DOCTORAL THESIS

Sustainable Mechanochemical Synthesis of Industrially Relevant Targets

Andrea Casagrande

TALLINNA TEHNIKAÜLIKOOL
TALLINN UNIVERSITY OF TECHNOLOGY
TALLINN 2026

TALLINN UNIVERSITY OF TECHNOLOGY
DOCTORAL THESIS
86/2026

Sustainable Mechanochemical Synthesis of Industrially Relevant Targets

Joint-supervision Estonia-France

ANDREA CASAGRANDE

TAL TECH PRESS

TALLINN UNIVERSITY OF TECHNOLOGY
School of Engineering
Virumaa College
This dissertation was accepted for the defence of the degree: 18/11/2026

Supervisor:

Dr. Allan Niidu
School of Engineering
Tallinn University of Technology
Tallinn, Estonia

Dr. Evelina Colacino
ICGM, URM 5253
University of Montpellier
Montpellier, France

Opponents:

Prof Dominique Agustin
University of Toulouse III Paul Sabatier
Toulouse, France

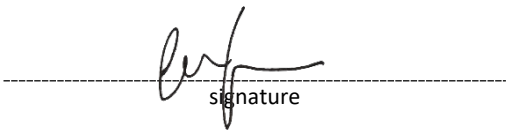
Prof Radovan Šebesta
Comenius University Bratislava
Bratislava, Slovakia

Prof Niclas Solin
Linköping University
Linköping, Sweden

Defence of the thesis: 14/12/2026, Montpellier, France

Declaration:
Hereby I declare that this doctoral thesis, my original investigation and achievement, submitted for the doctoral degree at Tallinn University of Technology has not been submitted for doctoral or equivalent academic degree.

Andrea Casagrande



signature

European Union
European Regional
Development Fund

Investing
in your future

Copyright: Andrea Casagrande, 2026
ISSN 2585-6901 (PDF)
ISBN 978-9916-80-610-4 (PDF)
https://doi.org/10.23658/taltech.86/2026

Casagrande, A. (2026). *Sustainable Mechanochemical Synthesis of Industrially Relevant Targets* [TalTech Press]. https://doi.org/10.23658/taltech.86/2026

TALLINNA TEHNIKAÜLIKOOL
DOKTORITÖÖ
86/2026

Tööstuslikult oluliste sihtühendite jätkusuutlik mehhanokeemiline süntees

Eesti ja Prantsusmaa ühisjuhendamine

ANDREA CASAGRANDE

TAL TECH
KIRJASTUS

List of Publications

The list of author's publications, based on which the thesis has been prepared:

I **Andrea Casagrande**, Rubén Solórzano-Rodríguez, Maria Carta, Francesco Delogu, Joris Vezzani, Allan Niidu, Evelina Colacino, Mechanochemical Amidation Mediated by 1,1'-Oxalyldiimidazole for the Synthesis of Agrochemicals, Chemistry – A European Journal, Volume 32, 2026, e71190. https://doi.org/10.1002/chem.71190

II Rubén Solórzano-Rodríguez, Nicolas Fantozzi, **Andrea Casagrande**, Christos M. Chatzigiannis, Corentin Bordier, Pietro Rando, Evelina Colacino, Safe and Sustainable by Design (SSbD) Synthesis of Food and Personal Care Ingredients by Mechanochemistry, ChemSusChem, Volume 19, 2026, e202502491. https://doi.org/10.1002/cssc.202502491

III Michael Patrascu, Damiana Meuti, Or Galant, Sally Nijem, Charles E. Diesendruck, **Andrea Casagrande**, Evelina Colacino, Michael Felderhoff, Sabrina Spatari, Sustainable pharmaceutical manufacturing based on mechanochemistry: A life cycle assessment of rac-Ibuprofen-Nicotinamide cocrystallization routes, Sustainable Chemistry and Pharmacy, Volume 51, 2026, 102422. https://doi.org/10.1016/j.scp.2026.102422.

List of additional publications related to the current work

IV **Andrea Casagrande**, Christos M. Chatzigiannis, Ken-ichi Otake, Joris Vezzani, Allan Niidu, Evelina Colacino, Scalable Amidation Reaction by Resonant Acoustic Mixing. Application to the Multi-Gram Scale Synthesis of Marketed Agrochemicals, *manuscript submitted*.

V Lea Čolakić,[‡] **Andrea Casagrande**,[‡] Goran Miletić, Ernest Meštrović, Evelina Colacino, Ivan Halasz, Breathing New Life into Old Processes: Continuous Mechanochemistry Enables Green Manufacturing of Essential Pharmaceuticals, *manuscript submitted*.

VI **Andrea Casagrande**, Yingzi Li, Laurence Brandon, Valerie Flaud, Dzmitry Kananovich, Riina Aav, Allan Niidu, Feliu Maseras, Evelina Colacino, Copper-Mediated Mechanochemical Nitrile Reduction in Mild Conditions Using Ammonia Borane and *in silico* Mechanistic Studies, *manuscript submitted*.

Author's Contribution to the Publications

Contribution to the papers in the thesis are:

I The author had a major role in the method development, synthesis and characterization of compounds used in the study. The author had a significant role in the preparation of the manuscript and a major role in the compilation of the supporting information.

II The author had a role in the method development, synthesis and characterization of compounds used in the study. The author had a major role in the greenness assessment calculations.

III The author had a major role in the DOZN™ based greenness assessment calculations.

IV The author had a major role in the method development, synthesis and characterization of compounds used in the study. The author had a significant role in the preparation of the manuscript and a major role in the compilation of the supporting information.

V The author had a major role in the method development, synthesis and characterization of one of the two compounds prepared in the study (phenytoin). The author had a significant role in the preparation of the manuscript and a major role in the compilation of the supporting information.

VI The author had a major role in the method development, synthesis and characterization of compounds used in the study. The author had a significant role in the preparation of the manuscript and a major role in the compilation of the supporting information.

Contents

List of Publications 5
List of additional publications related to the current work 6
Author's Contribution to the Publications 7
Contents 8
Introduction Générale 11
General Introduction 13
ABBREVIATIONS AND PICTOGRAMS 15
INTRODUCTION 17
1. Mechanochemical synthesis of agrochemicals 18
2. Food and personal-care ingredients synthesis in mechanochemistry 21
3. Mechanochemical equipment 22
3.1 Ball mills 22
3.2 Resonant Acoustic Mixer (RAM) 26
3.3 Twin Screw Extruder (TSE) 30
3.4 Approaches to Scale-Up : case studies 35
4. Green Chemistry metrics toolkits for the evaluation of mechanochemical processes 39
Introduction Chapitre I 41
I - Motivation and aims of the present work 42
Chapter I — Mechanochemical amidation mediated by 1,1'-oxalyldiimidazole for the synthesis of agrochemicals 43
1. Context 43
2. CDI-mediated amidation in vibrating ball mills 44
2.1 Gram-scale synthesis and the role of milling energy 46
2.2 *Step I* reaction kinetics 47
3. ODI-mediated amidation 47
3.1 Vibrating ball mills 47
3.2 Gram-scale synthesis: the planetary mill and the device effect 48
4. Solvent-free product recovery 49
5. Comparative greenness assessment 50
6. Conclusion 52
Introduction Chapitre II 53
II - Motivation and aims of the present work 54
Chapter II — Amide bond formation with *N,N,N',N'*-Tetramethylchloroformamidinium hexafluorophosphate (TCFH): from ball milling to resonant acoustic mixing at the multi-decagram scale. 55
1. Context 55
2. Establishing the reaction in ball mills 56
3. Transfer to the resonant acoustic mixer 59
3.1 Boscalid: a different reactivity 60
3.2 Comparison of the three technologies 61
3.3 TCFH against EDCI/Oxyma in LA-RAM 62

4. Scale-up by RAM 62
4.1 Aggregation of the by-product 64
4.2 Heat build-up, and the mechanical contribution 64
5. Solid-state characterization 66
6. Comparative greenness assessment 67
6.1 Comparing the three technologies 67
6.2 Comparing RAM with the solution routes 68
7. Conclusion 71

Introduction Chapitre III 73

III - Motivation and aims of the present work 74

Chapter III — Continuous Mechanochemical Manufacturing of Essential Medicines by Twin-Screw Extrusion 75
1. Context 75
2. Continuous synthesis of silver(I) sulfadiazine 76
3. Continuous synthesis of phenytoin 77
4. Benchmarking against the solution process 78
5. Conclusions 79

Introduction Chapitre IV 80

IV - Motivation and aims of the present work 81

Chapter IV — Mechanochemical Nitrile Reduction in Mild Conditions Using Ammonia Borane as Reducing Agent 82
1. Context 82
2. Reaction discovery: choosing the activator 83
3. Optimizing the stoichiometry 84
4. Optimizing the technical milling parameters 85
5. Substrate scope 86
6. Spectroscopic evidence for the copper–nitrile intermediate 87
7. Conclusions 89

Introduction Chapitre V 91

V - Motivation and aims of the present work 92

Chapter V — Mechanochemical Synthesis of Food and Personal-Care Ingredients by Ball Milling 93
1. Result and discussion 93
2. (S)-(-)-Perillartine 93
3. N-tert-butyl-α-phenylnitrone 95
4. Comparative Greenness Assessment 96
5. Conclusion 99

Introduction Chapitre VI 100

VI - Motivation and aims of the present work 101

Chapter VI — Scale-Up and Life Cycle Assessment of Mechanochemical *rac*-Ibuprofen:Nicotinamide Co-Crystallization 102
1. Context 102
2. Kilogram-scale co-crystallization by attritor and hammer milling 102
3. Green chemistry metrics 104

4. Life cycle assessment 105
4.1 Base case: global warming impact 105
4.2 Beyond global warming: the wider impact profile 106
4.3 Scenario analysis: decarbonizing electricity and solvent 106
5. Batch versus continuous mechanochemistry: EVM and HME compared 108
6. Conclusions 108
Conclusion Générale 109
General Conclusions 111
References 113
Acknowledgements 128
Abstract 129
Résumé 130
Lühikokkuvõte 131
Appendix 1 133
Appendix 2 153
Appendix 3 169
Appendix 4 185
Appendix 5 209
Appendix 6 319
Appendix 7 375
Curriculum Vitae 471
Elulookirjeldus 472

Introduction Générale

Les produits de la chimie fine sont présents partout dans la vie quotidienne. Les principes actifs pharmaceutiques, les produits phytosanitaires, les additifs alimentaires, les arômes, les parfums, les actifs cosmétiques et les colorants sont tous issus d'une synthèse chimique. La demande pour ces molécules continue d'augmenter, portée par la croissance démographique et par l'arrivée régulière de nouveaux produits sur le marché. Leur mode de production, en revanche, a peu changé. Il repose encore sur une synthèse en solution, conduite par lots (*batch)* et en plusieurs étapes, dans de grands volumes de solvant organique, avec chauffage, refroidissement et purification à chaque étape.

Le solvant est le principal point faible de cette approche. Dans un procédé *batch* typique de l'industrie pharmaceutique ou de la chimie fine, il représente 80 à 90 % de la masse totale engagée. Il constitue donc le premier contributeur au facteur E, c'est-à-dire à la masse de déchets produite par unité de masse de produit, qui reste élevée dans ces secteurs. À mesure que la réglementation environnementale se durcit, repenser la fabrication chimique selon les douze principes de la chimie verte n'est plus seulement un objectif académique, mais une nécessité industrielle et réglementaire.

La mécanochimie est l'une des technologies les plus prometteuses développées en réponse à ce constat. L'IUPAC la définit comme une réaction induite par l'absorption directe d'énergie mécanique. L'énergie est apportée par impact et cisaillement, directement sur les réactifs solides, et non par agitation d'une solution. Le solvant en masse est alors supprimé, en totalité ou en grande partie. Les technologies concernées sont le broyage à billes, le mélange acoustique résonant (RAM) et l'extrusion bi-vis (TSE), cette dernière ayant été retenue par l'IUPAC en 2019 parmi les dix technologies émergentes de la chimie. En vingt ans, la mécanochimie est passée du statut de curiosité de laboratoire à celui de plateforme de synthèse organique à part entière.

Deux questions restent cependant ouvertes. La première est celle de l'échelle : la plupart des protocoles publiés sont des preuves de concept réalisées sur quelques centaines de milligrammes. La seconde est celle de la preuve: l'avantage environnemental de la mécanochimie est souvent affirmé plutôt que mesuré. Le lever demande des outils dédiés, qu'il s'agisse des métriques de chimie verte ou de l'analyse de cycle de vie.

Ce travail de thèse aborde ces deux questions. Son objectif est d'appliquer la mécanochimie à la synthèse de molécules d'intérêt industriel et commercial, sans se limiter à un seul secteur de marché, et de quantifier le bénéfice environnemental de chaque voie développée. Les cibles retenues couvrent les produits phytosanitaires, les ingrédients de l'alimentation et des soins personnels issus de la biomasse renouvelable, et les formes solides pharmaceutiques. Dans chaque cas, le développement synthétique est associé à une évaluation chiffrée de la durabilité.

Le manuscrit s'ouvre sur un chapitre introductif, consacré à l'état de l'art de la mécanochimie appliquée à ces secteurs, aux équipements disponibles et aux outils d'évaluation de la durabilité. Le **chapitre I** décrit une amidation sans solvant activée par le 1,1'-oxalyldiimidazole (ODI), appliquée à la synthèse à l'échelle du gramme de trois fongicides commerciaux. Le **chapitre II** transfère une amidation médiée par le TCFH du broyeur à billes vers le mélange acoustique résonant, et montre une montée en échelle d'un facteur 160 sans réoptimisation. Le **chapitre III** passe du procédé discontinu au procédé continu, avec la préparation par extrusion bi-vis de deux médicaments

essentiels de l' Organisation Mondiale de la Santé (OMS), la sulfadiazine d'argent et la phénytoïne. Le **chapitre IV** change de registre : il ajoute une transformation nouvelle à la boîte à outils mécanochimique, la réduction des nitriles en amines primaires par le borane-ammoniac. Le **chapitre V** étend l'approche aux ingrédients de l'alimentation et des soins personnels, la périllartine et le *N*-*tert*-Butyl-α-phenylnitrone (PBN), et introduit des jarres en poly(oxyméthylène) sans fluor. Le **chapitre VI**, enfin, quitte la réaction isolée pour la comparaison de procédés : il évalue par analyse de cycle de vie plusieurs technologies mécanochimiques appliquées au co-cristal *rac*-ibuprofène:nicotinamide, face à une cristallisation conventionnelle en solvant. Une conclusion générale rassemble ces résultats et dégage les perspectives de ce travail.

General Introduction

Fine chemicals are present throughout everyday life. Active pharmaceutical ingredients, crop-protection agents, food additives, flavors, fragrances, cosmetic actives and dyes are all made by chemical synthesis. Demand for these molecules keeps rising, driven by population growth and by the steady arrival of new commercial products. The way they are made, in contrast, has changed little. It still relies on multi-step batch synthesis in solution, in large volumes of organic solvent, with heating, cooling and purification at every stage.

The solvent is the main weakness of this approach. In a typical pharmaceutical or fine-chemical batch process, it accounts for 80–90% of the total mass used. It is therefore the largest single contributor to the E-factor, the mass of waste generated per unit mass of product, which remains high across these sectors. As environmental regulation tightens, redesigning chemical manufacture around the Twelve Principles of Green Chemistry is no longer only an academic goal, but an industrial and regulatory necessity.

Mechanochemistry is one of the most promising technologies developed in response. IUPAC defines it as a reaction induced by the direct absorption of mechanical energy. The energy is delivered by impact and shear, directly on the solid reactants, rather than through a stirred solution. Bulk solvent is thus removed, in full or in large part. The technologies concerned are ball milling, resonant acoustic mixing (RAM) and twin-screw extrusion (TSE), the last of which was selected by IUPAC in 2019 as one of the ten emerging technologies in chemistry. Over twenty years, mechanochemistry has moved from a laboratory curiosity to a platform for organic synthesis in its own right.

Two questions nevertheless remain open. The first concerns scale: most published protocols are proofs of concept run on a few hundred milligrams. The second concerns proof: the environmental advantage of mechanochemistry is often asserted rather than measured. Answering it requires dedicated tools, whether green chemistry metrics or life cycle assessment.

This thesis addresses both questions. Its aim is to apply mechanochemistry to the synthesis of industrially and commercially relevant molecules, without restricting the work to a single market sector, and to quantify the environmental benefit of each route developed. The targets chosen span crop-protection agents, food and personal-care ingredients derived from renewable biomass, and pharmaceutical solid forms. In every case, synthetic development is coupled to a quantitative assessment of sustainability.

The manuscript opens with an introductory chapter on the state of the art of mechanochemistry in these sectors, on the available equipment, and on the tools used to assess sustainability. **Chapter I** describes a solvent-free amidation activated by 1,1'-oxalyldiimidazole (ODI), applied to the gram-scale synthesis of three marketed fungicides. **Chapter II** transfers a TCFH-mediated amidation from the ball mill to resonant acoustic mixing, and shows a 160-fold scale-up without re-optimization. **Chapter III** moves from batch to continuous processing, with the preparation by twin-screw extrusion of two World Health Organization (WHO) essential medicines, silver(I) sulfadiazine and phenytoin. **Chapter IV** changes register: it adds a new transformation to the mechanochemical toolbox, the reduction of nitriles to primary amines with ammonia borane. **Chapter V** extends the approach to food and personal-care ingredients, perillartine and *N*-*tert*-Butyl-α-phenylnitrone (PBN), and introduces fluorine-free poly(oxymethylene) milling jars. **Chapter VI**, finally, moves from the single reaction to the comparison of processes: it assesses, by life cycle assessment, several

mechanochemical technologies applied to the *rac*-ibuprofen:nicotinamide co-crystal, benchmarked against a conventional solvent-based crystallization. A general conclusion brings these results together and sets out the perspectives of this work.

ABBREVIATIONS AND PICTOGRAMS

η	Amount of LAG
ϕ	Filling Ratio
Φ_{MB}	Milling Ball(s) Filling Degree
AcOEt	Ethyl acetate
AE	Atom Economy
AM	Attritor Mill
API	Active Pharmaceutical Ingredient
AVO	Avobenzone
BRR	Ball-to-Reactant Ratio
CDI	1,1'-Carbonyldiimidazole
cEF	Complete E-Factor
COD	cyclooctadiene
CuAAC	Cu-catalysed Alkyne–Azide Cycloaddition
DCM	Dichloromethane
DGU	3a,6a-Diphenylglycoluril
DMF	Dimethylformamide
DMSO	Dimethyl sulfoxide
DSC	Differential Scanning Calorimetry
ECHA	European Chemicals Agency
EDCI	1-Ethyl-3-(3-dimethylaminopropyl)carbodiimide
E_{imp}	Energy per Impact
E_{tot}	Total Energy
EVM	Eccentric Vibrating Mill
GA	Grinding Auxiliaries
GA-RAM	Grinding Assisted-Resonant Acoustic Mixing
GHS	Globally Harmonized System
HATU	Hexafluorophosphate Azabenzotriazole Tetramethyl Uronium
HBTU	2-(1*H*-Benzotriazol-1-yl)-1,1,3,3-tetramethyluronium hexafluorophosphate
HM	Hammer Mill
HME	Hot Melt Extruder
IBU	Ibuprofen
ICH	International Council of Harmonisation
iGAL	Innovation Green Aspiration Level
IUPAC	International Union of Pure and Applied Chemistry
LAG	Liquid Assisted Grinding
LA-RAM	Liquid Assisted-Resonant Acoustic Mixing
MeOH	Methanol
NIC	Nicotinamide
NMI	*N*-Methylimidazole
NMP	1-Methyl-2-pyrrolidinone
OCT	Octinoxate
ODI	1,1'-Oxalyldiimidazole
OMS	Organisation Mondiale de la Santé
PBM	Planetary Ball Mill

PBN	*N*-*tert*-Butyl-α-phenylnitrone
PHE	Phenytoin
PMI	Process Mass Intensity
PMMA	Polymethylmethacrylate
POM	Polyoxymethylene
PP	Polypropylene
PTFE	Polytetrafluoroethylene
PXRD	Powder X-Ray Diffraction
PyBOP	(Benzotriazol-1-yloxy)tripyrrolidinophosphonium hexafluorophosphate
PyBrOP	Bromotripyrrolidinophosphonium hexafluorophosphate
RAM	Resonant Acoustic Mixing
REACH	Registration, Evaluation, Authorisation and Restriction of Chemicals
RME	Reaction Mass Efficiency
RPG	Relative Process Greenness
rpm	Rounds Per Minute
SDHI	Succinate Dehydrogenase Inhibitor
SME	Specific Mechanical Energy
SS	Stainless Steel
SSD	Silver Sulfadiazine
STY	Space Time Yield
TCFH	*N,N,N',N'*-Tetramethylchloroformamidinium hexafluorophosphate
THF	Tetrahydrofuran
TMU	Tetramethyl urea
TSE	Twin Screw Extrusion
VBM	Vibration Ball Mill
WHO	World Health Organization



Ball Milling



Resonant Acoustic Mixing



Twin Screw Extrusion

INTRODUCTION

The synthesis of organic molecules underpins virtually every sector of the modern economy. Active pharmaceutical ingredients, crop-protection agents, food additives and flavorings, fragrances and cosmetic actives, dyes, fine chemicals and the building blocks of advanced functional materials are all products of chemical manufacture, and global demand for them continues to rise in step with population growth, increasing prosperity and the continual development of new commercial products. Securing access to these molecules in sufficient quantity, at acceptable cost and with consistent quality has consequently become a central preoccupation of the chemical and process industries.

This expanding demand stands in tension with the environmental cost of the way such molecules are conventionally produced. The dominant manufacturing strategy remains multi-step, solution-phase batch synthesis conducted in large volumes of organic solvent, with substantial energy input and considerable waste generation at every stage. Solvents alone routinely account for the majority of the mass consumed in fine-chemical and pharmaceutical processes,[1] and are the single largest contributor to the process waste expressed by the E-factor (*i.e.* the mass of waste generated per unit mass of product) which remains stubbornly high across these sectors.[2] As environmental regulation tightens and the expectation of sustainable production intensifies, the imperative to redesign chemical manufacture around the Twelve Principles of Green Chemistry has shifted from an academic aspiration to a strategic and regulatory necessity.[3]

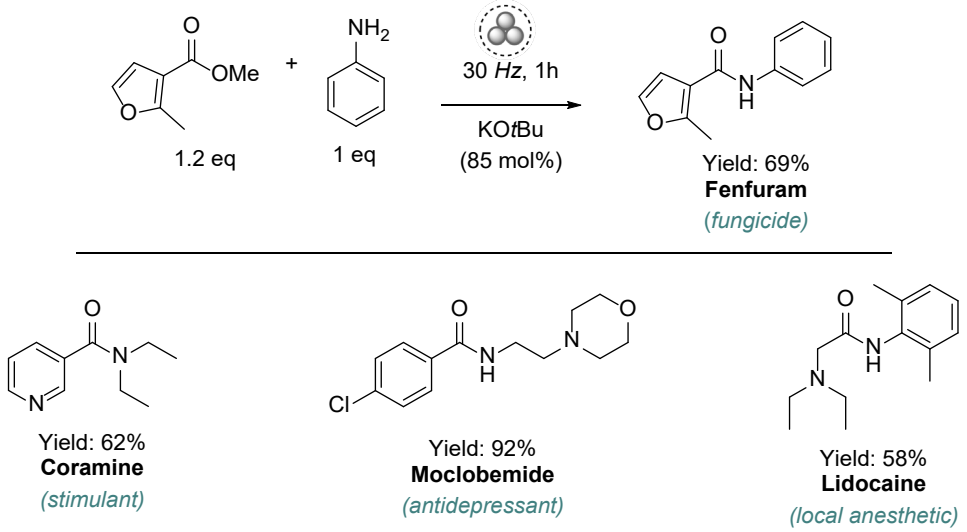
Among the enabling technologies developed in response to this imperative, mechanochemistry has emerged as one of the most promising. Defined by IUPAC as a chemical reaction induced by the direct transfer of mechanical energy,[4] mechanochemistry supplies the energy required to drive a transformation through impact and shear action directly on solid reactants, rather than through a stirred solution-phase. The more common technology to do this are ball mills, twin-screw extruders or, more recently, by resonant acoustic mixing (RAM). Its defining consequence is the elimination, partial or total, of the bulk solvent that otherwise dominates process mass and waste. Over the past two decades, mechanochemistry has matured from a laboratory curiosity into a versatile and increasingly well-understood platform for organic synthesis,[5,6] with documented gains in reaction rate, atom economy, waste reduction, and potentially lower costs,[7,8] relative to the corresponding solution-phase routes.[9,10]

Building on these foundations, this thesis examines how mechanochemistry can be applied to the sustainable synthesis of industrially and commercially important molecules, treated not as the concern of any single market sector but as a broad and heterogeneous class of high-value chemical products. The synthetic work developed in the following chapters spans agrochemicals, ingredients for the food and personal-care industries derived from renewable biomass, and pharmaceutical solid forms which are chosen as representative targets through which the scope, scalability and environmental credentials of mechanochemical manufacture can be assessed. Throughout, synthetic development is coupled to a quantitative evaluation of sustainability by means of green-chemistry metrics and life cycle assessment, so that the environmental advantages claimed for each mechanochemical route are substantiated by actual data.

1. Mechanochemical synthesis of agrochemicals

The synthesis of agrochemicals is undergoing already a fundamental shift as the limitations of traditional solution-based batch processing (*e.g.* high solvent waste, prolonged reaction cycles, and intensive energy requirements), become increasingly incompatible with green chemistry mandates. Mechanochemical synthesis, particularly high-energy ball milling, offers a transformative pathway for industrial-scale fungicide production. By leveraging mechanical shear and impact rather than liquid-phase diffusion, these methods significantly enhance reaction kinetics while minimizing the environmental footprint of high-volume chemical manufacturing.

The first contribution for the development of protocol that target directly a commercial agrochemical was in the framework of the development of direct amidation of esters done by Browne and coworkers,[11,12] that validates the shift toward solvent-minimized organic transformations, specifically in the synthesis of Fenfuram (Scheme 1). This work highlights how mechanochemical environments facilitate amides manufacture without the need of bulky coupling agents and reduced amount of base, aligning with the industry's broader goals of waste reduction and operational simplicity. This methodology offers several advantages. It delivers good to excellent yields within a short reaction time (1 hour of milling) and has been reported to be scaled up to the gram scale. Waste is kept low, owing in part to the near-stoichiometric reagent ratios. This is confirmed by the low process mass intensity (PMI) of the reaction: 1.94, compared with 59.28 for the closest solution-phase analogue reported by Yoon and co-workers[13] . Using this protocol, the scalability was limited only by the size of the jar in the mixer mill and was observably linear without yield loss from the 100 mg to the 2-3 g scale.



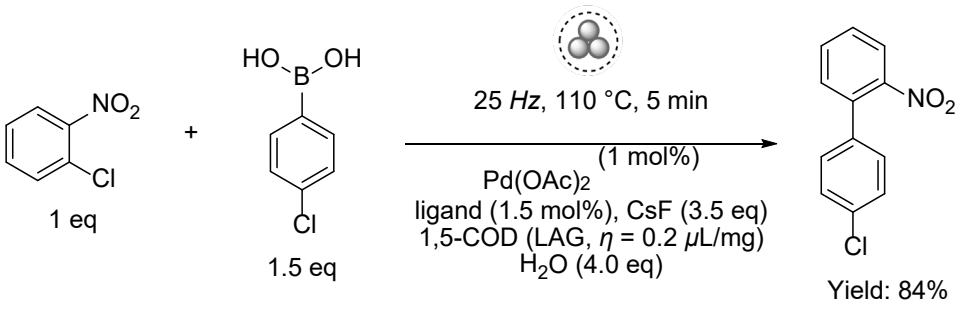
Scheme 1. Direct amidation of esters by ball milling and its application to the synthesis of Fenfuram, a fungicide, and selected active pharmaceutical ingredients.[11]

A definitive milestone in this field is the total mechanochemical synthesis of Boscalid, a vital fungicide produced at scales exceeding 1,000 tons annually. As detailed by Ito and coworkers (Scheme 2),[14] the process employs a rapid three-step sequence performed entirely within the milling jar, making resource of the huge development in synthetic

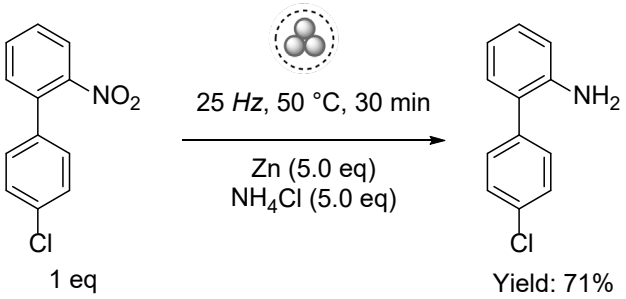
methodologies developments in the 5 years that have passed since the Browne's study. The synthesis of Boscalid breaks down in three steps:

- Suzuki–Miyaura Cross-Coupling:[15,16] The coupling of 2-chloronitrobenzene and 4-chlorophenylboronic acid is achieved in just 5 minutes. Technical optimization identified 2-dicyclohexylphosphino-2'-(N,N-dimethylamino)biphenyl (DavePhos) as the superior ligand and utilized 1,5-cyclooctadiene (1,5-cod) as a critical palladium stabilizer. High-temperature milling (internal temp. 110 °C), performed by heating the moving jar with a heat gun pointed to it, was essential to accelerate the transformation.
- Zinc-Mediated Béchamp Reduction:[17] The biaryl nitro intermediate is reduced to the corresponding amine using Zn powder and NH_4Cl. This step is completed in 30 minutes, a significant improvement over the 4–12 hours typical of solution-phase reductions.
- Amidation:[18] The final coupling with 2-chloronicotinyl chloride is achieved at 25 Hz in 30 minutes.

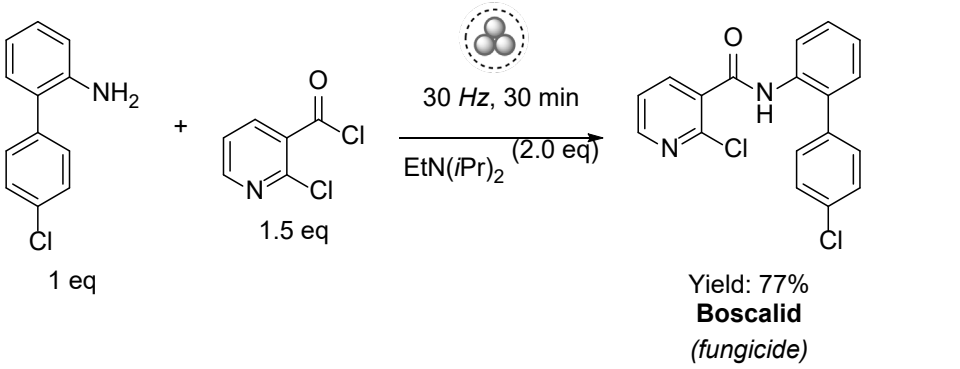
Suzuki-Miyaura cross-coupling:



Béchamp reduction:



Amidation:



***Scheme 2**. Full mechanochemical synthesis of Boscalid, performed in three steps.*[14–18]

The strategic importance of this protocol lies in its efficiency; the total reaction time is compressed to a little more than 1 hour, compared to the 30–36 hours required by traditional methods[19,20] while retaining high overall yields.

In Chapter I and II the number of mechanochemical syntheses for the preparation of five key succinate dehydrogenase inhibitor (SDHI) fungicides (*e.g.,* Fenfuram, Mepronil, Flutolanil, Boscalid and Fluxapyroxad) is expanded and these methods are benchmarked against the corresponding solution-based protocols, in order to precisely frame the importance of alternative, waste-minimized, focused strategies in the context of the preparation of such high-volume agrochemicals, where the large quantities required make waste minimization a key objective.

2. Food and personal-care ingredients synthesis in mechanochemistry

Beyond crop protection, mechanochemistry is increasingly applied to the high-value ingredients of the food and personal-care industries, where it pairs naturally with the valorization of natural and renewable feedstocks. Plant oils, terpenes, sugars and related bio-sourced molecules can be upgraded into useful products by milling or extrusion.[21] These sectors are large and under growing pressure to manufacture more cleanly, yet they remain comparatively underexplored by mechanochemical processing.

An illustrative example, again based on cyclodextrin inclusion complexes, is the work of Grepioni and coworkers on environmentally friendlier sunscreens.[22] By ball-milling *β*-cyclodextrin (*β*-CD) with the widely used UV filters avobenzone (AVO) and octinoxate (OCT), they obtained crystalline inclusion complexes in which the photodegradation of both filters was sharply reduced. Including the filters in the cyclodextrin cavity improves their photostability and is expected to limit their permeation through the skin, allowing lower amounts to be used in sun creams (Figure 1).

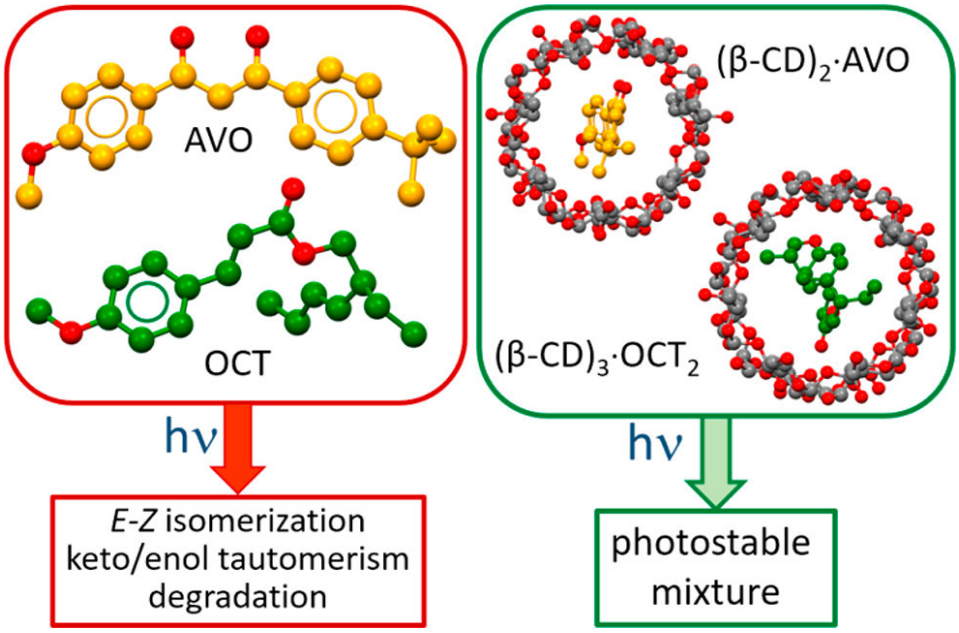
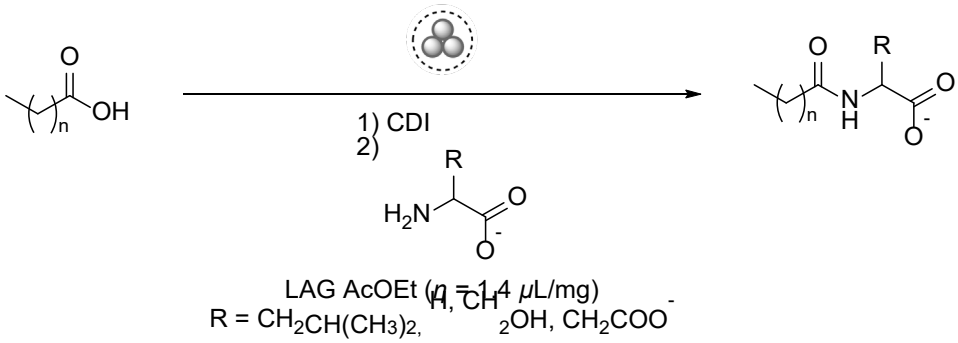


Figure 1. *Inclusion of avobenzone (AVO) and octinoxate (OCT) in β-cyclodextrin to enhance photostability. Reprinted with permission from ref. [22].*

Ball milling has also been used to prepare renewable surfactants for personal-care formulations. Nesterenko and coworkers developed a solvent-minimized, acylation of peptides obtained from silk sericin, a non-food biomass, using 1,1'-carbonyldiimidazole (CDI) to activate the fatty acid (Scheme 3). Model amino acids were acylated in up to 99% conversion in both vibrating and planetary ball mills, and the resulting silk lipopeptides lowered the surface tension of water to about 26 mN/m, indicating good potential as bio-based replacements for petroleum-derived surfactants.[23]



Scheme 3. *Ball milling synthesis of lipoamino acid surfactants.*

Chapter V extends this approach to two further marketable ingredients. It describes the multigram mechanochemical synthesis of the sweetener perillartine, prepared from the renewable Perilla-derived aldehyde perillaldehyde, and of the cosmetic antioxidant N-tert-butyl-α-phenylnitrone (PBN).[24] The work also introduces fluorine-free poly(oxymethylene) (POM) milling jars as a safer, more sustainable alternative to PTFE.

3. Mechanochemical equipment

3.1 Ball mills

The selection of a ball mill type is among the first and most consequential decisions in the design of a mechanochemical experiment. The motion kinematics governing each mill type[25] determine the nature, magnitude, and frequency of mechanical energy delivered to the sample, and consequently modulate reaction kinetics, selectivity, and scalability. At the laboratory scale, two principal ball-mill architectures are in common use: mixer/shaker mills and planetary mills, each presenting distinct advantages and limitations (Figure 2).[26–28]

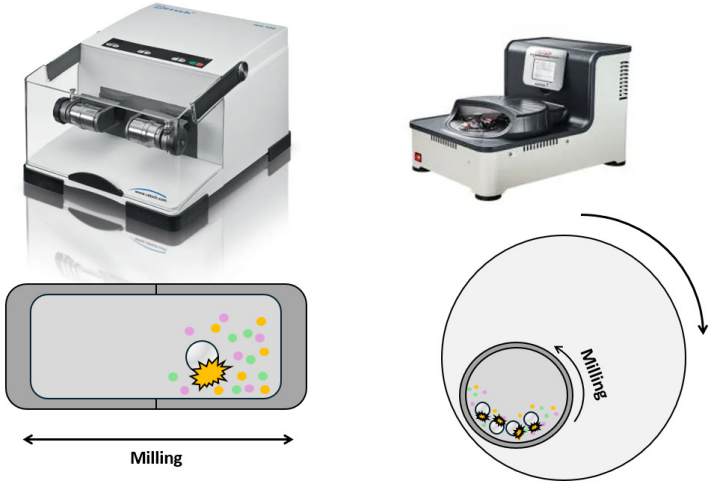


Figure 3. *Some commonly used ball mills and their mode of action. Top left: MM400 reproduced from Retsct webpage (https://www.retsch.com/). Top right: Pulverisette 7 Premium reproduced from Fritsch webpage (https://www.fritsch-international.com/).*

Mixer mills operate via a reciprocating back-and-forth linear (*i.e.* vibration ball mill (VBM)) or figure-of-eight oscillation of the milling jar (*i.e.* eccentric mixer mill such as Spex 8000 CertiPrep) at frequencies can go up to 30 to 50 Hz. In these devices, the primary force imparted to the sample arises from the high-velocity impact of one or a small number of milling balls against the walls of the jar. This geometry generates a predominantly impact-dominated energy transfer profile, characterized by high peak impact forces but relatively low shearing components.[29] The compact and simple design of mixer mills renders them particularly amenable to rapid screening of reaction conditions at the milligram-to-gram scale, typically accommodating jar volumes of 1.5 to 120 mL for VBM and up to 135 mL for the Spex 8000 CertiPrep. Planetary ball mills (PBM) operate on a fundamentally different kinematic principle. The milling jars are mounted eccentrically on a rotating disc (the 'sun wheel'), such that each jar undergoes a counter-directional rotation about its own axis while simultaneously orbiting around the central disc axis. This compound planetary motion generates both high-energy impact forces and pronounced shearing forces, as the milling balls are flung outwards by centrifugal acceleration and then detach from the jar wall when the direction of rotation reverses. The resulting energy input per impact event is generally higher than in mixer mills, making planetary mills better suited for larger-scale reactions (gram to multi-hundred-gram range) and for reactions requiring sustained high-energy input. Jar volumes for planetary mills commonly range from 12 mL to 500 mL, and maximum operational speeds for modern instruments (*e.g.* Fritsch P7 achieve speeds up to 1100 rpm; Retsch High Energy Ball Mill Emax, up to 2000 rpm).

3.1.1 Influence of Technical Parameters on Mechanochemical Reactions in Ball Milling

The reproducibility and translation of mechanochemical protocols between laboratories and across different instruments constitute a recognized challenge in the field. This challenge arises because the outcome of a milling reaction is not governed by a single, easily quantified variable, but rather by the cumulative mechanical energy delivered to the sample, a quantity that is a complex function of multiple instrumental and compositional parameters. Lungerich and coworkers[30] demonstrated convincingly that the commonly reported parameters of reaction time, rotational speed (rpm), and ball mass are insufficient on their own to achieve reliable cross-instrument reproducibility; instead, a cumulative energy criterion must be satisfied, irrespective of how that energy is delivered. The following sections discuss the principal parameters independently. More recently, Carta and Delogu studied the motion of a single ball in the most common oscillating mills. They combined piezoelectric impact sensors with numerical simulations. This gave the impact frequency, velocity and angle for jars with one-, two- and three-dimensional motion. They defined a specific milling intensity as the impact frequency times the impact energy, divided by the powder mass. This quantity scaled the reaction rates. Kinetic curves recorded at different intensities fell on a single curve when plotted against the total energy delivered to the powder.[25]

Oscillation frequency is the primary tunable energetic parameter. Friščić and coworkers provided the first in situ, real-time study of the effect of milling frequency on a mechanochemical organic reaction, employing *in situ* Raman spectroscopy to monitor the synthesis of a 2,3-diphenylquinoxaline derivative.[31] Their study revealed a pronounced dependence of reaction kinetics on small frequency variations and identified two distinct kinetic regimes at different frequencies, attributed to different mechanical activation modes. Crucially, the internal jar temperature, measured immediately after completion, was found to increase monotonically with frequency, suggesting that the

thermal contribution to reaction activation cannot be neglected even under apparently ambient milling conditions. In planetary mills, the rotational speed of the sun wheel (in rpm) directly governs the centrifugal acceleration experienced by the milling media; a linear relationship between speed and energy dose rate has been documented, though the precise relationship depends additionally on the disc-to-jar radius ratio and the speed ratio between the sun wheel and the individual jars.[28,30]

Milling time is the simplest adjustable parameter but should be interpreted in the context of the cumulative energy delivered, rather than as an independent variable. Excessive milling can lead to thermal degradation of products, polymorphic transitions, or over-grinding, wherein continued mechanical impact causes excessive defect formation, amorphization, particle agglomeration, and contamination from abrasion of the milling media; whilst insufficient milling results in incomplete conversion. The use of intermittent milling protocols, alternating between active milling and resting periods, has been employed to mitigate thermal build-up.[32] The relationship between milling time and reaction progress is most accurately determined by *in situ* monitoring techniques, which allow real-time tracking of conversion without requiring repeated interruptions to the milling process.[31,33]

The milling balls size and number constitute the primary mechanical transducers in any ball mill, and their properties exert a profound influence on reaction outcomes. The kinetic energy of a ball impact scales with ball mass (and therefore with the cube of its diameter for a given material), making ball size one of the most sensitive parameters for controlling energy input. Emmerling and coworkers conducted a systematic investigation of the role of ball mass and demonstrated the importance of the impacts:[34] reactions sensitive to energy input can undergo qualitatively different outcomes depending on whether larger or smaller balls are employed. Conversely, Boldyreva and coworkers showed that in some soft-matter model systems, ball mass and ball size may exert differential effects that are not straightforwardly predictable, complicating generalization.[35]

The milling media material, most commonly stainless steel (SS), zirconia (ZrO_2), tungsten carbide (WC), agate (SiO_2), polyamide, polyethylene terephthalate (PTFE), Polymethylmethacrylate (PMMA) or polyoxymethylene (POM), determines both the density (and thus impact energy for a given geometry) and the surface chemistry of the grinding interface (Figure 3).[6,35,36] Abrasion of the ball surface can lead to inadvertent contamination of the reaction mixture; stainless-steel balls may leach iron, nickel, or chromium species, which may act as adventitious catalysts. ZrO_2 balls provide chemical inertness and moderate density, making them suitable for reactions sensitive to metallic contamination. PTFE and polymeric balls offer the lowest densities and are preferred when minimal energy input and total chemical inertness are required (see also Chapter II). In the context of milling media one of the most conceptually novel departures from conventional ball-milling practice is the exploitation of the milling equipment itself (jars and balls) as catalytically active surfaces, a paradigm termed 'direct mechanocatalysis'.[37–43] In this approach, the milling media serve simultaneously as mechanical transducers (delivering kinetic energy to the reaction) and as heterogeneous catalysts (providing catalytically active surface sites for substrate activation and bond transformation). Because the catalyst is physically embodied in the milling equipment, product isolation requires only the removal of the milling balls from the reaction mixture, a significant practical advantage over conventional homogeneous or colloidal catalysis, where catalyst recovery can be arduous and costly.

The ball-to-reactant ratio (BRR), defined as the ratio of ball mass to total reactant mass, is a critical parameter governing both the stress energy transferred per impact and the kinetics of conversion. Emmerling and coworkers[44,45] employed *in situ* PXRD to demonstrate that increasing the BRR accelerates reaction times by increasing the impact stress per unit mass of sample, but does not affect the induction period characteristic of specific reaction systems. Burmeister and Kwade[28] conducted a comprehensive process-engineering analysis of planetary ball mills, establishing that the milling ball filling degree (Φ_{MB}) (*i.e*. the fraction of the jar volume occupied by milling balls) optimally falls near 0.3 for many reactions, with both higher and lower values leading to reduced energy transfer efficiency. The filling degree of the reactants relative to the void volume between the balls is an equally important but frequently underreported parameter.

Liquid-Assisted Grinding (LAG) has been a critical discovery enabling broad synthetic applicability, it is the practice of adding catalytic quantities of liquid (defined by the parameter η = volume of liquid per total mass of reactants, up to 1.0 μL/mg) to the milling jar.[46] Sub-stoichiometric amounts of solvent under LAG conditions can dramatically accelerate reaction rates, broaden substrate scope, and control selectivity. Effects are attributed to enhanced molecular mobility at reactive interfaces, plasticization of solid reactants, and solvent-mediated template effects. Closely related is the use of inert solid grinding auxiliaries (GAs), such as silica, sodium chloride, or alumina, which serve to improve powder flowability, prevent electrostatic agglomeration, and regulate the effective mechanical dose delivered to the substrates.



Figure 3. Different ball mill jars and balls of different materials. [a] 12 mL ZrO_2 Fristch jar for PBM. [b] 5 mL SS Retsch jar for VBM. [c] 10 mL ZrO_2 Retsch jar for VBM. [d] 10 mL Stainless Steel (SS) InSolido Technologies jar for VBM. [f] 50 mL SS Retsch jar for PBM. [g] 10 mL SS Fristch jar specific for the vertical VBM, the P23. [h] 10 mm Ø SS balls. [i] 9 mm Ø glass balls. [j] 7 mm Ø ZrO_2 balls. [k] 10 mm Ø Al_2O_3 balls.

3.2 Resonant Acoustic Mixer (RAM)

Resonant Acoustic Mixing (RAM) represents a comparatively recent but rapidly expanding approach that offers distinctive advantages in terms of scalability, operational simplicity, and the complete elimination of milling media (Figure 4).

RAM operates through the principle of acoustic resonance: the mixing vessel is affixed to a spring-mounted platform that oscillates vertically at or near the mechanical resonant frequency of the system. Unlike ball mills, RAM achieves reactivity by agitating materials at a low acoustic frequency (nominally 60 *Hz*), with energy input modulated through changes in the vertical acceleration experienced by the reaction vessel, tunable in the range of 0–100 *g*, where $g = 9.81\ m/s^2$ (force of gravity). The combination of a moderate operating frequency and a relatively large displacement amplitude (~14 mm peak-to-peak) generates an exceptionally high level of mixing energy compared to either ultrasonic mixers (which operate at very high frequency but with very small displacement) or conventional paint mixers (high displacement, very low frequency). The energy delivered to the reagent mixture is thus a function of both acceleration and time, and crucially, the absence of milling balls, jars, or any other impact media fundamentally distinguishes RAM from the classical mechanochemical toolkit.[47]

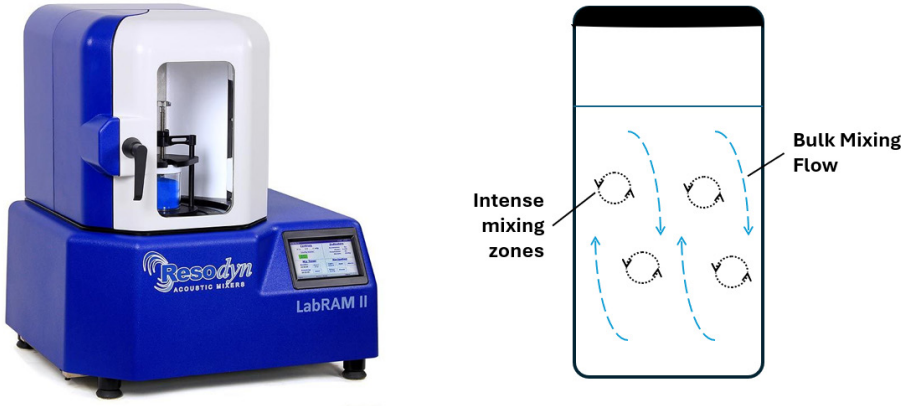
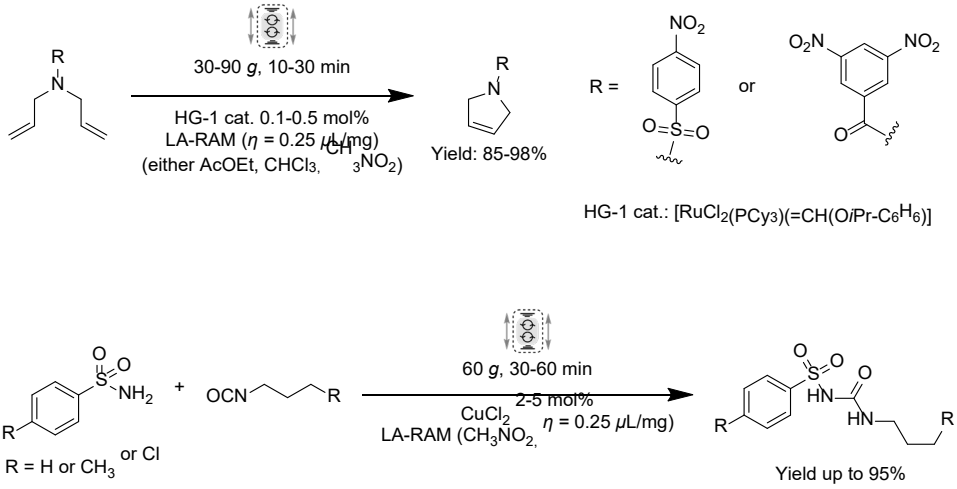


Figure 4. LabRAM II and the schematic representation of the mixing zones induced during operation. Reproduced from Resodyn™ webpage (https://resodynmixers.com/).

By generally avoiding the need for milling media, RAM enables simplification of reaction design, avoids product contamination resulting from chipping and abrasion of milling jars and balls, and it should facilitate the scale-up. These characteristics make RAM particularly well-suited for applications in pharmaceutical synthesis, where product purity is of paramount importance, and for the preparation of sensitive materials (*e.g.* explosives) where the impact forces inherent to ball milling would represent a safety or materials-integrity hazard.[48]

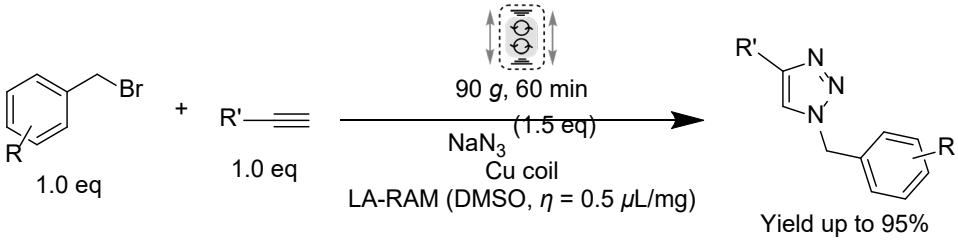
The first systematic application of RAM to catalytic organic mechanosynthesis was reported by Friščić and coworkers in 2022, who introduced it as a solvent-free, media-free platform for metal-catalyzed transformations.[49] Using Ru-catalyzed ring-closing metathesis and Cu-catalyzed sulfonamide–isocyanate coupling as model reactions, RAM was shown to be faster and operationally simpler than conventional ball milling, while also enabling the first mechanochemical example of Ru-catalyzed ene–ene and ene-yne

metathesis (Scheme 4). Notably, the methodology was readily scalable, as demonstrated by the straightforward 200-fold scale-up of Tolbutamide synthesis up to 30 g, without modification of reaction conditions, highlighting the practical advantages of RAM over traditional mechanochemical approaches.[49]



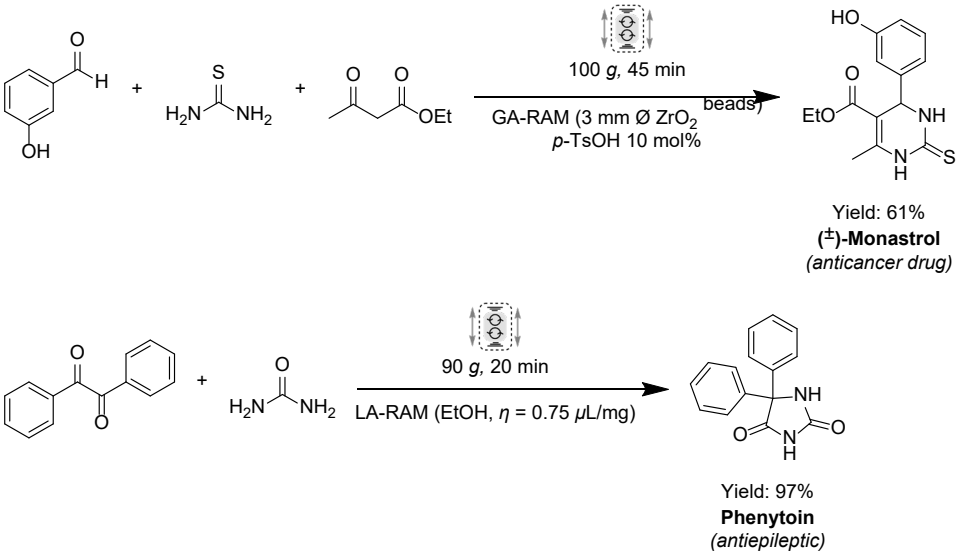
Scheme 4. The first examples of organic chemistry protocols involving RAM: ene-ene (or yne) metathesis (top) and isocyanate sulfonamide coupling (bottom).[49]

Subsequent work by the same group demonstrated the concept of direct mechanocatalysis under RAM conditions.[50] By introducing a simple copper coil as a heterogeneous catalyst, Cu-catalyzed alkyne–azide cycloaddition (CuAAC) reactions were conducted under RAM conditions, demonstrating that direct mechanocatalysis can occur in an entirely impact-free environment, driven solely by high-speed mixing of reagents against a metal surface (Scheme 5). Furthermore, real-time reaction monitoring using in situ Raman spectroscopy revealed zero-order reaction kinetics for several CuAAC reactions, consistent with a surface-based catalytic mechanism.[50]



Scheme 5. *First example of direct mechanocatalysis in RAM, applicated to CuAAC reaction.*[50]

In 2025, Colacino, Rivas and coworkers extended the RAM platform to multi-gram synthesis of pharmaceutically relevant targets through three representative organic transformations.[51] In selected cases, reaction efficiency was further enhanced through grinding-assisted RAM (GA-RAM), in which milling beads are introduced into the RAM vessel, either alone or in combination with a small amount of liquid in liquid-assisted RAM (LA-RAM). The reactions studied included the Knoevenagel condensation to vanillin barbiturate, the Biginelli multicomponent reaction to afford the anticancer drug (±)-Monastrol, and the Biltz rearrangement for the synthesis of the antiepileptic drug Phenytoin (Scheme 6). The processes were evaluated using green chemistry metrics and tools including Chem21 and DOZN 3.0 (*vide infra*), demonstrating that RAM technology outperforms the corresponding solution-based methods, representing an environmentally favorable alternative to conventional synthetic approaches.[51]



Scheme 6. *RAM multigram synthesis of (±)-Monastrol and Phenytoin.*[51]

One of the most compelling features of RAM as a mechanochemical platform is its capacity for direct and straightforward scale-up, which addresses one of the most persistent limitations of ball milling methodologies, where changes in reaction scale typically require re-optimization of a higher number of technical parameters linked to the necessity of convey efficiently the correct amount of energy to a more massive reaction scale.[30,52]

RAM reactions are readily and directly scaled up without any significant changes in reaction conditions, as demonstrated by the 200-fold scaling-up of the synthesis of the antidiabetic drug Tolbutamide, from hundreds of milligrams directly to 30 grams. The scalability of RAM was further demonstrated for the Biltz rearrangement, enabling the multi-gram synthesis of phenytoin under liquid-assisted RAM conditions without substantial modification of the optimized reaction parameters.[51] This represents a particularly striking result, as the identical reaction parameters (acceleration, time, and liquid additive loading) were applicable across this two-orders-of-magnitude scale range, a feat rarely achievable in ball-milling mechanochemistry without substantial process re-engineering.[49,51]

3.2.1 Influence of Technical Parameters on Mechanochemical Reactions in RAM

The gravitational acceleration (*g)* applied to the reaction vessel is the primary means by which energy input is controlled in RAM. Unlike in a conventional ball mill, the LabRAM instrument maintains a constant oscillation frequency corresponding to the mechanical resonant frequency of the device; instead, the amplitude of the oscillation is varied, thus altering the relative acceleration experienced by the powder particles. This has direct consequences for reaction outcome: the co-crystallization of carbamazepine and nicotinamide was monitored at two acceleration settings of 50 *g* and 100 *g*, with the higher acceleration affording faster and more complete conversion. The mechanistic rationale relates to comminution: higher accelerations are associated with increased particle–particle contact energies, leading to greater surface renewal and enhanced mass transport between solid reactants.[53]

RAM mixing efficiency is strongly linked to acceleration, and considerable variation in mixing efficiency can exist between different RAM models (*e.g.* LabRAM, LabRAM I, LabRAM II, OmniRAM, RAM 5, RAM 55) operating nominally at the same settings. This instrument-to-instrument variability has important practical implications for reaction reproducibility and protocol transfer, and underscores the need for careful characterization of individual instruments when quantitative comparisons are required.[54]

The filling ratio (ϕ), defined as the fraction of the vessel volume occupied by the reagent mixture, has been identified as a critical parameter for reaction control in RAM. Systematic investigation of Buchwald–Hartwig amination reactions under RAM conditions[55] revealed a clear relationship between reaction conversion and filling ratio (ϕ), providing a simple means to maximize conversion under scalable conditions. Specifically, underfilling the vessel leads to insufficient material contact and poor mixing, while overfilling suppresses the vigorous acoustic motion necessary for efficient energy transfer.[55]

A strategy termed liquid-assisted RAM (LA-RAM) is analogous to the well-established concept of liquid-assisted grinding (LAG) in ball milling, the introduction of sub-stoichiometric amounts of a liquid additive to RAM reactions which can profoundly influence reaction outcome. Like the ball milling equivalent liquid-to-solid ratio η (expressed in μL/mg) is the primary parameter describing liquid additive loading.[49,51]

All-in-all the filling ratio (ϕ), acceleration, and amount of liquid additive (η) collectively constitute three critical parameters that govern the design and optimization of scalable reactions under RAM conditions. Vessel geometry is an additional, often underappreciated parameter, as the dimensions and shape of the reaction vessel influence powder flow, the formation of mixing zones, and therefore the efficiency of mechanical-energy transfer and reaction progression under RAM conditions.[56] Understanding the interplay between these variables is essential for rational reaction development, yet their systematic investigation has only recently begun to appear in the literature, representing a significant opportunity for further fundamental research.

Reactions that respond poorly to media-free RAM, for example, systems that form viscous pastes or hard agglomerates that arrest bulk motion, can be promoted by grinding-assisted RAM (GA-RAM). The quantity of grinding media should be reported as a bead-to-powder mass ratio; for instance, 3 mm zirconia beads were used at a 1:1 ratio in representative GA-RAM reactions.[51] The beads enhance powder displacement, shearing, and deagglomeration, thereby maintaining effective mixing and increasing the

mechanical stress delivered to the reactants. GA-RAM can also be combined with LA-RAM when a liquid additive is required to adjust the reaction rheology. In the phenytoin synthesis, the benefit of pre-grinding KOH should instead be attributed cautiously to improved processing of the agglomerating mixture, while the major improvement arose from ethanol-induced rheological changes under LA-RAM conditions..[51]

Chapter II investigates how the distinct mixing regime of resonant acoustic mixing (RAM) affects a preparative amide-bond-forming reaction and identifies process parameters that differ from those established for vibratory ball milling (VBM). The study compares the influence of the physical state of the base: liquid N-methylimidazole (NMI) versus solid K_2HPO_4, and of reaction time on reaction outcome. Under the conditions examined, VBM benefited from shorter processing times and the solid base, whereas RAM gave improved results with liquid NMI and longer reaction times. These findings demonstrate that parameters optimized for VBM cannot necessarily be transferred directly to RAM, because the two technologies operate through different regimes of mixing and mechanical-energy transfer.

3.3 Twin Screw Extruder (TSE)

Among the suite of mechanochemical tools available to synthetic chemists, twin-screw extrusion (TSE) has emerged as a particularly transformative technology. Originally developed and optimized for the polymer processing and food manufacturing industries, TSE has been progressively adapted for reactive mechanochemical applications, enabling continuous, scalable, organic mechanosynthesis. Unlike ball milling, which operates in a batchwise regime with inherent limitations on throughput and scalability, TSE operates as a continuous-flow process, making it uniquely suited to industrial translation and process intensification.

A twin-screw extruder consists of two co-rotating or counter-rotating intermeshing screws housed within a modular barrel that can be heated (Figure 5). Solid reactants are continuously fed into the barrel, where they are subjected to a complex combination of compressive and shear mechanical forces as they are conveyed distally along the screw channels. The intermeshing geometry of the screws promotes intensive mixing and mechanical deformation of the solid feed material, generating sufficient localized energy to activate chemical reactions without the need for a bulk solvent medium.

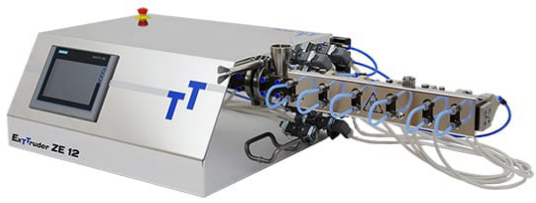


Figure 5. *A Three-Tec ZE 12 HMI, a benchtop extruder.[57] Reproduced from Three-Tec webpage (https://www.three-tec.ch/en/).*

The modular architecture of the TSE barrel is a critical feature of the platform from a synthetic chemistry perspective. Individual barrel segments can be independently kept at different temperatures, enabling a programmable temperature gradient along the length of the extruder. Equally important is the modular screw design: conveying elements, kneading blocks of variable offset angle, and reverse-pitch elements can be assembled in different sequences to produce tailored shear and mixing profiles appropriate to the specific mechanochemical transformation under investigation.[58]

Reagents can be introduced through two operational modes: starve-fed and flood-fed.[59] In starve-fed mode reagents are introduced into the extruder either as solids via gravimetric feeders or as liquids through injection ports positioned along the barrel. The latter capability enables the controlled delivery of LAG agents as well as glidants, which are solid additives that improve powder flow and prevent barrel motor blockages. In flood-fed mode, material is manually supplied in excess of the screw's conveying capacity directly in the barrel, so that the barrel remains fully filled with reactant throughout its length. Under these conditions, the fill level, and hence the compressive stress and residence time, are determined primarily by the screw geometry and rotational speed rather than by the feed rate. By contrast, in starve-fed mode, reagents are supplied at a set rate deliberately below the maximum conveying capacity of the screws, leaving a fraction of the barrel volume unfilled. This results in a lower and more controllable barrel fill level, reduced back-pressure, and a residence time that is directly adjustable through the feed rate independently of screw speed. Although manual flood feeding introduces greater variability in instantaneous feed rate compared to automated gravimetric systems, it nonetheless allows systematic investigation of screw configuration, barrel temperature, and screw speed effects on reaction outcome, which constitute the primary mechanochemical parameters of interest at the discovery and optimization stage.[58,60]

3.3.1 Effect of Technical Parameters on Mechanochemical Organic Reactions by TSE.
The outcome of mechanochemical reactions conducted by TSE is governed by a multi-dimensional parameter space that encompasses mechanical, thermal, and rheological variables. A systematic understanding of these parameters is essential both for reaction optimization and for the rational translation of chemistries from laboratory ball-milling scale to continuous extrusion.

Screw rotational speed (expressed in revolutions per minute, rpm) is the primary determinant of the shear rate, energy input per unit time, and residence time within the extruder. Higher screw speeds generate greater shear forces and promote more intensive mixing of reactant particles, which can increase reaction rates by increasing the frequency and efficiency of intermolecular contact at solid interfaces. Conversely, increasing screw speed reduces the average residence time of material within the barrel, which may lead to incomplete conversion if the intrinsic kinetics of the reaction aren't sufficiently rapid.

In the seminal study by Crawford and coworkers[61] on the TSE-mediated synthesis of condensation products including the Knoevenagel condensation, imine formation, aldol reaction, and Michael addition, a standard screw speed of 55 rpm was employed as a working condition that balanced efficient mixing with an adequate residence time for complete conversion. The authors observed that effective wetting of one reactant by another, which are the cases where one component is a liquid aldehyde at elevated temperature, was identified as a mechanistic prerequisite for these reactions under solvent-free extrusion conditions.[61]

The relationship between screw speed and conversion is not linear and is strongly reaction dependent. Computational fluid dynamics simulations of reactive extrusion processes have demonstrated that increasing screw speed and inlet flow rate simultaneously reduces the time available for reaction by shortening residence time, while the stagger angle of kneading blocks has the opposite effect, increasing mixing intensity without a proportional reduction in residence time.[62] These findings underscore the importance of treating screw speed as one component of an integrated parameter set rather than in isolation.

TSE allows precise, independent temperature control across distinct barrel zones, providing a level of thermal management unattainable in conventional ball-milling equipment.[63] This capability is particularly valuable for organic synthesis, where thermal activation may be required to overcome kinetic barriers, while excessive temperatures can promote unwanted side reactions or product decomposition.

Crawford and coworkers[61] investigated barrel temperatures ranging from ambient to 160 °C for their condensation reactions, reporting that partial product conversion was observed above 40 °C in certain cases, with full conversion achieved at higher temperatures where reactant melting points were exceeded.[61] The ability to operate above the melting point of one or more reactants is especially significant, as the resulting transient liquid phase dramatically enhances molecular mobility and reactive surface contact, effectively creating a quasi-liquid microenvironment at the solid interface consistent with the eutectic-mediated mechanism proposed for several mechanochemical condensation reactions, that was studied through a thorough Differential Scanning Calorimetry (DSC) analysis and wettability of the molten vanillin to the barbituric acid (Figure 5).

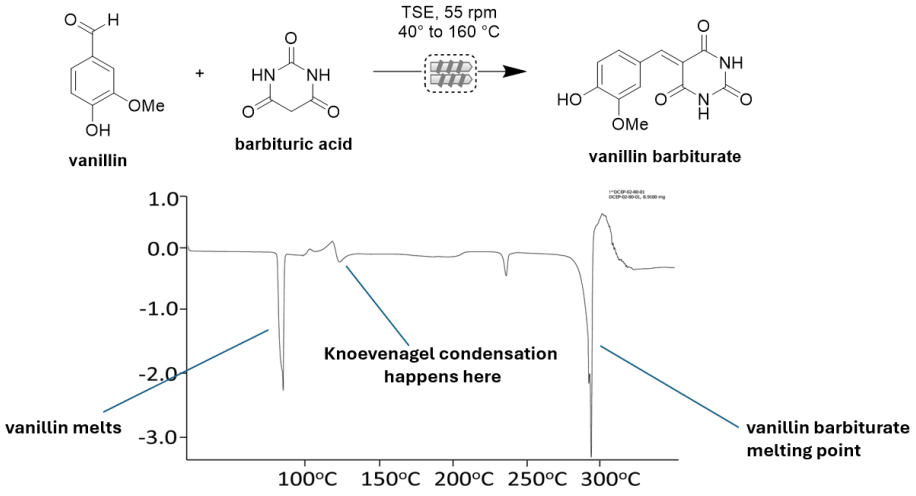


Figure 5. *TSE Knoevenagel condensation of vanillin and barbituric acid and DSC study of the reaction mixture. Readapted from ref. [61].*

The mass feed rate of solid reagents governs the fill level of the extruder barrel, which in turn determines the compressive stress experienced by the material and the effectiveness of screw-to-material energy transfer. An excessively low fill level results in insufficient inter-particle contact and mechanical energy dissipation, while an overfilled

barrel can lead to elevated torque demands, potential screw stalling due to motor blocking, and non-uniform processing. Feed rate also directly controls the space–time yield (STY) of the process, defined as the mass of product obtained per unit reactor volume per unit time (kg/m³h), which represents the primary metric of process efficiency for continuous manufacturing applications.[59,63] Optimization of feed rate thus requires balancing the competing demands of maximum productivity and sufficient dwell time for complete conversion, a trade-off that is intimately coupled to screw speed and barrel temperature.

In co-feeding configurations, where two or more solid reagents are delivered via separate gravimetric feeders, the stoichiometric ratio delivered to the extruder can be continuously varied by adjusting the relative feed rates of each component, providing a powerful handle for compositional optimization without halting the process.

The screw configuration (*e.g.* the specific sequence of conveying, kneading, and reverse-pitch elements assembled along the screw shaft) is arguably the most mechanically sophisticated parameter available to the TSE chemist. Kneading blocks, which consist of disc-shaped lobes staggered at defined offset angles relative to adjacent discs, are primarily responsible for generating the intense shear and dispersive mixing required to activate mechanochemical reactions (Figure 7).

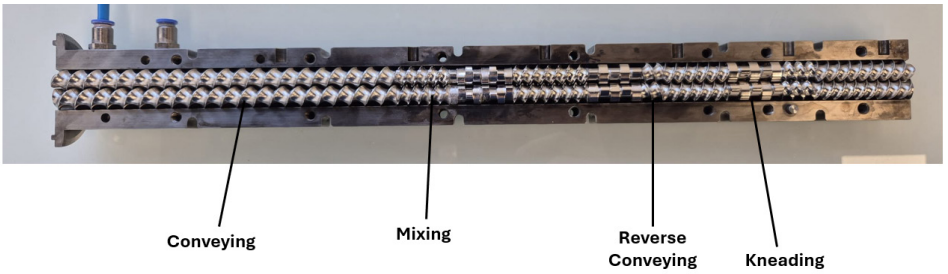


Figure 7. *Corotating twin screws hosted in half extrusion barrel. The picture shows the different modules (kneading, mixing, reverse and conveying) assembled.*

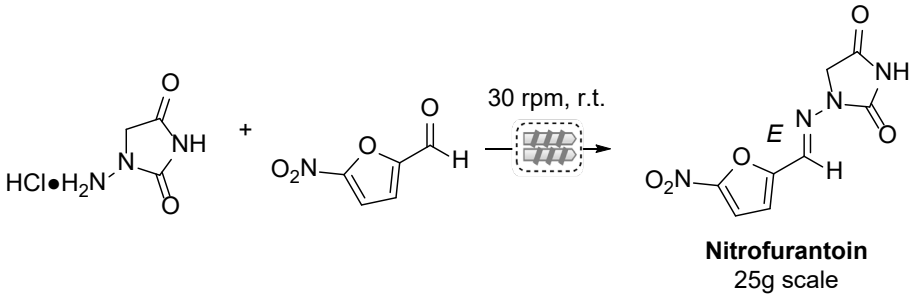
The offset angle of kneading elements has a direct and quantifiable effect on mixing efficiency and residence time: wider stagger angles generate greater shear but reduce axial conveyance, increasing residence time, whereas narrower angles favor forward conveyance at the expense of mixing intensity.[58,62] Reverse-pitch elements act as local barriers to forward flow, substantially increasing the fill level and dwell time in the preceding zone, which can be exploited to extend reaction time for slow-reacting substrates.

3.3.2 TSE as a Flow Mechanochemical Platform

The conceptual reframing of TSE as a "flow" mechanochemical technology, drawing an explicit parallel with the well-established field of continuous-flow solution-phase chemistry, has been a significant intellectual development that has broadened the community of researchers engaging with reactive extrusion. Browne and coworkers,[58] systematically documented the translation of reactions from batch ball-milling to flow-mode reactive extrusion, demonstrating that TSE operates within a continuous-flow paradigm characterized by steady-state operation, in-line analytics capability, and the possibility of telescoped, multi-step synthesis.[58]

Telescoped cascade processes represent one of the most compelling manifestations of the flow mechanochemical concept, wherein two or more sequential reactions are conducted in a single pass through the extruder, with intermediate products formed in upstream barrel zones serving directly as reactants in downstream zones. This approach eliminates isolation and purification steps between stages, dramatically reducing process complexity and waste generation relative to both solution-phase and batch mechanochemical analogues.

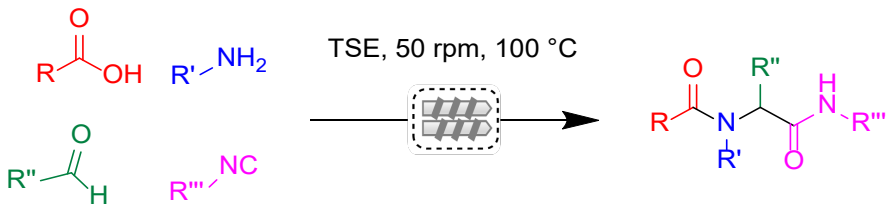
Crawford and co-workers demonstrated the continuous synthesis of nitrofurantoin, an antibiotic used to treat urinary tract infections, by twin-screw extrusion. The reaction involves condensation of 5-nitro-2-furaldehyde with 1-aminohydantoin hydrochloride to form the hydrazone linkage. Nitrofurantoin was obtained without added solvent or base and without workup. Reverse screw elements increased mixing and extended the residence time to approximately 40 min. Operation at room temperature and 30 rpm gave exclusively the E-isomer, with a space–time yield of 6.8×10^3 kg m^{-3} day^{-1} (Scheme 7).[64]



Scheme 7. *Nitrofurantoin synthesis done by TSE.*

The environmental performance of this route was subsequently evaluated by Galant and co-workers using life cycle assessment, alongside green chemistry and cost metrics. Compared with conventional solvent-based batch synthesis, TSE showed lower life cycle energy demand and lower impacts associated with climate change, human health and ecological health.[65]

Twin-screw extrusion has also been applied to the four-component Ugi reaction, which combines an aldehyde, an amine, a carboxylic acid and an isocyanide to form an α-acylaminoamide. Unlike a two-component hydrazone condensation, this transformation couples initial imine formation with subsequent C–C bond formation and acyl transfer, assembling four building blocks in one synthetic operation. El-Remaily and co-workers performed the reaction without added solvent or catalyst on a 200 mmol scale. The optimized model reaction afforded a 93% isolated yield at 100 °C and 50 rpm, with a residence time of approximately 15–20 min (Scheme 8).[66]



Scheme 8. *Multicomponent Ugi reaction, done via TSE on 200 mmol scale.*[66]

Chapter III describes the synthesis of two active pharmaceutical ingredients, that WHO as listed as Essential Medicines: silver(I) sulfadiazine and phenytoin. Silver(I) sulfadiazine had previously been prepared by ball milling[67]. Phenytoin had been synthesized by ball milling[68,69] and by RAM,[51] but never reported so far in a continuous process.

3.4 Approaches to Scale-Up : case studies

Translating mechanochemical reactions from laboratory scale to industrially relevant quantities remain one of the principal challenges facing the field or organic synthesis. In batch mechanochemical technologies such as vibratory and planetary mills, the energy density delivered to reactants is an intricate function of mill geometry, ball size, ball-to-powder mass ratio, oscillation frequency or rotational speed, and vessel fill level, parameters that do not scale linearly with vessel volume. Consequently, incremental scale-up has historically demanded engineered re-optimization at each production stage, often with non-trivial changes in conversion, selectivity, and product morphology. Notwithstanding these difficulties, the pharmaceutical and fine chemical industries represent particularly compelling contexts for scaling mechanochemical organic synthesis, given the twin imperatives of reducing solvent consumption and lowering the overall environmental footprint of agrochemicals and pharmaceuticals manufacture.

3.4.1 Batch Ball-Milling Technologies: Laboratory to Pilot Scale

In the context of ball milling-based technologies, a systematic study of the scalability of pharmaceutical co-crystal formation in batch was conducted by Felderhoff and coworkers, using the model system *rac*-ibuprofen:nicotinamide (*rac*-IBU:NIC).[70] The study benchmarked vibratory mills at gram scale, planetary mills at scales from approximately 2 g to a few hundred grams, and an industrial-scale Eccentric Vibrating Mill (EVM) at kilogram scale (Figure 8). It was demonstrated that complete co-crystal conversion, verified by powder X-ray diffraction (PXRD) and differential scanning calorimetry (DSC), could be achieved across all scales under LAG conditions, with the DSC profile providing a diagnostic two-endotherm fingerprint that unambiguously distinguished co-crystal from precursor material. Milling time, LAG solvent identity and volume, and ball-to-powder mass ratio were identified as the critical parameters governing conversion across scales and required careful re-optimization when transitioning from planetary to EVM operation. At kilogram scale, the industrial EVM (Siebtechnik ESM 236-1bs) successfully produced *rac*-IBU:NIC co-crystals in quantitative yield, constituting at the time of publication the first reported kilogram-scale mechanochemical synthesis of a pharmaceutical co-crystal using a batch process.[70]

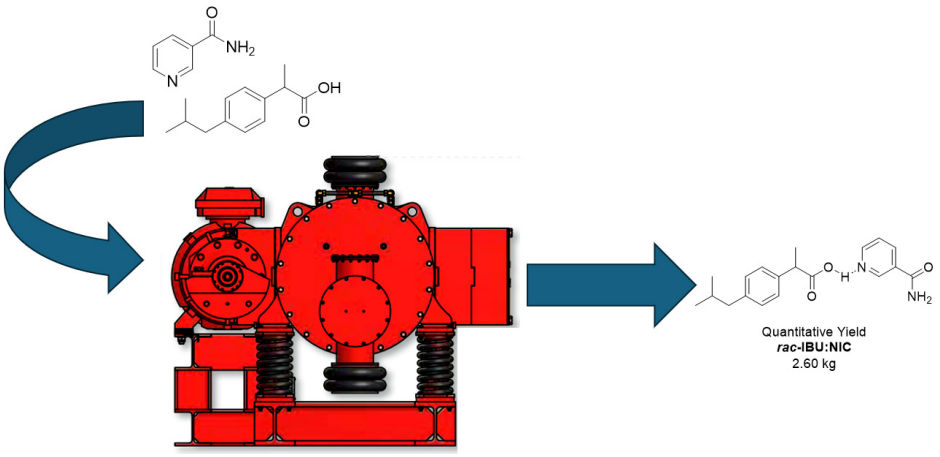


Figure 8. *Co-crystallization on Ibuprofen and Nicotinamide done in EVM, with quantitative yield on 2.60 kg scale.*[70] *EVM reproduced from Siebtechnik webpage (https://www.siebtechnik-tema.com/).*

Building on this foundation, the scope was subsequently expanded to large-scale pharmaceutical co-crystal mechanosynthesis by demonstrating kilogram-scale production using a drum mill,[71] a technology class ubiquitous in the mining and cement industries but previously unexplored for pharmaceutical co-crystallization. Using *rac*-IBU:NIC as the benchmark co-crystal system, a drum mill loaded with steel grinding media and operated under LAG conditions achieved quantitative yield of phase-pure co-crystal within 90 min. The drum mill configuration offers several practical advantages over EVM at large scale: greater volumetric capacity, lower energy consumption per unit mass of product, and simplified product isolation by sieving off the grinding media. Metal contamination analysis confirmed that iron and chromium levels arising from media abrasion were well within ICH guideline thresholds for daily intake, an important regulatory criterion for pharmaceutical manufacturing. Collectively, the *rac*-IBU:NIC case study spanning vibratory mills, planetary mills, EVM, and drum mill technologies provides a comprehensive scale-up trajectory for pharmaceutical co-crystals under mechanochemical conditions.[71]

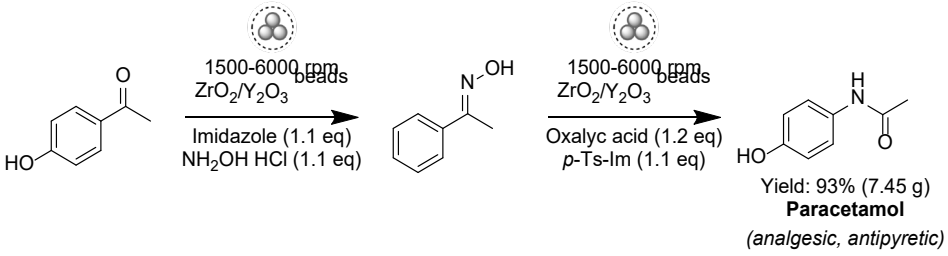
This scale-up trajectory sets the stage for Chapter VI, which turns from a single mill to a comparison among mechanochemical technologies themselves. Using the same *rac*-IBU:NIC system, it benchmarks several high-throughput routes against one another, eccentric vibratory, attritor and hammer milling, alongside continuous hot-melt extrusion, to establish how each performs at production-relevant rates and, in doing so, to demonstrate the scalability of mechanochemistry as a manufacturing technology. Their environmental performance is then placed on a quantitative footing through a cradle-to-gate life cycle assessment, benchmarked against conventional solution crystallization.

3.4.2 Bead Milling Technology: Continuous Processing and API Synthesis

Agitator bead mills (commercially exemplified by the Dyno®-mill, WILLY A. BACHOFEN AG) are stirred-media grinding devices in which a slurry or powder mixture is processed within a cylindrical vessel containing fine grinding beads (typically 0.3–3 mm diameter, composed of ZrO_2, glass, or SS) agitated by a rotating shaft fitted with disc or pin impellers. Unlike planetary and vibratory ball mills, bead mills can be operated in a

continuous pass-through mode, making them conceptually analogous to TSE in terms of process architecture. This continuous capability, combined with high throughput and the commercial availability of systems from laboratory (approximately 0.1 L chamber volume) to manufacturing scale (several hundred liters), positions bead milling as a strategically important bridging technology between laboratory ball-milling and large-scale continuous mechanochemistry for organic synthesis.

The first application of Dyno®-mill bead-milling technology to the mechanochemical synthesis of an active pharmaceutical ingredient was reported by Colacino and Gremaud in the context of the Beckmann rearrangement route to paracetamol[72] (Scheme 9), building on the previously reported ball-milling synthesis.[73] The Beckmann rearrangement, an acid-catalyzed oxime-to-amide isomerization constituting a key industrial step in paracetamol production, had previously required large volumes of polyphosphoric acid or related Brønsted acid media under solution-phase conditions.[74] In the bead-mill approach, mechanical activation substituted for bulk solvent across both the oxime synthesis step and the subsequent rearrangement, conducted sequentially in the Dyno®-mill under solvent-free or LAG conditions. Systematic optimization of bead-mill parameters, principally rotor speed (expressed as a percentage of maximum rpm), bead loading, and reaction time, identified conditions affording an overall isolated yield of paracetamol of 89%. Green metrics assessment demonstrated that the bead-milling route substantially outperformed the solution-based commercial process in terms of E-factor, atom economy, and process mass intensity (PMI), underscoring the environmental benefit of the mechanochemical approach.[72]



Scheme 9. *Beckmann rearrangement performed in a bead mill, for large scale synthesis of Paracetamol.*[72]

The generalizability of bead milling, as a scalable mechanochemical platform for amide bond forming reactions, was later on further demonstrated by Kappe and coworkers in the context of amide bond synthesis, one of the most prevalent and environmentally burdensome transformations in pharmaceutical manufacturing.[12] Conventional amide bond formation relies on hazardous solvents such as DMF and NMP, large excesses of coupling reagents, and added base. The bead-milling approach, employing only catalytic quantities of ethyl acetate as LAG agent, achieved isolated yields of up to 96% across a broad substrate scope without excess reagents or added base. E-factors as low as 1.5 and PMI values as low as 2.5 compared favorably with any existing amide coupling methodology. A 20-fold scale-up experiment, conducted without requiring re-optimization of core bead-mill parameters, delivered productivities of up to 2.89 kg/h, and product isolation required no organic solvents, relying solely on aqueous workup. The authors explicitly positioned bead milling as complementary to TSE within the continuous mechanochemical toolkit: while TSE affords superior temperature

programmability and screw configuration flexibility, bead mills benefit from broader industrial availability and lower equipment specialization requirements, reducing the barrier to adoption in existing pharmaceutical manufacturing infrastructure.[75]

3.4.3 Twin-Screw Extrusion: Continuous Mechanochemistry at Scale

Twin-screw extrusion (TSE) is distinguished from all the aforementioned technologies by its inherently continuous mode of operation, which fundamentally decouples production throughput from batch size. Increasing output requires simply operating the extruder for a longer duration or, for very large scales, employing a geometrically scaled-up machine according to well-established polymer processing engineering principles. Throughput is readily adjustable from grams per hour at laboratory scale to tens or hundreds of kilograms per hour in industrial configurations, without discontinuity of the process or requirement for re-optimization of the underlying process chemistry.[61] TSE provides several adjustable process parameters, including modular screw configuration, barrel temperature, feed rate and screw speed. Together, these parameters control material conveying, mixing and residence time, allowing the process to be adapted to different reaction mixtures. TSE therefore provides a route to continuous mechanochemical synthesis at manufacturing scale.

Transferring a reaction from batch ball milling to TSE requires access to suitable extrusion equipment and expertise in process development. Screw configuration and operating conditions must be selected to provide effective mixing and sufficient residence time while maintaining material transport through the barrel. The suitability of TSE therefore depends on both the reaction requirements and the processing behavior of the mixture. Mechanochemical scale-up consequently involves a complementary range of technologies. Their suitability depends on the required throughput, batch or continuous operation, equipment availability, contamination from milling media and reaction conditions.[58]

Vibratory and planetary ball mills retain their centrality as discovery and screening tools, providing rapid access to gram quantities of mechanochemical products with minimal capital investment. Eccentric vibratory mills and drum mills extend batch processing into the kilogram range and offer a practical route to large-scale pharmaceutical batch mechanochemistry using commercially available equipment.[70] Bead milling adds the option of quasi-continuous or multi-pass processing at high throughput, with proven scalability for both API synthesis (paracetamol via Beckmann rearrangement) and direct amide bond formation at productivities approaching 3 kg/h keeping a competitive sustainability profile.[72,75] RAM provides a media-free batch alternative suited to purity-sensitive substrates and multigram pharmaceutical synthesis where contamination from grinding media cannot be tolerated.[51] TSE stands apart from all these platforms through its combination of true continuous-flow operation, fully programmable process parameters, compatibility with in-line spectroscopic monitoring, and an engineering scale-up framework directly inherited from the polymer processing industry. The rational translation workflow that is increasingly emerging involves reaction discovery by ball milling, kinetic characterization by in situ monitoring, interim scale-up by bead milling or EVM, and ultimate continuous manufacturing by TSE, a staged progression that leverages the comparative strengths of each technology class and minimizes the risk associated with direct laboratory-to-production scale-up.

4. Green Chemistry metrics toolkits for the evaluation of mechanochemical processes

The environmental advantages of mechanochemistry over conventional solvent-based manufacturing, repeatedly invoked in narrative terms throughout the preceding sections, can be substantiated as objective, comparable, and reproducible improvements only through the application of dedicated green chemistry metric toolkits. Such toolkits operationalize the Twelve Principles of Green Chemistry[3] into quantitative or semi-quantitative scores that permit the benchmarking of a mechanochemical protocol against its solution-phase analogue without reliance on qualitative claims.

Four toolkits are particularly relevant to the present thesis and will be employed throughout the experimental chapters that follow; an exhaustive treatment of their underlying methodology, supplemented with case studies on the syntheses of active pharmaceutical ingredients (APIs) and agrochemicals, has been recently contributed by the present author and co-workers as a chapter of the Encyclopedia of Green Chemistry and is reproduced in Annex 4 for reference. A concise overview is provided here:

The CHEM21 toolkit, formulated by Clark and co-workers within the eponymous European consortium,[76] combines quantitative reaction descriptors (yield, atom economy, reaction mass efficiency, process mass intensity) with qualitative flag-based criteria (solvent classification, energy demand, occupational and environmental safety) graded on a green/amber/red scale, and is structured into four progressive assessment passes spanning the spectrum from preliminary discovery screening (zero-pass) to multi-kilogram manufacturing (third-pass). Its didactic clarity and ease of implementation through a freely available spreadsheet template have favored its widespread adoption for the comparative assessment of mechanochemical and benchmark solution protocols.[77]

The innovation Green Aspiration Level (iGAL) methodology, originally introduced as the GAL concept by Roschangar and coworkers[78] and subsequently refined into the iGAL[79] and iGAL 2.0[80] formulations, contextualizes the complete E-factor (cEF) of a given process within the synthetic complexity of the target molecule, the latter being quantified through the number of construction steps and the ideality metric. From these inputs, a Relative Process Greenness (RPG) score is generated that benchmarks the candidate route against an industry-average cEF reference value calibrated to the development phase of the project, thereby producing a sustainability indicator that is intrinsically API-relevant. The methodology is implemented through a web-based scorecard calculator and has been applied to the mechanochemical synthesis of the WHO essential anticancer drug imatinib, in which an RPG of 77% was achieved against 30% for the corresponding solution-based route.[81]

The DOZN Green Chemistry Evaluator, developed at MilliporeSigma,[9] converts the assessment against all twelve principles into a quantitative scoring scheme grouped into three categories (Group1: Improved Resource Use, Group 2: Increased Energy Efficiency, and Group 3: Reduced Human and Environmental Hazard) and condensed into a single normalized aggregate score in which lower values denote superior alignment with the principles. The tool draws upon Globally Harmonized System (GHS) hazard classifications, ensuring a reproducible and data-driven evaluation that has been successfully applied to comparative analyses of batch and continuous mechanochemical syntheses, as exemplified by the multi-platform benchmarking of the synthesis of the WHO essential medicine nitrofurantoin across vibratory ball milling, planetary ball milling, SPEX milling

and twin-screw extrusion for the version 2.0,[82] and, in its more recent DOZN 3.0 implementation, by the assessment, contributed in part by the present author, of the kilogram-scale mechanochemical co-crystallization of the *rac*-IBU:NIC pharmaceutical solid form across eccentric vibrating, attritor and hammer milling and hot-melt extrusion, benchmarked against the conventional ethanol-based crystallization route (Chapter VI).

The EcoScale, formulated by Van Aken, Strekowski and Patiny in 2006,[83] was the first widely adopted semi-quantitative tool for the assessment of reaction sustainability and remains a useful entry-level metric. From an ideal score of 100, penalty points are deducted according to six criteria (yield, price/availability of reagents, safety, technical set-up, temperature/time, and work-up/purification), the residual value offering an immediately interpretable indication of overall process quality. Owing to the structural simplicity of mechanochemical set-ups and the frequent absence of post-reaction work-up, the EcoScale tends to score mechanochemical protocols particularly favorably, as illustrated by the recent comparative assessments of the Beckmann rearrangement route to paracetamol implemented across vibratory milling,[73] planetary milling and twin-screw extrusion,[84] and agitator-bead milling.[72]

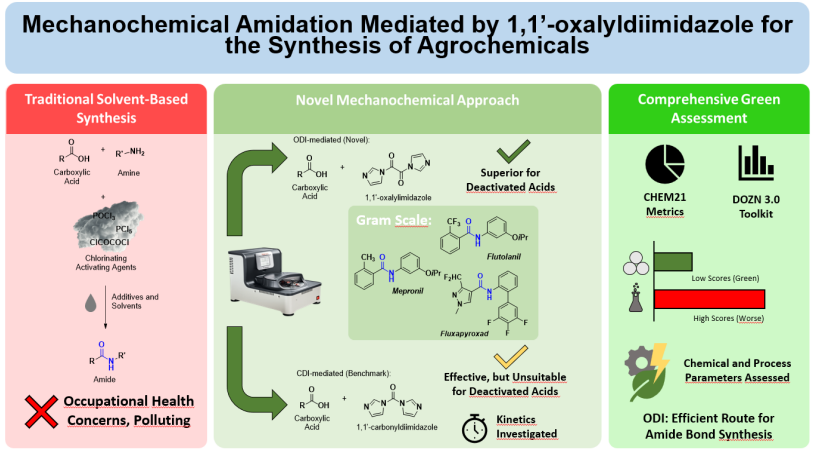
The combined use of these four toolkits, applied wherever appropriate to the protocols developed in the present thesis, provides the quantitative measure against which the green-chemistry credentials of each mechanochemical transformation will be assessed and compared with the corresponding solution-based counterparts.

Introduction Chapitre I

La mécanochimie constitue un outil précieux pour la synthèse organique. Elle permet aux réactions de se dérouler avec peu ou pas de solvant et réduit ainsi les déchets à la source. Son potentiel est particulièrement pertinent pour le secteur agrochimique, où la demande ne cesse d'augmenter, tandis que la pression pour produire de manière plus propre s'accroît en parallèle. De nombreux fongicides commercialisés comportent une liaison amide, dont la formation nécessite l'activation d'un acide carboxylique. L'agent d'activation est souvent la principale source de danger et de déchets stœchiométriques dans la synthèse. Le développement d'une amidation sûre, efficace et sans solvant constitue donc une étape importante vers une production plus respectueuse de l'environnement de ces composés.

Les objectifs spécifiques de ce chapitre étaient les suivants :

- Développer une amidation mécanochimique sans solvant pour la synthèse à l'échelle du gramme des fongicides commercialisés Mepronil, Flutolanil et Fluxapyroxad, en utilisant le 1,1'-carbonyldiimidazole (CDI) comme agent d'activation sûr ;
- Introduire le 1,1'-oxalyldiimidazole (ODI) comme alternative plus réactive au CDI, capable d'activer les acides fluorés peu réactifs que le CDI convertit difficilement ;
- Comparer les réactions réalisées avec le CDI et l'ODI dans des broyeurs à billes vibrants et planétaires, et identifier les paramètres chimiques, techniques et opératoires qui déterminent le rendement ;
- Suivre la cinétique réactionnelle aux premiers stades par des mesures de température et de pression en temps réel, afin de préciser le rôle de l'activation mécanique ;
- Concevoir une procédure de récupération permettant d'isoler les produits sans solvant organique ;
- Comparer les performances environnementales des voies mécanochimiques à celles des procédés correspondants en solution, à l'aide des outils CHEM21 et DOZN™ 3.0.



I - Motivation and aims of the present work

Mechanochemistry is a valuable tool for organic synthesis. It allows reactions to proceed with little or no bulk solvent and so reduces waste at the source. Its potential is especially relevant to the agrochemical sector, where demand keeps rising and the pressure to manufacture more cleanly grows in parallel. Many marketed fungicides are built around an amide bond and forming that bond requires the activation of a carboxylic acid. The activating agent is often the main source of hazard and stoichiometric waste in the synthesis. Developing a safe, efficient and solvent-free amidation is therefore an important step towards a greener production of these compounds.

The specific aims of this chapter were:

- to develop a solvent-free mechanochemical amidation for the gram-scale synthesis of the marketed fungicides Mepronil, Flutolanil and Fluxapyroxad, using 1,1'-carbonyldiimidazole (CDI) as a safe activating agent;
- to introduce 1,1'-oxalyldiimidazole (ODI) as a more reactive alternative to CDI, able to activate the deactivated, fluorinated acids that CDI converts poorly;
- to compare the CDI- and ODI-mediated reactions across vibrating and planetary ball mills, and to identify the chemical, technical and process parameters that govern the yield;
- to follow the early-stage reaction kinetics through real-time temperature and pressure measurements, to clarify the role of mechanical activation;
- to design a downstream recovery that isolates the products without organic solvents;
- to benchmark the greenness of the mechanochemical routes against the corresponding solution-based processes, using the CHEM21 and DOZN™ 3.0 toolkits.

Chapter I — Mechanochemical amidation mediated by 1,1′-oxalyldiimidazole for the synthesis of agrochemicals

1. Context

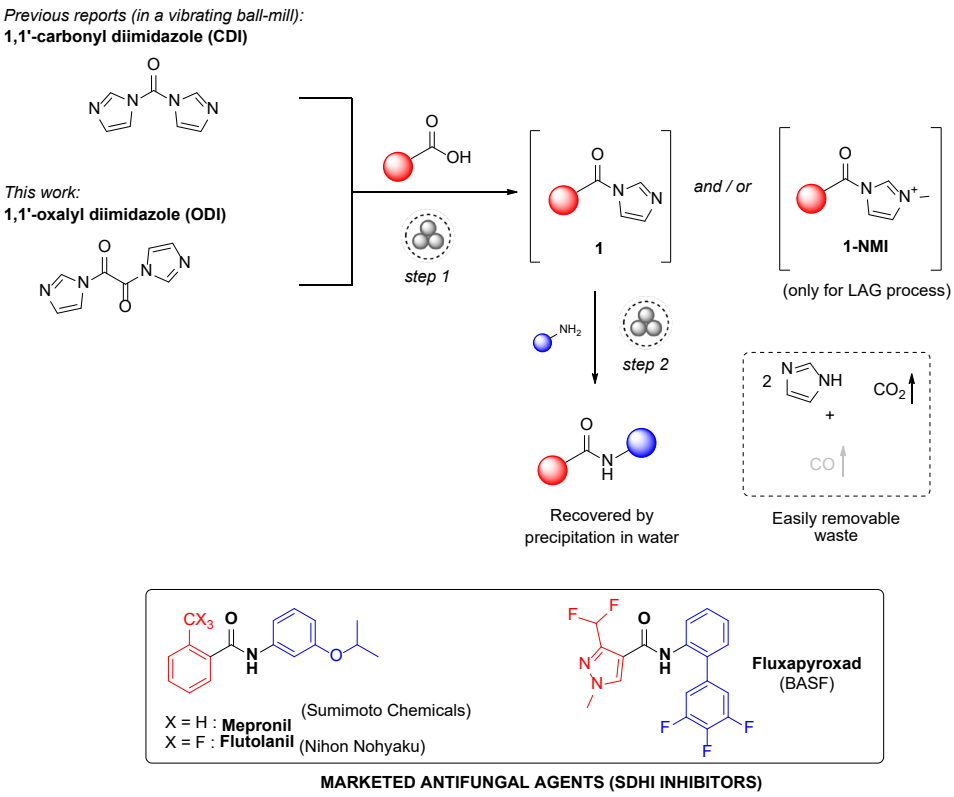
The amide bond is one of the most frequently formed linkages in the chemical industry, and it is central to many crop-protection agents.[85] As shown in the Introduction, mechanochemistry can build these molecules with far less solvent and waste than solution-phase routes. The challenge is to make such routes general, productive at scale, and demonstrably greener than the established processes they would replace.

Amide formation still depends on activating the carboxylic acid. Many of the reagents used for this purpose raise safety or sustainability concerns. Chlorinating agents such as $SOCl_2$, PCl_5 and $POCl_3$ are moisture-sensitive and release corrosive by-products. The widely used uronium and phosphonium coupling reagents (HATU, HBTU, PyBOP, PyBrOP) are efficient but generate large amounts of stoichiometric waste, which lowers atom economy and complicates purification.[86]

A cleaner option is 1,1′-carbonyldiimidazole (CDI). It is an affordable, bench-stable acyl-transfer reagent, and its only by-products are imidazole and carbon dioxide, both easily removed.[87] CDI has already been used mechanochemically to prepare amides,[88] ureas and carbamates.[89] It has one important limitation: it becomes inefficient with poorly nucleophilic, electron-poor acids, which fail to form the activated *N*-acyl imidazole intermediate **1**. This is exactly the situation met with fluorinated agrochemical building blocks.

To overcome this, we examined 1,1′-oxalyldiimidazole (ODI), a more reactive analogue of CDI.[90] ODI activates the same acids through the same intermediate **1** (see Scheme 10), but it is better suited to acids with unfavorable electronic properties. To the best of our knowledge, ODI had not previously been used to form amides, either in solution or by milling.

This chapter applies both reagents to the gram-scale, solvent-free synthesis of three marketed fungicides: Mepronil **9** (Sumitomo), Flutolanil **10** (Nihon Nohyaku) and Fluxapyroxad **11** (BASF), the last a high-value succinate-dehydrogenase-inhibitor with a global market estimated near 4 billion USD.[91] For each target, the key step is an amidation (Scheme 1). The work compares CDI- and ODI-mediated milling across vibrating and planetary ball mills, follows the early reaction kinetics, designs a solvent-free product recovery, and benchmarks the greenness of every route against the corresponding solution-based process using the CHEM21 and DOZN™ 3.0 toolkits.



Scheme 10. *Activating agents CDI and ODI, the shared N-acyl imidazole intermediate* ***1*** *(and the N-acyl methylimidazolium species* ***1-NMI*** *formed under LAG), and the three marketed agrochemicals prepared by amidation.*

2. CDI-mediated amidation in vibrating ball mills

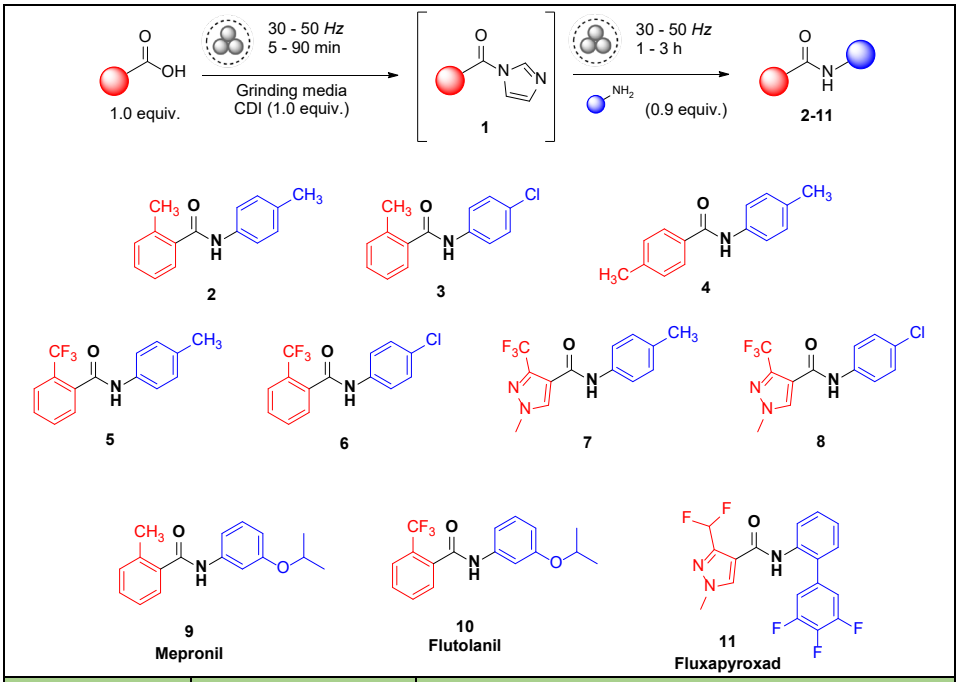
We first mapped the CDI route on a small library of anilides **2–11** in horizontal and vertical vibrating ball mills, using the one-pot, two-step sequence of Scheme 1: the acid is milled with CDI to give intermediate **1** (*step 1*), then the amine is added and milling continued (*step 2*). This scope let us separate the effects of the acid and of the amine, and it framed the more difficult preparation of the agrochemicals **9–11** (Table 1).

Two general trends emerged. First, steric hindrance was not a problem. With the same amine and the same milling conditions, the *ortho*-substituted acid gave a slightly higher yield than its *para*-isomer (98% for **2** *vs* 90% for **4**), the opposite of what is usually seen in solution.[92] Second, electronic effects dominated. Acids bearing fluorinated substituents consistently gave lower yields, because conversion to intermediate **1** was incomplete. A poorly nucleophilic amine in step 2 made things worse; the combination of a deactivated acid and a deactivated amine (compound **6**) failed under neat or LAG conditions and reached only 60% in a PTFE/ZrO_2 system at higher frequency.

The milling hardware mattered as much as the substrates. Zirconia grinding media gave the best average yields and were generally preferred over stainless steel. Adding an inorganic base (K_2CO_3, Cs_2CO_3, K_3PO_4) was detrimental in every case and could shut the reaction down. Heating during prolonged milling was also a factor: extending step 1 from 30 to 60 min dropped the yield of **2** to about 65%, consistent with degradation of

intermediate **1**. The same target reached 96% in a PTFE jar with a step-1 time of only 20 min, where frictional heating is reduced.

Table 1. *Reaction scope for CDI-mediated mechanochemical syntheses of amides 2–11 in vibrating ball-mills, in different processing conditions.*[a]



Entry[b]	Compound	Yield (%)		
		ZrO_2[b]	SS[b]	PFTE[c]
1	**2**	98	94	96
2	**3**	84	60	87
3	**4**	90	n.p.[d]	n.p.[d]
4	**5**	82	73	70
5	**6**	0	0	60
6	**7**	91	94	63
7	**8**	85	67	71
8	**9**	66	70	61
9	**10**	50	7	32
10	**11**	0	0	n.p.[d]

[a] Typical experimental procedure: the acid (1.0 equiv.) and the 1,1'-carbonyldiimidazole (CDI, 1.0 equiv.) were milled at a given frequency (30 or 50 *Hz*), during 5 –90 min. (*step1*). The amine (0.9 equiv.) was added, and the mixture was milled further for 1–3 h (*step2*). The reaction scale was 1.35 mmol, except when otherwise specified (c.f., the detailed mechanochemical process conditions are reported in the adjoined SI of the related publication, TableS2). [b] Horizontal vibrating ball-mill at 30*Hz* was used. [c] Vertical vibrating mill at 50*Hz* was used. [d] n.p. = not performed.

One result is worth singling out. Compound **8** combined a deactivated acid with a deactivated amine, yet still formed in good yield (77–85%). The *N*-methylpyrazole ring

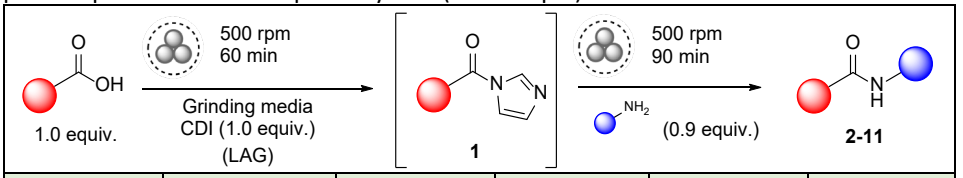
appears to offset, by induction, the strong electron-withdrawing effect of the trifluoromethyl group.

For the marketed targets, the vibrating-mill CDI route lacked generality. Each substrate needed its own conditions, and the fluorinated agrochemicals were poorly served: Mepronil **9** reached 70%, Flutolanil **10** only 50%, and Fluxapyroxad **11** did not form at all. Mepronil performed best, helped by the favorable electronics of *o*-toluic acid and by the fact that both the amine and intermediate **1** were liquids, which improved mixing.

2.1 Gram-scale synthesis and the role of milling energy

To raise productivity, the agrochemicals **9–11** were moved to a planetary ball mill (Fritsch's P7 Premium, here "P7P") on a 5.4 mmol scale. For each set of conditions, a published computational tool was used to estimate two energy quantities:[30] the cumulative kinetic energy delivered over the whole run (E_{tot}, in kJ) and the energy of a single ball–powder impact (E_{imp}, in mJ) (Table 2).

Table 2. CDI-mediated mechanochemical syntheses of marketed agrochemicals **9–11** in a PBM (P7P):[a] energetic considerations for selected experiments, as function of the process parameters for step1 and yields (after step 2).



Entry	Compound	Number of ZrO_2 balls / mm Ø	E_{imp} (mJ)	E_{tot} (kJ)	Yield (%)
1	9 Mepronil	25 / 5	11.3	31.1	3
2		50 / 5	11.3	62.8	73
3		648[b] / 3	2.8	149.6	60
4	10 Flutolanil	25 / 5	11.3	31.1	0
5		50 / 5	11.3	62.8	52
6		648[b] / 3	2.8	149.6	37
7	11 Fluxapyroxad	25 / 5	11.3	31.1	3
8		50 / 5	11.3	62.8	6
9		648[b] / 3	2.8	149.6	23[c]

[a] The filling degree was kept constant (ca. 60%) in all the experiments. The reaction scale was: 2.7 mmol (entries 1 and 4) in a 20 mL ZrO_2 jar or 5.4 mmol (entries 2,3, and 5–9) in a 45 mL ZrO_2 jar. Typical procedure in planetary ball-mill at 500 rpm: (*step 1*) acid (1.0 equiv.) and 1,1′-carbonyldiimidazole (1.0 equiv.) for 60m in; (*step 2*) amine (0.9equiv.) for 90 min. (*c.f.*, the detailed mechanochemical process conditions are reported in the adjoined SI of the related publication); [b] Equivalent to a total mass of 57.1 g of balls. [c] N-methylimidazole (NMI) was used in a LAG process (517.6 μL, η = 0.16 μL/mg).

These numbers showed clearly that more energy does not mean more product. For Mepronil **9**, milling with 50 × 5 mm balls (E_{imp} = 11.3 mJ, E_{tot} = 62.8 kJ) gave 73%. Using many small 3 mm balls raised the total energy 2.4-fold (149.6 kJ) but cut the per-impact energy to 2.8 mJ, and the yield fell to 60%. Halving the ball mass (25 × 5 mm, E_{tot} = 31.1

kJ) collapsed the yield to 3%. The yield therefore depends on the balance of impact energy and impact frequency, not on the total energy alone, and milling parameters have to be tuned for each system.

Fluxapyroxad **11** was the hardest case. Both its acid and its amine carry several fluorine atoms, so neat milling gave no product. An acceptable 23% was obtained only by adding *N*-methylimidazole (NMI) as a LAG additive (η = 0.16 μL/mg) in *step 1*. NMI plays several roles at once: it acts as the LAG liquid, as a base that forms a more reactive carboxylate, and as a competitor to imidazole, producing the more activated *N*-acyl methylimidazolium species **1-NMI**.[93] When K_2CO_3 was used instead of NMI, the reaction failed, which confirms that NMI itself is decisive here.

2.2 *Step I* reaction kinetics

The first step was followed in real time through internal temperature and pressure, using CO_2 release as a marker for the formation of intermediate **1**.[94] Control runs on CDI alone showed negligible decomposition, so the measured CO_2 could be assigned to the reaction. The profiles were sigmoidal, and their rates depended on the acid, decreasing in the order Fluxapyroxad **11** > Flutolanil **10** > Mepronil **9**.

A statistical model based on critical loading conditions reproduced the early-stage data and returned three parameters: the interface-generation rate *r*, the reaction probability (Π), and the fraction of powder activated per unit time (*k*). The interface-generation rate *r* was almost the same for all three substrates, while *k* and Π followed the same order as the rates. In short, fresh contact between the solid reactants is created at a similar pace in every case; once that contact exists, the local chemistry decides the outcome. The kinetic analysis also showed that mechanical activation drives only the earliest part of the reaction, after which the chemistry takes over. A full treatment of the model is given in the SI of the appended paper.

3. ODI-mediated amidation

Because CDI struggled with the deactivated acids, we turned to the more reactive ODI for the gram-scale synthesis of **9–11**. ODI and CDI are both imidazole-based and form the same intermediate **1**, but they differ in reactivity, selectivity and stability.

Using ODI means accepting the release of carbon monoxide during activation. In this set-up the gas is generated inside a sealed milling jar, so it stays in the reactor and can be handled with standard laboratory controls; jars fitted with gas valves allow it to be vented or collected. CO is, in any case, used industrially, for example in a well-known green ibuprofen process.[95] Solid ODI is also safer to handle than the liquid oxalyl chloride used for similar activations in solution: it has lower acute toxicity and no inhalation hazard, and neither reagent is currently restricted under ECHA REACH. CO evolution is therefore better seen as a process variable to manage by reactor design than as a reason to set the method aside.

3.1 Vibrating ball mills

In the vibrating mill, the ODI route followed the same overall trend as CDI: yields fell when deactivated acids were used (Figure 9). There were two notable differences. For the simple *o*-toluic substrates **2** and **3**, CDI unexpectedly out-performed ODI. After step 1 the CDI mixture was a dense paste while the ODI mixture was a clear liquid, and impact energy is transmitted less efficiently through a liquid; the lower melting point and partial decomposition of ODI likely contribute as well. The second difference concerned the LAG

additive: adding NMI was beneficial for CDI but detrimental for ODI, halving or switching off most reactions.

The picture reversed for the marketed fungicides. In the vibrating mill, ODI gave higher yields than CDI: 90% versus 66% for Mepronil **9**, and 84% versus 50% for Flutolanil **10** in stainless steel. Fluxapyroxad **11** did not form with either reagent.

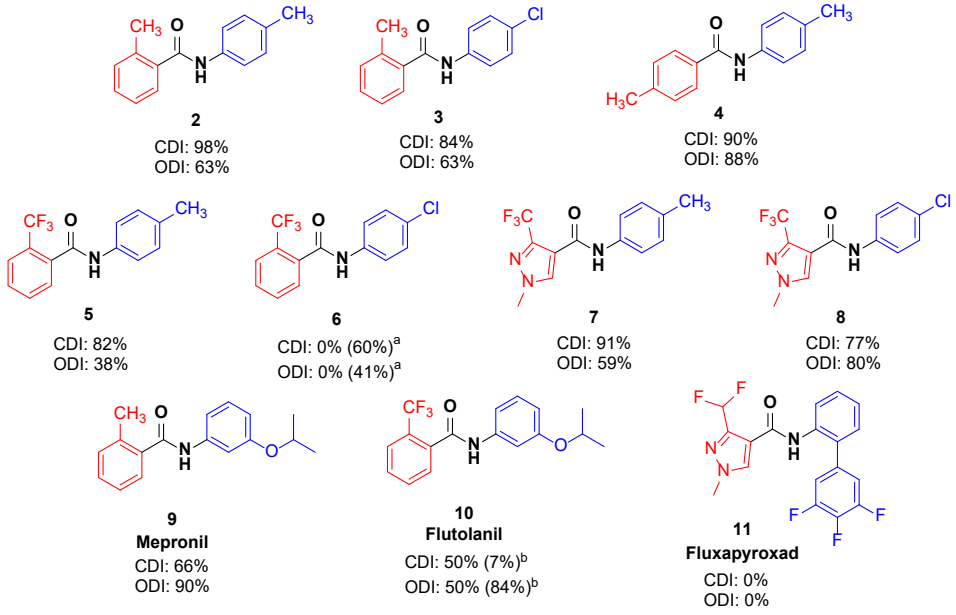


Figure 9. *Reaction scope for the ODI-mediated mechanochemical syntheses of amides 2–11 in a horizontal vibrating ball-mill (c.f., the reaction scale was 1.35 mmol; the detailed mechanochemical process conditions are reported in the SI of the appended article). The comparative results for the CDI-mediated amidation reaction in ZrO_2 grinding media (Table 1) are also indicated. Data in parenthesis refer to the reaction performed at 50 Hz for CDI and 30 Hz for ODI, with grinding media: (a) PTFE/ZrO2 or (b) stainless steel (SS). (c.f., the detailed mechanochemical process conditions are reported in the SI of the appended article).*

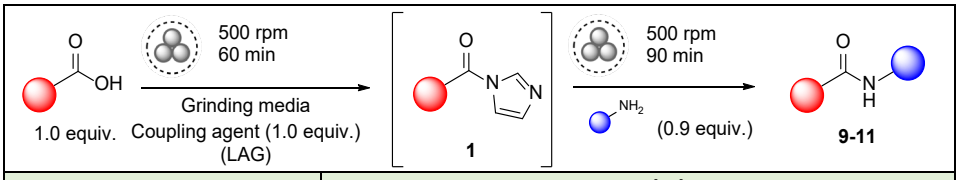
3.2 Gram-scale synthesis: the planetary mill and the device effect

The agrochemicals **9–11** were then prepared in two planetary mills, designated P6 and P7P, so that CDI and ODI could be compared under identical chemical and process conditions (Table 3). Across both devices, ODI out-performed CDI. The gains were largest in the P6 mill, where the yield of Mepronil **9** rose from 16% (CDI) to 93% (ODI).

The two mills are not equivalent. They differ in the geometry that governs how energy is delivered: the P7P reaches a higher acceleration (19.65 G) than the P6 (17.12 G) at the same disc speed. This explains a clear division of labor. The less reactive CDI needed the higher acceleration of the P7P. The more reactive ODI was better matched to the gentler P6, where its stronger driving force (helped by the extra CO it releases on activation) does not require as much energy, and where the more reactive intermediate is less likely to degrade. In the P6 runs we also used smaller 3 mm balls, which give frequent but lower-energy impacts, again protecting the reactive species. The two reagents are equally stable at room temperature over 24 h (measured with ATR-FTIR), so the difference is one of behavior under mechanical stress rather than shelf stability.

Fluxapyroxad **11** was the exception that needed everything at once. Its fluorinated acid and perfluorinated amine, both solids, required the higher acceleration of the P7P and LAG conditions. With NMI at η = 0.16 μL/mg, ODI in the P7P reached 66%, against 23% for the best CDI route. Neat milling gave no product in any mill, and raising the LAG amount to η = 0.4 μL/mg switched off all three reactions.

Table 3. *CDI- versus ODI-mediated yields for* ***9–11*** *in the P6 and P7P planetary mills.*[a]



		Yield (%)			
		CDI[b]		ODI[b]	
Entry	**Compound**	**P6**	**P7P[c]**	**P6[d]**	**P7P**
1	**Mepronil (9)**	16	73	**93**[e]	83
2	**Flutolanil (10)**	21	52	**64**[f]	55
3	**Fluxapyroxad (11)**	1[g]	23[g]	53[f,g]	**66**[d,g]

[a] Reaction scale was 5.4 mmol. Typical procedure in planetary ball-mill at 500 rpm, using 45 mL ZrO_2 milling jar, (*step 1*) acid (1.0 equiv.) and acylating agent (CDI or ODI, 1.0 equiv.); (*step 2*) amine (0.9 equiv.) for the specified times (c.f., the detailed mechanochemical process conditions are reported in the SI of the adjoined article); [b] 50 ZrO_2 balls (5 mm Ø, total weight: 19.2 g) were used except when otherwise specified; for *step 1*: 60 min, for *step 2*: 90 min; [c] Data reported already in Table 2, entries 2, 5 and 9; [d] 57.1 g of 3 mm Ø balls were used; [e] the reaction time was: for *step 1* - 75 min, for *step 2* - 90 min.; [f] The reaction time was 90 min (for both steps); [g] *N*-methylimidazole (NMI, 1.1 equiv.) was used in a LAG process (η = 0.16 μL/mg).

4. Solvent-free product recovery

The work-up usually undermines the green credentials of a mechanochemical reaction, so it was designed to avoid organic solvents entirely. For both the CDI and ODI routes, every target **2–11** was recovered by simple precipitation in water followed by filtration (Figure 10). The only by-products are gaseous CO_2 (and CO for ODI) from *step 1*, and the water-soluble imidazole released in *step 2*, which is washed away with the aqueous phase. For Fluxapyroxad **11**, diluted hydrochloric acid was used in place of water to dissolve the residual amine and NMI.

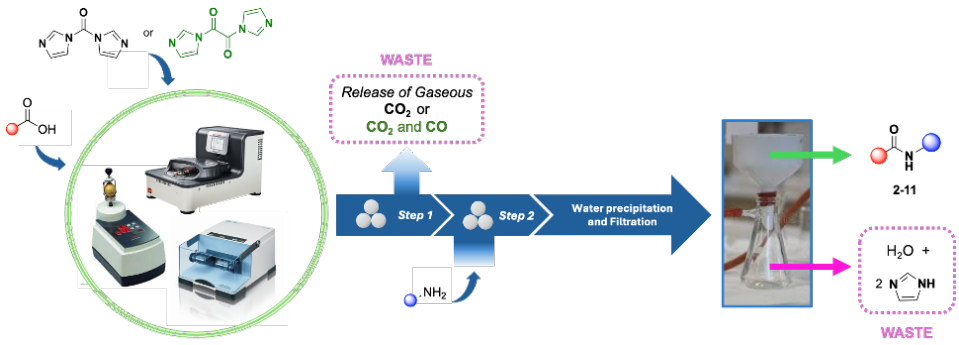


Figure 10. *Solvent-free downstream recovery of the targets by precipitation in water and filtration.*

5. Comparative greenness assessment

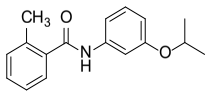
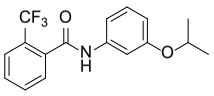
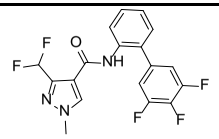
The environmental footprint of each route was quantified with two complementary toolkits, DOZN™ 3.0 and CHEM21, and compared with the most relevant solution-based process for each target.[76,96] The two toolkits gave converging conclusions.

In DOZN™ 3.0 a lower score is greener. For Mepronil **9**, the solution route scored better overall (aggregate 2.95), mainly because the milling work-up consumes water relative to the small amount of product; milling won only on energy efficiency, since it runs at room temperature instead of at 100 °C. For Flutolanil **10** and Fluxapyroxad **11**, both of which involve electron-poor reagents, the milling routes were greener across every group of principles, with aggregate scores 2.4- and 8.6-fold better than the solution processes. The advantage comes from avoiding organic solvents, from generating only water-soluble imidazole instead of HCl, and from a water-based recovery that replaces chromatography.

CHEM21 told the same story through mass-based metrics. Atom economy and reaction-mass efficiency alone might favor the solution routes, but process mass intensity (PMI) and *E*-factor, which count the work-up solvents, favor milling for every target except Mepronil. ODI gave the best figures of all. The clearest case is Fluxapyroxad **11**: the laboratory solution route, which relies on column chromatography, reaches a PMI of 742.7 and an *E*-factor of 741.7, more than nineteen times worse than the ODI milling route (PMI 37.8, *E*-factor 36.8). The milling routes also remove problematic solvents and reagents from the process, including DMF (now tightly regulated in the EU), dichloromethane (being phased out in the USA), diethyl ether (a severe fire hazard, flash point −45 °C), and the $PdCl_2$ used in the industrial carbonylation.[97]

One caveat applies. Mass-based metrics capture only part of the picture, and a full judgement of sustainability needs energy-based and life-cycle data measured at a comparable scale.[98] That kind of life-cycle analysis is developed for a different target in Chapter VI.

Table 4. *CHEM21 metrics (AE, RME, OE, PMI, E-factor) for the CDI, ODI and solution routes to* ***9–11****.*

	CDI (PBM) *vs* ODI (PBM) *vs* Solution																
																	
METRICS[a]	(**9**)					(**10**)					(**11**)[b]						
AE	61.4	*vs*	56.4	*vs*	80.8	64.2	*vs*	60.8	*vs*	69.0	67.9	*vs*	64.7	*vs*	62.8	*vs*	82.5
RME	40.5	*vs*	48.7	*vs*	61.8	31.2	*vs*	35.8	*vs*	54.9	14.6	*vs*	40.2	*vs*	50.5	*vs*	30.3
OE[c]	66.0	*vs*	86.3	*vs*	76.5	48.6	*vs*	58.9	*vs*	79.6	21.5	*vs*	62.2	*vs*	80.4	*vs*	36.8
PMI[d]	45.1	*vs*	35.4	*vs*	13.4	52.4	*vs*	43.3	*vs*	55.0	108.9	*vs*	37.8	*vs*	742.7	*vs*	60.4
$PMI_{reaction}$	2.5	*vs*	2.1	*vs*	6.3	3.2	*vs*	2.8	*vs*	50.4	8.0	*vs*	3.0	*vs*	28.7	*vs*	20.9
PMI_{workup}	42.6	*vs*	33.3	*vs*	7.2	49.2	*vs*	40.5	*vs*	4.6	100.9	*vs*	34.9	*vs*	714.0	*vs*	39.6
***E*-factor**	44.1	*vs*	34.4	*vs*	12.4	51.4	*vs*	42.3	*vs*	54.0	107.9	*vs*	36.8	*vs*	741.7	*vs*	59.4
Solvent	No solvent		No solvent		Xylene	No solvent		No solvent		DCM, DMF, THF	NMI (for LAG)		NMI (for LAG)		Et_2O, THF, AcOEt		ACN
Work-up, recovery	Water Precipitation, Filtration		Water Precipitation Filtration		Water washing	Water Precipitation, Filtration		Water Precipitation, Filtration		Crystalliz.	Water Precipitation, Filtration		Water Precipitation Filtration		Water Washing, Column chrom.		Trituration (Et_2O), Filtration
Health & safety																	
Main hazard statements	H360d		H331, H220, H360d, H372		H225, H302, H312, H314, H318, H330, H332, H372, H41	H360d		H331, H220, H360d, H372		H220, H225, H26(H280, H302, H30- H312, H314, H31- H319, H331, H33- H335, H336, H34- H350, H351, H360(H361, H370, H37- H373, H401, H411	H360d		H331, H220, H360d H372		H224, H225, H302, H304, H312, H314, H318, H319, H320, H330, H331, H335, H336, H351, H361, H373, H411		H220, H225, H280, H290, H302, H312, H314, H317, H318, H319, H331, H332, H335, H336, H351, H360D, H372, H400, H410, H412

Legend: Green flag: Preferred; Amber flag: Acceptable with some concerns; Red Flag: Undesirable. [a] Best values for AE, RME and OE is 100%, for PMI is 1 and E-Factor = PMI – 1.[2] When comparing two processes, the one with the lowest PMI will be greenest; [b] For Fluxapyroxad (11) the four columns are referred respectively to: CDI method in PBM, ODI method in PBM, solution-based method at laboratory scale, and industrial process; [c]$OE = \frac{RME}{AE}$ %;[99] [d] Where precise work-up chemical quantities were unavailable, estimates were derived as detailed in the ESI to ensure fair comparison.

6. Conclusion

A solvent-free mechanochemical method for amide-bond formation was developed and applied to a small library of anilides and to three marketed fungicides, Mepronil **9**, Flutolanil **10** and Fluxapyroxad **11**, on a gram scale. CDI is an effective, green activating reagent, but it is not suited to deactivated, fluorinated acids. For those substrates, the more reactive ODI proved to be a practical alternative, and it was used to form amides for the first time. The two reagents were compared systematically across vibrating and planetary ball mills, and the outcome was shown to depend on a careful balance of chemical, technical and process parameters: the choice of reagent, the grinding media, the milling device geometry, and the use of LAG.

Real-time kinetics showed that mechanical activation governs only the early stage of the reaction; once fresh reactant contact is created, the local chemical environment decides the result. A water-based recovery kept the process free of organic solvents from synthesis to isolation. Finally, both green-metrics toolkits agreed that, with the single exception of Mepronil, the milling routes were greener than the established solution processes, and that the ODI route was the greenest of all. These results show that amide synthesis by mechanochemistry is a credible route to industrially relevant molecules, and they set up the broader question, pursued in the following chapters, of how far this advantage extends to other product classes and to a full life-cycle assessment.

Introduction Chapitre II

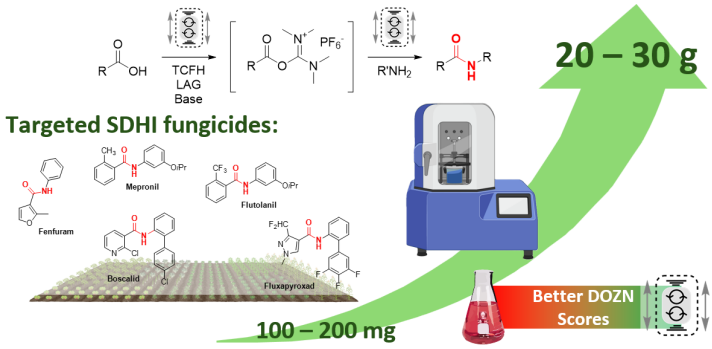
Le chapitre I a développé une amidation mécanochimique sans solvant avec le 1,1'-oxalyldiimidazole (ODI), en particulier pour les acides fluorés peu activés par le 1,1'-carbonyldiimidazole (CDI). La méthode a servi à préparer le Mépronil, le Flutolanil et le Fluxapyroxad à l'échelle du gramme, en broyeurs vibrants et planétaires.

La question suivante est celle de la montée en échelle. En broyage à billes, les billes occupent une partie du réacteur. Changer la taille du réacteur modifie aussi les trajectoires des billes, le mélange et le transfert d'énergie. Les conditions doivent donc souvent être réévaluées. Le *resonant acoustic mixing* (RAM) mélange les réactifs sans billes, ce qui libère plus de volume pour le mélange réactionnel. Un espace libre reste toutefois nécessaire pour le mouvement de la matière, et le remplissage optimal dépend du mélange et de la géométrie du réacteur. Le RAM offre ainsi une autre approche de la montée en échelle, dont les performances restent à évaluer.

Ce chapitre étudie une amidation médiée par le TCFH (hexafluorophosphate de *N,N,N',N'*-tétraméthylchloroformamidinium). Associé au *N*-méthylimidazole (NMI), le TCFH forme in situ un intermédiaire *N*-acyl imidazolium. Celui-ci permet de coupler des acides encombrés avec des amines peu nucléophiles. Les cibles sont cinq fongicides SDHI commercialisés : le Fenfuram, le Boscalid, le Mépronil, le Flutolanil et le Fluxapyroxad. Les trois derniers ayant été préparés au chapitre I, la voie TCFH peut être comparée aux voies CDI et ODI sur les mêmes produits.

Les objectifs spécifiques de ce chapitre étaient les suivants :

- établir l'amidation médiée par le TCFH des cinq fongicides dans des broyeurs à billes vibrants (VBM) et planétaires (PBM), et identifier les paramètres chimiques et opératoires qui déterminent le rendement ;
- transférer le protocole au RAM et déterminer lesquels de ces paramètres restent applicables et lesquels voient leur effet s'inverser avec le changement de mode de mélange ;
- porter la réaction en RAM à l'échelle de plusieurs dizaines de grammes, dans des réacteurs de 2,5 mL à 240 mL, et suivre les phénomènes physiques (rhéologie, échauffement du milieu, agrégation du sous-produit) qui apparaissent lorsque la masse augmente ;
- comparer les performances environnementales des trois technologies (VBM, PBM, RAM) entre elles et avec celles des voies industrielles correspondantes en solution, à l'aide des outils DOZN™ 3.0 et CHEM21.



II - Motivation and aims of the present work

Chapter I developed a solvent-free mechanochemical amidation using 1,1'-oxalyldiimidazole (ODI), with particular emphasis on fluorinated carboxylic acids that were poorly activated by 1,1'-carbonyldiimidazole (CDI). The method was applied to the gram-scale synthesis of Mepronil, Flutolanil and Fluxapyroxad in vibrating and planetary ball mills. These results established a route to the three fungicides and provided a basis for comparing different activating agents and processing technologies.

The next question concerns scale-up. In ball milling, the grinding media occupy part of the vessel volume, limiting the space available for the reaction mixture. Increasing the vessel size can also change ball trajectories, mixing and energy transfer, so operating conditions may need to be reassessed. In contrast, *resonant acoustic mixing* (RAM) can mix the reagents without grinding media, making more of the vessel volume available to the reaction mixture. This does not imply that the vessel is completely filled: sufficient free space must remain for material movement, and the appropriate filling level depends on the mixture and vessel geometry. RAM therefore offers an alternative approach to scale-up, whose performance must be assessed as the reaction loading increases.

This chapter investigates amidation mediated by *N,N,N',N'*-tetramethylchloroformamidinium hexafluorophosphate (TCFH). In combination with *N*-methylimidazole (NMI), TCFH generates an *N*-acyl imidazolium intermediate in situ, enabling the coupling of sterically hindered carboxylic acids with poorly nucleophilic amines. The targets are five marketed succinate dehydrogenase inhibitor (SDHI) fungicides: Fenfuram, Boscalid, Mepronil, Flutolanil and Fluxapyroxad. Mepronil, Flutolanil and Fluxapyroxad were also prepared in Chapter I, allowing the TCFH-mediated route to be compared with the CDI- and ODI-mediated routes for the same products.

The specific aims of this chapter were:

- to establish the TCFH-mediated amidation of the five fungicides in vibrating ball mills (VBM) and planetary ball mills (PBM), and to identify the chemical and process parameters that govern the yield;
- to transfer the protocol to RAM, and to establish which of those parameters carry over and which are inverted by the change of mixing regime;
- to scale the RAM reaction up to multi-decagram quantities, in vessels from 2.5 mL to 240 mL, and to follow the physical phenomena (rheology, heat build-up, by-product aggregation) that appear as the mass increases;
- to benchmark the three technologies (VBM, PBM, RAM) against each other and against the corresponding industrial solution-phase routes, using the DOZN™ 3.0 and CHEM21 toolkits.

Chapter II — Amide bond formation with *N,N,N′,N′*-Tetramethylchloroformamidinium hexafluorophosphate (TCFH): from ball milling to resonant acoustic mixing at the multi-decagram scale.

1. Context

Amide bond formation remains the single most frequently performed reaction in fine chemical manufacturing, and mechanochemical routes to it have been reviewed in detail. Its importance for crop protection was set out in Chapter I: many marketed fungicides carry an amide group, and the activation of the carboxylic acid that precedes it is usually the dirtiest step of the synthesis. The SDHI class is a good test case.[91] It is the fastest growing segment of the fungicide market, it is dominated by amides in which both fragments are aromatic and often electron-poor, and its industrial routes still rely on acyl chlorides.

N,N,N′,N′-Tetramethylchloroformamidinium hexafluorophosphate (TCFH) offers a different way in: combined with *N*-methylimidazole (NMI), it generates an *N*-acyl imidazolium ion in situ, which couples hindered acids with poorly nucleophilic amines under conditions that classical uronium reagents cannot handle.[100] Aav, Kananovich and co-workers showed that the same chemistry works by ball milling, and screened a range of bases for it.[101] The same group later extended TCFH-type reagents to the mechanochemical substitution of alcohols.[102] Under milling conditions, however, the reaction had only been run on a few hundred milligrams at a time.

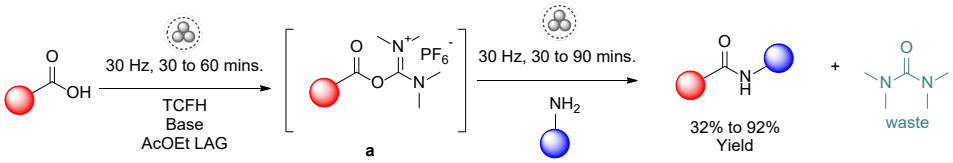
RAM offers a route past that constraint. The reagents are shaken by a vertical acoustic field, typically near 60 Hz, at accelerations of tens of *g*. Mixing is achieved by the resulting convective flow and by micro-mixing within the bulk, with no grinding media required.[49] The technique was first applied to co-crystals and drug formulations,[103] and to porous materials,[104] and more recently to organic synthesis: direct mechanocatalysis,[50] mechanoredox catalysis,[105] sulfonylguanidine synthesis,[106] and the multi-gram preparation of active pharmaceutical ingredients by Knoevenagel, Biginelli and Biltz reactions.[51] Direct comparisons of RAM against ball milling on the same reaction are still rare.[107]

Amide bond formation in RAM has one important precedent, reported while the present work was in progress. Lubell and co-workers used RAM to prepare amino esters, amides and peptides, with the aim of replacing the solvent-heavy protocols of solid-phase peptide synthesis.[108]

Scale is the point on which mechanochemical amidation is usually judged, and two answers to it have been proposed. One is to change the mill. Agitator bead milling has recently been used for amidation under liquid-assisted grinding with only small amounts of ethyl acetate, and delivered a twenty-fold scale-up at industrially relevant productivity.[16] The other is to remove the grinding media altogether, which is what RAM does. The second option has two practical advantages: the vessel can be filled with reagents instead of balls, and the acoustic field is applied in the same way whatever the vessel size, so a larger batch does not require a new set of milling parameters.

This chapter applies that idea to five marketed SDHI fungicides: Fenfuram **1**, Boscalid **2**, Mepronil **3**, Flutolanil **4** and Fluxapyroxad **5** (Scheme 11). Three of them (**3**, **4** and **5**) were also targets in Chapter I, which allows the TCFH route to be placed alongside the

CDI and ODI routes on the same molecules. To the best of our knowledge, this is the first amidation carried out in RAM under solvent-free conditions, the first applied to agrochemical targets, and the first performed at the multi-decagram scale. The reaction was first established in vibrating and planetary ball mills, then transferred to RAM, then scaled 160-fold, and finally assessed against the industrial solution-phase processes.



Scheme 11. T*he structures of the five SDHI fungicides with their originating companies, and the two-step mechanochemical amidation with TCFH, showing the activated intermediate* ***a*** *and the choice of base (K_2HPO_4 with AcOEt as LAG additive, η = 0.2 µL/mg, or neat NMI).*

2. Establishing the reaction in ball mills

The starting point was the milling protocol of Aav and co-workers,[101] with Fenfuram **1** as the model. The reaction is run in one pot but in two steps. The acid, TCFH and the base are milled first, which converts the acid into the activated species **a**. The amine is then added and milling is continued. Adding the amine at the start is counterproductive: it competes with the acid for TCFH and forms by-products that lower the yield.

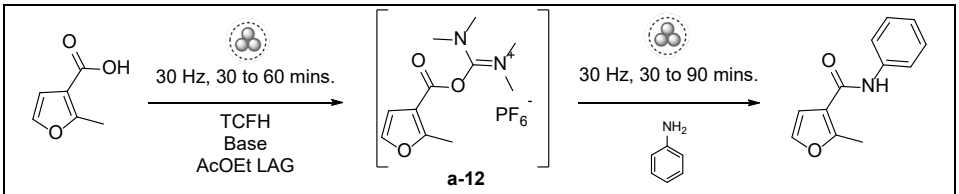
Two bases were retained from the published screening, K_2HPO_4 and NMI. They were chosen for their physical state rather than their strength. K_2HPO_4 is a solid and requires a LAG additive (AcOEt, η = 0.2 μL/mg); NMI is a liquid at room temperature and is used neat. The mixture therefore behaves quite differently in the two cases, which is what determines how force is transmitted from the grinding media to the reagents. The main results are collected in Table 5.

Milling time had the strongest effect, and shorter was better. The best result came from 60 min in step 1 followed by only 30 min in step 2 (78%, entry 3). Extending step 1 to 90 min cut the yield to less than half (31%, entry 2). Intermediate **a** is evidently reactive but fragile, and degrades once the mechanical input passes a certain threshold. Cutting *step 1* to 30 min was also detrimental (48%, entry 4), so the useful window is narrow.

The nature of the base mattered for a physical reason rather than a chemical one. Replacing solid K_2HPO_4 with liquid NMI dropped the yield from 64% to 45% (entries 1 and 5), even though NMI is normally what makes TCFH perform well in solution.[100] With NMI the mixture behaves more like a slurry than a powder, which damps the transfer of energy from the ball to the reagents. Across the whole substrate scope, the only exception was Fluxapyroxad **5**, which required NMI (Figure 11).

The device itself also changed the outcome. The Fritsch P23 uses egg-shaped jars, whereas the horizontal Retsch MM400 uses cylindrical ones. Jar geometry sets the ball trajectory, its time of flight and its angle of impact,[109] and under otherwise identical settings the P23 gave 57% against 64% for the MM400 (entries 1 and 6). Raising the frequency in the P23 from 30 to 50 *Hz* halved the yield again (33%, entry 7). More impacts at the same time means more opportunities to destroy **a**, which is consistent with the effect of milling time.

Table 5. *Selected conditions for the preparation of Fenfuram (**12**) in vibrating (VBM) and planetary (PBM) ball mills.*



Entry	Base	LAG[c] η	Mill	Jar	Ball(s)[d]	Frequency	Time first step	Time second step	Yield
1[a]	K_2HPO_4	0.2	MM400	10 ml ZrO_2	1×10 mm Ø ZrO_2	30 *Hz*	60 min.	60 min.	64%
2[a]	K_2HPO_4	0.2	MM400	10 ml ZrO_2	1×10 mm Ø ZrO_2	30 *Hz*	90 min.	60 min.	31%
3[a]	K_2HPO_4	0.2	MM400	10 ml ZrO_2	1×10 mm Ø ZrO_2	30 *Hz*	**60 min.**	**30 min.**	**78%**
4[a]	K_2HPO_4	0.2	MM400	10 ml ZrO_2	1×10 mm Ø ZrO_2	30 *Hz*	30 min.	30 min.	48%
5[a]	NMI	no	MM400	10 ml ZrO_2	1×10 mm Ø ZrO_2	30 *Hz*	60 min.	60 min.	45%
6[a]	K_2HPO_4	0.2	P23	10 ml ZrO_2	1×10 mm Ø ZrO_2	30 *Hz*	60 min.	60 min.	57%
7[a]	K_2HPO_4	0.2	P23	10 ml ZrO_2	1×10 mm Ø ZrO_2	50 *Hz*	60 min.	60 min.	33%
8[b]	K_2HPO_4	0.2	P7 Premium	45ml ZrO_2	50×7 mm Ø ZrO_2	500 rpm	**60 min.**	**60 min.**	**84%**

[a] Reaction conditions: 1.1 eq of 2-methyl-furanoic acid (0.66 mmol), 1.1 eq of TCFH (0.66 mmol), 0.8 eq of aniline (0.48 mmol), 3 eq of the indicated base (1.8 mmol). [b] Reaction conditions: 1.1 eq of 2-methyl-furanoic acid (2.64 mmol), 1.1 eq of TCFH (2.64 mmol), 0.8 eq of aniline (1.92 mmol), 3 eq of the indicated base (7.2 mmol). [c] LAG was always AcOEt at the η (μL/mg) value indicated. [d] For entries 1-5 a single Retsch's brand 10 mm diameter ZrO_2 ball weighting m = 3.3922 g. For entries 6,7 a single Fritsch's brand 10 mm diameter ZrO_2 ball weighting m = 2.9487 g. For entry 8, 50 Retsch's brand 7 mm diameter ZrO_2 balls were used, each weighting m = 1.0933 g.

Moving to the planetary mill improved matters on both counts. At four times the scale, the P7 Premium gave 84% (entry 8). Fifty small balls distribute the impacts more evenly and mix the powder better than a single large one, so the reagents are less prone to caking on the jar wall or around the ball. The remaining four targets were therefore scaled up in the PBM. The trend held across the scope, with Boscalid **2** as the sole exception (Figure 11), a reminder that the mill is only one of several parameters that decide the result.

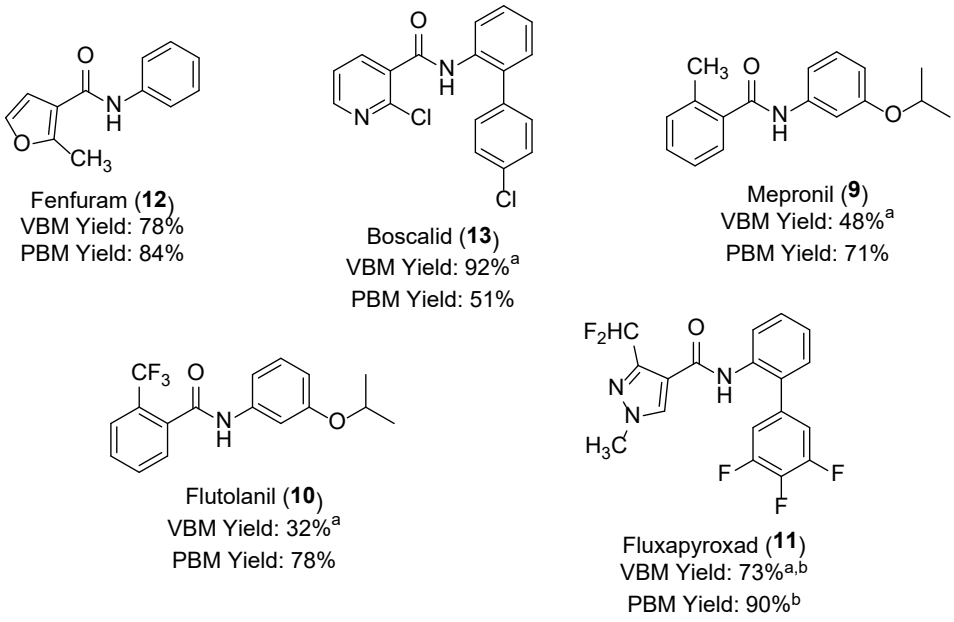
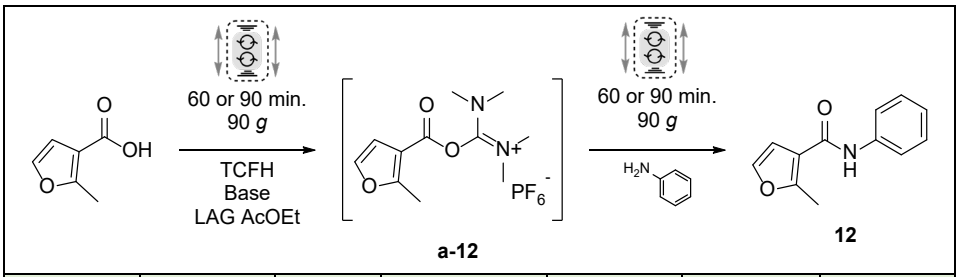


Figure 11. *Main reaction outcomes for the preparation in VBM and PBM of amide containing SDHI inhibitors. Yields are calculated from isolated products, VBM scale is 0.48 mmmol, PBM scale is 1.92 mmol [a] Second step time is 60 minutes. [b] Base used is NMI, no LAG used.*

3. Transfer to the resonant acoustic mixer

The RAM optimization started from the best milling conditions, again using Fenfuram **1** as the model, in 2.5 mL polypropylene (PP) vials at 90 *g* and 60 *Hz* (Table 6).

Table 6. *Selected conditions for the preparation of Fenfuram (**12**) in RAM.*



Entry	Base	LAG η	Ball(s)[b]	Time first step	Time second step	Yield
1[a]	K_2HPO_4	0.2	no	60 min.	60 min.	53%
2[a]	K_2HPO_4	0.2	no	90 min.	60 min.	41%
3[a]	K_2HPO_4	0.2	no	60 min.	90 min.	43%
4[a]	K_2HPO_4	0.2	2.8 g 2 mm Ø ZrO_2	60 min.	60 min.	36%
5[a]	NMI	no	no	60 min.	60 min.	79%
6[a]	**NMI**	**no**	**no**	**60 min.**	**90 min.**	**86%**
7[a]	no	no	no	60 min.	90 min.	7%

[a] Reaction conditions: 1.1 eq of 2-methyl-furanoic acid (0.8 mmol), 1.1 eq of TCFH (0.8 mmol), 0.8 eq of aniline (0.58 mmol), 3 eq of the indicated base (2.18 mmol), reaction performed in a 2.4 mL polypropylene (PP) screw top vial. [b] When indicated (entry 4) the ZrO_2 balls used were Retsch brand.

The most useful result is that the effect of the base is inverted. In RAM, NMI outperformed K_2HPO_4 by a wide margin (79% against 53%, entries 1 and 5), the opposite of what was seen in the ball mill. The two devices reward opposite rheologies. A ball mill needs a mixture solid enough to transmit an impact; RAM has no impact to transmit, and works instead by convective and micro-mixing driven by the acoustic field, which a fluid medium follows far more readily.

The response to time is inverted in the same way. With K_2HPO_4, lengthening either step was detrimental (41% and 43%, entries 2 and 3). With NMI, lengthening step 2 to 90 min raised the yield to 86% (entry 6), the best result obtained. A plausible reading is that the solid mineral base generates friction hotspots between abrading particles,[110] which degrade **a** and make long processing costly. A liquid base gives a homogeneous medium in which those hotspots do not form, so extra time simply improves conversion.

Adding grinding media confirmed the same picture from another direction. ZrO_2 beads have been reported to help co-crystal formation and to homogenize pharmaceutical suspensions in RAM,[103,111] but here 2.8 g of 2 mm beads lowered the yield to 36% (entry

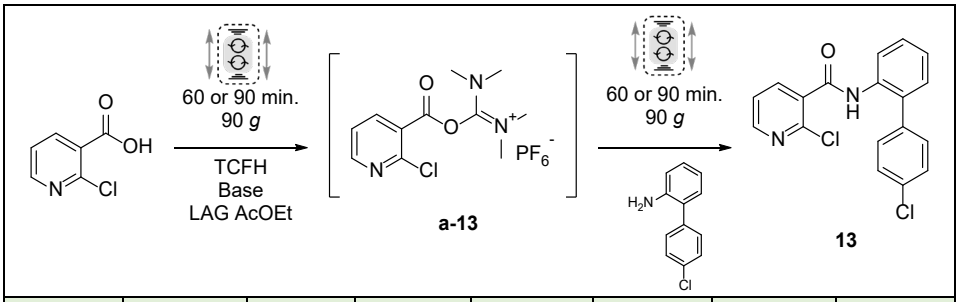
4). Grinding-assisted RAM behaves, in effect, like a vibrating mill locked at 60 *Hz*.[49,51] Even though these beads are small and carry much less momentum than the 10 mm balls used in the ball mill, they deliver impacts at a rate that intermediate **a** does not tolerate, exactly as entry 7 of Table 1 showed. Finally, omitting the base altogether gave only 7% (entry 7), which fixes the baseline for the discussion that follows.

3.1 Boscalid: a different reactivity

Boscalid **13** did not follow the pattern of the other four targets, and was optimized separately (Table 7). Its acid fragment carries a pyridine ring, which appears to change the reaction pathway.

Here K_2HPO_4 gave excellent yields (98%, entry 3) and NMI suppressed the reaction (31%, entry 7). This cannot be blamed on the amine, which is both hindered and deactivated by a chlorine substituent, and which should therefore react worse rather than better. The more likely explanation could be that a different, more electrophilic intermediate is involved. If the pyridine nitrogen of 2-chloronicotinic acid is protonated during activation, the resulting species (**a-13·HX**) would carry a more electron-poor carbonyl than the neutral one (**a-13**), and could couple readily even with a deactivated amine.

Table 7. *Selected conditions for the preparation of Boscalid (**13**) in RAM.*



Entry	Base	Base eq.	LAG η	Ball(s)[b]	Time first step	Time second step	Yield
1[a]	K_2HPO_4	3	0.2	no	60 min.	60 min.	94%
2[a]	K_2HPO_4	3	0.2	no	90 min.	60 min.	50%
3[a]	**K_2HPO_4**	**3**	**0.2**	**no**	**60 min.**	**90 min.**	**98%**
4[a]	K_2HPO_4	3	no	no	60 min.	60 min.	66%
5[a]	K_2HPO_4	3	0.4	no	60 min.	60 min.	93%
6[a]	K_2HPO_4	3	0.2	2.8 g 2 mm Ø ZrO_2	60 min.	60 min.	59%
7[a]	NMI	3	no	no	60 min.	60 min.	31%
8[a]	NMI	2.05	no	no	60 min.	60 min.	42%
9[a]	no	no	0.2	no	60 min.	90 min.	42%

[a] Reaction conditions: 1.1 eq of 2-methyl-furanoic acid (0.8 mmol), 1.1 eq of TCFH (0.8 mmol), 0.8 eq of aniline (0.58 mmol), 3 eq of the indicated base (2.18 mmol), reaction performed in a 2.4 mL polypropylene (PP) screw top vial. [b] When indicated (entry 6) the ZrO_2 balls used were Retsch brand.

Three observations support this. First, NMI is a good enough base to scavenge the pyridinium proton, which would convert **a-13·HX** back into the less reactive **a-13**; the yield then falls into line with what the electronics of the two fragments would predict. Second, halving the NMI loading to 2.05 equivalents, the amount that corresponds to η = 0.2 μL/mg if NMI is counted as the LAG liquid, reduced the inhibition (42%, entry 8). The effect of NMI is therefore stoichiometric, not catalytic. Third, a control run with K_2HPO_4 at η = 0.4 μL/mg was unaffected (93%, entry 5), which rules out the possibility that NMI acts simply by making the mixture too fluid. The effect is chemical.

The base-free experiments point the same way. Without any added base, Boscalid **13** was still isolated in 42% (entry 9), whereas Fenfuram **12** collapsed to 7% under equivalent conditions (Table 6, entry 7). The acid used for **12**, 2-methylfuran-3-carboxylic acid, has no basic site; 2-chloronicotinic acid does, and can partly cover the role of the external base. Taken together these results are consistent with an autocatalytic contribution, running alongside the conventional pathway. They do not prove it, and a dedicated mechanistic study would be needed to do so.

3.2 Comparison of the three technologies

The differences in reaction yield between the three technologies can be discussed in terms of mixing and the mode of mechanical activation (Figure 12). In a vibrating mill with a single ball, powder can adhere to the vessel walls and accumulate around the ball, a phenomenon known as the snowball effect.[112] A planetary mill with fifty balls distributes the material more effectively, whereas RAM mixes the reaction mixture without grinding media. RAM also avoids the ball–particle and ball–wall impacts involved in milling. The improved yields obtained under the optimized RAM conditions are consistent with effective mixing and reduced degradation of intermediate **a**. These contributions cannot, however, be separated on the basis of the yield data alone.

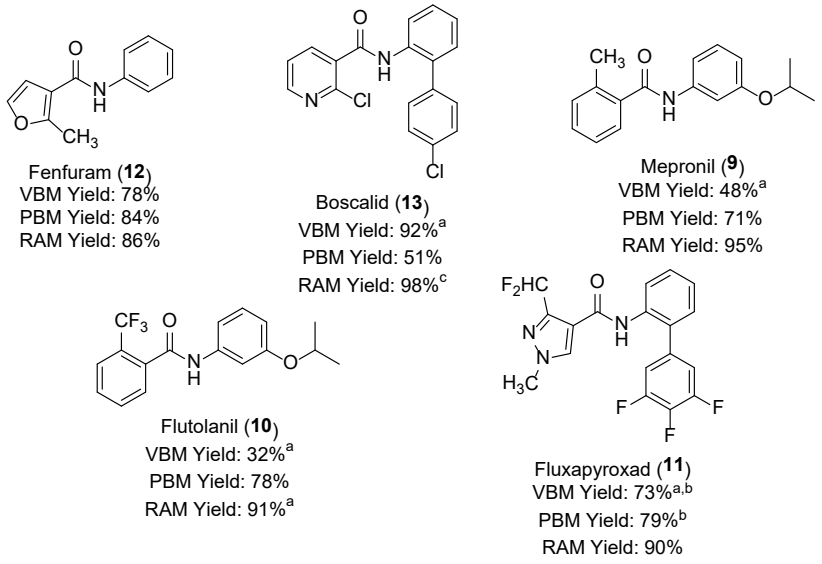


Figure 12. *Main reaction outcomes for the preparation in VBM, PBM and RAM of amide containing SDHI inhibitors. Yields are calculated from isolated products. [a] Second step time is 60 minutes. [b] Base used is NMI, no LAG used. [c] Base used is K_2HPO_4, LAG AcOEt (η = 0.2 µL/mg).*

3.3 TCFH against EDCI/Oxyma in LA-RAM

The EDCI/Oxyma protocol of Lubell and co-workers[108] appeared while this work was in progress. It was the only other LA-RAM amidation available, so the five targets were also prepared under its conditions. The comparison used the closest scales available for the two methods. The EDCI/Oxyma protocol (one step) used 3.34 mmol of acid in a 24 mL glass vessel. The TCFH protocol (two steps) used 8.00 mmol of acid (5.82 mmol of amine) in a 15 mL PTFE vessel. Both were run with 1,2-dimethoxyethane (DME, η = 0.9 µL/mg) at 80 *g* for 40 min. The TCFH runs therefore processed more material in a smaller vessel, which is the more demanding case. TCFH gave the higher yield for all five targets. EDCI/Oxyma gave only moderate to poor yields (22–56%). The gap was smallest for the hardest target, Boscalid **2** (29% against 22%).

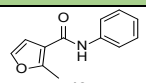
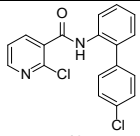
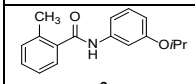
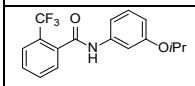
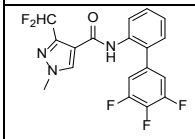
This result follows from what the two systems were designed for. EDCI/Oxyma was developed for peptides. It couples α-amino acid derivatives with fairly nucleophilic aliphatic amines. There, the main problem is to avoid epimerization, not to activate the acid. The targets of this chapter pose the opposite problem. Both partners are aromatic, and the amine is hindered, deactivated, or both. What is needed is a stronger activating agent, able to form a more electrophilic intermediate. TCFH meets that need. It also allows a higher throughput per unit of vessel volume, which matters for scale-up.

4. Scale-up by RAM

The point of moving to RAM was scalability, and this was tested by keeping the optimized protocol unchanged and simply increasing the vessel size. Reactions were run from 0.8 mmol up to 128 mmol of acid, a 160-fold increase. PTFE screw-top jars were used above

2.5 mL, for their chemical and thermal stability. No re-optimization of time, base or acceleration was carried out at any stage. The results are given in Table 8.

Table 8. *Scale-up of the RAM amidation for the five targets.*

Molecule	2.4 mL PP vial		15 mL PFTE jar		30 mL PFTE jar		120 mL PFTE jar		240 mL PFTE jar	
	Scale[a]	Yield	Scale[a]	Yield	Scale[a]	Yield	Scale[a]	Yield	Scale[a]	yield
 **12**	0.58 mmol	86% (100.1 mg)	5.82 mmol	98% (1.1467 g)	11.63 mmol	97% (9.3979 g)	46.55 mmol	100% (9.3679 g)	93.10 mmol	96% (18.0002 g)
 **13**	0.58 mmol	98% (194.7 mg)	5.82 mmol	29% (0.828 g)	11.63 mmol	58% (2.3344 g)	46.55 mmol	88% (14.1374 g)	93.10 mmol	67% (21.4600 g)
 **9**	0.58 mmol	95% (148.2 mg)	5.82 mmol	100% (1.5694 g)	11.63 mmol	100% (3.1424 g)	46.55 mmol	99% (12.4550 g)	93.10 mmol	91% (22.9012 g)
 **10**	0.58 mmol	91% (170.4 mg)	5.82 mmol	96% (1.8067 g)	11.63 mmol	100% (3.7717 g)	46.55 mmol	98% (14.7077 g)	93.10 mmol	96% (28.9370 g)
 **11**	0.58 mmol	90% (199.3 mg)	5.82 mmol	96% (2.1337 g)	11.63 mmol	95% (4.2123 g)	46.55 mmol	100% (17.6682 g)	93.10 mmol	99% (34.9914 g)

[a] Scale refers to the amount of the limiting reagent (the amine). Reaction condition followed the experiments conducted in the lowest scale: for compounds **9-12** the acid (1.1 eq), the TCFH (1.1 eq), NMI (3 eq) are mixed together for 60 minutes, then the jar is opened and the amine (0.8 eq) is added and the reaction mixture is furtherly mixed for 90 minutes; for compound **2** the acid (1.1 eq), the TCFH (1.1 eq), K_2HPO_4 (3 eq) and AcOEt LAG (η = 0.2 μL/mg) are mixed together for 60 minutes, then the jar is opened and the amine (0.8 eq) is added and the reaction mixture is furtherly mixed for 90 minutes.

Reactivity was essentially independent of scale. Four of the five targets stayed above 90% throughout, and the largest runs delivered 18.0 g of **12**, 22.9 g of **9**, 28.9 g of **10** and 35.0 g of **11** in a single batch. To our knowledge these are the largest organic synthesis reactions reported in RAM. The reaction is also robust to the acceleration setting: **12** was obtained quantitatively also at 45 *g*, half the standard value, which is worth noting for energy consumption at production scale.

The exception is again Boscalid **13**, which dropped to 29% in the 15 mL jar. Since this is the only outlier at this scale, the cause is most likely the geometry of that particular vessel. The 15 mL jar is only 34 mm tall, shorter even than the 2.5 mL vial used for the smallest reactions (45 mm). A short vessel limits the vertical travel of the material and hinders the convective loop that RAM relies on, so mixing and energy transfer both suffer. It was worth asking still how the other reported RAM amidation protocol performed with our substrate class as it was originally developed for the synthesis of peptides, so we prepared the five compounds with those conditions.[108] The separation is clear: EDCI/Oxyma gave 22–56% yield, which show a net underperformance of the EDCI as a coupling agent for our class of targets. This follows from what the two systems were built for. EDCI/Oxyma joins α-amino acid derivatives to comparatively nucleophilic

aliphatic amines, where the constraint is suppressing epimerization rather than activating the acid. The targets here pose the opposite problem. Both fragments are aromatic, and the amine is hindered, electronically deactivated, or both, so what is needed is a stronger activating agent, not a milder one.

4.1 Aggregation of the by-product

Part of the reason the yields hold up at scale seems to lie in something visible in the crude mixtures. In the runs with NMI, where the crude is a clear viscous liquid after step 1 and a darker, denser liquid after step 2, white solid spheres of varying diameter formed consistently at the larger scales (Figure 14a). These were isolated, washed with AcOEt and MeOH, and analyzed by ^{1}H NMR. They consist mainly of tetramethyl urea (TMU), the by-product released when TCFH activates the acid (Figure 14b). The minor signals present are most likely from crude adsorbed on the surface or trapped inside the aggregates as they grew.

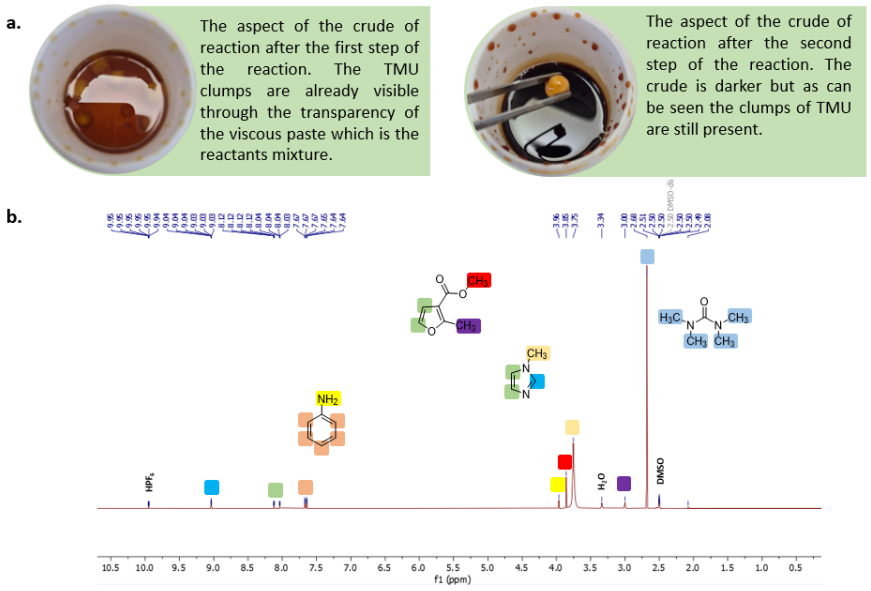


Figure 14. *a) Appearance of the crude after step 1 and step 2; b) ^{1}H NMR spectrum (d_6-DMSO) of an isolated aggregate, with the main signals assigned.*

This aggregation should help the reaction twice over. It removes TMU from the reacting phase, which pushes the equilibrium towards the product. It also creates soft solid domains that circulate through the mixture and improve homogenization, but without the abrasion of ZrO_2 or steel beads, which the results in Tables 6 and 7 show to be harmful here. In effect the system generates its own mixing aid.

4.2 Heat build-up, and the mechanical contribution

Heat is the other thing that changes with scale, since a larger mass dissipates it less efficiently. The behavior depended on the base. With NMI (**9-12**), the temperature reached about 40 °C after step 1, rose sharply to 60–65 °C as soon as the amine was added and mixed in, and reached roughly 90 °C internally by the end of step 2, with the

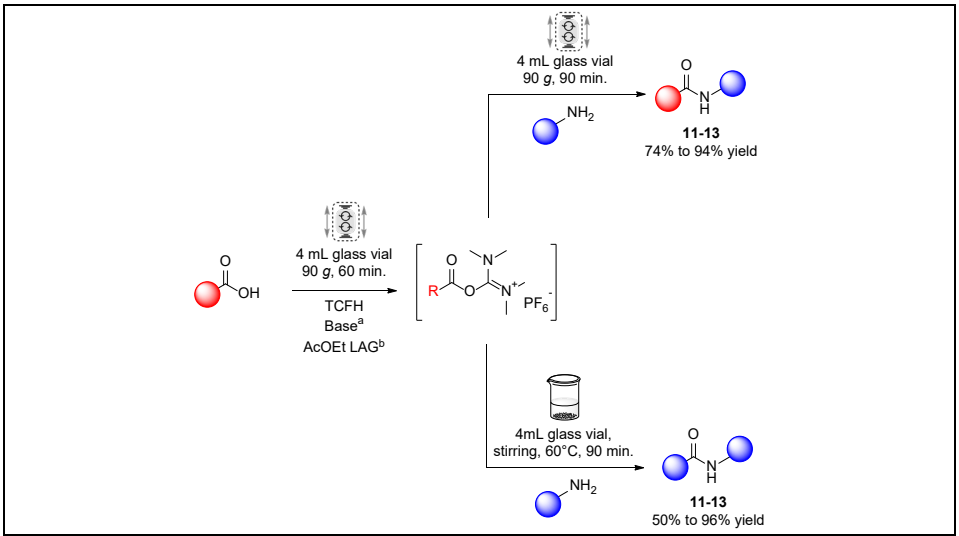
outer wall of the jar at about 65 °C. With K_2HPO_4 (**13**), abrasion between solid particles brought the mixture to 65 °C during step 1, but adding the amine produced no immediate rise, because the paste is too viscous for the solid amine to mix in quickly. After step 2 the wall reached 75 °C, implying 80–90 °C inside.

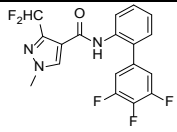
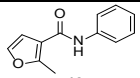
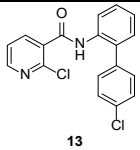
Since the mixture with NMI turns into a homogeneous fluid after step 1, resembling a deep eutectic solvent, it is fair to ask whether RAM is still doing anything mechanical in step 2, or whether it merely stirs a hot liquid. Control experiments were designed to answer this (Table 8). They were run on a small scale in 4 mL glass vials, where RAM produces no significant heating and the internal temperature stays at 30–40 °C, so that thermal and mechanical contributions can be separated. Step 1 was always run in RAM. Step 2 was then run either in RAM, or with conventional magnetic stirring in an oil bath at 60 °C.

The three substrates were chosen to span the range: **12** as the general model, **13** because it uses the solid base, and **11** because it combines a deactivated biphenyl amine like Boscalid (**13**) with the NMI using conditions of Fenfuram (**12**). For **12** the two routes are equivalent (96% and 94%). The crude is already fluid, adding aniline makes it more so, and aniline is a reasonable nucleophile, so heat and stirring suffice. For **13** the difference is large (50% against 74%). The crude is a viscous paste, the amine is a poorly nucleophilic solid, and without mechanical agitation the two do not meet. **11** sits in between (68% against 76%): the medium is fluid, but the amine is deactivated.

The conclusion is that the mechanical contribution of RAM is not decisive for easy systems, and becomes decisive exactly where solution chemistry also struggles, namely when a poor nucleophile has to be mixed into a difficult medium.

Table 8. *Second step under RAM against conventional stirring at 60 °C.*



Entry	Molecule	Yield (stirring)	Yield (RAM)
1[c]	 **11**	68%	76%
2[c]	 **12**	96%	94%
3[c]	 **13**	50%	74%

[a] Reaction conditions: acid (1.1 equiv., 1.5 mmol), TCFH (1.1 equiv., 1.5 mmol), base (3.0 equiv., 4.09 mmol), amine (0.8 equiv., 1.09 mmol) in a 4 mL glass vial. Step 1 was run in RAM at 90 *g* for 60 min in every case; step 2 was run either at 90 *g* for 90 min, or with magnetic stirring at 60 °C for 90 min. [b] AcOEt as LAG additive, η = 0.2 μL/mg.

5. Solid-state characterization

The products from the smallest RAM reactions were characterized by high-resolution synchrotron powder X-ray diffraction at beamline ID31 of the ESRF, and compounds **12**, **13**, **10** and **11** were also studied by microED. For Fenfuram **12** and Mepronil **9** no diffraction data had previously been reported, so these represent the first crystallographic characterization of the two compounds; their phase purity was verified by comparing the patterns against those of the starting materials and of TMU, and no impurity was detected. For Boscalid **13** and Fluxapyroxad **11**, the forms obtained by RAM followed by precipitation in water match the published structures, which had been obtained after column chromatography. For Flutolanil **10**, the pattern also matches the reported data, but the earlier work gave no preparation method for that form, so the present protocol provides a route to it.

6. Comparative greenness assessment

Two toolkits were applied, as in Chapter I: DOZN™ 3.0, which scores a process against the 12 Principles of Green Chemistry and where a lower score is greener,[99,113] and CHEM21, which combines mass-based metrics with a red/amber/green flagging of solvents, reagents and operations.[76] The assessment had two purposes: to compare the three mechanochemical technologies with each other, and to compare the optimized RAM protocol at its largest scale with solution routes that more closely match our protocol from a synthetic strategy point of view (*e.g.* acid activation followed by amine nucleophilic attack) and preferring industrial routes where possible.[114–118]

6.1 Comparing the three technologies

Across the three technologies, the DOZN™ scores improve steadily from VBM to PBM, then to laboratory-scale RAM, and finally to multi-decagram RAM (Figure 15). Two variables drive this. The first is yield, which changes with both scale and device. The second is the quantity of water, aqueous HCl and CaO consumed in the work-up, which is fixed by the internal volume of the vessel rather than by the amount of product.

The step from VBM to PBM is largely a yield effect: the jar is about four times larger and the reaction was scaled by the same factor, so the gain comes from the higher yields rather than from any change in material intensity. The step from ball milling to RAM is larger, and comes from volumetric efficiency. Because RAM needs no grinding media, a much higher ratio of reaction mass to vessel volume is possible, so proportionally less water and acid are needed for the precipitation. Scaling also costs nothing in re-optimization, and larger RAM batches have been reported to reach completion faster and to transfer energy more efficiently.[119]

Boscalid is the exception here too. Its yields are inconsistent across scales (92% in VBM and 98% in small-scale RAM, but 51% in PBM and 67% at large scale), which penalizes the resource-use group, and its work-up requires an extra basic wash.

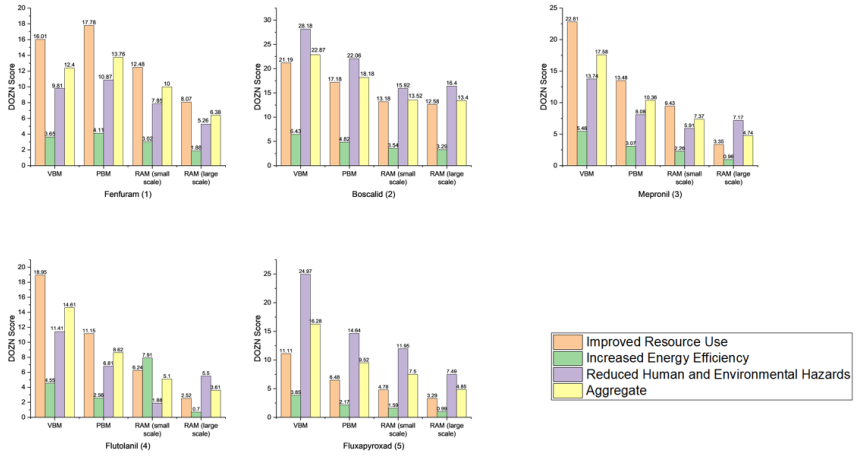


Figure 15. *Comparison of VBM vs PBM vs RAM (0.58 mmol scale, referred as "small scale") vs RAM (93.01 mmol scale, referred as "large scale") protocols for the synthesis of Fenfuram (**12**), Boscalid (**13**), Mepronil (**9**), Flutolanil (**10**), Fluxapyroxad (**11**) by DOZN™ 3.0 Quantitative Scoring tool. Legend: Aggregate score (**orange**), Group 1 (Improved Resource Use – **green**), Group 2 (Increased Energy Efficiency – **violet**), and Group 3 (Reduced Human and Environmental Hazards – **yellow**).*

6.2 Comparing RAM with the solution routes

The comparison against solution chemistry has to be made molecule by molecule, because the industrial routes differ considerably from one another. Each was matched to our protocol by adding, where necessary, the chlorination step required to reach the acyl chloride from the same carboxylic acid we start from, and in each case the mildest published chlorination was chosen so as not to load the comparison in our favor. Figure 16 gives the DOZN™ results and Table 6a and 6b the CHEM21 metrics.

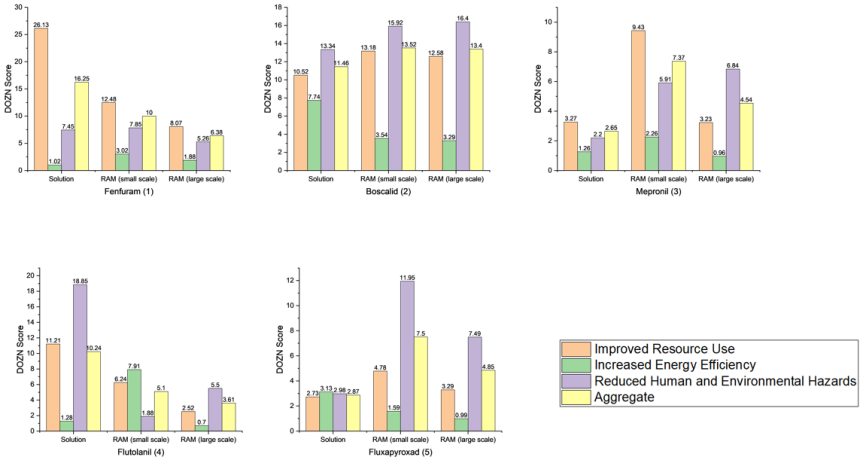
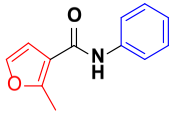
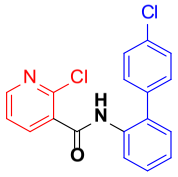
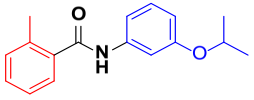


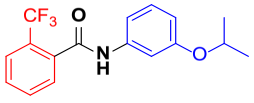
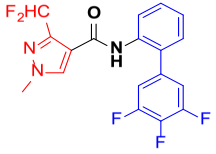
Figure 16. *Comparison of solution vs RAM (0.58 mmol scale, referred as "small scale") vs RAM (93.01 mmol scale, referred as "large scale") protocols for the synthesis of Fenfuram (**12**), Boscalid (**13**), Mepronil (**9**), Flutolanil (**10**), Fluxapyroxad (**11**) by DOZN™ 3.0 Quantitative Scoring tool. Legend: Aggregate score (**orange**), Group 1 (Improved Resource Use – **green**), Group 2 (Increased Energy Efficiency – **violet**), and Group 3 (Reduced Human and Environmental Hazards – **yellow**).*

Table 9. *Benchmark of "large scale" RAM protocol against solution-based protocols with CHEM21[76] for the synthesis of compounds* ***12****,[120]* ***13****[121] and* ***9****.[114]*

	RAM *vs* Solution								
									
METRICS[a]	(**12**)			(**13**)			(**9**)		
AE	40.3	*vs*	27.4	53.5	*vs*	64.4	47.4	*vs*	80.8
RME	29.6	*vs*	26.2	28.6	*vs*	58.7	34.0	*vs*	61.8
OE[b]	73.6	*vs*	95.4	53.5	*vs*	91.2	71.6	*vs*	76.5
PMI[c]	60.5	*vs*	65.7	101.1	*vs*	119.9	29.3	*vs*	13.4
$PMI_{reaction}$	5.0	*vs*	7.9	7.5	*vs*	110.1	4.2	*vs*	6.3
PMI_{workup}	55.6	*vs*	57.8	93.7	*vs*	9.8	25.1	*vs*	7.2
***E*-factor**	54.6	*vs*	64.7	92.7	*vs*	118.9	24.1	*vs*	12.4
Solvent	Water		ACN, AcOEt, PE	AcOEt, water		DCE, DCM, DMF, toluene, MeOH	Water		Xylene, water
Work-up, recovery	Water filtration		Column chromatography	Water filtration		Reduced pressure distillation, extraction, MeOH filtration	Water filtration		Water washing, reduced pressure evaporation
Health & safety									
Main hazard statements	H301, H311, H317, H318, H331, H341, H351, H372, H373, H400, H410, H302, H315, H318, H360D, H302, H311, H314, H318, H361d		H301, H311, H317, H318, H331, H341, H351, H372, H373, H400, H410, H224, H304, H315, H336, H411	H302, H315, H318, H360D		H225, H302, H304, H315, H319, H331, H335 H350, H226, H312, H319, H332, H360D, H22 H301, H311, H331, H370, H371, H228, H317 H351, H372, H331, H220, H360d, H372, H302 H315, H319, H361fd, H412, H225, H302, H311, H314, H318, H331, H335, H225, H304 H315, H336, H361d, H373, H412, H315, H31 H336, H351, H301, H331	H302, H315, H318, H360D, H302, H311, H314, H318 H361d		H302, H314, H318, H330, H372, H225, H302, H311, H314, H318, H331, H335, H225, H226, H304, H312, H315, H319, H332, H335, H373, H412

Legend: Green flag: Preferred; Amber flag: Acceptable with some concerns; Red Flag: Undesirable. [a] Best values for AE, RME and OE is 100%, for PMI is 1 and *E*-Factor = PMI – 1.[97] When comparing two processes, the one with the lowest PMI will be greenest; [b] $OE = {}^{RME}/_{AE} \times 100$; [c] Where precise work-up chemical quantities were unavailable, estimates were derived as detailed in the ESI to ensure fair comparison.

Table 10. *Benchmark of "large scale" RAM protocol against solution-based protocols with CHEM21[76] for the synthesis of compounds* ***10***[115,116] *and* ***11.***[117,118]

	RAM *vs* Solution					
						
METRICS[a]	(**10**)			(**11**)		
AE	52.0	*vs*	69.0	56.1	*vs*	73.1
RME	38.9	*vs*	60.9	44.2	*vs*	58.9
OE[c]	74.9	*vs*	88.1	78.7	*vs*	80.6
PMI[d]	24.5	*vs*	50.4	60.5	*vs*	16.3
PMI$_{reaction}$	3.6	*vs*	49.7	3.1	*vs*	8.9
PMI$_{workup}$	20.9	*vs*	0.7	57.4	*vs*	7.4
***E*-factor**	19.9	*vs*	49.4	56.4	*vs*	15.3
Solvent	Water		DCM, THF, *n*-hexane	Water		Et_2O, *n*-BuOH, water
Work-up, recovery	Water filtration		Distillation under reduced pressure, rectrystallization	Water filtration		Water washing, water filtration
Health & safety						
Main hazard statements	H302, H315, H318, H360D, H302, H311, H314, H318, H361d		H331, H220, H360d, H372, H301, H331, H351	H302, H315, H318, H360D, H410, H302, H311, H314 H318, H361d		H302, H319, H411, H224, H302, H336, H220, H280, H315, H318, H319, H332, H335, H412

Legend: Green flag: Preferred; Amber flag: Acceptable with some concerns; Red Flag: Undesirable. [a] Best values for AE, RME and OE is 100%, for PMI is 1 and *E*-Factor = PMI – 1.[97] When comparing two processes, the one with the lowest PMI will be greenest; [b] $OE = {RME}/{AE} \times 100$; [c] Where precise work-up chemical quantities were unavailable, estimates were derived as detailed in the ESI to ensure fair comparison.

The picture that emerges is consistent across the two toolkits. On the metrics that reward low molecular weight reagents, the solution routes usually win. TCFH is a bulky salt, and roughly a third of its mass is the PF_6^- counterion, which never appears in the product; this is what depresses AE and RME for **13, 9, 10, 11**. The only target where RAM leads on atom economy is Fenfuram **12**, where the published solution route uses a heavy phosphite coupling agent.[120]

On the metrics that count the whole process, the ranking changes. RAM gives the lower PMI and *E*-factor for **12**, **13** and **10**, because a simple aqueous precipitation replaces chromatography,[120] extraction[121] or recrystallisation.[116] The two cases where the solution route wins, **9** and **11**, both come down to the volume of water used in our precipitation, and Figure 5 shows that this figure improves as the batch size grows. It is a work-up problem, not a reaction problem.

The qualitative flags are where the mechanochemical route is unambiguously ahead. The RAM protocol runs at room temperature and, except for the small amount of AcOEt used as LAG additive for **13**, without solvent. It avoids acetonitrile and petroleum ether (**12**), dichloromethane, DMF, 1,2-dichloroethane and toluene (**13**), $POCl_3$ (**9**), oxalyl chloride, DCM, THF and *n*-hexane (**10**), and PCl_5 and diethyl ether (**11**). Several of these are severely restricted: DCM is being withdrawn from industrial use in the United States[122] and tightly controlled in the EU,[123] and DMF is restricted in Europe.[124] Against this, the RAM route has one recurring liability of its own: TMU, the by-product of TCFH, is classified as a teratogen, and this is what penalizes the hazard group of the DOZN™ score for **13** and **39**. Where the solution route uses a reagent whose own by-products are benign, as $POCl_3$ does with its phosphate salts, that trade-off can go against us.

7. Conclusion

A TCFH-mediated amidation established in the ball mill was transferred to resonant acoustic mixing and used to prepare five marketed SDHI fungicides. The transfer was not a simple translation. Two of the parameters that govern the milling reaction, the physical state of the base and the benefit of longer processing, are inverted in RAM, because a vibrating mill needs a mixture solid enough to transmit an impact whereas RAM needs one fluid enough to follow an acoustic field. Adding grinding media to RAM reproduced the drawback of milling without its advantage. Once these differences were understood, RAM outperformed both vibrating and planetary milling on every target.

The practical result is the scale-up. The optimized protocol was applied unchanged from 2.5 mL to 240 mL, a 160-fold increase, and delivered up to 35 g of product in a single batch with yields at or above 90% for four of the five compounds. No re-optimization was required at any step, which is precisely the property that ball milling lacks. Along the way, the aggregation of tetramethyl urea into soft solid spheres was identified as a likely self-assisting mixing effect, and control experiments showed that the mechanical contribution of RAM becomes decisive only when a poor nucleophile has to be mixed into a viscous medium.

The environmental assessment reveals both advantages and limitations of the RAM route. Compared with the corresponding solution-based processes, RAM consistently performs better in terms of energy consumption, solvent use and reagent hazards. It also generates less waste for three of the five targets. However, the high molar mass of TCFH limits atom economy, while the aqueous work-up requires further optimization for the two remaining targets to reduce waste. Increasing the batch size can improve process efficiency, but does not change the atom economy of a given reaction.

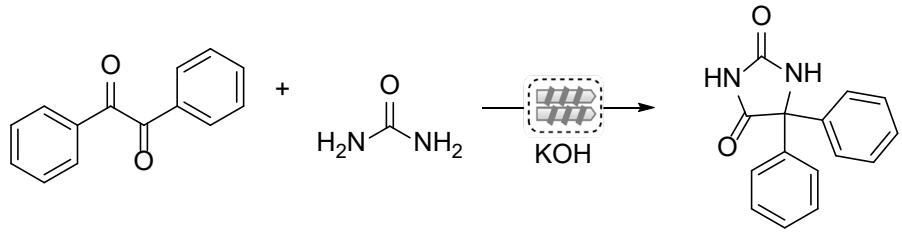
Taken with Chapter I, the results show that the choice of activating agent and the choice of mechanochemical device are not independent decisions, and that a route which is competitive at gram scale can become clearly advantageous once it is scaled. The following chapter turns from batch to continuous operation, which addresses the same throughput question from a different direction.

Introduction Chapitre III

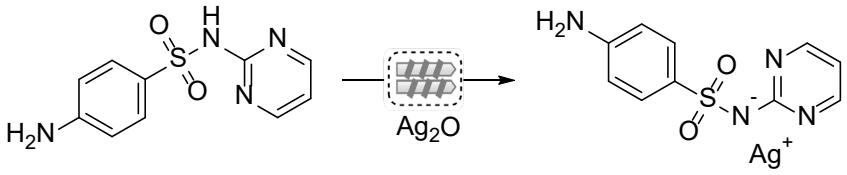
Les chapitres I à III ont montré que la mécanochimie réduit l'impact environnemental de la synthèse de petites molécules, depuis des réactions d'amidation individuelles jusqu'à un procédé de cocristallisation à l'échelle du kilogramme. Dans chaque cas, la réaction était encore réalisée en mode discontinu. Le traitement discontinu impose une limite stricte au débit de production et nécessite des manipulations manuelles entre les lots, ce qui ne correspond pas au fonctionnement habituel de la production pharmaceutique à grande échelle. L'extrusion bi-vis (TSE) permet de réaliser une réaction mécanochimique en continu, à l'aide d'équipements déjà familiers aux industries pharmaceutique et alimentaire. Ce chapitre examine si la TSE peut reproduire, voire accroître, les gains de durabilité déjà établis pour ces réactions en broyeur à billes.

Les objectifs spécifiques de ce chapitre étaient les suivants :

- transférer la synthèse mécanochimique de deux médicaments essentiels de l'Organisation mondiale de la Santé, la sulfadiazine d'argent(I) (**14**) et la phénytoïne (**15**), du broyage à billes en mode discontinu au traitement continu par extrusion bi-vis ;
- identifier une source d'argent pour la synthèse de **14** permettant d'éviter les déchets contenant des nitrates, et résoudre la structure d'un intermédiaire réactionnel jusqu'alors non décrit ;
- optimiser la base, la stœchiométrie, la température et la configuration des vis pour la synthèse continue de **15** ;
- confirmer la pureté de phase des deux produits par diffraction des rayons X sur poudre, et comparer la durabilité et la productivité des voies par TSE à celles des procédés correspondants en solution et des procédés mécanochimiques discontinus, à l'aide de l'outil CHEM21.



Phenytoin
(antiepileptic)



Silver Sulfadiazine
(antiseptic)

III - Motivation and aims of the present work

Chapters I to III showed that mechanochemistry lowers the environmental burden of small-molecule synthesis, from single amidation reactions to a kilogram-scale co-crystallization process. In every case, the reaction was still run in batch. Batch processing sets a hard limit on throughput and requires manual handling between runs, which is not how pharmaceutical manufacturing usually operates at scale. Twin-screw extrusion (TSE) offers a way to run a mechanochemical reaction continuously, using equipment already familiar to the pharmaceutical and food industries. This chapter tests whether TSE can reproduce, and even extend, the sustainability gains already established for these reactions in the ball mill.

The specific aims of this chapter were:

- to translate the mechanochemical synthesis of two World Health Organization essential medicines, silver(I) sulfadiazine (**14**) and phenytoin (**15**), from batch ball-milling to continuous processing by twin-screw extrusion;
- to identify a silver source for **14** synthesis that avoids nitrate-bearing waste, and to solve the structure of a previously unreported reaction intermediate;
- to optimize the base, the stoichiometry, the temperature, and the screw configuration for the continuous synthesis of **15**;
- to confirm the phase purity of both products by powder X-ray diffraction, and to benchmark the sustainability and the productivity of the TSE routes against the corresponding solution-based and batch mechanochemical processes, using the CHEM21 toolkit.

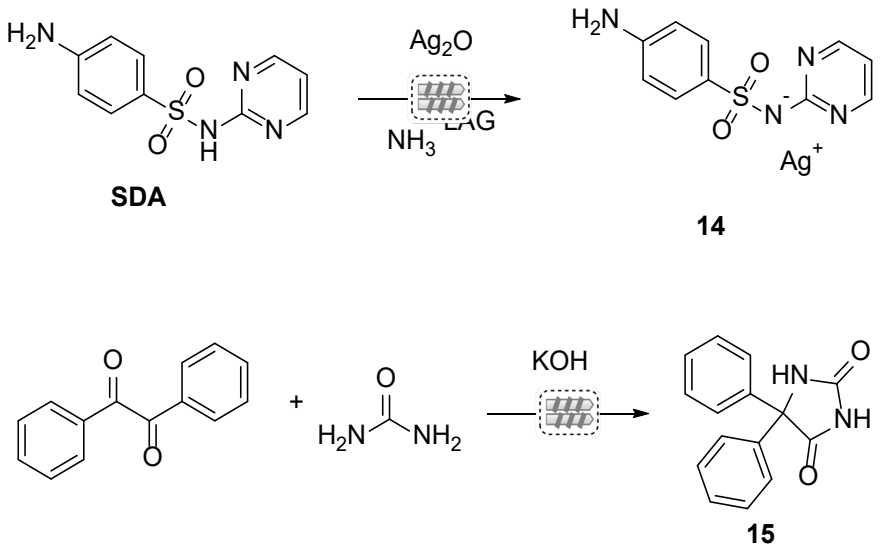
Chapter III — Continuous Mechanochemical Manufacturing of Essential Medicines by Twin-Screw Extrusion

1. Context

The pharmaceutical industry is under growing pressure to cut its carbon footprint without compromising product quality or supply. Solvents are the main contributor to this footprint. They can account for up to 90% of the mass used in a typical batch process, and their use, disposal, and associated drying and climate-control operations drive a large share of the sector's energy demand and greenhouse-gas emissions.[125,126] As shown in the general introduction, mechanochemistry offers a solvent-free or solvent-lean alternative that lowers Process Mass Intensity (PMI) and the E-factor, while keeping the critical quality attributes of the product unchanged.

Ball milling has been widely used to prepare active pharmaceutical ingredients (APIs) at laboratory scale.[127] Scaling this chemistry to production volumes, however, requires moving from batch to continuous processing. Twin-screw extrusion (TSE) was identified by IUPAC in 2019 as one of the top ten emerging technologies in chemistry, on the strength of its potential for sustainable, continuous synthesis.[128] The first mechanochemical API made by TSE was nitrofurantoin, reported in 2020.[63] That study also gave the first life-cycle comparison of a mechanochemical process against its solution-based counterpart, and found a substantially lower climate impact for the continuous route.[129] Since then, TSE has been used to prepare other generic APIs, including paracetamol and moclobemide, by adapting reactions first developed by ball milling.[58]

This chapter presents the continuous synthesis, by TSE, of two further APIs on the WHO Model List of Essential Medicines:[130] silver(I) sulfadiazine (**SSD**), a topical antiseptic, and phenytoin (**15**, diphenylhydantoin), an antiepileptic drug (Scheme 12). Both compounds had previously been prepared by ball milling[68,69] or by resonant acoustic mixing (RAM),[51] but never in a continuous process. The aim was to simplify the unit operations needed for their manufacture, and to establish whether the sustainability advantage already demonstrated for these reactions in batch could be preserved, or improved, under continuous operation.



Scheme 12. *Continuous mechanochemical routes to silver(I) sulfadiazine (**14**) from sulfadiazine (**SDA**) and Ag_2O, and to phenytoin (**15**) from benzil and urea, by TSE.*

2. Continuous synthesis of silver(I) sulfadiazine

SSD is conventionally made by mixing solutions of silver nitrate and sulfadiazine, followed by precipitation, filtration, and drying.[131] The process gives a good yield, but it consumes large volumes of water and generates nitrate-bearing effluent. A mechanochemical route already existed, using silver nitrate and a catalytic amount of aqueous ammonia in a ball mill.[67] To remove nitrate from the process entirely, we replaced silver nitrate with silver(I) oxide. This turns **14** formation into an acid–base neutralization: the oxide accepts the sulfonamide proton from sulfadiazine, and releases silver(I) to the deprotonated ligand. Water is the only stoichiometric by-product, and it is removed by simple drying.

Silver oxide is twice as efficient as silver nitrate, bearing the double amount of silver per mole: this raises the atom economy of the reaction from 85.0% (with $AgNO_3$) to 97.5% (with Ag_2O). The dry mixture of Ag_2O and sulfadiazine is stable and unreactive on its own, even after prolonged milling; a catalytic amount of aqueous ammonia is required to trigger the reaction, most likely by transiently stabilizing silver ions as the $[Ag(NH_3)_2]^+$ complex.

Real-time monitoring of the ball-milling reaction, by synchrotron powder X-ray diffraction (PXRD), revealed a short-lived crystalline intermediate that had not previously been reported. Its formation did not depend on the silver source used, which indicated that it contained silver ions but neither the counterion nor water. Because the intermediate was too unstable to isolate directly, its structure was solved from laboratory PXRD data collected under conditions designed to slow the reaction, using simulated annealing followed by solid-state DFT optimization. The refined structure (monoclinic, space group C2) showed sulfadiazine and silver ions arranged in one-dimensional chains, linked by hydrogen bonds into a three-dimensional network. Its unit-cell volume was slightly larger than that of the final **14** product, consistent with a lower-density, metastable structure that precedes the denser, final crystal form.

With the reaction pathway established, translating the synthesis to TSE proved straightforward. A 1:2 mixture of Ag_2O and sulfadiazine (12.1 g total) was hand-mixed and fed into the extruder, together with a few drops of aqueous ammonia added through a dedicated liquid-addition port. No further screw-profile optimization was required. The extrudate was an off-white, phase-pure powder, confirmed by PXRD to match the crystal structure of the approved drug product. The reaction proceeded at room temperature, at a rate of at least 10 g/h, and the product was recovered directly from the extruder, without any extraction or washing step.

3. Continuous synthesis of phenytoin

A straightforward way to prepare **PHE** is by the Biltz rearrangement: a base-promoted condensation between benzil and urea, followed by an intramolecular phenyl shift.[132] A competing dimerization gives 3a,6a-diphenylglycoluril (**DGU**) as the main by-product.

We first compared three non-hygroscopic hydroxide bases ($LiOH·H_2O$, NaOH, KOH) under neat extrusion at 80 °C. KOH gave the best yield of **15** (55%), consistent with the trend already observed in the ball mill.[133] The result follows from Hard and Soft Acid–Base theory: hydroxide, a hard base, pairs more strongly with harder cations ($Li^+ > Na^+ > K^+$), which reduces its availability to react. Weaker bases instead favoured the competing dimerization, with $LiOH·H_2O$ giving mostly **DGU** (21%) rather than **15** (3%).

With KOH confirmed as the base of choice, we screened the urea stoichiometry (1.0–1.6 equivalents) and the barrel temperature (70–100 °C). A slight excess of urea (1.4 equiv.) at 90 °C gave the best yield (61%). Temperature had only a modest effect within this range, though extrusion at room temperature still gave an acceptable yield (41%), showing that the reaction is exothermic enough to partly sustain itself once initiated by the mechanical input of the screws.

We also tested liquid-assisted grinding (LAG) with ethanol, which had previously given a near-quantitative yield of **15** by LA-RAM.[51] Under TSE, however, LAG improved the rheology of the mixture but did not outperform the optimized neat conditions (60% *vs*. 61% yield, respectively), and made manual feeding of the reagent mixture less reproducible due to the. Neat processing was therefore retained for the remaining optimization.

Finally, the screw configuration was modified to increase residence time and mixing, by introducing reverse-conveying elements at different points of the screw profile. The best-performing configuration gave 78% isolated yield after purging the barrel with urea to recover the residual extrudate, and only 5% of the **DGU** by-product (Table 11). The product was isolated by a solvent-minimized work-up: dissolution of the potassium salt of **15** in water, removal of the water-insoluble **DGU** by filtration, and precipitation of **15** by acidification with aqueous citric acid. PXRD confirmed that the isolated material matched the published crystal structure of phenytoin (CSD refcode PHYDAN03), and was consistent with samples obtained by LA-RAM and with a commercial reference standard.

Table 11. *Best-performing screw configuration for the continuous synthesis of phenytoin by TSE.*[a]

Entry	Screw profile	Screw speed (rpm)	Torque (Nm)[b]	Throughput (Kg/h)	SME[c] (kJ/kg)	Yield (%) 15[c]	
						without purge[d]	After purge[e]
1[d]	*configB*	30	7	32.0	2.5	57 (60)[f]	78 (70)[f]
2	*configB*	40	7	60.2	1.8	61	75
3	*configC*	30	10.5	32.3	3.7	48	76
4	*configC*	40	10.5	21.5	7.4	48	78
5[g]	*configB*	30	7	n.c.[h]	n.c.[h]	63	75

[a] Typical experimental procedure: 30.75 g total premix input mass composed of benzil (71.6 mmol, 15.21 g, 1.0 equiv.), urea (100.24 mmol, 6.08 g, 1.4 equiv.) and KOH (143.2 mmol, 9.46 g, 2.0 equiv.) was manually fed into the twin-screw extruder (25:1 length-to-diameter ratio, L/D). The screw (co-rotating) speed (rpm) was as specified, the barrel was heated at 90°C. Full screw-profile comparisons are given in the SI, Annex 6. [b] A torque value of about 1 N m corresponds to dry screw rotation (without chemicals). The torque value decreases to 5.5 – 6.0 N m upon the purging with urea started; [c] SME = Specific Mechanical Energy[58] calculated from the data set of the experiments before purging; [d] Yields were calculated on recovered extrudate mass before purging; [e] Yields were calculated assuming total recovery of initial premix mass input; [f] Reaction performed with EtOH in LAG conditions (η = 0.75 mL/g); [g] Experimental procedure: 61.50 g total premix input mass composed of benzil (143.3 mmol, 30.42 g, 1.0 equiv.), urea (200.62 mmol, 12.17 g, 1.4 equiv.) and KOH (286.6 mmol, 18.91 g, 2.0 equiv.), extruded at 90°C; [h] n.c. = not calculated.

4. Benchmarking against the solution process

The sustainability of both TSE routes was assessed with the CHEM21 toolkit,[76] using Process Mass Intensity (PMI) as the main quantitative metric, and benchmarked against the corresponding solution syntheses and the previously reported batch mechanochemical routes (ball milling and RAM).

For **14**, the conventional solution route has a total PMI of 62.9, driven almost entirely by the water used for dissolution, reaction, and washing. All the mechanochemical routes, whether by ball milling or by TSE, achieved a PMI close to the theoretical minimum of 1 (PMI ≈ 1.0–1.2), because they generate essentially no waste beyond the water by-product. Using Ag_2O instead of $AgNO_3$ gave a small further improvement in PMI, consistent with its higher atom economy. The TSE process also required proportionally less aqueous ammonia than the ball-milling process.

For **15**, the solution route has a much higher total PMI (221.6), because of the extractive work-up and recrystallization steps it requires. The mechanochemical routes lowered this considerably, though the improvement was less dramatic than for **14**, because **15** still needs a water-based work-up to remove the **DGU** by-product. The TSE route gave the lowest total PMI among the batch and continuous mechanochemical processes (68.4, against 93.9 for RAM and 383.6 for ball milling), mainly because the larger reaction scale used in TSE experiments diluted the fixed mass of work-up chemicals over more product.

Productivity followed a similar pattern. For **14**, TSE gave the highest throughput (10 g/h) of any route tested, and needed no downstream processing step, since the product was recovered directly from the extruder. For **15**, LA-RAM gave the highest instantaneous productivity in the short experiments compared here, but TSE is expected to overtake it over longer, steady-state runs, because continuous processing removes the repeated set-up, heating, and unloading steps that limit batch throughput.

5. Conclusions

Twin-screw extrusion reproduced, and in some respects extended, the sustainability advantages already established for these two reactions in batch. For **14**, replacing silver nitrate with silver(I) oxide removed nitrate waste from the process entirely, and gave a near-ideal PMI under both ball-milling and TSE conditions. Solving the structure of the previously unreported reaction intermediate also clarified the mechanistic pathway leading to the final crystal form. For **15**, systematic optimization of the base, the stoichiometry, the temperature, and the screw profile gave a phase-pure product at a competitive PMI, without needing liquid-assisted grinding.

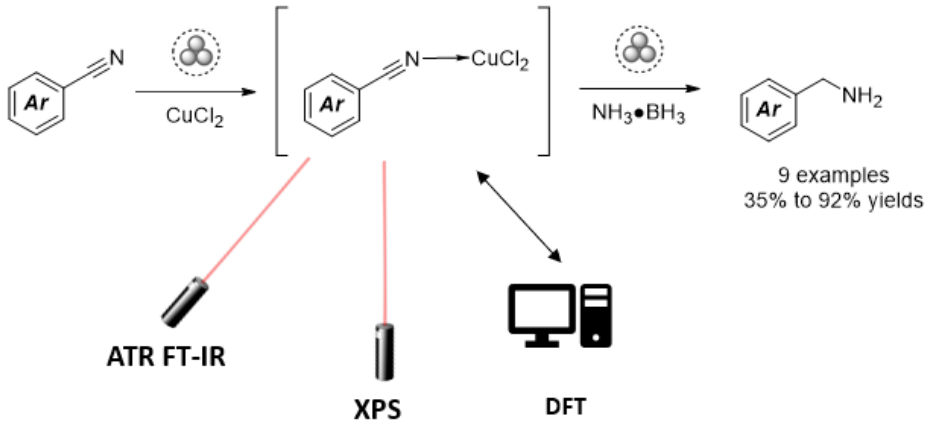
Beyond the specific chemistry, these results show that TSE can take a mechanochemical reaction already validated at small scale and run it continuously, with equipment compatible with existing pharmaceutical infrastructure. Continuous operation removes much of the downtime intrinsic to batch processing, and this advantage should grow as extrusion run times increase beyond the short, exploratory campaigns described here. Together with Chapters I to III, this chapter supports the broader conclusion of this thesis: that mechanochemical route redesign, and not only the incremental optimization of existing solution processes, is a credible strategy for reducing the environmental footprint of pharmaceutical and industrial manufacturing at scale.

Introduction Chapitre IV

Les chapitres I à III ont décrit la fabrication mécanochimique de molécules déjà commercialisées : des fongicides agrochimiques, un antiseptique et un médicament antiépileptique. Dans chaque cas, la mécanochimie a été utilisée pour obtenir une cible connue de manière plus propre que par la voie existante en solution. Ce chapitre déplace l'attention d'une molécule cible vers une réaction cible. L'objectif n'est plus de repenser le procédé de fabrication d'un produit existant, mais d'élargir la boîte à outils mécanochimique elle-même, en y ajoutant une transformation, la réduction d'un nitrile en amine primaire, qui n'avait jamais été réalisée par broyage à billes auparavant. Les amines primaires sont des éléments de base essentiels dans les secteurs pharmaceutique, agrochimique et de la chimie fine. Une voie sans solvant permettant de les obtenir à partir de nitriles facilement accessibles apporte donc une option véritablement nouvelle à la stratégie plus générale de synthèse durable par mécanochimie poursuivie tout au long de cette thèse.

Les objectifs spécifiques de ce chapitre étaient les suivants :

- développer un protocole mécanochimique sans solvant et à température ambiante pour la réduction des nitriles en amines primaires, en utilisant des agents réducteurs doux ;
- établir le champ d'application et les limites de la méthode sur un ensemble de nitriles aromatiques et benzyliques, et rationaliser les principales voies concurrentes ;
- caractériser le complexe intermédiaire cuivre–nitrile proposé par spectroscopie infrarouge à transformée de Fourier (FT-IR) et spectroscopie photoélectronique à rayons X (XPS), afin d'étayer l'hypothèse mécanistique d'une activation par un acide de Lewis.



IV - Motivation and aims of the present work

Chapters I to III described the mechanochemical manufacture of molecules that are already on the market: agrochemical fungicides, an antiseptic, an antiepileptic drug. In each case, mechanochemistry was used to reach a known target more cleanly than the existing solution-based route. This chapter shifts the focus from a target molecule to a target reaction. The aim is no longer to redesign the process for an existing product, but to extend the mechanochemical toolbox itself, by adding a transformation, the reduction of a nitrile to a primary amine, that had never been run under ball milling before. Primary amines are a key building block across pharmaceuticals, agrochemicals and fine chemicals, so a solvent-free route to access them from easily available nitriles adds a genuinely new option to the broader strategy of sustainable, mechanochemically enabled synthesis pursued throughout this thesis.

The specific aims of this chapter were:

- to develop a solvent-free, room-temperature mechanochemical protocol for the reduction of nitriles to primary amines, using mild reducing agents;
- to establish the scope and the limits of the method on a set of aromatic and benzylic nitriles, and to rationalize the main competing pathways;
- to characterize the proposed copper–nitrile intermediate complex by FT-IR and XPS spectroscopy and so support the mechanistic hypothesis of Lewis-acid activation.

Chapter IV — Mechanochemical Nitrile Reduction in Mild Conditions Using Ammonia Borane as Reducing Agent

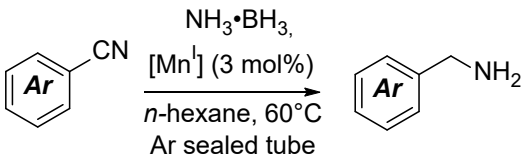
1. Context

Primary amines sit at the core of natural products, agrochemicals, dyes, polymers and a large share of marketed pharmaceuticals.[134,135] Reducing a nitrile is the most direct way to build them: it installs the CH_2–NH_2 group in a single step, from a precursor that is usually cheap and commercial. The C≡N triple bond, however, is thermodynamically robust, and far less reactive than nitro compounds, aldehydes, ketones or esters. Classical protocols therefore rely on stoichiometric hydride donors such as $LiAlH_4$, BH_3 or DIBAlH,[136] or on catalytic hydrogenation under harsh conditions, and both bring pyrophoric reagents, poor functional-group tolerance, metal-laden waste and flammable ethereal solvents.[137] Selectivity is a further difficulty, because the imine and amine intermediates are themselves nucleophilic, and compete for further reduction or condensation, giving mixtures of primary, secondary and tertiary amines.[138]

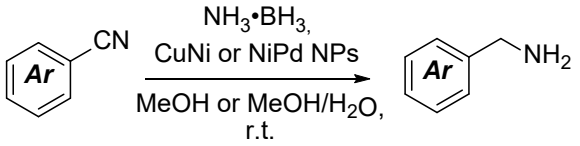
Catalytic hydrogenation with Ru, Rh, Ir, Fe, Co or Mn complexes is more atom-economic and chemoselective, but usually needs high temperature and pressure (up to 60 bar and 160 °C),[139–146] custom pincer-type phosphine ligands, and an external base to limit over-reduction.[147,148] Milder hydride- or hydrogen-transfer routes use boranes[149] or silanes.[150] Ammonia borane ($NH_3{\cdot}BH_3$, AB) is a particularly attractive option: a non-toxic, bench-stable solid carrying 19.6 wt% hydrogen, already used in solution to reduce imines, polarized olefins and carbonyls.[151,152] Applied to nitrile reduction, though, it has three recurring weaknesses. The homogeneous systems selective for primary amines depend on tailor-made ligands, whose multi-step, air-sensitive synthesis cancels much of the cost advantage of earth-abundant metals.[147,148] Most heterogeneous nanoparticle systems do not use AB as a hydride donor at all: it is dehydrogenated *in situ* to release H_2, so it serves only as a hydrogen-storage medium.[153,154] And the one catalyst-free protocol that does use AB as a true hydride donor requires refluxing diethyl ether at 120 °C in a sealed autoclave[155] (Scheme 13).

Mechanochemistry has meanwhile begun to build its own toolbox for reduction chemistry. $NaBH_4$ reduces nitrobenzenes with gold nanoparticles,[156] and, with LiCl to generate $LiBH_4$ *in situ*, esters to alcohols.[157] Diboronic species reduce alkynes, alkenes or nitro groups through *in situ* H_2 generation,[158,159] as do AB with solid NaCl,[160] ammonium formate with Pd/C[161] and silanes.[162–164] Zero-valent and low-reactive metals act as strong electron donors under mechanical agitation, since grinding activates passivated surfaces without anhydrous conditions or an inert atmosphere:[165] Ca and Mg have been used for solvent-free Birch reductions,[166] and Li, Na, Ca, Mg and Ba for Barbier- and Wurtz-type couplings[167] or Béchamp reductions.[17] Mechanical force can even drive single-electron transfer from piezoelectric materials,[164,168] and H_2 hydrogenation has been adapted to pressurizable jars.[169,170]

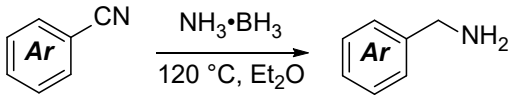
(a) Mn(I) catalysis:



(b) CuNi and NiPd nanoparticles catalysis:

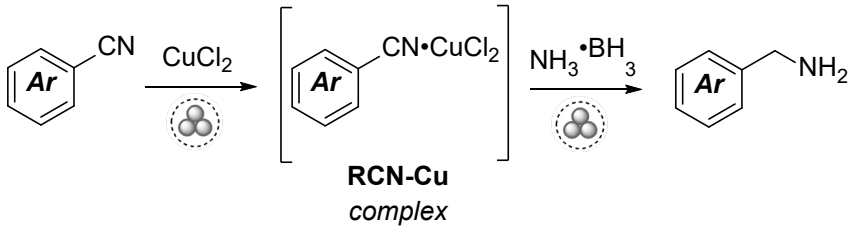


(c) Metal-free microwave-driven reduction:



Scheme 13. *Previous strategies for AB-mediated nitrile reduction, compared with the mechanochemical protocol developed in this chapter.*

Despite this progress, mechanochemical reductions remain scarce, and chemoselective ones especially so. To the best of our knowledge, none had been reported for reducing a nitrile to its primary amine. This chapter reports the first such protocol, using AB as the reductant and $CuCl_2$ as a mediator, through a two-step sequential activation in a single jar: $CuCl_2$ first coordinates the nitrile through its nitrogen lone pair (κ^1-N), polarizing the C≡N bond and raising the electrophilicity of the nitrile carbon; the activated substrate is then attacked by AB, used directly as a hydride donor rather than as a sacrificial H_2 source (Scheme 14).



Scheme 14. *Proposed general scheme of the mechanochemical nitrile reduction, mediated by an AB/$CuCl_2$ system.*

2. Reaction discovery: choosing the activator

A liquid benzyl cyanide was chosen as benchmark to study the reduction reaction in the ball-mill, exploring several borohydride reductants in a vibratory ball mill (ZrO_2 jar, single 10 mm ZrO_2 ball, 30 Hz). $NaBH_4$ and $LiBH_4$ gave no reaction, or only traces: a non-activated nitrile is too poor an electrophile to be reduced by these mild hydrides. The

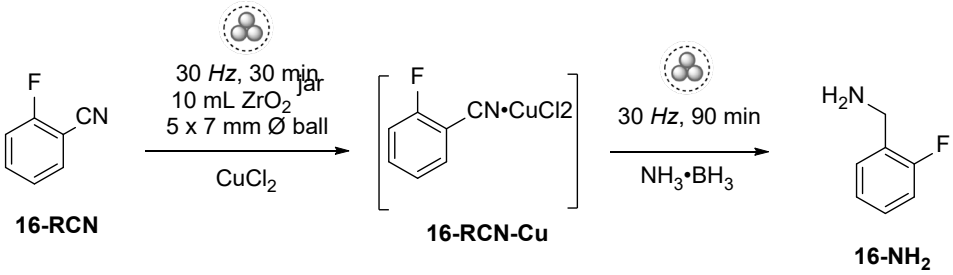
design that followed rested on a simple idea. If the nitrile carbon could be made more electrophilic beforehand, through κ^1-N coordination to a Lewis-acidic metal, the C≡N bond should reduce more easily. A first screening of Lewis acids ($MgCl_2$, $AlCl_3$, $ZrCl_4$, TiF_4, $FeCl_3$, $ZnCl_2$, $MnCl_2$), each pre-milled with the nitrile before adding $NaBH_4$, gave only moderate conversion at best.

To probe selectivity alongside activity, we moved to two halogenated substrates, solid *o*-iodobenzonitrile and liquid *o*-fluorobenzonitrile, so that competing dehalogenation could be tracked directly. The iodo-substrate gave high conversion with $NaBH_4/ZrCl_4$, but poor selectivity. Switching to AB, with anhydrous $CuCl_2$ as activator, changed the picture: 60% conversion to *o*-iodobenzylamine with only 20% dehydrohalogenation, where $NaBH_4/CuCl_2$ had given a complex mixture. $CuCl_2$ is therefore a σ-acceptor strong enough to polarize the C≡N bond and open it to attack by AB, and its affinity for the amine product may also help pull the reaction forward.

3. Optimizing the stoichiometry

We optimized the loading of $CuCl_2$ and AB on *o*-fluorobenzonitrile (**16-RCN**), reduced to *o*-fluorobenzylamine (**16-NH₂**, Table 11). Nitrile (1.0 equiv.) and $CuCl_2$ were milled together for 30 min at 30 Hz (*step 1*), then AB was added and milling continued for 90 min at 30 Hz (*step 2*).

Table 11. *Stoichiometry optimization for the reduction of* ***16-RCN*** *to* ***16-NH₂****.*



Entry	$CuCl_2$ equiv.	AB equiv.	Conversion[a] (%)	Yield of 1-NH_2[a] (%)
1	0.5	2	29%	16%
2	**0.5**	**5**	**100%**	**93% (92%[b])**
3	0.5	7	55%	33%
4	0.2	5	12%	12%
5	0.6	5	94%	92%
6	1	5	88%	2%
7	0.2	2	37%	13%

Typical experimental procedure: To a 10 mL ZrO_2 jar equipped with 5 x 7 mm Ø balls of the same material, the nitrile (1.5 mmol, 1.0 equiv.), $CuCl_2$ were milled for 30 minutes at 30 *Hz* in a mixer mill (*step 1*). After this milling time, AB was added, and the reaction mixture was further milled for 90 minutes at 30 *Hz* (*step 2*). [a] Calculated *via* ^{1}H qNMR, in $CDCl_3$ using cyclododecane as internal standard.[171] [b] Isolated yield.

The best loading was 0.5 equiv. $CuCl_2$ and 5 equiv. AB (entry 2), giving quantitative conversion and 92% isolated yield. Lowering AB to 2 equiv. left the reaction incomplete (entry 1); raising it to 7 equiv. also lowered conversion and yield (entry 3), consistent with

over-reduction of Cu(II) to inactive Cu(0), supported by visible metallic copper on the jar walls. A control without $CuCl_2$ gave no reaction at all. Below 0.5 equiv., $CuCl_2$ limited conversion through insufficient turnover (entry 4); at 1.0 equiv., conversion stayed high but selectivity collapsed to 2% (entry 6), which we attribute to a parasitic C–F activation pathway. The viable window is therefore narrow, 0.5–0.6 equiv. A further control (entry 7), at the same 1:10 Cu:AB ratio but lower absolute loadings, gave only 37% conversion, showing that the absolute amount of each reagent matters, not only their ratio.

4. Optimizing the technical milling parameters

We then examined milling time, ball number and size, frequency, jar geometry and grinding-media material. For each set-up, the cumulative nominal energy input (E_{tot}) and the nominal energy per ball–reactant impact (E_{imp}) were estimated with the open-source calculator published by Lungerich and coworkers,[30] as comparative rather than measured values (Table 12).

Table 12. *Technical parameter optimization for the reduction of* ***16-RCN*** *to* ***16-NH₂****.*

Entry	*f* (Hz)	Balls (n*Ø)	Energy			Yield[a]
			E_{tot} (kJ) (step 1)	E_{tot} (kJ) (step 2)	E_{imp} (mJ)	
1	30 Hz	5*7 mm	19.69	59.06	7.34	**93% (92%[b])**
2	30 Hz	4*7 mm	15.80	47.40	7.34	60%
3	30 Hz	3*7 mm	11.88	35.62	7.34	90%
4	30 Hz	2*7 mm	7.93	23.78	7.34	84%
5	30 Hz	6*5 mm	9.54	28.62	2.95	54%
6	30 Hz	4*5 mm	7.96	23.88	2.95	50%
7	30 Hz	1*10 mm	11.74	35.23	21.8	91%
8	25 Hz	1*10 mm	6.80	20.39	15.1	61%
9[c]	30 Hz	1*10 mm	11.60	34.81	21.5	34%

Typical experimental procedure: To a 10 mL ZrO_2 jar equipped with specified number and size of balls of the same material, the nitrile (1.5 mmol, 1.0 equiv.), $CuCl_2$ (0.75 mmol, 0.5 equiv.) were milled for the specified amount of time at the specified frequency in a MM400 mixer mill (*step 1*). After this milling time, NH_3BH_3 (7.5 mmol, 5 equiv.) was added, and the reaction mixture was further milled for the specified amount of time at the specified frequency (*step 2*). [a] Calculated *via* ^{1}H qNMR, in $CDCl_3$ using cyclododecane as internal standard.[171] [b] Isolated yield. [c] Mill used was Fritsch's P23 vertical mixer mill.

The number of balls had only a modest effect (entries 1, 3, 4); the small variations most likely reflect mixing efficiency, not total energy. E_{imp}, rather than E_{tot}, was the decisive parameter: 5 mm balls gave consistently lower yields than 7 mm balls even at matched E_{tot} (entry 4 *vs.* 6). 10 mm balls matched the 7 mm ones, in line with their higher E_{imp}, but were more prone to clumping on the ball itself, that hurt homogeneity and thus reproducibility.[112] Lowering the frequency from 30 to 25 *Hz* (entries 7 and 8) cut E_{imp} by about 30%, and the yield fell by a similar margin. Moving to a vertical mixer mill (entry

9), at nominally the same E_{tot} and E_{imp}, gave a much lower yield: the way energy is transferred, and not only its magnitude, clearly matters.

The jar material was equally important. PTFE jars built up pressure during milling, and stainless-steel balls corroded; ZrO_2, or another inert ceramic, is recommended for both. Milling time was fixed at 30 min for step 1 and 90 min for step 2: shorter times left the reaction incomplete, while over-milling lowered conversion again, because the Cu(0) formed in the jar, with residual oxygen, re-oxidizes the amine back to the nitrile.[172,173]

5. Substrate scope

Using the optimized conditions (Table 12, entry 1, 1.5 mmol scale), we applied the method to a focused panel of aromatic and benzylic nitriles. The crude was dissolved in methyl *tert*-butyl ether (MTBE), and the amine hydrochloride precipitated with HCl in cyclopentyl methyl ether (CPME); only the *ortho*-iodo substrate was isolated as the free amine by extraction, because a more pronounced benzylamine by-product prevented clean precipitation (Figure 16).

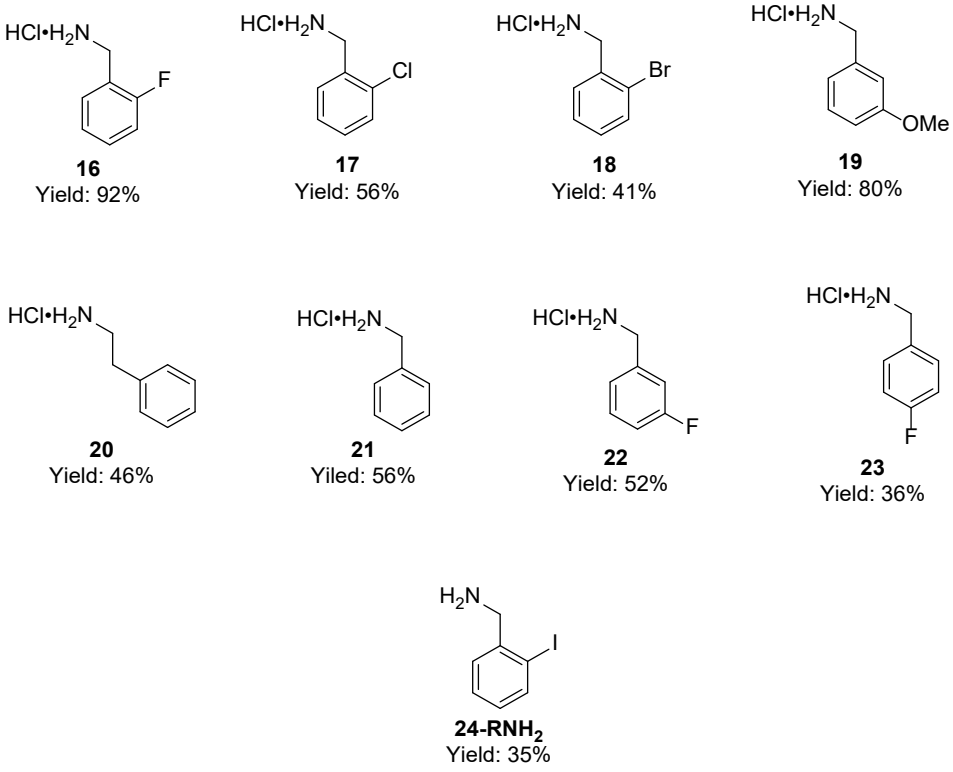


Figure 16. *Scope of the reaction.*

Across the *ortho*/*meta*/*para* fluorobenzonitriles, and the *ortho*-chloro and *ortho*-bromo analogues, the nitrile was reduced cleanly, with little to no dehalogenated by-product. The protocol is therefore chemoselective for the nitrile over the competing carbon–halogen bond, a pathway that often complicates nitrile reduction under classical metal/hydride conditions. Within the fluorinated series, isolated yield fell in the order *ortho* (92%) > *meta* (52%) > *para* (36%), tracking a growing contribution from a dibenzylic secondary amine by-product once the *ortho* relationship between nitrile and fluorine is

lost; the same trend appears for the parent benzonitrile (56%). Chelation of the copper center by the *ortho*-fluorine is one possible explanation, though no structural evidence is available yet. A related trend runs across the *ortho*-halogen series, F (92%) > Cl (56%) > Br (41%) > I (35%): the chloro- and bromo-substrates again track the secondary amine, while the iodo-substrate shows competing de-hydroiodination instead.

An electron-donating substituent was well tolerated (*meta*-methoxy, 80%), and the method is not confined to benzonitriles: phenylacetonitrile reduced to phenethylamine in 46% yield, again limited by the dialkylamine by-product. Isolated yields therefore range from moderate to good (35–92%), and conditions optimized on the *ortho*-fluoro substrate may need re-optimization elsewhere. The scope seems to depend less on the steric or electronic demand of the nitrile itself, and more on whether Cu(II) can engage the nitrogen lone pair as the mechanism requires.

6. Spectroscopic evidence for the copper–nitrile intermediate

To support the proposed κ^1-N activation mode, we characterized the complex between *o*-fluorobenzonitrile and $CuCl_2$ (**1-RCN-Cu**) by ATR FT-IR and XPS, on material recovered after step 1.

The IR spectrum (Figure 17) shows two bands in the C≡N stretching region: 2237.5 cm^{-1}, from residual free nitrile, and 2274.5 cm^{-1}, blue-shifted by +37 cm^{-1}, from the coordinated nitrile. A blueshift of this size is characteristic of end-on (κ^1-N) coordination to a Lewis-acidic metal:[174] σ-donation from the nitrile lone pair removes electron density from a weakly antibonding orbital, strengthening and shortening the C≡N bond. Because Cu(II) is d^9, π-backdonation is negligible and a positive shift is expected. Extending the milling time at 1:1 stoichiometry (30, 45, 60 min) shrank the free-nitrile band progressively, while two coordinated bands grew in, at 2254 and 2275 cm^{-1}, assigned to an open κ^1-N form and to a κ^2-N,F chelate in which the *ortho*-fluorine engages the second copper of a Cu_2Cl_4 dimer.

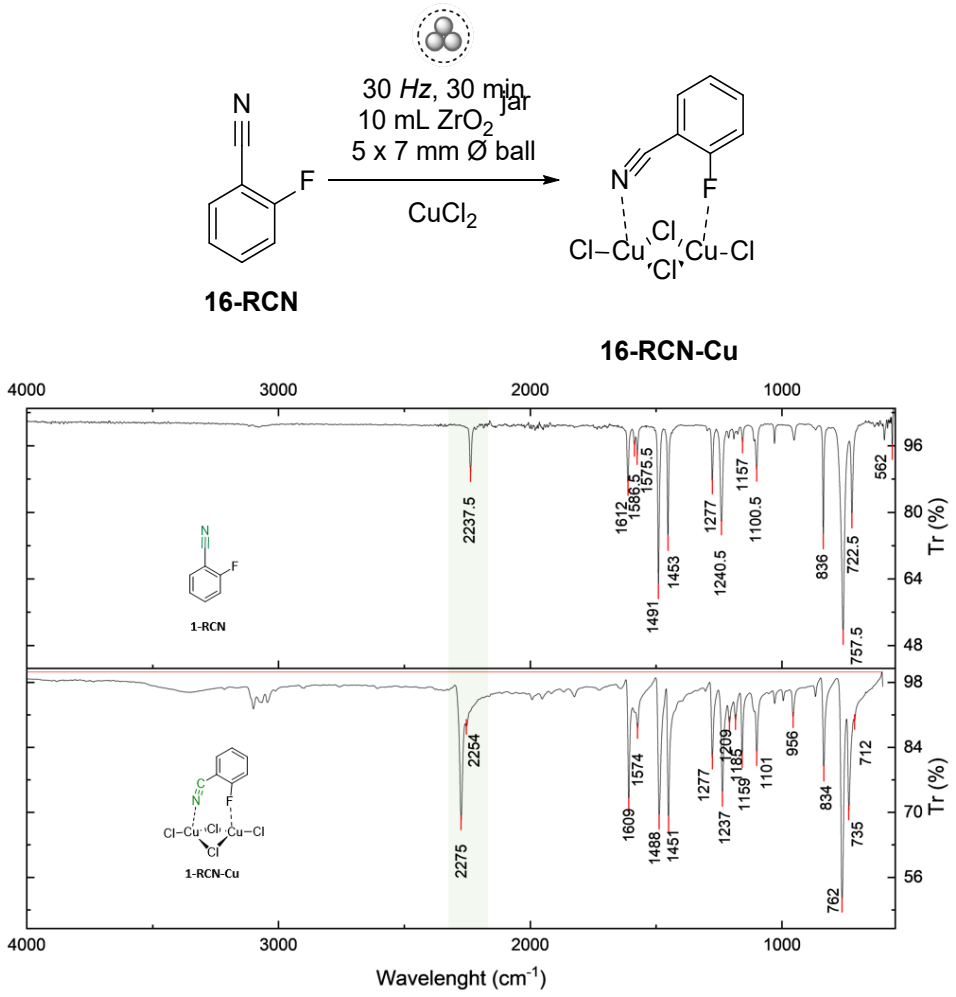


Figure 17. *Synthesis of* ***16-RCN-Cu*** *by milling, and ATR-FT-IR spectra of free* ***16-RCN*** *and of the crude mixture after milling.*

Aiming to elucidate the complex structure, XPS analyses were conducted (Figure 18). Because *o*-fluorobenzonitrile is a liquid, and poorly suited to solid-state acquisition under vacuum, we built a free-nitrile N 1s reference from the solid *ortho*-chloro, -bromo and -iodo analogues. Their binding energies were essentially identical (399.1–399.2 eV), so we adopted 399.2 eV as the reference, corroborated by the literature value for polymethacrylonitrile (399.6 eV).[175] On complexation, the N 1s shifts to 399.7 eV, consistent with σ-donation to Cu(II) depleting electron density at nitrogen (Table 13).[176]

The Cu $2p_{3/2}$ region resolves into two copper environments, each with its own shake-up satellite, a signature restricted to the open-shell $3d^9$ configuration of Cu(II) and absent for Cu(I) or Cu(0) (Figure 18).[177] One component, at 935.0 eV, matches uncoordinated $CuCl_2$ and is assigned to copper coordinated only by halogens; the other, at 932.5 eV, is assigned to the nitrogen-bound copper, whose lower binding energy reflects the electron density donated by the nitrile. The surface N:Cu (932.5 eV) ratio of about 1:1 matches a single κ^1-N-coordinated nitrile per nitrogen-bound copper.

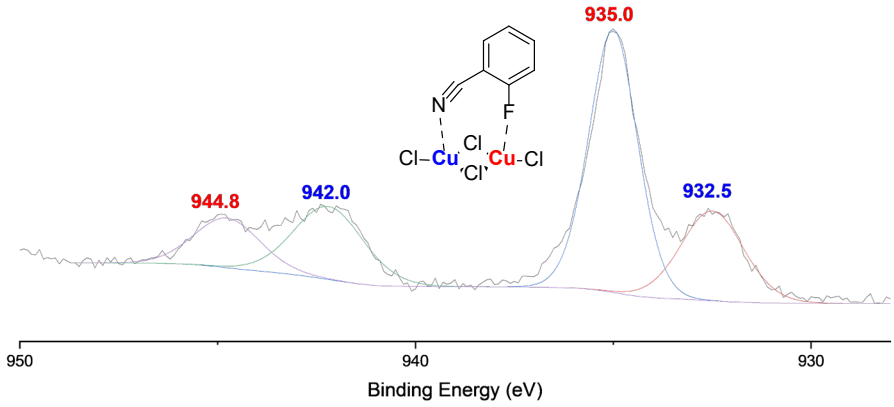


Figure 18. *Deconvoluted Cu $2p_{3/2}$ XPS spectrum of* ***16-RCN-Cu****, showing two Cu(II) environments (Cu–N at 932.5 eV; Cu–Cl at 935.0 eV) each with its own shake-up satellite, in agreement with the chelated κ^2-N,F structure.*

Table 13*. XPS core-level binding energies (eV) and surface atomic percentages of the Cu 2p, N 1s and Cl 2p regions of the* ***16-RCN-Cu*** *complex.*

Entry	Photoelectron	Binding Energy (eV)	Atomic %
1	Cu $2p_{3/2}$ (Cu···NC)	932.5	5.5
2	Cu $2p_{3/2}$ (Cu-Cl)	935.0	12.4
3	Cu $2p_{3/2}$ (sat)	942.2	5.0
4	Cu $2p_{3/2}$ (sat)	944.8	3.2
5	N 1s (N≡C)	399.7	6.9
6	Cl $2p_{3/2}$ (Cl-Cu)	199.0	66.8

The three observations, a blue-shifted C≡N stretch, a raised nitrile N 1s binding energy, and a lowered binding energy at the nitrogen-bound copper, all point the same way: κ^1-N coordination to Cu(II), and for the *ortho*-fluoro substrate a κ^2-N,F chelate.

7. Conclusions

This chapter reported the first mechanochemical protocol for reducing nitriles to primary amines, using ammonia borane as a genuine hydride donor and $CuCl_2$ as a Lewis-acidic activator. Optimization fixed the working stoichiometry (0.5 equiv. $CuCl_2$, 5 equiv. AB) and the milling parameters, and showed that the energy delivered per impact, not the cumulative energy input, predicts yield; ZrO_2 is the recommended jar and ball material. A panel of aromatic and benzylic nitriles reduced in moderate to good yield (35–92%), with over-alkylation to a dibenzylic secondary amine as the main competing pathway, while substrates bearing a nitro group, a reactive vinyl group, or a competing pyridine nitrogen fell outside the scope. FT-IR and XPS gave converging evidence for end-on κ^1-N coordination, identifying Lewis-acid activation of the nitrile as the design principle behind the reaction.

This chapter pursues a different objective from Chapters I to III. Those chapters targeted compounds that are already manufactured, and showed that mechanochemistry can produce them more sustainably than the solution routes it

replaces. Here the target is the reaction itself. Nitrile reduction had no ball-milling precedent, even though primary amines are central intermediates in pharmaceuticals, agrochemicals and fine chemicals. Establishing this transformation under milling conditions therefore adds a new entry to the mechanochemical toolbox. It supports the broader argument of this thesis: widening the range of reactions available to mechanochemistry is also a contribution to sustainable synthesis, alongside the cleaner re-synthesis of known targets.

Introduction Chapitre V

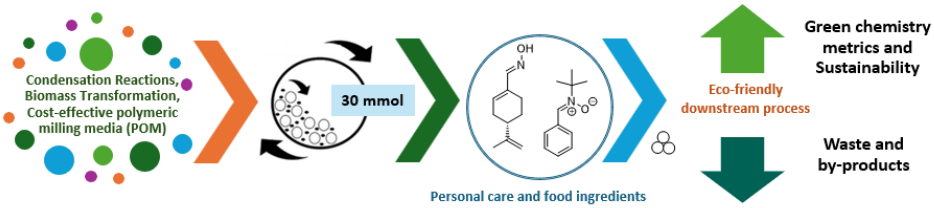
Les chapitres I à III ont montré que les méthodes mécanochimiques peuvent remplacer la synthèse en solution pour des produits agrochimiques et deux médicaments essentiels de l'OMS. Ce chapitre examine si la même approche convient aux ingrédients utilisés dans l'alimentation et les soins personnels, pour lesquels l'utilisation de solvants, la production de déchets et la pureté des produits sont des préoccupations tout aussi pressantes.

Deux cibles ont été sélectionnées. La première est la (*S*)-(−)-périllartine (**25**), un édulcorant naturel de type oxime obtenu à partir du (*S*)-périllaldéhyde, un aldéhyde terpénique renouvelable issu de l'huile de périlla. La seconde est la *N*-tert-butyl-α-phénylnitrone (PBN, **26**), un antioxydant utilisé dans les formulations cosmétiques. Toutes deux sont préparées par la même condensation d'un aldéhyde avec un sel d'hydroxylamine, une réaction simple bien adaptée au broyage sans solvant. Une synthèse antérieure de la PBN par broyage à billes dans un équipement en acier inoxydable avait été rapportée par Lamaty et ses collaborateurs,[182] mais le risque de contamination métallique rend ce dispositif inadapté à un ingrédient destiné aux soins personnels. Ce chapitre répond à cette limitation et étudie systématiquement l'effet des matériaux de broyage pour les deux cibles. Il introduit également des jarres en poly(oxyméthylène) (POM) fabriquées au laboratoire comme alternative sans fluor et sans métal aux réacteurs en PTFE plus couramment utilisés.

Les performances environnementales de chaque voie ont été évaluées par rapport à celles de la voie correspondante en solution à l'aide de trois outils complémentaires, CHEM21, DOZN™ 3.0 et EcoScale, afin que la comparaison prenne en compte conjointement l'efficacité massique, le profil de danger et l'impact des solvants.

Les objectifs spécifiques de ce chapitre étaient les suivants :

- préparer la (*S*)-(−)-périllartine (**25**) et la PBN (**26**) par broyage à billes vibrant et planétaire, à partir de précurseurs peu coûteux et facilement accessibles, et éviter les solvants organiques même lors de l'étape de récupération ;
- déterminer comment les matériaux de broyage (acier inoxydable, zircone, PTFE et POM fabriqué au laboratoire) et le choix de la base influencent la conversion et la sélectivité ;
- comparer les voies mécanochimiques aux voies correspondantes en solution à l'aide de trois outils de chimie verte (CHEM21, DOZN™ 3.0 et EcoScale), afin que la comparaison prenne également en compte le traitement postréactionnel.



V - Motivation and aims of the present work

Chapters I to III showed that mechanochemical methods can replace solution-phase synthesis for agrochemicals and two WHO's essentials medicines. This chapter asks whether the same approach works for ingredients used in food and personal care, where solvent use, waste generation, and product purity are equally pressing concerns.

Two targets were selected. The first is (*S*)-(−)-perillartine (**25**), a natural oxime sweetener obtained from (*S*)-perillaldehyde, a renewable terpene aldehyde from perilla oil. The second is *N*-tert-butyl-α-phenylnitrone (PBN, **26**), an antioxidant used in cosmetic formulations. Both are made by the same condensation of an aldehyde with a hydroxylamine salt, a simple reaction well suited to solvent-free milling. A prior synthesis of PBN by ball milling in stainless steel had been reported by Lamaty and coworkers,[178] but the risk of metal contamination makes that set-up unsuitable for a personal-care ingredient. This chapter addresses that limitation and maps the effect of the grinding media systematically for both targets. It also introduces in-house poly(oxymethylene) (POM) jars as a fluorine-free, metal-free alternative to more common PTFE vessels.

The greenness of each route was assessed against its solution-based counterpart using three complementary tools, Chem21, DOZN™ 3.0, and EcoScale, to ensure the comparison captures mass efficiency, hazard profile, and solvent impact together.

The specific aims of this chapter were:

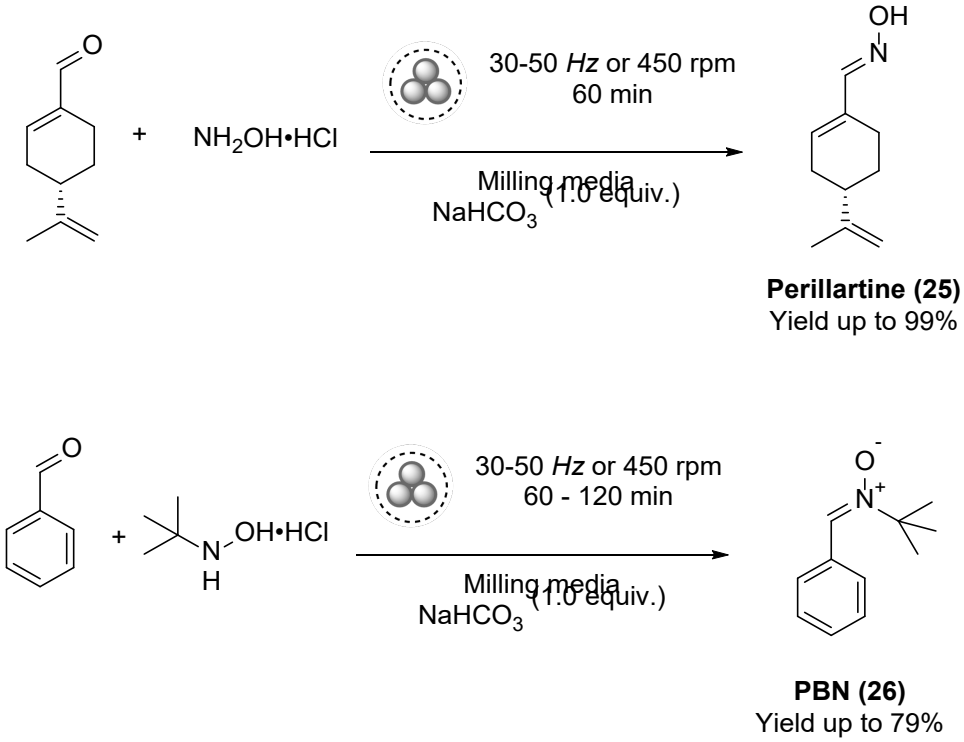
- To prepare (*S*)-(-)-perillartine (**25**) and PBN (**26**) by vibratory and planetary ball milling, from inexpensive and readily available precursors, and to avoid organic solvents even in the recovery step.
- To map how the milling media (stainless steel, zirconia, PTFE and in-house POM) and the choice of base affect conversion and selectivity.
- To benchmark the mechanochemical routes against their solution-based counterparts, using three green-chemistry tools (Chem21, DOZN™ 3.0 and EcoScale), so that the comparison also accounts for the work-up.

Chapter V — Mechanochemical Synthesis of Food and Personal-Care Ingredients by Ball Milling

1. Result and discussion

As set out in the general introduction, the value of a mechanochemical route is best judged on the whole workflow, and not on the isolated reaction. We therefore examined both targets under a range of milling conditions. We then carried the two best protocols through a full green assessment (see the comparative greenness assessment below).

Both **25** and **26** were prepared by the same one-step condensation. An aldehyde was milled with a hydroxylamine hydrochloride salt and one equivalent of base (Scheme 15). Both products have a low solubility in water. They were therefore recovered without organic solvent, by precipitation with aqueous sodium bisulfite (10% w/w), followed by filtration and drying. No chromatography or other waste intensive workup was needed at any stage.



Scheme 15. *Mechanochemical condensation of an aldehyde with a hydroxylamine to give (S)-(-)-perillartine (**1**) and PBN (**2**).*

2. (S)-(-)-Perillartine

Perillartine formed cleanly from the first attempt. We milled equimolar (*S*)-perillaldehyde, hydroxylamine hydrochloride and $NaHCO_3$ at 30 *Hz* for 1 h. We used a stainless-steel jar with two 7 mm steel balls. This gave perillartine (**25**) in 99% yield (Table 14, entry 1), with full selectivity for the *E*-oxime. The result needed no further optimization.

The milling parameters were not neutral, however. We kept the same steel jar, but we replaced the two 7 mm balls with fifteen smaller 5 mm balls. The yield then dropped to 73% (Table 14, entry 2), and unreacted aldehyde remained. The two set-ups deliver a similar total energy, but they differ in the energy per impact. The smaller balls transfer less energy per collision (3.6 *vs* 9.9 mJ).[30] A lower per-impact energy slows the condensation.[94] This leaves more time for a competing side reaction, the hydration of the aldehyde, to consume the starting material.

The jar material shaped this balance further. We replaced stainless steel with zirconia, under otherwise matched conditions. The yield rose from 73% to 91% (Table 14, entry 5), even though the cumulative energy was lower. We attribute this to heat management. Stainless steel conducts heat much better than zirconia. Reported values are about 15 $Wm^{-1}K^{-1}$ for austenitic stainless steel,[179] and only 2–3 $Wm^{-1}K^{-1}$ for dense yttria-stabilized zirconia near room temperature.[180] In the steel jar, more of the impact energy is dissipated as bulk heating, which favors the hydration side reaction. In the zirconia jar, the poorer conductivity keeps the energy more local, which favors the condensation. The broader point is that higher total energy did not lead to a higher yield.

The same trend is held in a planetary mill. Zirconia again outperformed stainless steel (98% *vs* 88%; Table 14, entries 13 and 14). Under the best conditions, up to 4.5 g of **25** was obtained in a single run.

We then treated the jar material as a design choice in its own right, and we introduced in-house POM jars. Across matched experiments, POM gave the highest yields, regardless of the ball material. It was ahead of zirconia, stainless steel and PTFE, and it matched optimized stainless steel. For example, POM gave 98% while PTFE gave 89% under the same conditions (Table 14, entries 9 and 8). POM therefore behaves as a practical, fluorine-free alternative to PTFE. It also avoids the metal abrasion associated with steel jars.[36]

The base also mattered. Sodium hydroxide gave no product, and only an off-colour paste. Sodium carbonate gave 78%. The milder $NaHCO_3$ remained the best choice. Dipotassium phosphate (K_2HPO_4) performed almost as well. Unlike $NaHCO_3$, it releases no CO_2 during milling. This is a useful feature for closed jars at a larger scale, where gas build-up is a safety concern. On this basis, the reaction was scaled to 30 mmol in a planetary mill, without loss of yield (90–91%).

Table 14. *Mechanochemical synthesis of (S)-(-)-perillartine (**25**) with different grinding media.*

Entry[a]	Jar	Ball	Balls (n)	Ø (mm)	m_{balls} (g)	E_{total} (kJ)	E_{impact} (mJ)	Yield (%)
1[b]	SS	SS	2	7	2.8	21.3	9.9	99
2[b]	SS	SS	15	5	7.6	57.3	3.6	73
3[b]	PTFE	SS	15	5	7.6	57.3	3.6	95
4[b]	POM	SS	15	5	7.6	57.3	3.6	96[a]
5[b]	ZrO_2	ZrO_2	15	5	6.2	46.9	2.9	91
6[b]	POM	ZrO_2	15	5	6.2	46.9	2.9	98
7[b,c]	PTFE	ZrO_2	15	5	6.2	46.9	2.9	90
8[b,c]	PTFE	SS	2	7	2.8	21.3	9.9	89
9[b,c]	POM	SS	2	7	2.8	21.3	9.9	98
10[d]	SS	SS	10	5	5.1	38.6	3.6	95
11[d]	PTFE	SS	8	5	4.1	30.9	3.6	98
12[d]	PTFE	ZrO_2	8	5	3.3	25.3	2.9	96
13[e]	ZrO_2	ZrO_2	30	5	12.4	18.6	6.0	98
14[e]	SS	SS	30	5	15.2	22.7	7.3	88[f]
15[c,e]	ZrO_2	ZrO_2	110	5	45.5	107.4	11.3	90[g]
16[c,e]	SS	SS	110	5	55.7	131.0	13.8	91[g]

[a] Reaction scale: 4.0 mmol except for entry 4 (2.0 mmol). Equimolar amounts of reagents were always used. 100% conversion was always obtained except for entry 2. The product was always recovered by precipitation using 10% aqueous $NaHSO_3$. [b] Reaction conditions: Horizontal vibrating ball-mill (MM400) 30 *Hz*, 1 h, 10 mL jar. The geometry of the milling vessel was identical, including for the in-house made POM jar. [c] K_2HPO_4 was used as base (1 equiv.), at 30 *Hz*, 1 h in a horizontal vibrating ball-mill (MM400). [d] Vertical vibrating ball-mill (P23): 50 *Hz*, 1 h. [e] Planetary ball-mill (P7 classic: entries 13 and 14; PM100: entries 15 and 16): 450 rpm, 1 h. The reaction scale was 4.0 mmol (entries 13 and 14) or 30 mmol (entries 15 and 16). [f] 10% of residual aldehyde was detected in the crude mixture (determined by 1H NMR analyses). [g] Corrected yield calculated from isolated product using qNMR, as (S)-perillaldehyde used in these batches contained a 10% of cuminaldehyde as an impurity.

3. N-tert-butyl-α-phenylnitrone

We next applied the same condensation to PBN. Here, benzaldehyde was milled with *N-tert*-butyl hydroxylamine hydrochloride and one equivalent of base. A solvent-free ball-milling synthesis of PBN in a stainless-steel jar had already been reported by our group, and it served as the benchmark (Table 15, entry 1, 100% yield).[10] Our aim was to find a milling set-up that avoids residual metal contamination, as we had done for perillartine. Such a set-up is better suited to a personal-care ingredient.

PBN proved more sensitive to the milling conditions than perillartine. We first used fifteen 5 mm steel balls at 30 *Hz* for 2 h. The cumulative energy was high (114.6 kJ), but the yield fell to 10%, and most of the starting material was recovered (Table 15, entry 2). This confirmed the trend seen for perillartine. A higher total energy does not help. Instead, it can favor the hydration side reaction.

We then held the cumulative energy constant and varied only the jar. The yield tracked the jar material. Replacing the steel jar with a softer polymeric jar (POM or PTFE) raised the yield to 45% (Table 15, entries 4 and 5). Among the combinations tested at 30 Hz, a POM jar with zirconia balls gave the best result (65%; Table 15, entry 6). A zirconia

jar with zirconia balls performed similarly (76%; Table 15, entry 3). Once again, softer or less conductive jars limited the heating that drives aldehyde hydration.

The behavior in the planetary mill was informative. A zirconia jar gave 79% (Table 15, entry 10), while a steel jar gave only 10% under otherwise similar conditions (Table 15, entry 11). This is notable, because the same steel benchmark had given a quantitative yield in the vibratory mill.[178] Zirconia therefore became the material of choice in the planetary mill. One combination was unproductive: a PTFE jar with zirconia balls gave no product at all (Table 15, entry 9), despite only a small difference in cumulative energy from a working set-up.

The *Z*-nitrone was formed with full selectivity in every case. The product was recovered by the same solvent-free work-up. Overall, PBN could be prepared in a useful yield (up to about 79%) in zirconia or POM jars. This was achieved without organic solvent, and without the residual metal expected from steel jars. The lower yields, relative to perillartine, reflect the greater sensitivity of this substrate to the energy and heat balance. They do not reflect a limitation of the solvent-free approach.

Table 15. *Mechanochemical synthesis of PBN (**26**) with different grinding media.*

Entry[a]	Jar	Ball	Balls (n)	Ø (mm)	m_{balls} (g)	E_{total} (kJ)	E_{impact} (mJ)	Yield (%)
1[b]	SS	SS	2	7	2.8	42.6	9.9	100[178]
2[c]	SS	SS	15	5	6.2	114.6	3.6	10
3[c]	ZrO_2	ZrO_2	15	5	6.2	93.8	2.9	76
4[c]	PTFE	SS	15	5	7.6	114.6	3.6	45
5[c]	POM	SS	15	5	7.6	114.6	3.6	45
6[c]	POM	ZrO_2	15	5	6.2	93.8	2.9	65
7[d]	SS	SS	10	5	5.1	38.6	3.6	74
8[d]	PTFE	SS	8	5	4.1	30.9	3.6	67
9[d]	PTFE	ZrO_2	8	5	3.3	25.3	2.9	0
10[e]	ZrO_2	ZrO_2	30	5	12.4	18.6	5.6	79
11[e]	SS	SS	30	5	15.2	22.8	7.3	10

[a] Reaction scale: 4.0 mmol, except for entry 7 (2.0 mmol). Equimolar amounts of reagents were always used. 100% conversion was always obtained except for entry 2. The product was always recovered by precipitation in aqueous NaHSO3 10% w/w. Legend: SS = Stainless steel. [b] Reaction conditions reported previously.[178] [c] Horizontal vibrating ball-mill (MM400) 30 *Hz*, 2 h, 10 mL jar. The geometry of the milling vessel was identical, including for the in-house-made POM jar. [d] Vertical vibrating ball-mill (P23): 50 *Hz*, 1 h, 5 mL (entries 8 and 9) or 10 mL (entry 7) jar. [e] Planetary ball-mill (P7 classic): 450 rpm, 1 h using K_2HPO_4 as base (1.0 equiv.). The reaction scale was 4.0 mmol (12 mL jar).

4. Comparative Greenness Assessment

We then compared each mechanochemical route with its solution-based counterpart. As noted in the general introduction, a single metric can be misleading. We therefore used three complementary tools: Chem21, DOZN™ 3.0 and EcoScore, which working principles are described in the introduction (Section 4) and in the Annex 4.[181] For each target, the solution protocol chosen for comparison was the one closest in reagents and work-up (Table 16).

The mass-based picture from Chem21 was clear. For **25**, every quantitative metric improved on milling. The process mass intensity (PMI) fell from 65 to 21, and the E-factor

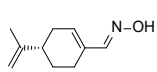
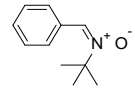
fell from 64 to 20 due to absence of solvent related waste production and resource efficient workup protocol that contributed to the amelioration of these metrics.[182] For **26**, the reagent-only metrics (atom economy and reaction mass efficiency) slightly favored the solution route. This was mainly because that route used a lower molecular weight base, and gave a higher yield. But this view is incomplete, because these metrics ignore the solvent. Once the solvent and the work-up were included, the mechanochemical route was far better. The PMI for **26** fell from 186 to 30, an almost six-fold reduction. For that target, the hazardous solvent (dichloromethane) and the silica used in the solution work-up accounted for more than 86% of the total PMI.

Also DOZN^{TM} 3.0 favored the mechanochemical route for both targets. For **25**, the aggregate score was about 7.5 times lower for milling than for solution (2.5 *vs* 18.7); a lower score is better. Likewise, the improvement came also in this case is mainly due to the removal of solvent, in both the reaction and the recovery.

The comparison of the two hazard-aware tools is worth spelling out, because it shows why one tool is not enough. The routes selected for **26** comparison where: the solution route that gives 97% yield but recovers the product from dichloromethane; and our milled route in a POM/ZrO_2 grinding media that gives 65% yield with an aqueous work-up (Table 2, entry 6). DOZN^{TM} 3.0 ranked the mechanochemical route as the greenest, because it penalized a lot the solvent heaviness of the solution-based route and the environmentally hazardous choice of the solvent used for recovery.

EcoScale scores remains competitive even if the difference between the difference in scores is minor (69 for the mechanochemical route *vs* 65 for the solution based method), the differences arise from different sources: for the solution the main penalties were due the concern related to the use of DCM and AcOEt in the column chromatography which resulted in the worse score, while the drawbacks for the mechanochemical route were due to the lower yield.

Table 16. *Comparison of green chemistry metrics by Chem21, DOZN™ and EcoScale toolkits for solution-based vs. mechanochemical methods in the preparation of (S)-(-) perillartine (**25**) and N-tert-butyl-α-phenylnitrone (PBN) (**26**).*

	Solution synthesis vs mechanochemical conditions					
Metrics[a,b] and Scores	 **(25)**			 **(26)**		
AE	40.0	vs	**54.4**	**58.5**	vs	56.1
RME	24.4	vs	**53.1**	**54.2**	vs	36.5
OE[c]	60.9	vs	**97.6**	**92.7**	vs	65.0
PMI	65.1[c]	vs	**21.3**	185.5[c]	vs	**29.9**
***E*-factor**	64.1[c]	vs	**20.3**	184.5[c]	vs	**28.9**
Solvent	H_2O		No solvent	CH_2Cl_2		No solvent
Work-up, recovery	Filtration, Recryst. (EtOAc, *c*-hex)		Filtration	Filtration (EtOAc, SiO_2)		Filtration
Health and safety	H301, H351, H371, H373, H400		H410	H301, H360fd, H371, H373, H401, H412		H330, H350, H370, H372
DOZN SCORES						
Group 1	23.2	vs	**3.0**	8.4	vs	**4.3**
Group 2	2.4	vs	**0.7**	1.9	vs	**0.0**
Group 3	16.6	vs	**2.3**	6.0	vs	**2.9**
Aggregate	18.7	vs	**2.5**	6.9	vs	**3.4**
EcoScale	41	vs	**75**	65	vs	**69**

Legend: Green flag = preferred; amber flag = acceptable with some concerns; red flag = undesirable; n.a. = not applicable. For EcoScale the score is classified as: excellent (≥75), acceptable (≥50), or inadequate (<50). [a] The optimum value for AE, RME, and OE is 100%; for E-factor, the optimum value is 0, with PMI = E factor +1.[2] When comparing two processes, the one with the lowest PMI will be the greenest. [b] Experimental protocols used for metrics calculations. Methods in solution: for (**1**), protocol published by Gröger and coworkers was used;[183] for (**26**), protocol published by Cid and coworkers was used.[184] Mechanochemical methods: for (**25**), Table 1 entry 6; for (**26**), Table 2, entry 6. [c] OE = RME AE × 100.

5. Conclusion

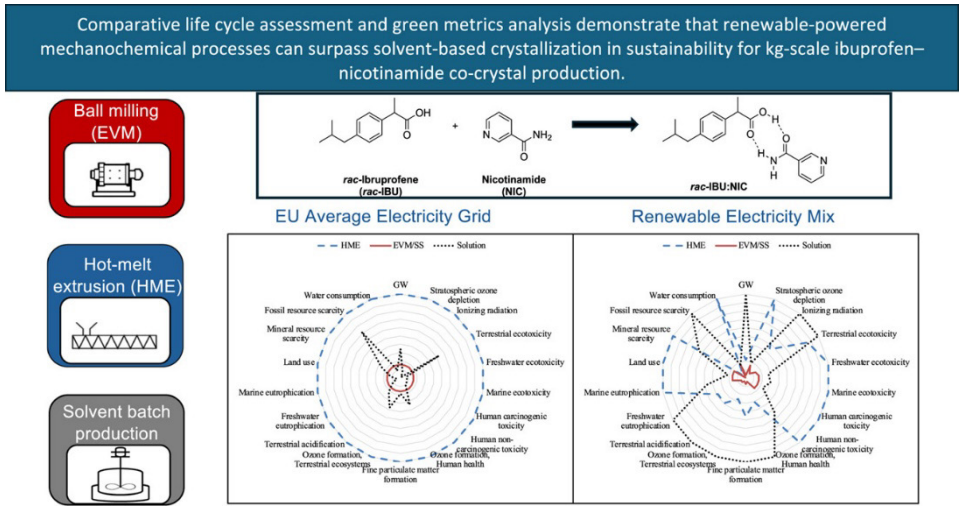
The study successfully scaled up mechanochemical synthesis of perillartine and PBN while showing that polymeric jars, especially POM, can be a safer and more sustainable alternative to traditional milling media. It emphasizes that mechanochemistry reduced solvent use, simplified work-up, and lowered environmental and safety risks overall, even when some individual metrics like yield were sometimes lower. This is a strong evidence that mechanochemical routes can be aligned with SSbD and green chemistry principles for food and personal care ingredients.

Introduction Chapitre VI

Les chapitres précédents ont montré que les voies mécanochimiques obtiennent de meilleurs résultats que la synthèse en solution selon les métriques de chimie verte fondées sur la masse. Ces métriques prennent en compte les réactifs et le traitement post-réactionnel, mais pas l'énergie ni les infrastructures. Ce chapitre passe de réactions individuelles à une comparaison complète des procédés de fabrication. En utilisant le *rac*-ibuprofène (*rac*-IBU), le cocristal pharmaceutique dont la préparation à l'échelle du kilogramme a déjà été présentée dans l'introduction, nous avons comparé quatre technologies mécanochimiques à un procédé conventionnel discontinu en solvant et évalué quantitativement chaque voie par une analyse du cycle de vie (ACV) du berceau à la porte.

Les objectifs spécifiques de ce chapitre étaient les suivants :

- compléter la comparaison des procédés mécanochimiques de préparation du *rac*-IBU à l'échelle du kilogramme en testant le broyage par attriteur (AM) et le broyage à marteaux (HM), aux côtés des voies déjà établies utilisant le broyeur vibrant excentrique (EVM) et l'extrusion à chaud (HME) ;
- comparer les métriques de chimie verte DOZN 3.0 de chaque voie mécanochimique viable à celles d'un procédé conventionnel de cristallisation discontinue dans l'éthanol ;
- examiner, par une analyse de scénarios, comment le profil environnemental de chaque voie évolue lorsque l'électricité provient de sources renouvelables et lorsque le procédé discontinu en solvant utilise de l'éthanol biosourcé ;
- identifier les conditions dans lesquelles la fabrication mécanochimique devient compétitive sur le plan environnemental par rapport à la cristallisation conventionnelle en solution, ou présente de meilleures performances.



VI - Motivation and aims of the present work

Previous chapters showed that mechanochemical routes score better than solution-based synthesis on mass-based green chemistry metrics. Those metrics count reagents and work-up, but not energy or infrastructure. This chapter turns from single reactions to a full manufacturing comparison. Using *rac*-ibuprofen:nicotinamide (*rac*-IBU:NIC), the pharmaceutical co-crystal already scaled to the kilogram in the introduction, we benchmarked four mechanochemical technologies against a conventional solvent-batch process, and we placed each route on a quantitative footing through a cradle-to-gate life cycle assessment (LCA).

The specific aims of this chapter were:

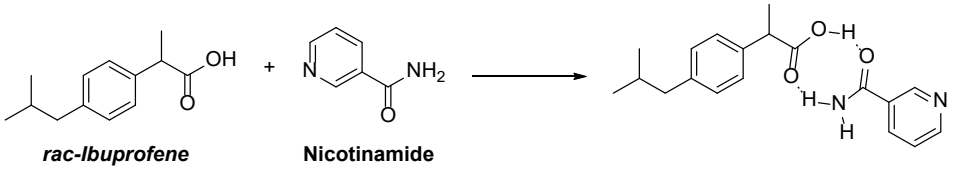
- to complete the kilogram-scale mechanochemical benchmark of *rac*-IBU:NIC by testing attritor milling (AM) and hammer milling (HM), alongside the eccentric vibrating mill (EVM) and hot-melt extrusion (HME) routes already established;
- to compare the DOZN 3.0 green chemistry metrics of every viable mechanochemical route against a conventional ethanol-based solvent-batch crystallization process;
- to test, through scenario analysis, how the environmental profile of each route changes when electricity is sourced from renewable generation, and when the solvent-batch process uses bio-based ethanol;
- to identify the conditions under which mechanochemical manufacturing becomes environmentally competitive with, or superior to, conventional solution crystallization.

Chapter VI — Scale-Up and Life Cycle Assessment of Mechanochemical *rac*-Ibuprofen:Nicotinamide Co-Crystallization

1. Context

Co-crystals are used to improve the solubility and dissolution rate of poorly soluble active pharmaceutical ingredients, without altering their covalent structure. The co-crystal of racemic ibuprofen with nicotinamide (*rac*-IBU:NIC) is a well-studied model system for this purpose, and it was used throughout this work as the benchmark pharmaceutical solid form (Scheme 16). As shown in the introduction (Section 3.4.1), its mechanochemical formation had already been demonstrated at the kilogram scale, in an eccentric vibrating mill and in a drum mill. What remained open was a direct comparison between several mechanochemical technologies, and a quantitative account of their environmental performance beyond mass-based metrics.

Chapters I and II showed, through the CHEM21, DOZN™ 3.0 and EcoScale toolkits, that mechanochemical routes generally outperform solution-based synthesis. These toolkits assess reagents, work-up and hazard, but they cannot capture the electricity consumed by a mill or the impact of the source used to generate it. A full judgement of sustainability needs a life cycle assessment, calculated at a comparable scale, a point already flagged at the close of Chapters I and II. This chapter developed that assessment for the first time for a mechanochemically produced pharmaceutical co-crystal.



***rac*-Ibuprofene (*rac*-IBU)** **Nicotinamide (NIC)** ***rac*-IBU:NIC**

Scheme 16. *Co-crystallization of rac-ibuprofen and nicotinamide to give the rac-IBU:NIC co-crystal.*

We compared five mechanochemical processes: an eccentric vibrating mill with a stainless-steel vessel (EVM/SS) and with an alumina vessel (EVM/Al_2O_3), an attritor mill (AM), a hammer mill (HM), and a hot-melt extruder (HME). Each was benchmarked against a solvent-batch ethanol crystallization process, representative of current industrial practice and built from a published patent.[185] The chapter first reports the DOZN™ 3.0 green metrics for every viable route, then develops a cradle-to-gate LCA for the routes carried through to full comparison. It closes by testing how far the environmental profile of mechanochemistry can improve once electricity is decarbonized.

2. Kilogram-scale co-crystallization by attritor and hammer milling

Attritor and hammer milling were used here to complete the technology comparison already opened by the EVM and drum mill work in the introduction. Nicotinamide and *rac*-ibuprofen were milled in equimolar amounts in both cases. In the attritor mill (0.5 L Teflon jar, zirconia balls, 1400 rpm), samples taken at 15, 60, 120 and 150 min showed

that conversion was already complete after 70 min. This time was therefore taken as the reference milling time for the scale-up calculations. Conversion was confirmed by PXRD and by a two-endotherm DSC profile (Figure 19a), the same diagnostic fingerprint used to follow co-crystal formation in the introduction. 1H-NMR of the isolated solid showed only the two expected components, with no by-product signals (Figure 19b).

The hammer mill (12 L alumina vessel, 140 rpm) was milled for a full 150 min but reached only 74% conversion. Because this fell well short of complete conversion, we excluded the hammer mill route from the environmental assessment that follows; it is retained here only as a negative result, since it shows that not every high-throughput mill is well suited to this reaction.

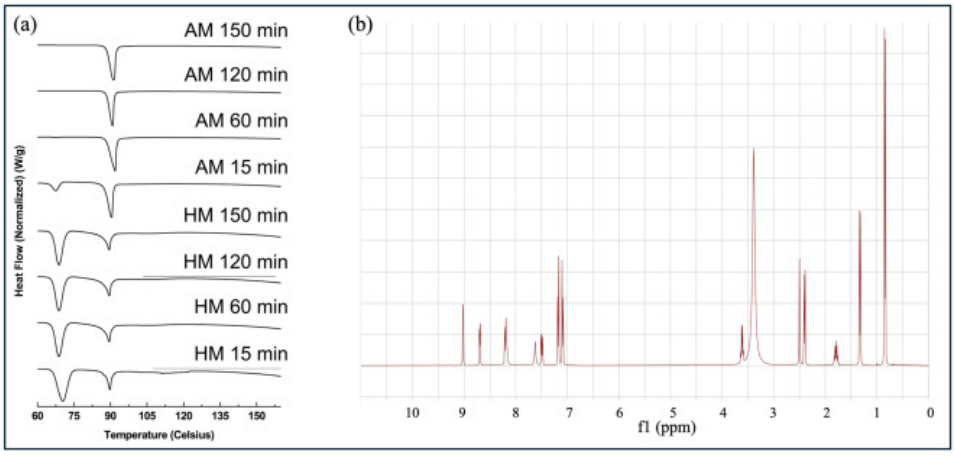


Figure 19. *Characterization of the AM and HM products. (a) DSC traces following co-crystal formation; the raw material and the co-crystal give clearly separated melting endotherms. (b) ^{1}H-NMR (DMSO-d_6) of the AM product after 120 min, showing no organic impurities.*

Table 17. *Kilogram-scale mechanochemical milling data obtained empirically in this study, used for the scaled-up process models and the LCA.*

Mill Type	Mass input (kg)	Mass output (kg)	Yield (%)	Time to reach yield (min.)	Energy consumption[a] (kWh)	Specific energy input (kWh/kg)	Internal volume (L)
EVM, SS[b]	2.80	2.80	100%	70	3.5	1.25	19.0
EVM, Al_2O_3[c]	1.40	1.40	100%	150	2.75	1.96	11.0
AM	0.15	0.15	100%	70	0.6	4	0.5
HM	2.2	2.2	74%	150	7.5	3.4	12

[a] Energy consumption was taken as the rated equipment power, a conservative upper bound. EVM data from Bodach and coworkers.[70] [b] EVM, using SS grinding media. [c] EVM, using alumina grinding media.

The EVM with the stainless-steel vessel was the most energy-efficient batch process, at 1.25 kWh per kg of product, less than a third of the specific energy of the attritor mill.

This single number already anticipates the LCA result below: within batch mechanochemistry, the choice of vessel and mill type has a direct, and large, effect on the electricity demand per kilogram of co-crystal.

3. Green chemistry metrics

We compared the DOZN 3.0 aggregate scores of the mechanochemical routes (EVM/SS, EVM/Al_2O_3, AM, and HME under two literature protocols)[82,186,187] against the solvent-batch process, run either with ethanol or with bio-ethanol.[185] All mechanochemical routes reached an aggregate score below 1, well ahead of the solvent-batch process (aggregate 1.76 for both ethanol and bio-ethanol) (Table 18).

Table 18. *DOZN 3.0 scores for the mechanochemical routes to rac-IBU:NIC, in batch and continuous, against the solvent-batch process.*[a,b]

Entry	Process	Grinding Media	Temperature (°C) / time (min)	Input / Output (kg)	DOZN™ 3.0 Scores[c]			
					Group 1	Group 2	Group 3	Aggregate
1	EVM	Al_2O_3	r.t. / 150	1.4 / 1.4[d]	0.28	0.00	0.47	0.34
2	EVM	SS	r.t. / 70	2.8 / 2.8[e]	0.28	0.00	0.47	0.34
3	AM	PFTE (ZrO_2 balls)	r.t. / 70	0.15 / 0.15	0.28	0.00	0.72	0.44
4	HME	SS	80 / 120	0.72 / 0.72[f]	0.28	0.07	0.47	0.34
5	HME	SS	90 / 120	0.1 / 0.1[g]	0.28	0.14	0.47	0.35
6	Solution	*n.a.*	60 / 360	1 / 1	1.07	2.70	1.76	1.50
7	Solution	*n.a.*	60 / 360	1 / 1	0.75	2.70	1.76	1.33

[a] Equimolar amount of *rac*-IBU and NIC were always processed. For the sake of comparison and normalization, the calculations are performed by assuming 100% mass recovery of the *rac*-IBU:NIC co-crystal. [b] Legend: Batch processes (entries 1–3) by (EVM, AM) *vs* continuous processes (entries 4–5) by HME, and solution process (entries 7–8), n.a.: Not applicable, r.t.: Room temperature. [c] Group 1: Improved resource use, Group 2: Increased energy efficiency, Group 3: Reduced human and environmental hazard. [d] The real (but not optimized) recovery reported in the original work was 81% of total mass input (1.14 kg). [e] The real (but not optimized) recovery reported in the original work was 94% of total mass input (2.64 kg). [f] Equimolar amount of *rac*-IBU (0.452 kg) and NIC (0.268 kg) were processes at a feed rate of 6 g/min with a screw speed of 50 rpm. [g] Equimolar amount of *rac*-IBU (0.063 kg) and NIC (0.037 kg) were processed at a feed rate of 0.05 kg/h with a screw speed of 30 rpm.

Every batch mill scored zero on Group 2, the energy-efficiency group, because milling runs at ambient temperature. HME needed heating to melt the reactants, which is penalized in Group 2, and the penalty grew with the process temperature: 0.07 at 80 °C against 0.14 at 90 °C. Even so, HME still matched the batch mills on the aggregate score, because its shorter processing time offset the heating penalty.

The AM route stood slightly apart, with a Group 3 score of 0.72 against 0.47 for the other mechanochemical routes. This came from a small increase in one of the resource-and-hazard-related sub-scores rather than from energy use, since AM shares the same ambient, solvent-free operation as EVM.

Replacing ethanol with bioethanol improved the solvent-batch process on Group 1 (1.07 to 0.75, entries 6 and 7) but doesn't reflect in a big enough improvement in the aggregate score (1.50 *vs* 1.33), since Group 2 depends on the heating step, not on the solvent's origin. This is the first sign of a pattern that runs through the rest of the chapter: reagent- and hazard-based metrics favor mechanochemistry outright, but energy, which DOZN 3.0 only captures as a temperature/time penalty, needed a full LCA to quantify properly.

4. Life cycle assessment

The LCA used a cradle-to-gate system boundary (Figure 20), covering upstream electricity, thermal energy and solvent supply, and the gate-to-gate co-crystallization step (mixing, heating, cooling, filtration, drying, recovery). The functional unit was 1 kg of isolated *rac*-IBU:NIC co-crystal, with identical feedstock masses (0.63 kg *rac*-IBU, 0.37 kg nicotinamide) assumed for every route, so that only the co-crystallization step itself was compared. Upstream API production was excluded from the comparison, since it is common to all routes; based on cradle-to-gate data for *rac*-ibuprofen alone, it was estimated separately at about 16.8 kg CO_2 eq. per kg of co-crystal. Background inventory data came from ecoinvent v3.11, with the EU-27 electricity mix as the baseline, and impacts were assessed with the ReCiPe 2016 midpoint (hierarchist) method.[188,189]

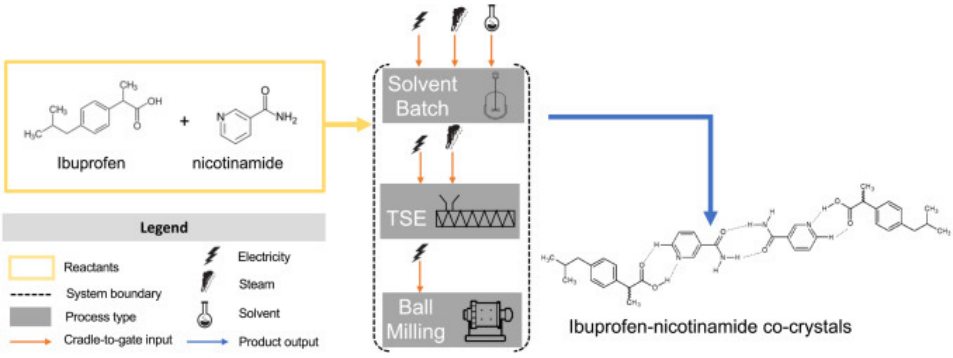


Figure 20. *Cradle-to-gate system boundaries for the solvent-batch, HME and ball-milling routes to rac-IBU:NIC. Reproduced with the permission of Elsevier from Reference 10.*

4.1 Base case: global warming impact

Under today's average European electricity mix, the EVM/SS route had the lowest global warming impact of all routes, nearly 50% below the solvent-batch benchmark (Figure 21). HME had the highest impact, about 3.5 times that of the solvent-batch process. This is the direct consequence of Table 1: HME needs more electrical and thermal energy per kilogram of product than any batch mill. The solvent-batch process itself performed better than HME and AM, mainly because ethanol is a comparatively benign solvent and 90% of it was recycled, which limits its net consumption.

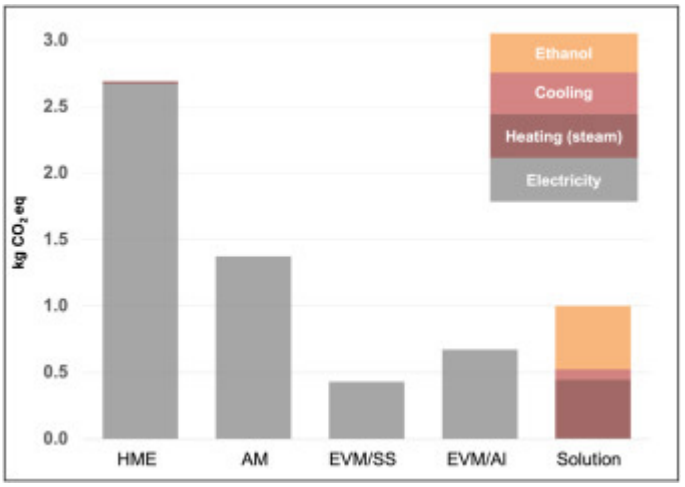


Figure 21. *Global warming impact of the mechanochemical routes and the solvent-batch process, base case (EU-27 electricity, fossil-based solvent). Reproduced with the permission of Elsevier from Reference 10.*

4.2 Beyond global warming: the wider impact profile

The picture changes once all 18 ReCiPe midpoint categories are considered. EVM/SS kept the lowest impact for five of them (global warming, terrestrial ecotoxicity, ozone formation, fossil resource scarcity, mineral resource scarcity) and was roughly on par with the solvent-batch process for two more (acidification, fine particulate matter). For most other categories, though, including human carcinogenic toxicity, the solvent-batch process performed better than every mechanochemical route. The reason traces back to the electricity mix: the EU-27 grid still draws 43% of its power from fossil sources, and electricity is the dominant contributor to impact for every mechanochemical route, batch or continuous.

4.3 Scenario analysis: decarbonizing electricity and solvent

Because the mechanochemical impact is tied almost entirely to electricity, we tested how the comparison shifts as the grid decarbonizes. Three scenarios were run in addition to the base case: (i) electricity from an 80/20 wind–photovoltaic mix; (ii) full electrification of all energy inputs on that same renewable mix; (iii) as (ii), but with the solvent-batch process also switched to fermentation-derived bioethanol (Figure 22).

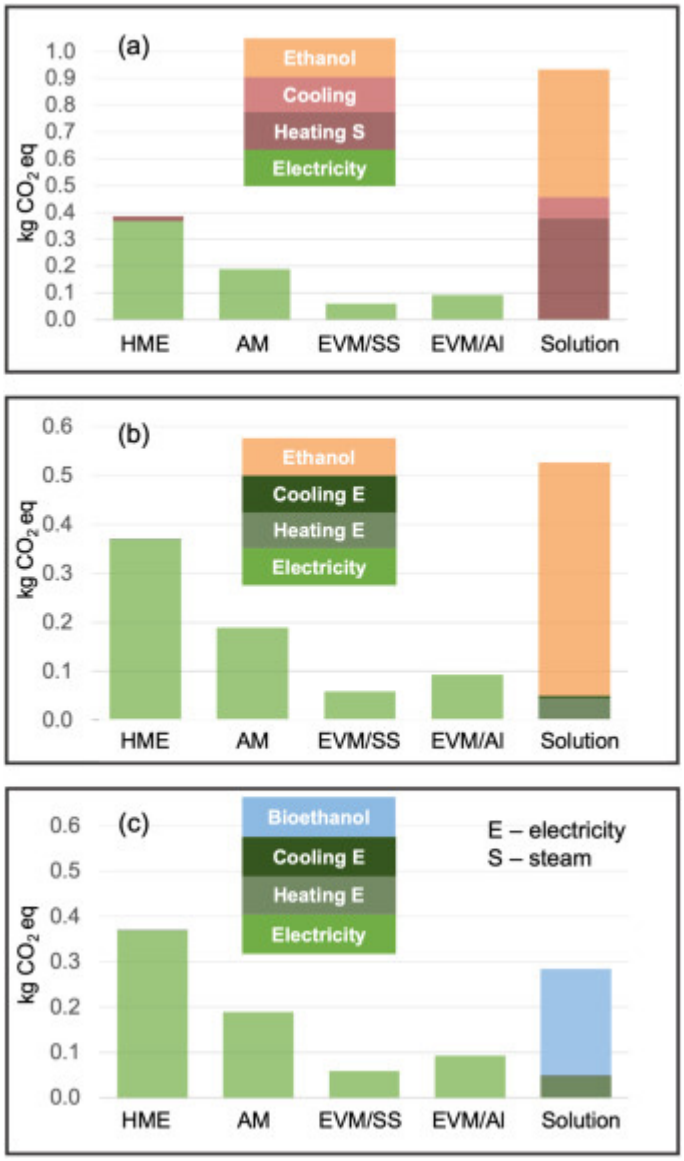


Figure 22. *Global warming potential of the mechanochemical routes against the solvent-batch process, under renewable electricity scenarios. Reproduced with the permission of Elsevier from Reference 10.*

Moving to renewable electricity lowered the global warming impact of every mechanochemical route and reduced that of EVM by more than 90% relative to the base case. Under this scenario, both EVM and HME became competitive with, or better than, the solvent-batch process, even when that process itself used bioethanol. Fossil resource scarcity followed the same trend, while human carcinogenic toxicity remained higher for most mechanochemical routes even under full renewable electrification, since this impact category is less sensitive to the electricity source than global warming is (see Annex 3 for full discussion).[190]

This result is structural, not incidental. The solvent-batch process's impact is tied to the manufacture of ethanol, which does not change with the electricity grid. Mechanochemistry's impact is tied almost entirely to electricity, and so it improves directly and proportionally as the grid decarbonizes. In a fully renewable-powered future, mechanochemical manufacturing of this co-crystal would very likely become the more sustainable choice on most impact categories, not only on global warming.

5. Batch versus continuous mechanochemistry: EVM and HME compared

EVM and HME sit at opposite ends of the mechanochemical process design space, and the LCA results make the trade-off explicit. EVM runs at ambient temperature and pressure, needs no heating step, and gave the lowest specific energy demand and the lowest life cycle impact of any route tested. Its batch mode, however, limits throughput and complicates integration with continuous downstream steps such as tableting. HME runs continuously, couples naturally to downstream formulation, and allows in-line monitoring, but its heating and screw operation raise its electrical and thermal demand, and with it its cradle-to-gate impact under a fossil-dominated grid

The choice between the two is therefore not only a question of chemistry, but of the energy system in which the plant operates. Under today's grid, EVM is the more defensible choice on environmental grounds. As the grid decarbonizes, HME's advantages in throughput and process integration could outweigh its current energy penalty, without its environmental profile becoming a limiting factor.

6. Conclusions

Five kilogram-scale mechanochemical routes to the *rac*-IBU:NIC co-crystal, EVM in two vessel materials, AM, HM and HME, were compared against a conventional solvent-batch process, first by green chemistry metrics and then by a cradle-to-gate LCA. HM did not reach full conversion within the timeframe tested and was excluded from the environmental comparison; every other mechanochemical route scored better than the solvent-batch process on the DOZN™ 3.0 aggregate, owing to the absence of solvent, high atom efficiency, and ambient operation.

The LCA told a more nuanced story. Under today's electricity mix, mechanochemical routes can carry a higher global warming and fossil resource burden than solvent-batch crystallization, because their footprint depends almost entirely on electricity, while the solvent-batch process benefits from a relatively benign, recyclable solvent. This changes sharply once renewable electricity is introduced: EVM's global warming impact fell by more than 90%, and both EVM and HME became competitive with the solvent-batch benchmark, even against bioethanol.

Taken together with Chapters I and II, this result completes the picture that mass-based green chemistry metrics alone cannot give: mechanochemistry's environmental case is strong on reagents and waste from the outset, and it becomes stronger, not weaker, as the electricity supply decarbonizes. This is the structural argument for treating mechanochemical manufacturing as a candidate technology for the ongoing transition to sustainable chemical and pharmaceutical production.

Conclusion Générale

L'objectif de ces travaux de thèse était d'évaluer dans quelle mesure la mécanochimie peut être utilisée pour la synthèse durable de molécules d'intérêt industriel, et d'appuyer chaque amélioration annoncée sur des données mesurées plutôt que sur des arguments généraux. Les molécules cibles couvrent quatre familles : les produits agrochimiques, les principes actifs pharmaceutiques, les ingrédients destinés à l'alimentation et aux soins personnels, et une forme solide pharmaceutique. Trois technologies ont été mises en œuvre : le broyage à billes, le mélange acoustique résonant (RAM) et l'extrusion bivis (TSE). Chaque voie de synthèse a été comparée à son équivalent en solution à l'aide de métriques de chimie verte, et, dans un cas, au moyen d'une analyse du cycle de vie complète.

Le chapitre I a permis de développer une amidation sans solvant, appliquée à l'échelle du gramme à trois fongicides commerciaux : le Mepronil, le Flutolanil et le Fluxapyroxad. Le CDI s'est révélé efficace pour la plupart des substrats, mais inadapté aux acides fluorés désactivés. Pour ces derniers, le 1,1′-oxalyldiimidazole (ODI) a été introduit et utilisé pour la première fois dans la formation de liaisons amide. Le suivi en temps réel de la température et de la pression a montré que l'activation mécanique ne gouverne que la première phase de la réaction. Une récupération en milieu aqueux a permis de s'affranchir des solvants organiques sur l'ensemble du procédé, et les deux outils d'évaluation ont classé la voie ODI comme la plus vertueuse parmi celles testées.

Le chapitre II a porté sur le transfert, du broyeur à billes vers le RAM, de l'amidation médiée par le TCFH appliquée à cinq fongicides SDHI commerciaux. Ce transfert n'a pas été une simple transposition : l'état physique de la base et l'effet d'un temps de traitement prolongé sont inversés d'une technologie à l'autre, car un broyeur vibrant exige un mélange suffisamment solide pour transmettre l'impact, alors que le RAM demande un milieu suffisamment fluide pour suivre le champ acoustique. Une fois ce point compris, le protocole a été appliqué sans modification de 2,5 mL à 240 mL, soit un facteur 160, et a fourni jusqu'à 35 g de produit par lot avec des rendements égaux ou supérieurs à 90 % pour quatre des cinq cibles. Aucune ré-optimisation n'a été nécessaire à aucune étape.

Le chapitre III a été consacré à la synthèse en continu, par extrusion bivis, de deux médicaments essentiels de l'OMS : la sulfadiazine argentique et la phénytoïne. Le remplacement du nitrate d'argent par l'oxyde d'argent(I) a supprimé les effluents nitratés du procédé, et la structure d'un intermédiaire jusqu'alors non décrit a été résolue. Pour la phénytoïne, l'optimisation de la base, de la stœchiométrie, de la température et du profil de vis a conduit à un produit de phase pure, sans recours au broyage assisté par liquide. L'extrusion bivis a donné le PMI total le plus faible des voies mécanochimiques comparées : 68,4, contre 93,9 pour le RAM et 383,6 pour le broyage à billes.

Le chapitre IV a établi la première réduction mécanochimique de nitriles en amines primaires, à l'aide de l'ammonia borane comme donneur d'hydrure et de $CuCl_2$ comme activateur acide de Lewis. Les nitriles aromatiques et benzyliques ont été réduits avec des rendements de 35 à 92 %. L'énergie délivrée par impact, et non l'énergie cumulée, s'est révélée être le paramètre prédictif du résultat. Les analyses FT-IR et XPS ont fourni des indications convergentes en faveur d'une coordination κ^1-N terminale du nitrile sur le cuivre.

Le chapitre V a décrit la préparation par broyage à billes de la perillartine et du PBN, respectivement un édulcorant de type oxime et un antioxydant cosmétique, à partir de précurseurs peu coûteux, avec une récupération par précipitation aqueuse et sans chromatographie. Des bols de broyage en poly(oxyméthylène) fabriquées au laboratoire ont été introduites comme alternative sans métal et sans fluor à l'acier et au PTFE, ce qui écarte le risque de contamination métallique pour des ingrédients destinés au contact humain.

Le chapitre VI a comparé cinq voies mécanochimiques à l'échelle du kilogramme conduisant au co-cristal *rac*-IBU:NIC, d'abord par les métriques de chimie verte, puis par une analyse du cycle de vie ‘’*cradle to gate*’’. Toutes les voies mécanochimiques abouties obtiennent un meilleur score agrégé DOZN™ 3.0 que le procédé conventionnel en solution. L'analyse du cycle de vie s'est révélée moins favorable dans le mix électrique actuel, ces voies dépendantes presque exclusivement de l'électricité. Avec une électricité renouvelable, l'impact sur le réchauffement climatique du broyage vibrant excentrique diminue de plus de 90 %, et cette technologie comme l'extrusion à chaud deviennent compétitives face au procédé de référence en solution.

Trois enseignements généraux se dégagent de ces travaux. D'abord, l'avantage d'une voie mécanochimique se joue sur l'ensemble du procédé et non sur la seule réaction : dans presque toutes les comparaisons présentées ici, c'est le traitement du brut réactionnel qui domine les métriques massiques. Ensuite, la chimie et l'équipement ne peuvent pas être optimisés séparément. Des paramètres favorables dans un broyeur vibrant peuvent être neutres, voire défavorables, en RAM, et le choix de l'agent d'activation est lié à celui de la technologie. Enfin, les métriques massiques sont nécessaires mais non suffisantes. Seule l'analyse du cycle de vie a montré que le bilan environnemental de la mécanochimie dépend en partie de la source d'électricité, et qu'il s'améliorera à mesure que celle-ci se décarbonera.

Certaines limites subsistent. L'économie d'atomes reste pénalisée par des agents d'activation de masse molaire élevée tels que le TCFH, le traitement aqueux n'a pas été optimisé pour toutes les cibles, et la dispersion de la chaleur aux échelles supérieures demande une étude complémentaire. Il s'agit là de problèmes pratiques plutôt que conceptuels.

La conclusion générale de ces travaux est que la reconception mécanochimique des voies de synthèse, associée à l'ajout de nouvelles transformations à la boîte à outils de la mécanochimie, constitue une stratégie efficace pour réduire l'empreinte environnementale de la production chimique en vue d’une mise à l’echelle industrielle dans le future.

General Conclusions

The aim of this thesis was to test how mechanochemistry can be used for the sustainable synthesis of industrially relevant molecules, and to support each claim of improvement with measured data rather than with general arguments. The work covered agrochemicals, active pharmaceutical ingredients, food and personal-care ingredients, and one pharmaceutical solid form. Three types of equipment were used: ball mills, resonant acoustic mixing (RAM), and twin-screw extrusion (TSE). Every route was benchmarked against its solution-based counterpart with green-chemistry metrics, and in one case with a full life cycle assessment. The main outcomes are summarized below.

- A solvent-free amidation was developed and applied to three marketed fungicides, Mepronil, Flutolanil and Fluxapyroxad, on a gram scale (**Chapter I**). CDI worked well for most substrates but failed on deactivated, fluorinated acids. For those, 1,1′-oxalyldiimidazole (ODI) was introduced, and used to form amides for the first time. Real-time temperature and pressure measurements showed that mechanical activation controls only the early part of the reaction. A water-based recovery kept the whole process free of organic solvents, and both toolkits ranked the ODI route as the greenest option tested.
- The TCFH-mediated amidation of five SDHI fungicides was transferred from the ball mill to RAM (**Chapter II**). The transfer was not direct: the physical state of the base and the benefit of longer processing are inverted between the two devices, because a mill needs a solid enough mixture to transmit an impact while RAM needs a fluid enough one to follow the acoustic field. Once this was understood, the protocol was applied unchanged from 2.5 mL to 240 mL, a 160-fold increase, and delivered up to 35 g per batch with yields at or above 90% for four of the five targets. No re-optimization was needed at any step. Counter to solution-based chemistry where optimization is required almost at every scale-up step.
- Two WHO essential medicines, silver(I) sulfadiazine and phenytoin, were prepared continuously by TSE (**Chapter III**). Replacing silver nitrate with silver(I) oxide removed nitrate waste from the sulfadiazine process, and the structure of a previously unreported intermediate was solved. For phenytoin, optimization of the base, the stoichiometry, the temperature and the screw profile gave a phase-pure product without liquid-assisted grinding. TSE gave the lowest total PMI of the mechanochemical routes compared (68.4, against 93.9 for RAM and 383.6 for ball milling).
- The first mechanochemical reduction of nitriles to primary amines was established, using ammonia borane as hydride donor and $CuCl_2$ as a Lewis-acidic activator (**Chapter IV**). Aromatic and benzylic nitriles were reduced in 35–92% yield. The energy delivered per impact, and not the cumulative energy input, was found to predict the outcome. FT-IR and XPS gave converging evidence for end-on κ^1-N coordination of the nitrile to copper.
- Perillartine and PBN, an oxime sweetener and a cosmetic antioxidant, were prepared by ball milling from inexpensive precursors, with recovery by aqueous precipitation and no chromatography (**Chapter V**). In-house poly(oxymethylene) jars were introduced as a metal-free and fluorine-free alternative to steel and PTFE, which removes the risk of metal contamination in ingredients intended for human contact.
- Five kilogram-scale mechanochemical routes to the *rac*-IBU:NIC co-crystal were compared with a conventional solvent-batch process by green metrics and by a

cradle-to-gate LCA (**Chapter VI**). All completed mechanochemical routes scored better on the DOZN™ 3.0 aggregate. The LCA was less favorable under the current electricity mix, because these routes depend almost entirely on electricity. With renewable electricity, the global warming impact of eccentric vibrating milling fell by more than 90%, and both it and hot-melt extrusion became competitive with the solvent-batch benchmark.

Taken together, these results support three general points. First, the advantage of a mechanochemical route is decided by the whole workflow and not by the reaction alone: in almost every comparison made here, the work-up dominated the mass-based metrics. Second, the chemistry and the equipment cannot be optimized separately. Parameters that improve a reaction in a vibrating mill can be neutral or harmful in RAM, and the choice of activating agent interacts with the choice of device. Third, mass-based metrics are necessary but not sufficient. Only the life cycle assessment showed that the environmental case for mechanochemistry rests partly on the electricity supply, and that it will strengthen as that supply decarbonizes.

Some limitations remain. Atom economy is still penalized by heavy activating agents such as TCFH, the aqueous work-up was not optimized for every target, and heat removal at larger scale needs further study. These are practical problems rather than conceptual ones. The broader conclusion of this thesis is that mechanochemical route redesign, together with the addition of new transformations to the mechanochemical toolbox, is a credible strategy for lowering the environmental footprint of chemical manufacturing at a scale that industry can use.

References

(1) Prat, D.; Wells, A.; Hayler, J.; Sneddon, H.; McElroy, C. R.; Abou-Shehada, S.; Dunn, P. J. CHEM21 Selection Guide of Classical- and Less Classical-Solvents. *Green Chem.* **2016**, *18* (1), 288–296. https://doi.org/10.1039/C5GC01008J

(2) Sheldon, R. A. The E Factor 25 Years on: The Rise of Green Chemistry and Sustainability. *Green Chem.* **2017**, *19* (1), 18–43. https://doi.org/10.1039/C6GC02157C

(3) Anastas, P. T.; Warner, J. C. *Green Chemistry: Theory and Practice*; Oxford University PressOxford, 2000. https://doi.org/10.1093/oso/9780198506980.001.0001

(4) Chemistry (IUPAC), T. I. U. of P. and A. *IUPAC - mechano-chemical reaction (MT07141)*. https://doi.org/10.1351/goldbook.MT07141

(5) Speight, I. R.; Ardila-Fierro, K. J.; Hernández, J. G.; Emmerling, F.; Michalchuk, A. A. L.; García, F.; Colacino, E.; Mack, J. Ball Milling for Mechanochemical Reactions. *Nat. Rev. Methods Primers* **2025**, *5* (1), 29. https://doi.org/10.1038/s43586-025-00401-2

(6) Stolle, A.; Szuppa, T.; Leonhardt, S. E. S.; Ondruschka, B. Ball Milling in Organic Synthesis: Solutions and Challenges. *Chem. Soc. Rev.* **2011**, *40* (5), 2317. https://doi.org/10.1039/c0cs00195c

(7) Fantozzi, N.; Volle, J.-N.; Porcheddu, A.; Virieux, D.; García, F.; Colacino, E. Green Metrics in Mechanochemistry. *Chem. Soc. Rev.* **2023**, *52* (19), 6680–6714. https://doi.org/10.1039/d2cs00997h

(8) Cuccu, F.; De Luca, L.; Delogu, F.; Colacino, E.; Solin, N.; Mocci, R.; Porcheddu, A. Mechanochemistry: New Tools to Navigate the Uncharted Territory of "Impossible" Reactions. *ChemSusChem* **2022**, *15* (17), e202200362. https://doi.org/10.1002/cssc.202200362

(9) Galant, O.; Cerfeda, G.; McCalmont, A. S.; James, S. L.; Porcheddu, A.; Delogu, F.; Crawford, D. E.; Colacino, E.; Spatari, S. Mechanochemistry Can Reduce Life Cycle Environmental Impacts of Manufacturing Active Pharmaceutical Ingredients. *ACS Sustainable Chem. Eng.* **2022**, *10* (4), 1430–1439. https://doi.org/10.1021/acssuschemeng.1c06434

(10) Patrascu, M.; Meuti, D.; Galant, O.; Nijem, S.; Diesendruck, C. E.; Casagrande, A.; Colacino, E.; Felderhoff, M.; Spatari, S. Sustainable Pharmaceutical Manufacturing Based on Mechanochemistry: A Life Cycle Assessment of Rac-Ibuprofen-Nicotinamide Cocrystallization Routes. *Sustainable Chem. Pharm.* **2026**, *51*, 102422. https://doi.org/10.1016/j.scp.2026.102422

(11) Nicholson, W. I.; Barreteau, F.; Leitch, J. A.; Payne, R.; Priestley, I.; Godineau, E.; Battilocchio, C.; Browne, D. L. Direct Amidation of Esters by Ball Milling. *Angew. Chem. Int. Ed.* **2021**, *60* (40), 21868–21874. https://doi.org/10.1002/anie.202106412

(12) Nikonovich, T.; Chatzigiannis, C. M.; Bordier, C.; Solorzano-Rodriguez, R.; Baier, D. M.; Ort, F. F.; Aav, R.; Leyssens, T.; Blanco-Ania, D.; Rutjes, F. P. J. T.; Kananovich, D.; Colacino, E. Mechanochemical Methods for Amide Bond Formation. *Chem. Rev.* **2026**, *126* (11), 6015–6080. https://doi.org/10.1021/acs.chemrev.5c00534

(13) Nguyen, Q.; Kim, T. S-Benzyl Isothiouronium Chloride as a Recoverable Organocatalyst for the Direct Reductive Amination of Ketones with Hantzsch Ester. *Synthesis* **2012**, *44* (13), 1977–1982. https://doi.org/10.1055/s-0031-1291125

(14) Nagao, A.; Kubota, K.; Ito, H. All-Step Mechanochemical Approach for the Rapid and Solventless Synthesis of Boscalid. *Synthesis* **2026**, *58* (06), 673–678. https://doi.org/10.1055/a-2744-6831

(15) Kubota, K.; Seo, T.; Ito, H. Solid-State Cross-Coupling Reactions of Insoluble Aryl Halides under Polymer-Assisted Grinding Conditions. *Faraday Discuss.* **2023**, *241*, 104–113. https://doi.org/10.1039/D2FD00121G

(16) Schneider, F.; Stolle, A.; Ondruschka, B.; Hopf, H. The Suzuki−Miyaura Reaction under Mechanochemical Conditions. *Org. Process Res. Dev.* **2009**, *13* (1), 44–48. https://doi.org/10.1021/op800148y

(17) Kubota, K.; Nagao, A.; Ito, H. Solvent-Free Zinc-Mediated Béchamp Reduction Using Mechanochemistry. *RSC Mechanochem.* **2025**, *2* (3), 389–393. https://doi.org/10.1039/D4MR00138A

(18) Schumacher, C.; Fritz, L.; Hanek, L. M.; Sidorin, V.; Brüx, D.; Bolm, C. Reshuffle Bonds by Ball Milling: A Mechanochemical Protocol for Charge-Accelerated Aza-Claisen Rearrangements. *Molecules* **2023**, *28* (2), 807. https://doi.org/10.3390/molecules28020807

(19) Takale, B. S.; Thakore, R. R.; Mallarapu, R.; Gallou, F.; Lipshutz, B. H. A Sustainable 1-Pot, 3-Step Synthesis of Boscalid Using Part per Million Level Pd Catalysis in Water. *Org. Process Res. Dev.* **2020**, *24* (1), 101–105. https://doi.org/10.1021/acs.oprd.9b00455

(20) Xu, J.; Lan, X.-B.; Xia, L.-J.; Yang, Y.; Cao, G. Synthesis and Process Optimization of Boscalid by Catalyst Pd-PEPPSI-IPrDtBu-An. *J. Serb. Chem. Soc.* **2021**, *86* (3), 247–256. https://doi.org/10.2298/JSC200330003X

(21) Len, C.; Duhan, V.; Ouyang, W.; Nguyen, R.; Lochab, B. Mechanochemistry and Oleochemistry: A Green Combination for the Production of High-Value Small Chemicals. *Front. Chem.* **2023**, *11*, 1306182. https://doi.org/10.3389/fchem.2023.1306182

(22) d'Agostino, S.; Azzali, A.; Casali, L.; Taddei, P.; Grepioni, F. Environmentally Friendly Sunscreens: Mechanochemical Synthesis and Characterization of β-CD Inclusion Complexes of Avobenzone and Octinoxate with Improved Photostability. *ACS Sustainable Chem. Eng.* **2020**, *8* (35), 13215–13225. https://doi.org/10.1021/acssuschemeng.0c02735

(23) Wehbe, L.; Bascou, R.; Nesterenko, A.; Guénin, E. Green Strategy for Sustainable Silk Lipopeptide Production Using Mechanochemistry. *ACS Sustainable Chem. Eng.* **2025**, *13* (5), 1882–1893. https://doi.org/10.1021/acssuschemeng.4c05049

(24) Solórzano-Rodríguez, R.; Fantozzi, N.; Casagrande, A.; Chatzigiannis, C. M.; Bordier, C.; Rando, P.; Colacino, E. Safe and Sustainable by Design (SSbD) Synthesis of Food and Personal Care Ingredients by Mechanochemistry. *ChemSusChem* **2026**, *19* (9), e202502491. https://doi.org/10.1002/cssc.202502491

(25) Carta, M.; Delogu, F. Ball Dynamics and Rate of Mechanically Induced Transformations in Oscillating Ball Mills. *Chemical Engineering Science* **2026**, *335*, 124495. https://doi.org/10.1016/j.ces.2026.124495

(26) James, S. L.; Adams, C. J.; Bolm, C.; Braga, D.; Collier, P.; Friščić, T.; Grepioni, F.; Harris, K. D. M.; Hyett, G.; Jones, W.; Krebs, A.; Mack, J.; Maini, L.; Orpen, A. G.; Parkin, I. P.; Shearouse, W. C.; Steed, J. W.; Waddell, D. C. Mechanochemistry: Opportunities for New and Cleaner Synthesis. *Chem. Soc. Rev.* **2012**, *41* (1), 413–447. https://doi.org/10.1039/C1CS15171A

(27) Colacino, E.; Carta, M.; Pia, G.; Porcheddu, A.; Ricci, P. C.; Delogu, F. Processing and Investigation Methods in Mechanochemical Kinetics. *ACS Omega* **2018**, *3* (8), 9196–9209. https://doi.org/10.1021/acsomega.8b01431

(28) Burmeister, C. F.; Kwade, A. Process Engineering with Planetary Ball Mills. *Chem. Soc. Rev.* **2013**, *42* (18), 7660. https://doi.org/10.1039/c3cs35455e

(29) Howard, J. L.; Cao, Q.; Browne, D. L. Mechanochemistry as an Emerging Tool for Molecular Synthesis: What Can It Offer? *Chemical Science* **2018**, *9* (12), 3080–3094. https://doi.org/10.1039/C7SC05371A

(30) Jafter, O. F.; Lee, S.; Park, J.; Cabanetos, C.; Lungerich, D. Navigating Ball Mill Specifications for Theory-to-Practice Reproducibility in Mechanochemistry. *Angew. Chem. Int. Ed.* **2024**, *63* (48), e202409731. https://doi.org/10.1002/anie.202409731

(31) Julien, P. A.; Malvestiti, I.; Friščić, T. The Effect of Milling Frequency on a Mechanochemical Organic Reaction Monitored by in Situ Raman Spectroscopy. *Beilstein J. Org. Chem.* **2017**, *13*, 2160–2168. https://doi.org/10.3762/bjoc.13.216

(32) Schmidt, R.; Martin Scholze, H.; Stolle, A. Temperature Progression in a Mixer Ball Mill. *Int. J. Ind. Chem.* **2016**, *7* (2), 181–186. https://doi.org/10.1007/s40090-016-0078-8

(33) Friščić, T.; Halasz, I.; Beldon, P. J.; Belenguer, A. M.; Adams, F.; Kimber, S. A. J.; Honkimäki, V.; Dinnebier, R. E. Real-Time and in Situ Monitoring of Mechanochemical Milling Reactions. *Nature Chem* **2013**, *5* (1), 66–73. https://doi.org/10.1038/nchem.1505

(34) Fischer, F.; Fendel, N.; Greiser, S.; Rademann, K.; Emmerling, F. Impact Is Important—Systematic Investigation of the Influence of Milling Balls in Mechanochemical Reactions. *Org. Process Res. Dev.* **2017**, *21* (4), 655–659. https://doi.org/10.1021/acs.oprd.6b00435

(35) Michalchuk, A. A. L.; Tumanov, I. A.; Boldyreva, E. V. Ball Size or Ball Mass – What Matters in Organic Mechanochemical Synthesis? *CrystEngComm* **2019**, *21* (13), 2174–2179. https://doi.org/10.1039/C8CE02109K

(36) Rappen, M. F.; Beissel, L.; Geisler, J.; Tietmeyer, S. T.; Graetz, S.; Borchardt, L. Polymer Vessels in Mechanochemical Syntheses: Assessing Material Performance. *RSC Mechanochemistry* **2024**. https://doi.org/10.1039/D4MR00059E

(37) Pickhardt, W.; Grätz, S.; Borchardt, L. Direct Mechanocatalysis: Using Milling Balls as Catalysts. *Chemistry – A European Journal* **2020**, *26* (57), 12903–12911. https://doi.org/10.1002/chem.202001177

(38) Hwang, S.; Grätz, S.; Borchardt, L. A Guide to Direct Mechanocatalysis. *Chem. Commun.* **2022**, *58* (11), 1661–1671. https://doi.org/10.1039/D1CC05697B

(39) Haley, R. A.; Zellner, A. R.; Krause, J. A.; Guan, H.; Mack, J. Nickel Catalysis in a High Speed Ball Mill: A Recyclable Mechanochemical Method for Producing Substituted Cyclooctatetraene Compounds. *ACS Sustainable Chem. Eng.* **2016**, *4* (5), 2464–2469. https://doi.org/10.1021/acssuschemeng.6b00363

(40) Fulmer, D. A.; Shearouse, W. C.; Medonza, S. T.; Mack, J. Solvent-Free Sonogashira Coupling Reaction via High Speed Ball Milling. *Green Chem.* **2009**, *11* (11), 1821. https://doi.org/10.1039/b915669k

(41) Vogt, C. G.; Grätz, S.; Lukin, S.; Halasz, I.; Etter, M.; Evans, J. D.; Borchardt, L. Direct Mechanocatalysis: Palladium as Milling Media and Catalyst in the Mechanochemical Suzuki Polymerization. *Angew. Chem. Int. Ed.* **2019**, *58* (52), 18942–18947. https://doi.org/10.1002/anie.201911356

(42) Sawama, Y.; Yasukawa, N.; Ban, K.; Goto, R.; Niikawa, M.; Monguchi, Y.; Itoh, M.; Sajiki, H. Stainless Steel-Mediated Hydrogen Generation from Alkanes and Diethyl Ether and Its Application for Arene Reduction. *Org. Lett.* **2018**, *20* (10), 2892–2896. https://doi.org/10.1021/acs.orglett.8b00931

(43) Martina, K.; Baricco, F.; Tagliapietra, S.; Moran, M. J.; Cravotto, G.; Cintas, P. Highly Efficient Nitrobenzene and Alkyl/Aryl Azide Reduction in Stainless Steel Jars without Catalyst Addition. *New J. Chem.* **2018**, *42* (23), 18881–18888. https://doi.org/10.1039/C8NJ04240C

(44) Kulla, H.; Fischer, F.; Benemann, S.; Rademann, K.; Emmerling, F. The Effect of the Ball to Reactant Ratio on Mechanochemical Reaction Times Studied by in Situ PXRD. *CrystEngComm* **2017**, *19* (28), 3902–3907. https://doi.org/10.1039/C7CE00502D

(45) Kulla, H.; Becker, C.; Michalchuk, A. A. L.; Linberg, K.; Paulus, B.; Emmerling, F. Tuning the Apparent Stability of Polymorphic Cocrystals through Mechanochemistry. *Cryst. Growth Des.* **2019**, *19* (12), 7271–7279. https://doi.org/10.1021/acs.cgd.9b01158

(46) Shan, N.; Toda, F.; Jones, W. Mechanochemistry and Co-Crystal Formation: Effect of Solvent on Reaction Kinetics. *Chem. Commun.* **2002**, *38* (20), 2372–2373. https://doi.org/10.1039/b207369m

(47) *How Resonant Acoustic Mixers Mix - RAM Mixers*. Resodyn Acoustic Mixers. https://resodynmixers.com/how-ram-mixes/ (accessed 2026-05-13)

(48) Anderson, S. R.; am Ende, D. J.; Salan, J. S.; Samuels, P. Preparation of an Energetic-Energetic Cocrystal Using Resonant Acoustic Mixing. *Propellants Explos. Pyrotech.* **2014**, *39* (5), 637–640. https://doi.org/10.1002/prep.201400092

(49) Gonnet, L.; Lennox, C. B.; Do, J.; Malvestiti, I.; Koenig, S. G.; Nagapudi, K.; Friščić, T. Metal-Catalyzed Organic Reactions by Resonant Acoustic Mixing. *Angew. Chem. Int. Ed.* **2022**, *61* (13). https://doi.org/10.1002/anie.202115030

(50) Lennox, C. B.; Borchers, T. H.; Gonnet, L.; Barrett, C. J.; Koenig, S. G.; Nagapudi, K.; Friščić, T. Direct Mechanocatalysis by Resonant Acoustic Mixing (RAM). *Chem. Sci.* **2023**, *14* (27), 7475–7481. https://doi.org/10.1039/D3SC01591B

(51) Chatzigiannis, C. M.; Scalzullo, S. M.; Colacino, E.; Rivas, M. E. Multigram-Scale Organic Synthesis by Resonant Acoustic Mixing: Application to the Sustainable Preparation of Active Pharmaceutical Ingredients. *ChemSusChem* **2025**, *18* (13), e202500110. https://doi.org/10.1002/cssc.202500110

(52) Suut-Tuule, E.; Schults, E.; Jarg, T.; Adamson, J.; Kananovich, D.; Aav, R. Scalable Mechanochemical Synthesis of Biotin[6]Uril. *ChemSusChem* **2025**, *18* (9), e202402354. https://doi.org/10.1002/cssc.202402354

(53) Michalchuk, A. A. L.; Hope, K. S.; Kennedy, S. R.; Blanco, M. V.; Boldyreva, E. V.; Pulham, C. R. Ball-Free Mechanochemistry: *In Situ* Real-Time Monitoring of Pharmaceutical Co-Crystal Formation by Resonant Acoustic Mixing. *Chem. Commun.* **2018**, *54* (32), 4033–4036. https://doi.org/10.1039/C8CC02187B

(54) Claydon, A. J.; Patil, A. N.; Gaulter, S.; Kister, G.; Gill, P. P. Determination and Optimisation of Resonant Acoustic Mixing (RAM) Efficiency in Polymer Bonded eXplosive (PBX) Processing. *Chem. Eng. Process.* **2022**, *173*, 108806. https://doi.org/10.1016/j.cep.2022.108806

(55) Gonnet, L.; Lennox, C. B.; Borchers, T. H.; Askari, M.; Wahrhaftig-Lewis, A.; Koenig, S. G.; Nagapudi, K.; Friščić, T. Establishing Parameters for Resonant Acoustic Mixing (RAM) Chemistry Using Buchwald-Hartwig Amination as a Model. *Green Chem.* **2026**, 10.1039.D6GC00784H. https://doi.org/10.1039/D6GC00784H

(56) Michalchuk, A. A. L.; Hope, K. S.; Kennedy, S. R.; Blanco, M. V.; Boldyreva, E. V.; Pulham, C. R. Ball-Free Mechanochemistry: In Situ Real-Time Monitoring of Pharmaceutical Co-Crystal Formation by Resonant Acoustic Mixing. *Chem. Commun.* **2018**, *54* (32), 4033–4036. https://doi.org/10.1039/c8cc02187b

(57) *ZE 12 HMI – Three-Tec*. https://www.three-tec.ch/. https://www.three-tec.ch/produkt/ze-12-hmi/ (accessed 2026-08-11)

(58) Bolt, R. R. A.; Leitch, J. A.; Jones, A. C.; Nicholson, W. I.; Browne, D. L. Continuous Flow Mechanochemistry: Reactive Extrusion as an Enabling Technology in Organic Synthesis. *Chem. Soc. Rev.* **2022**, *51* (11), 4243–4260. https://doi.org/10.1039/D1CS00657F

(59) *Reactive Extrusion: Principles and Applications*; Beyer, G., Hopmann, C., Eds.; Wiley-VCH: Weinheim, Germany, 2018. https://doi.org/10.1002/9783527801541

(60) Reynes, J. F.; Isoni, V.; García, F. Tinkering with Mechanochemical Tools for Scale Up. *Angew. Chem. Int. Ed.* **2023**, *62* (44). https://doi.org/10.1002/anie.202300819

(61) Crawford, D. E.; Miskimmin, C. K. G.; Albadarin, A. B.; Walker, G.; James, S. L. Organic Synthesis by Twin Screw Extrusion (TSE): Continuous, Scalable and Solvent-Free. *Green Chem.* **2017**, *19* (6), 1507–1518. https://doi.org/10.1039/C6GC03413F

(62) Wang, Y.-J.; Dai, C.-A.; Li, J.-H. Numerical Study of Tunable Photonic Nanojets Generated by Biocompatible Hydrogel Core-Shell Microspheres for Surface-Enhanced Raman Scattering Applications. *Polymers* **2019**, *11* (3), 431. https://doi.org/10.3390/polym11030431

(63) Crawford, D. E.; Porcheddu, A.; McCalmont, A. S.; Delogu, F.; James, S. L.; Colacino, E. Solvent-Free, Continuous Synthesis of Hydrazone-Based Active Pharmaceutical Ingredients by Twin-Screw Extrusion. *ACS Sustainable Chem. Eng.* **2020**, *8* (32), 12230–12238. https://doi.org/10.1021/acssuschemeng.0c03816

(64) Crawford, D. E.; Porcheddu, A.; McCalmont, A. S.; Delogu, F.; James, S. L.; Colacino, E. Solvent-Free, Continuous Synthesis of Hydrazone-Based Active Pharmaceutical Ingredients by Twin-Screw Extrusion. *ACS Sustainable Chem. Eng.* **2020**, *8* (32), 12230–12238. https://doi.org/10.1021/acssuschemeng.0c03816

(65) Galant, O.; Cerfeda, G.; McCalmont, A. S.; James, S. L.; Porcheddu, A.; Delogu, F.; Crawford, D. E.; Colacino, E.; Spatari, S. Mechanochemistry Can Reduce Life Cycle Environmental Impacts of Manufacturing Active Pharmaceutical Ingredients. *ACS Sustainable Chem. Eng.* **2022**, *10* (4), 1430–1439. https://doi.org/10.1021/acssuschemeng.1c06434

(66) Ali El-Remaily, M. A. E. A. A.; Soliman, A. M. M.; Elhady, O. M. Green Method for the Synthetic Ugi Reaction by Twin Screw Extrusion without a Solvent and Catalyst. *ACS Omega* **2020**, *5* (11), 6194–6198. https://doi.org/10.1021/acsomega.0c00369

(67) Sović, I.; Lukin, S.; Meštrović, E.; Halasz, I.; Porcheddu, A.; Delogu, F.; Ricci, P. C.; Caron, F.; Perilli, T.; Dogan, A.; Colacino, E. Mechanochemical Preparation of Active Pharmaceutical Ingredients Monitored by In Situ Raman Spectroscopy. *ACS Omega* **2020**, *5* (44), 28663–28672. https://doi.org/10.1021/acsomega.0c03756

(68) Konnert, L.; Reneaud, B.; de Figueiredo, R. M.; Campagne, J.-M.; Lamaty, F.; Martinez, J.; Colacino, E. Mechanochemical Preparation of Hydantoins from Amino Esters: Application to the Synthesis of the Antiepileptic Drug Phenytoin. *J. Org. Chem.* **2014**, *79* (21), 10132–10142. https://doi.org/10.1021/jo5017629

(69) Puccetti, F.; Lukin, S.; Užarević, K.; Colacino, E.; Halasz, I.; Bolm, C.; Hernández, J. G. Mechanistic Insights on the Mechanosynthesis of Phenytoin, a WHO Essential Medicine. *Chem. Eur. J.* **2022**, *28* (13), e202104409. https://doi.org/10.1002/chem.202104409

(70) Bodach, A.; Portet, A.; Winkelmann, F.; Herrmann, B.; Gallou, F.; Ponnusamy, E.; Virieux, D.; Colacino, E.; Felderhoff, M. Scalability of Pharmaceutical Co-Crystal Formation by Mechanochemistry in Batch. *ChemSusChem* **2024**, *17* (6), e202301220. https://doi.org/10.1002/cssc.202301220

(71) Schöbel, J.-H.; Winkelmann, F.; Bicker, J.; Felderhoff, M. Mechanochemical Kilogram-Scale Synthesis of *Rac* -Ibuprofen:Nicotinamide Co-Crystals Using a Drum Mill. *RSC Mechanochem.* **2025**, *2* (2), 224–229. https://doi.org/10.1039/D4MR00096J

(72) Geib, R.; Colacino, E.; Gremaud, L. Sustainable Beckmann Rearrangement Using Bead-Milling Technology: The Route to Paracetamol. *ChemSusChem* **2024**. https://doi.org/10.1002/cssc.202301921

(73) Mocci, R.; Colacino, E.; Luca, L. D.; Fattuoni, C.; Porcheddu, A.; Delogu, F. The Mechanochemical Beckmann Rearrangement: An Eco-Efficient "Cut-and-Paste" Strategy to Design the "Good Old Amide Bond." *ACS Sustainable Chem. Eng.* **2021**, *9* (5), 2100–2114. https://doi.org/10.1021/acssuschemeng.0c07254

(74) Fritch, J. R.; Fruchey, O. S.; Horlenko, T. Production of Acetaminophen. US4954652A, September 4, 1990. https://patents.google.com/patent/US4954652A/en (accessed 2026-10-05)

(75) Caboni, P.; Porcheddu, A.; Ötvös, S. B.; Kappe, C. O. Scalable Mechanochemical Synthesis of Amides Using Bead Milling Technology. *Green Chem.* **2026**, *28* (4), 2049–2055. https://doi.org/10.1039/D5GC04764A

(76) McElroy, C. R.; Constantinou, A.; Jones, L. C.; Summerton, L.; Clark, J. H. Towards a Holistic Approach to Metrics for the 21st Century Pharmaceutical Industry. *Green Chem.* **2015**, *17* (5), 3111–3121. https://doi.org/10.1039/C5GC00340G

(77) Fantozzi, N.; Volle, J.-N.; Porcheddu, A.; Virieux, D.; García, F.; Colacino, E. Green Metrics in Mechanochemistry. *Chem. Soc. Rev.* **2023**, *52* (19), 6680–6714. https://doi.org/10.1039/D2CS00997H

(78) Roschangar, F.; Sheldon, R. A.; Senanayake, C. H. Overcoming Barriers to Green Chemistry in the Pharmaceutical Industry – the Green Aspiration Level™ Concept. *Green Chem.* **2015**, *17* (2), 752–768. https://doi.org/10.1039/C4GC01563K

(79) Roschangar, F.; Zhou, Y.; Constable, D. J. C.; Colberg, J.; Dickson, D. P.; Dunn, P. J.; Eastgate, M. D.; Gallou, F.; Hayler, J. D.; Koenig, S. G.; Kopach, M. E.; Leahy, D. K.; Mergelsberg, I.; Scholz, U.; Smith, A. G.; Henry, M.; Mulder, J.; Brandenburg, J.; Dehli, J. R.; Fandrick, D. R.; Fandrick, K. R.; Gnad-Badouin, F.; Zerban, G.; Groll, K.; Anastas, P. T.; Sheldon, R. A.; Senanayake, C. H. Inspiring Process Innovation *via* an Improved Green Manufacturing Metric: iGAL. *Green Chem.* **2018**, *20* (10), 2206–2211. https://doi.org/10.1039/C8GC00616D

(80) Roschangar, F.; Li, J.; Zhou, Y.; Aelterman, W.; Borovika, A.; Colberg, J.; Dickson, D. P.; Gallou, F.; Hayler, J. D.; Koenig, S. G.; Kopach, M. E.; Kosjek, B.; Leahy, D. K.; O'Brien, E.; Smith, A. G.; Henry, M.; Cook, J.; Sheldon, R. A. Improved iGAL 2.0 Metric Empowers Pharmaceutical Scientists to Make Meaningful Contributions to United Nations Sustainable Development Goal 12. *ACS Sustainable Chem. Eng.* **2022**, *10* (16), 5148–5162. https://doi.org/10.1021/acssuschemeng.1c01940

(81) Nikonovich, T.; Jarg, T.; Martõnova, J.; Kudrjašov, A.; Merzhyievskyi, D.; Kudrjašova, M.; Gallou, F.; Aav, R.; Kananovich, D. Protecting-Group-Free Mechanosynthesis of Amides from Hydroxycarboxylic Acids: Application to the Synthesis of Imatinib. *RSC Mechanochem.* **2024**, *1* (2), 189–195. https://doi.org/10.1039/D4MR00006D

(82) Sharma, P.; Vetter, C.; Ponnusamy, E.; Colacino, E. Assessing the Greenness of Mechanochemical Processes with the DOZN 2.0 Tool. *ACS Sustainable Chem. Eng.* **2022**, *10* (16), 5110–5116. https://doi.org/10.1021/acssuschemeng.1c07981

(83) Van Aken, K.; Strekowski, L.; Patiny, L. EcoScale, a Semi-Quantitative Tool to Select an Organic Preparation Based on Economical and Ecological Parameters. *Beilstein J. Org. Chem.* **2006**, *2*. https://doi.org/10.1186/1860-5397-2-3

(84) Baier, D. M.; Rensch, T.; Dobreva, D.; Spula, C.; Fanenstich, S.; Rappen, M.; Bergheim, K.; Grätz, S.; Borchardt, L. The Mechanochemical Beckmann Rearrangement over Solid Acids: From the Ball Mill to the Extruder. *Chem. Methods* **2023**, *3* (4). https://doi.org/10.1002/cmtd.202200058

(85) Magano, J. Large-Scale Amidations in Process Chemistry: Practical Considerations for Reagent Selection and Reaction Execution. *Org. Process Res. Dev.* **2022**, *26* (6), 1562–1689. https://doi.org/10.1021/acs.oprd.2c00005

(86) De Figueiredo, R. M.; Suppo, J.-S.; Campagne, J.-M. Nonclassical Routes for Amide Bond Formation. *Chem. Rev.* **2016**, *116* (19), 12029–12122. https://doi.org/10.1021/acs.chemrev.6b00237

(87) Staab, H. A. New Methods of Preparative Organic Chmistry IV. Syntheses Using Heterocyclic Amides (Azolides). *Angew. Chem. Int. Ed.* **1962**, *1* (7), 351–367. https://doi.org/10.1002/anie.196203511

(88) Métro, T.-X.; Bonnamour, J.; Reidon, T.; Sarpoulet, J.; Martinez, J.; Lamaty, F. Mechanosynthesis of Amides in the Total Absence of Organic Solvent from Reaction to Product Recovery. *Chem. Commun.* **2012**, *48* (96), 11781–11783. https://doi.org/10.1039/c2cc36352f

(89) Lanzillotto, M.; Konnert, L.; Lamaty, F.; Martinez, J.; Colacino, E. Mechanochemical 1,1′-Carbonyldiimidazole-Mediated Synthesis of Carbamates. *ACS Sustainable Chem. Eng.* **2015**, *3* (11), 2882–2889. https://doi.org/10.1021/acssuschemeng.5b00819

(90) Murata, S. 1,1′-Oxalylimidazole, a New Reagent for Activation of Carboxylic Acid. *Chem. Lett.* **1983**, *12* (12), 1819–1820. https://doi.org/10.1246/cl.1983.1819

(91) *SDHI Fungicide Market Size & Share Outlook to 2031*. Mordor Intelligence. https://www.mordorintelligence.com/industry-reports/sdhi-fungicide-market (accessed 2026-07-03)

(92) Konnert, L.; Gauliard, A.; Lamaty, F.; Martinez, J.; Colacino, E. Solventless Synthesis of *N* -Protected Amino Acids in a Ball Mill. *ACS Sustainable Chem. Eng.* **2013**, *1* (9), 1186–1191. https://doi.org/10.1021/sc4001115

(93) Grzyb, J. A.; Shen, M.; Yoshina-Ishii, C.; Chi, W.; Brown, R. S.; Batey, R. A. Carbamoylimidazolium and Thiocarbamoylimidazolium Salts: Novel Reagents for the Synthesis of Ureas, Thioureas, Carbamates, Thiocarbamates and Amides. *Tetrahedron* **2005**, *61* (30), 7153–7175. https://doi.org/10.1016/j.tet.2005.05.056

(94) Vugrin, L.; Carta, M.; Lukin, S.; Meštrović, E.; Delogu, F.; Halasz, I. Mechanochemical Reaction Kinetics Scales Linearly with Impact Energy. *Faraday Discuss.* **2023**, *241*, 217–229. https://doi.org/10.1039/D2FD00083K

(95) US EPA, O. *Presidential Green Chemistry Challenge: 1997 Greener Synthetic Pathways Award*. https://www.epa.gov/greenchemistry/presidential-green-chemistry-challenge-1997-greener-synthetic-pathways-award (accessed 2026-07-03)

(96) Sharma, Dr. P.; Ponnusamy, E. DOZN^{TM} 3.0: A Quantitative Green Chemistry Evaluator for Sustainable Chemistry. *Sustain. Chem. Clim. Action* **2025**, *7*, 100129. https://doi.org/10.1016/j.scca.2025.100129

(97) Kielhorn, J.; Melber, C.; Keller, D.; Mangelsdorf, I. Palladium – A Review of Exposure and Effects to Human Health. *Int. J. Hyg. Environ. Health* **2002**, *205* (6), 417–432. https://doi.org/10.1078/1438-4639-00180

(98) Lucas, E.; Martín, A. J.; Mitchell, S.; Nabera, A.; Santos, L. F.; Pérez-Ramírez, J.; Guillén-Gosálbez, G. The Need to Integrate Mass- and Energy-Based Metrics with Life Cycle Impacts for Sustainable Chemicals Manufacture. *Green Chem.* **2024**, *26* (17), 9300–9309. https://doi.org/10.1039/D4GC00394B

(99) DeVierno Kreuder, A.; House-Knight, T.; Whitford, J.; Ponnusamy, E.; Miller, P.; Jesse, N.; Rodenborn, R.; Sayag, S.; Gebel, M.; Aped, I.; Sharfstein, I.; Manaster, E.; Ergaz, I.; Harris, A.; Nelowet Grice, L. A Method for Assessing Greener Alternatives between Chemical Products Following the 12 Principles of Green Chemistry. *ACS Sustainable Chem. Eng.* **2017**, *5* (4), 2927–2935. https://doi.org/10.1021/acssuschemeng.6b02399

(100) Beutner, G. L.; Young, I. S.; Davies, M. L.; Hickey, M. R.; Park, H.; Stevens, J. M.; Ye, Q. TCFH–NMI: Direct Access to *N* -Acyl Imidazoliums for Challenging Amide Bond Formations. *Org. Lett.* **2018**, *20* (14), 4218–4222. https://doi.org/10.1021/acs.orglett.8b01591

(101) Dalidovich, T.; Mishra, K. A.; Shalima, T.; Kudrjašova, M.; Kananovich, D. G.; Aav, R. Mechanochemical Synthesis of Amides with Uronium-Based Coupling Reagents: A Method for Hexa-Amidation of Biotin[6]Uril. *ACS Sustainable Chem. Eng.* **2020**, *8* (41), 15703–15715. https://doi.org/10.1021/acssuschemeng.0c05558

(102) Dalidovich, T.; Nallaparaju, J. V.; Shalima, T.; Aav, R.; Kananovich, D. G. Mechanochemical Nucleophilic Substitution of Alcohols via Isouronium Intermediates**. *ChemSusChem* **2022**, *15* (3), e202102286. https://doi.org/10.1002/cssc.202102286

(103) Nagapudi, K.; Umanzor, E. Y.; Masui, C. High-Throughput Screening and Scale-up of Cocrystals Using Resonant Acoustic Mixing. *Int. J. Pharm.* **2017**, *521* (1–2), 337–345. https://doi.org/10.1016/j.ijpharm.2017.02.027

(104) Titi, H. M.; Do, J.-L.; Howarth, A. J.; Nagapudi, K.; Friščić, T. Simple, Scalable Mechanosynthesis of Metal–Organic Frameworks Using Liquid-Assisted Resonant Acoustic Mixing (LA-RAM). *Chem. Sci.* **2020**, *11* (29), 7578–7584. https://doi.org/10.1039/D0SC00333F

(105) Effaty, F.; Gonnet, L.; Koenig, S. G.; Nagapudi, K.; Ottenwaelder, X.; Friščić, T. Resonant Acoustic Mixing (RAM) for Efficient Mechanoredox Catalysis without Grinding or Impact Media. *Chem. Commun.* **2023**, *59* (8), 1010–1013. https://doi.org/10.1039/D2CC06013B

(106) Gonnet, L.; Borchers, T. H.; Lennox, C. B.; Vainauskas, J.; Teoh, Y.; Titi, H. M.; Barrett, C. J.; Koenig, S. G.; Nagapudi, K.; Friščić, T. The " η -Sweet-Spot" (η_{max}) in Liquid-Assisted Mechanochemistry: Polymorph Control and the Role of a Liquid

Additive as Either a Catalyst or an Inhibitor in Resonant Acoustic Mixing (RAM). *Faraday Discuss.* **2023**, *241*, 128–149. https://doi.org/10.1039/D2FD00131D

(107) Vugrin, L.; Chatzigiannis, C.; Colacino, E.; Halasz, I. *In Situ* Raman Spectroscopy for Comparing Ball Milling and Resonant Acoustic Mixing in Organic Mechanosynthesis. *RSC Mechanochem.* **2025**, *2* (3), 482–487. https://doi.org/10.1039/D5MR00016E

(108) Maarouf-Mesli, N.; Desjardins-Michaud, J.; Imani, Z.; Ghosh, K.; Polyak, F.; Lubell, W. D. Solvent-Less Environmentally Benign Amino Ester, Amide, and Peptide Synthesis Enabled by Resonant Acoustic Mixing. *Green Chem.* **2026**, *28* (1), 264–276. https://doi.org/10.1039/D5GC04619J

(109) Broseghini, M.; D'Incau, M.; Gelisio, L.; Pugno, N. M.; Scardi, P. Effect of Jar Shape on High-Energy Planetary Ball Milling Efficiency: Simulations and Experiments. *Mater. Des.* **2016**, *110*, 365–374. https://doi.org/10.1016/j.matdes.2016.06.118

(110) Baláž, P.; Achimovičová, M.; Baláž, M.; Billik, P.; Cherkezova-Zheleva, Z.; Criado, J. M.; Delogu, F.; Dutková, E.; Gaffet, E.; Gotor, F. J.; Kumar, R.; Mitov, I.; Rojac, T.; Senna, M.; Streletskii, A.; Wieczorek-Ciurowa, K. Hallmarks of Mechanochemistry: From Nanoparticles to Technology. *Chem. Soc. Rev.* **2013**, *42* (18), 7571. https://doi.org/10.1039/c3cs35468g

(111) Leung, D. H.; Lamberto, D. J.; Liu, L.; Kwong, E.; Nelson, T.; Rhodes, T.; Bak, A. A New and Improved Method for the Preparation of Drug Nanosuspension Formulations Using Acoustic Mixing Technology. *Int. J. Pharm.* **2014**, *473* (1–2), 10–19. https://doi.org/10.1016/j.ijpharm.2014.05.003

(112) Boldyreva, E. Non-Ambient Conditions in the Investigation and Manufacturing of Drug Forms. *Curr. Pharm. Des.* **2016**, *22* (32), 4981–5000. https://doi.org/10.2174/1381612822666160804093120

(113) Anastas, P.; Warner, J. *Green Chemistry: Theory and Practice*; Oxford University Press: New York, 1998.

(114) Chiyomaru, I.; Kawada, S.; Takita, K. Compositions and Methods of Combatting Bacteria and Fungi Using 2-Methylbenzanilide Derivatives. US3937840A, February 10, 1976. https://patents.google.com/patent/US3937840A/en (accessed 2026-09-19)

(115) Patel, R. I.; Saxena, B.; Sharma, A. General Electron–Donor–Acceptor Complex Mediated Thioesterification Reaction via Site-Selective C–H Functionalization Using Aryl Sulfonium Salts. *Green Chem.* **2024**, *26* (19), 10265–10274. https://doi.org/10.1039/D4GC03768E

(116) Yabutani, K.; Ikeda, K.; Hatta, S.; Harada, T. Novel Benzoic Anilide Derivative and Fungicide Containing Same. US4093743A, June 6, 1978. https://patents.google.com/patent/US4093743A/en (accessed 2026-09-19)

(117) Zhang, Y.; Chen, Z.; Nie, J.; Zhang, F.-G.; Ma, J.-A. Development of Cyanopyrazoles as Building Blocks to Fungicide Fluxapyroxad and Analogues. *The Journal of Organic Chemistry* **2019**, *84* (11), 7148–7158. https://doi.org/10.1021/acs.joc.9b00819

(118) Gandi, V. R.; Bhosale, A. B.; Kini, P. A Process for Preparation of Carboxamide Compounds and Intermediates Thereof. WO2025074339A1, April 10, 2025. https://patents.google.com/patent/WO2025074339A1/en?oq=WO+2025%2f074339+A1 (accessed 2026-07-28)

(119) Michalchuk, A. A. L.; Boldyreva, E. V. Resonant Acoustic Mixing: Applications to Organic and Materials Synthesis. In *Encyclopedia of Green Chemistry*; Elsevier, 2025; pp 532–541. https://doi.org/10.1016/B978-0-443-15742-4.00121-6

(120) Zhang, L.; Ma, N.; Wang, M.; Gou, W.; Tian, J.; Xu, Q.; Zhao, C.; Li, C. (*O* -CF_3 PhO)$_3$ P as a Simple Coupling Reagent for Direct Amidation *via* Activation of Amines. *Org. Chem. Front.* **2024**, *11* (6), 1796–1803. https://doi.org/10.1039/D3QO01705B

(121) Garrido-García, P.; Quirós, I.; Milán-Rois, P.; Ortega-Gutiérrez, S.; Martín-Fontecha, M.; Campos, L. A.; Somoza, Á.; Fernández, I.; Rigotti, T.; Tortosa, M. Enantioselective Photocatalytic Synthesis of Bicyclo[2.1.1]Hexanes as Ortho-Disubstituted Benzene Bioisosteres with Improved Biological Activity. *Nat. Chem.* **2025**, *17* (5), 734–745. https://doi.org/10.1038/s41557-025-01746-7

(122) *Methylene Chloride; Regulation Under the Toxic Substances Control Act (TSCA)*. Federal Register. https://www.federalregister.gov/documents/2024/05/08/2024-09606/methylene-chloride-regulation-under-the-toxic-substances-control-act-tsca (accessed 2026-07-28)

(123) *Decision No 455/2009/EC of the European Parliament and of the Council of 6 May 2009 Amending Council Directive 76/769/EEC as Regards Restrictions on the Marketing and Use of Dichloromethane (Text with EEA Relevance)*; 2009; Vol. 137. http://data.europa.eu/eli/dec/2009/455(2)/oj (accessed 2026-07-28)

(124) *Commission Regulation (EU) 2021/2030 of 19 November 2021 Amending Annex XVII to Regulation (EC) No 1907/2006 of the European Parliament and of the Council Concerning the Registration, Evaluation, Authorisation and Restriction of Chemicals (REACH) as Regards N,N-Dimethylformamide (Text with EEA Relevance)*; 2021; Vol. 415. http://data.europa.eu/eli/reg/2021/2030/oj (accessed 2026-07-28)

(125) Constable, D. J. C.; Jimenez-Gonzalez, C.; Henderson, R. K. Perspective on Solvent Use in the Pharmaceutical Industry. *Org. Process Res. Dev.* **2007**, *11* (1), 133–137. https://doi.org/10.1021/op060170h

(126) Jiménez-González, C.; Curzons, A. D.; Constable, D. J. C.; Cunningham, V. L. Expanding GSK's Solvent Selection Guide—Application of Life Cycle Assessment to Enhance Solvent Selections. *Clean Technol. Environ. Policy* **2004**, *7* (1), 42–50. https://doi.org/10.1007/s10098-004-0245-z

(127) Colacino, E.; Porcheddu, A.; Charnay, C.; Delogu, F. From Enabling Technologies to Medicinal Mechanochemistry: An Eco-Friendly Access to Hydantoin-Based Active Pharmaceutical Ingredients. *React. Chem. Eng.* **2019**, *4* (7), 1179–1188. https://doi.org/10.1039/c9re00069k

(128) Gomollón-Bel, F. Ten Chemical Innovations That Will Change Our World: IUPAC Identifies Emerging Technologies in Chemistry with Potential to Make Our Planet More Sustainable. *Chem. Int.* **2019**, *41* (2), 12–17. https://doi.org/10.1515/ci-2019-0203

(129) Galant, O.; Cerfeda, G.; McCalmont, A. S.; James, S. L.; Porcheddu, A.; Delogu, F.; Crawford, D. E.; Colacino, E.; Spatari, S. Mechanochemistry Can Reduce Life Cycle Environmental Impacts of Manufacturing Active Pharmaceutical Ingredients. *ACS Sustainable Chem. Eng.* **2022**, *10* (4), 1430–1439. https://doi.org/10.1021/acssuschemeng.1c06434

(130) *WHO Model Lists of Essential Medicines*. https://www.who.int/groups/expert-committee-on-selection-and-use-of-essential-medicines/essential-medicines-lists (accessed 2026-07-21)
(131) Borges, Á. D. L.; Ponte, G. D.; Federman Neto, A.; Carvalho, I. Síntese de sulfadiazina e sulfadiazina de prata em escala semi-micro: prática experimental em síntese de fármacos. *Quím. Nova* **2005**, *28*, 727–731. https://doi.org/https://doi.org/10.1590/S0100-40422005000400030
(132) Biltz, H.; Slotta, K. Über Die Herstellung von Hydantoinen. *J. Prakt. Chem.* **1926**, *113* (1), 233–267. https://doi.org/10.1002/prac.19261130121
(133) Ortiz-Trankina, L. N.; Crain, J.; Williams, C., III; Mack, J. Developing Benign Syntheses Using Ion Pairs via Solvent-Free Mechanochemistry. *Green Chem.* **2020**, *22* (11), 3638–3642. https://doi.org/10.1039/d0gc01116a
(134) Hayes, K. S. Industrial Processes for Manufacturing Amines. *Appl. Catal. A Gen.* **2001**, *221* (1–2), 187–195. https://doi.org/10.1016/S0926-860X(01)00813-4
(135) Flick, A. C.; Leverett, C. A.; Ding, H. X.; McInturff, E.; Fink, S. J.; Helal, C. J.; DeForest, J. C.; Morse, P. D.; Mahapatra, S.; O'Donnell, C. J. Synthetic Approaches to New Drugs Approved during 2018. *J. Med. Chem.* **2020**, *63* (19), 10652–10704. https://doi.org/10.1021/acs.jmedchem.0c00345
(136) Seyden-Penne, J.; Seyden-Penne, J. *Reductions by the Alumino- and Borohydrides in Organic Synthesis*, 2. ed.; Wiley-VCH: New York Weinheim, 1997.
(137) Caddick, S.; Judd, D. B.; Lewis, A. K. de K.; Reich, M. T.; Williams, M. R. V. A Generic Approach for the Catalytic Reduction of Nitriles. *Tetrahedron* **2003**, *59* (29), 5417–5423. https://doi.org/10.1016/S0040-4020(03)00858-5
(138) Natte, K.; Jagadeesh, R. V. Amines By Reduction. In *Kirk-Othmer Encyclopedia of Chemical Technology*; Kirk-Othmer, Ed.; Wiley, 2021; pp 1–34. https://doi.org/10.1002/0471238961.0113091419030809.a01.pub3
(139) Reguillo, R.; Grellier, M.; Vautravers, N.; Vendier, L.; Sabo-Etienne, S. Ruthenium-Catalyzed Hydrogenation of Nitriles: Insights into the Mechanism. *J. Am. Chem. Soc.* **2010**, *132* (23), 7854–7855. https://doi.org/10.1021/ja102759z
(140) de Bellefon, C.; Fouilloux, P. Homogeneous and Heterogeneous Hydrogenation of Nitriles in a Liquid Phase: Chemical, Mechanistic, and Catalytic Aspects. *Catal. Rev.* **1994**, *36* (3), 459–506. https://doi.org/10.1080/01614949408009469
(141) Feller, M. Hydrogenation of Nitriles and Imines for Hydrogen Storage. *Phys. Sci. Rev.* **2019**, *4* (3). https://doi.org/10.1515/psr-2018-0033
(142) Chen, J.; Jiao, Y.; Qin, X.; Cai, X.; Wang, M.; Diao, J.; Wang, L.; Li, C.; Ren, P.; Wen, X.; Wang, N.; Rong, J.; Xiao, D.; Liu, H.; Ma, D. Atomic-Dispersed Rh Enables Efficient Catalytic Nitrile Hydrogenation: Size Effect and Metal-Dependent Effect. *ACS Catal.* **2023**, *13* (13), 8354–8361. https://doi.org/10.1021/acscatal.3c01562
(143) Chin, C. S.; Lee, B. Hydrogenation of Nitriles with Iridium-Triphenylphosphine Complexes. *Catal. Lett.* **1992**, *14* (1), 135–140. https://doi.org/10.1007/BF00764228
(144) Bornschein, C.; Werkmeister, S.; Wendt, B.; Jiao, H.; Alberico, E.; Baumann, W.; Junge, H.; Junge, K.; Beller, M. Mild and Selective Hydrogenation of Aromatic and Aliphatic (Di)Nitriles with a Well-Defined Iron Pincer Complex. *Nat. Commun.* **2014**, *5* (1), 4111. https://doi.org/10.1038/ncomms5111
(145) Liu, W.; Sahoo, B.; Junge, K.; Beller, M. Cobalt Complexes as an Emerging Class of Catalysts for Homogeneous Hydrogenations. *Acc. Chem. Res.* **2018**, *51* (8), 1858–1869. https://doi.org/10.1021/acs.accounts.8b00262

(146) Elangovan, S.; Topf, C.; Fischer, S.; Jiao, H.; Spannenberg, A.; Baumann, W.; Ludwig, R.; Junge, K.; Beller, M. Selective Catalytic Hydrogenations of Nitriles, Ketones, and Aldehydes by Well-Defined Manganese Pincer Complexes. *J. Am. Chem. Soc.* **2016**, *138* (28), 8809–8814. https://doi.org/10.1021/jacs.6b03709

(147) Lyu, Q.; Qian, X.; Su, Y.; Wang, Y.; Li, L.; Wang, Z.; Ma, Y.; Sun, W.-H. Efficiently Robust Transfer Hydrogenation of Nitriles to Methylamines Achieved by Using Manganese Complexes. *J. Catal.* **2026**, *459*, 116925. https://doi.org/10.1016/j.jcat.2026.116925

(148) Sarkar, K.; Das, K.; Kundu, A.; Adhikari, D.; Maji, B. Phosphine-Free Manganese Catalyst Enables Selective Transfer Hydrogenation of Nitriles to Primary and Secondary Amines Using Ammonia–Borane. *ACS Catal.* **2021**, *11* (5), 2786–2794. https://doi.org/10.1021/acscatal.0c05406

(149) Hayrapetyan, D.; Khalimon, A. Y. Catalytic Nitrile Hydroboration: A Route to N,N-Diborylamines and Uses Thereof. *Chem. - Asian J.* **2020**, *15* (17), 2575–2587. https://doi.org/10.1002/asia.202000672

(150) Li, B.; Sortais, J.-B.; Darcel, C. Amine Synthesis via Transition Metal Homogeneous Catalysed Hydrosilylation. *RSC Adv.* **2016**, *6* (62), 57603–57625. https://doi.org/10.1039/c6ra10494k

(151) Faverio, C.; Boselli, M. F.; Medici, F.; Benaglia, M. Ammonia Borane as a Reducing Agent in Organic Synthesis. *Org. Biomol. Chem.* **2020**, *18* (39), 7789–7813. https://doi.org/10.1039/D0OB01351J

(152) Yang, X.; Fox, T.; Berke, H. Ammonia Borane as a Metal Free Reductant for Ketones and Aldehydes: A Mechanistic Study. *Tetrahedron* **2011**, *67* (37), 7121–7127. https://doi.org/10.1016/j.tet.2011.06.104

(153) Yu, C.; Fu, J.; Muzzio, M.; Shen, T.; Su, D.; Zhu, J.; Sun, S. CuNi Nanoparticles Assembled on Graphene for Catalytic Methanolysis of Ammonia Borane and Hydrogenation of Nitro/Nitrile Compounds. *Chem. Mater.* **2017**, *29* (3), 1413–1418. https://doi.org/10.1021/acs.chemmater.6b05364

(154) Göksu, H.; Ho, S. F.; Metin, Ö.; Korkmaz, K.; Mendoza Garcia, A.; Gültekin, M. S.; Sun, S. Tandem Dehydrogenation of Ammonia Borane and Hydrogenation of Nitro/Nitrile Compounds Catalyzed by Graphene-Supported NiPd Alloy Nanoparticles. *ACS Catal.* **2014**, *4* (6), 1777–1782. https://doi.org/10.1021/cs500167k

(155) Ding, M.; Chang, J.; Mao, J.-X.; Zhang, J.; Chen, X. Noncatalyzed Reduction of Nitriles to Primary Amines with Ammonia Borane. *J. Org. Chem.* **2022**, *87* (24), 16230–16235. https://doi.org/10.1021/acs.joc.2c01727

(156) Menuel, S.; Léger, B.; Addad, A.; Monflier, E.; Hapiot, F. Cyclodextrins as Effective Additives in AuNP-Catalyzed Reduction of Nitrobenzene Derivatives in a Ball-Mill. *Green Chem.* **2016**, *18* (20), 5500–5509. https://doi.org/10.1039/C6GC00770H

(157) Mack, J.; Fulmer, D.; Stofel, S.; Santos, N. The First Solvent-Free Method for the Reduction of Esters. *Green Chem.* **2007**, *9* (10), 1041. https://doi.org/10.1039/b706167f

(158) Cuccu, F.; Basoccu, F.; Fattuoni, C.; Porcheddu, A. Mechanically Accelerated Catalytic Hydrogenation: Correlating Physical State, Reaction Rate, and Interface Area. *Green Chem.* **2024**, *26* (4), 1927–1934. https://doi.org/10.1039/D3GC03783E

(159) Toyama, Y.; Nakamura, T.; Horikawa, Y.; Morinaka, Y.; Ono, Y.; Yagi, A.; Itami, K.; Ito, H. Rh-Catalyzed Mechanochemical Transfer Hydrogenation for the Synthesis

of Periphery-Hydrogenated Polycyclic Aromatic Compounds. *Chem. Sci.* **2025**, *16* (21), 9117–9124. https://doi.org/10.1039/d5sc01489a

(160) Mkrtchyan, S.; Purohit, V. B.; Shalimov, O.; Karpun, Y.; Prajapati, R. V.; Prajapati, V. D.; Bielec, B.; Addová, G.; Filo, J.; Jin, P.; Wang, C.; Katayev, D.; Iaroshenko, V. O. Photo and Mechanochemically Induced Reduction of Nitroarenes Using Ammonia Borane. *Org. Chem. Front.* **2026**, *13* (3), 874–883. https://doi.org/10.1039/D5QO01451D

(161) Portada, T.; Margetić, D.; Štrukil, V. Mechanochemical Catalytic Transfer Hydrogenation of Aromatic Nitro Derivatives. *Molecules* **2018**, *23* (12), 3163. https://doi.org/10.3390/molecules23123163

(162) Li, A. Y.; Segalla, A.; Li, C.-J.; Moores, A. Mechanochemical Metal-Free Transfer Hydrogenation of Carbonyls Using Polymethylhydrosiloxane as the Hydrogen Source. *ACS Sustainable Chem. Eng.* **2017**, *5* (12), 11752–11760. https://doi.org/10.1021/acssuschemeng.7b03298

(163) Hanek, L. M.; Bolm, C. Mechanochemical Hydrodeoxygenations. *Eur. J. Org. Chem.* **2026**, *29* (22), e202501222. https://doi.org/10.1002/ejoc.202501222

(164) Ai, Z.; Liu, M.; Wang, X.; He, X.; Zhang, X.; Lian, Z. Mechanochemical Piezoelectric Catalysis: Advancing the Hydrogenation of Alkenes. *Adv. Sci. n/a* (n/a), e76446. https://doi.org/10.1002/advs.76446

(165) Nallaparaju, J. V.; Aav, R.; Kananovich, D. Mechanochemistry: A Transformative Technique for the Synthesis of Polar Organometallics from Zero-Valent Metals. *ChemPlusChem* **2026**, *91* (1), e202500445. https://doi.org/10.1002/cplu.202500445

(166) Nallaparaju, J. V.; Satsi, R.; Merzhyievskyi, D.; Jarg, T.; Aav, R.; Kananovich, D. G. Mechanochemical Birch Reduction with Low Reactive Alkaline Earth Metals. *Angew. Chem. Int. Ed.* **2024**, *63* (20). https://doi.org/10.1002/anie.202319449

(167) Kondo, K.; Lowe, M.; Davison, N.; Waddell, P. G.; Armstrong, R. J.; Lu, E.; Kubota, K.; Ito, H. Mechanochemical Synthesis of Organosodium Compounds through Direct Sodiation of Organic Halides. *Nat. Synth* **2026**, *5* (5), 669–679. https://doi.org/10.1038/s44160-025-00949-7

(168) Sudrajat, H.; Hsu, H.-Y.; Jérôme, F.; Colmenares, J. C. Mechanoredox-Catalyzed Organic Synthesis with Piezoelectric Materials: Quo Vadis? *ChemCatChem* **2025**, *17* (6), e202401814. https://doi.org/10.1002/cctc.202401814

(169) Bhatnagar, S.; Felderhoff, M.; Schöbel, J.-H. Solvent-Free Mechanocatalytic Reduction of Nitro Compounds with Hydrogen Gas and Its Application in the Synthesis of Drugs and Their Intermediates. *Adv. Synth. Catal.* **2025**, *367* (19), e70071. https://doi.org/10.1002/adsc.70071

(170) Mayer, M.; Wohlgemuth, M.; Salomé Straub, A.; Grätz, S.; Borchardt, L. Hydrogenation of Organic Molecules via Direct Mechanocatalysis. *Angew. Chem. Int. Ed.* **2025**, *64* (16), e202424139. https://doi.org/10.1002/anie.202424139

(171) Jarg, T.; Tamm, J.; Suut-Tuule, E.; Lootus, K.-M.; Kananovich, D.; Aav, R. How Reliable Is Internal Standard Method in Monitoring Mechanochemical Synthesis? A Case Study of Triphenylmethane in HPLC-UV-MS Analysis of Hemicucurbit[*n*]Urils. *RSC Mechanochem.* **2025**, *2* (4), 507–515. https://doi.org/10.1039/D4MR00145A

(172) Xu, B.; Hartigan, E. M.; Feula, G.; Huang, Z.; Lumb, J.; Arndtsen, B. A. Simple Copper Catalysts for the Aerobic Oxidation of Amines: Selectivity Control by the

Counterion. *Angew. Chem. Int. Ed.* **2016**, *55* (51), 15802–15806. https://doi.org/10.1002/anie.201609255

(173) Patil, R. D.; Gupta, M. K. Methods of Nitriles Synthesis from Amines through Oxidative Dehydrogenation. *Adv. Synth. Catal.* **2020**, *362* (19), 3987–4009. https://doi.org/10.1002/adsc.202000635

(174) Casella, G.; Fonseca Guerra, C.; Carlotto, S.; Sgarbossa, P.; Bertani, R.; Casarin, M. New Light on an Old Debate: Does the RCN–PtCl2 Bond Include Any Back-Donation? RCN←PtCl2 Backbonding vs. the IR νC≡N Blue-Shift Dichotomy in Organonitriles–Platinum(Ii) Complexes. A Thorough Density Functional Theory – Energy Decomposition Analysis Study. *Dalton Trans.* **2019**, *48* (34), 12974–12985. https://doi.org/10.1039/c9dt02440a

(175) Beamson, G.; Briggs, D. *High Resolution XPS of Organic Polymers: The Scienta ESCA300 Database*; Wiley: Chichester, 1992.

(176) Cano, A.; Avila, Y.; Avila, M.; Reguera, E. Structural Information Contained in the XPS Spectra of Nd10 Metal Cyanides. *J. Solid State Chem.* **2019**, *276*, 339–344. https://doi.org/10.1016/j.jssc.2019.05.021

(177) Biesinger, M. C. Advanced Analysis of Copper X-ray Photoelectron Spectra. *Surf. Interface Anal.* **2017**, *49* (13), 1325–1334. https://doi.org/10.1002/sia.6239

(178) Colacino, E.; Nun, P.; Colacino, F. M.; Martinez, J.; Lamaty, F. Solvent-Free Synthesis of Nitrones in a Ball-Mill. *Tetrahedron* **2008**, *64* (23), 5569–5576. https://doi.org/10.1016/j.tet.2008.03.091

(179) Mills, K. C.; Su, Y.; Li, Z.; Brooks, R. F. Equations for the Calculation of the Thermo-Physical Properties of Stainless Steel. *ISIJ International* **2004**, *44* (10), 1661–1668. https://doi.org/10.2355/isijinternational.44.1661

(180) Schlichting, K. W.; Padture, N. P.; Klemens, P. G. Thermal Conductivity of Dense and Porous Yttria-Stabilized Zirconia. *J. Mater. Sci.* **2001**, *36* (12), 3003–3010. https://doi.org/10.1023/A:1017970924312

(181) Casagrande, A.; Niidu, A.; Aav, R.; Kananovich, D.; Colacino, E. Green Chemistry Tools in Mechanochemistry. In *Encyclopedia of Green Chemistry*; Elsevier, 2025; pp 550–571. https://doi.org/10.1016/B978-0-443-15742-4.00116-2

(182) Sheldon, R. A.; Arends, I. W. C. E.; Hanefeld, U. *Green Chemistry and Catalysis*; Wiley, 2007. https://doi.org/10.1002/9783527611003

(183) Betke, T.; Rommelmann, P.; Oike, K.; Asano, Y.; Gröger, H. Cyanid-freie Und Breit Anwendbare Enantioselektive Syntheseplattform Für Chirale Nitrile Durch Einen Biokatalytischen Zugang. *Angew. Chem.* **2017**, *129* (40), 12533–12538. https://doi.org/10.1002/ange.201702952

(184) Morales, S.; Guijarro, F. G.; Alonso, I.; García Ruano, J. L.; Cid, M. B. Dual Role of Pyrrolidine and Cooperative Pyrrolidine/Pyrrolidinium Effect in Nitrone Formation. *ACS Catal.* **2016**, *6* (1), 84–91. https://doi.org/10.1021/acscatal.5b01726

(185) Qiuxiang Yin; Zhiming Shen; Junbo Gong; Baohong Hou; Meijing Zhang; Jingkang Wang; Chuang Xie; Ying Bao; Zhao Wang; Lina Zhou. Preparation Method of Ibuprofen-Nicotinamide Eutectic Crystals. CN103304476A, September 18, 2013. https://patents.google.com/patent/CN103304476A/en (accessed 2026-07-09)

(186) Maniruzzaman, M.; Zhang, J.; Thakkar, R. Pharmaceutical Composition Containing Cocrystals for Additive Manufacturing. WO2022036290A1, February 17, 2022. https://patents.google.com/patent/WO2022036290A1/en (accessed 2026-09-19)

(187) Dhumal, R. S.; Kelly, A. L.; York, P.; Coates, P. D.; Paradkar, A. Cocrystalization and Simultaneous Agglomeration Using Hot Melt Extrusion. *Pharm. Res.* **2010**, *27* (12), 2725–2733. https://doi.org/10.1007/s11095-010-0273-9

(188) Van Zelm, R.; Hennequin, T.; Huijbregts, M. A. J. Performing Life Cycle Impact Assessment with the Midpoint and Endpoint Method ReCiPe. *Nat. Protoc.* **2025**, *20* (12), 3400–3411. https://doi.org/10.1038/s41596-025-01207-y

(189) Huijbregts, M. A. J.; Steinmann, Z. J. N.; Elshout, P. M. F.; Stam, G.; Verones, F.; Vieira, M.; Zijp, M.; Hollander, A.; van Zelm, R. ReCiPe2016: A Harmonised Life Cycle Impact Assessment Method at Midpoint and Endpoint Level. *Int. J. Life Cycle Assess.* **2017**, *22* (2), 138–147. https://doi.org/10.1007/s11367-016-1246-y

(190) Billen, P.; Leccisi, E.; Dastidar, S.; Li, S.; Lobaton, L.; Spatari, S.; Fafarman, A. T.; Fthenakis, V. M.; Baxter, J. B. Comparative Evaluation of Lead Emissions and Toxicity Potential in the Life Cycle of Lead Halide Perovskite Photovoltaics. *Energy* **2019**, *166*, 1089–1096. https://doi.org/10.1016/j.energy.2018.10.141

Acknowledgements

This thesis was carried out as a joint doctoral project between the University of Montpellier and Tallinn University of Technology. The work was supported by Campus France, under the French-Estonian cooperation programme coordinated by the Embassy of France in Estonia.

I would like to thank my supervisors, Dr. Evelina Colacino and Dr. Allan Niidu, for their guidance and support. They made my time in both France and Estonia a source of scientific and personal growth. I am also grateful to them for giving me the opportunity to carry out my doctorate in two countries. This experience will remain very valuable to me.

I thank my colleagues and friends in Montpellier, with whom I shared the laboratory and the fume hoods: Christos, Rubén, Corentin, Alessia, Luigi and Marzia. Thank you for your help with laboratory work and for your company outside of it.

I am grateful to the staff of the Department of Chemistry and Biotechnology in Tallinn. In particular, I thank Prof. Riina Aav and Dr. Dzmitry Kananovich for hosting me in their laboratory. Their advice improved the quality of this work. I also thank my colleagues and friends there: Tania, Tania, Jaga, Margo, Nastya, Ece, Annette, Nora and Misha. Thank you for the good times in the laboratory and in Tallinn.

I would like to thank the people I met during these almost four years in Montpellier and Tallinn. Thank you for the new experiences, the laughter and the friendships we built together. In Montpellier, I thank Elena, Stefano, Rishit, Mery, Rodrigo, Vanessa, Nikola, Andrea, Gabriele, Alberto, Riccardo, Michel, Ariella, Jules and Austin. In Tallinn, I thank Tommy, Merili, Michele, Zhé, Alessia, Gaia, Maria, Thibaud, Leonardo, Teddy and Margarita. These memories will stay with me.

I thank Zoé for her support, and for being close to me, first as a friend and then as a partner, during this time.

I thank Gianluca and Luca. We decided together to leave Rome and start our PhDs in France, and I am very grateful for the bond we strengthened in these years.

I am also grateful to everyone who waited for me in Rome and made each visit feel as if I had never left. First of all, my family. I also thank Andrea, Elisabetta, Davide, Andrea, Flavia, Alessandro, Giorgia, Chiara, Andrea, Aurora, Luca, Ludovica and Enrico, for the moments we shared in Rome and across Europe and the world.

This work would not have been possible without all of you.

Abstract

Mechanochemical Synthesis of Industry-Important Molecules

Organic solvents still dominate chemical manufacturing, accounting for most of the waste and much of the energy demand. Mechanochemistry offers a different route: mechanical force, applied in a ball mill, an acoustic mixer, or an extruder, allows reactions to run with little or no solvent. This thesis asks how far that idea can be taken for molecules already on the market, and whether the resulting processes are measurably cleaner. Six studies are presented, each pairing a synthetic development with a quantitative sustainability assessment. The first chapter introduces 1,1′-oxalyldiimidazole (ODI) as a coupling agent for solvent-free amide bond formation, applied on gram scale to three marketed fungicides: Mepronil, Flutolanil, and Fluxapyroxad. Compared directly with 1,1′-carbonyldiimidazole (CDI), ODI proves better suited to deactivated, fluorinated substrates, where the yield gain reaches +77%. Recovery uses water alone.

The second chapter addresses throughput. A TCFH-mediated amidation of five SDHI fungicides is transferred from ball milling to resonant acoustic mixing (RAM). The protocol then transfers unchanged from 2.5 to 240 mL, a 160-fold increase, giving up to 35 g per batch.

The third chapter moves to continuous operation. Twin-screw extrusion prepares two WHO essential medicines, silver(I) sulfadiazine and phenytoin. Replacing silver nitrate with silver(I) oxide removes nitrate waste, and a previously unreported intermediate is structurally characterized.

The fourth chapter widens the reaction toolbox. Nitriles are reduced to primary amines by ball milling for the first time, using ammonia borane as hydride donor and copper(II) chloride as Lewis-acidic activator. FT-IR and XPS support end-on nitrile coordination as the activating step.

The fifth chapter turns to food and personal-care ingredients: the sweetener (*S*)-(−)-perillartine and the antioxidant *N*-*tert*-butyl-α-phenylnitrone, both made by condensation on multigram scale with no organic solvent at any stage. In-house poly(oxymethylene) jars are introduced as a fluorine-free alternative to PTFE.

The sixth chapter measures a process rather than making a molecule. Five kilogram-scale routes to the *rac*-ibuprofen:nicotinamide cocrystal are compared by cradle-to-gate life cycle assessment. Under the current electricity mix, mechanochemistry is not automatically the lower-impact option; under renewable electricity, its global warming impact falls by more than 90%.

Together, these studies span agrochemicals, medicines, consumer ingredients, and a new transformation. They show that mechanochemistry can deliver marketed molecules with almost no solvent, and that the sustainability gain can be measured rather than assumed.

Résumé

Synthèse mécanochimique de molécules d'intérêt industriel

Les solvants organiques dominent encore la production chimique, où ils représentent l'essentiel des déchets et une grande partie de la demande énergétique. La mécanochimie propose une autre voie : la force mécanique, appliquée dans un broyeur à billes, un mélangeur acoustique ou une extrudeuse, permet de conduire des réactions avec peu ou pas de solvant. Cette thèse examine jusqu'où cette approche peut être portée pour des molécules déjà commercialisées, et si les procédés obtenus sont réellement plus propres. Six études sont présentées, chacune associant un développement synthétique à une évaluation quantitative de la durabilité.

Le premier chapitre introduit le 1,1'-oxalyldiimidazole (ODI) comme agent de couplage pour la formation de liaisons amide sans solvant, appliqué à l'échelle du gramme à trois fongicides commerciaux : le Mépronil, le Flutolanil et le Fluxapyroxad. Comparé directement au 1,1'-carbonyldiimidazole (CDI), l'ODI se révèle mieux adapté aux substrats désactivés et fluorés, où le gain de rendement atteint +77 %. La récupération se fait dans l'eau seule.

Le deuxième chapitre traite de la productivité. Une amidation médiée par le TCFH, appliquée à cinq fongicides SDHI, est transférée du broyage à billes vers le mélange acoustique résonant (RAM). Le protocole est ensuite transposé sans modification de 2,5 à 240 mL, soit un facteur 160, et fournit jusqu'à 35 g par lot.

Le troisième chapitre passe au mode continu. L'extrusion bi-vis permet de préparer deux médicaments essentiels de l'OMS : la sulfadiazine d'argent(I) et la phénytoïne. Le remplacement du nitrate d'argent par l'oxyde d'argent(I) élimine les déchets nitratés, et un intermédiaire jusqu'ici non décrit est caractérisé structuralement.

Le quatrième chapitre élargit la boîte à outils réactionnelle. Les nitriles sont réduits en amines primaires par broyage à billes pour la première fois, avec l'ammoniaborane comme donneur d'hydrure et le chlorure de cuivre(II) comme activateur acide de Lewis. L'IRTF et l'XPS confirment une coordination terminale du nitrile comme étape d'activation.

Le cinquième chapitre porte sur des ingrédients alimentaires et cosmétiques : l'édulcorant (*S*)-(−)-périllartine et l'antioxydant *N*-*tert*-butyl-α-phénylnitrone, tous deux préparés par condensation à l'échelle de plusieurs grammes, sans solvant organique à aucun stade. Des jarres de broyage en poly(oxyméthylène) fabriquées au laboratoire sont introduites comme alternative sans fluor au PTFE.

Le sixième chapitre mesure un procédé plutôt qu'il ne fabrique une molécule. Cinq voies à l'échelle du kilogramme vers le cocristal *rac*-ibuprofène:nicotinamide sont comparées par analyse du cycle de vie du berceau à la porte. Avec le mix électrique actuel, la mécanochimie n'est pas automatiquement l'option à plus faible impact ; avec une électricité renouvelable, son impact sur le réchauffement climatique diminue de plus de 90 %.

Ensemble, ces études couvrent les produits agrochimiques, les médicaments, les ingrédients de grande consommation et une transformation nouvelle. Elles montrent que la mécanochimie peut fournir des molécules commercialisées presque sans solvant, et que le gain de durabilité peut être mesuré plutôt que supposé.

Lühikokkuvõte

Keemiatööstuses on endiselt valdavalt kasutusel orgaanilised lahustid, mis moodustavad sealjuures suurema osa tööstusjääkidest ning märkimisväärse osa protsesside energiavajadusest. Mehhanokeemia pakub uutmoodi lahenduse: tänu kuulveskis, akustilises seguris või ekstruuderis rakendatavale mehaanilisele jõule on võimalik reaktsioone läbi viia kas väikese koguse või täielikult ilma lahustita. Käesolev doktoritöö uurib, kui ulatuslikult on võimalik seda lähenemist juba turul leiduvate molekulide puhul rakendada ja kas väljatöötatud protsessid on ka mõõdetavalt puhtamad. Esitatakse kuus uurimust, millest igaüks ühendab sünteesi väljatöötamise jätkusuutlikkuse kvantifitseerimisega. Esimeses peatükis tutvustatakse 1,1'-oksalüüldiimidasooli (ODI) sidumisreagendina lahustivaba amiidsideme moodustamiseks, mida rakendatakse grammiskaalas kolmele turul olevale fungitsiidile: mepronüül, flutolanüül ja fluksapüroksaad. Võrreldes 1,1'-karbonüüldiimidasooliga (CDI), on ODI deaktiveeritud ja fluoritud substraatide jaoks sobivam sidumisagent, mida tõestab 77%-ni ulatuv saagise kasv. Produkt eraldatakse ainult vee abil. Teine peatükk käsitleb tootlikkust. Viie SDHI-fungitsiidi TCFH-sõltuv amidatsioon viiakse kuuljahvatuselt üle resonantsakustilisele segamisele (ingl *resonant acoustic mixing*, RAM), mistõttu kaks veskireaktsiooni parameetrit pöörduvad vastupidiseks. Kuigi protokoll ise jääb seejuures muutumatuks, kasvab protokolli maht 160-kordselt 2,5 ml-lt 240 ml-ni, tootes kuni 35 g partii kohta. Kolmas peatükk läheb üle pidevale protsessile. Kaksikkruvi-ekstrusiooni teel valmistatakse kaks WHO esmatähtsat ravimit: hõbesulfadiasiin ja fenütoiin. Tänu hõbenitraadi asendamisele hõbeoksiidiga on võimalik ära hoida nitraatjäätmete teke, lisaks õnnestub määrata varem kirjeldamata vaheühendi struktuur. Neljas peatükk laiendab reaktsioonide tööriistakasti. Esmakordselt redutseeritakse kuulveskit kasutades nitriilid primaarseteks amiinideks, kasutades ammoniaakboraani hüdriididoonorina ning vask(II)kloriidi Lewise happe tüüpi aktivaatorina. Nitriili otsmist koordinatsiooni aktiveeriva etapina toetavad nii FT-IR kui ka XPS. Viies peatükk keskendub toidu ja enesehoolduse koostisainetele: magusainele (*S*)-(−)-perillartiin ja antioksüdandile *N*-*tert*-butüül-α-fenüülnitroon, mida mõlemat valmistatakse mitmegrammises skaalas kondensatsiooni teel, vajamata üheski etapis orgaanilisi lahusteid. Tutvustatakse laboris valmistatud polüoksümetüleennõusid kui fluorivaba alternatiivi PTFE-le. Kuues peatükk tegeleb molekulide valmistamise asemel hoopis protsessi mõõtmisega. Kasutades „hällist väravani" elutsükli hindamist, võrreldakse viit teed *rac*-ibuprofeen:nikotiinamiidi kokristalli tootmiseks kilogrammiskaalas. Arvestades praegu levinud elektrienergia jaotusega, ei saa automaatselt väita, et mehhanokeemia oleks keskkonnale väikseima mõjuga valik, kuid vaid taastuvenergiat kasutades langeb selle mõju kliimasoojenemisele enam kui 90%. Ülaltoodud uurimused hõlmavad valdkondi nagu agrokemikaalid, ravimid, tarbekaupade koostisained kui ka üht uut keemilist muundamist. Tänu sellele on võimalik väita, et mehhanokeemia võimaldab turul olevate molekulide peaaegu lahustivaba tootmist ning et nende protsesside jätkusuutlikkust on võimalik kvantifitseerida, mitte vaid eeldada.

Appendix 1

Publication I

A. Casagrande, R. Solorzano-Rodriguez, M. Carta, F. Delogu, J. Vezzani, A. Niidu, E. Colacino. Mechanochemical Amidation Mediated by 1,1'-Oxalyldiimidazole for the Synthesis of Agrochemicals. *Chem. Eur. J.*, **2026**, *32*, e71190.

Reproduced by permission of John Wiley and Sons.

Check for updates

Chemistry – A European Journal

ChemEurJ Chemistry Europe
European Chemical Societies Publishing

RESEARCH ARTICLE OPEN ACCESS

Mechanochemical Amidation Mediated by 1,1'-Oxalyldiimidazole for the Synthesis of Agrochemicals

Andrea Casagrande[1,2] | Rubén Solorzano-Rodriguez[1] | Maria Carta[3] | Francesco Delogu[3] | Joris Vezzani[1] | Allan Niidu[2] | Evelina Colacino[1]

[1]ICGM, CNRS, ENSCM, Univ. Montpellier, Montpellier, France | [2]Virumaa College, Tallinn University of Technology, Tallinn, Estonia | [3]Department of Mechanical, Chemical and Materials Engineering, University of Cagliari, Cagliari, Italy

Correspondence: Evelina Colacino (evelina.colacino@umontpellier.fr)

Received: 23 March 2026 | **Revised:** 7 May 2026 | **Accepted:** 12 May 2026

Keywords: 1,1'-carbonyl diimidazole (CDI) | 1,1'-oxalyl diimidazole (ODI) | agrochemicals | amide bond | ball-milling | energy | green metrics

ABSTRACT

The synthesis of amide moieties, essential components in both pharmaceuticals and agrochemicals, traditionally involves environmentally hazardous and polluting processes. This study presents a novel mechanochemical method to form amide bond using 1,1'-oxalyl diimidazole (ODI) as activating agent, and evaluates its applicability in synthesizing agrochemicals such as Mepronil, Flutolanil, and Fluxapyroxad at gram-scale. The mechanochemical kinetics underlying the synthesis of the three mentioned compounds was also investigated. The new method was compared with the similar 1,1'-carbonyl diimidazole (CDI)-mediated mechanochemical amidation previously reported. Results demonstrate that ODI-mediated synthesis outperforms in the case of deactivated acids. Energetic considerations and technical process parameters are also discussed to provide quantitative technology assessment. A comprehensive analysis by green chemistry metrics with CHEM21 and DOZN^{TM} 3.0 toolkits, underscores the potential benefits of the mechanochemical approach, compared with the solvent-based protocols for the preparation of marketed agrochemicals.

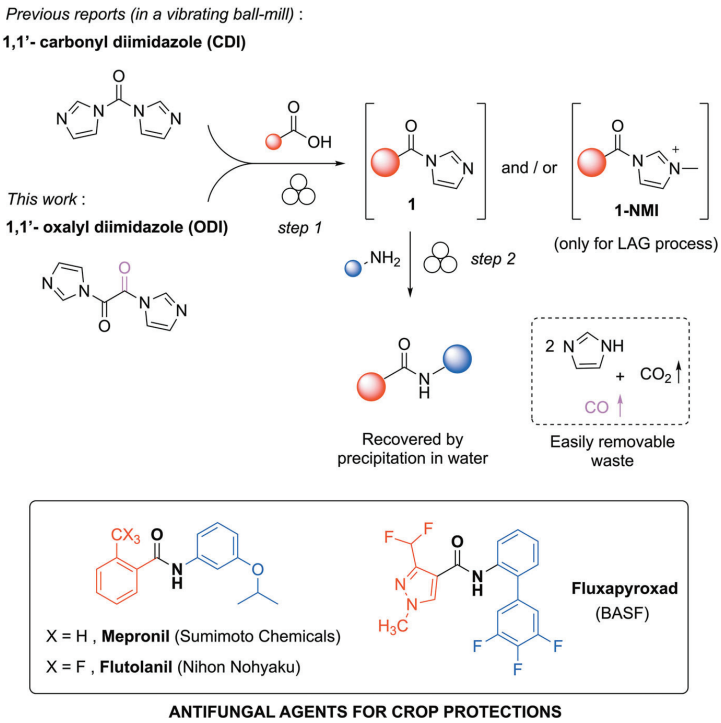
1 | Introduction

The synthesis of amide bonds is one of the most used transformations in industry [1], with applications encompassing organic synthesis and material functionalization [2], and widely used also in drug discovery [3] and in the preparation of active pharmaceutical ingredients [4] and crop protecting agrochemicals [5]. The efforts undertaken to discover active compounds for crop protection have recently intensified with the objectives of enhancing the selective control of insects, weeds, and fungal pathogens as well as reducing toxicological and environmental concerns [6]. This is part of the strategies aimed at improving crop yields to account for the increase in global population and the changes in regulation [7, 8]. Developing efficient and sustainable synthetic routes to access strategic agrochemicals cannot be postponed any longer in the light of the upward jump in global agricultural pesticide production rose from 1.80 million metric tons in 1990 to 3.73 million metric tons of active ingredients in 2023 [9].

In this regard, the superior green performance [10], reduced energy demand [11], minimized waste production, and avoidance of hazardous solvents [12, 13] exhibited by mechanochemical methods show great promise. They meet not only the criteria of Safe and Sustainable by Design (SSbD), but are consistent with the recently launched *IUPAC Guiding Principles of Responsible Chemistry* [14].

In this work, we propose exactly a mechanochemical synthesis of three antifungal agents marketed for crop protection, Mepronil [15], Flutolanil [16, 17], and Fluxapyroxad [18, 19],

This is an open access article under the terms of the Creative Commons Attribution License, which permits use, distribution and reproduction in any medium, provided the original work is properly cited.
© 2026 The Author(s). *Chemistry - A European Journal* published by Wiley-VCH GmbH.



SCHEME 1 | Activating agents CDI and ODI and preparation of marketed agrochemicals by amidation reaction.

with a high global market size. As evident from Scheme 1, the key step is an amidation reaction. Generally, amide bond formation remains challenging because carboxylic acid activation often depends on coupling/activating reagents that present either safety concerns or poor sustainability [2]. Chlorinating agents such as $SOCl_2$, PCl_5, and $POCl_3$ are air- and moisture-sensitive and may release toxic, corrosive byproducts, including SO_2 and HCl, during the reaction, while widely used new generation uronium and phosphonium coupling reagents, such as hexafluorophosphate azabenzotriazole tetramethyl uronium (HATU), hexafluorophosphate benzotriazole tetramethyl uronium (HBTU), (benzotriazol-1-yloxytripyrrolidinophosphonium hexafluorophosphate (PyBOP), and bromo(tripyrrolidin-1-yl)phosphanium hexafluorophosphate (PyBrOP), despite their efficiency typically produce significant stoichiometric waste, resulting in low atom economy and difficult purification. Compared with their current industrial syntheses, which require hazardous and/or polluting compounds, controlled atmosphere, heavy purification procedures, mechanochemical processes can be expected to provide an improved eco-footprint [10, 20–23]. The advantages offered by mechanochemical processing go well beyond solvent avoidance. For instance, the experimental set-up is simple, new reactivities can be explored [24], solubility, or steric hindrance [25] of the reactants are no longer an issue, chemical space can be expanded [26], and reaction rates can be higher [27–32].

Additional advantage come from the choice of reagents for amidation reactions under mechanochemical processing conditions [33]. A safer alternative to the hazardous isocyanates, (tri)phosgene, or chloroformates typically used in the industry, is 1,1'-carbonyl diimidazole (CDI), which is a highly efficient and user-friendly acyl transfer agent, affordable and readily available in bulk quantities, making it ideal for large-scale applications. It is also a valid alternative to the most commonly used coupling/activating agents that, despite their efficiency, display poor atom economy.

CDI has been effectively employed in the solution synthesis of carbonates, ureas, amides, urethanes, and esters [34–36], as well as in peptide coupling reactions [37–41]. In pharmaceutics, CDI is particularly valued for its ability to produce APIs in a clean environment [42, 43], since its byproducts—imidazole and carbon dioxide—are relatively benign and easily removed. Moreover, compared with other coupling agents currently used in amide synthesis, associated waste is less harmful, and the use of resources is improved (e.g., better atom economy). CDI was also successfully used in the mechanochemical preparation of amides [44], ureas [45–48], (including the Lossen rearrangement to hydantoins) [49] and carbamates [50].

Since CDI becomes less efficient with poorly nucleophilic, deactivated acids, the use of 1,1'-oxalyldiimidazole [51] (ODI) was explored. ODI is a more reactive analogue of CDI, and particularly suitable to react with carboxylic acid having unfavorable electronic properties, which fail to deliver the activated *N*-acyl imidazole intermediate **1** (*first step*, Scheme 1) when CDI is used.

15213765, 0, Downloaded from https://chemistry-europe.onlinelibrary.wiley.com/doi/10.1002/chem.71190 by Andreas Casagrande - Université de Montpellier , Wiley Online Library on [25/06/2026]. See the Terms and Conditions (https://onlinelibrary.wiley.com/terms-and-conditions) on Wiley Online Library for rules of use; OA articles are governed by the applicable Creative Commons License

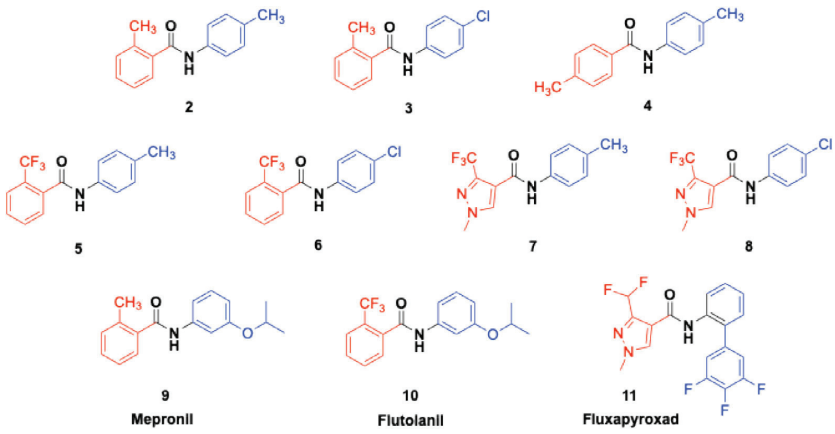


FIGURE 1 | Reaction scope to compare the efficiency of CDI versus ODI-mediated synthesis of amides by mechanochemical processing.

In this respect, it is worth noting that very few reports deal with the use of ODI in solution to prepare carboxylic acid anhydrides [52], esters (e.g., 1,4-dihydroquinoxaline-2,3-diones) [53], nitriles, formiates and formamides [52], cyclic hydrazides (e.g., piperazine-2,3-diones and their tautomers) [54, 55], or as a ligand in inorganic synthesis [56] and for chemiluminescent detection [57]. Surprisingly, no reports deal either with the use of ODI-mediated synthesis of amide in solution nor by mechanochemical processing.

We used the new mechanochemical method we developed to prepare three marketed agrochemicals (Scheme 1), and extended the reaction scope (Figure 1), to better compare the efficiency of CDI- vs ODI-mediated mechanochemical synthesis of amides (see Table S3, Supporting Information for a comparison of CDI vs ODI in solution-based synthesis). The results are discussed in terms of technical and processing parameters, and corresponding energy inputs [58].

The ecological footprint of the ODI-mediated syntheses for three marketed agrochemicals was also evaluated by green chemistry metrics [10], and assessed by CHEM21 [59] and DOZN [12, 60, 61] toolkits. The scores with the solution-based manufacturing processes, and with the corresponding CDI-mediated syntheses by mechanochemistry.

2 | Results and Discussion

1,1′-Carbonyldiimidazole (CDI)-mediated activation to amides. The CDI-mediated preparation of selected targets, including the agrochemicals Mepronil (**9**), Flutolanil (**10**), and Fluxapyroxad (**11**) (Scheme 1 and Figure 1) was explored first, to fully enlighten and disclose similarities and differences with their corresponding ODI-mediated reactions. Table 1 sums-up the best mechanochemical reaction conditions identified for each target.

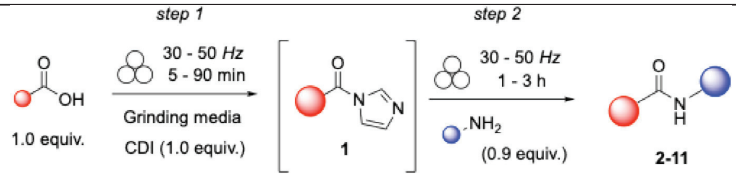
In general, for the preparation of compound **2** (Table 1, entry 1), the use of higher amounts of amines (up to 1.2 equivalents) decreased the yield of the reaction, while traces of products were obtained if an inorganic base was added in the second step (e.g., K_2CO_3, Cs_2CO_3, K_3PO_4), independently on the mechanochemical process conditions used at 30 Hz. This trend was also observed for the preparation of compound **4** (Table 1, entry 3), for which the reactants (the acid and the amine) exhibit electronic properties similar to those employed for compound **2**. However, it is also worth to notice that, in the same mechanochemical processing conditions for both steps using ZrO_2 as milling media, with the same amine (e.g., *p*-methyl aniline), the methyl *ortho*-substituted carboxylic acid delivered a slightly better yield (98%) than the corresponding *para*-substituted substrate (90%), suggesting that, differently than in solution, steric hindrance is not detrimental when mechanochemical conditions are used [25].

The optimization of the milling time in step 1 was also necessary. Indeed, in the preparation of compound **2**, yields dropped to *ca*. 65% (for both SS, stainless steel and ZrO_2 grinding media) by extending the reaction time in *step 1* from 30 to 60 min, probably due to degradation of the *N*-acyl derivative **1,** as a consequence of the heating effects at both microscopic and/or macroscopic levels, resulting from friction and impacts, that cannot be ruled out, leading to an increase in bulk temperature. This hypothesis could be confirmed by repeating the reaction in a polytetrafluoroethylene (PTFE) milling jar (Table 1, entry 1 and Supporting Information), delivering a comparable high yield (96%, at 50 Hz), even though the reaction time for step 1 was reduced to 20 min. Cycled milling was also investigated to possibly reduce the heating effects due to continuous milling, however, no benefits were observed.

In addition to mechanochemical processing conditions, the optimization of the reactions needed to account also for the electronic properties of the amine added in the second step of the reaction. For example, in the preparation of compound **3,** involving a poorly nucleophilic amine (*p*-chloro aniline), the degradation of the *N*-acyl derivative **1** could be more important due to the slower kinetics of addition of the amine, delivering yields generally lower compared to compound **2** (Table 1, entries 1 vs 2), especially when SS was used as grinding media. These considerations are in coherence also with the reactivity trend observed for the set of

15213765, 0, Downloaded from https://chemistry-europe.onlinelibrary.wiley.com/doi/10.1002/chem.71190 by Andreu Casagrande - Université de Montpellier , Wiley Online Library on [25/06/2026]. See the Terms and Conditions (https://onlinelibrary.wiley.com/terms-and-conditions) on Wiley Online Library for rules of use; OA articles are governed by the applicable Creative Commons License

TABLE 1 | Reaction scope for CDI-mediated mechanochemical syntheses of amides **2–11** in vibrating ball-mills, in different processing conditions.[a]



Entry[b]	Compound	Yield (%)		
		ZrO_2[b]	SS[b]	PTFE[c]
1	**2**	**98**	94	96
2	**3**	84	60	**87**
3	**4**	**90**	n.p.[d]	n.p.[d]
4	**5**	**82**	73	70
5	**6**	0	0	**60**
6	**7**	91	**94**	63
7	**8**	**85**	67	71
8	**9**	66	**70**	61
9	**10**	**50**	7	32
10	**11**	0	0	n.p[d]

[a]Typical experimental procedure: the acid (1.0 equiv.) and the 1,1'-carbonyldiimidazole (CDI, 1.0 equiv.) were milled at a given frequency (30 or 50 *Hz*), during 5–90 min. (*step 1*). The amine (0.9 equiv.) was added, and the mixture was milled further for 1–3 h (*step 2*). The reaction scale was 1.35 mmol, except when otherwise specified (*c.f.*, the detailed mechanochemical process conditions are reported in the Supporting Information and Table S2).
[b]Horizontal vibrating ball-mill at 30 *Hz* was used.
[c]Vertical vibrating mill at 50 *Hz* was used.
[d]n.p. = not performed.

compounds **5**, **6**, and **10** (Table 1, entries 4, 5, and 9 respectively), generating the same *N*-acyl imidazole intermediate **1** from 2-trifluoromethyl benzoic acid, allowing to isolate the effect of the amines used in the second step.

If steric effects seemed not to be responsible for the outcome of the reactions, electronic effects on both the starting carboxylic acid and the amine were important. This was particularly evident by comparing three sets of compounds: *set 1* (**2**, **4**, **5**, and **7**), *set 2* (**3**, **6**, and **8**), and *set 3* (**9** and **10**). For each set, the amine selected for the second step did not vary (*p*-methyl aniline, *p*-chloro aniline, or *m*-isopropyloxy aniline, respectively), allowing to isolate the effect of the electronic properties of different carboxylic acids. As a general trend, and as expected, the carboxylic acids bearing fluorinated substituents delivered lower yields of the final amides, regardless of the milling conditions used. Indeed, the conversion of the fluorinated carboxylic acids to the corresponding *N*-acyl derivative **1** was never complete, as indicated by TLC and qualitative GC-MS analyses of the crude after the first step, showing the presence of the starting (unreacted) carboxylic acid. Worst results were obtained when a poorly nucleophilic amine was used for step 2, as for compound **6** (Table 1, entry 5). At 30 *Hz*, by neat milling or in liquid assisted grinding (LAG) conditions using *N*-methyl imidazole (NMI), in different processing mechanochemical conditions, the reactions failed. An acceptable 60% yield could be obtained at higher milling frequency (50 *Hz*) in PTFE/ZrO_2 milling system, extending the reaction time for both steps, to 90 and 180 min respectively. Worth noting is the preparation of compound **5** in comparison with compound **6** (Table 1, entries 4 vs 5, respectively), the only difference being the nucleophilicity of (solid) anilines used.

Even though, for both compounds, the presence of a trifluoromethyl group on the starting carboxylic acid was not optimal for the formation of the corresponding activated *N*-acyl intermediate **1**, the reaction could occur when the more nucleophilic (and low melting, m.p. 45°C) *p*-toluidine was used (entry 4) instead of *p*-chloro aniline (m.p. 72°C). In this case, SS or ZrO_2 grinding media were also suitable, and the reaction times were shorter for both steps.

However, if the combination of a deactivated carboxylic acid with a deactivated amine was unsuccessful in promoting the reactions in both *step 1* (formation of the *N*-acyl derivative **1**) and *step 2* (amidation) for compound **6** (entry 5), the same trend was not observed in the preparation of compound **8** (entry 7). In this case, despite the unfavorable electronic properties of the substrates (the acid and the amine) the reaction was really satisfying in different milling conditions (entry 7, and Supporting Information). This result can be explained evoking a cooperative effect due to the presence of the *N*-methyl pyrazole moiety mitigating, by inductive effects, the strong electron-withdrawing character of the trifluoro methyl substituent. Along the same line, and by comparing compounds **5** and **7** (entries 4 and 6, respectively), higher yields were obtained when 1-methyl-3-(trifluoromethyl)-1*H*-pyrazole-4-carboxylic acid was used, even

15213765, 0, Downloaded from https://chemistry-europe.onlinelibrary.wiley.com/doi/10.1002/chem.71190 by Andreu Casagrande - Université de Montpellier , Wiley Online Library on [25/06/2026]. See the Terms and Conditions (https://onlinelibrary.wiley.com/terms-and-conditions) on Wiley Online Library for rules of use; OA articles are governed by the applicable Creative Commons License

though the differences in yields between the targets are less relevant, being the electron-rich *p*-toluidine used in the second step.

The mechanochemical CDI-mediated amidation reaction in a vibrating ball mill using SS as grinding media, was previously reported [44]. For the reaction scope investigated (Figure 1), the addition of an inorganic base (e.g., K_2CO_3, Cs_2CO_3, K_3PO_4) was tested, but it was detrimental in all the reaction and mechanochemical processing conditions explored, leading to low yields or to the inhibition of the reaction. For all the targets **2–11**, SS was not the best option except for compound **7** (entry 6). This deviation can be attributed to the specific rheology of the reaction, the crude being a viscous paste.

Therefore, the exploration of other mechanochemical processing conditions was a must, with ZrO_2 grinding media being generally more appropriate for the CDI-mediated amidation in the ball-mill, delivering higher average yields, even for the less reactive combination of reagents (in both steps).

The CDI-mediated amidation reaction in both horizontal and vertical vibrating ball-mills lacked general applicability for our reaction scope and *ad hoc* reaction conditions should be developed for each target, requiring a continuous remodulation of the mechanochemical parameters, depending on the target to prepare. In particular, the method had limited applicability when deactivated substrates (e.g., fluorinated carboxylic acids and/or poorly nucleophilic amines) were used, delivering modest yields for preparing the marketed agrochemicals Mepronil (**9**), Flutolanil (**10**) and Fluxapyroxad (**11**) (Table 1, entries 8–10). As a matter of fact, in that series, Mepronil (**9**) delivered the highest yield (70%). This is not surprising, not only because of the favorable electronic properties for both the *ortho*-toluic acid and the 3-isopropoxy aniline, but also due to the physical state of the amine (a liquid) and the reaction intermediate. Indeed, after the first step, the *N*-acyl derivative **1** was a viscous liquid, and the mixing with the amine was facilitated being the 3-isopropoxy aniline also a liquid.

For all the compounds prepared, the formation of the corresponding symmetrical ureas, a typical byproduct in CDI-mediated reactions, was never observed, as shown by GC-MS analyses of the crude reaction mixture (just after milling).

With the purpose of preparing the marketed agrochemicals Mepronil (**9**), Flutolanil (**10**), and Fluxapyroxad (**11**) with high productivity and on gram scale, the CDI-mediated amidation reaction for these selected targets was implemented in a planetary ball-mill (herein referred to as P7P), using zirconia as grinding media (Table 2).

For each set of mechanochemical processing parameters investigated (Table 2), a publicly accessible computational tool [58] was employed to quantify the kinetic energy imparted by the milling media to the reactants upon impact. The analysis differentiated between the cumulative kinetic energy transferred to the reaction mixture over the entire milling duration (E_{total}, in kJ) and the energy associated with a single ball-molecule collision event (E_{impact}, in mJ). The total mass of the milling balls (total m_{balls}) was also incorporated into the calculations, given its direct contribution to the magnitude of E_{total} via momentum transfer and impact frequency.

Therefore, for the agrochemical targets **9–11**, the analysis was conducted considering the mechanochemical processing conditions for *step 1* only, accounting for the formation of the activated *N*-acyl derivative **1** (Table 2). From the extent of success of the first step, it depends essentially the yield of the entire process. The higher the conversion of the starting acid is, the better the yield will be, especially in the case of Mepronil (**9**) and Flutolanil (**10**), having in common 3-isopropyl aniline added in the second step, providing electron-donating effect by induction.

In the mechanochemical preparation of Mepronil (**9**), a 73% yield was obtained by milling the reactants at 500 rpm in a ZrO_2 jar (45 mL, 5.4 mmol scale) with 50×5 mm balls of the same material (Table 2, entry 2, and Supporting Information). However, when the experiment was repeated by replacing the 50×5 mm balls (entry 2) with 25×5 mm balls (entry 1), in a 20 mL ZrO_2 jar (2.7 mmol scale), the yield dropped to 3%. Even though the energy delivered to the reactants during each single impact ($E_{impact} = 11.3$ mJ) was identical for both experiments (entries 1 and 2), the lower cumulative total energy ($E_{total} = 31.1$ kJ) could have slowed down the transformation rate into the corresponding *N*-acyl derivative **1**.

Along the same line, at higher cumulative total energy ($E_{total} = 149.6$ kJ) and in reaction conditions set to provide higher stress frequency (S_F) [62, 63] enabling more impacts per unit of time (entry 3), with a 2.4-fold total cumulative energy ($E_{total} = 149.6$ kJ vs 62.8 kJ in entry 2), the yield was moderate (60%). Indeed, the energy delivered to the reactants during each single impact ($E_{impact} = 2.8$ mJ vs 11.3 mJ in entry 2) was four times lower, with a consequent less efficient conversion of *ortho*-toluic acid into the activated intermediate **1**, delivering a lower yield after the second step (60%, entry 3).

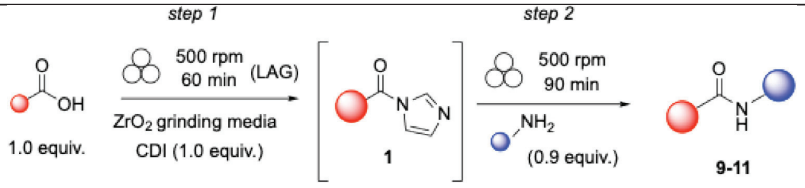
This result confirms that greater energy inputs do not consistently yield higher conversion or yields, emphasizing the need for precise optimization of milling parameters rather than reliance on energy intensity alone in the design of efficient mechanochemical protocols. Indeed, the optimization of a mechanochemical reaction is multifactorial and the reactivity of the system needs fine tuning of several variables, accounting also for the rheological behaviors of the mixture and the chemical reactivity of each chemical entity.

This statement finds further confirmation when comparing the outputs for the preparation of Mepronil (**9**) and Flutolanil (**10**), under identical mechanochemical processing conditions (e.g., Table 2, entries 2 vs 5, and 3 vs 6). Even though both values for E_{impact} and E_{total} were identical, yields were quite different, accounting for differences in the electronic properties of the starting acids (*o*-CH_3-benzoic acid and *o*-CF_3-benzoic acid, respectively).

This is particularly evident in the case of the mechanochemical preparation of Fluxapyroxad (**11**) (Table 2, entries 7–8), when prepared in identical energetic and processing conditions, already successful for targets **9** and **10** (entries 2 and 5).

15213765, 0, Downloaded from https://chemistry-europe.onlinelibrary.wiley.com/doi/10.1002/chem.71190 by Andreu Casagrande - Université de Montpellier , Wiley Online Library on [25/06/2026]. See the Terms and Conditions (https://onlinelibrary.wiley.com/terms-and-conditions) on Wiley Online Library for rules of use; OA articles are governed by the applicable Creative Commons License

TABLE 2 | CDI-mediated mechanochemical syntheses of marketed agrochemicals **9–11** in a planetary mill (P7P):[a] energetic considerations for selected experiments, as function of the process parameters for step 1 and yields (after step 2).



Entry	Compound	Number of ZrO_2 balls / mm Ø	E_{impact} (mJ)	E_{tot} (kJ)	Yield (%)
1	9 Mepronil	25 / 5	11.3	31.1	3
2		50 / 5	11.3	62.8	73
3		648[b] / 3	2.8	149.6	60
4	10 Flutolanil	25 / 5	11.3	31.1	0
5		50 / 5	11.3	62.8	52
6		648[b] / 3	2.8	149.6	37
7	11 Fluxapyroxad	50 / 5	11.3	62.8	3
8		648[b] / 3	2.8	149.6	6
9		648[b] / 3	2.8	149.6	**23**[c]

[a]The filling degree was kept constant (*ca*. 60%) in all the experiments. The reaction scale was: 2.7 mmol (entries 1 and 4) in a 20 mL ZrO_2 jar or 5.4 mmol (entries 2, 3, and 5–9) in a 45 mL ZrO_2 jar. Typical procedure in planetary ball-mill at 500 rpm: (*step 1*) acid (1.0 equiv.) and 1,1′-carbonyldiimidazole (1.0 equiv.) for 60 min; (*step 2*) amine (0.9 equiv.) for 90 min. (*c.f.*, the detailed mechanochemical process conditions are reported in the Supporting Information);
[b]Equivalent to a total mass of 57.1 g of balls.
[c]*N*-methylimidazole (NMI) was used in a LAG process (517.6 μL, $\eta = 0.16$ µL/mg).

The mechanochemical synthesis of Fluxapyroxad (**11**) (entry 7) was in this case not productive. Several different attempts by neat milling were fully unsuccessful (0% yield) with no conversion of the starting materials, due to the highly deactivated nature of both reactants, presenting several electron-withdrawing fluorine atoms on both the acid (involved in the first step) and the amine (involved in the second one). Moreover, the mechanochemical processing conditions outperforming for Mepronil (**9**) and Flutolanil (**10**) (Table 2, entries 2 and 5) were not effective for the CDI-mediated synthesis of Fluxapyroxad (**11**) in P7P ball-mill, delivering only 3% yield (Table 2, entry 7). In the optimal mechanochemical processing conditions (accounting for the simultaneous adjustment of chemical, technical and process parameters), an acceptable yield of 23% (Table 2, entry 9) could be reached only upon the addition of *N*-methylimidazole (NMI, $\eta = 0.16$ µL/mg, 1.1 equiv.) in the first step of the mechanochemical synthesis. Indeed, as observed already in solution, carbamoyl imidazole intermediates (**1**, Scheme 1) lack adequate reactivity toward nucleophilic attack, necessitating activation through alkylation of the distal nitrogen of the imidazole nucleus [64].

The key role played by NMI could be due to several effects and reactions, occurring in parallel or simultaneously. Thus, NMI can act as: i) LAG solvent, ii) base generating, in the first step, a more reactive carboxylate, also due to donor mesomeric effects of the pyrazole ring, and iii) competitor with imidazole, in the formation of a more activated, formally charged, *N*-acyl methyl imidazolium intermediate **1-NMI** (Schemes 1 and 2), facilitating the reaction with the severely deactivated amine. Additionally, being NMI a liquid, its contribution from a rheological standpoint to a better mix of the reaction crude cannot be excluded.

However, although the reaction was somehow effective in the presence of NMI, when K_2CO_3 was employed instead, the reaction was unsuccessful when fluorinated/deactivated substrates were used, indirectly confirming the pivotal role played by NMI for the success of this specific transformation.

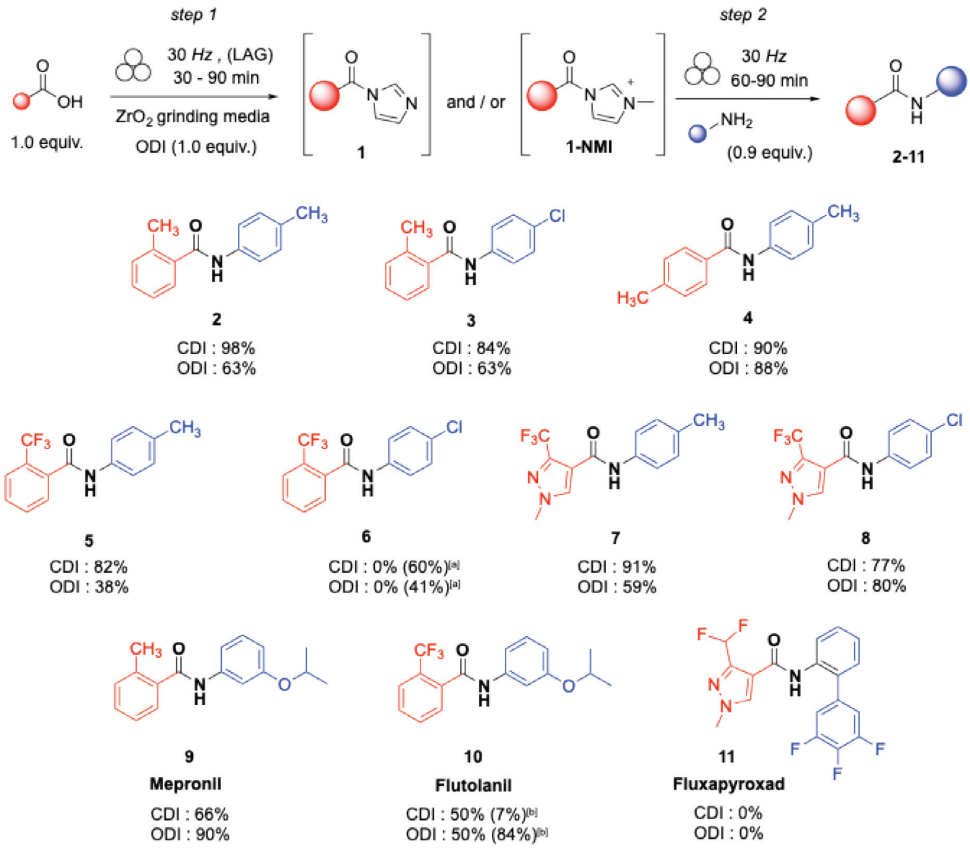
Although the CDI-mediated amidation leading to the marketed agrochemicals **9–11** was not satisfactory when vibrating ball-mills were used (Table 1), their gram-scale preparation was possible in planetary ball-mills (Table 2), milling in neat (entries 2 and 5, for mepronil **9** and Flutolanil **10**, respectively) or LAG conditions (entry 9, for Fluxapyroxad **11**).

2.1 | Kinetic Investigations

Kinetic investigations [65] were also conducted to extract and interpret the kinetic curves obtained from real-time temperature, *T*, and pressure measurements during the mechanochemical *one-pot*/two-step CDI-mediated amidation leading to Mepronil **9**, Flutolanil **10**, and Fluxapyroxad **11**. Since only the first step shows an appreciable pressure rise associated with CO_2 formation, the analysis was focused on this stage.

To accurately interpret the pressure profile, it is first necessary to understand how the application of mechanical forces affects gas evolution during milling, where energy is transferred to the material through impulsive collisions. This energy

15213765, 0, Downloaded from https://chemistry-europe.onlinelibrary.wiley.com/doi/10.1002/chem.71190 by Andrea Casagrande - Universite de Montpellier , Wiley Online Library on [25/06/2026]. See the Terms and Conditions (https://onlinelibrary.wiley.com/terms-and-conditions) on Wiley Online Library for rules of use; OA articles are governed by the applicable Creative Commons License



SCHEME 2 | Reaction scope for the ODI-mediated mechanochemical syntheses of amides **2–11** in a horizontal vibrating ball-mill (*c.f.*, the reaction scale was 1.35 mmol; the detailed mechanochemical process conditions are reported in the Supporting Information and Table S2). The comparative results for the CDI-mediated amidation reaction in ZrO_2 grinding media (Table 1) are also indicated. Data in parenthesis refer to the reaction performed at 50 *Hz* for CDI and 30 *Hz* for ODI, with grinding media: (a) PTFE/ZrO_2 or (b) stainless steel (SS). (*c.f.*, the detailed mechanochemical process conditions are reported in the Supporting Information).

input leads to both mechanical activation and localized heating arising from plastic deformation and friction. Consequently, the observed pressure increase, results from a combination of thermal expansion of pre-existing gas and the formation of CO_2 generated by the reaction. Therefore, to obtain reliable kinetic curves describing the amount of CO_2 produced, these two contributions must be properly disentangled during the data analysis. Therefore, to obtain reliable kinetic curves describing the amount of CO_2 produced, these two contributions must be properly disentangled during the data analysis, by extracting the kinetic curves from pressure data, and analyzing them by kinetic modelling (*c.f.*, Section S3 in the Supporting Information).

Real-time pressure measurements tracked CO_2 evolution during CDI-mediated activation (step 1), serving as a kinetic marker for *N*-acyl imidazole formation (Figures S9,S10, Supporting Information). Control experiments conducted by ball-milling CDI alone, confirmed negligible CDI decomposition, attributing pressure increases solely to reaction-derived CO_2 (Figure S8, Supporting Information). Kinetic profiles showed sigmoidal shapes with substrate-dependent rates: Fluxapyroxad (**11**) reacted fastest, followed by Flutolanil (**10**) and Mepronil (**9**) (Figure S9, Supporting Information).

The early-stage of the reaction appears to be driven by mechanical input, transitioning later to reaction-driven regimes. This is particularly evident for Flutolanil (**10**), where discontinuous milling confirmed the primary role of initial mechanical activation (Figures S9,S10 of Supporting Information). The statistical kinetic model (Equations 8–12, Supporting Information) allows to rationalize the global kinetics from critical loading conditions (CLCs), extracting key parameters such as interface generation rate (r), reaction probability (α), and powder activation fraction (k). By fitting early-stage data revealed that the reaction kinetics are substrate (acid)-dependent, with decreasing kinetics in the order Fluxapyroxad (**11**) > Flutolanil (**10**) > Mepronil (**9**) for both k and α, while r remained almost constant, confirming that

15213765, 0, Downloaded from https://chemistry-europe.onlinelibrary.wiley.com/doi/10.1002/chem.71190 by Andrea Casagrande - Université de Montpellier , Wiley Online Library on [25/06/2026]. See the Terms and Conditions (https://onlinelibrary.wiley.com/terms-and-conditions) on Wiley Online Library for rules of use; OA articles are governed by the applicable Creative Commons License

chemical reactivity dominates after activated surfaces are formed (Figures S11,S12 of Supporting Information).

This analysis quantitatively benchmarks the limited CDI reactivity upon mechanical stress for deactivated substrates (acids), justifying the use of ODI-mediated activation for enhanced reactivity. A more comprehensive discussion on the kinetic investigation, including the explanation of the kinetic model is presented in the Supporting Information (*c.f.*, Section S3).

2.2 | 1,1′-Oxalyldiimidazole (ODI)-Mediated Activation to Amides

Even though CDI was a valid coupling agent for amidation reactions in the vibrating ball-mill (Table 1), with the best average outputs obtained by using hard grinding media (mainly ZrO_2), the method resulted in low to moderate reactivity in the presence of deactivated acids (Table 1), even when more energetic mechanochemical processing conditions in a planetary ball-mill were applied (Table 2, entries 4–9). Therefore, in the quest of a more reactive coupling agent, 1,1'-oxalyldiimidazole (ODI) was used as an alternative acylating agent to CDI, to prepare the target agrochemicals **9**–**11**, at multigram scale (5.4 mmol). The comparison of ODI with CDI is particularly relevant since both are imidazole-based coupling agents and work via the formation of the same ***N***-acyl imidazole intermediate. However, they differ in reactivity, selectivity, and applications (Table S3, Supporting Information).

However, the use of ODI also requires consideration of carbon monoxide evolution during the activation step. In the present mechanochemical set-up, however, gas formation takes place inside a sealed milling jar, so the evolved gas remains confined to the reactor and can be managed by appropriate and standard laboratory safety precautions and engineering controls to fully mitigate operator risks. In particular, the use of milling jars, commercially available or in-house made, equipped with gas-handling valves provide a practical means to channel the gas in a controlled manner, for venting, for gas-solid reactions or for subsequent collection or recycling [66–68]. CO gas itself is industrially employed, demonstrating its viability, also in the green synthesis of Active Pharmaceutical Ingredient [69, 70]. Despite the concerns that can be raised on the evolution of CO gas during the synthesis, solid ODI exhibits lower acute dermal/oral toxicity and lacks inhalation hazards, unlike its liquid counterpart oxalyl chloride (ClCOCOCl), often used in solution for similar purposes, at both laboratory scale [71, 72] and in pharmaceutical manufacturing [73–75] (e.g., for acid chloride formation) or materials synthesis [76]. By the time of this contribution, to the best of our knowledge, no ECHA REACH (European Chemical Agency Registration, Evaluation, Authorization and Restriction of Chemicals) regulations prohibit both oxalyl dihalides (including oxalyl chloride) or ODI at laboratory, research, or industrial scales. ODI was therefore selected for activating carboxylic acids otherwise not efficiently converted when CDI was used, while preserving the practical advantages of the mechanochemical processing, including solvent-free processing and simplified workup. In this context, CO evolution should be viewed as a process parameter to be managed by suitable reactor design and operational control, rather than as a factor that negates the synthetic value of the ODI-mediated approach.

Recommended to be used in dry conditions for best performance (though more tolerant than some others), no special precautions or sophisticated experimental milling set-up were needed to promote the ODI-mediated synthesis of amides in a vibrating ball-mill, and a similar one-pot/two-step approach as for the CDI-mediated amidation described so far (Scheme 2).

In the preparation of targets **2** and **3** sharing *o*-toluic acid (melting at 102°C–104°C) as starting material and generating the same *N*-acyl derivative **1** and imidazole (melting at 90°C–91°C) as by-product, CDI unexpectedly overperformed over ODI coupling agent, and independently on the electronic nature of the amines (m.p. 44°C–45°C for *p*-toluidine and 71°C for *p*-chloroaniline, respectively) added in the second step. However, even though the entropic pool is higher for the ODI-mediated reaction, both the rheology of the reaction mixtures and the melting points of the activating agents (m.p. for CDI 113°C–115°C while ODI decomposes directly at 87°C–92°C [51]), also need to be accounted to explain the reactivity trends observed.

Indeed, in the same milling conditions, the crude mixture after the first step resulted in a dense and compact paste when CDI was used, while a clear liquid was observed for ODI. Even though some decomposition of the more reactive ODI could not be excluded during milling, the transmission of the energy during the impacts could have been more effective when CDI was used, possibly less affected by elastic dispersion than for the reactions making use of ODI.

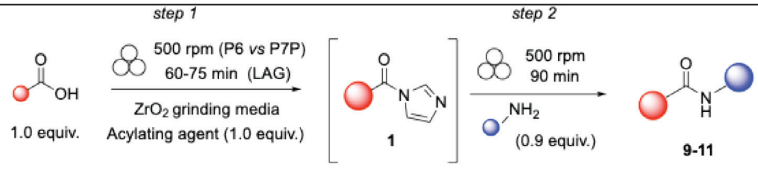
Along the same line, and differently than CDI-mediated reactions, in the case of ODI, the addition of liquid NMI as LAG solvent ($\eta = 0.16\ \mu L/mg$) in the first step proved to be detrimental, switching off the reactions (0% yield for both compounds **2** and **3**). Except for target **6**, for which the use of NMI was beneficial, in all the other cases, and independently on the mechanochemical processing conditions used, yields were halved compared to the values obtained in neat grinding conditions.

Generally speaking, the reactivity trend for the ODI-mediated amidation reaction in the vibrating ball-mill was very similar to the corresponding processes involving CDI, with an important drop in yields observed when deactivated acids were used (compounds **2**, **3**, and **9** vs **5**, **6**, and **10**, respectively, Scheme 2).

However, for compound **6** and independently on the activating agent used (CDI or ODI), the output of the reaction strongly depended on the mechanochemical processing parameters used. Indeed, PTFE/ZrO_2 grinding media outperformed ZrO_2, even though the CDI-mediated process required higher milling frequency (50 Hz) and longer reaction time in step 1 (90 min) compared to ODI-mediated synthesis (at 30 Hz during 60 min for step 1). Along the same line, SS grinding media proved to be more suitable than ZrO_2 for the preparation of Flutolanil **10** (84% vs 49% yield respectively, Scheme 2), confirming the importance of the fine tuning of the mechanochemical processing parameters, in addition to the chemical reactivity of a specific substrate or reactant.

15213765, 0, Downloaded from https://chemistry-europe.onlinelibrary.wiley.com/doi/10.1002/chem.71190 by Andreu Casagrande - Université de Montpellier , Wiley Online Library on [25/06/2026]. See the Terms and Conditions (https://onlinelibrary.wiley.com/terms-and-conditions) on Wiley Online Library for rules of use; OA articles are governed by the applicable Creative Commons License

TABLE 3 | Mechanochemical syntheses of marketed agrochemicals **9–11** in planetary ball mills:[a] comparative assessment as function of the chemical (CDI vs ODI-mediated methods) and technical process parameters.



		Yield (%)			
		CDI[b]		ODI[b]	
Entry	Compound	P6	P7P[c]	P6[d]	P7P
1	**9** Mepronil	16	73	**93**[e]	83
2	**10** Flutolanil	21	52	**64**[f]	55
3	**11** Fluxapyroxad	1[g]	23[g]	53[f g]	**66**[d g]

[a]Reaction scale was 5.4 mmol. Typical procedure in planetary ball-mill at 500 rpm, using 45 mL ZrO_2 milling jar, (step 1) acid (1.0 equiv.) and acylating agent (CDI or ODI, 1.0 equiv.); (step 2) amine (0.9 equiv.) for the specified times (*c.f.*, the detailed mechanochemical process conditions are reported in the Supporting Information and Table S2);
[b]50 ZrO_2 balls (5 mm ∅, total weight: 19.2 g) were used except when otherwise specified; for step 1: 60 min, for step 2: 90 min;
[c]Data reported already in Table 2, entries 2, 5 and 9;
[d]57.1 g of 3 mm ∅ balls were used;
[e]The reaction time was: for step 1: 75 min, for step 2: 90 min.;
[f]The reaction time was 90 min (for both steps);
[g]*N*-methylimidazole (NMI, 1.1 equiv.) was used in a LAG process ($\eta = 0.16$ mL/mg).

Despite the several attempts to disclose a general mechanochemical method, the ODI-mediated amidation reaction in the vibrating ball-mill only outperformed CDI in the preparation of the fungicides Mepronil (**9**) and Flutolanil (**10**), and the optimization plan remained extremely cumbersome for each of the substrates. The best results are reported in Scheme 2. Furthermore, similarly to the CDI-mediated amidation reaction in the vibrating ball-mill, the preparation of Fluxapyroxad (**11**) was unsuccessful under all the (neat or LAG) mechanochemical processing conditions tested.

Our previous findings showed that the CDI-mediated amidation reactions delivered acceptable (but still moderate) yields of Mepronil (**9**), Flutolanil (**10**) and Fluxapyroxad (**11**) (Table 2, entries 2, 5, and 9, respectively), in a planetary ball-mill, in neat or LAG conditions, when other (mechano)chemical processing conditions failed. Therefore, the gram-scale synthesis of these specific targets (**9–11**) was implemented using two different mechanochemical devices, referred to as P6 and P7P and the results were compared for both CDI- and ODI-mediated synthesis, in the same optimized processing conditions (Table 3).

Overall, data in Table 3 clearly indicate that, regardless of the planetary milling device used (P6 or P7P), the multigram scale ODI-mediated amidation reactions outperformed the corresponding CDI method. In particular, for all compounds **9–11**, ODI conditions were more effective particularly with the P6 planetary ball-mill, with incremental yields in the range of 43%–86% (Table 3, entries 1–3 – CDI vs ODI in P6 experiments), and to a lesser extent in the P7P, with a maximum yield increase of 33% for Fluxapyroxad (**11**) (Table 3, entry 3 – CDI vs ODI in P7P experiments).

For the set of experiments carried out in the P6 planetary mill, Mepronil (**9**) was the compound displaying the highest yield increase (entry 1, 16% vs 93%) under ODI conditions, probably due to the favorable electronic and rheological properties of both the reactants towards both activation/addition steps. In the case of Flutolanil (**10**), this trend was confirmed even though the yield increase observed for ODI conditions was 43% (entry 2, 21% vs 64%), and lower than for Mepronil (**9**). This is not surprising, considering the deactivated nature of the starting *o*-trifluoromethyl benzoic acid, also requiring longer reaction times for both steps (90 min each). In the case of Fluxapyroxad (**11**) ODI-mediated amidation outperformed CDI (entry 3, 1% vs 53% CDI vs ODI, respectively) but LAG conditions using NMI were necessary, with an optimized $\eta = 0.16$ μL/mg value. While LAG was necessary for the preparation of Fluxapyroxad (**11**) in all the mechanochemical conditions tested (Table 3, entry 3), no improvements were observed when it was used in the synthesis of both Mepronil (**9**) and Flutolanil (**10**). Moreover, a complete reaction inhibition was observed for all the targets (**9–11**) when η value was increased up to 0.4 μL/mg.

In general, for both CDI and ODI methods, the reaction in the planetary ball-mill was facilitated by the presence of a liquid reagent (the amine) in the reaction mixture (Table 3, entries 1 and 2), while the addition of *N*-methylimidazole (NMI, Table 3, entry 3) in LAG conditions (η = 0.16 μL/mg) was necessary for both solid and deactivated reagents, delivering better yields

15213765, 0, Downloaded from https://chemistry-europe.onlinelibrary.wiley.com/doi/10.1002/chem.71190 by Andreu Casagrande - Université de Montpellier , Wiley Online Library on [25/06/2026]. See the Terms and Conditions (https://onlinelibrary.wiley.com/terms-and-conditions) on Wiley Online Library for rules of use; OA articles are governed by the applicable Creative Commons License

compared to the mechanochemical processing condition in dry media.

This trend was particularly evident in the case of Fluxapyroxad (**11**) especially when P7P was used (Table 3, entry 3) and for which the use of NMI was crucial to achieve acceptable yields. The solid fluorinated amine is particularly deactivated towards nucleophilic attack on the activated *N*-acyl imidazole intermediate **1** (and/or **1-NMI**) due to the strong electron-withdrawing effect of three fluorine atoms on the aryl ring. Indeed, the sets of experiments in P7P for both CDI- (6% vs 23%, neat vs LAG respectively) and ODI- (traces vs 66%, neat vs LAG, respectively) mediated syntheses, showed that the lowest yields were obtained in the absence of NMI, and independently on the mechanochemical processing conditions explored, and again, with a switch-off of the reaction (for all the targets, **9–11**) at η = 0.4 μL/mg.

In comparative terms, for Fluxapyroxad (**11**), the use of ODI as coupling/activating agent was competitive in comparison with CDI, for P6 and particularly P7P, also suggesting that the more reactive ODI is better suited for deactivated substrates/intermediates. For agrochemicals **9–11**, the preparation using CDI as activating agent performed better in the P7P planetary ball-mill. However, differences were observed when ODI was used with the P6 planetary ball mill, delivering better results for agrochemicals **9** and **10**, while P7P proved more efficient for preparing Fluxapyroxad (**11**). These results can be explained by considering the relative reactivity of CDI vs ODI. They display similar melting points (119°C vs 114°C–116°C, respectively) and they deliver the same activated *N*-acyl imidazole intermediate **1** (and/or **1-NMI**), which allows to rule out the possibility of a more favorable rheology for the reactions involving ODI as a consequence of a macroscopic melt.

CDI and ODI display the same stability at room temperature, upon aging, however, their relative stability under identical mechanical stress can be different. Commercial samples of CDI and ODI were equally stable during 24 h at room temperature, as shown by ATR FT-IR analyses, sampling at t = 0 , 6, and 24 h. However, differences may arise upon mechanochemical processing. Therefore, the better reactivity of ODI was justified by its more favorable entropic pool compared to CDI, with the release of an additional CO molecule, which should help the reaction to evolve favorably towards the activated *N*-acyl imidazole intermediate **1**, an aspect that becomes important especially in the case of poorly nucleophilic acids.

Clearly, yields were also dependent on a specific technical parameter, namely the ball-milling device used. While keeping all other technical parameters identical (e.g., milling media, size and number of milling balls, milling jar volume and shape, filling degree and ball to mass ratio), as well as the reaction scale (5.4 mmol), chemical conditions (neat or LAG), and mechanochemical process parameters (milling speed and reaction time), significant differences were observed.

The two different planetary ball-milling devices used, referred to P6 and P7P, differ in: (i) the distance between the axis of the sun wheel and the axis of the bowl (referred to as *r* in mm), and (ii) the ratio of rotation between the sun wheel and the bowl (referred to as ^{i}relativ), providing different main accelerations (G) resulting in a same sun disc speed (i.e., 500 rpm), (Table S4, Supporting Information).

Therefore, the higher acceleration (19.65 G, 192.77.1 m sec^{-2}) provided by the P7P planetary ball-mill was appropriate for the preparation of the target agrochemicals **9–11** via reactions involving CDI (Table 3, entries 1–3), less reactive than ODI, and for which the P7P was the most suitable planetary ball-mill. Being the reactivity of CDI lower compared to ODI, it is not surprising that, under identical mechanochemical conditions at the same sun disc speed (e.g., 500 rpm), and for the same substrate, a higher acceleration (energy) was needed to promote the reaction (Table S4, Supporting Information), without degradation of the very reactive *N*-acyl-imidazole active specie and/or the CDI itself. The shallower energy requirement for a reactive collision was also modulated by using milling balls of smaller diameter (Table 3, 3 mm balls were used for the ODI-mediated synthesis in P6 planetary ball-mill), to ensure a high frequency of collision per unit of time, but still delivering lower kinetic energy at each single impact, thereby also preserving ODI and the very reactive *N*-acyl-imidazole active species from degradation, which reflects into overall higher yields, also at gram scale, for the experiments conducted in the P6 planetary ball-mill.

Therefore, in general, if the CDI activating agent resulted more suitable for experiments conducted in the P7P, the use of the P6 seemed to be more appropriate when the more reactive ODI was used (Table 3, entries 1 and 2), for which less energy is required, having a stronger entropic pull in reacting with the acid. However, in the case of Fluxapyroxad **11** (Table 3, entry 3), the unfavorable electronic properties (i.e., a fluorinated acid and a perfluorinated amine) and the physical state of the reagents (solids) required *ad hoc* process conditions. In particular, and synergistically: i) a higher acceleration (energy) to promote the reaction, with the P7P planetary ball-mill resulting the most appropriate, independently on the activating agent used (CDI vs ODI) and ii) LAG conditions to form a more reactive *N*-acyl intermediate (e.g., **1-NMI**) were needed. Indeed, by neat grinding, no reaction was observed in all cases, for both CDI or ODI-mediated reactions, when either P6 or P7P planetary mills were used.

When it comes to product recovery, and to keep the generally demonstrated environmental-friendly approach of mechanochemical reactions [10], the eco-design has to also concern the downstream processes.

Therefore, in general, if the CDI activating agent resulted more suitable for experiments conducted in the P7P, the use of the P6 seemed to be more appropriate when the more reactive ODI was used (Table 3, entries 1 and 2), for which less energy is required, having a stronger entropic pull in reacting with the acid. However, in the case of Fluxapyroxad **11** (Table 3, entry 3), the unfavorable electronic properties (i.e., a fluorinated acid and a perfluorinated amine) and the physical state of the reagents (solids) required *ad hoc* process conditions. In particular, and synergistically: i) a higher acceleration (energy) to promote the reaction, with the P7P planetary ball-mill resulting the most appropriate, independently on the activating agent used (CDI vs ODI) and ii) LAG conditions to form a more reactive *N*-acyl intermediate (e.g., **1-NMI**) were needed. Indeed, by neat grinding, no reaction was observed in all

15213765, 0, Downloaded from https://chemistry-europe.onlinelibrary.wiley.com/doi/10.1002/chem.71190 by Andrea Casagrande - Université de Montpellier , Wiley Online Library on [25/06/2026]. See the Terms and Conditions (https://onlinelibrary.wiley.com/terms-and-conditions) on Wiley Online Library for rules of use; OA articles are governed by the applicable Creative Commons License

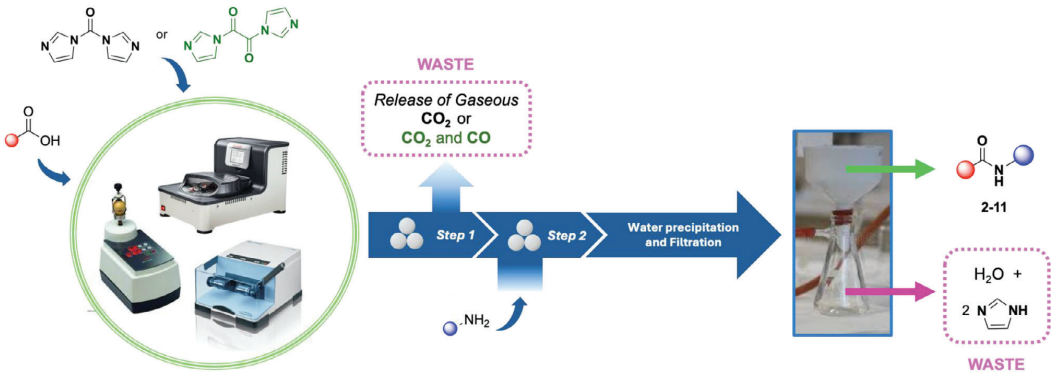


FIGURE 2 | Downstream and eco-friendly process for recovering the final targets, with no need of organic solvents.

cases, for both CDI or ODI-mediated reactions, when either P6 or P7P planetary mills were used.

When it comes to product recovery, and to keep the generally demonstrated environmental-friendly approach of mechanochemical reactions [10], the eco-design has to also concern the downstream processes.

Solvent use during work-up continues to be one of the most significant challenges that diminishes the advantages of mechanochemical reactions. Therefore, special attention was also devoted to downstream operations, implementing a straightforward recovery of the final targets without the use of organic solvents, by minimizing the use of toxic/hazardous additional chemicals and the amount of waste generated. Therefore, the final targets **2–11** (for both CDI- and ODI-mediated amidation) were universally recovered by precipitation in water, followed by filtration, the only waste being gaseous CO_2 and CO (from for ODI) in the first step, and the water-soluble imidazole, generated in the second step (Figure 2).

2.3 | Comparative Greenness Assessment of Mechanochemical Versus Solution-Based Processes by Green Chemistry Metrics

The eco-footprint of the mechanochemical processes was quantitatively assessed by an array of green chemistry metrics calculations [10, 13], using the Chem21 [59], and DOZN^{TM} 3.0 [12, 60, 61, 77] tools (*c.f.*, excel files in the Supporting Information). These metrics represent essential tools that should guide the design and optimization of synthetic protocols, particularly when the objective is sustainability and environmental compatibility. The evaluations performed using the DOZN toolkit were paired with calculations with Chem21 to secure an even more objective and quantitative approach to the evaluation of greenness, sustainability and safety of the process. Therefore, green metrics such as atom economy (AE) [78], real mass economy (RME) [79], process mass intensity (PMI) [80], and optimum efficiency (OE) [59] were calculated along with the assessment for solvent and reagent choice, reaction and workup setup, and hazards. The scores obtained with both toolkits, were compared with the corresponding solution-based preparation methods.

In particular, for the three agrochemicals **9–11**, metrics were calculated for both CDI and ODI-mediated mechanochemical syntheses at gram-scale in planetary ball-mills, selecting the methods delivering the best yields (Table 3 and Supporting Information). No CDI- or ODI-mediated synthesis in solution are known for the agrochemicals **9–11**. Therefore, the solution-based procedures to access Mepronil **9** [15], Flutolanil **10** [16, 17] and Fluxapyroxad **11** [18, 19] were selected from the literature among those that were most closely related to the mechanochemical synthetic methods used herein, to ensure a robust and meaningful comparison. For Fluxapyroxad specifically, the comparison was performed against both a laboratory-scale synthesis [19] and the industrial method [81], as the former mirrors the activation of acid/amine addition approach, while the latter offers a realistic benchmark against established manufacturing methods.

2.4 | DOZN Assessment

The evaluation of greenness using DOZN^{TM} 3.0 [61] is presented in Figure 3 (and Supporting Information). The tool quantitatively assesses adherence to the twelve principles of green chemistry and has become a valuable approach for evaluating mechanochemical manufacturing processes of commercially relevant molecules in comparison to solution-based approaches at different scales. DOZN^{TM} tool operates by assigning a score, from 0 to 100 for each of the twelve green principles [60], which are subsequently aggregated into three principle-based groups reflecting thematic similarities: Improved Resource Use (principles 1, 2, 7, 8, 9, 11 – Group 1), Increased Energy Efficiency (principle 6, Group 2), and Reduced Human and Environmental Hazard (principles 3, 4, 5, 10, 12 – Group 3). An overall *aggregate score* is calculated as the mean of all twelve principle scores. The lower the value, the greener the process, with the optimum *aggregate score* value being below 1.

In the case of Mepronil (**9**), solution-based synthesis outperformed both CDI- or ODI- mediated amide bond synthesis by milling, delivering better scores for Groups 1 and 3 (3.59 and 2.57

15213765, 0, Downloaded from https://chemistry-europe.onlinelibrary.wiley.com/doi/10.1002/chem.71190 by Andreu Casagrande - Université de Montpellier , Wiley Online Library on [25/06/2026]. See the Terms and Conditions (https://onlinelibrary.wiley.com/terms-and-conditions) on Wiley Online Library for rules of use; OA articles are governed by the applicable Creative Commons License

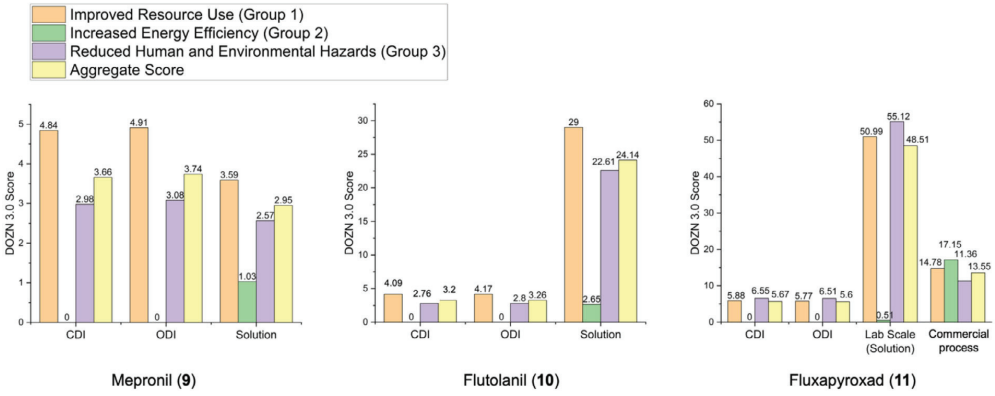


FIGURE 3 | Comparison of solution-based versus planetary ball mill (PBM) syntheses for both CDI- and ODI-mediated amidation reaction, by DOZN^{TM} 3.0 quantitative scoring tool. Legend: *Group 1* (Improved Resource Use – **orange**), *Group 2* (Increased Energy Efficiency – **green**), *Group 3* (Reduced Human and Environmental Hazards – **violet**), and Aggregate score – **yellow**.

respectively), as well as for the aggregate (2.95). Performance in this instance is primarily constrained by water consumption relative to product recovery during the work-up (Figure 2). However, this parameter could be further improved at larger scale, particularly if the solvent (water) is recycled for subsequent workups. The only advantage of the mechanochemical approach was observed for Group 2 (energy efficiency), being the reactions performed at room temperature and atmospheric pressure (instead of heating at 100°C) [15]. Contrarily, for the preparation of Flutolanil (**10**) and Fluxapyroxad (**11**), both involving electron-withdrawing reagents and substrates, and consistently with the experimental data, both CDI- and ODI-mediated mechanochemical synthesis outperformed the respective solution-based methods for each group of principles, and with 2.4- and 8.6-fold better aggregate scores for both targets, respectively.

For both Flutolanil (**10**) and Fluxapyroxad (**11**), although lower yields were obtained by both mechanochemical methods (CDI and ODI-based) compared to solution-based counterparts, scores for Group 1 and Group 3 resulted better. This is explained mainly by two factors that play a major role in the general economy of the synthetic methods by mechanochemistry. For Group 1 (improved resource use) the better scores resulted not only by the avoidance of solvents (e.g., DMF, CH_2Cl_2, Et_2O), but also in the strategies employed for the activation of the acid and for the isolation of the final product. By mechanochemistry, for both CDI and ODI activating agent, imidazole is generated as by-product. Being water soluble, it can be washed by water. Conversely, solution-based routes make use of stoichiometric amount of chlorinating agents to activate the starting carboxylic acid (e.g., oxalyl chloride [16] and PCl_5 [19] for Flutolanil **10** and Fluxapyroxad **11**, respectively), which produce HCl as a by-product and necessitate subsequent neutralization with basic additives (i.e., triethylamine or pyridine), directly inflating resource consumption and negatively affecting also Group 3 (reduced human and environmental hazards). Group 3 displayed better scores for the mechanochemical protocols, through systematic elimination of hazardous solvents (DMF, dichloromethane, and diethyl ether) and substitution of air sensitive chlorinating reagents (e.g., PCl_3 or oxalyl chloride), needing controlled inert gas atmosphere, by safer and air stable imidazole-based coupling agents (i.e., CDI and ODI). This approach allowed to reduce substantially the occupational health risks and environmental contamination, as their reaction with atmospheric moisture do not generate hazardous acids (e.g., gaseous HCl or phosphoric acid) and exothermic heat. Additionally, the work-up conducted directly into the milling jar further reduces both acute occupational health risks and environmental contamination, by employing only water or dilute hydrochloric acid, further minimizing exposure to organic solvents and volatile organic compounds. The staggering difference in scores in the case of Fluxapyroxad (**11**) can be further justified by looking at the difference in the workup procedure. The solution-based protocol needs column chromatography to purify the final compound, extensively dispendious in terms of polluting resources (e.g., silica, petroleum ether mainly), while the mechanochemical counterpart rely only on precipitation in acidified water (Figure 2).

When it comes to Group 2 (increased energy efficiency), the score accounts for any deviation from room standard conditions, which are room temperature and atmospheric pressure. The mechanochemical methods (for both CDI and ODI) operated at room-temperature and in significantly shorter reaction times compared to their solution-based counterparts. Indeed, the activation of the acid was the less efficient for each of the targets **9–11**. In the case of Mepronil (**9**), the reaction with $POCl_3$ required 3 h at 100°C [15], for Flutolanil (**10**), the reaction by oxalyl chloride needed cooling to 0°C [16], and in the case of the industrial synthesis of Fluxapyroxad (**11**), the reaction occurs in an autoclave under high pressure of CO (9 bar), at high temperatures (130°C) and for a prolonged time (20 h) [81], yielding the worst overall score in this category across the entire assessment.

In general, for all the agrochemicals **9–11**, when comparing CDI vs ODI method by milling, similar scores where always obtained for each group of principles and for the aggregate scores. The minimal variations between the two mechanochemical approaches reflect their inherent similarity in terms of resource consumption patterns, stoichiometry, and reaction conditions, which do not

15213765, 0, Downloaded from https://chemistry-europe.onlinelibrary.wiley.com/doi/10.1002/chem.71190 by Andreu Casagrande - Université de Montpellier , Wiley Online Library on [25/06/2026]. See the Terms and Conditions (https://onlinelibrary.wiley.com/terms-and-conditions) on Wiley Online Library for rules of use; OA articles are governed by the applicable Creative Commons License

generate sufficient differentiation in the assessment by DOZN™ 3.0.

2.5 | CHEM21 Assessment

Assessment by CHEM21 [59] (Table 4 and Supporting Information) quantitatively compares methods through green metrics, including the Overall Efficiency (OE), which enables direct comparison across different reaction classes, a feature not consistently achievable with Atom Economy (AE) or Reaction Mass Efficiency (RME). As intrinsic atom- or mass-efficiency varies among transformations, OE provides a more broadly applicable and discriminating metric for assessing synthetic efficiency [59]. Chem21 takes into account also other qualitative criteria that facilitate the assessment of energy efficiency, safety, and potential environmental and health risks. The evaluation framework employs a categorical flag system with clear visual indicators to enhance interpretability and enabling the identification of reaction performance across distinct sustainability dimensions. Each criterion is designated by a color-coded flag: green denotes "preferred," amber signifies "acceptable with some concerns," and red indicates "undesirable."

For the three agrochemical targets **9**–**11**, AE, RME and OE alone might suggest an advantage for methodologies in solution. With the exception of Mepronil (**9**) however, metrics such as PMI and E-factor point to the opposite direction, accounting quantitatively for the resources used in the whole process, which also include the solvents used in the workup (included in the value of $PMI_{work\text{-}up}$), and not only the yield (Table 4).

The mechanochemical methods, particularly the ODI-mediated amidation, demonstrated superior performance not only in comparison with solution-based routes for each of the targets (**9-11**), but also respect to CDI-mediated method, with the lowest *E*-factor and the most favorable PMI values (Table 4). Despite the generally lower yields of the mechanochemical methods compared to solution-based protocols, the better metrics are explained by the absence of solvents (that constitute 66%–96% of the total reaction mass), and the systematic elimination of basic additives required in the solution protocols to neutralize the HCl (or HBr) generated as by-products. Especially in the case of Fluxapyroxad (**11**) the laboratory scale amidation in solution results in a PMI of 742.7 and an *E*-factor of 741.7, over 19-fold worse than the ODI mechanochemical route (PMI 37.8 and *E*-factor 36.8). This dramatic gap is due to the use of column chromatography as a purification method, which consumes disproportionate resources. This is quantified by the values of $PMI_{work\text{-}up}$ (34.9 vs 714.0, Table 4) in favor for the mechanochemical route. However, in the industrial process the purification conducted by trituration in Et_2O, followed by filtration, delivered greatly improved PMI and *E*-factor values (60.4 and 59.4 respectively). The improvement of the total PMI value is also reflected in $PMI_{work\text{-}up}$ values, which is the value that improves most (Table 4). Nonetheless and although PMI and *E*-factor metrics for the mechanochemical methods with ODI (at 5.4 mmol scale) are better than those of the industrial process, the comparison is not fully realistic. Indeed, mass-based metrics need to be integrated with energy-based and life cycle assessments to determine the sustainable footprint of each process [82], ideally at a similar scale.

As for DOZN™ 3.0, Chem21 also substantiated mechanochemical superiority through systematic elimination of hazardous solvents and reactants. Solution-based procedures rely on solvents with significant occupational and environmental liabilities. The synthesis of Flutolanil (**10**) requires *N,N*-dimethylformamide (DMF), already subject to strict regulations for industrial use in the EU [83], and dichloromethane (DCM), which is banned for most commercial and industrial uses and is undergoing a complete phase-out in USA [84]. At laboratory scale, the synthesis of Fluxapyroxad (**11**) makes use of diethyl ether, characterized by an exceptionally low flash point (−45°C) and low autoignition temperature (160°C), representing a severe fire and explosion hazard, while at industrial scale, toxic and polluting $PdCl_2$ [85] is used for the carbonylation reaction using CO gas under high pressure.

By contrast, the CDI/ODI-mediated mechanochemical protocols operate under metal- and solvent-free conditions (or require only minimal amounts of solvent by LAG process with NMI), with potentially better environmental footprint, also in terms of downstream processing, as the final targets are recovered by precipitation in water, instead of: i) employing *n*-hexane for crystallization in the case of Flutolanil (**10**), and ii) purification by column chromatography for Fluxapyroxad (**11**). Therefore, the PBM route, skipping the need for wasteful workup procedures, along with the easier experimental setup that avoids the use of hazardous chemicals, shows in the CHEM21 assessment a better overall performance, even when yields are lower than those of the solution-based methods considered for the assessment.

Overall, with the exception of Mepronil (**9**), in all cases, and independently on the assessment tool used (DOZN™ 3.0 or CHEM21), the mechanochemical methods displayed superiority in terms of overall greenness, in comparison to the solution-based counterparts, at laboratory scale.

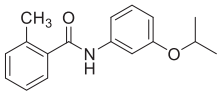
3 | Conclusion

We developed a mechanochemical method for amide bond formation was disclosed and applied to the preparation of a library, including three marketed agrochemicals, Mepronil (**9**), Flutolanil (**10**), and Fluxapyroxad (**11**) at gram-scale. Therefore, 1,1'-oxalyldimidazole (ODI) was used as valid alternative to the green activating agent 1,1'-carbonyldiimidazole (CDI), not suitable for deactivated acids (e.g., containing fluorinated substituents). The mechanochemical amidation reactions by both CDI and ODI were systematically compared and the reactivity profiles investigated by both vibrating ball-mill (VBM) and planetary ball-mill (PBM). Accordingly, different mechanochemical processing conditions, set by adjusting chemical variables (e.g., neat grinding vs LAG processes), technical (e.g., type of ball-mills, milling media, size and number of milling balls, milling jar volume) and process (e.g., operating frequency, and reaction time) parameters were explored. Kinetic investigation for the CDI-mediated synthesis was also performed. Kinetic analysis suggests that mechanical activation dominates only the early reaction stages. Kinetic datasets were interpreted based on a kinetic model that allows bridging global and local kinetics. It appears that the fraction of powder effectively processed per unit time as well as the reaction probability depend strongly

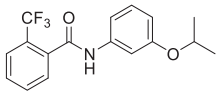
15213765, 0, Downloaded from https://chemistry-europe.onlinelibrary.wiley.com/doi/10.1002/chem.71190 by Andreu Casagrande - Université de Montpellier , Wiley Online Library on [25/06/2026]. See the Terms and Conditions (https://onlinelibrary.wiley.com/terms-and-conditions) on Wiley Online Library for rules of use; OA articles are governed by the applicable Creative Commons License

TABLE 4 | Comparison of CHEM21 [60] assessment for solution-based versus PBM protocol using CDI or ODI as a coupling agents for the synthesis of compounds (**9**), (**10**), and (**11**) (for the full assessment, *c.f.*, Supporting Information).

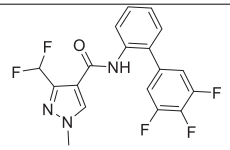
CDI (PBM) versus ODI (PBM) versus Solution



(**9**)



(**10**)



(**11**)[b]

Metrics[a]	(9)					(10)					(11)[b]				
AE	61.4	vs	56.4	vs	80.8	64.2	vs	60.8	vs	69.0	67.9	vs	64.7	vs	62.8	vs	82.5
RME	40.5	vs	48.7	vs	61.8	31.2	vs	35.8	vs	54.9	14.6	vs	40.2	vs	50.5	vs	30.3
OE[c]	66.0	vs	86.3	vs	76.5	48.6	vs	58.9	vs	79.6	21.5	vs	62.2	vs	80.4	vs	36.8
PMI[d]	45.1	vs	35.4	vs	13.4	52.4	vs	43.3	vs	55.0	108.9	vs	37.8	vs	742.7	vs	60.4
$PMI_{reaction}$	2.5	vs	2.1	vs	6.3	3.2	vs	2.8	vs	50.4	8.0	vs	3.0	vs	28.7	vs	20.9
PMI_{workup}	42.6	vs	33.3	vs	7.2	49.2	vs	40.5	vs	4.6	100.9	vs	34.9	vs	714.0	vs	39.6
***E*-factor**	44.1	vs	34.4	vs	12.4	51.4	vs	42.3	vs	54.0	107.9	vs	36.8	vs	741.7	vs	59.4
Solvent	No solvent		No solvent		Xylene	No solvent		No solvent		DCM, DMF, THF	NMI (for LAG)		NMI (for LAG)		Et_2O, THF,AcOEt		ACN
Work-up, recovery	Water Precipitation, Filtration		Water Precipitation, Filtration		Water washing	Water Precipitation, Filtration		Water Precipitation, Filtration		Crystalliz.	Water Precipitation, Filtration		Water Precipitation, Filtration		Water Washing, Column chrom.		Trituration (Et_2O), Filtration
Health & safety																	
Main hazard statements	H360d		H331, H220, H360d, H372		H225, H302, H312, H314, H318, H330, H332, H372, H412	H360d		H331, H220, H360d, H372		H220, H225, H260, H280, H302, H304, H312, H314, H315, H319, H331, H332, H335, H336, H341, H350, H351, H360d, H361, H370, H372, H373, H401, H411	H360d		H331, H220, H360d, H372		H224, H225, H302, H304, H312, H314, H318, H319, H320, H330, H331, H335, H336, H351, H361, H373, H411		H220, H225, H280, H290, H302, H312, H314, H317, H318, H319, H331, H332, H335, H336, H351, H360D, H372, H400, H410, H412

Legend: Green flag: Preferred; Amber flag: Acceptable with some concerns; Red Flag: Undesirable.

[a]Best values for AE, RME and OE is 100%, for PMI is 1 and *E*-Factor = PMI − 1 [87]. When comparing two processes, the one with the lowest PMI will be greenest

[b]For Fluxapyroxad (**11**) the four columns are referred respectively to: CDI method in PBM, ODI method in PBM, solution-based method at laboratory scale, and industrial process

[c]$OE = \frac{RME}{AE} \times 100$ [60];

[d]Where precise work-up chemical quantities were unavailable, estimates were derived as detailed in the Supporting Information to ensure fair comparison.

15213765, 0, Downloaded from https://chemistry-europe.onlinelibrary.wiley.com/doi/10.1002/chem.71190 by Andrea Casagrande - Universita de Mompellier , Wiley Online Library on [25/06/2026]. See the Terms and Conditions (https://onlinelibrary.wiley.com/terms-and-conditions) on Wiley Online Library for rules of use; OA articles are governed by the applicable Creative Commons License

on the substrate nature following the trend Fluxapyroxad **11** > Flutolanil **10** > Mepronil **9**. These findings indicate that, once molecular contact is established, the local chemical environment plays a decisive role in determining the likelihood of chemical transformation. For the three selected agrochemicals **9–11**, the yields obtained were discussed in terms of total cumulative energy (E_{total} in kJ) and energy delivered to the reactants during each single impact (E_{impact} in mJ). Additionally, the reactivity profiles of both CDI and ODI by PBM were investigated, showing different stability as a function of the mechanochemical stress delivered, modulated by specific planetary mill geometries (e.g., Table 4). The selection of 1,1- oxalyl diimidazole (ODI) over 1,1'-carbonyldiimidazole (CDI) when appropriate, represents a pragmatic and new approach to promote amide synthesis by mechanochemistry [33], especially when reactivity constraints (mostly, unfavorable electronic factors) require more reactive coupling agents, as demonstrated for Flutolanil (**10**) and Fluxapyroxad (**11**).

For both CDI- and ODI-mediated mechanochemical syntheses of marketed molecules of interest for agrochemical industry (**9-11**), the eco-footprint was assessed by using two different tools for green chemistry metrics calculations (DOZN^{TM} 3.0 and CHEM21 tools). The results were compared to the most pertinent solution-based processes. The tools delivered converging outputs in the evaluation of the mechanochemical approaches as a whole, and despite the formation of CO as by product from the ODI-mediated synthesis [69, 70]. Indeed, the assessment of a method for its sustainability, whatever the method is, cannot focus exclusively only on the evaluation of 'one specific reagent' or a specific by product formed, but should consider the process as a whole (i.e., efficiency, productivity, safety, costs, including PMI data, operational simplicity, downstream operations, waste treatment etc.). Specifically, while solution-based chemistry for the preparation of Mepronil (**9**) already demonstrates acceptable performance and sustainability, in the case of Flutolanil (**10**) and Fluxapyroxad (**11**), both CDI- and ODI-mediated mechanochemical synthesis delivered better green chemistry metrics (despite their lower productivity) than the comparative solution-based processes, with no organic solvents used, at any stage, from synthesis to recovery of the final products, with waste easily removed in water, confirming once again, that amide synthesis by mechanochemistry constitutes a promising route [33].

Author Contributions

Andrea Casagrande: experimental investigations, formal analysis and green metrics. **Rubén Solorzano-Rodriguez**: review and editing (green chemistry metrics). **Joris Vezzani**: DSC analyses. **Maria Carta**: writing (section on kinetics), review and editing. **Francesco Delogu**: writing (section on kinetics), review and editing. **Evelina Colacino**: funding acquisition, conceptualization, supervision, writing – original draft, review and editing. **Allan Niidu**: funding acquisition, review and editing. All authors have approved the final version of the manuscript.

Acknowledgments

A.C. is grateful to Campus France and Tallinn Technological University (TalTech) for the Ph.D. fellowship (co-tutelle de thèse France-Estonie). E.C. and A.N. are grateful to Campus France and French-Estonian cooperation Programme Hubert Curien France-Estonia (PHC PARROT 2021–2023). A.N. is grateful to the French Embassy in Estonia for the mobility grant (2024). E.C. is grateful to Gladys Da Conceiçao (Fritsch, France) for providing technical parameters for planetary ball-mills (P6 and P7 Premium, reported in Table S4, Supporting Information).

Open access publication funding provided by COUPERIN CY26.

Conflicts of Interest

The authors declare no conflicts of interest.

Data Availability Statement

The data that support the findings of this study are available in the supplementary material of this article.

References

1. J. Magano, "Large-Scale Amidations in Process Chemistry: Practical Considerations for Reagent Selection and Reaction Execution," *Organic Process Research & Development* 26 (2022): 1562–1689.

2. R. M. de Figueiredo, J.-S. Suppo, and J.-M. Campagne, "Nonclassical Routes for Amide Bond Formation," *Chemical Reviews* 116 (2016): 12029–12122.

3. J. Boström, D. G. Brown, R. J. Young, and G. M. Keserü, "Expanding the Medicinal Chemistry Synthetic Toolbox," *Nat Rev Drug Discovery* 17 (2018): 709–727.

4. J. R. Dunetz, J. Magano, and G. A. Weisenburger, "Large-Scale Applications of Amide Coupling Reagents for the Synthesis of Pharmaceuticals," *Organic Process Research & Development* 20 (2016): 140–177.

5. B. Luo, Y. Hu, Y. Wu, M. Liu, and K. Fang, "Comprehensive Overview of Pyrazole Amide Derivatives as Novel Pesticides for Crop Protection and Pest Management," *Journal of Agricultural and Food Chemistry* 73 (2025): 30582–30600.

6. C. Lamberth, S. Jeanmart, T. Luksch, and A. Plant, "Current Challenges and Trends in the Discovery of Agrochemicals," *Science* 341 (2013): 742–746.

7. H. C. J. Godfray, J. R. Beddington, I. R. Crute, et al., "Food Security: The Challenge of Feeding 9 Billion People," *Science* 327 (2010): 812–818.

8. M. W. A. Phillips, "Agrochemical Industry Development, Trends in R&D and the Impact of Regulation," *Pest Management Science* 76 (2020): 3348–3356.

9. Food and Agriculture Organisation of United Nations (FAO): https://www.fao.org/faostat/en/#data/RP/visualize (accessed February 22, 2026).

10. N. Fantozzi, J.-N. Volle, A. Porcheddu, D. Virieux, F. García, and E. Colacino, "Green Metrics in Mechanochemistry," *Chemical Society Reviews* 52 (2023): 6680–6714.

11. O. Galant, G. Cerfeda, A. S. McCalmont, et al., "Mechanochemistry Can Reduce Life Cycle Environmental Impacts of Manufacturing Active Pharmaceutical Ingredients," *ACS Sustainable Chemistry & Engineering* 10 (2022): 1430–1439.

12. P. Sharma, C. Vetter, E. Ponnusamy, and E. Colacino, "Assessing the Greenness of Mechanochemical Processes With the DOZN 2.0 Tool," *ACS Sustainable Chemistry & Engineering* 10 (2022): 5110–5116.

13. A. Casagrande, A. Niidu, R. Aav, D. Kananovich, and E. Colacino, *Encyclopedia of Green Chemistry*, First Edition, ed. B. Török, (Elsevier, 2025), 2550–2571.

14. IUPAC Guiding Principles of Responsible Chemistry https://iupac.org/responsible-chemistry/(accessed February 22, 2026).

15. I. Chiyomaru, S. Kawada, and K. Takita, "US3937840A," (1976), https://patents.google.com/patent/US3937840A/en?oq=US3937840A.

16. R. I. Patel, B. Saxena, and A. Sharma, "General Electron–donor–acceptor Complex Mediated Thioesterification Reaction via Site-selective

15213765, 0, Downloaded from https://chemistry-europe.onlinelibrary.wiley.com/doi/10.1002/chem.71190 by Andrea Casagrande - Université de Montpellier , Wiley Online Library on [25/06/2026]. See the Terms and Conditions (https://onlinelibrary.wiley.com/terms-and-conditions) on Wiley Online Library for rules of use; OA articles are governed by the applicable Creative Commons License

C–H Functionalization Using Aryl Sulfonium Salts," *Green Chemistry* 26 (2024): 10265–10274.

17. K. Yabutani, K. Ikeda, S. Hatta, and T. Harada, "US4093743A," (1977).

18. As an Example, Fluxapyroxad (Sercadis is a top-tier Succinate dehydrogenase Inhibitors (SDHI) Fungicide Class With an Estimated Global Market Size of 3.9-4.0 Billions USD,in 2025, https://www.mordorintelligence.com/industry-reports/sdhi-fungicide-market#:~:text=SDHI%20Fungicide%20Market%20Analysis%20by,%25%20CAGR%20over%202026%2D2031, (accessed February 16, 2026).

19. Y. Zhang, Z. Chen, J. Nie, F.-G. Zhang, and J.-A. Ma, "Development of Cyanopyrazoles as Building Blocks to Fungicide Fluxapyroxad and Analogues," *Journal of Organic Chemistry* 84 (2019): 7148–7158.

20. K. J. Ardila-Fierro and J. G. Hernández, "Sustainability Assessment of Mechanochemistry by Using the Twelve Principles of Green Chemistry," *ChemSusChem* 14 (2021): 2145–2162.

21. E. Colacino, V. Isoni, D. Crawford, and F. García, "Upscaling Mechanochemistry: Challenges and Opportunities for Sustainable Industry," *Trends in Chemistry* 3 (2021): 335–339.

22. F. Gomollón-Bel, "Ten Chemical Innovations That Will Change Our World: IUPAC Identifies Emerging Technologies in Chemistry With Potential to Make Our Planet More Sustainable," *Chemistry International* 41 (2019): 12–17.

23. F. Gomollón-Bel, "Mechanochemists Want to Shake up Industrial Chemistry," *ACS Central Science* 8 (2022): 1474–1476.

24. F. Cuccu, L. De Luca, F. Delogu, et al., "Mechanochemistry: New Tools to Navigate the Uncharted Territory of "Impossible" Reactions," *Chemsuschem* 15 (2022): e202200362.

25. L. Konnert, F. Lamaty, J. Martinez, and E. Colacino, "Solventless Mechanosynthesis of N-Protected Amino Esters," *Journal of Organic Chemistry* 79 (2014): 4008–4017.

26. J. G. Hernández and C. Bolm, "Altering Product Selectivity by Mechanochemistry," *Journal of Organic Chemistry* 82 (2017): 4007–4019.

27. O. V. Lapshin, E. V. Boldyreva, and V. V. Boldyrev, "Role of Mixing and Milling in Mechanochemical Synthesis (Review)," *Russian Journal of Inorganic Chemistry* 66 (2021): 433–453.

28. J. M. Ottino, *The Kinematics of Mixing: Stretching, Chaos and Transport*, (Cambridge University Press, 1989) ISBN 9780521368780.

29. S. Mateti, M. Mathesh, Z. Liu, et al., "Mechanochemistry: A Force in Disguise and Conditional Effects Towards Chemical Reactions," *Chemical Communications* 57 (2021): 1080–1092.

30. N. Q. Vo, S. Odunuga, P. Bellon, and R. S. Averback, "Forced Chemical Mixing in Immiscible Alloys During Severe Plastic Deformation at Elevated Temperatures," *Acta Materialia* 57 (2009): 3012–3019.

31. E. Juaristi and C. G. Avila-Ortiz, "Salient Achievements in Synthetic Organic Chemistry Enabled by Mechanochemical Activation," *Synthesis* 55 (2023): 2439–2459.

32. A. A. Michalchuk, I. A. Tumanov, V. A. Drebushchak, and E. V. Boldyreva, "Advances in Elucidating Mechanochemical Complexities via Implementation of a Simple Organic System," *Faraday Discussions* 170 (2014): 311–335.

33. T. Nikonovich, C. Chatzigiannis, C. Bordier, et al., *Chemical Reviews* (2026), in press, https://doi.org/10.1021/acs.chemrev.5c00534.

34. H. A. Staab, "Reaktionsfähige Heterocyclische Diamide Der Kohlensäure," *Justus Liebigs Annalen der Chemie* 609 (1957): 75–83.

35. H. A. Staab, "Reaktionsfähige N-Carbonsäureester und N-Carbonsäureamide des Imidazols und Triazols," *Justus Liebigs Annalen der Chemie* 609 (1957): 83–88.

36. H. A. Staab, "New Methods of Preparative Organic Chmistry IV. Syntheses Using Heterocyclic Amides (Azolides)," *Angewandte Chemie International Edition in English* 1 (1962): 351–367.

37. G. W. Anderson and R. Paul, "N,N'-Carbonyldiimidazole, A New Reagent for Peptide Synthesis," *Journal of the American Chemical Society* 80 (1958): 4423–4423.

38. J. Gante, "Peptide Syntheses via N-(1-Imidazolylcarbonyl)- and N-(1-Imidazolylthiocarbonyl)-Amino Esters," *Angewandte Chemie International Edition in English* 5 (1966): 315.

39. R. Paul and G. W. Anderson, "N,N'-Carbonyldiimidazole, a New Peptide Forming Reagent[1]," *Journal of the American Chemical Society* 82 (1960): 4596–4600.

40. A. K. Saha, H. Rapoport, and P. Schultz, "1,1'-Carbonylbis(3-methylimidazolium) Triflate: An Efficient Reagent for Aminoacylations," *Journal of the American Chemical Society* 111 (1989): 4856–4859.

41. J.-S. Suppo, G. Subra, M. Bergès, R. Marcia de Figueiredo, and J.-M. Campagne, "Inverse Peptide Synthesis via Activated α-Aminoesters," *Angewandte Chemie International Edition* 53 (2014): 5389–5393.

42. D. J. Dale, J. Draper, P. J. Dunn, et al., "The Process Development of a Scaleable Route to the PDE5 Inhibitor UK-357,903," *Organic Process Research & Development* 6 (2002): 767–772.

43. D. J. Dale, P. J. Dunn, C. Golightly, et al., "The Chemical Development of the Commercial Route to Sildenafil: A Case History," *Organic Process Research & Development* 4 (2000): 17–22.

44. T.-X. Métro, J. Bonnamour, T. Reidon, J. Sarpoulet, J. Martinez, and F. Lamaty, "Mechanosynthesis of Amides in the Total Absence of Organic Solvent From Reaction to Product Recovery," *Chemical Communications* 48 (2012): 11781–11783.PMID: 23108313.

45. L. Konnert, M. Dimassi, L. Gonnet, F. Lamaty, J. Martinez, and E. Colacino, "Poly(ethylene) Glycols and Mechanochemistry for the Preparation of Bioactive 3,5-disubstituted Hydantoins," *RSC Advances* 6 (2016): 36978–36986.

46. M. Lupacchini, A. Mascitti, L. Tonucci, N. d'Alessandro, E. Colacino, and C. Charnay, "From Molecules to Silicon-Based Biohybrid Materials by Ball Milling," *ACS Sustainable Chemistry & Engineering* 6 (2018): 511–518.

47. L. Konnert, L. Gonnet, I. Halasz, et al., "Mechanochemical Preparation of 3,5-Disubstituted Hydantoins From Dipeptides and Unsymmetrical Ureas of Amino Acid Derivatives," *Journal of Organic Chemistry* 81 (2016): 9802–9809.

48. A. Mascitti, M. Lupacchini, R. Guerra, et al., "Poly(ethylene glycol)s as Grinding Additives in the Mechanochemical Preparation of Highly Functionalized 3,5-disubstituted Hydantoins," *Beilstein Journal of Organic Chemistry* 13 (2017): 19–25.

49. A. Porcheddu, F. Delogu, L. De Luca, and E. Colacino, "From Lossen Transposition to Solventless "Medicinal Mechanochemistry"," *ACS Sustainable Chemistry & Engineering* 7 (2019): 12044–12051.

50. M. Lanzillotto, L. Konnert, F. Lamaty, J. Martinez, and E. Colacino, "Mechanochemical 1,1′-Carbonyldiimidazole-Mediated Synthesis of Carbamates," *ACS Sustainable Chemistry & Engineering* 3 (2015): 2882–2889.

51. S. Murata, "1,1′-oxalyldiimidazole, a New Reagent for Activation of Carboxylic Acid," *Chemistry Letters* 12 (1983): 1819–1820.

52. T. Kitagawa, H. Sasaki, and N. Ono, "A Useful Method for the Conversion of Aldehyde Oximes Into Nitriles Using 1,1'-oxalyldiimidazole," *Chemical and Pharmaceutical Bulletin* 33 (1985): 4014–4016.

53. A. Nefzi, M. A. Giulianotti, and R. A. Houghten, "Solid-phase Synthesis of Branched Thiohydantoin Benzimidazolinethiones and Branched Thiohydantoin Tetrahydroquinoxalinediones," *Tetrahedron Letters* 41 (2000): 2283–2287.

54. Z. Liu, W. Chen, M. A. Giulianotti, and R. A. Houghten, "Solid-phase Synthesis of 2,3,4,5-tetrahydro-1H-benzo[e][1,4]Diazepine Derivatives," *Tetrahedron Letters* 52 (2011): 4112–4113.

55. M. Menichincheri, D. Ballinari, A. Bargiotti, et al., "Catecholic Flavonoids Acting as Telomerase Inhibitors," *Journal of Medicinal Chemistry* 47 (2004): 6466–6475.

15213765, 0, Downloaded from https://chemistry-europe.onlinelibrary.wiley.com/doi/10.1002/chem.71190 by Andrea Casagrande - Université de Montpellier , Wiley Online Library on [25/06/2026]. See the Terms and Conditions (https://onlinelibrary.wiley.com/terms-and-conditions) on Wiley Online Library for rules of use; OA articles are governed by the applicable Creative Commons License

56. T. C. Stamatatos, S. P. Perlepes, C. P. Raptopoulou, et al., "Initial Use of 1,1′-oxalyldiimidazole for Inorganic Synthesis: Decomposition of the Ligand as a Means to the Preparation of an Imidazole- and Oxalate(-2)-containing, 1D Copper(II) Complex," *Inorganic Chemistry Communications* 12 (2009): 402–405.

57. J. H. Lee, J.-E. R. Rho, T.-H. D. Rho, and J. G. Newby, "Advent of Innovative Chemiluminescent Enzyme Immunoassay," *Biosensors and Bioelectronics* 26 (2010): 377–382.

58. O. F. Jafter, S. Lee, J. Park, C. Cabanetos, and D. Lungerich, "Navigating Ball Mill Specifications for Theory-to-Practice Reproducibility in Mechanochemistry," *Angewandte Chemie International Edition* 63 (2024): e202409731, https://lungerich-group.github.io, The online tool is available under, accessed December 23, 2025.

59. C. R. McElroy, A. Constantinou, L. C. Jones, L. Summerton, and J. H. Clark, "Towards a Holistic Approach to Metrics for the 21st Century Pharmaceutical Industry," *Green Chemistry* 17 (2015): 3111–3121.

60. A. DeVierno Kreuder, T. House-Knight, J. Whitford, et al., "A Method for Assessing Greener Alternatives between Chemical Products Following the 12 Principles of Green Chemistry," *ACS Sustainable Chemistry & Engineering* 5 (2017): 2927–2935, DOZN™ is a universal tool, suitable for scoring any process, no matter the activation technique used, once the Detailed Experimental/Process Conditions Are Known. The DOZN™ tool is accessible free of charge here, https://bioinfo.merckgroup.com/dozn (accessed June 27, 2025).

61. P. Sharma and E. Ponnusamy, "DOZN™3.0: a Quantitative Green Chemistry Evaluator for Sustainable Chemistry," *Sustainable Chemistry for Climate Action* 7 (2025): 100129, https://www.sciencedirect.com/science/article/pii/S2772826925000744.

62. R. Schmidt, C. F. Burmeister, M. Baláž, A. Kwade, and A. Stolle, "Effect of Reaction Parameters on the Synthesis of 5-Arylidene Barbituric Acid Derivatives in Ball Mills," *Organic Process Research & Development* 19 (2015): 427–436.

63. A. Stolle, R. Schmidt, and K. Jacob, "Scale-up of Organic Reactions in Ball Mills: Process Intensification With Regard to Energy Efficiency and Economy of Scale," *Faraday Discuss* 170 (2014): 267–286.

64. J. A. Grzyb, M. Shen, C. Yoshina-Ishii, W. Chi, R. S. Brown, and R. A. Batey, "Carbamoylimidazolium and Thiocarbamoylimidazolium Salts: Novel Reagents for the Synthesis of Ureas, Thioureas, Carbamates, Thiocarbamates and Amides," *Tetrahedron* 61 (2005): 7153–7175.

65. L. Vugrin, M. Carta, S. Lukin, E. Meštrović, F. Delogu, and I. Halasz, "Mechanochemical Reaction Kinetics Scales Linearly With Impact Energy," *Faraday Discussions* 241 (2023): 217–229.

66. S. Bhatnagar, M. Felderhoff, and J.-H. Schöbel, "Solvent-Free Mechanocatalytic Reduction of Nitro Compounds With Hydrogen Gas and Its Application in the Synthesis of Drugs and Their Intermediates," *Advanced Synthesis & Catalysis* 367 (2025): e70071.

67. F. Puccetti, T. Rinesch, S. Suljić, K. Rahimi, A. Herrmann, and C. Bolm, "NMR in Operando Monitoring of Mechanochemically Accelerated Sublimations," *Chem* 9 (2023): 1318–1332.

68. S. Reichle, M. Felderhoff, and F. Schüth, "Mechanocatalytic Room-Temperature Synthesis of Ammonia From Its Elements Down to Atmospheric Pressure," *Angewandte Chemie International Edition* 60 (2021): 26385–26389.

69. For an example on the use of CO in industrial settings: P. T. Anastas and M. M. Kirchhoff, "Origins, Current Status, and Future Challenges of Green Chemistry," *Accounts of Chemical Research* 35 (2002): 686–694.

70. For an example on the use of CO in industrial settings: BHC Company, "BHC Company Ibuprofen Process. In The Presidential Green Chemistry Challenge Awards Program: Summary of 1997 Award Entries and Recipients; EPA744-S-97-001," (1998): 2, U.S. Environmental Protection Agency, Office of Pollution Prevention and Toxics: Washington, DC.

71. S. F. E. Hansen and T. Ulven, "Oxalyl Chloride as a Practical Carbon Monoxide Source for Carbonylation Reactions," *Organic Letters* 17 (2015): 2832–2835, https://pubs.acs.org/doi/10.1021/acs.orglett.5b01252.

72. J. Wang, Y. Yin, X. He, et al., "Nickel-Catalyzed Highly Selective Reductive Carbonylation Using Oxalyl Chloride as the Carbonyl Source," *ACS Catalysis* 13 (2023): 8161–8168.

73. C. A. Rudd Gretton, "Prescription Digital Therapeutics WO20260041667A1," (2026).

74. J. R. Murphy, P. S. Bury, N. A. Wagstaff, P. S. Hinchliffe, and S. E. Osbourn, "Salt Forms of Bis(3-(2-(Dimethylamino)ethyl)-1H-indol-4-yl) 3,3′-Oxydipropionate," (2025), WO2025238258A1.

75. C. Feilding-Mellen and T. Mason, "Pharmaceutical Compositions Comprising 5-Methoxy-N,N-Dimethyltryptamine (5-MeO-DMT)," (2025), WO2025068714A1.

76. E. Jeong, S. Kim, J.-H. Lim, et al., "Compound, Electrolyte for Rechargeable Lithium Battery Including the Same, and Rechargeable Lithium Battery Including the Same," (2026), US20260011782A1.

77. C. M. Chatzigiannis, S. M. Scalzullo, E. Colacino, and M. E. Rivas, "Multigram-Scale Organic Synthesis by Resonant Acoustic Mixing: Application to the Sustainable Preparation of Active Pharmaceutical Ingredients," *ChemSusChem* 18 (2025): e202500110.

78. B. Trost, "The Atom Economy—A Search for Synthetic Efficiency," *Science* 254 (1991): 1471–1477.

79. M. G. T. C. Ribeiro and A. A. S. C. Machado, "Greenness of Chemical Reactions – limitations of Mass Metrics," *Green Chemistry Letters and Reviews* 6 (2013): 1–18.

80. J. Martínez, J. F. Cortés, and R. Miranda, "Green Chemistry Metrics, A Review," *Processes* 10 (2022): 1274.

81. T. Zierke, J. Rheinheimer, M. Rack, et al., "WO2008145740A1," (2008).

82. E. Lucas, A. J. Martín, S. Mitchell, et al., "The Need to Integrate Mass- and Energy-based Metrics With Life Cycle Impacts for Sustainable Chemicals Manufacture," *Green Chemistry* 26 (2024): 9300–9309.

83. Regulation (EU) 2021/2415, L2415/2016 http://data.europa.eu/eli/dir_impl/2021/2415/oj (accessed January 2, 2026).

84. U.S EPA Regulation: Risk Management for Methylene Chloride Available at https://www.epa.gov/assessing-and-managing-chemicals-under-tsca/risk-management-methylene-chloride (Accessed November 19, 2025).

85. J. Kielhorn, C. Melber, D. Keller, and I. Mangelsdorf, "Palladium – A Review of Exposure and Effects to human Health," *International Journal of Hygiene and Environmental Health* 205 (2002): 417–432.

86. R. A. Sheldon, "The E Factor: Fifteen Years On," *Green Chemistry* 9 (2007): 1273.

87. D. C. Braddock, P. D. Lickiss, B. C. Rowley, et al., "Tetramethyl Orthosilicate (TMOS) as a Reagent for Direct Amidation of Carboxylic Acids," *Organic Letters* 20 (2018): 950–953.

88. B. F. Cain, "2-Acyloxymethylbenzoic Acids. Novel Amine Protective Functions Providing Amides with the Lability of Esters," *Journal of Organic Chemistry* 41 (1976): 2029–2031.

89. J. Liu, Q. Liu, H. Yi, et al., "Visible-Light-Mediated Decarboxylation/Oxidative Amidation of α-Keto Acids With Amines Under Mild Reaction Conditions Using O_2," *Angewandte Chemie International Edition* 53 (2014): 502–506.

90. S. Mkrtchyan, M. Jakubczyk, S. Lanka, et al., "Mechanochemical Transformation of CF_3 Group: Synthesis of Amides and Schiff Bases," *Advanced Synthesis & Catalysis* 363 (2021): 5448–5460.

91. B. Picard, T. Fukuyama, and I. Ryu, "Phosphine-Free Aminocarbonylation Using Pd/DBU Catalyst: Carbonylative Coupling of Aryl Iodides and Amines," *Journal of Organic Chemistry* 88 (2023): 5220–5225.

92. U. Troppmann, W. Mayer, S. Koltzenburg, R. Israels, A. Bauder, and U. Schlotterbeck, "US8735321B2," (2009).

15213765, 0, Downloaded from https://chemistry-europe.onlinelibrary.wiley.com/doi/10.1002/chem.71190 by Andreu Casagrande - Université de Montpellier , Wiley Online Library on [25/06/2026]. See the Terms and Conditions (https://onlinelibrary.wiley.com/terms-and-conditions) on Wiley Online Library for rules of use; OA articles are governed by the applicable Creative Commons License

93. S.-P. Wang, C. W. Cheung, and J.-A. Ma, "Direct Amidation of Carboxylic Acids With Nitroarenes," *Journal of Organic Chemistry* 84 (2019): 13922–13934.

94. Y. Wang, B. Tian, Y. Li, et al., "A Sustainable and Versatile Cellulose-Based CO Surrogate for Carbonylative Reactions," *ChemSusChem* 17 (2024): e202301324.

Supporting Information

Additional supporting information can be found online in the Supporting Information section.

The authors have cited additional references within the Supporting Information [15–17, 19, 65, 87–94]. The data supporting this article, including ^{1}H, $^{13}C\{^{1}H\}$ and $^{19}F\{^{1}H\}$ NMR, FT-IR (ATR) spectra, DSC analyses for compounds **2–11**, excel spreadsheets for green chemistry metrics calculations by Chem21 and DOZN 3.0 tools data input are available as part of the Supplementary Information.

Supporting File 1: chem71190-sup-0002-DataFile.zip.

15213765, 0, Downloaded from https://chemistry-europe.onlinelibrary.wiley.com/doi/10.1002/chem.71190 by Andreas Casagrande - Université de Montpellier , Wiley Online Library on [25/06/2026]. See the Terms and Conditions (https://onlinelibrary.wiley.com/terms-and-conditions) on Wiley Online Library for rules of use; OA articles are governed by the applicable Creative Commons License

Appendix 2

Publication II

R. Solórzano-Rodríguez, N. Fantozzi, A. Casagrande, C. M. Chatzigiannis, C. Bordier, P. Rando, E. Colacino. Safe and Sustainable by Design (SSbD) Synthesis of Food and Personal Care Ingredients by Mechanochemistry. *ChemSusChem*, **2026**, *19 (9)*, e202502491.

Reproduced by permission of John Wiley and Sons.

Check for updates

ChemSusChem

Chemistry Europe
European Chemical Societies Publishing
ChemSusChem

RESEARCH ARTICLE OPEN ACCESS

Safe and Sustainable by Design (SSbD) Synthesis of Food and Personal Care Ingredients by Mechanochemistry

Rubén Solórzano-Rodríguez[1] | Nicolas Fantozzi[1] | Andrea Casagrande[1,2] | Christos M. Chatzigiannis[1] | Corentin Bordier[1] | Pietro Rando[3] | Evelina Colacino[1]

[1]ICGM, Univ Montpellier, CNRS, ENSCM, Montpellier, France | [2]Virumaa Kolledž, Tallinn University of Technology, Ida-Viru maakond, Estonia | [3]CRB Benelux BV, Maastricht, The Netherlands

Correspondence: Evelina Colacino (evelina.colacino@umontpellier.fr)

Received: 1 November 2025 | **Revised:** 17 March 2026 | **Accepted:** 18 March 2026

Keywords: active ingredients | biomass transformation | green chemistry metrics | mechanochemistry | polymeric jars

ABSTRACT

The preparation of perillartine, a potent marketed sweetener, and *N*-tert-butyl-α-phenylnitrone (PBN), a most commonly used free-radical spin-trap used in personal care formulation, endowed with antioxidant, neuroprotective, and anti-aging properties, was studied by vibrating and planetary ball-milling. The reactivity in polymeric jars, such as PTFE and in-house made polyoxymethylene (POM), was evaluated and compared to the most commonly used stainless steel and zirconium oxide milling media. This investigation revealed an insightful correlation while also accounting for the energy involved in each transformation. Assessment of the processes by green chemistry metrics and tools (*e.g.*, Chem21, DOZN 3.0 and EcoScale) showed that mechanochemical approaches offer a Safe and Sustainable by Design (SSbD) approach also complying with the IUPAC guiding principles of a responsible chemistry. The reduced solvent consumption, the simplified purification procedures, and lower associated environmental and safety hazards are strongly aligned with the green chemistry principles.

1 | Introduction

The need for environmentally sustainable chemical processes has become a critical focus for modern science and industry, driving significant interest in green chemistry approaches. Traditionally, chemical processes rely on hazardous solvents, require substantial energy inputs, and produce significant amounts of waste, posing challenges to both environmental sustainability and economic efficiency. The transition to greener chemical methods supports the United Nations' 17 Sustainable Development Goals (UN SDGs) [1], promoting practices that minimize waste, improve resource efficiency, and enhance safety. In particular, mechanochemistry has been identified as a transformative technology that directly contributes to achieving several of these goals (the link between mechanochemistry and the UN SDGs appeared for the first time in the literature in [2]; the concept was further expanded in [3]). IUPAC highlighted mechanochemistry as a key technology for sustainable chemical synthesis [4], offering a solvent-free alternative to traditional processes and a powerful approach to implement the 12 principles of green chemistry [5, 6]. In pharmaceutical and fine chemical manufacturing, solvents typically account for 80%–90% of the reaction mass [7], 75% of the energy consumption, and up to 50% of the global warming potential, posing a substantial issue that needs to be addressed [8]. In contrast, mechanochemical methods exhibit improved green metrics [9, 10], including lower energy requirements, reduced waste generation, and improved safety by avoiding toxic solvents. When appropriately designed and assessed, such mechanochemical processes are Safe and Sustainable by Design (SSbD). Additionally, in our believe, they comply with the framework of "IUPAC guiding principles of responsible chemistry" [11] recently unveiled and calling on scientists, educators, industry

Rubén Solórzano-Rodríguez and Nicolas Fantozzi contributed equally to this work.

This is an open access article under the terms of the Creative Commons Attribution License, which permits use, distribution and reproduction in any medium, provided the original work is properly cited.

© 2026 The Author(s). *ChemSusChem* published by Wiley-VCH GmbH.

professionals, policymakers, and future chemists to direct their work toward addressing the pressing challenges facing humanity.

One particularly illustrative example where mechanochemical processes and green chemistry principles work in synergy is the synthesis of high-value compounds derived from natural or renewable resources. Here, we describe the mechanochemical synthesis of (*S*)-(-)-perillartine (**1**) and *N*-*tert*-butyl-α-phenylnitrone (**2**, PBN) from inexpensive, readily available precursors, using protocols that minimize waste generation and are SSbD-compliant (Scheme 1). (*S*)-(-)-Perillartine, also known as perilla sugar, is a potent, Food and Drug Administration (FDA)-approved [12] semisynthetic sweetener (approximately 2000 times sweeter than sucrose) that has attracted attention due to its potential biological activities. It is derived from *Perilla frutescens*, a crop widely distributed in East Asian countries and commonly used not only in cuisine, but also in traditional medicine due to its diverse pharmacological properties [13–17]. The synthesis of perillartine typically involves the condensation reaction of perillaldehyde, with hydroxylamine hydrochloride [18, 19]. Perillaldehyde is a natural compound extracted from *P. frutescens* and used as food additive for flavoring and in perfumery to add spiciness.

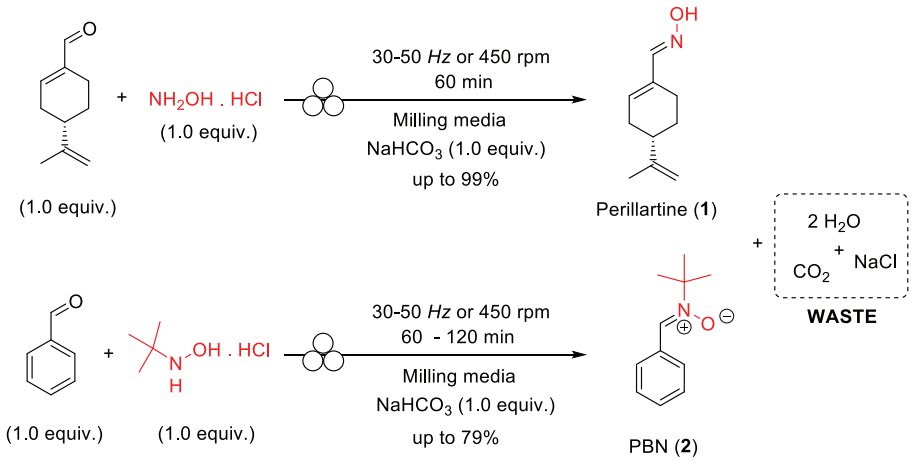
Recently, green alternative synthetic protocols were reported using electrochemical [20] and chemoenzymatic [21] procedures. Despite their efficiency, these methods require uncommon experimental setups limiting their broader applicability.

We previously described the mechanochemical preparation of oximes as key intermediates for the Beckman rearrangement to amides [22, 23]. Aldoxymes were also prepared by a mechanochemical condensation reaction of arylaldehydes with hydroxylamine [24]. Herein, we extended the study to the mechanochemical preparation of aldoxime (*S*)-(-)-Perillartine (**1**) by ball-milling. Beyond the simplicity of the experimental setup, the reactions do not require anhydrous conditions or the use of organic solvents, including in the downstream process to recover the final product (Figure 1).

Similarly, *N*-*tert*-butyl-*α*-phenylnitrone (**2**, PBN) is a well-known free-radical spin trap that exhibits neuroprotective and antiaging properties [25–31]. Due to its antioxidant properties and its ability to mitigate oxidative stress-related conditions, it has attracted interest from both academia and industry. Its main application lies in personal care, and it is registered as a cosmetic ingredient in CosIng, the European Commission's database of cosmetic substances and ingredients [32].

Commonly used solvent-based methods to synthesize nitrones involve mainly i) condensation reactions of *N*-monosubstituted hydroxylamines, ii) oxidation of different substrates (*N*,*N*-disubstituted hydroxylamines, secondary amines, *N*-alkyl-α-amino acids, imines and isoxazolidines), iii) reactions of oximes with electrophiles, and iv) reaction of nitro compounds with aldehydes under reductive conditions [33]. Specifically, synthetic procedures for PBN reported in the literature, either solution-based or microwave-assisted processes, rely on the first approach [34–37]. A preliminary report on the mechanochemical synthesis of nitrones was first investigated by one of us [38].

In parallel to long-lasting and ongoing work targeting the preparation of Active Pharmaceutical Ingredients (APIs) by different mechanochemical methods (both in batch and in continuous) [23, 39–42], we wish to expand the application of mechanochemical processing to other value-added molecules to new market sectors, such as food and personal care, where sustainability is still poorly addressed. Therefore, we report the mechanochemical preparation of the sweetener perillartine from a naturally occurring, and abundant renewable product of commercial interest, the flavoring agent *Perilla frutescens* and expand further the preparation of the antioxidant *N*-*tert*-butyl-α-phenylnitrone (**2**, PBN), under different processing conditions. This includes the use of polyoxymethylene (POM) as grinding media, quite unexplored in organic synthesis, expanding the range of mechanochemical processing conditions by introducing new metal and fluorine-free milling media (POM), offering a more sustainable, healthier, and less expensive option compared to polytetrafluoroethylene (PTFE) jars. Indeed, per- and polyfluoroalkyl substances (PFAS) are progressively recognized as persistent environmental pollutants, and PTFE falls within this chemical class. By providing a fluorine-free option, polyoxymethylene (POM) is consistent with a proactive Safe and Sustainable by Design framework, thereby reducing potential future risks associated with persistent



SCHEME 1 | Mechanochemical preparation of (*S*)-(-)-perillartine (**1**) and *N*-*tert*-butyl-α-phenylnitrone (PBN, **2**).

1864564x, 2026, 9, Downloaded from https://chemistry-europe.onlinelibrary.wiley.com/doi/10.1002/cssc.202502491 by Andrea Cusumano - Universite de Montpellier , Wiley Online Library on [22/06/2026]. See the Terms and Conditions (https://onlinelibrary.wiley.com/terms-and-conditions) on Wiley Online Library for rules of use; OA articles are governed by the applicable Creative Commons License

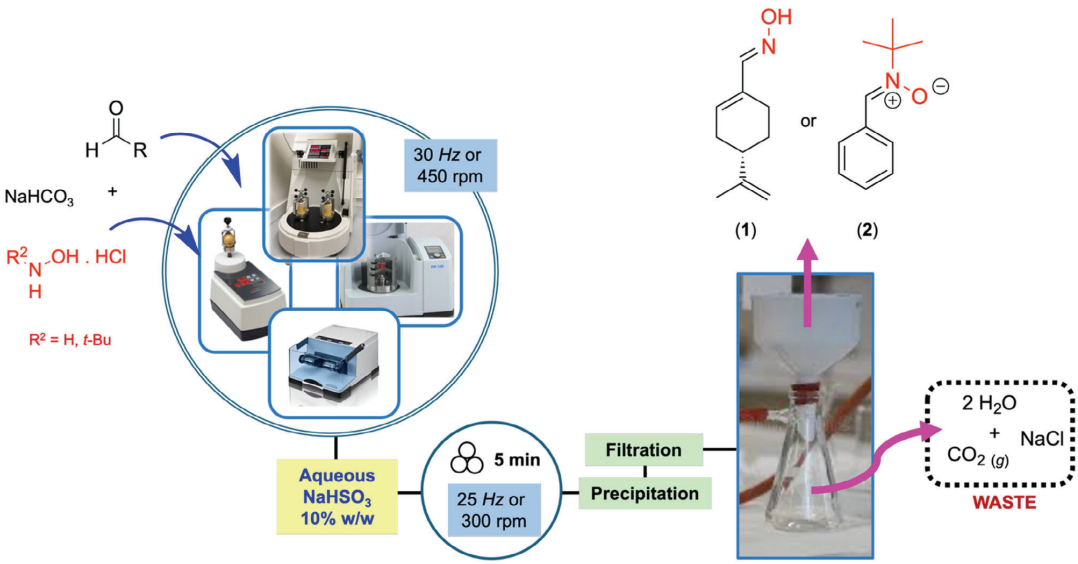


FIGURE 1 | Downstream and eco-friendly process for recovering (*S*)-(-)-perillartine (**1**) and *N*-*tert*-butyl-α-phenylnitrone (PBN, **2**), with no need of organic solvents. Images of the milling equipment were reproduced by kind permission of (a) Retsch (GmbH, Germany) for vibrating ball-mill (MM400) and PM100 (planetary mill), and (b) Fritsch (GmbH, Germany) for vibrating ball-mill (P23) and P7 Classic line (planetary mill).

pollutants. In addition, POM represents also suitable alternative to stainless steel (SS), as it can prevent or reduce the likelihood of residual metal contamination arising from abrasion of the milling media.

The mechanochemical protocol herein developed is robust and transferable across different common milling platforms (vibratory and planetary), which is essential for its practical adoption by the wider chemical community. The study is completed by an in-depth analysis of the process's full eco-footprint, which is a key contribution that moves beyond simple reaction yields. The comprehensive and quantitative green assessment of the entire workflow includes the often-neglected downstream processing by an array of green chemistry metrics calculations [9, 10], using Chem21 [43], DOZN 3.0 [41, 44, 45], and Eco-scale [46] tools. The scores are compared with the corresponding solution-based preparation methods, validating the mechanochemical method's alignment with SSbD principles and the IUPAC Guiding Principles of Responsible chemistry [11].

2 | Results and Discussion

The mechanochemical synthesis of (*S*)-(-)-perillartine (**1**) and PBN (**2**) was explored under different mechanical stresses (vibrating and planetary ball-milling) and milling media. Both compounds were synthesized through a direct condensation reaction between equimolar amounts of the corresponding aldehyde and hydroxylamine hydrochloride salt, in the presence of one equivalent of $NaHCO_3$ (Scheme 1). Taking advantage of their low solubility in water, (S)-(-)-perillartine (**1**) and PBN (**2**) were readily recovered from the crude reaction mixture using three simple steps: precipitation with aqueous sodium bisulfite (10% w/w), filtration, and drying. No organic solvents were required, even during downstream processing, making the entire workflow —from synthesis to recovery—both straightforward and eco-friendly (Figure 1).

To evaluate the influence of different grinding media on the outcome of the reaction, jars in stainless steel (SS), zirconium oxide, and two polymeric materials such as polytetrafluoroethylene (PTFE) and polyoxymethylene (POM) were compared. SS and zirconium oxide are well-established grinding media due to their chemical resistance and availability. However, the release of metal impurities due to the abrasion of hard grinding media cannot be excluded, especially when SS is used [47, 48]. On the other hand, polymeric vessels have recently emerged as cost-effective, alternatives to the conventional metallic and ceramic jars. Poly(methyl methacrylate) (PMMA) is the most commonly used polymeric material especially for in situ monitoring purposes [49].

However, its chemical compatibility and mechanical resistance are somehow limited, and in some cases not so effective as other harder and denser milling media [50] for covalent bond forming reactions (for a comparative example on the use of PMMA *vs* SS/ZrO_2 grinding media in the synthesis of an Active Pharmaceutical Ingredient (Dantrolene): a) synthesis in SS or ZrO_2 jars [51]; b) synthesis in SS or ZrO_2 jars [52]). Ertalyte jars were also used for metal-free mechanochemical oxidation reactions [53].

The choice of the polymeric jars can be tailored to meet specific mechanochemical process requirements, such as chemical and thermal resistance, transparency to UV-Vis, X-ray radiation or Raman beam, or mechanical resistance to abrasion [54]. PTFE excels in chemical and thermal resistance; however, PTFE vessels tend to deform due to their inherent softness. POM, although less resistant than PTFE in terms of chemical and thermal stability, allows for stronger, stiffer vessel construction, minimizing deformation during milling and potentially inducing different

18645564, 2026, 9, Downloaded from https://chemistry-europe.onlinelibrary.wiley.com/doi/10.1002/cssc.202502491 by Andrea Casagrande - Université de Montpellier , Wiley Online Library on [22/06/2026]. See the Terms and Conditions (https://onlinelibrary.wiley.com/terms-and-conditions) on Wiley Online Library for rules of use; OA articles are governed by the applicable Creative Commons License

mechanical stresses [55–57]. POM jars proved to be resistant over repeated runs, with no visual abrasion or deformation. Contrarily to hard material such as SS or ZrO_2, for which the amount of residual "leached" metal can be measured directly from the crude mixture (e.g., by ICP-MS methods), leachate analyses for POM vessels are beyond the scope of this process-study. Indeed, it would be necessary to manufacture "ad hoc" in situ monitoring devices, able to detect "online" the gaseous byproducts generated by the degradation of POM under mechanochemical processing. The technical advancements and experimental setups available nowadays in the field of "real-time in situ/in operando monitoring of mechanochemical reactions," make use of PXRD diffractometers, RAMAN probes, or thermal cameras. These techniques are not suitable for detecting the gaseous byproducts generated by POM depolymerization (in case this would occur). Whether at some point, other "analytical facilities" coupled to milling devices were to become available in the future, still, suitable analytical methods should be disclosed. Indeed, the main byproduct that could be generated by degradation of POM (due to heat, UV exposure, or chemical attack) comes from its depolymerization back to its monomer units (formaldehyde), especially when POM is heated above ~230°C or burned [55–57]. We exclude that these extreme conditions can be reached in our processing conditions, ruling out already the hypothesis of the degradation of POM vessels. Other secondary degradation products such as formic acid and carbon monoxide (CO) could also be formed through oxidation of formaldehyde (if any). CO_2 and MeOH (most rarely, it is formed in trace amounts depending on the presence of moisture and additives) could also be formed when the POM material is subjected to even higher temperatures or flames. Again, we exclude the formation of these secondary degradation byproducts of POM (and generated from formaldehyde) during the mechanochemical processing conditions reported in our manuscript.

One advantage of polymeric jars is their compatibility with various ball (or bead) materials, which allows to isolate (understand) the effects of the ball composition while keeping the jar material constant. For each of the mechanochemical processing conditions explored (Tables 1 and 2), a freely accessible online tool [59] was used to calculate the kinetic energy of the milling balls transferred to the molecules upon impact, distinguishing between the total energy ($E_{total,}$ in kJ) transferred to the reaction mixture during milling, and the energy per single impact (E_{impact}, in mJ) between the ball and the molecules. The total mass (total m_{balls}) was also considered, due to its contribution to the total kinetic energy (E_{total}).

Therefore, in the case of the mechanochemical preparation of (*S*)-(-)-perillartine (**1**), and already since the first trial, (*S*)-(-)-perillartine (**1**) was obtained in 99% yield by milling equimolar amounts of the reactants at 30 Hz during 1 h in a SS jar (10 mL) with 2 x 7 mm balls of the same material (Table 1, entry 1). No further optimization was needed, highlighting the intrinsic

TABLE 1 | Selection of data for mechanochemical processing conditions using different grinding media or their combinations, in the preparation of (*S*)-(-)-perillartine (**1**).

Entry[a]	Jar material	Ball material	Number of balls	Diameter (Ø mm)	*Total* m_{balls} (g)[a]	E_{total} (kJ)	E_{impact} (mJ)	Yield (%)
1[b]	SS	SS	2	7	2.8	21.3	9.9	99
2[b]	SS	SS	15	5	7.6	57.3	3.6	73
3[b]	PTFE	SS	15	5	7.6	57.3	3.6	95
4[b]	**POM**	SS	15	5	7.6	57.3	3.6	**96**[a]
5[b]	ZrO_2	ZrO_2	15	5	6.2	46.9	2.9	91
6[b]	**POM**	ZrO_2	15	5	6.2	46.9	2.9	**98**
7[b,c]	PTFE	ZrO_2	15	5	6.2	46.9	2.9	90
8[b,c]	PTFE	SS	2	7	2.8	21.3	9.9	89
9[b,c]	**POM**	SS	2	7	2.8	21.3	9.9	**98**
10[d]	SS	SS	10	5	5.1	38.6	3.6	95
11[d]	PTFE	Stainless steel	8	5	4.1	30.9	3.6	98
12[d]	PTFE	ZrO_2	8	5	3.3	25.3	2.9	96
13[e]	ZrO_2	ZrO_2	30	5	12.4	18.6	6.0	98
14[e]	SS	SS	30	5	15.2	22.7	7.3	88[f]
15[c,e]	ZrO_2	ZrO_2	110	5	45.5	107.4	11.3	90[g]
16[c,e]	SS	SS	110	5	55.7	131.0	13.8	91[g]

[a]*Reaction scale:* 4.0 mmol except for entry 4 (2.0 mmol). Equimolar amounts of reagents were always used. 100% conversion was always obtained except for entry 2. The product was always recovered by precipitation using 10% aqueous $NaHSO_3$. The weight for each type of milling ball used for the experiments is given in Table S1. The electrical energy consumption associated with the milling experiments is reported in Table S2. Legend : SS = Stainless steel.
[b]*Reaction conditions*: Horizontal vibrating ball-mill (MM400) 30 Hz, 1 h, 10 mL jar. The geometry of the milling vessel was identical, including for the in house-made POM jar.
[c]K_2HPO_4 was used as base (1 equiv.), at 30 Hz, 1 h in a horizontal vibrating ball-mill (MM400).
[d]Vertical vibrating ball-mill (P23): 50 Hz, 1 h.
[e]Planetary ball-mill (P7 classic: entries 13 and 14; PM100: entries 15 and 16): 450 rpm, 1 h. The reaction scale was 4.0 mmol (entries 13 and 14) or 30 mmol (entries 15 and 16).
[f]10% of residual aldehyde was detected in the crude mixture (determined by ^{1}H NMR analyses).
[g]Corrected yield calculated from isolated product using qNMR, as (*S*)-perillaldehyde used in these batches contained a 10% of cuminaldehyde [58] as an impurity.

18645564x, 2026, 9, Downloaded from https://chemistry-europe.onlinelibrary.wiley.com/doi/10.1002/cssc.202502491 by Andrea Casagrande - Université de Montpellier , Wiley Online Library on [22/06/2026]. See the Terms and Conditions (https://onlinelibrary.wiley.com/terms-and-conditions) on Wiley Online Library for rules of use; OA articles are governed by the applicable Creative Commons License

TABLE 2 | Selection of mechanochemical processing conditions using different grinding media or their combinations, in the preparation of *N-tert*-butyl-α-phenylnitrone (PBN, **2**).

Entry[a]	Jar material	Balls material	Number of balls	Diameter (Ø mm)	*Total* m_{balls} (g)	E_{total} (kJ)	E_{impact} (mJ)	Yield (%)
1[b]	SS	SS	2	7	2.8	42.6	9.9	100 [38]
2[c]	SS	SS	15	5	6.2	114.6	3.6	10
3[c]	**ZrO_2**	ZrO_2	15	5	6.2	93.8	2.9	**76**
4[c]	PTFE	SS	15	5	7.6	114.6	3.6	45
5[c]	POM	SS	15	5	7.6	114.6	3.6	45
6[c]	**POM**	ZrO_2	15	5	6.2	93.8	2.9	**65**
7[d]	SS	SS	10	5	5.1	38.6	3.6	74
8[d]	PTFE	SS	8	5	4.1	30.9	3.6	67
9[d]	PTFE	ZrO_2	8	5	3.3	25.3	2.9	0
10[e]	**ZrO_2**	ZrO_2	30	5	12.4	18.6	5.6	**79**
11[e]	SS	SS	30	5	15.2	22.8	7.3	10

[a]*Reaction scale:* 4.0 mmol, except for entry 7 (2.0 mmol). Equimolar amounts of reagents were always used. 100% conversion was always obtained except for entry 2. The product was always recovered by precipitation in aqueous $NaHSO_3$ 10% w/w. The weight for each type of milling ball used for the experiments is given in Table S1. The electrical energy consumption associated with the milling experiments is reported in Table S2. *Legend*: SS = Stainless steel.
[b]Reaction conditions reported previously [38].
[c]Horizontal vibrating ball-mill (MM400) 30 Hz, 2 h, 10 mL jar. The geometry of the milling vessel was identical, including for the in-house-made POM jar.
[d]Vertical vibrating ball-mill (P23): 50 Hz, 1 h, 5 mL (entries 8 and 9) or 10 mL (entry 7) jar.
[e]Planetary ball-mill (P7 classic): 450 rpm, 1 h using K_2HPO_4 as base (1.0 equiv.). The reaction scale was 4.0 mmol (12 mL jar).

efficiency of mechanochemistry in facilitating condensation reactions. However, when the experiment was repeated by replacing the 2 × 7 mm balls (entry 1) by 15 × 5 mm (entry 2), the yield dropped to 73%, due to uncomplete conversion of the aldehyde.

The lower amount of energy delivered to the reactants during each single impact (E_{impact} = 3.6 mJ) could slow down the transformation rate into the product [60], in favor of other side reactions, such as hydration reaction of the starting aldehyde, as a consequence of a higher cumulative total energy (E_{total} = 57.3 kJ). However, heating effects at microscopic and/or macroscopic levels, produced during friction and impacts, cannot be excluded. In the case of SS, having higher thermal conductivity (λ) (14.9 W/mK) compared to zirconia (in the range 1.7–2.7 W/mK) [61], the hydration reaction of aldehyde could be favored, due to a higher heating dissipation promoting a rise in bulk temperature.

On the contrary, in ZrO_2, its significantly lower thermal conductivity potentially limiting heat dissipation, the condensation reaction is favored by local temperature rises. This trend was also confirmed when ZrO_2 (entry 5) was used instead of SS (entry 2): the yield increased to 91%, despite the lower cumulative total energy (E_{total} = 46.9 kJ vs. 57.3 kJ in entry 2), as a consequence of the lower density of ZrO_2 in comparison to stainless steel [50]. This observation suggests that higher energy input does not necessarily correlate with higher yield, providing valuable insights into the distinct reactivity profiles of mechanochemical reactions.

Along the same line, other comparative experiments in a planetary ball-mill (entries 13 and 14), differing only in the nature of the milling media, showed that zirconia outperformed stainless steel, affording a 98% yield versus 88%, respectively. ^{1}H NMR analyses of the latter revealed a 10% residual amount of unreacted aldehyde. In the best conditions for the planetary mill, up to *ca.* 4.5 g of (*S*)-(-)-perillartine (**1**), could be obtained in one run. To better understand the influence of the milling media and isolate the effect of the jar material, hard vessels were replaced with softer polymeric jars made of PTFE or POM. The milling conditions were adjusted to maintain a constant cumulative total energy (E_{total}) across experiments (entries 3–4, 5–7, and 1, 8, 9), by varying the type (SS or ZrO_2), size (Ø = 5 or 7 mm), and number (2, 8, 10, or 15) of milling balls (Table 1).

The results showed that the outcome of the reaction depended primarily on the jar material. POM consistently delivered higher yields compared to ZrO_2 (entries 6 vs. 5), stainless steel (entries 4 vs. 2), and PTFE (entries 9 vs. 8), regardless of the ball material used. Yields obtained in POM were even comparable to those obtained in SS jars under optimized conditions (entries 9 vs. 1).

Chemical parameters need also to be considered. Therefore, the influence of the base was also examined. Therefore, for comparative purposes with $NaHCO_3$, bases such as NaOH and Na_2CO_3 were also tested, using identical mechanochemical reaction and work-up, as those outperforming for the synthesis of perillartine **2** using POM jars (Table 1, entry 6). In the case of NaOH as a base, no product was formed upon precipitation (0% yield). The crude was an orange paste, very different from the white powder usually obtained for perillartine (**2**). When Na_2CO_3 was used, the isolated yield increased to 78%, but it was still lower than the benchmark experiment (Table 1, entry 6), delivering 98% yield. These experiments confirmed, furthermore, the validity of the mechanochemical method, with $NaHCO_3$ being the optimal base for this transformation.

High yields were maintained when $NaHCO_3$ was replaced by K_2HPO_4 (entries 7–9, 15, and 16), regardless of reaction scale (4.0 or 30 mmol) or milling conditions. Notably, when E_{total} was kept constant at 21.3 kJ (entries 8 and 9) and milling was performed at 30 Hz in either POM or PTFE jars, POM again outperformed PTFE (98% vs. 89% yield, respectively).

The reaction was also successfully scaled up to 30 mmol in a planetary ball mill (entries 15 and 16), giving comparable yields

18645564, 2026, 9, Downloaded from https://chemistry-europe.onlinelibrary.wiley.com/doi/10.1002/cssc.202502491 by Andrea Casagrande - Université de Montpellier , Wiley Online Library on [22/06/2026]. See the Terms and Conditions (https://onlinelibrary.wiley.com/terms-and-conditions) on Wiley Online Library for rules of use; OA articles are governed by the applicable Creative Commons License

regardless of the milling media used (SS or ZrO_2). From a process development perspective, this is advantageous, as it circumvents potential limitations related to the cost or availability of ZrO_2 vessels for large-scale applications, and potential constraint in machinery.

Although K_2HPO_4 sometimes gave slightly lower yields than $NaHCO_3$, it offers an important operational benefit: unlike $NaHCO_3$, it does not release CO_2 during the reaction. This eliminates the risk of pressure buildup in closed milling vessels, which can become a critical issue at larger scales.

In general, (*S*)-(-)-perillartine (**1**) was obtained in very good to excellent yields (up to 99%) and with full selectivity toward the *E*-regioisomer. The pure product was recovered by avoiding the use of organic solvents and chromatographic purifications, by a straightforward precipitation/filtration sequence of operations. The reaction was efficient regardless of the type of milling media or combinations thereof, milling frequency used (30 or 50 Hz), scale (4.0 or 30 mmol), or type of milling device used (Table 1). Even though the nature of the polymeric material constituting the jars [54] can affect both conversions and yields [51, 52], herein the reaction can also be facilitated by its favorable rheology, as the starting aldehyde is a liquid, absorbed onto the solid reagents. As soon as the reaction proceeds to completion, a solid cake is formed, recovered as fine, dry powder after the aqueous work-up (Figure 1).

Similarly, the mechanochemical preparation of *N*-tert-butyl-α-phenylnitrone (PBN, **2**; *Z*-regioisomer) was investigated (Scheme 1 and Table 2), focusing on the influence of the milling jar composition—including combinations of different milling materials—on reaction productivity. In the case of polymeric jars made of PTFE or POM, balls composed of either SS or zirconia were used. The results were evaluated in terms of mechanochemical processing conditions and compared to those previously reported for a vibrating ball mill (Table 2, entry 1) [38], where stainless steel was used as milling media. The rationale was to identify an alternative milling setup that avoids residual metal contamination, particularly for applications involving human use or consumption, as previously demonstrated in the mechanochemical synthesis of (*S*)-(-)-perillartine (**1**). At 30 Hz, in reaction conditions set to provide higher stress frequency (S_F) [62, 63] enabling more impacts per unit of time (entry 2), with a 3-fold total cumulative energy (E_{total} = 114.6 vs. 42.6 kJ in entry 1), the yield dropped drastically (10%) and the conversion of starting materials remained low. This trend confirmed the observation and considerations made so far for the preparation of (*S*)-(-)-perillartine (**1**) (Table 1, entries 1 and 2). By keeping constant the total cumulative energy (E_{total} = 114.6 kJ, entries 2, 4, and 5), the reaction output was strictly dependent on the material used for the milling jar. Thus, PBN (**2**) yield increased to 45% by replacing SS jar by "softer" polymer vessels, probably due to the lower thermal conductivity diminishing the extent of hydration reaction of the aldehyde, such as POM or PTFE. At 30 Hz, among the possible combinations, PTFE/POM with SS/ZrO_2 balls, POM/ZrO_2 combination was the best, confirming the potential of this polymeric material as a valuable alternative to the commonly used PTFE. Also, Teflon is a fluoropolymer, and any potential residue from leaching could be problematic —especially in applications involving human consumption. From an environmental perspective as well, this is a concern, given that fluoropolymers like Teflon are highly persistent in the environment.

At a lower total cumulative energy (in the range *ca.* 31–39 kJ, entries 7 and 8), yields were increased up to 74%, as the milling frequency was 50 Hz, for PTFE/SS ball combination or in SS (both jar and balls). However, for PTFE, by replacing SS balls (entry 8) with ZrO_2 ones (entry 9), despite a relatively small difference in the total cumulative energy [$\Delta(E_{total}) = 5.6$ kJ], reagents were not converted (0% yield).

Comparable yields were obtained when ZrO_2 milling media was used to prepare PBN (**2**), in both vibrating and planetary ball-mill (76% and 79% yield, entries 3 and 10, respectively), with ZrO_2 becoming the material of choice in this last case. Indeed, even if the benchmark experiment in the vibrating ball-mill (entry 1) [38] delivered quantitative yield of PBN (**2**) in SS, the same reaction in the planetary ball-mill was not efficient (10% yield, entry 11), despite the little difference in the total cumulative energy [$\Delta(E_{total}) = 4.6$ kJ, entries 10 vs. 11)]. This could be due to a more favorable balance between mechanical stress and less important macroscopic thermal effects for reactions carried out in ZrO_2 (entries 2 vs. 3, and 10 vs. 11).

As expected, for this transformation, the output of the reactions was mainly dependent on the interplay between technical (e.g., type of ball-mill and milling media, milling jar volume and shape, size and number of milling balls, ball to mass ratio, and filling degree) and process parameters (e.g., operating frequency and reaction time) [9, 62, 63], confirming, once more, that the optimization of a mechanochemical reaction is multifactorial and the reactivity of the system needs fine tuning of several variables. Independently on the yields and the processing conditions used, the *Z*-regioisomer was always obtained with full selectivity.

Similarly to (*S*)-(-)-perillartine (**1**), PBN (**2**) was easily recovered without the use of organic solvents (Figure 1). The melting point measured for PBN (**2**) after work-up by precipitation of the crude in aqueous $NaHSO_3$ (10%) was 70°C–71°C, closely matching the value reported in the literature (71°C–72°C), whether the product was recovered by recrystallization from hexane [64], or by evaporation in vacuo from dichloromethane [38]. This fact suggested that the same solid form could have been formed in all cases, aspect of particular interest especially when dealing with drugs [65], or any substance for which the stability of crystalline properties over time and/or under varying environmental conditions is essential [66].

2.1 | Comparative Greenness Assessment of Mechanochemical vs. Solution-Based Processes

Several methods were previously reported for the solution-based synthesis of (*S*)-(-)-perillartine (**1**) and *N-tert*-butyl-α-phenylnitrone (PBN, **2**), briefly described below for context and comparative purposes. Mostly, (*S*)-(-)-perillartine (**1**) was prepared by dissolving hydroxylamine hydrochloride and sodium carbonate in water, followed by the gradual addition of perillaldehyde. After 2 h reaction, a liquid–liquid extraction was performed using ethyl acetate. Further purification using column chromatography with cyclohexane/ethyl acetate afforded perillartine in 62% yield [18, 19]. Another method, although similar, did not report yield and therefore could not be directly compared [67]. More recently, electrochemical [20] and chemoenzymatic [21] synthesis of (*S*)-

1864564x, 2026, 9, Downloaded from https://chemistry-europe.onlinelibrary.wiley.com/doi/10.1002/cssc.202502491 by Andrea Cusumano - Université de Montpellier , Wiley Online Library on [22/06/2026]. See the Terms and Conditions (https://onlinelibrary.wiley.com/terms-and-conditions) on Wiley Online Library for rules of use; OA articles are governed by the applicable Creative Commons License

(-)-perillartine (**1**) were described. In the first, (*S*)-(-)-perillartine (**1**) was obtained after 10 h in 90% yield through the generation of NH_2OH by the electrocatalytic reduction of KNO_3 in water, using a multilayered Zn nanosheet catalyst as electrode, needed for the addition of perillaldehyde under acidic conditions. On the other hand, the chemoenzymatic method relies on the oxidation of perillyl alcohol by *Acetobacter* spp., followed by in situ condensation of perillaldehyde with an excess of aqueous hydroxylamine hydrochloride (1.5 equiv.). This approach afforded (*S*)-(-)-perillartine (**1**) in 96% yield after 48 h, after purification by column chromatography.

When compared with the mechanochemical method presented herein in Table 1, the solution-based protocols already exhibit several limitations. The classical preparation of aldoximes [19], although using water as solvent, requires a larger solvent volume and results in significantly lower 58% yield impacting negatively the overall green metrics. The more recent electrochemical [20] and chemoenzymatic [21] processes afforded comparable yields (96% and *ca*. 90%, respectively) to the mechanochemical process (Table 1). However, these methods rely on specialized electrochemical setups or bacterial cultures, which are often less accessible in standard synthetic laboratories. In contrast, the mechanochemical approach employed here requires the use of common milling equipment, making it more practical and easier to implement in most research and industrial settings. Moreover, the mechanochemical protocol avoids the use of metals as catalysts and provides similar or even superior yields, while drastically reducing reaction times from 10–48 h to 1 h.

In the case of *N-tert*-butyl-α-phenylnitrone (PBN, **2**), most of the solution-based methods for its preparation rely on the use of slight excess of pyrrolidine as a base and dichloromethane as the solvent. Under these conditions, PBN (**2**) was reported to be formed after 15 min [35, 36].

By substituting dichloromethane with a less harmful mixture of water and methanol, reaction time increased to 6 h. Solventless procedures were also reported in the literature. In one example, microwave-assisted activation was used to afford PBN (**2**) in 86% yield after 2 min of microwave irradiation at about 140°C, after purification by column chromatography [34]. In another case, PBN (**2**) was obtained in 90% yield by stirring a mixture of benzaldehyde and *N-tert*-butyl hydroxylamine hydrochloride in the presence of a 2.5-fold excess of magnesium oxide under an inert atmosphere for 24 h, after recrystallization from highly volatile solvents (VOS), namely a harmful dichloromethane/diethyl ether mixture [37].

Although these solution-based protocols reported the formation of PBN (**2**) in a shorter time (2–15 min vs. 60–120 min for the mechanochemical methods), they rely on either the use of energy-intensive microwave heating or the use of dichloromethane, a toxic solvent recently banned from the majority of industrial and commercial applications due to its environmental persistence and risks to human health [68, 69]. In contrast, the proposed mechanochemical protocols (Table 2) avoid the use of solvents, including in the downstream process (Figure 1), no heating is required, and only aqueous waste, not containing harmful compounds, is generated while maintaining a high yield.

However, beyond these qualitative considerations, already harnessing the advantages of mechanochemistry to conduct organic syntheses [70], a quantitative assessment of the eco-footprint of mechanochemical methods vs. solution-based approaches is always needed.

Indeed, mechanochemistry has emerged as a powerful approach for enhancing green metrics in chemical processes [9, 10] and their sustainability profiles [45, 71], in comparison with the solution-based counterparts. Herein, the green chemistry metrics of the chemical transformations described above (Scheme 1 and Tables 1 and 2) were calculated using Chem21 [43], while the DOZN [41, 44, 45] and EcoScale [46] toolkits evaluate each process based on the 12 Principles of Green Chemistry and the reaction efficiency and downstream process, respectively. The developed mechanochemical methods were compared against the corresponding solution-based processes. The protocols selected for (*S*)-(-)-perillartine (**1**) [18] and *N-tert*-butyl-α-phenylnitrone (PBN, **2**) [36] synthesis were chosen based on similarities in chemical reagents and work-up procedures.

2.1.1 | Green Metrics assessment by Chem21 tool [43]

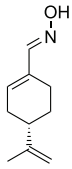
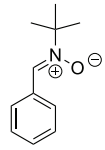
The assessment by Chem21 tool combines both quantitative and qualitative indicators to evaluate the sustainability of a process (Table 3). Quantitative factors include yield, selectivity, and key metrics such as atom economy (AE) [73], reaction mass efficiency (RME) [74], optimum efficiency (OE) [43], process mass intensity (PMI) [75], and *E*-factor [75]. These parameters were calculated for (*S*)-(-)-perillartine (**1**) and *N-tert*-butyl-α-phenylnitrone (PBN, **2**), synthesized by both mechanochemical and solution-based methods, to compare the environmental impact of each approach (see Table 3 and Excel spreadsheets in the Supporting Information). Notably, the inclusion of OE offers an advantage over AE and RME, as it accounts for variations inherent to different chemical processes. Optimum efficiency (OE) metric enables direct comparative assessment across disparate reaction classes [43]. A capability not consistently afforded by metrics such as atom economy (AE) or reaction mass efficiency (RME). This discrepancy arises from the fact that certain transformations are intrinsically atom- or mass-efficient, whereas others are not, rendering OE a more broadly applicable and discriminating metric for evaluating the efficiency of diverse synthetic methodologies [69].

In addition to numerical metrics, Chem21 evaluates qualitative factors such as energy efficiency, safety, and potential environmental and health hazards associated with the chemicals and processes used. For each factor, a clear visual scoring system is assigned: green for "preferred," amber for "acceptable with some concerns," and red for "undesirable," ensuring an intuitive and transparent evaluation of sustainability.

For the mechanochemical synthesis of (*S*)-(-)-perillartine (**1**), all quantitative metrics were improved compared to the solution-based procedure [18]: AE was increased due to the use of a lower molecular weight base (sodium hydrogen carbonate instead of sodium carbonate); RME was improved due to stoichiometric use of reagents; OE was close to the optimal value of 100%; and PMI and *E*-factor, which take into account solvents and work-up procedures, were substantially reduced due to the low solvent requirements inherent to the mechanochemical method, including the downstream process. In terms of qualitative evaluation, the nature of the solvents used for the work-up process (water, green flag vs. cyclohexane, amber flag), as well as

1864564x, 2026, 9, Downloaded from https://chemistry-europe.onlinelibrary.wiley.com/doi/10.1002/cssc.202502491 by Andrea Casagrande - Université de Montpellier , Wiley Online Library on [22/06/2026]. See the Terms and Conditions (https://onlinelibrary.wiley.com/terms-and-conditions) on Wiley Online Library for rules of use; OA articles are governed by the applicable Creative Commons License

TABLE 3 | Comparison of green chemistry metrics by Chem21 toolkit for solution-based *vs.* mechanochemical methods in the preparation of (*S*)-(-)-perillartine (**1**) and *N-tert*-butyl-α-phenylnitrone (PBN) (**2**).

	Solution synthesis vs. mechanochemical conditions					
	 (**1**)			 (**2**)		
METRICS[a,b]						
AE	40.0	vs.	54.4	58.5	vs.	56.1
RME	24.4	vs.	53.1	54.2	vs.	36.5
OE[c]	60.9	vs.	97.6	92.7	vs.	65.0
PMI	65.1	vs.	21.3	185.5	vs.	29.9
***E*-factor**	64.1	vs.	20.3	184.5	vs.	28.9
Solvent	H_2O		No solvent	CH_2Cl_2		No solvent
Work-up, recovery	Liquid extraction, Recryst. (EtOAc, *c*-C_6H_{12})		Filtration	Filtration (EtOAc, SiO_2)		Filtration ($NaHSO_3$ aq.)
Health and safety	H410, H411 H301, H351, H371, H373, H400		n.a.	H330, H350, H370, H372 H301, H360FD, H371, H373, H401, H412		n.a.

[a]The optimum value for AE, RME, and OE is 100%; for *E*-factor, the optimum value is 0, with PMI = E factor +1 [72]. When comparing two processes, the one with the lowest PMI will be the greenest.
[b]Experimental protocols used for metrics calculations. Methods in solution: for (**1**), reference [18] was used; for (**2**), reference [36] was used. Mechanochemical methods: for (**1**), Table 1 entry 6; for (**2**), Table 2, entry 6.
[c]$OE = \frac{RME}{AE} \times 100$. *Legend*: **Green flag** = preferred; **amber flag** = acceptable with some concerns; **red flag** = undesirable; n.a. = not applicable.

the quantity of reagents used (stoichiometric, amber flag vs. excess, red flag), further favored the mechanochemical method over the solution-based one (also see Supporting Information).

In contrast, for *N-tert*-butyl-α-phenylnitrone (PBN, **2**), the quantitative assessment revealed differences in the values of AE, RME, and OE (Table 3).

This result arises from the fact that these metrics only consider the reagents involved (i.e., their molecular weight and stoichiometry) and not the solvents. Specifically, AE metric for the solution-based method was slightly better because a lower molecular weight base was used (pyrrolidine instead of sodium hydrogen carbonate), while RME and OE were favored for the solution method due to a higher yield (97% vs. 65% for the mechanochemical method in Table 2, entry 6). However, assessing the greenness of a process solely on these metrics might be biased. When solvents were included in the calculations, an approximately 6-fold decrease in PMI and *E*-factor values could be observed in favor of the mechanochemical process. The qualitative evaluation also supported this finding, highlighting the use of hazardous solvents (dichloromethane) and silica during the purification step, which account for more than the 86% of the total PMI for PBN (**2**), in comparison with the mechanochemical method selected for the calculations, using POM/ZrO_2 as milling media (65% yield, Table 2, entry 6). In this case, even if the yield of the mechanochemical process was lower (65% vs. 97% for the solution process [18]), the metrics accounting for the work-up procedures were still better (*c.f.*, Excel spreadsheet in the Supporting Information), harmful solvents were not used, and the value of PMI for the mechanochemical process remained lower compared to the PMI calculated of the solution-based protocol. These quantitative evaluations support the potential of mechanochemistry as a "Safe and Sustainable by Design" (SSbD) approach for organic synthesis and emphasize the need for green chemistry metrics to account for downstream processing. Indeed, solvent use during work-up remains one of the most significant challenges undermining the benefits of mechanochemical reactions. Moreover, the safety and the hazards for each process need to be considered. Ideally, environmental impact should be evaluated through Life Cycle Assessment (LCA); however, such data are not always available or accessible, even for solution-based methods at an industrial scale [71].

2.1.2 | Assessment by DOZN 3.0 toolkit

DOZN 3.0 toolkit evaluates chemical processes based on the 12 Principles of Green Chemistry [76], grouping them into three main categories: i) *Group 1*: Improved Resource Use, which considers principles 1, 2, 7, 8, 9, and 11; ii) *Group 2*: Increased Energy Efficiency, which includes principle 6 and evaluates deviations

1864564x, 2026, 9, Downloaded from https://chemistry-europe.onlinelibrary.wiley.com/doi/10.1002/cssc.202502491 by Andrea Casagrande - Université de Montpellier , Wiley Online Library on [22/06/2026]. See the Terms and Conditions (https://onlinelibrary.wiley.com/terms-and-conditions) on Wiley Online Library for rules of use; OA articles are governed by the applicable Creative Commons License

from ambient conditions regarding temperature and pressure; and iii) *Group 3*: Reduced Human and Environmental Hazards, which includes principles 3, 4, 5, 10, and 12, assessing waste generation, its severity, and the hazard profile of the final product. For each group, an individual score is calculated and then normalized to an aggregate value (referred to as "aggregate score") and calculated by the average of the individual scores of each green chemistry principle. It provides a quantitative measure of the overall greenness of a process, with values approaching zero indicating greater sustainability. When comparing two processes, the one with the lower aggregate score is considered the more environmentally benign.

The comparison of DOZN 3.0 scores for the preparation of (*S*)-(-)-perillartine (**1**) and *N*-*tert*-butyl-α-phenylnitrone (PBN, **2**) is shown in Figure 2A (and in the Excel spreadsheet in the Supporting Information). For both compounds, the aggregate DOZN 3.0 scores favor the mechanochemical approach, indicating a lower overall environmental impact relative to the solution-based methods. In the case of (*S*)-(-)-perillartine (**1**), the scores for *Group 1* (Improved Resource Use) and *Group 3* (Reduced Human and Environmental Hazards) were significantly improved mainly due to the elimination of solvents for both the reaction and the recovery of the product, and for the simplified work-up procedure.

Notably, analysis of the individual scores for *N*-*tert*-butyl-α-phenylnitrone (PBN, **2**) shows that the difference arises primarily from *Group 3* (Reduced Human and Environmental Hazards), mainly attributed to the use of dichloromethane and pyrrolidine in the solution-based process [18], and not to a difference in yields (97% vs. 65% for solution vs. mechanochemistry), or reagents stoichiometry, used in equimolar amounts in both methods. For both compounds and synthetic methods (mechanochemical or solution), *Group 2* (Increased Energy Efficiency) does not contribute significantly to the final score, as all reactions were performed at room temperature and at atmospheric pressure, with only the use of reduced pressure in filtration processes and solvent evaporation (for the solution-based process). It is important to note that the *Group 2* (Increased Energy

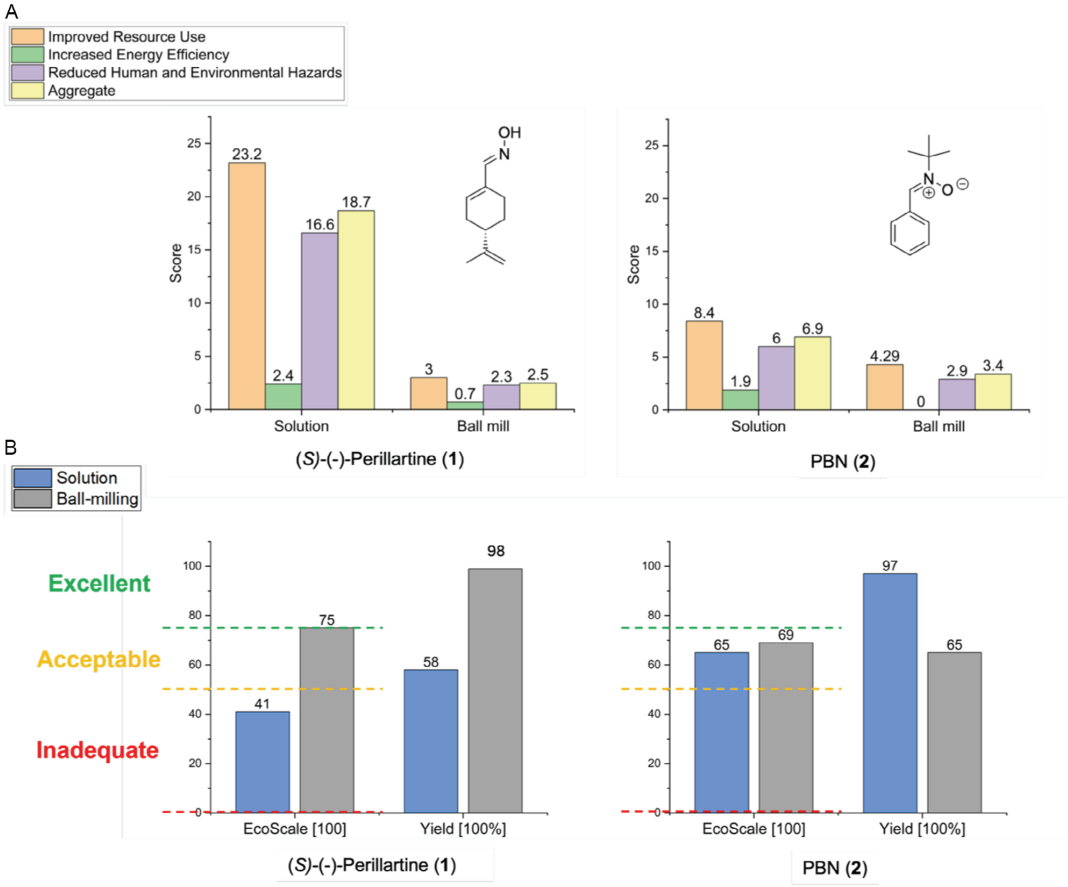


FIGURE 2 | Comparison of solution-based vs. mechanochemical synthesis for (*S*)-(-)-perillartine (**1**) and *N*-*tert*-butyl-α-phenylnitrone (PBN, **2**). (A) By DOZN 3.0 Quantitative Scoring tool [44, 45]. Legend: *Group 1* (Improved Resource Use—**orange**), *Group 2* (Increased Energy Efficiency—**green**), *Group 3* (Reduced Human and Environmental Hazards—**violet**), and Aggregate score—**yellow**; (B) by EcoScale tool [46]. Legend: excellent (≥75), acceptable (≥50), or inadequate (<50). Experimental protocols used for metrics calculations. Methods in solution: for (**1**), reference [18] was used; for (**2**), reference [36] was used. Mechanochemical methods: for (**1**), Table 1 entry 6; for (**2**), Table 2, entry 6.

1864564x, 2026, 9, Downloaded from https://chemistry-europe.onlinelibrary.wiley.com/doi/10.1002/cssc.202502491 by Andrea Casagrande - Université de Montpellier , Wiley Online Library on [22/06/2026]. See the Terms and Conditions (https://onlinelibrary.wiley.com/terms-and-conditions) on Wiley Online Library for rules of use; OA articles are governed by the applicable Creative Commons License

Efficiency) scores for the mechanochemical protocols may be artificially favorable in the DOZN 3.0 assessment. This is due to the software's assumption that reactions performed at room temperature consume minimal energy, without accounting for the actual electrical consumption of the milling equipment. This limitation should be considered when interpreting DOZN 3.0 outputs for mechanochemical processes, especially in the context of a fair comparison with solution-based methods.

For both compounds, aggregate scores for the mechanochemical methods (2.5 and 3.4, respectively, for **1** and **2**) were lower than the aggregate scores for the corresponding solution-based syntheses (18.7 and 6.9, respectively). In the case of (*S*)-(-)-perillartine (**1**), the aggregate score for the mechanochemical method was *ca.* 7.5 times lower than for solution-based synthesis.

2.1.3 | Assessment using EcoScale toolkit [46]

The EcoScale toolkit is a semi-quantitative assessment method designed to evaluate the efficiency and sustainability of synthetic routes by integrating multiple factors, including yield, cost, safety, technical setup, and environmental impact [46] (Figure 2B, Figure S4 and Excel spreadsheet in the Supporting Information). Each process starts with an initial ideal score of 100, from which penalty points are subtracted based on specific drawbacks such as hazardous reagents, excessive solvent use, high energy consumption, or complex purification steps. The final score classifies the process into one of three categories: excellent (≥75), acceptable (≥50), or inadequate (<50).

For the solution-based synthesis of (*S*)-(-)-perillartine (**1**) [18], the main score (41) is primarily the result of the lower yield (58%) and greater safety hazards linked to the use of cyclohexane and ethyl acetate during the work-up procedure. In contrast, the mechanochemical process (using POM/ZrO_2 milling media, Table 1 entry 6) avoided the use of harmful chemicals or organic solvents also for the recovery of the product, achieving a score of (75), the only penalty being safety hazards associated with the unavoidable use of hydroxylamine hydrochloride, which is indeed the reagent. Therefore, also in this case, the mechanochemical method outperformed compared to the solution-based one.

In the case of *N-tert*-butyl-α-phenylnitrone (PBN, **2**), similar scores are obtained for both solution (65 score) and mechanochemical methods (69 score, using POM/ZrO_2 milling media, Table 2 entry 6), although differences arise from different sources. For the solution process, the main penalty involved safety concerns due to the use of dichloromethane, ethyl acetate, and silica gel used for the recovery of the product, whereas a lower yield accounts for the main drawback in the mechanochemical process. Interestingly, despite the lower yield of the mechanochemical method (65%, Table 2 entry 6) in comparison with the solution synthesis (97% yield), the EcoScale values remain competitive, confirming once again the favorable ecofootprint of mechanochemistry if the reaction and all the postreaction operation are well designed.

2.1.4 | Comparison between the green assessment tools: DOZN 3.0 vs. EcoScale

Depending on the tool chosen for metrics calculations and the reaction protocols selected, the assessment of the greenness of the processes can lead to different conclusions. Therefore, for the sake of comparisons, and to demonstrate that only one single tool is not sufficient to determine which process is the best from the point of view of the eco-footprint, DOZN 3.0 and EcoScale were considered, both allowing to quantitatively evaluate also the safety and hazards (not scored in Chem21). The preparation of PBN (**2**) was used as benchmark and three methods were compared: in solution (97% yield) [36], and by ball milling, using as milling media SS (Method A, 100% yield) [38], or the POM/ZrO_2 combination (Method B, 65% yield, Table 2, entry 6) (Figure S4 in the Supporting Information).

As a result, based on DOZN 3.0 output (Figure S4), Method B resulted in the best with the lowest aggregate score (3.4), followed by the synthesis in solution [36], having a much better score (6.9) than the mechanochemical method A [38] (scoring 22.2). The high aggregate score for the mechanochemical Method A [38] is a consequence of the postreaction operation to recover the final product by precipitation/filtration of the salts in dichloromethane, impacting on both *Group 1* (Improved Resource Use) and *Group 3* (assessing waste generation, its severity, and the hazard profile of the final product) scores. In particular, very high scores were obtained for the green chemistry principle #1 (Prevention, in *Group 1* — scoring 100) and principle #3 (Safety, in *Group 3* — scoring *ca.* 63).

However, the assessment is completely reversed when EcoScale is used (Figure S4), with the mechanochemical Method A [38] being the greenest, followed by Method B and then solution synthesis [36]. The assessment is mainly driven by the yield of the reaction. No penalty points are given if the reaction is quantitative, but the penalty points increase dramatically as soon as the yield decreases. Therefore, in the case of Method A [38] (100% yield), there was no penalty, and the mechanochemical method falls in the "excellent zone" (score 88, Figure S4). For Method B (Table 2, entry 6), a 65% yield accounted for −17 penalty points (with the maximum value being −50 points). Consequently, Method B was classified in the "acceptable" zone with an EcoScale score of 69. Whether the mechanochemical process selected for the calculations delivered higher yield, the EcoScale score increased. For example, for the process conducted in ZrO_2 (Table 2, entry 3), a yield of 76% accounted for a five-point penalty gain, bringing the mechanochemical process again in the "excellent" zone. However, the EcoScale fails to consider the amount of solvent used (organic or not) and the waste generated, and it does not give the same importance or weight as DOZN 3.0 for the environmental, safety, and societal implications, which make its use not so common for greenness assessment, as it can be seen in the case of Method A, when comparing Ecoscale and DOZN 3.0 scores.

In summary, all assessments presented herein converge on a common conclusion: mechanochemistry offers an efficient approach to synthesize (*S*)-(-)-perillartine (**1**) and *N-tert*-butyl-α-phenylnitrone (PBN, **2**), particularly by simplifying reaction setup and work-up procedures and eliminating the need for hazardous reagents and solvents, with better green chemistry metrics in comparison with the solution-based methods.

3 | Conclusion

The unprecedented, multigramscale mechanochemical preparation of (*S*)-(-)-perillartine (**1**), a potent sweetener, and *N-tert*-

18645564c, 2026, 9, Downloaded from https://chemistry-europe.onlinelibrary.wiley.com/doi/10.1002/cssc.202502491 by Andrea Casagrande - Université de Montpellier , Wiley Online Library on [22/06/2026]. See the Terms and Conditions (https://onlinelibrary.wiley.com/terms-and-conditions) on Wiley Online Library for rules of use; OA articles are governed by the applicable Creative Commons License

butyl-α-phenylnitrone (PBN, **2**) a well-known free-radical spin trap that exhibits antioxidant, neuroprotective, and anti-aging properties were described, and the influence of different mechanochemical processing conditions was studied. The use of "softer" polymeric jars (PTFE or POM) was considered as valid alternative to "harder" milling materials (SS or ZrO_2). The use of POM milling media is, to the best of our knowledge, still underexplored in the field of mechanochemistry, and this work highlights its benefits compared to more traditional jars. In some cases, it demonstrated better performance than PTFE, positioning it as a valuable and potentially more sustainable alternative at reduced cost. This claim is based on the broader context of avoiding fluoropolymers, given the growing environmental and health concerns surrounding per- and polyfluoroalkyl substances (PFAS), progressively identified as persistent environmental pollutants, the chemical class to which PTFE belongs. By offering a fluorine-free alternative, POM aligns with a proactive "Safe and Sustainable by Design" strategy, mitigating future risks associated with persistent pollutants. Moreover, POM is also a valid alternative to SS, preventing or diminishing the probability of residual metal impurities due to abrasion of the milling media. Although, at present, POM jars are not commercially available, proper scale-up would require the manufacture of larger POM jars (for batch) or POM-coated screws (for continuous processes such as twin-screw extrusion). When it comes to the use of planetary ball-mills, the jars should be designed and manufactured to resist at the high energetic conditions provided by planetary ball-mills, usually not compatible with "soft" polymeric materials (e.g., PTFE, PMMA, POM), which would break or deform during the milling process. These engineering aspects, however, lie beyond the scope of the current manuscript. By analogy with PTFE, which has already led to marketed large-scale solutions, we believe that the present study on POM provides the necessary foundation to serve as a reference for future developments.

The comparative assessment of mechanochemical and solution-based methods for the synthesis of (*S*)-(-)-perillartine (**1**) and *N*-*tert*-butyl-α-phenylnitrone (PBN, **2**) highlights the environmental benefits of mechanochemistry. The comprehensive sustainability assessment performed by a comparative green evaluation using multiple complementary tools (Chem21, DOZN 3.0, and EcoScale) covering the entire process, including the downstream work-up, showed that mechanochemical approaches consistently led to reduced solvent use, simplified work-up procedures, and lower associated environmental and safety risks. This in-depth analysis of the processes' full eco-footprint is a key contribution that moves beyond simple reaction yields.

Although some individual parameters, such as yield or atom economy, were initially more favorable in the solution-based protocols, the overall performance of the mechanochemical methods demonstrated a lower environmental impact and greater alignment with green chemistry principles. In addition, the byproducts and waste generated by these methods exhibit minimal or no toxicity to humans and the environment. Ball-milling conditions differ significantly from conventional experimental setups [77], and as such, we could not assume that the *E*,*Z*-isomeric ratio would mirror that observed under standard conditions in solution. Through comparison with literature spectral data, we determined that the products synthesized under ball-milling conditions were consistent with those previously reported and with full selectivity toward the regioisomers *E*-(**1**) [21] and the more stable form *Z* [78] for PBN (**2**).

This work contributes to the field by bridging practical synthesis with detailed sustainability analysis. Specifically, its novelty lies in (i) applying mechanochemistry to synthesize high-value, marketable ingredients (e.g., perillartine) for the food and personal care sectors [79] from an abundant, renewable biomass-derived aldehyde (e.g., perillaldehyde) [80], using fluorine-free polymeric jars; (ii) demonstrating the process's robustness and versatility across different, commonly used milling platforms; (iii) closely working with manufacturers for mechanochemical devices (for both batch and continuous processes) to design new reactors, or to retool and retrofit existing devices for new applications, at different scales; and (iv) providing a comprehensive green assessment of the entire workflow, including the often-neglected downstream processing, which validates the method's alignment with SSbD principles and the IUPAC Guiding Principles of Responsible chemistry [11].

We hope that this contribution will stimulate the curiosity of the scientific community and contribute to a circular economy mindset, by transforming a readily available natural raw material from *Perilla frutescens* into a commercially relevant product. Our study bridges the gap between green chemistry metrics and industrial application, and it demonstrates that mechanochemical protocols are not only sustainable and efficient but can also deliver products of tangible economic significance, thereby linking practical synthesis with sustainability principles. The cross-fertilization among several market sectors raises awareness on innovation opportunities for a more sustainable chemical industry, which should also result in new developments in mechanochemistry. Mechanochemical routes can become synthetically superior to the current manufacturing processes in solution, upon further developments at process-level.

Author Contributions

Evelina Colacino: conceptualization, project administration, data curation, funding acquisition, supervision, resources, writing, review and editing. **Nicolas Fantozzi**: investigation, formal analysis, writing – original draft. **Rubén Solórzano-Rodríguez**: conceptualization, data curation, formal analysis, writing – original and final draft, supervision, visualization, review and editing. **Andrea Casagrande**: investigation, formal analysis, validation. **Christos M. Chatzigiannis** and **Corentin Bordier**: visualization, review and editing. **Pietro Rando**: review and editing, funding.

Acknowledgments

This article is based upon work from COST Action CA18112 "Mechanochemistry for Sustainable Industry," supported by COST (European Cooperation in Science and Technology) [82–85]. COST (European Cooperation in Science and Technology) is a funding agency for research and innovation networks, helping to connect research initiatives across Europe and enable scientists to grow their ideas by sharing them with their peers. This boosts their research, career, and innovation www.cost.eu [86]. E.C. and N.F. acknowledge Région Occitanie (France) for the Pre-Maturation 2020 – MECHAPI grant (ESRPREMAT – 00262). E.C. and A.C. acknowledge Campus France and Tallinn Technological University (TalTech) for the Ph.D. fellowship (co-tutelle de thèse France-Estonia). E.C., R.S.R., C.M.C., and C.B. acknowledge IMPACTIVE (Innovative Mechanochemical Processes to synthesize green ACTIVE pharmaceutical ingredients) [87, 88], the research project

1864564x, 2026, 9, Downloaded from https://chemistry-europe.onlinelibrary.wiley.com/doi/10.1002/cssc.202502491 by Andrea Casagrande - Université de Montpellier , Wiley Online Library on [22/06/2026]. See the Terms and Conditions (https://onlinelibrary.wiley.com/terms-and-conditions) on Wiley Online Library for rules of use; OA articles are governed by the applicable Creative Commons License

funded from the European Union's Horizon Europe research and innovation program (European Health and Digital Executive Agency) under grant agreement No. 101057286. Views and opinions expressed are however those of the authors only and do not necessarily reflect those of the European Union or the European Health and Digital Executive Agency. Neither the European Union nor the granting authority can be held responsible for them. The initial set of experiments for the mechanochemical synthesis of (*S*)-(-)-perillartine (**1**) was conceived in 2021 by the main author for the Master Programme "Ingénierie des cosmétiques, arômes et parfums" (ICAP), at the Faculty of Science (Department of Chemistry) of the University of Montpellier (France). Then, the set of experiments was further implemented by the main author at the occasion of the 4th Training School on "Mechanochemical Synthesis and kinetics" (13–16 June, 2022—Cagliari, Italy) organized by the COST Action CA18112 "Mechanochemistry for Sustainable Industry" (MechSustInd, 2019–2023) and chaired by Prof. Francesco Delogu (Università degli Studi di Cagliari, Italy).

Open access publication funding provided by COUPERIN CY26.

Funding

This study was supported by European Cooperation in Science and Technology (CA18112), Région Occitanie Pyrénées-Méditerranée (Pre-Maturation 2020 – MECHAPI grant (ESRPREMAT – 00262), European Health and Digital Executive Agency (101057286), Campus France - French Embassy in Estonia.

Conflicts of Interest

The authors declare no conflicts of interest.

Data Availability Statement

The data that support the findings of this study are available in the supplementary material of this article.

References

1. United Nations, Sustainable Development Goals (UN SDGs), (accessed January 27, 2025), *Available at:* https://sdgs.un.org/goals.

2. D. Virieux, F. Delogu, A. Porcheddu, F. García, and E. Colacino, "Mechanochemical Rearrangements," *The Journal of Organic Chemistry* 86 (2021): 13885–13894.

3. J. Alić, M.-C. Schlegel, F. Emmerling, and T. Stolar, "Meeting the UN Sustainable Development Goals with Mechanochemistry," *Angewandte Chemie International Edition* 63 (2024): e202414745.

4. F. Gomollón-Bel, "Ten Chemical Innovations That Will Change Our World: IUPAC Identifies Emerging Technologies in Chemistry with Potential to Make Our Planet More Sustainable," *Chemistry International* 41 (2019): 12–17.

5. E. Colacino, V. Isoni, D. Crawford, and F. Garcia, "Upscaling Mechanochemistry: Challenges and Opportunities for Sustainable Industry," *Trends in Chemistry* 3 (2021): 335–339.

6. K. J. Ardila-Fierro and J. G. Hernández, "Sustainability Assessment of Mechanochemistry by Using the Twelve Principles of Green Chemistry," *ChemSusChem* 14 (2021): 2145–2162.

7. D. J. C. Constable, C. Jimenez-Gonzalez, and R. K. Henderson, "Perspective on Solvent Use in the Pharmaceutical Industry," *Organic Process Research & Development* 11 (2007): 133–137.

8. C. Jiménez-González, A. D. Curzons, D. J. C. Constable, and V. L. Cunningham, "Cradle-to-Gate Life Cycle Inventory and Assessment of Pharmaceutical Compounds," *The International Journal of Life Cycle Assessment* 9 (2004): 114–121.

9. N. Fantozzi, J.-N. Volle, A. Porcheddu, D. Virieux, F. García, and E. Colacino, "Green Metrics in Mechanochemistry," *Chemical Society Reviews* 52 (2023): 6680–6714.

10. A. Casagrande, A. Niidu, R. Aav, D. Kananovich, and E. Colacino, "Green Chemistry tools in Mechanochemistry," in *Encyclopedia of Green Chemistry*, edited by B. Török (Elsevier, 2025) pp.550–571.

11. IUPAC Guiding Principles of Responsible Chemistry, https://iupac.org/responsible-chemistry/, (accessed July 31, 2025).

12. FDA's Global Substance Registration System, https://www.fda.gov/industry/fda-data-standards-advisory-board/fdas-global-substance-registration-system, (accessed May 15, 2025).

13. X.-L. Chang, Z.-L. Zhao, X.-L. Li, H. Xu, Y. Sun, and W.-H. Wang, "Extraction and Advanced Adsorbents for the Separation of Perillaldehyde from Perilla frutescens (L.) Britton var. crispa f. viridis Leaves," *Food Science and Technology Research* 20 (2014): 189–199.

14. T. Hou, V. R. Netala, H. Zhang, Y. Xing, H. Li, and Z. Zhang, "Perilla frutescens: A Rich Source of Pharmacological Active Compounds," *Molecules* 27 (2022): 3578.

15. M. Igarashi and Y. Miyazaki, "A Review on Bioactivities of Perilla: Progress in Research on the Functions of Perilla as Medicine and Food," *Evidence-Based Complementary and Alternative Medicine (e-CAM)* 2013 (2013): 925342.

16. H. Kong, B. Zhou, X. Hu, X. Wang, and M. Wang, "Protective Effect of Perilla (Perilla frutescens) Leaf Essential Oil on the Quality of a Surimi-Based Food," *Journal of Food Processing and Preservation* 42 (2018): e13540.

17. Y. Xiao, L. Xiao, M. Li, et al., "Perillartine Protects Against Metabolic Associated Fatty Liver in High-Fat Diet-Induced Obese Mice," *Food & Function* 14 (2023): 961–977.

18. T. Betke, P. Rommelmann, K. Oike, Y. Asano, and H. Gröger, "Cyanide-Free and Broadly Applicable Enantioselective Synthetic Platform for Chiral Nitriles through a Biocatalytic Approach," *Angewandte Chemie International Edition* 56 (2017): 12361–12366.

19. Bousquet, E. W., in *Organic Syntheses Collective Volume 2*, edited by A. H. Blatt, (John Wiley and Sons, 1943), 313–315.

20. C. Xue, S. Jia, J. Jiao, et al., "Highly Efficient Electrosynthesis of Oximes from Nitrates and Carbonyl Compounds in Acidic Media," *Green Chemistry* 26 (2024): 9869–9873.

21. P. Zambelli, A. Pinto, D. Romano, et al., "One-Pot Chemoenzymatic Synthesis of Aldoximes from Primary Alcohols in Water," *Green Chemistry* 14 (2012): 2158–2161.

22. R. Mocci, E. Colacino, L. De Luca, C. Fattuoni, A. Porcheddu, and F. Delogu, "The Mechanochemical Beckmann Rearrangement: An Eco-efficient "Cut-and-Paste" Strategy to Design the "Good Old Amide Bond"," *ACS Sustainable Chemistry & Engineering* 9 (2021): 2100–2114.

23. R. Geib, E. Colacino, and L. Gremaud, "Sustainable Beckmann Rearrangement using Bead-Milling Technology: The Route to Paracetamol," *ChemSusChem* 17 (2024): e202301921.

24. Z. T. Bhutia, A. Das, M. Biswas, A. Chatterjee, and M. Banerjee, "7-Oxa-4-thia-1-aza-bicyclo[3.2.1]octane 4,4-Dioxides: Mechanochemical Synthesis by Tandem Michael Addition–1,3-Dipolar Cycloaddition of Aldoximes and Evaluation of Antibacterial Activities," *European Journal of Organic Chemistry* 2018 (2018): 506–514.

25. X. Cao and J. W. Phillis, "α-Phenyl-tert-butyl-nitrone Reduces Cortical Infarct and Edema in Rats Subjected to Focal Ischemia," *Brain Research* 644 (1994): 267–272.

26. J. Folbergrová, Q. Zhao, K. Katsura, and B. K. Siesjö, "N-tert-butyl-alpha-phenylnitrone Improves Recovery of Brain Energy State in Rats Following Transient Focal Ischemia," *Proceedings of the National Academy of Sciences* 92 (1995): 5057–5061.

1864564x, 2026, 9, Downloaded from https://chemistry-europe.onlinelibrary.wiley.com/doi/10.1002/cssc.202502491 by Andrea Casagrande - Université de Montpellier , Wiley Online Library on [22/06/2026]. See the Terms and Conditions (https://onlinelibrary.wiley.com/terms-and-conditions) on Wiley Online Library for rules of use; OA articles are governed by the applicable Creative Commons License

27. S. Kuroda, K.-i. Katsura, L. Hillered, T. E. Bates, and B. K. Siesjö, "Delayed Treatment with α-Phenyl-N-tert-butyl Nitrone (PBN) Attenuates Secondary Mitochondrial Dysfunction after Transient Focal Cerebral Ischemia in the Rat," *Neurobiology of Disease* 3 (1996): 149–157.

28. J. Marco-Contelles, "α-Phenyl-N-tert-Butylnitrone and Analogous α-Aryl-N-alkylnitrones as Neuroprotective Antioxidant Agents for Stroke," *Antioxidants* 13 (2024): 440.

29. R. A. Floyd, K. Hensley, M. J. Forster, J. A. Kelleher-Anderson, and P. L. Wood, "Nitrones as Neuroprotectants and Antiaging Drugs," *Annals of the New York Academy of Sciences* 959 (2002): 321–329.

30. R. A. Floyd and K. Hensley, "Nitrone Inhibition of Age-Associated Oxidative Damage," *Annals of the New York Academy of Sciences* 899 (2000): 222–237.

31. G. T. Balogh, K. Vukics, Á. Könczöl, Á. Kis-Varga, A. Gere, and J. Fischer, "Nitrone Derivatives of Trolox as Neuroprotective Agents," *Bioorganic & Medicinal Chemistry Letters* 15 (2005): 3012–3015.

32. European Commission database for information on cosmetic substances and ingredients (CosIng): accessed May 21, 2025, https://ec.europa.eu/growth/tools-databases/cosing/. For *N*-tert-Butyl-α-phenylnitrone, EC no : 222-168-8.

33. S.-I. Murahashi and Y. Imada, "Synthesis and Transformations of Nitrones for Organic Synthesis," *Chemical Reviews* 119 (2019): 4684–4716.

34. M. M. Andrade, M. T. Barros, and R. C. Pinto, "Exploiting Microwave-Assisted Neat Procedures: Synthesis of N-aryl and N-alkylnitrones and Their Cycloaddition En Route for Isoxazolidines," *Tetrahedron* 64 (2008): 10521–10530.

35. D. Corbisiero, T. Fantoni, L. Ferrazzano, et al., "Fast MacMillan's Imidazolidinone-Catalyzed Enantioselective Synthesis of Polyfunctionalized 4-Isoxazoline Scaffolds," *ACS Omega* 7 (2022): 26919–26927.

36. S. Morales, F. G. Guijarro, I. Alonso, J. L. G. Ruano, and M. B. Cid, "Dual Role of Pyrrolidine and Cooperative Pyrrolidine/Pyrrolidinium Effect in Nitrone Formation," *ACS Catalysis* 6 (2016): 84–91.

37. R. Hammami, P. Maldivi, C. Philouze, et al., "Synthesis of 4-Phosphinylpyrrolidin-3-ones via [3+2] Cycloaddition of Nitrones with Phosphinylallenes," *Advanced Synthesis & Catalysis* 365 (2023): 1385–1390.

38. E. Colacino, P. Nun, F. M. Colacino, J. Martinez, and F. Lamaty, "Solvent-Free Synthesis of Nitrones in a Ball-Mill," *Tetrahedron* 64 (2008): 5569–5576.

39. E. Colacino, A. Porcheddu, C. Charnay, and F. Delogu, "From Enabling Technologies to Medicinal Mechanochemistry: an Eco-Friendly Access to Hydantoin-Based Active Pharmaceutical Ingredients," *Reaction Chemistry & Engineering* 4 (2019): 1179–1188.

40. D. E. Crawford, A. Porcheddu, A. S. McCalmont, F. Delogu, S. L. James, and E. Colacino, "Solvent-Free, Continuous Synthesis of Hydrazone-Based Active Pharmaceutical Ingredients by Twin-Screw Extrusion," *ACS Sustainable Chemistry & Engineering* 8 (2020): 12230–12238.

41. C. M. Chatzigiannis, S. M. Scalzullo, E. Colacino, and M. E. Rivas, "Multigram-Scale Organic Synthesis by Resonant Acoustic Mixing: Application to the Sustainable Preparation of Active Pharmaceutical Ingredients," *ChemSusChem* 18 (2025): e202500110.

42. A. Porcheddu, F. Delogu, L. De Luca, and E. Colacino, "From Lossen Transposition to Solventless "Medicinal Mechanochemistry"," *ACS Sustainable Chemistry & Engineering* 7 (2019): 12044–12051.

43. C. R. McElroy, A. Constantinou, L. C. Jones, L. Summerton, and J. H. Clark, "Towards a Holistic Approach to Metrics for the 21st Century Pharmaceutical Industry," *Green Chemistry* 17 (2015): 3111–3121.

44. A. De Vierno Kreuder, T. House-Knight, J. Whitford, et al., "A Method for Assessing Greener Alternatives between Chemical Products Following the 12 Principles of Green Chemistry," *ACS Sustainable Chemistry & Engineering* 5 (2017): 2927–2935. DOZN is a universal tool; suitable for scoring any process, no matter the activation technique used, once the detailed experimental/process conditions are known. The DOZN tool is accessible free of charge here/ https://bioinfo.merckgroup.com/dozn (accessed June 27, 2025).

45. P. Sharma, C. Vetter, E. Ponnusamy, and E. Colacino, "Assessing the Greenness of Mechanochemical Processes with the DOZN 2.0 Tool," *ACS Sustainable Chemistry & Engineering* 10 (2022): 5110–5116.

46. K. Van Aken, L. Strekowski, L. Patiny, "EcoScale, a Semi-Quantitative Tool to Select an Organic Preparation Based on Economical and Ecological Parameters," *Journal of Organic Chemistry* 2 (2006): 3. The EcoScale tool is accessible free of charge here: https://ecoscale.cheminfo.org (accessed June 11, 2025).

47. F. Basoccu, P. Caboni, and A. Porcheddu, "Mechanochemistry: Unravelling the Impact of Metal Leaching in Organic Synthesis," *ChemSusChem* 18 (2025): e202402547.

48. L. Konnert, M. Dimassi, L. Gonnet, F. Lamaty, J. Martinez, and E. Colacino, "Poly(ethylene) Glycols and Mechanochemistry for the Preparation of Bioactive 3,5-Disubstituted Hydantoins," *RSC Advances* 6 (2016): 36978–36986.

49. T. Friščić, I. Halasz, P. J. Beldon, et al., "Real-Time and In Situ Monitoring of Mechanochemical Milling Reactions," *Nature Chemistry* 5 (2013): 66–73.

50. For stainless steel (SS): the hardness is typically in the range of 5.5 to 6.0 Mohs depending on the type of steel; the density is in the range 7.7 to 8.1 g/cm^3. For zirconium oxide (ZrO_2): the hardness is typically in the range 8.0 to 8.5 Mohs; the density (when stabilised by Yttria) is 6.0 g/cm^3.

51. I. Sović, S. Lukin, E. Meštrović, et al., "Mechanochemical Preparation of Active Pharmaceutical Ingredients Monitored by In Situ Raman Spectroscopy," *ACS Omega* 5 (2020): 28663–28672.

52. E. Colacino, A. Porcheddu, I. Halasz, et al., "Mechanochemistry for "No Solvent, No Base" Preparation of Hydantoin-Based Active Pharmaceutical Ingredients: Nitrofurantoin and Dantrolene," *Green Chemistry* 20 (2018): 22973–22977.

53. A. Porcheddu, F. Delogu, L. De Luca, C. Fattuoni, and E. Colacino, "Metal-Free Mechanochemical Oxidations in Ertalyte Jars," *Beilstein Journal of Organic Chemistry* 15 (2019): 1786–1794.

54. M. F. Rappen, L. Beissel, J. Geisler, S. T. Tietmeyer, S. Grätz, and L. Borchardt, "Polymer Vessels in Mechanochemical Syntheses: Assessing Material Performance," *RSC Mechanochemistry* 1 (2024): 386–392.

55. M. Biron, *Thermoplastics and Thermoplastic Composites: Technical Information for Plastics Users* (Elsevier Science, 2007).

56. F. Bedoui and B. Fayolle, *Polyoxymethylene Handbook* (2014), pp. 241–255.

57. J. S. DesVeaux and K. M. Knauer, "Harnessing Plastic Depolymerization Products to Upcycle Mixed Waste into High-Value Chemicals," *Chem* 11 (2025): 102485.

58. Cuminaldehyde is used commercially in perfumes and other cosmetics and listed in the European Commission database for information on cosmetic substances and ingredients (CosIng) : https://ec.europa.eu/growth/tools-databases/cosing/details/39410. For Cuminaldehyde: EC n° 204-516-9, (accessed May 25, 2025).

59. O. F. Jafter, S. Lee, J. Park, C. Cabanetos, and D. Lungerich, "Navigating Ball Mill Specifications for Theory-to-Practice Reproducibility in Mechanochemistry," *Angewandte Chemie International Edition* 63 (2024): e202409731. The online tool is available at: https://lungeric-hgroup.github.io (accessed May 28, 2025).

60. L. Vugrin, M. Carta, S. Lukin, E. Meštrović, F. Delogu, and I. Halasz, "Mechanochemical Reaction Kinetics Scales Linearly with Impact Energy," *Faraday Discussions* 241 (2023): 217–229.

1864564x, 2026, 9, Downloaded from https://chemistry-europe.onlinelibrary.wiley.com/doi/10.1002/cssc.202502491 by Andrea Casagrande - Université de Montpellier , Wiley Online Library on [22/06/2026]. See the Terms and Conditions (https://onlinelibrary.wiley.com/terms-and-conditions) on Wiley Online Library for rules of use; OA articles are governed by the applicable Creative Commons License

61. For Zirconia: https://www.azom.com/properties.aspx?ArticleID=133, For SS: https://www.engineeringtoolbox.com/stainless-steel-specific-heat-thermal-conductivity-vs-temperature-d_2225.html (accessed May 28, 2025).

62. R. Schmidt, C. F. Burmeister, M. Baláž, A. Kwade, and A. Stolle, "Effect of Reaction Parameters on the Synthesis of 5-Arylidene Barbituric Acid Derivatives in Ball Mills," *Organic Process Research & Development* 19 (2015): 427–436.

63. A. Stolle, R. Schmidt, and K. Jacob, "Scale-up of Organic Reactions in Ball Mills: Process Intensification with Regard to Energy Efficiency and Economy of Scale," *Faraday Discussions* 170 (2014): 267–286.

64. M. Shimizu, I. Shibuya, Y. Taguchi, S. Hamakawa, K. Suzuki, and T. Hayakawa, "Oxidation of Sulfides to Sulfoxides with 3-Aryl-2-Tert-Butyloxaziridines under High Pressure," *Journal of the Chemical Society, Perkin Transactions* 1 (1997): 3491–3492.

65. *Polymorphism in the Pharmaceutical Industry: Solid Form and Drug Development*, edited by R. Hilfiker, (Wiley-VCH, 2006), pp. 2211–2234.

66. D.-K. Bucar, R. W. Lancaster, and J. Bernstein, "Disappearing Polymorphs Revisited," *Angewandte Chemie International Edition* 54 (2015): 6972–6993.

67. S. O. Baumann, M. Bendova, M. Puchberger, and U. Schubert, "Modification of Titanium Isopropoxide with Aromatic Aldoximes," *European Journal of Inorganic Chemistry* 2011 (2011): 573–580.

68. European Chemicals Agency Substances resticted under REACH, https://echa.europa.eu/substances-restricted-under-reach (accessed May 2, 2025).

69. United States Environmental Protection Agency, https://www.epa.gov/assessing-and-managing-chemicals-under-tsca/risk-management-methylene-chloride, (accessed May 2, 2025).

70. For an overview of the advantages of mechanochemistry vs solution-based methods, please refer to Figure 3 in reference 9.

71. O. Galant, G. Cerfeda, A. S. McCalmont, et al., "Mechanochemistry Can Reduce Life Cycle Environmental Impacts of Manufacturing Active Pharmaceutical Ingredients," *ACS Sustainable Chemistry & Engineering* 10 (2022): 1430–1439.

72. R. A. Sheldon, "The E factor: Fifteen Years on," *Green Chemistry : An International Journal and Green Chemistry Resource* 9 (2007): 1273–1283.

73. B. Trost, "The Atom Economy—A Search for Synthetic Efficiency," *Science* 254 (1991): 1471–1477.

74. W. Wang, J. Lü, L. Zhang, and Z. Li, "Real Atom Economy and Its Application for Evaluation the Green Degree of a Process," *Frontiers of Chemical Science and Engineering* 5 (2011): 349–354.

75. R. A. Sheldon, W. C. E. Arends, and U. Hanenfeld, *Green Chemistry and Catalysis* (Wiley, 2007) pp.1–47.

76. P. T. Anastas and J. C. Warner, *Green Chemistry: Theory and Practice* (Oxford University Press, 2000).

77. I. R. Speight, K. J. Ardila-Fierro, J. G. Hernández, et al., "Ball Milling for Mechanochemical Reactions," *Nature Reviews Methods Primers* 5 (2025): 29.

78. L. W. Boyle, M. J. Peagram, and G. H. Whitham, "The Relative Reactivities of 'normal' and Angle Strained Cyclo-Olefins in 1,3-Dipolar Cycloaddition Reactions. Rotational Barriers in Nitrones," *Journal of the Chemical Society B: Physical Organic* (1971): 1728–1733.

79. Perillartine is a molecule of commercial relevance. Recent market analyses show that the global perillartine market was valued at USD 145.8 million in 2024 and is projected to reach USD 287.6 million by 2033, growing at a 7.8% CAGR (Compound Annual Growth rate). For more details, please see: Perillartine Market Size, Growth & Forecast Report 2033. https://datahorizzonresearch.com/perillartine-market-55259 (accessed September 15, 2025). The food and beverage sector accounts for the largest share of demand, while the pharmaceutical segment is the fastest growing due to the compound's antioxidant, antimicrobial, and anti-inflammatory activities. The cosmetics and personal care industry also increasingly incorporates perillartine in anti-aging and skin-protective products.

80. The global perillaldehyde market is estimated at USD 104.6 million in 2025, projected to reach USD 153.4 million by 2035 (CAGR ≈ 3.9%). For more details, please see: Perillaldehyde Market - Global Market Analysis Report 2035, (accessed September 15, 2025).

81. X.-Y. Yuan, M. Z., and S. W. Ng, "Perillartine," *Acta Crystallographica* E65 (2009): o2149.

82. For more information on COST Action CA18112 'Mechanochemistry for Sustainable Industry' (MechSustInd), https://www.mechsustind.eu/ (accessed April 6, 2026).

83. J. Biela, M. Stalla, L. Rabe, D. Machado, G. Evers, and S. Ansems, *Impact Assessment Study on Innovation in COST Actions* (November 2024) - https://www.cost.eu/uploads/2025/01/COST-Impact-Assessment-Innovation-112024.pdf (accessed March 2, 2025).

84. J. G. Hernández, I. Halasz, D. E. Crawford, et al., "European Research in Focus: Mechanochemistry for Sustainable Industry (COST Action MechSustInd)" *European Journal of Organic Chemistry* 2020 (2020): 8–9.

85. COST Annual Report 2025, "Success stories" 20–21; https://www.cost.eu/uploads/2026/03/COST-Annual-Report-2025.pdf.

86. COST, European Cooperation in Science and Technology, https://www.cost.eu/ (accessed May 2, 2025).

87. IMPACTIVE: Innovative Mechanochemical Processes to synthesize green ACTIVE pharmaceutical ingredients, https://mechanochemistry.eu/, (accessed April 10, 2026).

88. J. Sáenz de la Torre, L. Flamarique, F. Gomollon-Bel, and E. Colacino, "Mechanochemistry in Europe: Where We Come from and Where We are Now," *Open Research Europe* 5 (2025): 73.

Supporting Information

Additional supporting information can be found online in the Supporting Information section. The authors have cited additional references within the Supporting Information [81]. The data supporting this article, including ^{1}H and ^{13}C NMR, FT-IR (ATR) spectra for compounds (**1**) and (**2**), excel spreadsheets for green chemistry metrics calculations by Chem21, DOZN tools and EcoScale data input are available as part of Supplementaty Information.

1864564x, 2026, 9, Downloaded from https://chemistry-europe.onlinelibrary.wiley.com/doi/10.1002/cssc.202502491 by Andrea Casagrande - Université de Montpellier , Wiley Online Library on [22/06/2026]. See the Terms and Conditions (https://onlinelibrary.wiley.com/terms-and-conditions) on Wiley Online Library for rules of use; OA articles are governed by the applicable Creative Commons License

Appendix 3

Publication III

M. Patrascu, D. Meuti, O. Galant, S. Nijem, C. E. Diesendruck, A. Casagrande, E. Colacino, M. Felderhoff, S. Spatari. Sustainable pharmaceutical manufacturing based on mechanochemistry: A life cycle assessment of rac-Ibuprofen–Nicotinamide cocrystallization routes. *Sustainable Chemistry and Pharmacy*, **2026**, *51*, 102422.

Reproduced by permission of Elsevier.

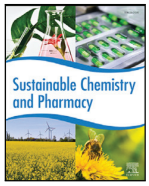
Sustainable Chemistry and Pharmacy 51 (2026) 102422



Contents lists available at ScienceDirect

Sustainable Chemistry and Pharmacy

journal homepage: www.elsevier.com/locate/scp



Sustainable pharmaceutical manufacturing based on mechanochemistry: A life cycle assessment of *rac*-Ibuprofen-Nicotinamide cocrystallization routes

Michael Patrascu [a,b,c,*], Damiana Meuti [a], Or Galant [d], Sally Nijem [e], Charles E. Diesendruck [e,c], Andrea Casagrande [f,h], Evelina Colacino [f], Michael Felderhoff [g], Sabrina Spatari [d,b,c]

[a] *Technion Israel Institute of Technology, Faculty of Chemical Engineering, Haifa 3200003, Israel*
[b] *Technion Israel Institute of Technology, Grand Technion Energy Program, Haifa 3200003, Israel*
[c] *Technion Israel Institute of Technology, The Resnick Sustainability Center for Catalysis, Haifa 3200003, Israel*
[d] *Technion Israel Institute of Technology, Faculty of Civil and Environmental Engineering, Haifa, Israel*
[e] *Technion Israel Institute of Technology, Schulich Faculty of Chemistry, Haifa, Israel*
[f] *ICGM, Univ. Montpellier, CNRS, ENSCM, 34293 Montpellier, France*
[g] *Department of Heterogeneous Catalysis, Max-Planck-Institut fur Kohlenforschung, Kaiser-Wilhelm-Platz 1, 45470 Mulheim an der Ruhr, Germany*
[h] *Virumaa College, Tallinn's University of Technology, Ehitajate tee 5, 19086, Tallinn, Estonia*

ARTICLE INFO

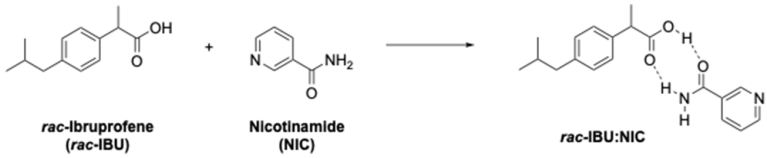
Keywords:
Mechanochemistry
Ball milling
Active pharmaceutical ingredients
Life cycle assessment
Green chemistry

ABSTRACT

Mechanochemistry is emerging as a sustainable alternative to solvent-based synthesis, yet its environmental and process-scale performance for pharmaceutical applications remains underexplored. This work assesses the environmental sustainability and process efficiency of mechanochemical versus conventional solution-based routes for producing *rac*-ibuprofen–nicotinamide (*rac*-IBU:NIC) co-crystals, a model pharmaceutical solid form. Experimental data from kilogram-scale eccentric vibrating milling (EVM), attritor mill (AM) and hammer mill (HM) were integrated with process modeling, green chemistry metrics, and cradle-to-gate life cycle assessment (LCA). Mechanochemical performance in batch (EVM, AM and HM) and continuous configurations (hot melt extrusion, HME) was benchmarked against an ethanol-based crystallization process representative of current industrial practice. Green metrics results confirmed that all mechanochemical routes achieved lowest aggregate scores, outperforming the solvent-batch process, demonstrating superior greenness due to solvent elimination, high atom economy, and ambient operation. LCA results, however, indicated higher global warming and fossil resource impacts for some mechanochemical systems compared to the solvent-batch process under fossil-based electricity, reflecting their reliance on electrical power. Scenario analyses revealed that renewable electricity dramatically lowers these impacts, reducing the global warming potential of EVM by more than 90 % and rendering both EVM and HME environmentally competitive with the solvent-batch process, even when considering a green solvent such as bio-ethanol. Mechanochemistry not only eliminates solvent use but also aligns with the global transition to renewable energy, since its impacts scale directly with the cleanliness of the electricity supply, positioning it as a viable pathway toward greener pharmaceutical manufacturing.

* Corresponding author at: Technion Israel Institute of Technology, Faculty of Chemical Engineering, Haifa 3200003, Israel.
E-mail address: michael@technion.ac.il (M. Patrascu).

https://doi.org/10.1016/j.scp.2026.102422
Received 24 November 2025; Received in revised form 23 February 2026; Accepted 18 April 2026
Available online 27 April 2026
2352-5541/© 2026 Published by Elsevier B.V.



Scheme 1. Reaction to form *rac*-IBU:NIC co-crystal.

1. Introduction

One of the major challenges in the preparation of co-crystals in solution arises from the differing solubility of solid blends, making the targeting of specific polymorphs challenging. Mechanochemical methods can offer a solution to this issue, sometimes allowing access to co-crystals that would otherwise be unattainable via solution methods (Linberg et al., 2024; Hasa et al., 2016). Yet, despite the large number of literature examples and wide applicability, mechanochemical methods for co-crystal synthesis are primarily limited to small-scale laboratory preparation (Braga et al., 2013; Xiao et al., 2023). Exploring the scalability of co-crystal preparation without solvents reveals the full potential of mechanochemistry as a key enabling technology for sustainable industrial synthesis. The environmental impact of mechanochemical processes for preparing active pharmaceutical ingredients (APIs) was quantitatively assessed based on the Twelve Principles of Green Chemistry (Sharma et al., 2022) using DOZN™ toolkit (Kreuder et al., 2017). DOZN™ is a universal scoring tool, enabling the evaluation of any process irrespective of the activation technique, as long as detailed experimental and process parameters are defined. That study evaluated the potential to greatly reduce material inputs to API production, namely the direct elimination of solvents, and reduced need for excess reactants, which improve certain green chemistry metrics like process mass intensity and E-factor. Furthermore, life cycle assessment (LCA) has been used to understand the impact that mechanochemical and other novel processes can have on upstream supply chains for manufacturing specific APIs (Galant et al., 2022; Spatari et al., 2023; Hallamasek et al., 2024). Galant et al. demonstrated mechanochemistry's low environmental impact, including waste reduction and up to 85% reduction in greenhouse gas emissions, as well as a cost reduction estimated at 12% when predicted for scaling API manufacture (Galant et al., 2022). Applying LCA methods to mechanochemical processes is a burgeoning area of research with promise for attaining industrial scale-up. Recently it was used to evaluate the synthesis of organic chemicals through twin-screw extrusion, showing favorable life cycle environmental metrics (Galant et al., 2023) as well as processing of inorganic chemicals used for battery manufacture (Arfelis et al., 2023).

The co-crystal of racemic ibuprofen (*rac*-IBU), a widely used nonsteroidal anti-inflammatory drug, with water-soluble nicotinamide (NIC) serves as a well-known example in the pharmaceutical industry for enhancing the dissolution and absorption of active pharmaceutical ingredients (APIs), thereby accelerating the onset of therapeutic action. The co-crystallization reaction is depicted in Scheme 1. While the industrial production of this co-crystal typically relies on solution-based methods, various alternative techniques have been explored. These include batch processes such as manual grinding with a mortar and pestle, ball milling under neat (Fischer et al., 2016; Guerain et al., 2020; Skorupska et al., 2017) or liquid-assisted conditions (Friščić and Jones, 2009), and continuous methods like twin-screw extrusion (TSE) (Kelly et al., 2012) and hot melt extrusion (HME) (Karimi-Jafari et al., 2019, 2021; Dhumal et al., 2010).

Notably, mechanochemical co-crystallization via extrusion has achieved production rates between 0.025 and 0.2 kg/h, with optimal results observed at 90 °C and screw speeds of 20–50 rpm (Madanayake et al., 2023). However, batch mechanochemical approaches remain limited to laboratory-scale yields, typically producing up to 1.0 g of *rac*-IBU:NIC cocrystals after 40 min of grinding at 50 Hz using stainless steel media (Fischer et al., 2016).

More recently, the use of industrial eccentric vibrating mill to prepare kilogram-scale of *rac*-IBU:NIC cocrystals was demonstrated (Bodach et al., 2024), as well as using a drum mill (Schöbel et al., 2025) and attritor mill (Triller et al., 2025). Therefore, despite the growing interest in continuous flow operations (Galant et al., 2021), the vast majority of fine chemical, pharmaceutical and biopharmaceutical industries operate in batch, not only for synthesis but also on the formulation side (e.g., for powder mixing, granulation, coating etc.). The development of large-scale batch mode mechanochemical processes is still an appealing alternative to continuous flow mechanochemistry. Moreover, a major challenge in the production of co-crystals of APIs is the transfer of processes in the gram-scale from laboratory preparations to the kg-scale for commercial production.

Over the last two decades, a growing number of studies have turned to life cycle assessment (LCA) as a method to evaluate the environmental impacts of manufacturing active (Tao et al., 2023; Davies et al., 2024; Ma et al., 2025) and excipient (Riazi et al., 2019; Wang et al., 2021) pharmaceutical ingredients. Most of these studies focused on the cradle-to-gate manufacture of the API following industrial solvent-batch processing routes to benchmark multiple APIs, while other studies evaluated possible economic and environmental benefits of process intensification and continuous flow technologies (Galant et al., 2022; Ott et al., 2014; Yaseneva et al., 2016; Grimaldi et al., 2021). Recent studies have combined LCA methods with evaluation using green chemistry metrics as screening tools to compare emerging green chemicals manufacturing approaches to conventional alternatives (Maga et al., 2024; Blömer et al., 2024). The cradle-to-gate greenhouse gas (GHG) emissions intensity for numerous APIs varies significantly, ranging from 10 to over 1000 kg CO_2 eq. per kg (Wernet et al., 2010; Lee et al., 2016; Parvatker et al., 2019). Moreover, studies have concluded that API production is complex and can require more that 200 inputs just within the gate-to-gate production (Jiménez-González and Overcash, 2014).

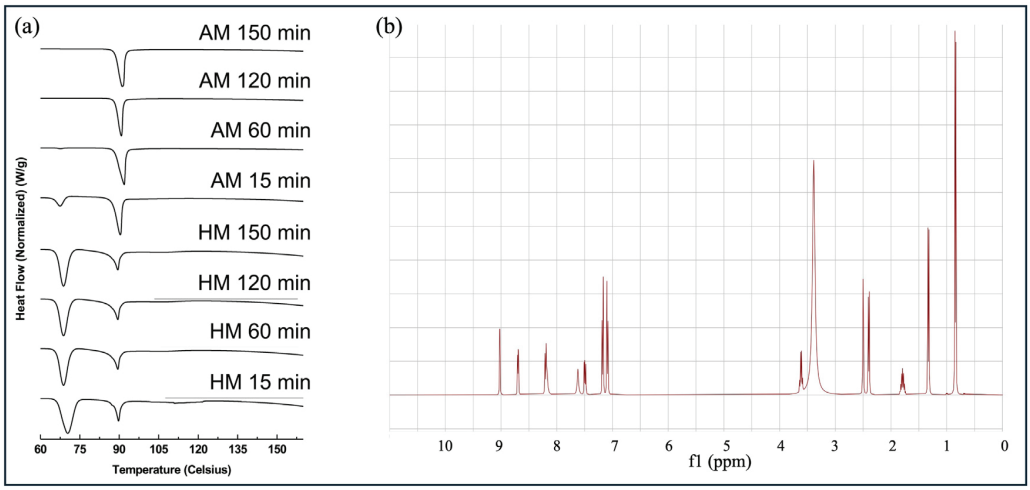


Fig. 1. Characterization of the AM/HM product: (a) Differential scanning calorimetry (DSC) following the *rac*-IBU:NIC co-crystal formation in AM and HM. Reactant and product are both crystalline showing clear and different melting points. Exotherm at 72 °C represents a raw material, and at 90 °C the co-crystal. (b) ^{1}H-NMR (400 Mhz, DMSO-d6) of *rac*-IBU:NIC co-crystal after 120 min of milling in AM. No organic impurities are seen.

A complete cradle-to-gate evaluation of *rac*-IBU:NIC requires life cycle inventory data for production of the API (*rac*-IBU) and nicotinamide. Siegert et al. (2020) evaluated the cradle-to-grave processes involved in *rac*-IBU production and consumption, including metabolism and by-product release into municipal wastewater treatment processes, as well as the packaging materials and their post-use impacts. The work tracked environmental impacts from cradle-to-gate processes and described the downstream processes following consumption of *rac*-IBU tablets used by individuals for treatment. The authors report a cradle-to-gate GHG intensity of 27 kg CO_2 eq. per kg *rac*-IBU. Wang et al. examined the life cycle impacts of two alternative *rac*-IBU tablet formulations and include the processing steps, wet granulation, fluid bed drying, and tablet compaction (Wang et al., 2021). Their work compared the impacts of alternative excipient formulations used in the *rac*-IBU tablet while maintaining the same quantity and production route for the API itself. Grimaldi et al. (2021) examined efficiency gains over the production cycle of *rac*-IBU when using enzymatic catalysts in continuous flow production.

Industrial-scale LCA benchmarks for nicotinamide have not been previously reported to the best of our knowledge. In this work, our objective is to compare the environmental impact of mechanochemical and solvent processes, which use green solvents, in the formation of *rac*-IBU-NIC co-crystal production, by green chemistry metrics and LCA methods. We analyze various types of ball-mills, HME and solvent-batch processes assuming identical production of *rac*-IBU and nicotinamide (Vitamin B3) feedstocks for the formulation of the co-crystal *rac*-IBU:NIC.

2. Methods

2.1. Experimental

In this work we use data from recent experiments conducted using state-of-the-art batch mechanochemical equipment to produce the *rac*-IBU:NIC co-crystals, as detailed below.

2.1.1. Eccentric vibrating mills (EVM)

Detailed experimental procedure has been described previously (Bodach et al., 2024). The mechanochemical synthesis of *rac*-IBU:NIC cocrystals was performed using industrial eccentric vibratory mills. These devices, commonly employed in mineral and metallurgical processing, generate combined elliptical, circular, and linear oscillations, resulting in enhanced media acceleration and efficient energy transfer. Equimolar mixtures of *rac*-IBU and nicotinamide were processed in two mills with identical vibration amplitudes (horizontal 11–12 mm, vertical 7–8 mm), differing only in vessel material; stainless steel or alumina. Total powder inputs were 2.8 kg and 1.4 kg for the respective vessels. Each batch was milled for 150 min at ambient temperature, with samples withdrawn at 15, 60, 120, and 150 min for ex situ PXRD and DSC analysis. Complete conversion to the *rac*-IBU:NIC cocrystal was achieved, affording isolated yields of 2.63 kg (stainless steel) and 1.14 kg (Al_2O_3). No additional crystalline or amorphous phases were detected. The process proceeded quantitatively without liquid additives or external heating, demonstrating efficient solvent-free co-crystallization at kilogram scale.

2.1.2. Attritor mill (AM)

Nicotinamide (55.4 g, 1 eq.) was grinded with *rac*-Ibuprofen (94.6 g, 1 eq.) using attritor mill (Netzsch model PE 075) equipped with 0.5 L Teflon jar and 600 g of 1 mm zirconia balls. The mixture was milled for 150 min at 1400 rpm. Samples were collected after 15, 60, 120 and 150 mins and characterized via XRD (see the SI) and differential scanning calorimetry (DSC, Fig. 1(a)) without any purification, indicating the ideal milling time is 70 min. This was assumed to be the milling time for the scaled-up calculations which follow. At the end of the procedure, the sticky solid was removed from the mill and the spheres were manually separated from the solid. To verify the chemical purity of the co-crystal, a sample from AM was dissolved in DMSO-d6 and analyzed by 1H-NMR. As observed in Fig. 1(b), the NMR shows only peaks of the 2 chemical components — *rac*-IBU and nicotinamide. There are no additional peaks of any chemical by-products.

2.1.3. Hammer mill (HM)

Nicotinamide (812.6 g, 1 eq.) was grinded with *rac*-IBU (1387.4 g, 1 eq.) using electrical double disk hammer mill (MX-6) equipped with 12.0 L alumina jar. The mixture was milled for 150 mins at 140 rpm. Samples were collected after 15, 60, 120 and 150 mins and characterized via XRD (see the SI) and DSC Fig. 1 without any purification. At the end of the procedure, the material was a flowing solid and was simply poured from the reactor into a large beaker. The product was obtained with 74% yield. Due to the poor yield obtained even after 150 min we did not include this process in the following environmental impacts assessment.

2.2. Green chemistry metrics

Mechanochemistry is closely aligned with the 12 principles of green chemistry (Anastas and Warner, 2000; Colacino et al., 2021), although these principles serve only as a conceptual guideline rather than a quantitative evaluation framework. Various methods are currently used to assess the greenness of a process, and several green chemistry metrics were calculated for an objective evaluation of the environmental profile of mechanochemical methods (in batch and in continuous) (Fantozzi et al., 2023), in comparison with the solution-batch counterparts. Among them, the DOZN™ toolkit (Kreuder et al., 2017; Sharma et al., 2022) measures quantitatively the compliance with the 12 principles of green chemistry. Not only does it assign a score to each of them, it also categorizes them into 3 groups: Group 1 (G1), encompassing principles 1, 2, 7, 8, 9, and 11, which focus on resource optimization; Group 2 (G2), consisting solely of principle 6, which evaluates the energy efficiency of the process; and Group 3 (G3), which includes principles 3, 4, 5, 10, and 12, assessing reductions in human and environmental hazards.

The individual greenness scores for each principle are compiled into a normalized value, termed aggregate score, which quantifies the overall greenness of a process on a scale from 0 to 100: the process is considered green when the aggregate score is equal to or below 1, with zero being the most desirable value.

2.3. LCA

2.3.1. Goal and scope definition

The environmental performance of *rac*-IBU:NIC co-crystallization by mechanochemical and solvent-batch methods was evaluated using life cycle assessment (LCA) according to ISO 14040/44 standards (International Organization for Standardization, 2006a,b). A cradle-to-gate system boundary was defined, Fig. 2, encompassing upstream raw material and energy supply chains as well as gate-to-gate co-crystallization operations—mixing, heating, cooling, filtration, drying, and product recovery. We assume production in Central Europe with background data on input electricity, thermal energy and solvent where needed as supplied in today's market.Equipment construction and facility infrastructure were excluded, as their contribution per functional unit is deemed negligible and differences among the alternatives studied are also likely small. Overall, the partial contribution of the co-crystallization step is small compared to the impact of the *rac*-IBU reactant production process, which we have estimated to be ca. 16.8 kg CO_2 eq. (per 1 kg of co-crystal product) based on cradle-to-gate LCA findings by Siegert et al. (2020). Thus, in this study we show the differences between the various production processes for the co-crystallization step only.

The functional unit was 1 kg of isolated *rac*-IBU:NIC co-crystals. Feedstocks (0.63 kg *rac*-IBU, 0.37 kg nicotinamide) were assumed identical for all routes; therefore, upstream API production was excluded. Material and energy inventories were derived from process data (Table 1) and scaled using the methodology of Piccinno et al. (2016). LCI data for materials and energy were obtained from the ecoinvent v3.11 database (Wernet et al., 2010) (attributional, allocation at point of substitution model) within SimaPro 10.3, with the EU-27 electricity mix, which reflects the fuel mix for electricity production until end of 2024.

Solvent-batch data were developed from a published patent (Yin et al., 2013), assuming 90% ethanol recycling and 10% solvent losses (Geisler et al., 2004). For mechanochemical processes, electrical energy inputs were estimated from rated power and operational time, giving conservative upper bounds. Scenario analyses assessed renewable energy (wind/PV and hydro-based electricity) and bioethanol substitution. No co-products were generated.

The LCA thus isolates and compares the cradle-to-gate crystallization stage across process routes, clarifying how mechanochemistry's sustainability depends on the decarbonization of electricity supply systems.

2.3.2. Life cycle inventory

Life cycle inventory models were developed for the five mechanochemical processes and solvent-batch benchmark for producing *rac*-IBU:NIC co-crystals. Process engineering calculations were used to develop the LCI of each alternative following methods described by Piccinno et al. (2016). The cradle-to-gate LCI data and model equations for each alternative are summarized in the Supporting Information and elaborated upon herein.

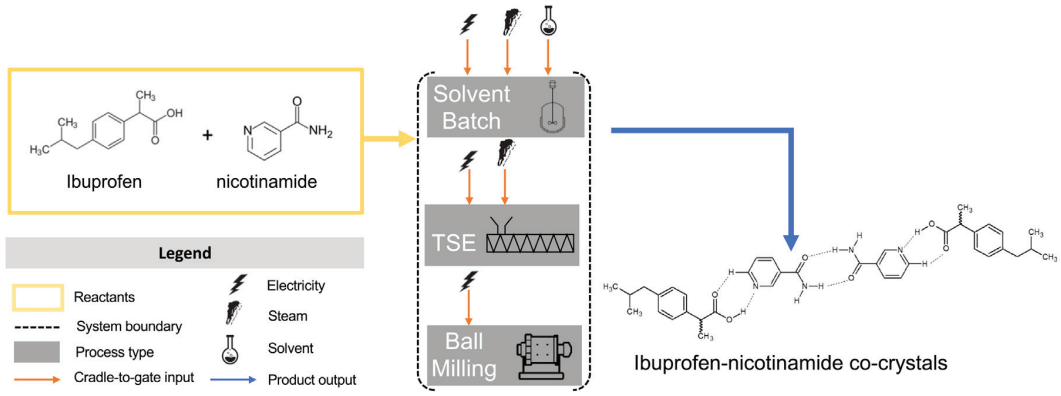


Fig. 2. System boundaries for the 'cradle-to-gate' production of *rac*-IBU:NIC co-crystals by classical solvent-batch processes, HME and ball milling.

Table 1
Milling in batch data obtained empirically in this study.

Mill type	Mass input [kg]	Mass output [kg]	Yield [%]	Time to reach yield [min]	Energy consumption [kWh]	Specific energy input [kWh/kg]	Internal volume [L]
EVM steel (Bodach et al., 2024)	2.80	2.80	100	70	3.5	1.25	19.0
EVM alumina (Bodach et al., 2024)	1.40	1.40	100	150	2.75	1.96	11.0
AM	0.15	0.15	100	70	0.6	4	0.5
HM	2.2	2.2	74	150	7.5	3.4	12

2.3.3. *Mechanochemical synthesis in batch*

The empirical data presented in Table 1 were used for the scaled-up calculations and LCA. Power consumption, which is the one most significant LCI item, has been conservatively taken as the maximum equipment power rating. From Table 1 it is clear that EVM with steel vessel is the most energy efficient batch mechanochemical process with specific energy of only 1.25 kWh/kg. The LCI data is given in Table S11. Note that due to the poor yield obtained in HM even after 150 min we did not include this process in the environmental impacts assessment.

2.3.4. *HME*

The material and energy balances data for the 'gate-to-gate' production of *rac*-IBU:NIC co-crystals through HME were calculated from a patent (Maniruzzaman et al., 2022), allowing construction of a scaled-up chemical process simulation model based on ThermoFisher twin-screw extruder equipment (Swanborough, 2025). The lab scale extruder operates 8 barrels performing the following steps: *rac*-IBU and nicotinamide are put into a twin-screw feeder (Leistritz ZSE 12 HP-PH 12 mm) at room temperature (barrel 1) at a feed rate of 6 g/min. Then, the reactants are conveyed (barrel 2) to the first mixing zones (barrels 3–4) to assure the thorough mixing of the two ingredients. In the second mixing zone (barrel 5) the temperature is set to 80 °C, melting one or both ingredients and reach molecular level. Then, the melt is conveyed to barrel 6 to vent any accumulated moisture out of the barrel. Finally, barrels 7 and 8 are used to cool down the extrudates close to ambient temperature, inducing crystallization, and convey materials out of the barrel. Detailed data, assumptions and calculations can be found in Section 1 of the SI, Tables S1–S3. Figure S1 shows a schematic of the process. To produce 1 kg *rac*-IBP:NCT co-crystals, the required energy for mixing/conveying is 28 MJ, whereas the heating zone (barrel 5) requires additional 0.16 MJ of energy, both of which are supplied from electricity.

2.3.5. *Solvent batch*

Material and energy balances for the solvent-batch process were calculated based on a patent (Yin et al., 2013). The energy requirements for each unit operation were assessed by chemical process scale-up approximations developed by Piccinno et al. (2016). Specific assumptions on the system boundary and LCI are summarized in Section 2 of the SI, Tables S4–S9. A detailed process flow diagram is given in Fig. 3. Detailed data, assumptions and calculations can be found in Section 2 of the SI, Tables S4–S10. Solvent recycling is considered after product filtration and drying, assuming a 10% solvent loss (Geisler et al., 2004). The feed to the system is composed of 628.1 g of *rac*-IBU and 371.9 g of nicotinamide (1:1 molar ratio) which are dissolved in an ethanol–water mixture solvent (5:1 v/v). The yield per-pass of the eutectic product is assumed to be 56% based on the reported patent (Yin et al., 2013). Unreacted reactants are recycled together with 80% of the solvent such that the total reactants mass in the reactor is 1122.2 g of *rac*-IBU and 664.6 g of nicotinamide. 10% of the reactor solvent is further recycled after drying and condensation. The batch

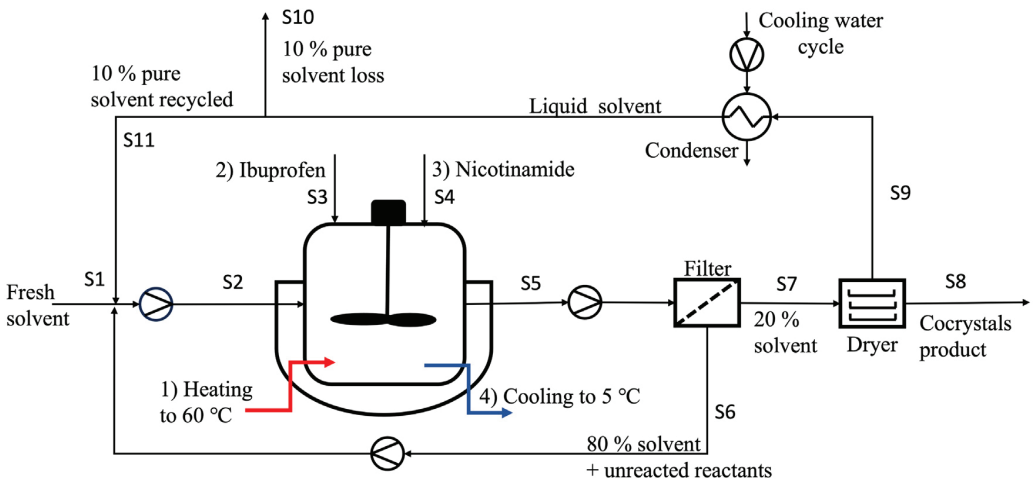


Fig. 3. Process flow diagram of the simulated solvent-batch process.

crystallization is conducted as follows: After dissolving completely under stirring at 60 °C, the solution is cooled at a rate of 8 °C/h. At 20 °C, grains begin to appear. Then, the temperature is reduced to 5 °C and crystals are grown for 1 h. The crystal slurry is then filtered and dried at 20 °C for 8 h to obtain 1000 g of white crystalline *rac*-IBU:NIC co-crystals.

2.3.6. Life cycle impact assessment

We use the ReCiPe 2016 Midpoint (Hierarchist) V1.11 life cycle impact assessment (LCIA) method (Huijbregts et al., 2017) to compare the life cycle environmental impacts of global warming, fossil resource scarcity, human carcinogenic and non-carcinogenic toxicity, terrestrial eco-toxicity and marine eco-toxicity for the different alternative production processes of *rac*-IBU:NIC co-crystals. This midpoint LCIA method has been used to evaluate emerging mechanochemical processes for producing API by TSE (Galant et al., 2022) and benchmark them with conventional production routes. More generally, it has been used to benchmark emerging technology with conventional alternatives as in earlier work on water management (Wang et al., 2013), renewable energy sources for electricity (Billen et al., 2019), resource recovery in water treatment (Kar et al., 2023) and consumer products (Riazi et al., 2019). Summary of all LCIA can be found in the SI, Section 3, Tables S11–S16. Material flows and PMI indicator are given in Table S18.

2.3.7. Scenario analysis

To investigate environmental hotspots, uncertainties and opportunities for reducing the environmental impact of co-crystal production, we tested scenarios in which electricity inputs are sourced from renewable electricity sources and ethanol solvent is derived from bio-ethanol produced from Maize (corn) and cellulosic feedstocks. The renewable electricity source, taken from an average mix in Switzerland from the ecoinvent database, assumes the majority of power is supplied by sources available today; hydropower (94%); wind, solar and geothermal (2.5%); biomass (1.4%); and the remainder includes residual nuclear and fossil fuel sources and has a global warming intensity of 10.6 g CO_2 eq. per kWh. The renewable electricity mix contrasts with our baseline estimates, which assumes electricity is supplied from the average European electricity grid (EU 27). The European average electricity grid takes an average of supply to 27 European countries, with the majority of power sources coming from France and Germany (30%) based on the 2024 medium voltage EU grid mix data from ecoinvent 3.11. We further discuss the implications of greater sources of wind power on the margin as expected in IEA forecasts for 2030. Data for fermentative ethanol were taken from literature and consider a mixture of edible crops, including corn (Xu et al., 2022) and winter crops (Spatari et al., 2020) and cellulosic feedstocks (Pourhashem et al., 2013). The data on the global warming intensity of ethanol solvent are summarized in SI Table S17. Overall, this scenario analysis aims to understand the sensitivity of external inputs to the process, in particular the current energy transition, which can change supply of energy and chemical feedstocks, including solvents.

3. Results and discussion

3.1. Green chemistry metrics

The synthesis of *rac*-IBP:NIC crystals was tested at the kg scale (up to ca. 3 kg) in various types of milling devices, as detailed in Table 1. Herein, DOZN™ 3.0 was used to compare the greenness of mechanochemical preparation of *rac*-IBU:NIC cocrystal under different mechanochemical processes in batch, notably by eccentric vibration mill (Bodach et al., 2024) (EVM), attritor mill (AM)

Table 2
Comparative DOZN™ 3.0 scores for the mechanochemical preparation of *rac*-IBU:NIC in batch vs. in continuous (by HME), and against the solution-based counterpart[a,b].

Entry	Process	Grinding media	Temperature, °C/time, min	Input, kg/Output, kg	DOZN™ 3.0 Scores[c]			
					G1	G2	G3	Aggregate
1	EVM (Bodach et al., 2024)	Al_2O_3	r.t/150	1.4/1.4[d]	0.28	0.00	0.47	0.34
2	EVM (Bodach et al., 2024)	SS	r.t./70	2.8/2.8[e]	0.28	0.00	0.47	0.34
3	AM	PTFE (ZrO_2 balls)	r.t. d/70	0.15/0.15	0.28	0.00	0.72	0.44
4	HME (Maniruzzaman et al., 2022)	SS	80/120	0.72/0.72[f]	0.28	0.07	0.47	0.34
5	HME (Dhumal et al., 2010)	SS	90/120	0.1/0.1[g]	0.28	0.14	0.47	0.35
6	Solution (Yin et al., 2013)	n.a	60/360	1/1	1.07	2.7	1.76	1.50
7	Solution (Yin et al., 2013)	n.a	60/360	1/1	0.75	2.70	1.76	1.33

[a] Equimolar amount of *rac*-IBU and NIC were always processed. For the sake of comparison and normalization, the calculations are performed by assuming 100% mass recovery of the *rac*-IBU:NIC co-crystal.

[b] Legend: Batch processes (entries 1–3) by (EVM, AM) vs continuous processes (entries 4–5) by HME, and solution process (entries 7–8), n.a.: Not applicable, SS: Stainless steel, r.t.: Room temperature.

[c] G1: Improved resource use, G2: Increased energy efficiency, G3: Reduced human and environmental hazard.

[d] The real (but not optimized) recovery reported in the original work was 81% of total mass input (1.14 kg).

[e] The real (but not optimized) recovery reported in the original work was 94% of total mass input (2.64 kg).

[f] Equimolar amount of *rac*-IBU (0.452 kg) and NIC (0.268 kg) were processes at a feed rate of 6 g/min with a screw speed of 50 rpm.

[g] Equimolar amount of *rac*-IBU (0.063 kg) and NIC (0.037 kg) were processed at a feed rate of 0.05 kg/h with a screw speed of 30 rpm.

and hammer mill (HM), in continuous by hot melt extrusion (Dhumal et al., 2010; Maniruzzaman et al., 2022) (HME) and to compare them with the solution based process (Yin et al., 2013). The detailed calculations are available as a separate excel file, as integral part of the SI.

The processes in EVM and HME have been previously reported, while the ethanol solution process is ubiquitously used in the chemical industry. Similarly to our previous report on EVM, the co-crystallization was tested in AM and HM using stoichiometric quantities, filling the mills to their limit to obtain the maximal output. As seen in Table 2, the AM is quite efficient in this co-crystallization reaction, while the HM is not able to achieve full conversion even after 2.5 h.

Each of the mechanochemical processes displayed excellent aggregate scores, below 1, outperforming the solution-based method (Table 1, entries 1–5 vs entries 6-7). For G1 and G3, scores were practically identical, because they use the same reactants in equimolar amounts of raw materials (*rac*-IBU and NIC), with a slightly higher G3 value for AM (entry 3), which makes the corresponding aggregate score slightly higher than for the other mechanochemical processes. These scores serve to evaluate the quantity of waste generated, how severe their effects are, and the degree of associated hazards.

The difference among each mechanochemical process lies mainly in the reaction scale and product throughput, with favorable G1 scores when resources (raw materials) are used efficiently, especially when no by-products are formed. Indeed, the formation of *rac*-IBU:*rac*-IBU, and/or NIC:NIC dimers (Khansary et al., 2020), sometimes observed by HME due to external energy input such as heating, was never observed by processing the reactants in batch.

Score differences emerge primarily in Group 2 (energy efficiency). Batch mechanochemical milling processes received a score of zero because they operate entirely under ambient temperature and pressure conditions, incurring no temperature/pressure penalty in the DOZN 3.0 framework (entries 1–3). In contrast, HME required heating to achieve complete conversion of the raw materials into *rac*-IBU:NIC, which introduced energy penalties based on the temperature severity factors and reaction duration. This resulted in higher Group 2 scores for HME and a corresponding linear increase in aggregate DOZN scores with rising process temperature (entries 4–5).

Comparison to the solution-based counterpart (entries 6–7), mechanochemical processes highlight the benefits both in terms of throughput and processing. The overall worse performance of solution-batch chemistry in Groups 1 and 3 reflects the downside related not only to the use of solvents, for both the reaction and the recovery of the final product, but also a less efficient use of resources, due to a solvent loss (see Fig. 3 and increased waste. Group 2 score results were affected by the need to heat (at 60 °C) for prolonged time (3 h).

Interestingly, and compared to HME processes (entries 5 and 6), in which heating is done to higher temperatures (80 and 90 °C, respectively), reaction times for the continuous process were shorter, turning out to be more beneficial. Based on these considerations, and considering the scores (G1, G2, G3 and aggregate) for each process, mechanochemical methods remain more advantageous than the solution-based counterparts. The environmental impact of solution based processes can be partially mitigated if biobased resources are used. Indeed, for the classical batch process (entries 7 and 8), Group 1 score was reduced when ethanol was replaced by bio-ethanol (1.07 vs 0.75, respectively), with a mild improvement of the aggregate score (1.50 vs 1.33, respectively).

However, when comparing mechanochemical processes, the choice of the suitable technology should account not only the energetic considerations, which might be slightly more favorable for batch processing, but also for the ease of product recovery and the overall throughput per unit of time, parameters that are specific to each equipment. Therefore, a systematic technology and economic assessment should be conducted for each reaction explored, to identify the technology that suits best with the specific process under investigation.

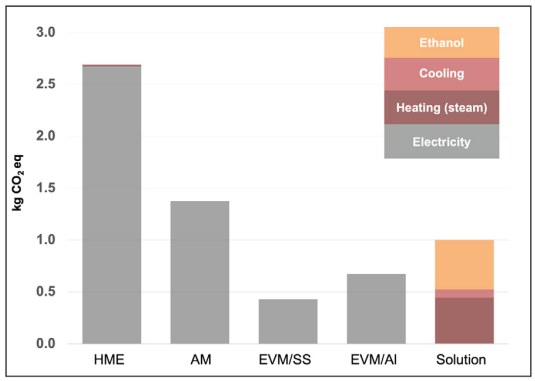


Fig. 4. Global warming impact of the various mechanochemical routes versus the solvent batch process using non-renewable electricity.

3.2. Life cycle assessment

Fig. 4 compares the global warming impact of the various co-crystallization processes under the base-case assumption of fossil-based energy. Among the mechanochemical routes, the eccentric vibrating mill with stainless steel media (EVM/SS) exhibits the lowest impact, owing to its relatively modest electricity demand—even under conservative assumptions of power input. In contrast, the HME process shows the highest burden, with a footprint about 3.5 times larger than that of the solvent-batch route. Interestingly, the traditional solution-batch process performs better than HME and AM. This advantage stems from the use of ethanol, a relatively benign solvent, combined with solvent recycling, which markedly reduces its net consumption compared to earlier studies (Galant et al., 2022, 2023). Overall, the results highlight a fundamental trade-off: mechanochemical approaches avoid the use of solvents but remain energy-intensive, making their performance highly dependent on electricity sources. Conversely, solution-based processing benefits from solvent recycling and the choice of a green solvent, enabling competitive environmental performance despite relying on solvent use. Nonetheless, the EVM/SS configuration achieves nearly a 50% reduction in global warming impact relative to the solvent-batch benchmark, which underscores the observation that specific mechanochemical designs can outperform conventional solution methods, even under the current energy supply scenario.

We evaluated the 18 midpoint impacts of all co-crystal production alternatives following the ReCiPe 2016 midpoint hierarchical method (Huijbregts et al., 2017; van Zelm et al., 2025). SI Figure S2 and Table S14 summarize results from the 18 impact categories, including global warming impact Fig. 4. Although global warming impact is lowest for the EVM/SS route compared to all mechanochemical and solvent-batch routes, this trend holds only for five impact categories (global warming, terrestrial ecotoxicity, ozone formation, fossil resource scarcity and mineral resource scarcity). Additionally, acidification potential and fine particulate matter formation are approximately on par for EVM/SS and the solvent-batch process. The HME, HM and AM mechanochemical routes have higher impacts compared to the solvent-batch route and EVM/Al varies depending upon the impact category. For the solvent-batch process, the major source of impact relates to both the ethanol solvent, assumed produced from ethylene (petroleum-derived) feedstock and heat from industrial steam, which also relies on fossil fuels. As noted above, electricity impacts dominate for all mechanochemical routes to co-crystal formation, where the electricity is assumed taken as the average European electricity grid from 27 member states, and includes power plants that combust fossil fuels (see SI Figure S4A), including 43% from fossil fuel resources, but 39% from nuclear and 8% from hydro-electric power, a mix that results in a net cradle-to-gate global warming impact 340 g CO_2 eq. per kWh from electricity input. These findings call for further analysis of renewable electricity for the mechanochemical system and renewable solvents for the solvent-batch system, which we explore in the scenario analysis, assuming electricity is sourced from onshore wind power.

3.2.1. Scenario analysis

Since the impact of the mechanochemical processes relies exclusively on the electric power supplied, a study of the impact of the source of energy is warranted. Whilst there is limited control over the environmental burden associated with solvent and reactants manufacturing, as it is not within the ‘gate-to-gate’ process, the energy associated with the ‘gate-to-gate’ process can be adjusted and optimized by different approaches (through energy recovery from other sources, such as incineration or renewable energy). The efficiency of energy recovery from other sources depends on the type of energy source and technology used. We have considered four alternative scenarios: (a) All energy forms are based on fossil fuels and today’s European Electricity grid (base-case, Fig. 4). (b) Electricity only is based on renewable mix of 80/20% wind and PV power. (c) All energy forms are electrified and based on renewable mix of 80/20% wind and PV power power. (d) Same as (c) on top of using ethanol produced by fermentation using renewable feedastocks. Fig. 5 shows the global warming impact for scenarios (b)–(d), while Fig. 6 and Fig. 7 show the fossil resource scarcity (FR) and human carcinogenic toxicity impacts, respectively, for scenarios (a) to (c). We exclude the option of incorporating

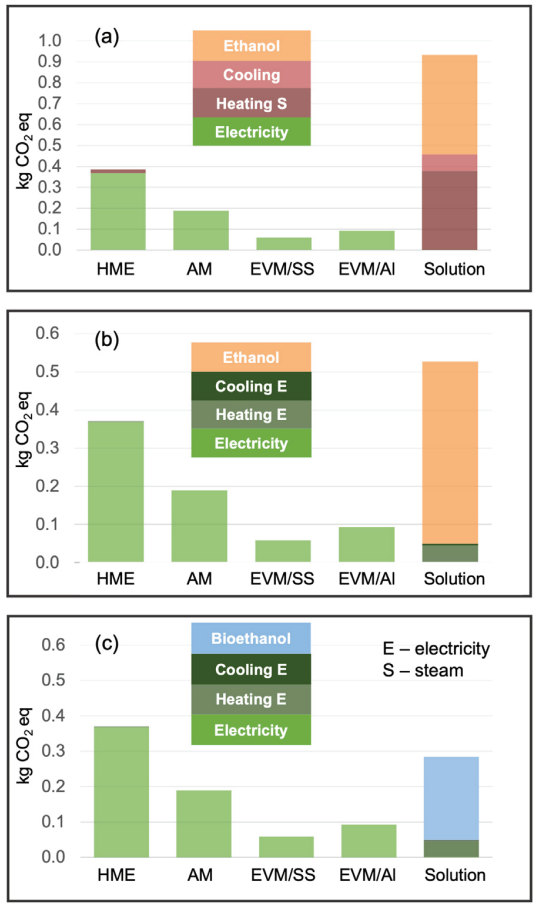


Fig. 5. Global warming potential in kg CO_2 eq. of the various mechanochemical routes versus the solvent-batch process. (a) Electricity from renewable resources (mix of 80/20% wind and PV power). (b) Electrification of all energy sources to renewable. (c) Electrification of all energy sources to renewable, and ethanol from renewable resources.

ethanol solvent from renewable (corn) feedstock, which is due both to the large fertilizer inputs for growing corn and their fossil-fuel intensity, and energy involved in conversion to ethanol (MacLean and Spatari, 2009; Wang et al., 2012). Although we exclude impacts estimate for use of ethanol derived from corn (except for the GW impact), we note that corn-derived ethanol remains fossil energy intensive due to fertilizer application and energy requirements during crop production as well as the energy needs for converting the feedstock to ethanol. Yet, when sourced from second generation feedstocks (lignocellulose), ethanol approaches also a near-zero energy intensity per kg solvent used (Wang et al., 2012). All impacts are reduced due to the transition of energy sources to renewable (from wind) in all examined processes. When transitioning to renewable energy source, solvent-batch can be less favorable due to solvent use, depending on the source of ethanol from renewable resources (bioethanol), see Fig. 5(c). Ethanol derived from first generation crops such as corn or barley can reach negative GWI depending on whether combined with advanced feedstocks and carbon capture and storage (Xu et al., 2022; Spatari et al., 2020). Moreover, emerging second generation ethanol technologies that use agricultural residues or dedicated energy crops can arrive at very low GWI (−2 to −25 g CO_2 eq. per kg ethanol) depending on co-products and land management (Pourhashem et al., 2013; Yang et al., 2020) and very negative GWI (−52 to −4800 g CO_2 eq. per kg ethanol) depending on whether using perennial grass feedstocks, the co-products involved and whether including carbon capture and storage (Gelfand et al., 2020; Lask et al., 2021).

EVM has lower global warming (Fig. 4) and fossil resource scarcity (Fig. 6(a)) impacts compared to the solution process even for the fossil based energy, the base-case, scenario a. However, other impacts are higher for EVM (and all other mechanochemistry routes) compared to the solution process under this scenario, such as the human carcinogenic toxicity, Fig. 7(a).

Although renewable, wind/solar-based, electricity favors mechanochemistry routes compared to solvent-batch for many impacts (see Figs. 5(b) and 6(c)), some ReCiPe LCIA impacts are mixed. For example, human carcinogenic toxicity, Fig. 7(b), and terrestrial

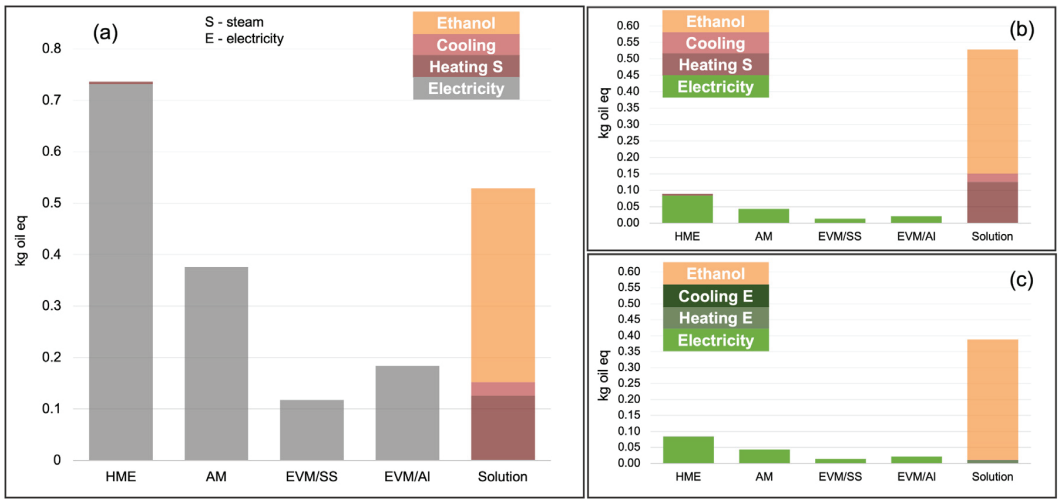


Fig. 6. Fossil resource scarcity of the various mechanochemical routes versus the solvent batch process for various scenarios: (a) Energy from fossil fuels. (b) Only electricity from renewable (mix of 80/20% wind and PV power). (c) Electrification of all energy sources to renewable (mix of 80/20% wind and PV power).

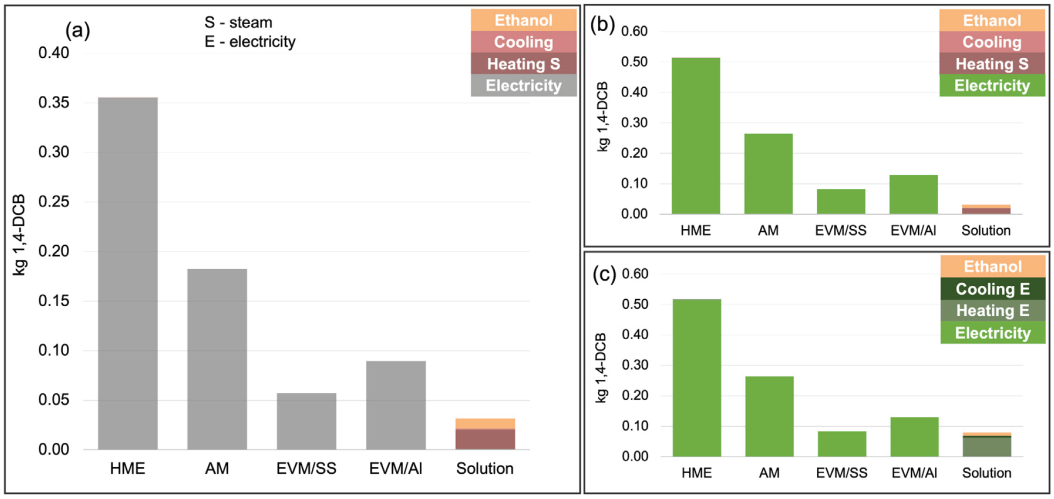


Fig. 7. Human carcinogenic toxicity of the various mechanochemical routes versus the solvent-batch process. (a) Energy from fossil fuels. (b) Only electricity from renewable (mix of 80/20% wind and PV power). (c) Electrification of all energy sources to renewable (mix of 80/20% wind and PV power).

ecotoxicity (See SI Figure S3 and Table S15) are higher for all mechanochemical routes, except EVM/SS, as compared with solvent-batch production. Accompanied by significant reductions to climate change impacts by reducing global warming effects, some other impact categories follow different trends. Onshore wind occupies land and its life cycle maintenance and infrastructure imparts impacts (emissions to air, water and land) primarily related to the materials involved in the infrastructure. Earlier studies surveyed those impacts (Arvesen and Hertwich, 2012), noting that human toxicity impacts can range from 16–70 g 1–4 DCB eq. per kWh. This is still lower than the human toxicity impact from coal power plants, which can be three orders of magnitude higher than those of renewable power sources like solar photovoltaics (Billen et al., 2019). Yet, future electricity grids are likely to combine multiple renewable sources, including hydroelectric power, which is part of today's EU electricity grid (see SI Figure S4), as well as non-renewable sources like nuclear power, which reduce GHG emissions but also have other LCIA impacts.

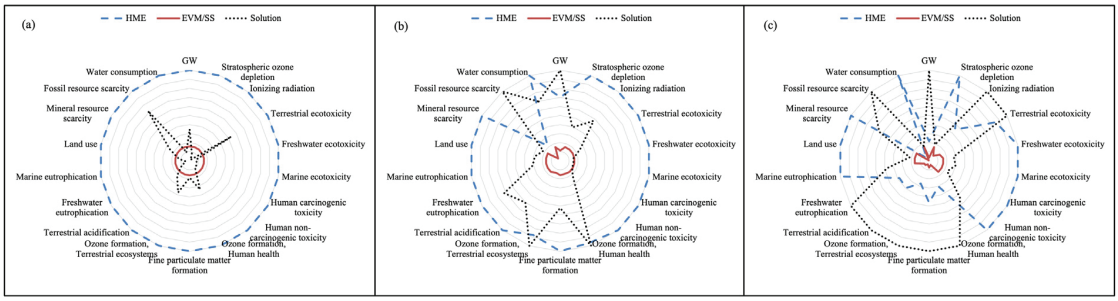


Fig. 8. Normalized relative impacts (maximum value is 1, minimum value is 0) for the batch (EVM/SS) and continuous (HME) mechanochemical routes vs. the traditional solvent-batch process for three scenarios: (a) The base-case. (b) Electrification of all energy sources to renewable (mix of 80/20% wind and PV power). (c) Electrification of all energy sources to renewable power based on Swiss mix (94% hydro).

To understand the range of environmental impacts for the mechanochemical processes and the solvent-batch system, we compare the processes that show upper and lower bound ReCiPe impact ranges – HME and EVM/SS – with the solvent-batch process. These processes also represent both continuous (HME) and batch (EVM) mechanochemistry methods. In Fig. 8 the relative impact for each category is depicted for three scenarios: (a) The base-case (b) Scenario c which is investigated above (electrification of energy sources based on mix of 80/20% wind and PV power) (c) Another renewable scenario where the power is based on the Swiss mix (94% hydro). ReCiPe 2016 impacts for the three electricity grids are presented in SI Figure S5.

When electricity is sourced from today's average EU grid, HME impacts are the highest, the EVM/SS impacts are lower (16% of the HME values for all impacts, due to the lower specific power consumption), whereas the solution (solvent-batch) process is favored for most impacts. Nonetheless, for seven impact categories (global warming, terrestrial ecotoxicity, ozone formation, fossil resource scarcity, fine particulate matter formation, terrestrial acidification, and mineral resource scarcity) the EVM/SS has the lowest impact even for the base-case.

When moving to an all renewable-supplied electricity grid of 80/20% mix of wind and PV respectively, Fig. 8(b), the EVM/SS system has consistently the lowest impacts among the three alternatives, exemplifying the superiority of this method. The solvent-batch process, however, outperforms HME for 13 impact categories even under the renewable power scenario. It is interesting to examine the impact of a different renewable mix. Assuming all electric power comes from the Swiss renewable mix (94% hydro) we study in impacts in Fig. 8(c). In this case even the HME outperforms solvent-batch in many more environmental categories (e.g. ionizing radiation, fine particulate matter formation etc.), including a significant relative reduction in global warming impact.

These findings demonstrate that mechanochemistry's environmental ranking is dynamically tied to energy-system decarbonization. In a renewable-dominated future, mechanochemical synthesis may become the unequivocally more sustainable choice, yet life cycle impacts aside from global warming will need to be addressed with that energy transition. Furthermore, process optimization when scaling this early-stage technology must aim to minimize electricity demand.

Beyond the influence of energy sourcing, process configuration and scalability also determine the overall potential of mechanochemical manufacturing. Comparing batch operation in the eccentric vibrating mill (EVM) with continuous processing by hot melt extrusion (HME) reveals complementary strengths and trade-offs. The EVM configuration offers operational simplicity, straightforward maintenance, and flexible batch scaling through modular parallelization, which fits well with existing batch-oriented pharmaceutical infrastructure. It operates at ambient temperature and pressure, eliminating heating requirements and resulting in lower specific energy demand per kilogram of product, as evidenced by the lowest life cycle impact among mechanochemical routes. However, the discontinuous nature of EVM limits throughput and may complicate integration with continuous downstream steps. Conversely, HME enables steady-state operation, in-line monitoring, and direct coupling with downstream formulation processes such as granulation or tableting. These advantages come at the cost of higher electrical and thermal energy input due to controlled heating and screw operation, increasing its cradle-to-gate impact when fossil electricity dominates. From an engineering and LCA perspective, the selection between batch and continuous mechanochemistry thus depends on production scale, product consistency needs, and available renewable energy infrastructure. In a decarbonized energy system, HME's process intensification potential could outweigh its current energy penalties, while EVM remains an efficient and robust choice under conventional power systems.

4. Conclusions

In this work, we compared the production of *rac*-IBU:NIC cocrystals via mechanochemical methods (ball milling in several configurations and hot-melt extrusion) against a conventional solvent-batch crystallization route. The evaluation combined green chemistry metrics (DOZN™ toolkit) with a rigorous life cycle assessment (LCA) under cradle-to-gate system boundaries. Experimental data from kilogram-scale mechanochemical trials were coupled with scaled process simulations to generate material and energy balances for each route.

The green metrics analysis showed that all mechanochemical approaches achieved superior aggregate scores compared to the solvent-batch method. The absence of solvents, high atom efficiency, and operation at ambient conditions (for batch mills) translated

into lower waste generation and improved resource use. Continuous hot-melt extrusion carried a penalty in the energy efficiency category, but still outperformed the solvent-based process overall.

In contrast, the LCA results revealed that mechanochemical processes can exhibit high global warming potential and fossil resource use depending on the specific mechanochemical route used when powered by fossil-based electricity, primarily due to their exclusive reliance on electric power. The solvent-batch route benefited from the relatively benign profile of ethanol as solvent and the possibility of solvent recycling. Nevertheless, scenario analyses demonstrated that when electricity is supplied from renewable sources, the environmental profile of mechanochemistry improves dramatically, surpassing the solvent-batch benchmark in all cases. This effect is structural; while the environmental burden of solvent-based processes is tied to solvent production regardless of energy decarbonization, mechanochemistry's footprint is directly proportional to the cleanliness of the electricity mix. Thus, mechanochemistry not only addresses issues of solvent use and process efficiency but also offers a pathway that is synergistic with the ongoing global transition toward renewable energy in chemical manufacturing.

CRediT authorship contribution statement

Michael Patrascu: Writing – review & editing, Writing – original draft, Visualization, Validation, Supervision, Resources, Methodology, Investigation, Formal analysis, Data curation, Conceptualization. **Damiana Meuti:** Writing – original draft, Visualization, Formal analysis, Data curation. **Or Galant:** Writing – original draft, Methodology, Investigation, Formal analysis, Data curation. **Sally Nijem:** Methodology, Data curation. **Charles E. Diesendruck:** Writing – review & editing, Supervision, Resources, Methodology, Investigation, Formal analysis, Data curation. **Andrea Casagrande:** Software, Formal analysis, Data curation. **Evelina Colacino:** Writing – review & editing, Supervision, Resources, Project administration, Methodology, Investigation, Funding acquisition, Data curation, Conceptualization. **Michael Felderhoff:** Data curation. **Sabrina Spatari:** Writing – review & editing, Writing – original draft, Validation, Supervision, Software, Resources, Methodology, Investigation, Formal analysis, Data curation, Conceptualization.

Declaration of competing interest

The authors declare that they have no known competing financial interests or personal relationships that could have appeared to influence the work reported in this paper.

Acknowledgments

This article is based upon work from COST Action CA18112 'Mechanochemistry for Sustainable Industry', supported by COST (European Cooperation in Science and Technology) (COST, 2025a; Biela et al., 2024; Hernández et al., 2020).

cost EUROPEAN COOPERATION IN SCIENCE & TECHNOLOGY

Funded by the European Union

COST (European Cooperation in Science and Technology) is a funding agency for research and innovation networks, helping to connect research initiatives across Europe and enable scientists to grow their ideas by sharing them with their peers. This boosts their research, career and innovation. www.cost.eu (COST, 2025b). E.C. and A.C. acknowledge Campus France and Tallinn Technological University (TalTech), France for the Ph.D. fellowship (co-tutelle de thèse France-Estonia). Views and opinions expressed are however those of the authors only and do not necessarily reflect those of the European Union or HaDEA. Neither the European Union nor the granting authority can be held responsible for them. The authors would like to thank BASF Pharma Solutions and Midas Pharma for providing *rac*-IBU in large amount.

Appendix A. Supplementary data

Supplementary material related to this article can be found online at https://doi.org/10.1016/j.scp.2026.102422.

Data availability

Data will be made available on request.

References

Anastas, P.T., Warner, J.C., 2000. Green Chemistry. Oxford University PressOxford, http://dx.doi.org/10.1093/oso/9780198506980.001.0001.

Arfelis, S., Malpartida, I., Lair, V., Caldeira, V., Sazdovski, I., Bala, A., i Palmer, P.F., 2023. Life cycle assessment on calcium zincate production methods for rechargeable batteries. Sci. Total Environ. 866, 161094. http://dx.doi.org/10.1016/j.scitotenv.2022.161094.

Arvesen, A., Hertwich, E.G., 2012. Assessing the life cycle environmental impacts of wind power: A review of present knowledge and research needs. Renew. Sustain. Energy Rev. 16, 5994–6006. http://dx.doi.org/10.1016/j.rser.2012.06.023.

Biela, J., Stalla, M., Rabe, L., Machado, D., Evers, G., Ansems, S., 2024. Impact assessment study on innovation in COST actions. URL: https://www.cost.eu/uploads/2025/01/COST-Impact-Assessment-Innovation-112024.pdf.

Billen, P., Leccisi, E., Dastidar, S., Li, S., Lobaton, L., Spatari, S., Fafarman, A.T., Fthenakis, V.M., Baxter, J.B., 2019. Comparative evaluation of lead emissions and toxicity potential in the life cycle of lead halide perovskite photovoltaics. Energy 166, 1089–1096. http://dx.doi.org/10.1016/j.energy.2018.10.141.

Blömer, J., Maga, D., Röttgen, J., Wu, Z., Hiebel, M., Eilebrecht, S., Jentsch, S., Eggers, N., 2024. Assessment of chemical products and processes: Green metrics and life cycle assessment – a comparison. Chem. Ing. Tech. 96, 561–574. http://dx.doi.org/10.1002/cite.202300229.

Bodach, A., Portet, A., Winkelmann, F., Herrmann, B., Gallou, F., Ponnusamy, E., Virieux, D., Colacino, E., Felderhoff, M., 2024. Scalability of pharmaceutical co-crystal formation by mechanochemistry in batch. ChemSusChem 17, http://dx.doi.org/10.1002/cssc.202301220.

Braga, D., Maini, L., Grepioni, F., 2013. Mechanochemical preparation of co-crystals. Chem. Soc. Rev. 42, 7638. http://dx.doi.org/10.1039/c3cs60014a.

Colacino, E., Isoni, V., Crawford, D., García, F., 2021. Upscaling mechanochemistry: Challenges and opportunities for sustainable industry. Trends Chem. 3, 335–339. http://dx.doi.org/10.1016/j.trechm.2021.02.008.

COST, 2025a. COST action CA18112 mechanochemistry for sustainable industry. https://www.mechsustind.eu/. (Accessed 30 September 2025).

COST, 2025b. COST: European cooperation in science and technology. https://www.cost.eu/ (Accessed 30 September 2025).

Davies, J.F., McAlister, S., Eckelman, M.J., McGain, F., Seglenieks, R., Gutman, E.N., Groome, J., Palipane, N., Latoff, K., Nielsen, D., Sherman, J.D., Patel, P., Wong, T., Harknett, E., Wong, S., Watson, S., Gemmell-Smith, M., Laing, S., Cooper, I., Bakogianis, A., Nasteka, A., Hay, J., Taylor-Smith, R., Reilly, S., Wallace, C., Mills, L., Pinder, A., Back, M., Damm, E., Goudie, C., Wong, J., Wilkinson, A., Mohamed, A., Silk, E., Mitchard, M., Qureshi, N., Shatananda, L., George, D., Davenport, T., Skingle, A., Cooper, M., Sharif, S., Harding, K., O'Docherty, A., Hawkins, T., Pooley, S., Myo, J., Hamid, H.K., Davis, G., 2024. Environmental and financial impacts of perioperative paracetamol use: a multicentre international life-cycle assessment. Br. J. Anaesth. 133, 1439–1448. http://dx.doi.org/10.1016/j.bja.2023.11.053.

Dhumal, R.S., Kelly, A.L., York, P., Coates, P.D., Paradkar, A., 2010. Cocrystalization and simultaneous agglomeration using hot melt extrusion. Pharm. Res. 27, 2725–2733. http://dx.doi.org/10.1007/s11095-010-0273-9.

Fantozzi, N., Volle, J.-N., Porcheddu, A., Virieux, D., García, F., Colacino, E., 2023. Green metrics in mechanochemistry. Chem. Soc. Rev. 52, 6680–6714. http://dx.doi.org/10.1039/D2CS00997H.

Fischer, F., Wenzel, K.-J., Rademann, K., Emmerling, F., 2016. Quantitative determination of activation energies in mechanochemical reactions. Phys. Chem. Chem. Phys. 18, 23320–23325. http://dx.doi.org/10.1039/C6CP04280E.

Friščić, T., Jones, W., 2009. Recent advances in understanding the mechanism of cocrystal formation via grinding. Cryst. Growth Des. 9, 1621–1637. http://dx.doi.org/10.1021/cg800764n.

Galant, O., Aborome, A., McCalmont, A.S., James, S.L., Patrascu, M., Spatari, S., 2023. LCA as a tool to detect environmental "hot spots" in early-stage mechanochemical synthesis of organic dyes. ACS Sustain. Chem. Eng. 11, 12155–12165. http://dx.doi.org/10.1021/ACSSUSCHEMENG.3C03290/ASSET/IMAGES/LARGE/SC3C03290_0007.JPEG, URL: https://pubs.acs.org/doi/full/10.1021/acssuschemeng.3c03290.

Galant, O., Cerfeda, G., McCalmont, A.S., James, S.L., Porcheddu, A., Delogu, F., Crawford, D.E., Colacino, E., Spatari, S., 2022. Mechanochemistry can reduce life cycle environmental impacts of manufacturing active pharmaceutical ingredients. ACS Sustain. Chem. Eng. 10, 1430–1439. http://dx.doi.org/10.1021/ACSSUSCHEMENG.1C06434/SUPPL_FILE/SC1C06434_SI_001.PDF, URL: https://pubs.acs.org/doi/pdf/10.1021/acssuschemeng.1c06434.

Galant, O., Donmez, H.B., Barner-Kowollik, C., Diesendruck, C.E., 2021. Flow photochemistry for single-chain polymer nanoparticle synthesis. Angew. Chem. Int. Ed. 60, 2042–2046. http://dx.doi.org/10.1002/anie.202010429.

Geisler, G., Hofstetter, T.B., Hungerbühler, K., 2004. Production of fine and speciality chemicals: Procedure for the estimation of LCIs. Int. J. Life Cycle Assess. 9, 101–113. http://dx.doi.org/10.1007/BF02978569/METRICS, URL: https://link.springer.com/article/10.1007/BF02978569.

Gelfand, I., Hamilton, S.K., Kravchenko, A.N., Jackson, R.D., Thelen, K.D., Robertson, G.P., 2020. Empirical evidence for the potential climate benefits of decarbonizing light vehicle transport in the U.S. with bioenergy from purpose-grown biomass with and without BECCS. Environ. Sci. Technol. 54, 2961–2974. http://dx.doi.org/10.1021/acs.est.9b07019.

Grimaldi, F., Tran, N.N., Sarafraz, M.M., Lettieri, P., Morales-Gonzalez, O.M., Hessel, V., 2021. Life cycle assessment of an enzymatic ibuprofen production process with automatic recycling and purification. ACS Sustain. Chem. Eng. 9, 13135–13150. http://dx.doi.org/10.1021/acssuschemeng.1c02309.

Guerain, M., Guinet, Y., Correia, N., Paccou, L., Danède, F., Hédoux, A., 2020. Polymorphism and stability of ibuprofen/nicotinamide cocrystal: The effect of the crystalline synthesis method. Int. J. Pharm. 584, 119454. http://dx.doi.org/10.1016/j.ijpharm.2020.119454.

Hallamasek, S., Ubbenjans, V., Lapkin, A.A., 2024. Life cycle assessment of a process for paracetamol flow synthesis from bio-waste derived beta pinene. Sustain. Chem. Pharm. 40, 101629. http://dx.doi.org/10.1016/j.scp.2024.101629.

Hasa, D., Miniussi, E., Jones, W., 2016. Mechanochemical synthesis of multicomponent crystals: One liquid for one polymorph? A myth to dispel. Cryst. Growth Des. 16, 4582–4588. http://dx.doi.org/10.1021/acs.cgd.6b00682.

Hernández, J.G., Halasz, I., Crawford, D.E., Krupicka, M., Baláž, M., André, V., Vella-Zarb, L., Niidu, A., García, F., Maini, L., Colacino, E., 2020. European research in focus: Mechanochemistry for sustainable industry (COST action MechSustInd). Eur. J. Org. Chem. 2020 (1), 8–9. http://dx.doi.org/10.1002/ejoc.201901718, URL: https://chemistry-europe.onlinelibrary.wiley.com/doi/abs/10.1002/ejoc.201901718, arXiv:https://chemistry-europe.onlinelibrary.wiley.com/doi/pdf/10.1002/ejoc.201901718.

Huijbregts, M.A.J., Steinmann, Z.J.N., Elshout, P.M.F., Stam, G., Verones, F., Vieira, M., Zijp, M., Hollander, A., van Zelm, R., 2017. ReCiPe2016: a harmonised life cycle impact assessment method at midpoint and endpoint level. Int. J. Life Cycle Assess. 22, 138–147. http://dx.doi.org/10.1007/s11367-016-1246-y.

International Organization for Standardization, 2006. ISO 14040:2006 - Environmental management — Life cycle assessment — Principles and framework. https://Www.Iso.Org/Standard/37456.Html.

International Organization for Standardization, 2006. ISO 14044:2006 - Environmental management — Life cycle assessment — Requirements and guidelines. https://Www.Iso.Org/Standard/38498.Html.

Jiménez-González, C., Overcash, M.R., 2014. The evolution of life cycle assessment in pharmaceutical and chemical applications – a perspective. Green Chem. 16, 3392–3400. http://dx.doi.org/10.1039/C4GC00790E.

Kar, S., Singh, R., Gurian, P.L., Hendricks, A., Kohl, P., McKelvey, S., Spatari, S., 2023. Life cycle assessment and techno-economic analysis of nitrogen recovery by ammonia air-stripping from wastewater treatment. Sci. Total Environ. 857, 159499. http://dx.doi.org/10.1016/j.scitotenv.2022.159499, URL: https://www.sciencedirect.com/science/article/pii/S0048969722065986.

Karimi-Jafari, M., Soto, R., Albadarin, A.B., Croker, D., Walker, G., 2021. In-line Raman spectroscopy and chemometrics for monitoring cocrystallisation using hot melt extrusion. Int. J. Pharm. 601, 120555. http://dx.doi.org/10.1016/j.ijpharm.2021.120555.

Karimi-Jafari, M., Ziaee, A., Iqbal, J., O'Reilly, E., Croker, D., Walker, G., 2019. Impact of polymeric excipient on cocrystal formation via hot-melt extrusion and subsequent downstream processing. Int. J. Pharm. 566, 745–755. http://dx.doi.org/10.1016/j.ijpharm.2019.06.031.

Kelly, A., Gough, T., Dhumal, R., Halsey, S., Paradkar, A., 2012. Monitoring ibuprofen–nicotinamide cocrystal formation during solvent free continuous cocrystallization (SFCC) using near infrared spectroscopy as a PAT tool. Int. J. Pharm. 426, 15–20. http://dx.doi.org/10.1016/j.ijpharm.2011.12.033.

Khansary, M.A., Walker, G., Shirazian, S., 2020. Incomplete cocrystalization of ibuprofen and nicotinamide and its interplay with formation of ibuprofen dimer and/or nicotinamide dimer: A thermodynamic analysis based on DFT data. Int. J. Pharm. 591, 119992. http://dx.doi.org/10.1016/j.ijpharm.2020.119992.

Kreuder, A.D., House-Knight, T., Whitford, J., Ponnusamy, E., Miller, P., Jesse, N., Rodenborn, R., Sayag, S., Gebel, M., Aped, I., Sharfstein, I., Manaster, E., Ergaz, I., Harris, A., Grice, L.N., 2017. A method for assessing greener alternatives between chemical products following the 12 principles of green chemistry. ACS Sustain. Chem. Eng. 5, 2927–2935. http://dx.doi.org/10.1021/acssuschemeng.6b02399.

Lask, J., Rukavina, S., Zorić, I., Kam, J., Kiesel, A., Lewandowski, I., Wagner, M., 2021. Lignocellulosic ethanol production combined with CCS—A study of GHG reductions and potential environmental trade-offs. GCB Bioenergy 13, 336–347. http://dx.doi.org/10.1111/gcbb.12781.

Lee, C.K., Khoo, H.H., Tan, R.B.H., 2016. Life cyle assessment based environmental performance comparison of batch and continuous processing: A case of 4-D-erythronolactone synthesis. Org. Process. Res. Dev. 20, 1937–1948. http://dx.doi.org/10.1021/acs.oprd.6b00275.

Linberg, K., Sander, P.C., Emmerling, F., Michalchuk, A.A.L., 2024. *In situ* investigation of controlled polymorphism in mechanochemistry at elevated temperature. RSC Mechanochemistry 1, 43–49. http://dx.doi.org/10.1039/D3MR00019B.

Ma, L., Li, J., Zhang, H., Xu, L., 2025. Life cycle assessment and economic analysis of aspirin production. Sustain. Chem. Pharm. 44, 101963. http://dx.doi.org/10.1016/j.scp.2025.101963.

MacLean, H.L., Spatari, S., 2009. The contribution of enzymes and process chemicals to the life cycle of ethanol. Environ. Res. Lett. 4, 014001. http://dx.doi.org/10.1088/1748-9326/4/1/014001.

Madanayake, S.N., Manipura, A., Thakuria, R., Adassooriya, N.M., 2023. Opportunities and challenges in mechanochemical cocrystallization toward scaled-up pharmaceutical manufacturing. Org. Process. Res. Dev. 27, 409–422. http://dx.doi.org/10.1021/acs.oprd.2c00314.

Maga, D., Röttgen, J., Blömer, J., Wu, Z., Greuel, M., Hiebel, M., Zeidler-Fandrich, B., Eilebrecht, S., 2024. How to measure the greenness of chemicals? A case study on butadiene production applying green metrics and life cycle assessment. Chem. Ing. Tech. 96 (5), 688–697. http://dx.doi.org/10.1002/cite.202300231, URL: https://onlinelibrary.wiley.com/doi/abs/10.1002/cite.202300231, arXiv:https://onlinelibrary.wiley.com/doi/pdf/10.1002/cite.202300231.

Maniruzzaman, M., Zhang, J., Thakkar, R., 2022. Pharmaceutical composition containing cocrystals for additive manufacturing. WO/2022/036290.

Ott, D., Kralisch, D., Denčić, I., Hessel, V., Laribi, Y., Perrichon, P.D., Berguerand, C., Kiwi-Minsker, L., Loeb, P., 2014. Life cycle analysis within pharmaceutical process optimization and intensification: Case study of active pharmaceutical ingredient production. ChemSusChem 7, 3521–3533. http://dx.doi.org/10.1002/cssc.201402313.

Parvatker, A.G., Tunceroglu, H., Sherman, J.D., Coish, P., Anastas, P., Zimmerman, J.B., Eckelman, M.J., 2019. Cradle-to-gate greenhouse gas emissions for twenty anesthetic active pharmaceutical ingredients based on process scale-up and process design calculations. ACS Sustain. Chem. Eng. 7, 6580–6591. http://dx.doi.org/10.1021/acssuschemeng.8b05473.

Piccinno, F., Hischier, R., Seeger, S., Som, C., 2016. From laboratory to industrial scale: a scale-up framework for chemical processes in life cycle assessment studies. J. Clean. Prod. 135, 1085–1097. http://dx.doi.org/10.1016/J.JCLEPRO.2016.06.164.

Pourhashem, G., Adler, P.R., McAloon, A.J., Spatari, S., 2013. Cost and greenhouse gas emission tradeoffs of alternative uses of lignin for second generation ethanol. Environ. Res. Lett. 8, 025021. http://dx.doi.org/10.1088/1748-9326/8/2/025021.

Riazi, B., Zhang, J., Yee, W., Ngo, H., Spatari, S., 2019. Life cycle environmental and cost implications of isostearic acid production for pharmaceutical and personal care products. ACS Sustain. Chem. Eng. 7, 15247–15258. http://dx.doi.org/10.1021/acssuschemeng.9b02238.

Schöbel, J.-H., Winkelmann, F., Bicker, J., Felderhoff, M., 2025. Mechanochemical kilogram-scale synthesis of *rac*-ibuprofen:nicotinamide co-crystals using a drum mill. RSC Mechanochemistry 2, 224–229. http://dx.doi.org/10.1039/D4MR00096J.

Sharma, P., Vetter, C., Ponnusamy, E., Colacino, E., 2022. Assessing the greenness of mechanochemical processes with the DOZN 2.0 tool. ACS Sustain. Chem. Eng. 10, 5110–5116. http://dx.doi.org/10.1021/acssuschemeng.1c07981.

Siegert, M.-W., Saling, P., Mielke, P., Czechmann, C., Emara, Y., Finkbeiner, M., 2020. Cradle-to-grave life cycle assessment of an ibuprofen analgesic. Sustain. Chem. Pharm. 18, 100329. http://dx.doi.org/10.1016/j.scp.2020.100329.

Skorupska, E., Kaźmierski, S., Potrzebowski, M.J., 2017. Solid state NMR characterization of ibuprofen:Nicotinamide cocrystals and new idea for controlling release of drugs embedded into mesoporous silica particles. Mol. Pharm. 14, 1800–1810. http://dx.doi.org/10.1021/acs.molpharmaceut.7b00092.

Spatari, S., Galant, O., Diesendruck, C.E., 2023. Life cycle assessment. In: Mechanochemistry and Emerging Technologies for Sustainable Chemical Manufacturing. CRC Press, Boca Raton, pp. 93–104. http://dx.doi.org/10.1201/9781003178187-5.

Spatari, S., Stadel, A., Adler, P.R., Kar, S., Parton, W.J., Hicks, K.B., McAloon, A.J., Gurian, P.L., 2020. The role of biorefinery co-products, market proximity and feedstock environmental footprint in meeting biofuel policy goals for winter barley-to-ethanol. Energies 13, 2236. http://dx.doi.org/10.3390/en13092236.

Swanborough, A., 2025. A practical approach to scale-up from bench-top twin-screw extruders, URL: http://www.pinetwork.org/pubs/Alan%20Swanborough.pdf (Accessed 30 September 2025).

Tao, Y., Zhu, S., Smith, J., Lakhani, N., You, F., 2023. Environmental sustainability of the globalized pharmaceutical supply chains: The case of tenofovir disoproxil fumarate. ACS Sustain. Chem. Eng. 11, 6510–6522. http://dx.doi.org/10.1021/acssuschemeng.2c06518.

Triller, S., Winkelmann, F., Schöbel, J.-H., Felderhoff, M., 2025. Utilizing an attritor mill for solvent-free mechanochemical synthesis of *rac*-ibuprofen:nicotinamide co-crystals. RSC Mechanochemistry http://dx.doi.org/10.1039/D5MR00020C.

van Zelm, R., Hennequin, T., Huijbregts, M.A.J., 2025. Performing life cycle impact assessment with the midpoint and endpoint method ReCiPe. Nat. Protoc. http://dx.doi.org/10.1038/s41596-025-01207-y.

Wang, D., Cheow, W.S., Amalina, N., Faiezin, M., Hadinoto, K., 2021. Selecting optimal pharmaceutical excipient formulation from life cycle assessment perspectives: A case study on ibuprofen tablet formulations. J. Clean. Prod. 292, 126074. http://dx.doi.org/10.1016/j.jclepro.2021.126074.

Wang, R., Eckelman, M.J., Zimmerman, J.B., 2013. Consequential environmental and economic life cycle assessment of green and gray stormwater infrastructures for combined sewer systems. Environ. Sci. Technol. 47 (19), 11189–11198, PMID: 23957532, http://dx.doi.org/10.1021/es4026547, https://doi.org/10.1021/es4026547.

Wang, M., Han, J., Dunn, J.B., Cai, H., Elgowainy, A., 2012. Well-to-wheels energy use and greenhouse gas emissions of ethanol from corn, sugarcane and cellulosic biomass for US use. Environ. Res. Lett. 7, 045905. http://dx.doi.org/10.1088/1748-9326/7/4/045905.

Wernet, G., Conradt, S., Isenring, H.P., Jiménez-González, C., Hungerbühler, K., 2010. Life cycle assessment of fine chemical production: a case study of pharmaceutical synthesis. Int. J. Life Cycle Assess. 15, 294–303. http://dx.doi.org/10.1007/s11367-010-0151-z.

Xiao, Y., Wu, C., Hu, X., Chen, K., Qi, L., Cui, P., Zhou, L., Yin, Q., 2023. Mechanochemical synthesis of cocrystal: From mechanism to application. Cryst. Growth Des. 23, 4680–4700. http://dx.doi.org/10.1021/acs.cgd.3c00183.

Xu, H., Lee, U., Wang, M., 2022. Life-cycle greenhouse gas emissions reduction potential for corn ethanol refining in the USA. Biofuels Bioprod. Biorefining 16, 671–681. http://dx.doi.org/10.1002/bbb.2348.

Yang, M., Baral, N.R., Anastasopoulou, A., Breunig, H.M., Scown, C.D., 2020. Cost and life-cycle greenhouse gas implications of integrating biogas upgrading and carbon capture technologies in cellulosic biorefineries. Environ. Sci. Technol. 54, 12810–12819. http://dx.doi.org/10.1021/acs.est.0c02816.

Yaseneva, P., Hodgson, P., Zakrzewski, J., Falß, S., Meadows, R.E., Lapkin, A.A., 2016. Continuous flow Buchwald–Hartwig amination of a pharmaceutical intermediate. React. Chem. Eng. 1, 229–238. http://dx.doi.org/10.1039/C5RE00048C.

Yin, Q., Shen, Z., Gong, J., Hou, B., Zhang, M., Wang, J., Xie, C., Bao, Y., Wang, Z., Zhou, L., 2013. Preparation Method of Ibuprofen-Nicotinamide Eutectic Crystals. Tianjin University.

Appendix 4

Publication IV

A. Casagrande, A. Niidu, R. Aav, D. Kananovich, E. Colacino. Green Chemistry Tools in Mechanochemistry. In *Encyclopedia of Green Chemistry*, Vol. 2 (Ed.: B. Török), Elsevier, Amsterdam, **2025**, pp. 550–571.

Reproduced by permission of Elsevier.

Green Chemistry Tools in Mechanochemistry

Andrea Casagrande, ICGM, University of Montpellier, CNRS, ENSCM, Montpellier, France and Tallinn University of Technology, Tallinn, Estonia
Allan Niidu, Riina Aav, and Dzmitry Kananovich, Tallinn University of Technology, Tallinn, Estonia
Evelina Colacino, ICGM, University of Montpellier, CNRS, ENSCM, Montpellier, France

© 2024 Elsevier Inc. All rights are reserved, including those for text and data mining, AI training, and similar technologies.

Introduction 1
Mechanochemical Techniques and Devices 2
Mechanochemistry and Twelve Principles of Green Chemistry 4
Prevention 4
Atom Economy 5
Safer Chemical Synthesis 6
Designing Safer Chemicals 6
Safer Solvents and Auxiliaries 7
Energy Efficiency 7
Use of Renewable Feedstock 7
Reduce Derivatives 8
Catalysis 8
Design for Degradation 8
Real-Time Analysis for Pollution Prevention 8
Inherently Safer Chemistry for Accident Prevention 9
Green Chemistry Metric Toolkits 9
CHEM21 10
iGAL 10
DOZN 12
EcoScale 15
Life Cycle Assessment 17
Conclusions 20
Acknowledgments 20
References 20

Abstract

Mechanochemistry has gained increasing prominence in organic synthesis, with the potential to revolutionize industrial synthesis of active pharmaceutical ingredients (APIs) and other valuable targets. This technology offers a promising avenue for achieving greener and more sustainable processes compared to traditional solution-based synthetic protocols. Accordingly, it is important to employ and continue developing toolkits and metrics to comprehensively assess the environmental impact of these processes. These toolkits enable both quantitative and qualitative greenness assessments, facilitating comparisons with established solution-based protocols, promoting innovations, and guiding process development. Here, we present the utilization of key green chemistry tools designed for this purpose, demonstrating their usefulness through case study analysis.

Introduction

Over the last century, the intensification of human activities, particularly in the chemical industry, has had profound negative effects on the environment, including the disruption of the ozone layer, global warming, and pollution of water, air, and land, as well as the excessive exploitation and depletion of natural resources. Recognizing the need to tackle these challenges and minimize negative impacts that pose threats to future generations, the development of innovative methodologies for performing chemical transformations under the umbrella of green (*1*) and sustainable chemistry has come into the spotlight. As defined by the International Union of Pure and Applied Chemistry (IUPAC), sustainable chemistry involves "the design, manufacture, and use of environmentally benign chemical products and processes that prevent pollution, reduce or eliminate the use and generation of hazardous waste, and reduce risk to human health and the environment" (*2*). This definition encapsulates the core principles driving advances in chemical sciences today, emphasizing that sustainable chemistry covers broader aspects, including long-term societal and environmental impacts, and extends the focus of green chemistry, which primarily aims at developing less hazardous chemical processes (*3*).

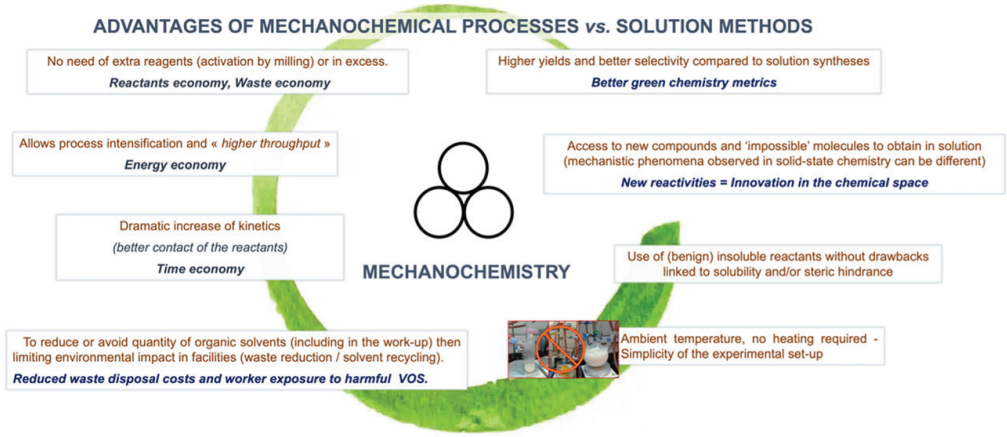


Fig. 1 Advantages of mechanochemical processes *vs* solution-based syntheses. Reproduced with the permission of Royal Society of Chemistry (*10*).

Mechanochemistry, as defined by IUPAC, involves chemical reactions that are induced by the direct absorption of mechanical energy (*4*). This activation technique is typically applied to enhance reactivity of solid chemicals, resulting in the generation of reactive sites on surfaces during grinding, shearing, and stretching, enabling reactions to occur upon contact of solid particles (*5*). Furthermore, efficient mixing of solids or solid-liquid mixtures in mechanochemical apparatus facilitate mass transfer and promote chemical reactions in heterogeneous media. The phenomenon of chemical reactions induced by grinding is known from ancient times. The term "mechanochemistry" was first introduced by Wilhelm Ostwald in 1891, who considered mechanochemistry as one of the four principal chemical disciplines, alongside thermochemistry (activation with heat), photochemistry, and electrochemistry (*6*,*7*). Although mechanochemistry is not a novel concept, it remained peripheral to mainstream solution chemistry for a long time and has gained renewed attention only in recent decades. This renaissance is driven by the pursuit of sustainable chemistry, as mechanochemistry enables solvent-free chemical reactions, thereby eliminating the need for potentially toxic organic solvents, which are predominantly derived from fossil fuels. In 2019, IUPAC included reactive extrusion, a mechanochemical technique, among the top 10 world-changing chemical innovations with the potential to make the world more sustainable (*8*).

Beyond environmental benefits, mechanochemically driven, solvent-free reactions offer several practical advantages over traditional way to perform reactions in homogenous solution (*9*,*10*). Thus, mechanochemical reactions feature significantly reduced reaction times and independence from reactants' solubility. The high reaction rates allow operation at ambient temperatures rather than using thermal activation, leading to notable improvements in yields and selectivity by using simple technical setups (**Fig. 1**).

Moreover, the unique reaction medium of mechanochemistry compared to solution chemistry can also produce unexpected outcomes, enabling the discovery of new reactions and unusual reactivity (*11*), thus opening new frontiers in chemical science (*12*).

These benefits have been demonstrated in various applications, including the preparation of advanced inorganic materials (*6*), co-crystals (*13*) coordination polymers (*14*), supramolecular structures (*14*), biomass valorization (*15*) and organic synthesis (*16*), including the synthesis of active pharmaceutical ingredients (APIs) (*17*).

In this chapter, we focus on the green chemistry aspects of mechanochemistry, emphasizing its alignment with the twelve principles of green chemistry (*18*,*19*) and highlighting how this technology advances the sustainability of chemical processes, as demonstrated by relevant green chemistry metrics (*10*,*20*). This is further substantiated by reported examples of applying green chemistry metrics and toolkits to showcase the improvements of batch and continuous-flow mechanochemical methods compared to traditional solvent-based approaches.

Mechanochemical Techniques and Devices

Progressing from the archaic manual grinding with mortar and pestle known from ancient times, the contemporary mechanochemistry relies on the use of various automated devices (**Fig. 2**, **Table 1**). The setups ensure rapid and efficient mixing of solid reactants, enabling efficient mass transfer and collision of solid particles in concentrated multicomponent and multiphase reaction media.

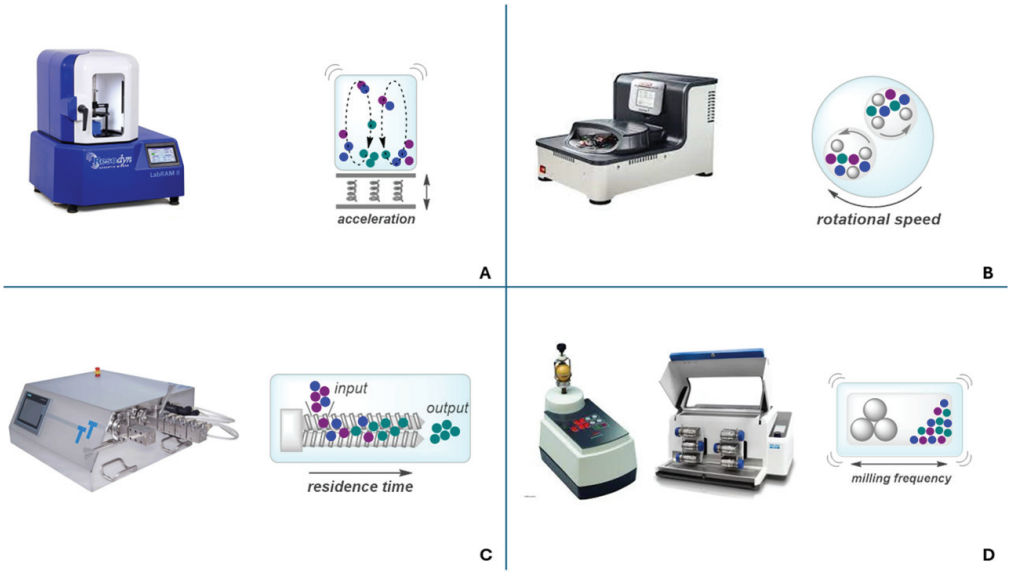


Fig. 2 Examples of instruments to run mechanochemical reactions and their working principle. A – Resodyn Resonant Acoustic Mixer, B – Fritsch Pulverisette 7 Premium, C – Three-Tec ZE 5–12 Hybrid, D – Fritsch Pulverisette 23 (left) and Retsch Mixer Mill 500 Vario (right). Reproduced with the permission of Resodyn Acoustic Mixers (A, https://resodynmixers.com/), Fritsch (B and C, left; https://www.fritsch-international.com/), Three-Tec (C, https://www.three-tec.ch) and Retsch (D, right; https://www.retsch.com/).

Table 1 Mechanochemical devices and selected technical details (*21*).

Device	*Capacity*	*Energy related parameter*	*Mode*
Vibrational ball mill	1.5 to 125 mL	Frequency (up to 50 Hz)	Batch
Planetary ball mill	12 to 900 mL	Rotations per minute (up to 1100 rpm)	Batch
Eccentric miller	3.2 to 1522 L	Rotations per minute (*e.g.*, 1500 rpm) with variable amplitudes	Batch and continuous
Dyno-mill	0.5 to 612 L	Mill drive (up to 250 kWh)	Batch and continuous
Twin-screw extruder	0.3 kg/h to 2.5 t/h	Residence time, torque force, temperature	Continuous
Resonant acoustic mixer	Up to 420 Kg in batch Up to 2.2 t/h in continuous	Acceleration (up to 100 *g*)	Batch and continuous

The most common setups to run mechanochemical transformations are *ball milling devices* that can be categorized based on motion involved to mix solid chemical and thus the resultant forces applied to them (*21*,*22*). *Vibrating ball mills* (VBM) are one of the most widespread and convenient instruments for laboratory use, allowing to perform mechanochemical typically in a gram scale. In VBM, tightly closed jars with reagents are rapidly shacked, oscillating with up to 50 Hz frequency. The mixing and grinding are achieved by using milling balls of various dimensions and chemical composition. Typically, the jars and balls are manufactured from various inert hard materials, such as stainless steel, zirconium oxide, silicon or tungsten carbide, and polymers like PMMA, PTFE, polyamide, *etc*. The material of the jar and balls can significantly influence the reaction outcome, being affected by different chemical composition and hardness (*4*,*21*). Catalytic reactions can also be performed by selecting a proper material (*23*). As a downside, abrasion may occur, including leaking of metal, that contaminates the product.

Planetary ball mills (PBM) work similarly to VBM but can be equipped larger volume jars, opening to batch scale up possibilities, but in this system the jars are rotated to a certain number of rotations per minute, applying centrifugal force and milling balls to mix the chemicals.

Specialized ball mills such as *eccentric vibrating millers* (*24*,*25*) and *bead-mills* (*e.g.*, Dyno-mill (*26*,*27*)) are suitable for further scale up. Additional opportunity for scale-up in continuous flow regime is offered by *twin-screw extruders* (TSE) (*21*,*28*), that knead

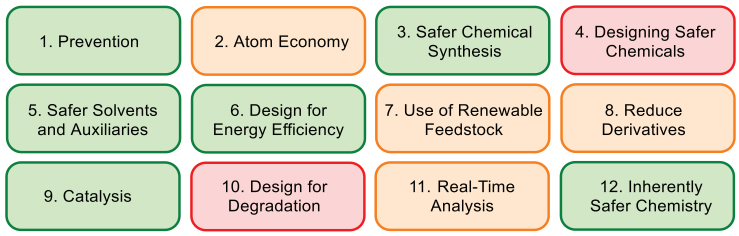


Fig. 3 The 12 principles of green chemistry and their relevance to mechanochemistry (*18*). *Legend*: (green = most attainable, red = least attainable).

and mix the reagents in between two screw that rotate in opposite directions. Temperature of the reactor in which the screws reside, the profile (geometry) of the screws and the residence time are the three most important parameters that can be varied in TSE.

Resonant acoustic mixers (RAM) enable the transfer the mechanical energy through sound waves to the reaction mixture allocating the reaction container on a spring system (*29*). In this setup, the milling media is absent, that prevents abrasion and contamination of product. The amount of energy transferred to the reaction mixture is modulated by varying the acceleration imparted to it (expressed in multiples of acceleration constant $g = 9.81\ \mathrm{m/s^2}$). Industrial RAM devices are designed to mix multi-kg scale mixtures, what makes them potentially suitable for performing upscaled mechanochemical reactions.

Not all mechanochemical reactions are necessarily conducted completely solvent-free. The performance of some reactions can be improved by adding small amount of liquid, which act as lubricants and solvating agents, enhancing mixing and reaction kinetics. This technique is known as liquid-assisted grinding (LAG) (*30*), described by the parameter η (μL mg^{-1}).

$$\eta = \frac{volume\ \ of\ \ liquid\ \ additive\ (\mu L)}{total\ \ mass\ \ of\ \ the\ \ reagents\ (mg)}$$

Typical η values for a mechanochemical reaction range from 0 to 1 μL mg^{-1}. When the value exceeds this range, the reaction mixture is classified as a slurry with values up to 10 μL mg^{-1}. Above this, the reaction is considered homogeneous in solution. These ranges are approximate and influenced by specific properties of the chemical entities involved, such as solubility in the LAG liquid. The liquid-to-solid ratio and the rheological properties of the reaction mixture may also change during the reaction. Generally, the phase composition has a profound impact on reaction rates (*31*), and controlling the texture of the reaction media is crucial. In this regard, in contrast to liquid additives, inert solids (*e.g.*, silica, sodium sulfate, sodium chloride) can sometimes be advantageously used as grinding additives.

Mechanochemistry and Twelve Principles of Green Chemistry

The ties between mechanochemistry and green chemistry can be demonstrated through alignment with the twelve fundamental principles of green chemistry formulated by Anastas and Warner (*1*) (**Fig. 3**). These principles are frequently referenced to advocate the green nature of mechanochemical transformations (*18*) and to emphasize their advantages over conventional solution-based chemistry (*10*). This concept was comprehensively analyzed (*19*) establishing links with all twelve principles and illustrated by selected examples. However, the relevance of various principles differs significantly, ranging from direct to rather tangential connection that are not specifically attributable to mechanochemistry. In **Fig. 3**, this varying level of interaction is indicated with color codes, with the most closely associated principles marked in green (predominant cases) and weakly or not specifically relevant ones shown in amber and red (*18*).

To avoid qualitative assessments based on green chemistry principles as narratives, it is essential to quantify and measure the green chemistry characteristics of a chemical process, providing a scoring system or values that can be aligned with each of the twelve principles. In this regard, *green chemistry metrics* have been suggested to serve as objective and verifiable indicators, allowing for unbiased and non-speculative evaluation (*10*,*20*). Besides quantifying aspects related to certain principles of green chemistry, these metrics are also intended to serve as clear indicators of improvements, or *vice versa*, disadvantages introduced during the development of a given chemical process. Comparison with a benchmarking approach is required in this case. Typically, closely related solution-based methodologies are used as a backdrop to reveal the advantages of newly designed mechanochemical methods.

In this section, we provide a discussion on the relevance of each of the twelve principles (*1*) to mechanochemistry, along with an overview of the most useful green chemistry metrics aligned with these principles, which are commonly used as indicators of improvement.

Prevention

"It is better to prevent waste than to treat or clean up waste after it has been created": The prevention principle is perhaps the most important among the twelve principles of green chemistry and is frequently referenced when discussing the green chemistry

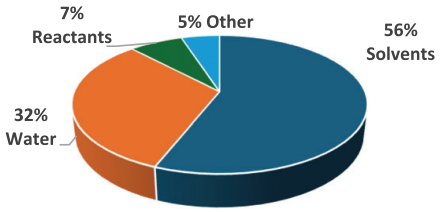


Fig. 4 Composition by mass of the types of material used to manufacture APIs (*32*).

advantages of mechanochemistry. Solvents generally account for 80–90% of mass utilization in typical batch manufacturing of pharmaceuticals or fine chemicals (*32*) (**Fig. 4**), making them the primary contributors to waste generation. In this context, the total absence or significantly reduced use of solvents in mechanochemical processes establishes a clear connection with the principle of prevention, avoiding the generation of excessive solvent-based waste.

The quantitative assessment of generated waste can be performed using various green chemistry metrics that quantify efficiency of mass utilization, such as *Process Mass Intensity* (PMI) (*33*). PMI indicates the amount of materials required to produce a unit mass of product and is defined as (Eq. 1).

$$PMI = \frac{total\ \ mass\ \ used\ \ in\ \ the\ \ process(kg)}{mass\ \ of\ \ product(kg)} \tag{1}$$

The total mass used in the process includes all process materials, such as raw materials, reagents, solvents, water, and auxiliary chemicals involved in all production stages, including the chemical reaction, work-up, isolation, and purification.

Closely linked and historically preceding PMI is the and *Environmental Factor* (*E*-Factor) (*34*), defined as (Eq. 2).

$$E\ \ Factor = \frac{mass\ \ of\ \ waste(kg)}{mass\ \ of\ \ the\ \ product\ \ of\ \ interest(kg)} \tag{2}$$

This metric focuses on the amount of waste generated in a process and is similar to PMI, as shown by their mathematical relationship (Eq. 3).

$$E\ Factor = PMI - 1 \tag{3}$$

The closer PMI is to 1 (and *E*-Factor to 0), the less waste-intensive the process is. It is worth noting that some contributors to the *E*-Factor and PMI may be excluded from calculations if required (*e.g.*, recycled solvents, water). A standardized approach to using *E*-Factors in the pharmaceutical industry was proposed by Roschangar and co-workers (*35*), who introduced the *complete* *E*-Factor (cEF) to account for all materials involved, while the *simple* *E*-Factor (sEF) metric discounts water and solvents.

The calculation of PMI or *E*-Factor is commonly performed for mechanochemical processes when comparing them with benchmarking solvent-based approaches. Mechanochemical reactions, occurring in the absence of bulk solvents or with minimal solvent quantities (LAG), significantly reduce waste generation, which is reflected in dramatically reduced PMI and *E*-Factor values. Further reduction in PMI values also encourages improvements in isolation and purification protocols, which often require classical methods of solvent treatment. For example, filtration with treatment using minimal amounts of solvent can be a better option than aqueous work-up and extraction.

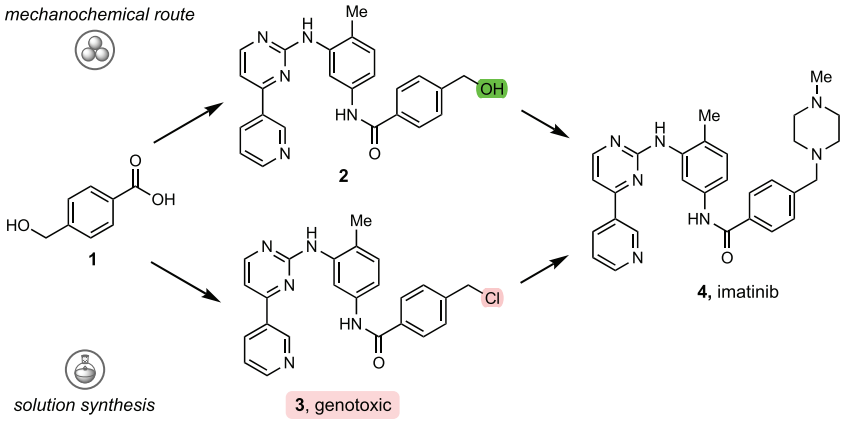
Atom Economy

"Synthetic methods should be designed to maximize incorporation of all materials used in the process into the final product": This principle encourages the maximal incorporation of atoms from the starting materials into the product. The corresponding green chemistry metric, *atom economy* (AE) (*36*), is defined as (Eq. 4).

$$AE = \frac{formula\ \ weight\ \ product\left(\frac{kg}{kmol}\right)}{formula\ \ weight\ \ of\ \ all\ \ reactants\ \ used\ \ in\ \ reaction\left(\frac{kg}{kmol}\right)} \tilde{n} 100 \tag{4}$$

The ideal case of 100% Atom Economy (AE) ensures that no additional products (potential waste) are generated in a reaction. However, this condition is only satisfied in specific classes of chemical reactions, such as addition, rearrangement, and isomerization. Since AE is attributed to a chemical reaction rather than the methodology used to perform it, AE has no direct link with mechanochemistry. Nevertheless, AE reflects the theoretical maximal efficiency of reactant utilization according to ideal stoichiometry and in the absence of any side processes. In actual processes, an excess of chemicals is often used to drive the reaction to completion, and side reactions are common. This real-case scenario can be better reflected by calculating *Reaction Mass Efficiency* (RME) (*37*), which considers yields, the actual molar quantities of reactants, along with the concepts of atom efficiency (Eq. 5).

$$RME = \frac{mass\ \ of\ \ product(kg)}{total\ \ mass\ \ of\ \ reactants\ \ used\ \ in\ \ reaction(kg)} \tilde{n} 100 \tag{5}$$



Scheme 1 Mechanochemical synthesis of imatinib **4** bypassing a genotoxic intermediate **3**.

The closer RME is to 100 %, the less waste-intensive the process is. Regarding mechanochemistry, mechanochemical conditions often enhance reaction rates, allowing for the avoidance of excess chemicals to complete the reaction. Furthermore, ambient temperature operation and the enhanced reactivity of low-reacting solids (compared to their behavior in solution) can result in improved yields and better selectivity due to suppressed side processes. These improvements are reflected in better RME values for mechanochemical processes. Closely related to RME is the *Real Atom Economy* (RAE) metric, which is defined in a similar manner (*38*).

Safer Chemical Synthesis

"Wherever practicable, synthetic methods should be designed to use and generate substances that possess little or no toxicity to human health and the environment": Employing mechanochemical conditions for synthesis frequently allows the substitution of toxic chemicals with less toxic alternatives. Such replacements are often not possible or inefficient in solution due to low solubility and insufficient reactivity of the replacement chemicals. For example, toxic organic amine bases (triethylamine, DIPEA, DMAP) can be substituted with safer inorganic salts such as phosphates and carbonates of sodium and potassium (*39*,*40*). Highly toxic potassium cyanide has been replaced with potassium ferricyanide $K_3[Fe(CN)_6]$ to run Strecker-type reaction in a ball mill (*41*). 1,1′-Carbonyldiimidazole (CDI) has been validated as a highly efficient activator for carboxylic acids in the synthesis of amides (*42*) and carbamates (*43*) under ball milling conditions. This reagent produces by-products with low acute toxicity (CO_2 and imidazole), providing an alternative to toxic chemicals employed for the same purpose, such as $SOCl_2$ and oxalyl chloride. Along this line, and similarly to CDI, *N*-acylbenzotriazoles are also versatile reagents, with the benzotriazole-1-yl group acts as substitute agent for halogen, easily displaced by nucleophiles. They are usually stable in the air and are more reactive than the corresponding *N*-acylimidazoles. They were used to prepare pentapeptides labeled with biotin, such as the biotin-Ahx-RGDfV-NH_2, containing the well-known arginine –glycine–aspartic acid (RGD)-motif, which is the main recognition site of the cell adhesion integrin receptors (*44*).

The advantages of mechanochemical synthesis can be leveraged to re-route synthetic pathways used in the preparation of APIs (*45*), thereby avoiding the generation of (geno)toxic intermediates. In a recent example, the anti-cancer drug imatinib **4** (**Scheme 1**) was prepared via a two-step mechanochemical synthesis in a ball mill from 4-(hydroxymethyl)benzoic acid (**1**), bypassing the chlorinated intermediate **3** with genotoxic properties commonly used in solvent-based commercial routes (*46*). The hydroxy-containing intermediate **2** obtained in the mechanochemical route showed no genotoxic potential according to *in silico* assessment.

The toxic properties of chemicals are usually expressed through LD_{50} or EC_{50} values and other similar quantitative parameters. However, relevant toxicological data can be unavailable, and toxic effects vary greatly depending on the mechanism of action, administration route, affected species, etc (*47*). The toxicity of chemicals is routinely assessed in most common green chemistry metrics and toolkits (see section "Green Chemistry Metric Toolkits" below). Cumulative toxic effects can be quantified in life-cycle assessment studies (see section "Life Cycle Assessment") by using the 1,4-dichlorobenzene (1,4-DCB) equivalent as a reference unit to calculate the toxic impact of all chemicals involved.

Designing Safer Chemicals

"Chemical products should be designed to preserve efficacy of function while reducing toxicity": This principle advocates for the design of chemical products that have no adverse effects on human health and the environment while maintaining their functionality. This principle has no apparent link to mechanochemistry since it can be attributed to any branch of chemical

science, encouraging the use of safe-by-design chemicals. Nevertheless, in relation to mechanochemistry, it can be considered as an extension of the previously discussed principle of safer chemical synthesis. In this regard, mechanochemical processing methods encourage the design of novel reagents and the discovery of new uses for known solid materials (such as inorganic salts and polymers) as safer reagents for organic synthesis. Prominent examples illustrating this concept include the discovery of piezoelectric materials (such as $BaTiO_3$) to trigger organic redox reactions in a ball mill (*48*,*49*) and the use of commodity plastics to initiate radical reactions under similar conditions (*50*). Additional notable examples from recent literature include the use of calcium hypochlorite as chlorine source in the mechanochemical preparation of *N*-chlorinated hydantoins as antibacterial agents for polymer textiles (*51*), glucose as a protic source in mechanochemical Birch reduction (*52*), ferric nitrate for the preparation of nitro compounds from alkenes (*53*), and nanocellulose serving as both a reductant and a reaction medium under ball milling conditions (*54*).

Safer Solvents and Auxiliaries

"The use of auxiliary substances (e.g., solvents, separation agents, etc.) should be made unnecessary wherever possible and, innocuous when used": Besides being major contributors to waste generation (see Section "Prevention"), solvents also significantly impact process safety and overall toxicity. For example, the use of highly flammable diethyl ether or toxic solvents like dimethylformamide (DMF), benzene, or dichloromethane (DCM) poses considerable danger. Although mechanochemistry greatly reduces the need for solvents and diminishes the associated safety concerns, LAG technique still requires small quantities of solvents. Furthermore, work-up, isolation, and purification of the product may still necessitate intensive solvent use. These needs call for the use of safer and more sustainable solvents and auxiliary chemicals in mechanochemical synthesis as well. From a green chemistry standpoint, the harmful properties of solvents can be scored to classify them as preferable (so-called "green solvents"), problematic, hazardous, or highly hazardous (*55*). The use of green solvents as LAG agents and for subsequent work-up is encouraged. Advances in the synthesis of amides using mechanochemistry serve as a good illustration of how mechanochemistry helps to alleviate solvent-related safety concerns. DMF and DCM are the two most preferred solvents for the amide synthesis (*56*), both recently restricted for use in the EU and the USA (*57*,*58*). In contrast, mechanochemical amide couplings can be performed without any solvent at all by using CDI as a coupling reagent (*42*), while other amide coupling agents are compatible with green organic solvents (ethyl acetate, γ-valerolactone) as LAG additives (*39*,*59*,*60*). Whether, the mechanochemical amidation methods affords a high-purity product through simple work-up, involving only washing with water and filtration, thus avoiding the use of additional solvents and auxiliary chemicals for extraction and purification, green chemistry metrics might not be always favorable, due to intrinsically low atom economy displayed by methodologies making use of the most common coupling agents (*e.g.*, HATU, COMU, EDC, *etc.*).

Energy Efficiency

"Energy requirements should be recognized for their environmental and economic impacts and should be minimized. Synthetic methods should be conducted at ambient temperature and pressure": Mechanochemical reactions are typically run without external heating and under ambient pressure, yet they are completed in shorter times than analogous reactions in solution, resulting in low energy consumption. The striking acceleration effect in the absence of thermal activation can be attributed, among other factors, to the high effective concentrations of reactants (*61*). Nevertheless, highly energy-demanding processes (for example, direct amidation(*62*)) still require elevated temperatures to achieve reasonable reaction rates and high product yields. There is potential to improve the energy yield of mechanochemical transformations (*63*), which may also vary depending on the instrument used and the production scale. The examples below illustrate lower overall energy requirements of mechanochemical processes compared to benchmark approaches in solution or gas phase reactions. For example, iron-catalyzed synthesis of ammonia from hydrogen and nitrogen have been reported to achieve impressively high conversion (yielding up to 82.5 vol% NH_3) in a ball mill at a low temperature of 45°C and ambient (1 bar) pressure (*64*), along with the protocol reported for the same Haber-Bosch type process, involving mechanocatalysis at room temperature and ambient pressure (yielding up to 0.2 vol% NH_3 over 50 h) (*65*). This is strikingly different from the energy-intensive conditions of the industrial Haber-Bosch process, which operates at 450°C and 200 bar pressure. The superior energy efficiency of mechanochemical Suzuki-Miyaura cross-coupling in a ball mill, compared to microwave and ultrasound activation, has been validated through a life cycle assessment (LCA) study (*66*). Among green chemistry tools, LCA provides the most comprehensive analysis of materials and energy flows involved, making it an appropriate tool for the quantitative assessment of energy efficiency. As a representative example, energy efficiency of mechanochemical synthesis of the World Health Organization (WHO) Essential medicine nitrofurantoin (benchmarked *vs* conventional solution approach) by using TSE technology is showcased in Section "Life Cycle Assessment".

Use of Renewable Feedstock

"A raw material or feedstock should be renewable rather than depleting whenever technically and economically practicable": Although the use of renewable and sustainable resources is essential for any type of chemical technology, the application of mechanochemical methods can significantly enhance the use of renewables and increase the circularity of materials through degradation at the end of life (discussed in Section "Design for Degradation" below). Mechanochemical processing has shown

advantages in the processing and valorization of biomass, including the transformation of biopolymers such as cellulose, chitin, and lignin (15,67–69). More sustainable replacements for scarce resources can become feasible with the help of mechanochemical activation. For example, the increased reactivity of metals under ball milling conditions allows for the substitution of scarce lithium with earth-abundant calcium and magnesium in mechanochemical Birch reduction (70).

Reduce Derivatives

"Unnecessary derivatization (use of blocking groups, protection/deprotection, temporary modification of physical/chemical processes) should be minimized or avoided if possible, because such steps require additional reagents and can generate waste": In organic synthesis, this principle emphasizes the design of more efficient and shorter synthetic pathways to target products. It aims to incorporate a minimal number of preparative steps while achieving maximum complexity and maintaining desired product selectivity. The lack of selectivity and efficiency in many common organic reactions often necessitates the use of protection and activation groups, leading to additional steps for protection, deprotection, and activation. This creates a demand for more selective and specialized methods, as well as improved activation techniques in organic synthesis, thereby expanding the diversity of the synthetic toolbox. In this regard, mechanochemistry, with its unique characteristics, satisfy these requirements and perfectly complements the portfolio of modern methods available to synthetic chemists. It is important to note that the rational development of improved approaches is hardly possible without understanding the driving forces involved, which requires studies that provide fundamental insight into the underlying mechanisms.

The advantages of mechanochemistry in achieving precise control over selectivity have been showcased multiple times and features one of the distinct advantages of mechanochemical organic synthesis (12). Performing chemical transformation in solid phase also offers opportunity to synthesize complex products in a single step by leveraging enhanced intermolecular interaction (71) or by performing multicomponent reactions with *in-situ* generated intermediates, such as organometallic compounds (72,73). Successful activation-group-free synthesis can be illustrated by the direct preparation of carboxamides from carboxylic acids and amines using TSE technology (62). Base-free (74) or protecting-group-free (46) reactions can also be performed streamlining the synthesis of APIs and resulting in a lower number of synthetic operations/steps, thereby improving green chemistry metrics (see Section "iGAL" below for an example).

An additional appealing aspect is the possibility to activate and directly use natural mineral feedstock for incorporating desired atoms into organic molecules, avoiding the prior generation of more reactive but more toxic chemicals and/or multi-step synthesis of complex reagents. For instance, mechanochemical activation in a ball mill has been shown to enable the direct use of fluorspar (CaF_2) as a fluorine source for forging sulfur-fluorine and carbon-fluorine bonds in organic molecules (75).

Catalysis

"Catalytic reagents (as selective as possible) are superior to stoichiometric reagents": Catalytic transformations hold fundamental significance in chemistry, and these processes can also be performed under mechanochemical conditions, including multiple examples of highly efficient transition metal-mediated (76) and organocatalytic transformations (77). However, mechanochemistry offers a particularly unique approach to running catalytic reactions by utilizing catalytically active sites on the surface of milling media or the working surfaces of the instruments used, a method known as *direct mechanocatalysis*. This methodology was pioneered by the Mack *et al.* and further developed by Borchardt group (78,79). In its original variant, it involved the use of milling jars, balls or pellets made from catalytically active metals such as copper, nickel, silver, or palladium. This technique facilitates the straightforward recovery of the catalyst without significant contamination of the reaction mixture. An adaptation of this method to RAM has been recently demonstrated, with copper-catalyzed alkyne-azide click-coupling (CuAAC) reactions being performed on the surface of a copper coil (80). Continuous direct mechanocatalytic Suzuki-Miyaura coupling in TSE has also been achieved by using a TSE instrument with Pd-coated extruder screws or barrel (81).

Design for Degradation

"Chemical products should be designed so that at the end of their function they break down into innocuous degradation products and do not persist in the environment": Although this principle does not have a specific tie with mechanochemistry, mechanochemical methods have proved their efficiency in facilitating the chemical degradation of polymers (82,83) and destruction of toxic halogenated pollutants (84–86). These examples verify that mechanochemistry can provide a platform for developing advanced mineralization and remediation techniques, thereby promoting better recirculation of materials. Furthermore, ball milling has been demonstrated as a convenient approach for characterizing oxidative mechanochemical degradation profiles of APIs, forming the corresponding oxidation products after very short reaction times (87).

Real-Time Analysis for Pollution Prevention

"Analytical methodologies need to be further developed to allow for real-time, in-process monitoring and control prior to the formation of hazardous substances": In recent years, significant efforts have been made to develop techniques suitable for real-

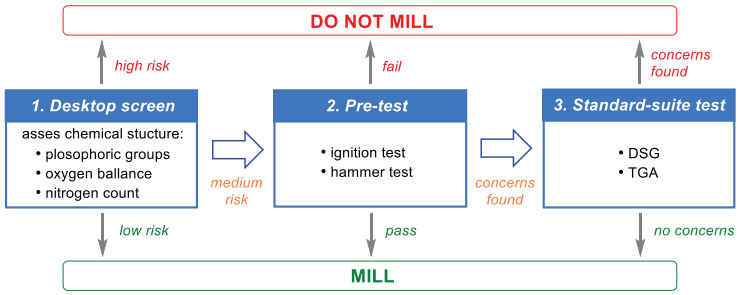


Fig. 5 Proposed safety assessment flow chart for implementation of ball milling for organic synthesis (*93*).

time analysis of mechanochemical reactions (*88*,*89*). These tools aim to enhance fundamental understanding of the driving forces behind mechanochemistry and provide convenient methods for monitoring the progress of reactions without interruption. Recent commercially available developments include temperature and pressure monitoring milling devices. More specialized setups, which may not be readily available in common laboratories, can offer in-depth information on the real-time progress of reactions. Examples include *in-situ* synchrotron PXRD (*90*), Raman spectroscopy (*91*), and in-operando solid-state NMR (*92*). However, the widespread adoption of these techniques is still limited by the need for sophisticated instrumentation and high costs, which may not always be accessible.

Inherently Safer Chemistry for Accident Prevention

"Substances and the form of a substance used in a chemical process should be chosen to minimize the potential for chemical accidents, including releases, explosions, and fires": As was mentioned before (Section "Safer Solvents and Auxiliaries"), eliminating solvents mitigates the solvent-associated hazards. Nevertheless, other hazards of chemical synthesis still must be meticulously assessed. In this regard, several safety issues specific to mechanochemistry can be outlined. Many of these concerns stem from the rapid reaction rates in concentrated media during mechanochemical processing. For example, an exothermic process completed in a short time may result in thermal runaway, overpressure the reactor, and even in explosion. From a safety standpoint, solvents are beneficial for efficient heat dissipation as they serve as excellent heat sinks (*93*). Besides the thermal risks, any potential gas release in a closed milling vessel must be considered as a hazard, especially evolution of flammable or toxic gases or vapors. Generation of highly reactive particles of pyrophoric materials during milling (powders of metals, metal hydrides, *etc*.) is also common and should be considered as a safety risk (*94*). The explosion risk is heightened by shock-, friction-, impact-, and thermosensitive reactants, products or intermediates. Moreover, same dangers may arise when milling mixtures of reductants with oxidants. Noise produced by mechanochemical devices was considered as an additional disadvantage (*93*). The severity of these hazards is different across the various mechanochemical techniques. For instance, resonance acoustic milling (RAM) technology was developed for safe mixing of primary explosives and explosive formulations (*95*).

Safety considerations for laboratory-scale chemical synthesis by ball milling have been systematically analyzed by Priestley, Brownie, and co-workers (*93*). A safety assessment workflow was designed to ensure that safety risks associated with mechanochemical reactions are minimized before conducting experimental work and further scaling up (**Fig. 5**). The proposed workflow for chemical screening involves three steps: (i) desktop screening to check all reaction chemicals for explosive properties based on specific criteria (carbon atoms per plosophoric group, oxygen balance, nitrogen content) to classify risk levels; (ii) preliminary ignition and hammer tests for thermal and impact sensitivity; (iii) advanced testing with differential scanning calorimetry (DSC) and thermogravimetric analysis (TGA) to assess thermal instability and gas evolution. It worth adding that besides assessment of individual compounds as focused on the mentioned study, mixtures of reactants that might react violently or even explosively must be also evaluated by following a similar workflow. Typically, such risks are associated with mixtures of reductants and oxidants. The prevalence of redox reactions in the organic synthetic toolbox underscores the critical importance of such analyses prior to experimental tests and especially before scaling up operations. Proper evaluation and risk assessment for these reactions are essential to ensuring a safe mechanochemical implementation, forthcoming scale-up and industrial adaptation.

Green Chemistry Metric Toolkits

Several toolkits have been developed to assess and quantify the environmental impact and sustainability of chemical processes, as well as their alignment with the twelve principles of green chemistry. These toolkits aim to provide holistic, objective, and standardized measures to evaluate various green chemistry-related aspects of chemical reactions, such as waste generation, energy

efficiency, toxicity, and the use of renewable resources. By applying these metrics, the greenness of different methodologies can be compared, and areas for further improvement can be identified, allowing for informed decisions to develop more sustainable and environmentally friendly chemical processes. In this section, we showcase examples of the use of various green chemistry metric toolkits for the analysis of mechanochemical processes.

CHEM21

The CHEM21 toolkit was developed within the framework of the CHEM21 project (Chemical Manufacturing Methods for the 21st Century Pharmaceutical Industries) by James Clark and co-workers (*96*). It aims to evaluate sustainability of reactions, encompassing a comprehensive and holistic range of quantitative and qualitative criteria to determine how green a reaction is. For example, the quantitative parameters include such parameters as yield, selectivity, atom economy (AE), reaction mass efficiency (RME), process mass intensity (PMI). Qualitative criteria allow assessment of energy efficiency, safety, environmental and health hazards. The scoring system is designed with visual and easy-to-interpret indicators. A green, amber or red 'flag' is assigned to each assessed criterion, where green denotes 'preferred', amber is 'acceptable with some issues' and red is 'undesirable'. The structure of the toolkit is designed to provide a level of detail and complexity appropriate for different research stages. Assessments can be performed at four different levels, from initial screening of reaction conditions (zero-pass) to multi-kilogram manufacturing (third pass). For laboratory scale, zero and first pass assessments are sufficient. The use of the toolkit at these levels is user-friendly and straightforward, involving filling out an Excel spreadsheet. The toolkit is also well-designed for educational purposes, as it facilitates easy tracking of outcome origins and clear identification of methodological bottlenecks, thereby promoting critical thinking. However, use of non-quantitative flag-based scoring system at the first pass might be considered as a limitation if comparison of similar protocols is required.

The toolkit was used to reveal green chemistry advantages of a mechanochemical amidations (*39*) using uronium-type coupling reagents (COMU and TCFH, **Table 2**) in comparison with benchmarking solvent-based method (with COMU) (*97*).

Mechanochemical amide coupling of Cbz-protected L-phenylalanine **5** and ethyl 4-aminobenzoate (benzocaine, **6**) was performed in a vibrating ball mill with a slight excess of COMU (1.1 equiv.) or TCFH reagents (1.1–1.3 equiv.), and significant excess of base (K_2HPO_4, 3 equiv.), under liquid-assisted grinding (LAG) conditions, using a small amount of ethyl acetate ($\eta = 0.19\ \mu L\ mg^{-1}$). This procedure resulted in 92 or 96% yields of amide **7**, that was higher than in benchmarking solution method (70%). The isolation of the reaction products was readily performed by filtration and water wash for the mechanochemical process, whereas column chromatography was required in conventional solution approach. Green metrics such as reaction mass efficiency (RME) and product mass intensity (PMI) showed unambiguously that mechanochemical procedures outperformed solution-based method. Thus, PMI for COMU/K_2HPO_4 system was over 7-fold lower (196.3 *vs* 1464.7 in solution), underlining that mechanochemical reaction produced less waste. Furthermore, safer and sustainable solvents such as water and ethyl acetate were utilized in the mechanochemical protocols, contrasting with the use of toxic DMF. However, major safety concerns arise from the use of stoichiometric amide coupling reagents, which may pose environmental, safety or health hazards themselves (*98*,*99*), or from products derived from them (such as tetramethyl urea). Moreover, the use of these coupling reagents reduces the atom economy of the reactions. These critical points clearly indicate that further development of mechanochemical amidation methods is required, preferably avoiding amide coupling reagents (*62*). In addition, the CHEM21 toolkit has recently been employed for the green chemistry assessment of the mechanochemical synthesis of the anti-cancer drug imatinib (*46*) and the preparation of a polyaromatic amide with aggregation-induced emission behavior (*100*).

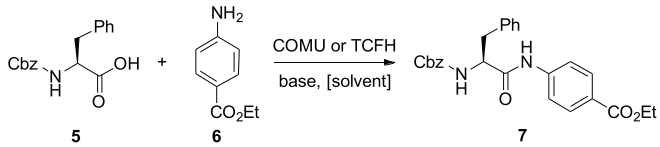
iGAL

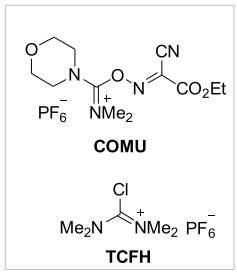
The *Green Aspiration Level* (GAL) concept was first formulated by Roschangar, Sheldon and Senanayake in 2015 as a process performance metric that quantifies the environmental impact of producing a specific pharmaceutical agent while considering the complexity of the synthetic process for producing the target molecule (*35*). The GAL is a standardized metric derived from average development phase-dependent *E*-factors for the pharmaceutical industry. It also accounts for the complexity of a synthetic route and enables the measurement of *relative process greenness* (RPG) for newly designed routes by comparing the respective complete *E*-factor (*c*EF) with a benchmarking GAL value. This approach effectively visualizes whether any green chemistry improvement has been achieved. The methodology has further evolved into the '*Innovation Green Aspiration Level*' (iGAL) methodology (*101*) and its second generation, iGAL 2.0 (*102*). The iGAL methodology can be applied using a scorecard web calculator (*103*).

In mechanochemistry, the iGAL approach was applied to highlight the green chemistry benefits of the mechanochemical synthesis of imatinib (*46*) **4** (**Scheme 2**), an anticancer drug included in the World Health Organization's List of Essential Medicines. This was compared with the benchmark early-stage development solvent-based methodology (*104*). The target active pharmaceutical ingredient (API) was prepared with an 86% total yield and HPLC purity of 99% through a two-fold C–N bond construction sequence. This involved EDC-mediated amide coupling of 4-(hydroxymethyl)benzoic acid **1** with aromatic amine **8**, followed by nucleophilic substitution of the isouronium-activated hydroxyl group in the amide intermediate **2** with 1-methylpiperazine **9**.

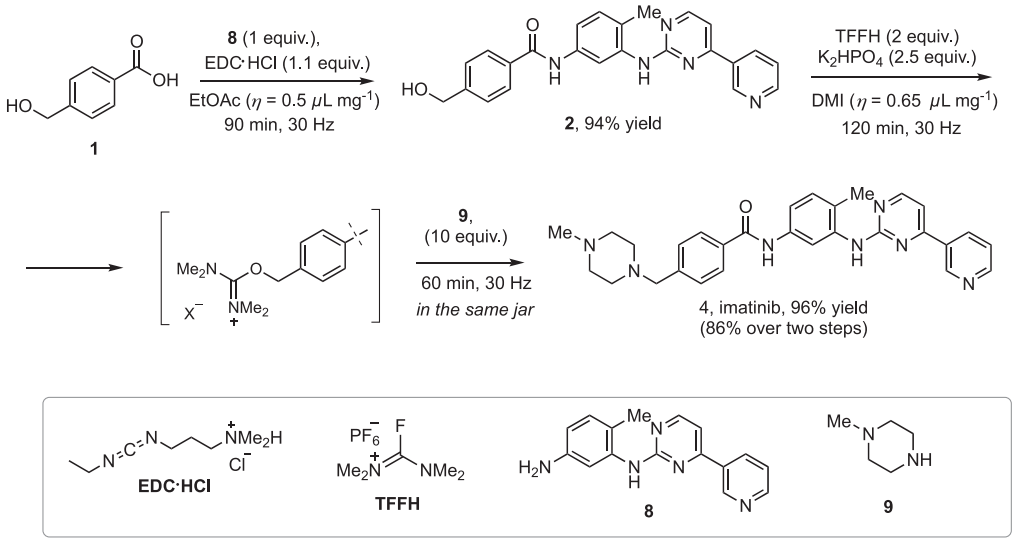
The mechanochemical method demonstrated an excellent relative process greenness (RPG) of 77% which is much higher when compared to the RPG (30%) of the solution-based method (**Fig. 6**). The latter involves prior activation of **1** by conversion into the

Table 2 Comparison of green metrics for mechanochemical and solution-based amidation reactions based on CHEM21 toolkit.





Metrics	Mechanochemistry		Solution
	COMU / K_2HPO_4	TCFH / K_2HPO_4	COMU / DIPEA in DMF
Yield (%)	96	92	70
Atom economy (%)	50	60	50
RME (%)	46	53	35
PMI (total), including:	196.3	203.7	1464.7
PMI (reactants)	3.4	3.1	3.7
PMI (solvent)	0.6	0.6	18.9
PMI (work-up)	192.3	200	1442.2
Solvent choice	EtOAc, water	EtOAc, water	DMF
Work-up, isolation	filtration	filtration	chromatography
Health and safety			
Main hazard statements	H302, H312	H360	H226, 312, 332, 360



Scheme 2 Mechanochemical synthesis of imatinib (*46*).



Fig. 6 Graphical illustration of green chemistry innovation in the mechanochemical synthesis of imatinib by iGAL scorecard. Reproduced from Ref. (*46*) with permission from the Royal Society of Chemistry).

corresponding chloride by reaction with $SOCl_2$ as additional non-constructive step. Importantly, the mechanochemical approach exhibits a lower waste output of 2.22 times when compared to the average value at early development stage.

The iGAL approach also measures the impact of synthesis complexity, demonstrating how well the process design aligns with the 8th principle (Reduce Derivatives, see Section "Reduce Derivatives"). *Process complexity* is evaluated based on the number of construction steps (complexity = 2 in the example considered, **Fig. 6**), excluding steps for activation, protection, and deprotection. The *ideality* metric reflects the contribution of construction steps, defined as the ratio of constructive steps to the total step count (*105*).

DOZN

DOZN 2.0 Green Chemistry Evaluator is a free web-based software developed at MilliporeSigma (*106*) that helps to quantitatively assess any process against the twelve principles of green chemistry, and to enable objective comparisons of the processes. DOZN 2.0 uses readily available data including and not limited to the data present in the Globally Harmonized System of Classification and Labeling of Chemicals (GHS). The tool assigns an individual score to each principle, with the lowest score reflects a better adherence to the green chemistry principles. The principles are divided in three groups (Improved Resource Use, Increased Energy Efficiency and Reduced Human and Environmental Hazard) and an average score is calculated for each group. The normalized

score obtained by the three groups of principles is referred to as '*aggregate score*'. Closer to zero the aggregate score is, greener is the process.

The first category (Group 1), *Improved Resource Use*, includes the principles that aims waste reduction and resources use efficiency and groups the principle 1, 2, 7, 8, 9 and 11. For each of the principles in this group, a severity score is calculated using a dedicated equation (*20*). For example, the first principle, *Waste Prevention*, is quantified based on how the generated waste in a process is then disposed of, incineration being the worst possible output and recovery for recycling or waste-to-energy/energy-from-waste being the best.

The second category (Group 2), *Increased Energy Efficiency*, considers only the 6th principle, and measures energy consumption based on reaction times and the severity of pressure and temperature deviations from standard conditions.

However, the score obtained for a reaction in solution (upon heating or in cryogenic conditions) might not be directly comparable to the score obtained for a reaction conducted by mechanochemistry, being the experimental set-ups very different.

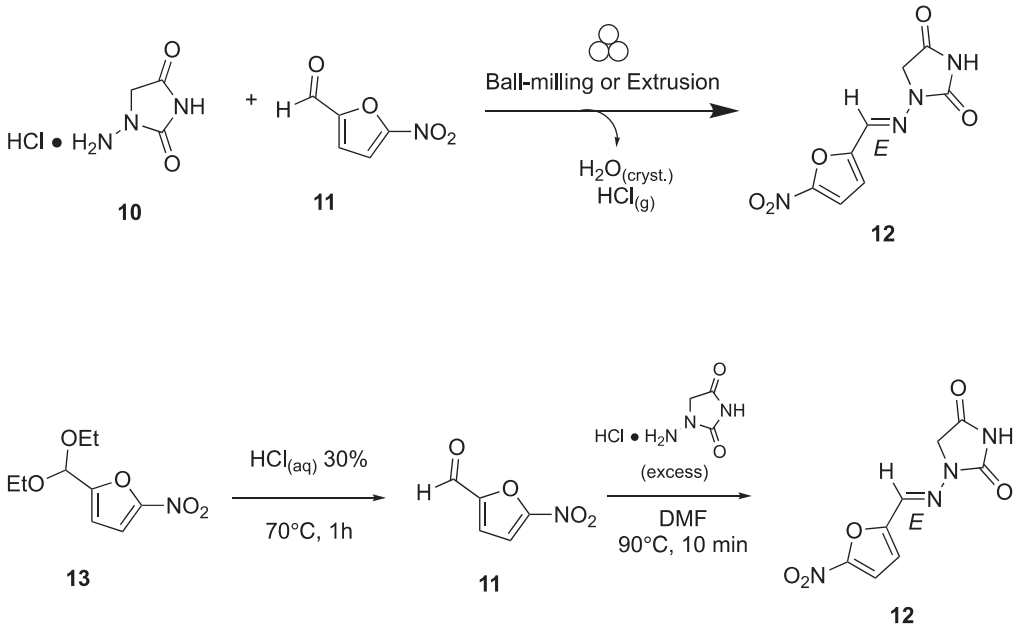
The third category (Group 3), *Reduced Human and Environmental Hazard*, makes use of the data from GHS to calculate a cumulative score that groups the principles 3, 4, 5, 10, and 12.

For example, principle 3 encouraging safer chemical synthesis is quantified assigning a value, ranging from 1 to 5, to indicate how hazardous a reactant is, with 5 being the most hazardous. This score is determined considering various toxicological effects, including acute toxicity, skin irritation, reproductive toxicology, carcinogenicity, *etc*.

The *aggregate score* is at last the normalized average of the score for each group of principles. However, while the DOZN tool is advantageous as an easy-to-use online resource that provides quantitative assessment, its comprehensive and complex calculation methodology can make it unclear to users what specific modifications to the reaction conditions are needed to improve their scores.

The DOZN tool was used by Colacino and co-worker (*20*) to assess the greenness of mechanochemical process for the synthesis of nitrofurantoin **12**, a World Health Organization (WHO) essential medicine (*107*). More specifically, three mechanochemical batch processes were compared: one performed in a vibrating ball mill, one in a planetary ball mill, and one in a SPEX mill, along with a continuous flow mechanochemical synthesis using TSE technology (*74*,*108*). In turn, the mechanochemical methods were compared with the commercial synthesis in solution (*109*) (**Scheme 3** shows the synthetic path for mechanochemical and solution based synthesis).

The DOZN scores of mechanochemical processes are displayed in **Fig. 7**. Although the aggregate scores for each process are generally good and does not show big differences, in depth analysis on each of different DOZN categories helps to elucidate the main differences for each process. For the first category, *Improved Resource Use* (Group 1 of principles), the higher scores for vibrating and planetary mill are due to the lower yields compared to SPEX mill which mean that a higher mass of waste is



Scheme 3 The mechanochemical pathway to nitrofurantoin **12** (top) (*74*,*108*), and the commercial batch-synthesis in solution (bottom) (*109*).

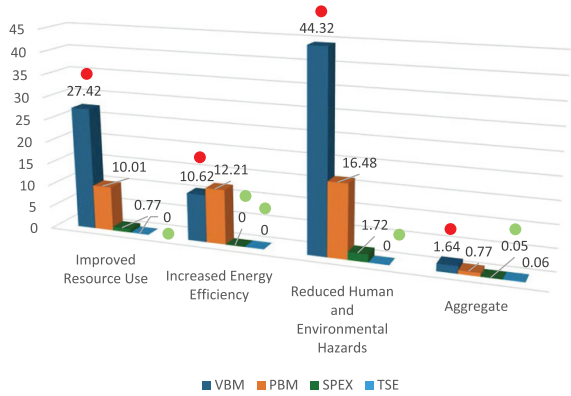


Fig. 7 DOZN score comparison between vibrational ball mill (VBM), planetary ball mill (PBM), SPEX mill (SPEX) and twin-screw extrusion (TSE) mechanochemical processes in the synthesis of nitrofurantoin **12**. Red dots indicate the worst score, while green dots indicate the best ones. Adapted from Ref. (*20*). with the permission of American Chemical Society.

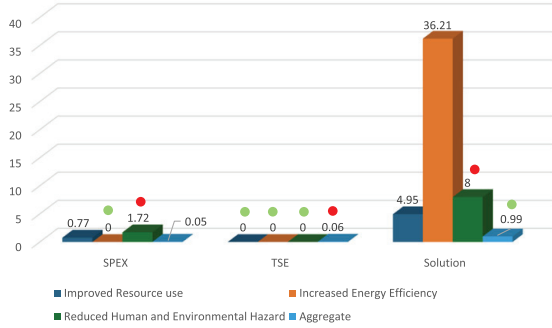


Fig. 8 Data comparison for each of the four DOZN categories between SPEX miller, twin-screw extrusion (TSE) and the standard in solution protocol. Red dots indicate the worst score, while green dots indicate the best ones. Adapted from Ref. (*20*). with the permission of American Chemical Society.

generated (*20*). The second category (Group 2), *Energy Efficiency*, accounts for: i) any deviations of the process from standard conditions, *i.e.*, from pressure and room temperature, and ii) '*time economy*' intended for the reaction to occur and to be worked-up. Therefore, the better scores were obtained for mechanochemical processes in batch (in a SPEX mill) and in continuous (by TSE), for which no work-up was needed. Lastly, the third category (Group 3), *Reduced Human and Environmental Hazard*, shows the biggest difference in scores for all four processes compared. This can be again attributed to amount of waste generated (and their toxicity), also related to the yield. The reaction performed in the vibrating mill delivered a lower yield compared to the other milling devices, thus resulting in a greater waste production and consequently in higher assigned score.

A better productivity (over 15 min) was obtained by TSE (3.47 g) *vs.* SPEX mill (1.49 g). Moreover, the best performing SPEX mill and twin-screw extruder (TSE) were compared to the commercial solution-based batch synthesis, the results for each of the three DOZN categories are shown in **Fig. 8**.

Contributing most to the worst overall scores for the solution-based synthesis is category 2 which is participated by the sole principle 6, *Design for Energy Efficiency*. The worst score in this case is due to the need of using excess of reagents, heating and cooling the reaction, a requirement that is not needed for mechanochemical reactions, but is also linked to a vastly greater energy consumption. For the other two categories, by looking at the scores of each principle, it shows that the solvent-less nature of the mechanochemistry processes greatly affects positively the scores, because far less waste is produced, moreover the waste is further reduced, and the used resources are better implemented as both SPEX mill and TSE do not need work up process to isolate the final product. Resuming, by looking at the DOZN scores, although the aggregate score of 0.99 for the standard solution protocol is not bad, the great advantage of running the mechanochemical alternative lies mostly in the greater energy efficiency in which the differences are sharper and also given the better yield along the simpler reaction protocol which brings advantages in terms of less

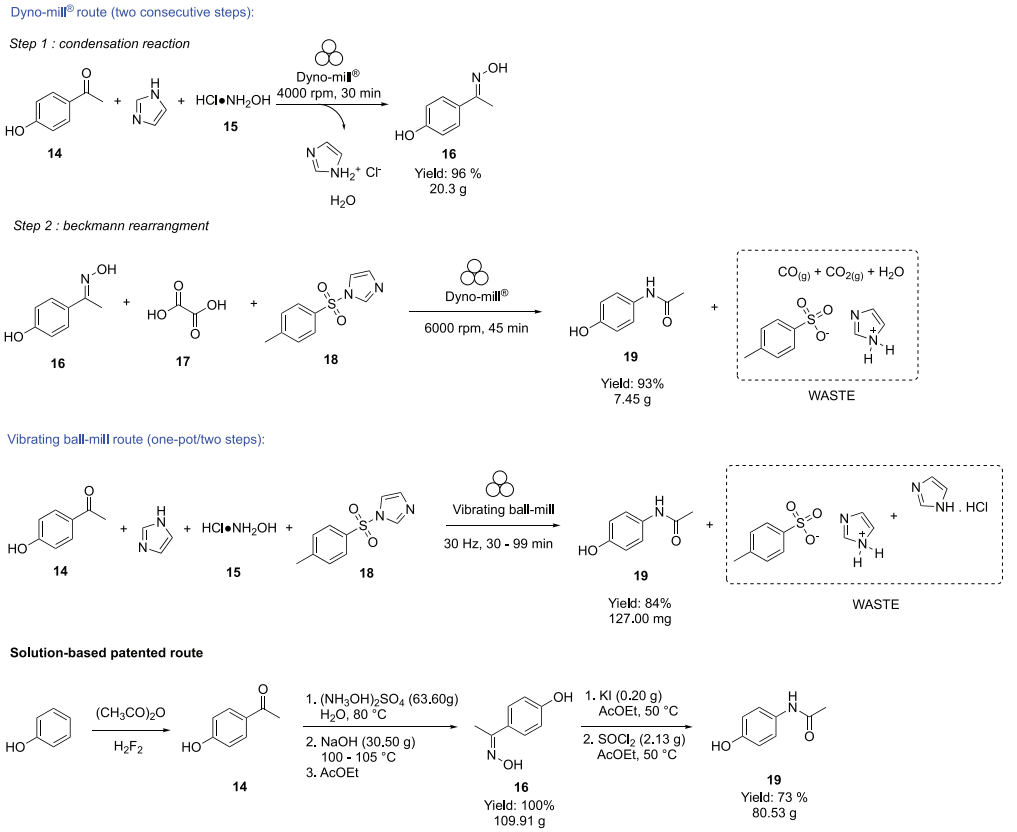
hazards for humans and environment alike. It is thus clear that running the synthesis of nitrofurantoin **12** mechanochemically is greener and easier to perform and consequently also more economically advantageous.

EcoScale

EcoScale is the first toolkit developed to semi-quantitatively assess the sustainability of a reaction protocol (*110*). This web-based software (*111*), equipped with an integrated database of chemicals, uses a system of six parameters to assign a score from 1 to 100. An ideal score of 100 represents a chemical reaction with inexpensive, non-toxic, and environmentally benign reagents, that reaches completion under ambient conditions in a short time, delivering product in quantitative yield. Penalty points are deducted based on how much the analyzed protocol deviates from these ideal expectations.

This toolkit was used to compare four mechanochemical protocols for the synthesis of paracetamol (WHO essential medicine) through Beckmann rearrangement (*112*–*114*), along with the standard solvent-based commercial route (Hoechst-Celanese protocol, referred to as H.-C.) (*115*).

In first place a comparison of synthetic paths that lead from *p*-hydroxyacetophenone (piceol) **14** that passes through condensation with hydroxylamine hydrochloride **15** to give the oxime **16**, then via Beckmann rearrangement to paracetamol **19** (**Scheme 4**) (*112*,*114*). This is suitable for comparison with the commercial route (*115*), which starts with a Friedel-Crafts on phenol to give **14**, then condensation of hydroxylamine to give **16** and then the Beckmann rearrangement to give paracetamol **19**.



Scheme 4 Paracetamol synthetic routes. On the top the mechanochemical protocol that uses the Dyno-mill (*114*), in the middle the mechanochemical protocol that uses the vibrational ball-mill (*112*) and on the bottom the Hoechst-Celanese route (*115*).

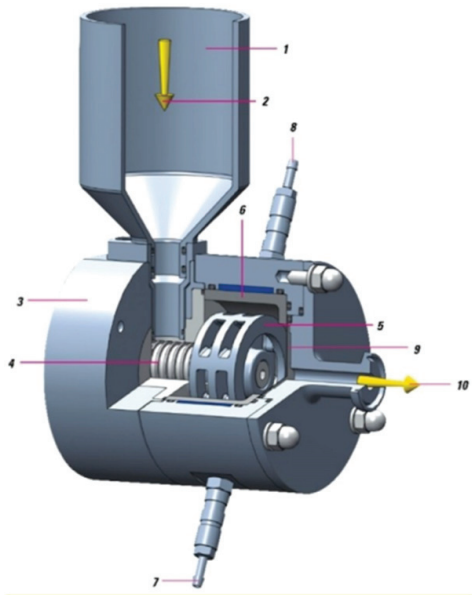


Fig. 9 Schematic representation of a Dyno-mill. 1- Feed hopper, 2 – Product inlet, 3 – Seal housing for lip seal or double mechanical seal, 4 – Screw conveyor, 5 – Dyno-Accelerator, 6 – Coolable grinding container, 7 – Cooling inlet, 8 – Cooling outlet, 9 – Grinding media separator or sieve plate, 10 – Lid outlet. Reproduced from Ref. (*114*). with the permission of John Wiley and Sons.

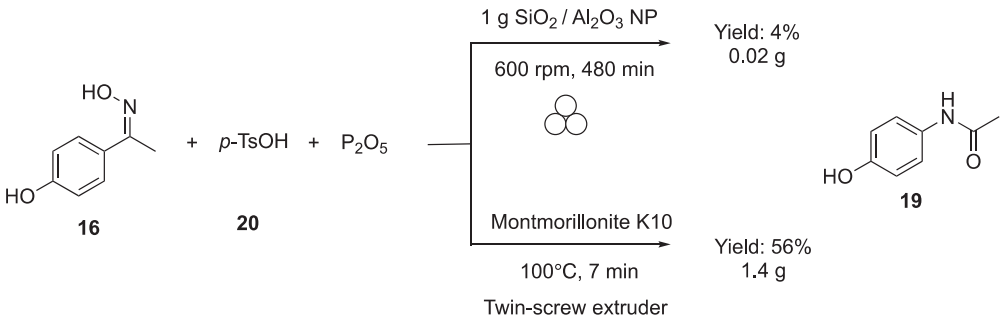
Table 3 EcoScale scores and penalty points for the mechanochemical VBM (*112*) and Dyno-mill (*113*) processes compared with the commercial Hoechst-Celeste route in solution (*115*). Green cells indicate best results, red one's worst results

Entry	Parameters	VBM[112]	Dyno-mill®[114]	H.-C. route[115]
1	Yield	-8	-5	-13
2	Price/availability	-10	-6	-8
3	Safety	-20	-20	-40
4	Technical set-up	0	0	-2
5	Temperature/time	0	0	-7
6	Workup and purification	-10	-1	-7
	EcoScale	52	68	23

Based on the seminal article making use of a vibrational ball mill (*112*), leading to mg-quantities of the target API, the multi-gram scale mechanochemical synthesis of paracetamol **19** was successfully translated in an agitator bead mill (*114*) (the Dyno-mill, **Fig. 9**), operating in batch, semi-continuous or continuous mode, depending on the experimental set-up.

The results for each synthetic pathway are presented in **Table 3**.

As can be seen from **Table 3**, it is clear that the standard solution-based route has the lowest EcoScale score, that is due mainly to lower overall yield and the necessity to use more hazardous and not environmentally friendly chemicals such as thionyl chloride ($SOCl_2$). A point worth to note is the 0 penalty for the parameters 4 and 5 which are typical and intrinsic of a



Scheme 5 Schemes for Beckmann rearrangement protocol in: PBM and by TSE (*113*).

Table 4 EcoScale scores and penalty points for the four mechanochemical protocols (**Schemes 4** and **5**). Green cells indicate best results, red one's worst results

Entry	Parameters	VMB[112]	Dyno-mill®[114]	PBM[113]	TSE[113]
1	Yield	-8	-6	-48	-22
2	Price/availability	-10	-8	-15	-15
3	Safety	0	0	0	0
4	Technical set-up	0	0	0	0
5	Temperature/time	0	0	-1	0
6	Workup and purification	-10	0	-13	-13
	EcoScale	72	86	23	50

mechanochemical protocol, due to the aforementioned simplicity in the setup and the reactions that progress generally faster without the need for thermal excursions.

Following through, the Beckmann rearrangement to paracetamol **19** (*112*,*114*) was also adapted for planetary mill (PBM) (*113*) and twin-screw extrusion (TSE) (*113*) (**Scheme 5**). The green chemistry metrics analysis of the four methods allows for a comparison of the various possibilities that mechanochemistry offers in terms of batch milling methods, different reagents involved, and production scale.

Table 4 makes a comparison among the above-mentioned two-step mechanochemical methods to access paracetamol in batch (by VBM, PBM and Dyno-mill) and in continuous (by Twin screw extrusion). For sake of comparison, only the data for the last step (Beckmann rearrangement) were considered for the Eco-scale calculations.

In this case, the best score of the Dyno-mill protocol can be explained by the overall better yield and process intensification compared to PBM and TSE protocols, with yield dropping at 4% for the reaction performed in PBM.

Life Cycle Assessment

Life cycle assessment (LCA) has been used as a tool to evaluate resource consumption, environmental and human health impacts of various products, also including chemicals. The tool is widely adopted in numerous engineering fields to guide public policy regarding climate change impact. In the chemicals sector it allows to measure the sustainability of process design and calculate the environmental burden of products that rely on specific chemicals throughout their life cycle (*116*). LCA provides a much more comprehensive insight into the environmental footprint of a process compared to the basic green chemistry metrics mentioned

above. However, this level of analysis requires more extensive data collection, making it more practical to use at a later stage of process development and increased production scale, which are promising for industrial implementation.

LCA was applied to the synthesis of nitrofurantoin **12** (**Scheme 3**) comparing two routes according to ISO 14040/44 standards: (*117*–*119*)

(1) Patented solvent-based synthesis (*109*).
(2) Mechanochemical synthesis using twin screw extrusion (*108*).

Firstly, system boundaries were defined (**Fig. 10**) and then life cycle inventory (LCI) was calculated. The former included inputs (energy and materials) to the synthesis of starting materials, the main product, and relevant waste and emissions. Functional unit of said calculations was chosen 1 kg on nitrofurantoin. There were some assumptions made to the system boundaries and life cycle inventory:

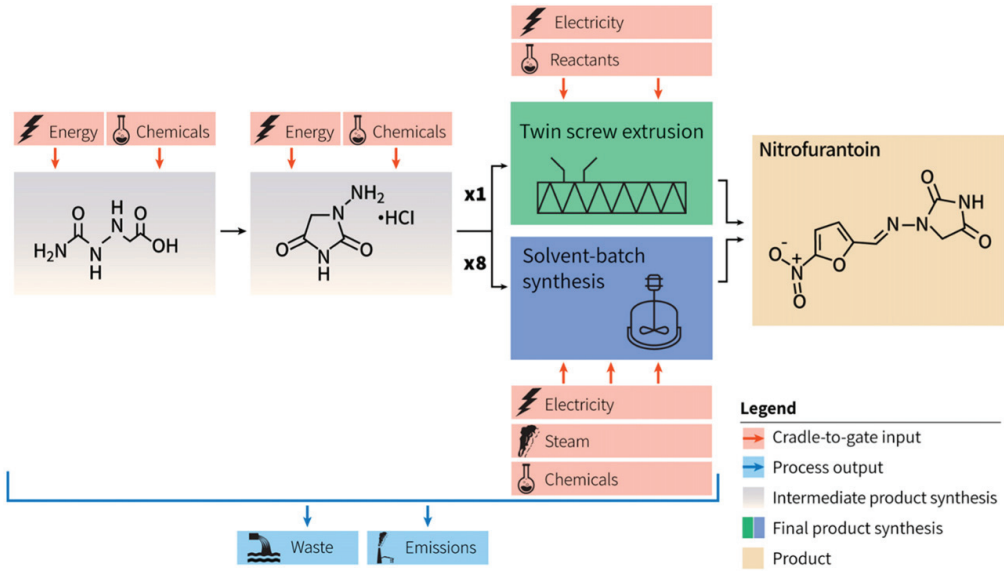


Fig. 10 System boundaries as defined by Galant *et al.*(*119*) Reproduced with the permission of American Chemical Society.

Table 5 Comparison of LCI of 1 kg nitrofurantoin produced through TSE and solvent-based process (*119*).

Mechanochemical process	*Energy requirement/chemicals amount*	*Solvent-based process*	*Energy requirement/chemicals amount*
Input		**Input**	
5-nitrofurfural, kg	0.59	5-nitrofurfural, kg	0.59
1-aminohydantoin hydrochloride, kg	0.64	1-aminohydantoin hydrochloride, kg	5.15
50% NaOH, kg	2.28×10^{-5}	Water, kg	4.47
25% NaOClO, kg	1.45×10^{-4}	30% HCl, kg	0.17
Water, kg	2.85×10^{-5}	50% NaOH	0.08
TSE energyconsumption, kWh	6.61	1% NaOH, kg	4.12
Scrubber energy consumption, kWh	1.19×10^{-4}	Water for purification, kg	10.31
Output		**Output**	
Wastewater for treatment, kg	2×10^{-4}	Wastewater for treatment, kg	19.15
n.a.	n.a.	Electricity, kWh	0.02
n.a.	n.a	Steam, MJ	5.22

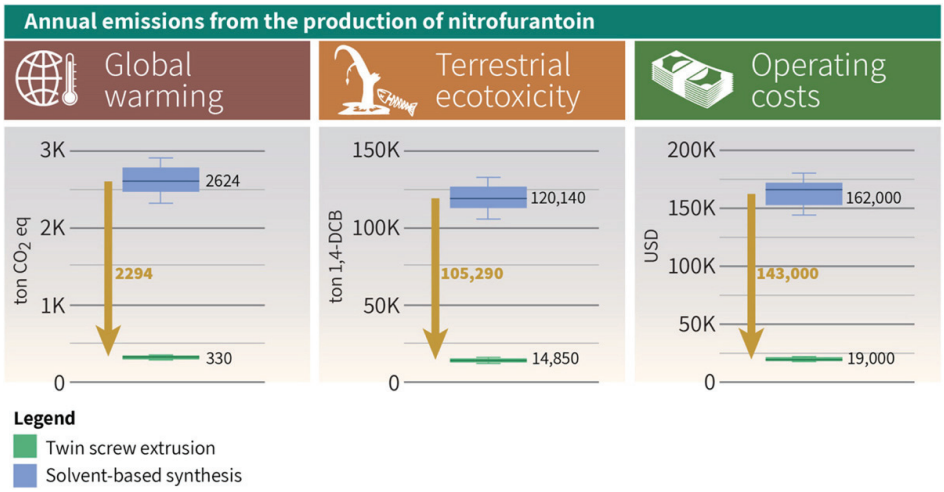


Fig. 11 Annual emissions from the production of nitrofurantoin **12**. Reproduced from Ref. (*119*). with the permission of American Chemical Society.

Table 6 Selected LCIA results for TSE and solvent-based process (*119*).

Environmental impact	*Units*	*TSE*	*Solvent-based*
Global warming	kg CO_2 eq	76	610
Fossil resource scarcity	kg oil eq	24	190
Human non-carcinogenic toxicity	kg 1,4-DCB	81	640
Terrestrial ecotoxicity	kg 1,4-DCB	0.32	2800
Freshwater ecotoxicity	kg 1,4-DCB	31	250
Ionization radiation	kBq Co-60 eq	7.9	56

(1) In transportation stage emissions from the logistics were excluded and it was assumed as the amount of chemicals required for the solvent-based synthesis was higher than in the case of mechanochemical synthesis, the environmental impacts from the solvent-based synthesis should also be higher.
(2) 5-Nitrofurfural environmental impact was omitted since it was absent in Ecoinvent database (*120*) and the amount of 5-nitrofurfural in both synthetic routes is the same. Therefore, it was deemed that relative results would not be affected, only the absolute values would be.
(3) If some materials were used in the processes constantly without replacing, then their contribution to the overall environmental impact was negligible.
(4) Wastewater treatment was omitted, and main waste streams and the quantity of wastewater were reported.

After setting the system boundaries life cycle inventory (LCI) was calculated to evaluate the materials and energy required to produce 1 kg of nitrofurantoin **12**. Already here the potential benefit of twin screw extruder-based process became apparent as the mass and energy flow of the system was remarkably lower than in the case of solvent-based process (**Table 5**).

Then, based on the obtained data, LCA was carried out using SimaPro (*121*) software and ReCiPe 2016 midpoint hierarchist method (*122*) to compare relative environmental impact of the two processes. Global warming, fossil resource scarcity, human non-carcinogenic toxicity, terrestrial ecotoxicity, freshwater ecotoxicity, and ionization radiation were assessed among others (**Fig. 11** and **Table 6**).

As one can see from the **Table 6**, according to *Life Cycle Impact assessment* (LCIA) method, the environmental impact of solvent-based nitrofurantoin synthesis process is an order of magnitude higher than that of twin-screw extrusion-based process in all

categories presented. Therefore, it is safe to say that in the current case mechanochemistry has proven to be far superior method for the chemical processing (*123*).

Conclusions

Mechanochemistry is an age-old technique that has received renewed interest due to its ability to conduct organic reactions with minimal or no solvent use by milling and grinding solid reactants together. This reduced reliance on solvents aligns well with the twelve principles of green chemistry, resulting in decreased environmental impact, enhanced safety, and improved cost-effectiveness. Furthermore, mechanochemical methods offer opportunities to improve the efficiency of valorizing biomass, mineral resources, and waste, thereby enhancing material circularity.

Green chemistry metrics are essential for quantifying and measuring these advantages, providing a scoring system and verifiable indicators aligned with each of the twelve principles. Holistic sustainability assessments can be achieved using respective green chemistry toolkits and, at a more comprehensive level, through life cycle assessment (LCA).

This chapter demonstrated through selected cases of mechanochemical pharma-relevant transformations how various green chemistry metric toolkits (CHEM21, iGAL, DOZN, EcoScale) and LCA analyses showcase the superior greenness of laboratory-scale developments compared to traditional solution-based approaches. The clear advantages of mechanochemistry make it highly appealing as an industrial production method (*124*,*125*), supported by existing mechanochemical instrumentation like twin-screw extruders (TSE), resonant acoustic mixers (RAM), and eccentric mills.

Mechanochemistry holds considerable yet largely untapped potential to revolutionize industrial chemistry, leading to a better environmental footprint. Further development finalized to improve and expand the portfolio of existing synthetic methods, including their adaptation for scaled-up preparations is an ongoing process.

In this context, green chemistry metrics analysis can provide a useful guide to optimize the performance of mechanochemical processes, serving as objective indicators that encourage successful developments and prevent the emergence of hotspots.

Acknowledgments

A.C. is grateful to Campus France and Tallinn Technological University (TalTech) for the PhD fellowship (co-tutelle de thèse France-Estonie). E.C. and A.N. are grateful to Campus France and French-Estonian cooperation Programme Hubert Curien France-Estonia (PHC PARROT 2021–2023). This contribution is mainly based upon work from COST Action CA18112 Mechanochemistry for Sustainable Industry (*126*–*128*), supported by COST (European Cooperation in Science and Technology) a funding agency for research and innovation networks (www.cost.eu). E.C., R.A. and D.K. are also grateful to European Union's Horizon 2021–2027 research and innovation program for the generous funding under grant agreement No 101057286 (IMPACTIVE) (*129*).

References

1. Anastas, P.; Warner, J. Green Chemistry: Theory and Practice. **1998**, New York: Oxford University Press.
2. OECD Workshop on Sustainable Chemistry. Sustainable Chemistry – Definition & Statement; **1999**. Available at: https://iupac.org/who-we-are/committees/sustainable-chemistry/#:~:text=Sustainable%20chemistry%20is%20the%20design,human%20health%20and%20the%20environment. (accessed 15 July, 2024)
3. Tundo, P.; Anastas, P.; Black, D.St.C.; *et al.* Pure Appl. Chem. **2000**, *72*, 1207–1228.
4. Horie, K.; Barón, M.; Fox, R.B.; *et al.* Pure Appl. Chem. **2004**, *76*, 889–906.
5. Ferguson, M.; Moyano, M.S.; Tribello, G.A.; *et al.* Chem. Sci. **2019**, *10*, 2924–2929.
6. Baláž, P.; Achimovičová, M.; Baláž, M.; *et al.* Chem. Soc. Rev. **2013**, *42*, 7571–7637.
7. Xu, C.; De, S.; Balu, A.M.; Ojeda, M.; Luque, R. Chem. Commun. **2015**, *51*, 6698–6713.
8. Gomollón-Bel, F. Chem. Int. **2019**, *41*, 12–17.
9. Do, J.-L.; Friščić, T. Synlett **2017**, *28*, 2066–2092.
10. Fantozzi, N.; Volle, J.-N.; Porcheddu, A.; *et al.* Chem. Soc. Rev. **2023**, *52*, 6680–6714.
11. Cuccu, F.; De Luca, L.; Delogu, F.; *et al.* ChemSusChem **2022**, *15*, e202200362.
12. Howard, J.L.; Cao, Q.; Browne, D.L. Chem. Sci. **2018**, *9*, 3080–3094.
13. Braga, D.; Maini, L.; Grepioni, F. Chem. Soc. Rev. **2013**, *42*, 7638–7648.
14. Friščić, T. Chem. Soc. Rev. **2012**, *41*, 3493–3510.
15. Cova, C.M.; Luque, R. BMC Chem. Eng. **2019**, *1*, 16.
16. Margetić, D.; Štrukil, V. Mechanochemical Organic Synthesis. **2016**, Elsevier.
17. Tan, D.; Loots, L.; Friščić, T. Chem. Commun. **2016**, *52*, 7760–7781.
18. Colacino, E.; Isoni, V.; Crawford, D.; García, F. Trends Chem. **2021**, *3*, 335–339.
19. Ardila-Fierro, K.J.; Hernández, J.G. ChemSusChem **2021**, *14*, 2145–2162.
20. Sharma, P.; Vetter, C.; Ponnusamy, E.; Colacino, E. ACS Sustain. Chem. Eng. **2022**, *10*, 5110–5116.
21. Reynes, J.F.; Isoni, V.; García, F. Ange. Chem. Int. Ed. **2023**, *62*, e202300819.
22. Colacino, E.; Carta, M.; Pia, G.; *et al.* ACS Omega **2018**, *3*, 9196–9209.
23. Hwang, S.; Grätz, S.; Borchardt, L. Chem. Commun. **2022**, *58*, 1661–1671.
24. For an example of eccentric vibrating mills, please see: https://www.siebtechnik-tema.com/eccentric-vibrating-mills/ (accessed July 15, 2024).

25. For an application of eccentric vibrating mills, please see: Bodach, A.; Portet, A; Winkelmann, F. *et al.* ChemSusChem **2024**, *17*, e202301220.
26. For an example of bead-mill technology, please see: https://www.wab-group.com/en/products/dyno-mill-ubm/ (accessed, July 15, 2024)
27. For an application of bead-mill, please see: Geib, R.; Colacino, E; Gremaud, L. ChemSusChem **2024**, *17*, e202301921.
28. Bolt, R.R.A.; Leitch, J.A.; Jones, A.C.; Nicholson, W.I.; Browne, D.L. Chem. Soc. Rev. **2022**, *51*, 4243–4260.
29. Gonnet, L.; Lennox, C.B.; Do, J.; *et al.* Angew. Chem. Int. Ed. **2022**, *61*, e202115030.
30. Bowmaker, G.A. Chem. Commun. **2013**, *49*, 334–348.
31. Hutchings, B.P.; Crawford, D.E.; Gao, L.; Hu, P.; James, S.L. Angew. Chem. Int. Ed. **2017**, *56*, 15252–15256.
32. Henderson, R.K.; Jiménez-González, C.; Constable, D.J.C.; *et al.* Green Chem. **2011**, *13*, 854–862.
33. Jimenez-Gonzalez, C.; Ponder, C.S.; Broxterman, Q.B.; Manley, J.B. Org. Process Res. Dev. **2011**, *15*, 912–917.
34. Sheldon, R.A.; Arends, I.W.C.E.; Hanefeld, U. Wiley-VCH verlarg GmbH & co. Green Chemistry & Catalysis. **2007**, Germany: KGaA Weiheim.
35. Roschangar, F.; Sheldon, R.A.; Senanayake, C.H. Green Chem. **2015**, *17*, 752–768.
36. Trost, B. Science **1991**, *254*, 1471–1477.
37. Curzons, A.D.; Mortimer, D.N.; Constable, D.J.C.; Cunningham, V.L. Green Chem. **2001**, *3*, 1–6.
38. Wang, W.; Lü, J.; Zhang, L.; Li, Z. Front. Chem. Sci. Eng. **2011**, *5*, 349–354.
39. Dalidovich, T.; Mishra, K.A.; Shalima, T.; *et al.* ACS Sustain. Chem. Eng. **2020**, *8*, 15703–15715.
40. Konnert, L.; Gauliard, A.; Lamaty, F.; Martinez, J.; Colacino, E. ACS Sustain. Chem. Eng. **2013**, *1*, 1186–1191.
41. Bolm, C.; Mocci, R.; Schumacher, C.; *et al.* Angew. Chem. Int. Ed. **2018**, *57*, 2423–2426.
42. Métro, T.-X.; Bonnamour, J.; Reidon, T.; *et al.* Chem. Commun. **2012**, *48*, 11781–11783.
43. Lanzillotto, M.; Konnert, L.; Lamaty, F.; Martinez, J.; Colacino, E. ACS Sustain. Chem. Eng. **2015**, *3*, 2882–2889.
44. Gonnet, L.; Tintillier, T.; Venturini, N.; *et al.* ACS Sustain. Chem. Eng. **2017**, *5*, 2936–2941.
45. Porcheddu, A.; Delogu, F.; De Luca, L.; Colacino, E. ACS Sustain. Chem. Eng. **2019**, *14*, 12044–12051. 7.
46. Nikonovich, T.; Jarg, T.; Martõnova, J.; *et al.* RSC Mechanochemistry **2024**, *1*, 189–195.
47. Egorova, K.S.; Ananikov, V.P. Organometallics **2017**, *36*, 4071–4090.
48. Kubota, K.; Pang, Y.; Miura, A.; Ito, H. Science **2019**, *366*, 1500–1504.
49. Schumacher, C.; Hernández, J.G.; Bolm, C. Angew. Chem. Int. Ed. **2020**, *59*, 16357–16360.
50. Kubota, K.; Jiang, J.; Kamakura, Y.; *et al.* J. Am. Chem. Soc. **2024**, *146*, 1062–1070.
51. Konnert, L.; Dimassi, M.; Gonnet, L.; *et al.* RSC Adv. **2016**, *6*, 36978–36986.
52. Kondo, K.; Kubota, K.; Ito, H. Chem. Sci. **2024**, *15*, 4452–4457.
53. Patra, S.; Nandasana, B.N.; Valsamidou, V.; Katayev, D. Adv. Sci. **2024**, *11*, 2402970.
54. Mkrtchyan, S.; Purohit, V.B.; Zapletal, J.; Shalimov, O.O.; Iaroshenko, V.O. ACS Sustain. Chem. Eng. **2024**, *12*, 1–9.
55. Prat, D.; Wells, A.; Hayler, J.; *et al.* Green Chem. **2016**, *18*, 288–296.
56. Sabatini, M.T.; Boulton, Lee T.; Sneddon, H.F.; Sheppard, T.D. Nat. Catal. **2019**, *2*, 10–17.
57. Sherwood, J.; Albericio, F.; de la Torre, B.G. ChemSusChem **2024**, *17*, e202301639.
58. EPA Press Office. Biden-Harris Administration Finalizes Ban on Most Uses of Methylene Chloride, Protecting Workers and Communities from Fatal Exposure; **2024**.
59. Pétry, N.; Benakki, H.; Clot, E.; *et al.* Beilstein J. Org. Chem. **2017**, *13*, 2169–2178.
60. Porte, V.; Thioloy, M.; Pigoux, T.; *et al.* Eur. J. Org. Chem. **2016**, *2016*, 3505–3508.
61. Pladevall, B.S.; de Aguirre, A.; Maseras, F. ChemSusChem **2021**, *14*, 2763–2768.
62. Stolar, T.; Alić, J.; Talajić, G.; *et al.* Chem. Commun. **2023**, *59*, 13490–13493.
63. Politov, A.; Golyazimova, O. Faraday Discuss. **2014**, *170*, 345–356.
64. Han, G.-F.; Li, F.; Chen, Z.-W.; *et al.* Nat. Nanotechnol. **2021**, *16*, 325–330.
65. Reichle, S.; Felderhoff, M.; Schüth, F. Angew. Chem. Int. Ed. **2021**, *60*, 26385–26389.
66. Schneider, F.; Szuppa, T.; Stolle, A.; Ondruschka, B.; Hopf, H. Green Chem. **2009**, *11*, 1894–1899.
67. Shen, F.; Xiong, X.; Fu, J.; *et al.* Renew. Sustain. Energy Rev. **2020**, *130*, 109944.
68. Hajiali, F.; Jin, T.; Yang, G.; *et al.* ChemSusChem **2022**, *15*, e202102535.
69. Gaudino, E.Calcio; Cravotto, G.; Manzoli, M.; Tabasso, S. Chem. Soc. Rev. **2021**, *50*, 1785–1812.
70. Nallaparaju, J.V.; Satsi, R.; Merzhyievskyi, D.; *et al.* Angew. Chem. Int. Ed. **2024**, *63*, e202319449.
71. Kaabel, S.; Stein, R.S.; Fomitšenko, M.; *et al.* Angew. Chem. Int. Ed. **2019**, *58*, 6230–6234.
72. Yin, J.; Stark, R.T.; Fallis, I.A.; Browne, D.L. J. Org. Chem. **2020**, *85*, 2347–2354.
73. Varma Nallaparaju, J.; Nikonovich, T.; Jarg, T.; *et al.* Angew. Chem. Int. Ed. **2023**, *62*, e202305775.
74. Colacino, E.; Porcheddu, A.; Halasz, I.; *et al.* Green Chem. **2018**, *20*, 2973–2977.
75. Patel, C.; André-Joyaux, E.; Leitch, J.A.; *et al.* Science **2023**, *381*, 302–306.
76. Porcheddu, A.; Colacino, E.; De Luca, L.; Delogu, F. ACS Catal. **2020**, *10*, 8344–8394.
77. Williams, M.T.J.; Morrill, L.C.; Browne, D.L. ChemSusChem **2022**, *15*, e202102157.
78. Haley, R.A.; Mack, J.; Guan, H. Inorg. Chem. Front. **2017**, *4*, 52–55.
79. Pickhardt, W.; Grätz, S.; Borchardt, L. Chem. Eur. J. **2020**, *26*, 12903–12911.
80. Lennox, C.B.; Borchers, T.H.; Gonnet, L.; *et al.* Chem. Sci. **2023**, *14*, 7475–7481.
81. Chantrain, V.; Rensch, T.; Pickhardt, W.; Grätz, S.; Borchardt, L. Chem. Eur. J. **2024**, *30*, e202304060. https://doi.org/10.1002/chem.202304060.
82. Lee, H.W.; Yoo, K.; Borchardt, L.; Kim, J.G. Green Chem. **2024**, *26*, 2087–2093.
83. Kaabel, S.; Therien, J.P.D.; Deschênes, C.E.; *et al.* Proc. Nat. Acad. Sci. **2021**, *118*, e2026452118. 29.
84. Rowlands, S.A.; Hall, A.K.; McCormick, P.G.; *et al.* Nature **1994**, *367*. 223–223.
85. Birke, V.; Schütt, C.; Burmeier, H.; Ruck, W. Fresenius Environ. Bull. **2011**, *20*, 2794–2805.
86. Zhang, K.; Huang, J.; Yu, G.; *et al.* Environ. Sci. Technol. **2013**, *47*, 6471–6477.
87. Kaiser, R.P.; Krake, E.F.; Backer, L.; *et al.* Chem. Commun. **2021**, *57*, 11956–11959.
88. Michalchuk, A.A.L.; Emmerling, F. *Angew. Chem. Int. Ed.* **2022**, *61*, e202117270; Angew. Chem. **2022**, *134*, e202117270.
89. Ardila-Fierro, K.J.; Hernández, J.G. Angew. Chem. Int. Ed. **2024**, *63*, e202317638.
90. Friščić, T.; Halasz, I.; Beldon, P.J.; *et al.* Nat. Chem. **2013**, *5*, 66–73.
91. Lukin, S.; Užarević, K.; Halasz, I. Nat. Protoc. **2021**, *16*, 3492–3521.
92. d'Anciães, I.; Silva, A.; Bartalucci, E.; Bolm, C.; Wiegand, T. Adv. Mater. **2023**, *35*. 2304092.
93. Priestley, I.; Battilocchio, C.; Iosub, A.V.; *et al.* Org. Process. Res. Dev. **2023**, *27*, 269–275.
94. Vilaivan, T. ACS Chem. Health Saf. **2022**, *29*, 132–134.
95. Beckel, E.; Oyler, K.; Mehta, N.; *et al.* Propellants Explos. Pyrotech. **2021**, *46*, 697–704.
96. McElroy, C.R.; Constantinou, A.; Jones, L.C.; Summerton, L.; Clark, J.H. Green Chem. **2015**, *17*, 3111–3121.
97. El-Faham, A.; Albericio, F. J. Pept. Sci. **2010**, *16*, 6–9.

98. Sperry, J.B.; Minteer, C.J.; Tao, J.; *et al.* Org. Proc. Res. Dev. **2018**, *22*, 1262–1275.
99. Graham, J.C.; Trejo-Martin, A.; Chilton, M.L.; *et al.* Chem. Res. Toxicol. **2022**, *35*, 1011–1022.
100. Cyniak, J.S.; Kasprzak, A. RSC Adv. **2024**, *14*, 13227–13236.
101. Roschangar, F.; Zhou, Y.; Constable, D.J.C.; *et al.* Green Chem. **2018**, *20*, 2206–2211.
102. Roschangar, F.; Li, J.; Zhou, Y.; *et al.* ACS Sustain. Chem. Eng. **2022**, *10*, 5148–5162.
103. Green Chemistry Innovation Scorecard Calculator, https://www.acs.org/greenchemistry/research-innovation/tools-for-green-chemistry/green-chemistry-innovation-scorecard-calculator.html (accessed 15 July, 2024)
104. Liu, Y.-F.; Wang, C.-L.; Bai, Y.-J.; *et al.* Org. Proc. Res. Dev. **2008**, *12*, 490–495.
105. Gaich, T.; Baran, P.S. J. Org. Chem. **2010**, *75*, 4657–4673.
106. DeVierno Kreuder, A.; House-Knight, T.; Whitford, J.; *et al.* ACS Sustain. Chem. Eng. **2017**, *5*, 2927–2935.
107. World Health Organization. Model List of Essential Medicines – 23rd List; **2023**.
108. Crawford, D.E.; Porcheddu, A.; McCalmont, A.S.; *et al.* ACS Sustain. Chem. Eng. **2020**, *8*, 12230–12238.
109. Li, X.; Zhang, F. Method for Preparing and Refining Nitrofurantoin; **2009**, CN101450941
110. Van Aken, K.; Strekowski, L.; Patiny, L. Beilstein J. Org. Chem. **2006**, *2*, 3.
111. EcoScale, https://ecoscale.cheminfo.org (accessed 15 July, 2024)
112. Mocci, R.; Colacino, E.; Luca, L.De; *et al.* ACS Sustain. Chem. Eng. **2021**, *9*, 2100–2114.
113. Baier, D.M.; Rensch, T.; Dobreva, D.; *et al.* Chem. Methods **2023**, *3*, e202200058.
114. Geib, R.; Colacino, E.; Gremaud, L. ChemSusChem. **2024**, e202301921.
115. Fritch, J.R.; Fruchey, O.S.; Horlenko, T. USPTO **1990**, *4954652*.
116. Parvatker, A.G.; Eckelman, M.J. ACS Sustain. Chem. Eng. **2019**, *7*, 350–367.
117. EN ISO 14040:2006/A1:2020. International Organization For Standardization: Geneva, **2020**.
118. EN ISO 14044:2006/A1:2020, International Organization For Standardization: Geneva, **2020**.
119. Galant, O.; Cerfeda, G.; McCalmont, A.S.; *et al.* ACS Sustain. Chem. Eng. **2022**, *10*, 1430–1439.
120. Wernet, G.; Bauer, C.; Steubing, B.; *et al.* Int. J. Life Cycle Assess. **2016**, *21*, 1218–1230.
121. SimaPro, 9.0.0.49, Pre Consultants: The Netherlands.
122. Huijbregts, M.A.J.; Steinmann, Z.J.N.; Elshout, P.M.F.; *et al.* Int. J. Life Cycle Assess. **2017**, *22*, 138–147.
123. Lim, X. C.&E.N. **2020**, *98* (38).
124. Gomollón-Bel, F. ACS Cent. Sci. **2022**, *8*, 1474–1476.
125. Gomollón-Bel, C.F. C&EN Glob. Enterp. **2022**, *100*, 21–22.
126. For more information on COST Action CA18112'Mechanochemistry for Sustainable Industry': http://www.mechsustind.eu/ (accessed July 24, 2024).
127. Hernández, G.; Halasz, I.; Crawford, D.E.; *et al.* Eur. J. Org. Chem.. **2020**, 8–9.
128. Baláž, M.; Vella-Zarb, L.; Hernández, J.G.; *et al.* Chem. Today **2019**, *37*, 32–34.
129. For more information on Horizon Europe. Innovative Mechanochemical Processes to synthesize green ACTIVE pharmaceutical ingredients (IMPACTIVE). Available at: https://mechanochemistry.eu/ (accessed: July 24, 2024).

Appendix 5

Publication V

A. Casagrande, C. M. Chatzigiannis, K.-i. Otake, J. Vezzani, A. Niidu, E. Colacino. Scalable Amidation Reaction by Resonant Acoustic Mixing: Application to the Multi-Gram Scale Synthesis of Marketed Agrochemicals. **2026**, *submitted to a peer-reviewed journal*.

10 November 2026

Scalable Amidation Reaction by Resonant Acoustic Mixing. Application to the multi-gram scale synthesis of marketed Agrochemicals

Andrea Casagrande[1,2], Christos M. Chatzigiannis[1], Ken-ichi Otake[3], Joris Vezzani[1], Allan Niidu[2], Evelina Colacino[1]

1. ICGM, ENSCM
2. Virumaa College, Tallinn's University of Technology
3. Kitagawa Laboratory, Kyoto University

Abstract

Industrial amide bond formation in agrochemical manufacture still relies on low-molecularweight chlorinating agents and dipolar aprotic solvents. Herein, five marketed SDHI fungicides, Fenfuram (1), Boscalid (2), Mepronil (3), Flutolanil (4) and Fluxapyroxad (5), were prepared by TCFH-mediated one-pot/two-step amidation across three mechanochemical platforms (VBM, PBM and LA-RAM). The optimal reaction environment proved platform-dependent: ball-milling favoured solid K2HPO4, whereas LA-RAM required liquid N-methylimidazole acting as both base and grinding liquid, and added grinding media (GA-RAM) lowered the yield through degradation of the activated acyl intermediate. LA-RAM was the most efficient and most readily scalable platform, delivering 1–5 in 67–99% yield on a 93 mmol scale (up to 34.9 g per batch, a 160-fold scale-up) at room temperature in 2.5 h at η # 0.2 μL mg-1 of ethyl acetate, without re-optimisation. HR-PXRD and microED confirmed the crystalline forms for agrochemicals 2, 4 and 5, and gave the first structures of 1 and 3. DOZN™ 3.0 and CHEM21 assessments showed reduced waste, elimination of POCl3, oxalyl chloride, DMF and CH2Cl2, and PMI halved for 4 (24.5 vs 50.4).

Posted on 10 November 2026 — CC-BY 4.0 — This is a preprint and has not been peer reviewed. Data may be preliminary. — https://doi.org/10.26434/chemrxiv.15011959/v1

Scalable Amidation Reaction by Resonant Acoustic Mixing. Application to the multi-gram scale synthesis of marketed Agrochemicals

Andrea Casagrande,[a,b] Christos M. Chatzigiannis,[a] Ken-ichi Otake,[c] Joris Vezzani,[a] Allan Niidu[b] and Evelina Colacino[a,*]

[a]ICGM, Univ. Montpellier, CNRS, ENSCM, 34293 Montpellier, France. *E-mail : evelina.colacino@umontpellier.fr

[b]Virumaa College, Tallinn's University of Technology, Ehitajate tee 5, 19086, Tallinn, Estonia

[c] Institute for Integrated Cell-Material Sciences (iCeMS), Kyoto University, Kitagawa Laboratory, iCeMS Research Bldg., 2F, Yoshida-Honmachi, Sakyo-ku, Kyoto, 606-8501, Japan

Abstract

Industrial amide bond formation in agrochemical manufacture still relies on low-molecular-weight chlorinating agents and dipolar aprotic solvents. Herein, five marketed SDHI fungicides, Fenfuram (**1**), Boscalid (**2**), Mepronil (**3**), Flutolanil (**4**) and Fluxapyroxad (**5**), were prepared by TCFH-mediated one-pot/two-step amidation across three mechanochemical platforms (VBM, PBM and LA-RAM). The optimal reaction environment proved platform-dependent: ball-milling favoured solid K_2HPO_4, whereas LA-RAM required liquid *N*-methylimidazole acting as both base and grinding liquid, and added grinding media (GA-RAM) lowered the yield through degradation of the activated acyl intermediate. LA-RAM was the most efficient and most readily scalable platform, delivering **1**–**5** in 67–99% yield on a 93 mmol scale (up to 34.9 g per batch, a 160-fold scale-up) at room temperature in 2.5 h at $\eta \leq 0.2$ μL mg^{-1} of ethyl acetate, without re-optimisation. HR-PXRD and microED confirmed the crystalline forms for agrochemicals **2**, **4** and **5**, and gave the first structures of **1** and **3**. DOZN™ 3.0 and CHEM21 assessments showed reduced waste, elimination of $POCl_3$, oxalyl chloride, DMF and CH_2Cl_2, and PMI halved for **4** (24.5 *vs* 50.4).

Introduction

Among the many reactions employed in modern chemical manufacturing, amide bond construction remains one of the most important.[1] Its significance arises from its broad utility in organic synthesis and materials science,[2] as well as its central role in medicinal chemistry,[3] pharmaceutical manufacturing,[4] and the preparation of agrochemical products used for crop protection.[5] Considering the steady growth of the global agrochemicals market,[6-8] driven by the demand for increased agricultural productivity amid shrinking arable land and a growing global

population,[9] and changes in regulation,[10] the development of more sustainable practices to access marketed active ingredients for crop protection is a societal and an economic need.

From a sustainability standpoint, amidation reactions under mechanochemical processing have gained increasing attention,[11, 12] in alternative to established methodologies in solution. Indeed, mechanochemical methods, when properly designed, brings a significantly improved environmental footprint,[13, 14] and they represent a great promise to reduce dependence on energy-intensive operations,[15, 16] and lower waste generation in solvent-free (or low-solvent) processing conditions. Such advantages (not exhaustively listed) position mechanochemical processes among the strategies most consistent with contemporary goals for sustainable innovation (aligning with the Safe and Sustainable by Design, SSbD framework) and responsible chemistry.[17, 18] Nevertheless, mechanochemical methods relying on resonant acoustic mixing (RAM) to amide bond formation has remained, to the best of our knowledge, limited and mostly confined to the preparation peptides on Rink amide solid support,[19] or solvent-less,[20] using a carbodiimide (DIC or EDCI) as coupling agent in the presence of the additive Oxyma.

The mechanochemical synthesis by ball-milling of Fenfuram (**1**)[21] and Boscalid (**2**)[22] was previously described, respectively by direct amidation of esters[21] or by using acyl chloride and an organic base[23] (Figure 1). We recently reported the mechanochemical synthesis by ball-milling of marketed agrochemicals such as Mepronil (**3**), Flutolanil (**4**) and Fluxapyroxad (**5**), mediated by 1,1'-oxalyldiimidazole (ODI), allowing the amide bond formation from deactivated acids, when similar commonly used coupling agents such as 1,1'-carbonyldiimidazole (CDI) failed or underperformed.[24] Agrochemicals **1-5** belong to Succinate Dehydrogenase Inhibitor (SDHI) fungicides, representing a fast-growing sub-segment within the broader agrochemical market, particularly in the fungicide category of phytopharmaceuticals.[7, 8, 25]

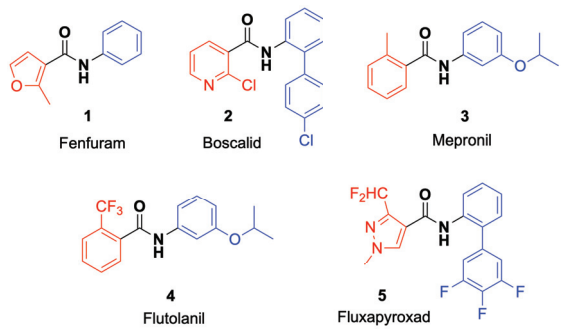


Figure 1. Marketed SDHI fungicides prepared by ball-milling and by RAM, selected for this work.

Considering the commercial value of SDHI fungicides, we report herein the development of more sustainable, multigram-scale preparation of such an important class of phyto-pharmaceuticals **1-5** using mechanochemical processing conditions by Liquid-assisted resonant acoustic mixing (LA-RAM), with a particular emphasis on amide bond formation mediated by *N,N,N',N'*-tetramethylchloroformamidinium hexafluorophosphate (TCFH) as coupling agent.[26] Previously used for the mechanochemical preparation by ball-milling of amides[27] and in substitution reactions on alcohols,[28] at laboratory scale, its efficiency and performance at scale, by RAM was never explored so far.

Herein, scalability was investigated up to 128 mmol and the results were systematically assessed against those achieved by vibrating ball-mill (VBM) and planetary ball-mill (PBM) and towards the LA-RAM amidation reaction mediated by EDCl/Oxyme,[19, 20] published during the preparation of this manuscript. CHEM21[29] and DOZN^{TM} 3.0[30-32] green chemistry tools confirmed a promising overall environmental performance for mechanochemical methods, in comparison with previously published procedures in solution.

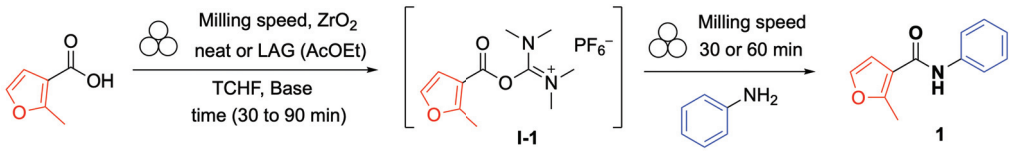
Moreover, X-ray powder diffraction (PXRD) and Microcrystal Electron Diffraction (microED) analyses showed that, for Boscalid (2), Flutolanil (**4**) and Fluxapyroxad (**5**), the same crystalline structures as the marketed phytopharmaceuticals were obtained. For Fenfuram (**1**) and Mepronil (**3**), the crystalline structure was never disclosed so far, and it is reported here for the first time.

Results and discussion

Ball-milling syntheses of phytopharmaceuticals 1-5. Preliminary experiments focused on the mechanochemical synthesis of Fenfuram (**1**) selected as benchmark.

Following the one-pot/two-step TCFH-mediated amidation previously reported,[27] selected chemical (*e.g.,* type of base, neat milling or in liquid-assisted grinding, LAG, conditions), technical (*e.g.*, type of ball-mill - VBM or PBM - milling jar volume and shape) and process (*e.g.*, milling speed at 30 or 50 *Hz* and 500 rpm) parameters were initially investigated at small scale by VBM (10 mL jar, 0.48 mmol scale), using zirconium oxide as milling media. Then, PBM was used for a 4-fold scale-up (1.92 mmol scale) in 45 mL jars (Table 1).

Table 1. Selected mechanochemical conditions for the synthesis of Fenfuram (**1**) by ball-milling (VBM and PBM) at different scales.[a]



Entry	Type of Mill	Jar volume (mL) / Speed	Time (min)		Yield (%)
			Step 1	Step 2	
1	VBM - MM400	10 / 30 Hz	60	60	64
2		10 / 30 Hz	90	60	31
3		10 / 30 Hz	60	30	**78**
4		10 / 30 Hz	30	30	48
5[b]		10 / 30 Hz	60	60	45
6		10 / 30 Hz	60	90	60
7	VBM - P23	10 / 30 Hz	60	60	57
8		10 / 50 Hz	60	60	33
9	PBM - P7P	45 / 500 rpm	60	60	**84**
10		45 / 500 rpm	60	90	57

[a] All the reactions were conducted in zirconium oxide jars of the specified volume, using AcOEt as LAG solvent (η = 0.2 mL/mg) and K_2HPO_4 (3.0 equiv.) as a base, except when otherwise specified. The detailed mechanochemical reaction conditions are described in ESI: Method A1 (for entries 1-5), Method A2 (for entries 6 and 7), and Method B (for entry 8); [b] the base was *N*-methylimidazole (NMI, 3.0 equiv.) in neat grinding conditions.

A first set of experiments (entry 1-4) aimed to investigate the reaction time for each individual step. At a milling speed of 30 *Hz*, using TCFH as coupling agent, dipotassium phosphate (K_2HPO_4, 3.0 equiv.) as a base, and AcOEt as LAG solvent (h = 0.2 mL/mg), the best results were obtained for shorter milling times for both steps, during 60 min and 30 min respectively (entry 4). Longer milling times (for both steps) gave lower yields suggesting a possible degradation of the intermediate **I-1**, especially after step 1 (entry 2). By decreasing the reaction time for both steps (entry 4), the yield dropped, most probably due to a limited amount of intermediate I-1 formed after the first step, due to an incomplete conversion of the starting acid.

Additional experiments investigated the effect of extending Step 2 to 90 min (entries 6 and 10 for VBM and PBM, respectively) while maintaining Step 1 at 60 min. Under VBM conditions (30 Hz), **1** was isolated in 60% yield, compared with 64% and

78% when step 2 lasted 60 and 30 min, respectively. Under PBM conditions (500 rpm), extending Step 2 from 60 to 90 min decreased the isolated yield from 84% to 57%. Prolonged milling during step 2 therefore provided no improvement under the conditions examined.

The effect of the base was also investigated. Previous findings, both in solution[33] and by milling[27] showed that N-methylimidazole (NMI, a liquid) proved to be equally effective than K_2HPO_4 (a solid) for the TCFH-mediated amidation reaction. Therefore, the reaction was repeated using NMI instead. Being a liquid, it can act at the same time as base and as LAG solvent, which made not necessary the addition of AcOEt, used in the experiments involving solid K_2HPO_4 (entry 5). Whether the amount of NMI used for the experiment (3.0 equiv., 142.8 mL) is accounted in the calculation of the 'η value' or not, the reaction can still be classified as mechanochemical,[34] with $0.34 < \eta < 0.54$ mL/mg respectively. However, Fenfuram (**1**) was obtained in a lower 45% yield (entry 5 vs entry 1), probably due to an unfavourable rheology of the reaction, possibly because the combined presence of liquid NMI and aniline produced a more fluid mixture that dampened ball impacts during the second step, rather than the chemical interactions between the base and other reagents, especially since NMI is typically employed to enhance the performance of TCFH.[27, 33]

While jar geometry (cylindrical *vs* egg-shaped), affecting the way forces are applied to the reaction mixture,[35-37] seemed not to have a relevant influence on the reaction outcome at the same milling speed and reaction conditions (entry 1 *vs* entry 7), processing parameters such as the milling speed proceed to be crucial (entry 7 vs entry 8), with a drop in yield (33%) when the reaction was conducted at 50 Hz. The higher frequency results in more frequent impacts within the same timeframe, increasing the likelihood of degradation of the active intermediate **I-1**, somehow confirming previous observations (entry 2) on its stability under milling.

These selected reactivity studies (entries 1-10) were functional towards the implementation of the reaction in the planetary ball-mill (entry 9) at a 4-fold scale (1.92 mmol), leading Fenfuram (**1**) in an 84% yield after the first trial (*c.f.*, Method B, ESI), with no further optimisation needed.

Having identified the optimal reaction and processing conditions for the synthesis of Fenfuram (**1**), the scope of the TCFH-mediated amidation methodology was extended to the preparation of phytopharmaceuticals **2–5**. The target compounds were synthesized using both vibrational ball milling (VBM) and 4-fold upscaled by planetary ball milling (PBM) to evaluate the applicability and robustness of the optimized protocol across

different mechanochemical platforms (Table 2, and Methods A1, A2 and B in the ESI). The better results were obtained in a PBM, with the exception of Boscalid (**2**), obtained in a 92% yield at 50 *Hz* in a VBM.

Table 2. TCFH-mediated mechanochemical amidation reaction to phytopharmaceuticals **1-5**, by ball-milling (VBM and PBM) in conditions, and comparison with the 1,1'-oxalyl diimidazole (ODI)-mediated reaction in a PBM,[24] and by LA-RAM.

	Yields (%) by Ball-milling *vs* RAM				
Compound	**VBM**[b]	**PBM**[c]	**TCFH Method**[a,d]	**ODI Method**[24] **VBM / PBM**	**TCFH Method by RAM**[d,e]
(**1**)	78	**84**	A1, A2, B	n.p.[f]	**86**
(**2**)	**92**	51	A2, B	n.p.[f]	**98**
(**3**)	48	**71**	A1, B	90 / 93	**95**
(**4**)	32	**78**	A1, B	50 / 64	**91**
(**5**)	73	**79**	A1, B	0 / 53	**90**

[a] All the reactions were conducted using AcOEt as LA-RAM solvent (η = 0.2 mL/mg) and K_2HPO_4 (3.0 equiv.) as a base, except for Fluxapyroxad (**5**) involving neat grinding with NMI (3.0 equiv.) as a base; [b] The reaction scale was 0.48 mmol; [c] The reaction scale was 1.92 mmol; [d] The detailed mechanochemical reaction conditions are described in ESI; [e] RAM conditions (Method C1, ESI): carboxylic acid (0.80 mmol), TCFH (0.80 mmol), and base (2.40 mmol) in a 2.5 mL polypropylene vial, without grinding media; *step 1*: 90 *g*, 60 min; *step 2*: addition of amine (0.58 mmol), followed by 90 *g*, 90 min. NMI was used as the base for compounds **1** and **3–5**; K_2HPO_4 was used for Boscalid (**2**). [f] n.p. = not performed.

It is worth to observe that the use of TCFH as activating agent, combined with NMI, acting as both the base and the LAG solvent, was crucial for achieving satisfying yields for Fluxapyroxad (**5**) in both VBM and PBM, especially given the deactivated (fluorinated) nature of both the acid and the amine reactants, outperforming also in comparison with the our previously reported ODI-mediated amidation reaction.[24] The comparison with previously reported solution-based methodologies to phytopharmaceuticals **1-5** is reported in Table S12 (*c.f.*, ESI) and discussed separately within this manuscript in the section dedicated to green chemistry metrics.

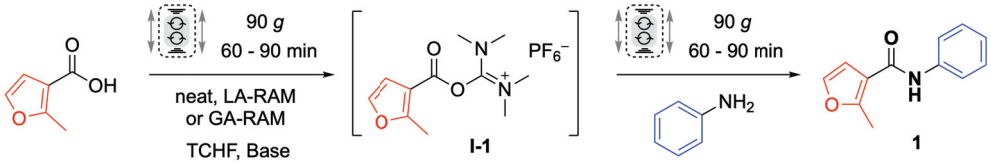
Liquid-assisted Resonant Acoustic Mixing (LA-RAM) syntheses of phytopharmaceuticals 1-5. The mechanochemical methodology established through a systematic investigation of the milling parameters, reaction reactivity, and potential bottlenecks of the TCFH-mediated amidation under ball-milling conditions, provided the necessary understanding of these factors prior to transferring the reaction to resonant acoustic mixing (RAM)

activation.[38] Based on these findings, Fenfuram (**1**) was selected as the benchmark substrate for the optimization of the RAM processing conditions (Table 3).

The simultaneous execution of multiple mechanochemical reactions in a single run, conceptually identical to the seminal report on '*parallel mechanochemistry*' platforms,[39] allowed the efficient screening of multiple experimental parameters (*e.g.*, vessel material and geometry, vessel filling degree, reactant ratios, additives, solvent and/or amount screening for LA-RAM, or acceleration) reducing the time and effort needed for reaction optimization. An in-house made multi-samples holder allowed for the processing of up to 16 samples simultaneously, greatly increasing throughput compared to standard single-jar adapter. The system uses adapters with 6 or 14 positions, accommodating vials of various sizes (from minimum of 2 mL up to 20 mL).

Interesting correlations and differences emerge when comparing the reactivity trends observed under resonant acoustic mixing (RAM, Table 3) with those previously obtained by ball milling (BM, Table 1).

Table 3. Selected LA-RAM processing conditions for the synthesis of Fenfuram (**1**).[a]



Entry	Base	LA-RAM [η] = [mL/mg]	Balls	Time (min)		Yield (%)
				Step 1	Step 2	
1	K_2HPO_4	0.2	NO	60	60	53
2	K_2HPO_4	0.2	NO	90	60	41
3	K_2HPO_4	0.2	NO	60	90	43
4[b]	K_2HPO_4	0.2	YES[b]	60	60	36
5	NMI	-	NO	60	60	79
6	**NMI**	-	NO	60	90	**86**
7	NO	-	NO	60	90	7

All the reactions were conducted in a 2.4 mL polypropylene (PP) screw top vial, using AcOEt as LA-RAM (η = 0.2 mL/mg), at 90 *g* for the specified times. *Reaction conditions*: for *step 1*: 2-methyl-furanoic acid (0.8 mmol, 1.1 equiv.), TCFH (0.8 mmol, 1.1 equiv.) and K_2HPO_4 or NMI (3.0 equiv.) as a base; for *step 2*: aniline (0.58 mmol, 0.8 equiv.). The detailed mechanochemical reaction conditions are described in ESI (*c.f.*, Method C1); [b] GA-RAM by adding ZrO_2 grinding balls (2 mm ∅, m_{tot} = 2.8 g).

In the RAM-activated experiments, employing K_2HPO_4 as base (entries 1-3), Fenfuram (**1**) was obtained only in moderate yields (36–53%), regardless of the duration of the reaction over the two individual steps. Although the highest yield within this series (53%) was obtained using 60 min (in step 1), followed by 60 min (in step 2) (entry 1), modifying the processing times resulted in only marginal changes, suggesting that the reaction time alone was not the primary factor governing reaction efficiency. In contrast, replacing solid K_2HPO_4 with liquid *N*-methylimidazole (NMI) led to a marked improvement in product formation, with isolated yields increasing to 79–86% (entries 5 and 6), indicating that NMI effectively promotes the TCFH-mediated amidation under RAM conditions, and longer reaction times, contrarily to the mechanochemical conditions for BM (Table 1).

These differences can be rationalized by considering the distinct operating principles of BM and RAM. In ball milling, efficient energy transfer relies on repeated impacts between the milling media and the reaction mixture, favouring mixtures with more solid-like rheological properties that efficiently transmit mechanical forces while minimizing energy dissipation. In contrast, RAM relies on resonant acoustic vibrations rather than ball impacts, and efficient mixing is promoted by the rheological properties of the reaction medium. Under these conditions, the presence of a liquid base such as NMI increases the fluidity of the reaction mixture, facilitating more homogeneous mixing through the combined effects of acoustic micro-mixing at 60 *Hz* and intensified mixing at high acceleration (90 *g*).[40, 41] Consequently, the liquid-assisted system appears to provide a more favourable environment for the TCFH-mediated amidation under RAM conditions.

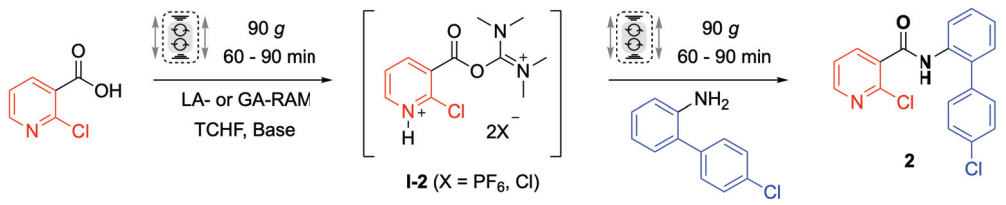
Along the same line, the presence of the solid inorganic base promotes interparticle abrasion during mixing,[42] generating localized friction-induced local heating that may accelerate the degradation of the activated acyl intermediate (**I-1**), thereby reducing the overall yield. In contrast, the more homogeneous and fluid reaction medium produced by NMI is expected to dissipate mechanical energy more uniformly, minimizing localized overheating while maintaining efficient mixing. Under these conditions, prolonged processing can favour complete conversion of the reactants without significant decomposition of the reactive intermediate **I-1**. Control experiments performed in the absence of NMI resulted in only 7% product formation (entry 7), confirming its essential role in promoting the amidation process, not merely acting as a base, but as an essential liquid additive. Overall, these results demonstrated that, in contrast to the BM process (Table 1), where the highest yields were achieved using

K_2HPO_4, herein the chemical environment provided by NMI has a substantially greater influence on the reaction outcome than variations in the reaction time over the individual steps, indicating that the optimal reaction environment is highly dependent on the mode of mechanical activation.

Additional evidence supporting the proposed degradation of the reactive intermediate (**I-1**) can be obtained by considering the grinding-assisted RAM (GA-RAM) experiment (entry 4, Table 3). The incorporation of ZrO_2 grinding media into RAM has previously been shown to facilitate cocrystal formation,[43] improve the homogeneity of pharmaceutical suspensions,[44] and in the synthesis of the antiepileptic drug phenytoin.[45] However, under the present reaction conditions, the addition of grinding media resulted in a marked decrease in product yield, indicating that their beneficial effect is not universally transferable across mechanochemical transformations. This observation is consistent with the behaviour previously observed under ball-milling conditions, where excessive mechanical activation was associated with reduced product formation owing to the degradation of the activated intermediate (**I-1**) (Table 1, entries 6 and 7). A similar phenomenon appears to occur under GA-RAM conditions.[45] The introduction of grinding media into the RAM vessel effectively superimposes impact events onto the resonant acoustic agitation, creating a hybrid activation mode that has been conceptually compared to a vertical ball mill operating at a fixed frequency of 60 Hz. Although the ZrO_2 balls employed in the GA-RAM experiment (entry 4) were considerably smaller (2 mm diameter) than the 10 mm diameter grinding media used in the BM experiments and therefore possessed lower individual impact energies, their rapid oscillatory motion may substantially increase the frequency of collisions. The resulting high-frequency mechanical impacts could generate localized stress sufficient to promote decomposition of the highly reactive intermediate (**I-1**), thereby reducing the overall reaction yield. These findings suggest that, for the present TCFH-mediated amidation, the advantages of enhanced mixing provided by grinding-assisted RAM are outweighed by the detrimental effects of excessive mechanical activation.

Mechanistic considerations: the case of Boscalid (2). A separate discussion is needed for the optimization of the synthesis of Boscalid (**2**), as the presence of a pyridine ring in the carboxylic acid component resulted in a reactivity profile distinct from that observed for Fenfuram (**1**) and the other substrates investigated.

Table 4. Selected LA-RAM processing conditions for the synthesis of Boscalid (**2**).[a]



Entry	Base (equiv.)	LA-RAM [η] = [mL/mg]	Balls	Time (min) # step		Yield (%)
				# 1	# 2	
1	K_2HPO_4 (3.0)	0.2	NO	60	60	94
2	K_2HPO_4 (3.0)	0.2	NO	90	60	50
3	**K_2HPO_4** (3.0)	0.2	NO	60	90	**98**
4	K_2HPO_4 (3.0)	-	NO	60	60	66
5	K_2HPO_4 (3.0)	0.4	NO	60	60	93
6[b]	K_2HPO_4 (3.0)	0.2	YES[b]	60	60	59
7	NMI (3.0)	-	NO	60	60	31
8	NMI (2.05)	-	NO	60	60	42
9	NO	0.2	NO	60	90	42

[a] All the reactions were conducted in a 2.4 mL polypropylene (PP) screw top vial, using AcOEt as LA-RAM (η = 0.2 mL/mg), at 90 *g* for the specified times. *Reaction conditions*: for *step 1*: 2-chloro nicotinic acid (0.8 mmol, 1.1 equiv.), TCFH (0.8 mmol, 1.1 equiv.) and K_2HPO_4 or NMI (3.0 equiv.) as a base; for *step 2*: 4'-chloro-[1,1'-biphenyl]-2-amine (0.58 mmol, 0.8 equiv.). The detailed mechanochemical reaction conditions are described in ESI (*c.f.*, Method C1); [b] GA-RAM by adding ZrO_2 grinding balls (2 mm ∅, m_{tot} = 2.8 g).

This deviation from the general trend suggests that the heteroaromatic moiety influences the course of the TCFH-mediated amidation, potentially through differences in the activation of the carboxylic acid, the stability of the activated intermediate **I-2**, or competing side reactions. Although further mechanistic studies would be required to elucidate the origin of this behaviour, the results indicate that Boscalid (**2**) represents a particular case within the investigated phytopharmaceuticals investigated and therefore merits separate consideration (Table 4).

When K_2HPO_4 was employed as the base, the reaction proceeded efficiently across a range of LA-RAM processing conditions, affording high yields (93–98%, entries 1, and 5), with little differences upon variations in the processing times of the individual steps, with the optimal conditions being achieved using 60/90 min reaction time sequence (entry 3). For this substrate, the solid inorganic base K_2HPO_4 provided

the suitable reaction environment under RAM conditions without requiring extensive optimization of the mechanical parameters. Notably, this enhanced reactivity cannot be attributed to the nature of the amine, 4'-chloro-[1,1'-biphenyl]-2-amine, which is sterically hindered and electronically deactivated due to the presence of the electron-withdrawing chlorine. The unusual reactivity observed could reflect a mechanistic divergence, potentially involving the formation of an even more reactive intermediate than initially expected.

The unexpectedly high efficiency observed for the amidation of Boscalid (**2**) in the presence of the solid inorganic base K_2HPO_4 may be rationalized by considering a possible activating role of the pyridine ring of 2-chloronicotinic acid. The pyridine nitrogen may participate in the initial activation of the carboxylic acid by TCFH, facilitating the formation of the reactive acyl intermediate **I-2**. Furthermore, the electron-deficient nature of the resulting activated carbonyl species, exacerbated by the formation of a pyridinium salt (**I-2**) leading to a a more electrophilic acyl intermediate, may enhance its reactivity toward the sterically and electronically deactivated 4'-chloro-[1,1'-biphenyl]-2-amine added in the second step. Such an interplay between substrate activation and enhanced electrophilicity of the acyl-activated intermediate **I-2**, could account for the high efficiency of the amidation reaction under the optimized RAM conditions. Further evidence supporting a possible autocatalytic contribution of the pyridine ring can be inferred from the results reported in entries 7–8 (Table 4). The introduction of NMI resulted in a significant inhibition of the reaction, affording the lowest yields observed under the investigated conditions (31–42%). This behaviour may be explained by considering the ability of NMI to interact with the pyridinium species involved in the activation process. By acting as a proton acceptor, NMI could disrupt the proton-transfer equilibrium associated with intermediate **I-2**, thereby decreasing the electrophilicity of the activated acyl species and reducing its reactivity toward the sterically hindered and electronically deactivated 4′-chloro-[1,1′-biphenyl]-2-amine. These results suggest that, in the case of Boscalid (**2**) synthesis, maintaining the pyridinium-assisted activation pathway may be critical for achieving efficient amidation.

Further insight into the role of NMI can be obtained from entry 8, in which the amount of NMI was reduced to match the previously optimised LA-RAM conditions at η = 0.2 μL/mg, assuming NMI itself acts as the liquid additive. Under these conditions, the inhibitory effect was less pronounced compared with entry 7, likely due to the lower concentration of NMI present in the reaction mixture. This trend suggests that the detrimental effect of NMI is concentration-dependent and arises from its direct

interaction with the reaction pathway rather than from a modification of the mechanical environment alone. In other words, NMI does not appear to function as a catalytic additive in this transformation; instead, its presence likely perturbs the activation process through a stoichiometric interaction with the reactive intermediate **I-2**.

The selected NMI loading was based on previous experiments using ethyl acetate as a LA-RAM additive at η = 0.2 μL/mg, while avoiding the use of three equivalents of NMI, which was anticipated to generate an excessively fluid reaction mixture with unfavourable rheological properties. However, comparison with the K_2HPO_4-based experiment performed at a higher LA-RAM coefficient (η = 0.4 μL/mg, entry 5, Table 3) indicates that increased fluidity alone does not account for the reduced reaction efficiency observed with NMI. Indeed, the higher liquid content in the K_2HPO_4 system did not negatively affect the reaction outcome, suggesting that the inhibitory effect originates primarily from the chemical nature of NMI rather than from altered mixing behaviour or energy transfer within the reaction mixture.

Indeed, the implementation of grinding-assisted RAM (GA-RAM) through the addition of ZrO_2 balls did not improve the reaction efficiency (entry 6), instead leading to a reduced yield. This behaviour is consistent with the trends previously observed for Fenfuram (**1**), where the introduction of additional impact events can promote degradation of reactive intermediate **I-2** rather than enhancing productive mixing.

Additional support for the proposed role of the pyridine moiety in promoting the amidation reaction can be obtained from entry 9 (Table 4), particularly when compared with the analogous base-free experiment performed for Fenfuram (**1**) (entry 7, Table 3). These results indicate that the 2-chloronicotinic acid component of Boscalid (**2**) retains a significant degree of reactivity even in the absence of an external base, affording the desired product in moderate yield (42%). This behaviour contrasts with the synthesis of Fenfuram (**1**), where the absence of base resulted in only 7% product formation. The lower reactivity of the 2-methylfuran-3-carboxylic acid substrate can be attributed to the absence of a basic heteroaromatic moiety capable of participating in proton-transfer processes during activation of the carboxylic acid. Although the reduced yield observed for Boscalid (**2**) under 'base-free' conditions (entry 9) indicates that the external base remains important for achieving optimal conversion, the residual reactivity is consistent with the proposed involvement of the pyridine ring in facilitating the activation process. This contribution may operate alongside other activation pathways and could account, at least in part, for the enhanced efficiency observed for this substrate. The observed acceleration does not, by itself, establish an autocatalytic mechanism. Changes in

mixture consistency, phase distribution, and mixing efficiency during the reaction may contribute to this behavior. In particular, the formation of TMU may modify the liquid content and reaction environment. The present data do not distinguish these possible contributions or demonstrate catalysis by a reaction-generated species.

Mechanochemical methodology validation across different mechanochemical platforms and product recovery. Overall, these results emphasize the importance of considering both chemical and mechanical parameters when transferring mechanochemical methodologies across different substrates. In the optimal LA-RAM conditions, while NMI-assisted conditions were advantageous for Fenfuram (**1**), Boscalid (**2**) showed superior performance under K_2HPO_4-mediated LA-RAM.

The generality of the optimized TCFH-mediated amidation reaction across different mechanochemical platforms is further highlighted in Table 2, where the yields obtained for preparing the phytopharmaceuticals **1-5** using VBM, PBM, and RAM are compared. The overall yield trends highlight the importance of evaluating multiple mechanochemical technologies during methodology development, as the mode of mechanical activation can have a pronounced influence on reaction efficiency. In the present study, planetary ball milling (PBM) outperformed vibrational ball milling (VBM), while resonant acoustic mixing (RAM) provided a further improvement over the optimized protocol in the PBM. Starting from a chemically robust TCFH-mediated amidation methodology, previously shown to efficiently promote amide bond formation by ball-milling,[27] the progression from VBM to PBM and ultimately to RAM demonstrates that technological optimization can be as important as chemical optimization in maximizing reaction performance.

The superior performance of PBM and RAM in the preparation of the phytopharmaceuticals **1-5** can be rationalized by considering the different mixing and energy-transfer mechanisms associated with each technology. In VBM, the reaction mixture was prone to adhering to the reactor walls or accumulating around the milling ball. The *snowball effect*, limited efficient contact between the reactants and reduced the effectiveness of mechanical activation.[46, 47] In the PBM, the planetary motion of the milling vessel combined with the use of a higher number of milling balls, may enhances homogenization of the reaction mixture, resulting in an improved mass transfer and overall better yields of phytopharmaceuticals **1-5**. In the case of LA-RAM activation, the acoustic streaming (upon vibrations at 60 Hz), combined with high-acceleration oscillatory motion at a defined '*g*', allowed efficient particle mixing at micro- and

macroscopic level (fluidization phenomena) and frequent interparticle contacts. Moreover, the absence of grinding media compared to ball-milling, also minimized localized impact events and mechanical abrasion that, for the present TCFH-mediated amidation, may be responsible for the degradation of the active intermediates.

Independently on the mechanochemical platform used, phytopharmaceuticals **1-5** were recovered upon an eco-friendly and straightforward work-up procedure that avoids organic solvents. Due to their low solubility in water, compounds **1-5** were recovered from the crude reaction mixture through precipitation in water followed by a filtration ensuring that the entire workflow, from synthesis to recovery, the use of organic solvent remaining limited only to the amount used for the liquid-assisted processes (LAG or LA-RAM).

Comparative studies: TCFH- ***vs*** **EDCl/Oxyma-mediated mechanochemical amidation by LA-RAM.** During the preparation of this manuscript, amidation reactions by LA-RAM mediated by EDCl/Oxyma activating system was reported for the synthesis of peptides.[20] Therefore, to further validate the TCFH-mediated amidation herein described to prepare the phytopharmaceuticals **1-5**, and for sake of comparison, their synthesis was repeated in the same reaction conditions of the recently published methodology[20] at the closest-matched scale (3.34 mmol) available for both TCFH- and EDCl/Oxyma-mediated approaches (Table S2, ESI). The comparison was most appropriately made using the closest comparable reaction scales available for the two methodologies: 3.34 mmol of carboxylic acid in a 24 mL glass vessel for the one-pot/one-step EDCI/Oxyma protocol,[20] and 8.00 mmol of acid (5.82 mmol of amine, limiting reagent) in a 15 mL PTFE vessel for the one-pot/two-step TCFH-mediated protocol (*c.f.*, Methods C1-C2, ESI). Both mixtures were reacted in the presence of 1,2-dimethoxyethane (DME, η = 0.9 μL/mg) as LA-RAM solvent at 80 *g* for 40 minutes. Notably, the latter processes a substantially larger amount of material was processed in a smaller reaction volume, corresponding to a considerably higher volumetric productivity. Despite these more demanding conditions, the TCFH-mediated methodology consistently outperformed the EDCI/Oxyma approach (affording only moderate-to-poor yields), for all target compounds **1-5** (Table S2, ESI). This advantage was particularly evident for the most challenging substrate, Boscalid (**2**), for which the TCFH-mediated synthesis afforded a slightly higher isolated yield (29% *vs*. 22%). AcOEt (η = 0.9 μL/mg) was also used as LA-RAM solvent to prepare the two targets delivering respectively the best and the worst results upon application of the previously reported procedure with DME[20] (Table S2, entries 2 and 4, ESI). The rationale behind

this choice relies on the observation that AcOEt proved to be successful for our experiments, and to benchmark it with the EDCl/Oxyma method explored in the original publication.[20] As a result (Table S2, entries 2 and 4, ESI), yields for Boscalid (**2,** 17%) and Flutolanil (**4**, 45%) prepared by LA-RAM-mediated EDCl/Oxyma coupling reaction with AcOEt (η = 0.9 μL/mg) delivered even lower yields than with DME (η = 0.9 μL/mg) (Table S2, entries 2 and 4, ESI).

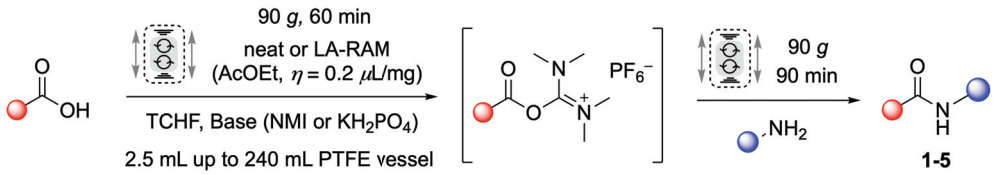
These findings are consistent with the original design rationale of the EDCI/Oxyma system,[20] which was developed and optimized primarily for peptide bond formation. In such transformations, coupling typically involves α-amino acid derivatives and relatively nucleophilic aliphatic amines, where minimizing epimerization rather than maximizing carboxylic acid activation is the principal challenge. In contrast, the SDHI targets **1-5** investigated in this work present a substantially more demanding coupling scenario. In every case, both coupling partners are aromatic, while the amine component is sterically hindered and/or electronically deactivated by electron-withdrawing substituents, resulting in reduced nucleophilicity.

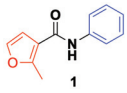
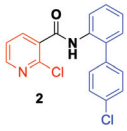
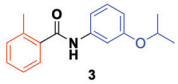
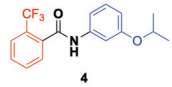
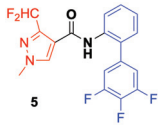
Under these conditions, efficient amidation requires a coupling reagent capable of generating a more electrophilic activated acyl intermediate. The superior performance of TCFH under mechanochemical conditions is therefore consistent with its stronger activating ability, enabling efficient coupling even with poorly nucleophilic aromatic amines.

Taken together, these observations underline that the TCFH-mediated protocol not only provides improved synthetic performance but also enables higher space-time and volumetric process efficiency, reinforcing its potential as a practical and scalable mechanochemical amidation methodology.

It should be noted that the EDCI/Oxyma data are reported as qNMR yields, whereas the values obtained for the TCFH-mediated protocol correspond to isolated yields (Table S2, ESI). Since isolated yields include product recovery and purification losses, direct quantitative comparison should be interpreted with caution. Nevertheless, the superior performance of the TCFH methodology despite this more stringent basis of evaluation suggests that its practical advantage may be greater than the reported values alone imply, especially when scalability is targeted.

Table 5. Scalability of the TCFH-mediated LA-RAM amidation for compounds (**1–5**).



Target	2.5 mL PP vial		15 mL PTFE vessel		30 mL PTFE vessel		120 mL PTFE vessel		240 mL PTFE vessel[b]	
	Scale[a] (mmol)	Yield (%) amount (mg)	Scale[a] (mmol)	Yield (%) amount (g)	Scale[a] (mmol)	Yield (%) amount (g)	Scale[a] (mmol)	Yield (%) amount (g)	Scale[a] (mmol)	Yield (%) amount (g)
 **1**	0.58	86 100.1	5.82	98 1.1467	11.63	97 2.3	46.55	100 9.4	93.10	96 18.0
 **2**	0.58	98 194.7	5.82	29 0.828	11.63	58 2.3	46.55	88 14.1	93.10	67 21.5
 **3**	0.58	95 148.2	5.82	100 1.6	11.63	100 3.1	46.55	99 12.5	93.10	91 22.9
 **4**	0.58	91 170.4	5.82	96 1.8	11.63	100 3.7	46.55	98 14.7	93.10	96 28.9
 **5**	0.58	90 199.3	5.82	96 2.1	11.63	95 4.2	46.55	100 17.7	93.10	99 34.9

[a] The initial reaction charge occupied approximately 70% of the vessel volume, estimated visually. This represents the apparent bulk fill level, including interparticle voids, rather than the true volume fraction of solid reactants. Differences in powder packing may therefore affect the actual fill level between formulations. The reaction scale refers to the amount of the limiting reagent (the amine). The reaction conditions followed the experiments conducted at the lowest scale (*c.f.*, Method C1, ESI). For compounds **1, 3- 5**: *step 1:* the acid (1.1 equiv.) and *N,N,N',N'*-tetramethylchloroformamidinium hexafluorophosphate (TCFH, 1.1 equiv.) were added in the presence of a base. For accessing compound **2**, the base was dipotassium phosphate (K_2HPO_4, 3.0 equiv.) and AcOEt (η = 0.2 μL/mg) was used as liquid-assisted RAM (LA-RAM) solvent. For accessing compounds **1, 3-5** the base was *N*-methylimidazole (NMI, 3.0 equiv.). The mixture was reacted at 90 *g* for 60 min. *Step 2*. After this time the amine (0.8 equiv.) was added, and the reaction mixture was further mixed at 90 *g* for 90 min.; [b] Method C2 was used (*c.f.*, ESI).

Scalability studies for LA-RAM syntheses of phytopharmaceuticals 1-5 and thermal effects. To demonstrate the robustness and scalability of the TCFH-mediated LA-RAM amidation, each target compound (**1–5**) was synthesized at progressively increasing reaction scales, reaching up to a 160-fold increase relative to the initial reaction. This evaluation was designed to verify that the optimized reaction conditions could be translated to higher-throughput syntheses while maintaining reaction efficiency.

PTFE screw-cap jars were selected for the scale-up experiments because of their superior chemical and thermal stability compared with the 2.5 mL polypropylene (PP) vials used for the initial 0.8 mmol-scale reactions. Table 5 (c.f., see also Figure S1, ESI) summarizes the reaction scales investigated, the corresponding reaction vessels employed, the isolated yields and the amount obtained under each set of conditions.

The results clearly demonstrate that the methodology is consistent across the different scales and overall independent on the target, being highly effective for preparations at multigram (and potentially larger) scales, with the highest amount obtained across the investigation being 34.5 g over 3 h reaction (over two steps), for Fluxapyroxad (**5**), a target particularly challenging to synthesise. The solid fluorinated aromatic amine is significantly deactivated toward nucleophilic attack on the activated acyl intermediate generated in the first step owing to the strong electron-withdrawing effect exerted by the three fluorine substituents on the aromatic ring. The TCFH-mediated amidation by LA-RAM applied to the preparation of this challenging target outperformed independently on the scale, compared to our previously reported amidation reaction mediated by 1,1-oxalylimidazole (ODI).[24]

In the case of Boscalid (**2**), particularly for the experiment conducted with 8 mmol of starting acid, yield notably decreased (29% yield, 5.82 mmol scale) (Figure S1, ESI). Given that this is the only significant outlier at this reaction scale, the lower yield is more plausibly attributed to the geometry of the reaction vessel than to the chemistry of the transformation itself. The 15 mL PTFE jar used for this experiment is the shortest vessel investigated (34 mm in height), even shorter than the 2.5 mL PP vial used for the initial 0.8 mmol-scale reactions (45 mm). Such a reduced aspect ratio may limit the vertical oscillatory motion of the reaction mixture under resonant acoustic mixing, diminishing convective particle circulation and the frequency of effective particle-particle contacts. The resulting decrease in mixing efficiency and mechanical energy transfer provides a plausible explanation for the reduced reaction performance.

One factor that may contribute to the consistently high yields obtained, even upon scaling the reaction up to 160-fold, is the occurrence of distinct physical phenomena within the reaction mixture at larger scales. In the reactions leading to targets **1, 3-5**, where NMI was employed as the base, the crude reaction mixture evolved from a clear, homogeneous viscous liquid after the activation step to a darker, denser phase following amine addition. Concomitantly, white spherical agglomerates of varying diameter were consistently observed (Figure 2).



Figure 2. Appearance of the reaction mixture after the first step (*left*, viscous paste) and the second step (*right*), showing the formation and persistence of macroscopic aggregates.

^{1}H NMR analysis of the isolated aggregates after dissolution in DMSO-d_6 revealed signals attributable to tetramethyl urea (TMU), the stoichiometric byproduct of the TCFH-mediated activation step. However, this analysis does not establish the physical state or composition of the aggregates before dissolution The aggregates may retain liquid TMU within a matrix of other reaction components or salts, although their precise composition remains unresolved. The formation of these aggregates may influence the rheological properties of the reaction mixture and its mixing behavior under LA-RAM conditions: the presence of these soft, in situ formed solid domains may promote efficient mixing of larger quantities of reactants in a non-destructive manner, unlike conventional grinding media such as ZrO2 or stainless-steel balls (GA-RAM), which could otherwise damage fragile intermediates. In this way, the system may achieve better homogenization while preserving the integrity of reactive species, ultimately supporting the observed scalability and high yields.

Heat buildup represents an additional factor that may affect the reaction outcome, particularly at larger reaction scales. As the total mass of the reaction mixture increases, heat dissipation becomes progressively less efficient, leading to greater thermal accumulation that may influence the balance between productive reaction pathways and competing degradation processes.

This phenomenon was observed for all substrates, although the thermal profiles (measured through an infrared handheld thermometer directed at the external surface of the reaction jar or at the reaction mixture immediately after opening the jar at the end of the reaction), differed depending on whether NMI or K_2HPO_4 was employed as the base. For substrates **1**, **3-5,** where NMI was used, the internal temperature of the reaction mixture reached approximately 40 °C after the activation step. Upon addition of the

amine, a rapid temperature increase to 60–65 °C was observed, coinciding with the immediate homogenization of the reaction mixture. By the end of the second reaction step, the internal temperature had increased further to approximately 90 °C, whereas the outer wall of the reaction vessel reached around 65 °C. These observations indicate that significant heat is generated during the course of the reaction and that thermal accumulation becomes substantial under scale-up conditions, where heat dissipation is less efficient, thus suggesting that thermal management may become an important parameter during process scale-up.

In contrast, Boscalid (**2**), for which K_2HPO_4 was employed as the base, exhibited a markedly different thermal profile. After the activation step, the internal temperature of the reaction mixture reached approximately 65 °C, which may be attributed to frictional heating arising from the abrasive interactions between the solid inorganic base and the other solid components of the reaction mixture. However, unlike the NMI-mediated systems, no appreciable increase in temperature was observed following the addition of the amine. This behaviour is likely related to the highly viscous rheology of the reaction mixture after the first step, which may delay the efficient dispersion of the solid amine upon its addition, and consequently slowed both mixing/solubilisation and the onset of the amidation reaction, possibly associated to exothermic phenomena.

High-pressure sealed-crucible DSC screening of the premixed Fenfuram reaction formulation revealed a broad exothermic event peaking at 98.3 °C and additional exothermic events at higher temperatures (Figure S2, ESI). These results establish exothermic activity in the formulation and highlight the need for further thermal assessment before extending the process beyond the demonstrated scale.

Conversely, when NMI was employed as the base, the reaction mixture evolved into a homogeneous fluid after the first activation step. This lower-viscosity phase likely promoted rapid mixing upon addition of the amine, facilitating efficient contact between the reactants. Such efficient homogenization may explain the immediate increase in temperature observed after amine addition, as the exothermic amidation reaction can proceed more rapidly in a well-mixed system. This behavior is consistent with the enhanced reaction performance observed under these conditions.

Following the second reaction step, the external temperature of the reaction vessel reached approximately 75 °C, suggesting that the internal temperature of the reaction mixture was likely in the range of 80–90 °C.

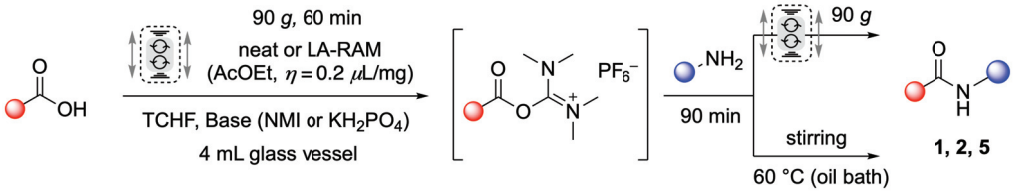
Comparison between TCFH-mediated amidation by LA-RAM *vs* conventional heating (effect of the temperature). To distinguish the contribution of thermal effects from that of LA-RAM activation, a series of control experiments was designed using three representative substrates. Fenfuram (**1**) was selected as the benchmark reaction for this study, Boscalid (**2**) was chosen to represent systems employing the solid base K_2HPO_4, and Fluxapyroxad (**5**) was included because it incorporates the same sterically hindered and electronically deactivated biphenyl amine as Boscalid (**2**) while using NMI as the base, thereby enabling the influence of the base to be evaluated independently of amine reactivity. The outcomes of these experiments are summarized in Table 6.

To investigate the respective contributions of mechanical activation and temperature during the second step of the reaction, a series of control experiments was designed. The visual inspection of the crude after the first step indicated the formation of a liquid phase, it was hypothesized that the amidation could proceed predominantly as a liquid-phase reaction, with RAM serving primarily to promote efficient mixing rather than directly providing the mechanical activation required for bond formation.

To test this hypothesis, only the second reaction step was varied. The activation step was performed under the optimized LA-RAM conditions (90 *g*, 60 min) in all cases. Subsequently, the activated reaction mixture was either processed by RAM at 90 *g* for 90 min or stirred in an oil bath maintained at 60 °C for 90 min without further mechanical activation. The experiments were carried out at a small reaction scale (1.09 mmol, 4 mL glass vial) to minimize thermal effects associated with RAM operation. Under these conditions, no appreciable temperature increase was observed during RAM processing, and the internal temperature remained between approximately 30 and 40 °C throughout the reaction. This experimental design enabled the influence of mechanical activation during the second step to be evaluated independently from the heat generated during larger-scale LA-RAM experiments.

As shown in Table 6, the influence of LA-RAM activation during the second reaction step depends strongly on the intrinsic reactivity of the substrate and the rheological properties of the reaction mixture.

Table 6. Comparison between fully mechanochemical two-step TCFH-mediated amidation protocols *vs* hybrid approach combining LA-RAM (step 1) and conventional stirring at 60 °C in an oil bath (step 2).[a]



Entry	Compound	Base	LA-RAM [η] = [mL/mg]	Yield (%)	
				Stirring (oil bath)	LA- RAM
1	**1**	NMI	-	96	94
2	**2**	K_2HPO_4	0.2	50	74
3	**5**	NMI	-	68	76

[a] All the reactions were conducted in a 4 mL glass screw top vial, using AcOEt as LA-RAM (η = 0.2 mL/mg), at 90 *g* for the specified times. *Reaction conditions*: for *step 1*: acid (1.5 mmol, 1.1 equiv.), TCFH (1.5 mmol, 1.1 equiv.) and K_2HPO_4 or NMI (4.09 mmol, 3.0 equiv.) as a base; for *step 2*: amine (1.09 mmol, 0.8 equiv.). The detailed mechanochemical reaction conditions are described in ESI (*c.f.*, Method C1).

For Fenfuram (**1**), no significant difference was observed between the reaction performed under RAM and that conducted under conventional stirring. Following the activation step, the crude reaction mixture is a homogeneous fluid that becomes even less viscous upon addition of the aniline (a liquid). Under these conditions, efficient mixing can be achieved by conventional stirring, while heating at 60 °C provides sufficient thermal energy to promote amidation. Together with the relatively high nucleophilicity of the amine partner, these factors account for the comparable reaction efficiencies observed under both conditions.

In contrast, a markedly different behaviour was observed for Boscalid (**2**). After the activation step, the reaction mixture forms a highly viscous paste, and the subsequent addition of a solid, sterically hindered and electronically deactivated amine further exacerbates mixing limitations. Under conventional stirring, the poor dispersion of the reactants results in a substantial decrease in reaction efficiency. Under LA-RAM conditions, however, the intense acoustic mixing promotes more effective homogenization of the reaction mixture, improving reactant contact and leading to significantly higher yields.

Fluxapyroxad (**5**) represents an intermediate case. Similar to Fenfuram (**1**), the activated reaction mixture remains fluid after the first step and can therefore be stirred

efficiently. However, the amine component exhibits reduced nucleophilicity, analogous to that of Boscalid (**2**). Consequently, although heating and conventional stirring are sufficient to achieve moderate conversion, LA-RAM consistently affords higher yields, indicating that efficient mixing alone does not fully account for the improved performance. Rather, the mechanical environment generated by resonant acoustic mixing appears to facilitate the amidation of less reactive substrates by enhancing the frequency and uniformity of productive reactant interactions.

Collectively, these results indicate that, once the activated intermediate has been generated, thermal energy and conventional stirring are sufficient to promote amidation in highly reactive and homogeneous systems. However, as substrate reactivity decreases and the reaction mixture becomes more viscous or heterogeneous, the enhanced mixing characteristics of LA-RAM become increasingly important, enabling more efficient reactant contact and ultimately improving reaction efficiency.

Analyses at the solid-state: High-Resolution Powder X-Rays Diffraction (PXRD) and Microcrystal Electron Diffraction (MicroED). Considering the significant impact of crystalline forms on material properties and performance in the pharmaceutical field,[48, 49] the products obtained from the smallest-scale LA-RAM reactions (0.5 mmol) were subjected to solid-state structural characterization. All compounds (**1–5**) were analysed by high-resolution synchrotron powder X-ray diffraction (PXRD), while compounds **1-3**, and **5** were further investigated by microcrystal electron diffraction (MicroED) to obtain single-crystal structural information (Figures S8-S12 and Tables S3-S7, ESI).

For Fenfuram (**1**) and Mepronil (**3**), no previous crystallographic data were identified in the literature; therefore, the structures reported herein represent the first X-ray diffraction characterization of these compounds. For all the samples **1-5**, the phase purity of the isolated crystalline products was confirmed by comparison of the experimental PXRD patterns with those of the corresponding starting materials and potential reaction byproducts, including tetramethyl urea (TMU), generated from the TCFH activation step. No additional reflections attributable to impurities were observed, confirming the formation of the pure crystalline phases. For Boscalid (**2**) and Fluxapyroxad (**5**), revealed that the crystalline forms obtained through the present mechanochemical synthesis under LA-RAM conditions, followed by aqueous precipitation of the products, are consistent with the previously reported crystallographic data.[50]

Table 7. Space groups for phytopharmaceuticals **1-5**.

Entry	Compound	Space group	[Refcode]	Ref.
1	Fenfuram (**1**)	$Pna2_1$	2584567[a]	-
2	Boscalid (**2**)	P $2_1/c$	[NOZKOF02]	[50]
3	Mepronil (**3**)	Pbcn	2584567[a]	-
4	Flutolanil (**4**)	*P*-1[51]	[KUYVOQ]	[51]
5	Fluxapyroxad (**5**)	Pbca	[IDECIH]	[50]

[a] Deposition number for the structure deposited in Cambridge Crystallographic Data Centre (CCDC).

Notably, these structures were previously obtained following conventional solution-phase purification by column chromatography, demonstrating that the LA-RAM methodology provides access to the same crystalline forms through a simplified isolation procedure. Finally, for Flutolanil (**4**), the obtained crystal structure was also found to be consistent with previously reported data.[51] However, as the previous report did not provide a synthetic procedure for accessing this crystalline form, the present work establishes a reproducible preparation route for its formation under mechanochemical conditions. Table 7 sums-up the space groups identified for all the compounds **1-5**, prepared by LA-RAM and after work-up.

Greenness assessment of LA-RAM *vs* Solution-based synthesis by green chemistry metrics. To evaluate the environmental sustainability of the TCFH-mediated amidation, green chemistry assessment was carried out employing complementary tools: DOZN™[30-32] and the CHEM21 toolkit.[29] DOZN™ provides a quantitative evaluation of a process's alignment with the 12 Principles of Green Chemistry, scoring them individually and further consolidated into three thematic groups: *Improved Resource Use* (Principles 1, 2, 7, 8, 9, and 11; Group 1), *Increased Energy Efficiency* (Principle 6; Group 2), and *Reduced Human and Environmental Hazard* (Principles 3, 4, 5, 10, and 12; Group 3). The overall environmental performance is expressed as an aggregate score, calculated as the arithmetic mean of the scores for the twelve individual principles. Lower aggregate scores correspond to greener processes, with values below 1 indicating optimal sustainability performance.

The CHEM21 toolkit, on the other hand, combines quantitative green chemistry metrics (Atom Economy AE, Reaction Mass Efficiency RME, Optimum efficiency OE, Process mass intensity, PMI, *E*-factor) with a qualitative flagging system categorizing

solvents, reagents, products (and byproducts), operational parameters (*e*.g., temperature, work-up, mode of operation, use of catalysts) and hazard profiles (with particular focus on diagnostic H-statements from the GHS classification of substances employed), into green (Recommended), amber (Hazardous), and red (To be avoided) categories.

This dual assessment was conducted with two complementary objectives. The first was to extend the technological comparison of the three mechanochemical platforms (VBM, PBM, and RAM) by incorporating a green chemistry evaluation, reflecting the central premise of mechanochemistry as a sustainable alternative to conventional solution-based synthesis. The second was to compare the environmental performance of the optimized large-scale LA-RAM protocol with that of the industrial manufacturing routes currently employed for the target active ingredients **1-5**, thereby assessing its potential to provide a more sustainable manufacturing strategy.

Assessment by DOZN™ 3.0 tool (Figures S13, S14 and excel spreadsheets in ESI). This analysis provided valuable insight into the differences in green chemistry performance among the mechanochemical technologies investigated (Figure S13, ESI). Among the variables contributing most significantly to the DOZN™ scores, two are particularly influential: (i) the reaction yield (observed to be also dependent on the mechanochemical platform used), and (ii) the quantities of reagents and chemicals required for the synthesis and during the workup.

For each target compound (**1–5**), the variation in the aggregate DOZN™ score as a function of the synthetic platform (solution-phase synthesis, VBM, PBM, and LA-RAM) is presented in Figure 3 (see also Figure S13, ESI). A clear and consistent trend is observed across all targets: the transition from VBM to PBM, followed by LA-RAM at laboratory scale and, ultimately, at the multi-gram scale, results in progressively lower (i.e., more favorable) scores across all groups of the Green Chemistry Principles. This systematic improvement is reflected in a corresponding decrease in the overall aggregate DOZN™ score, highlighting the enhanced environmental performance achieved especially for mechanochemical activation by LA-RAM, with the lowest aggregate scores across the mechanochemical platforms investigated.

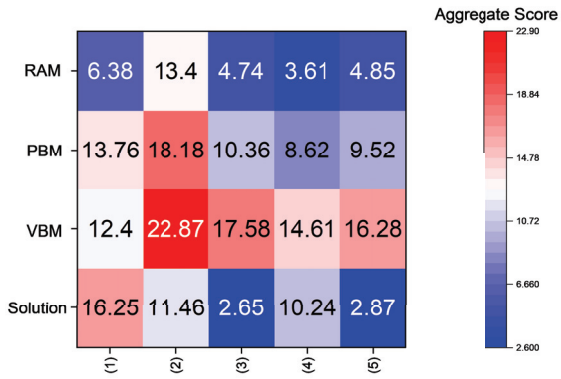


Figure 3.Aggregate scores calculated by DOZN^{TM} 3.0 for phytopharmaceuticals **1-5**, prepared in solution and by mechanochemical processing by VBM, PBM (Method B, ESI) and LA-RAM (at scale). The detailed calculations are reported in ESI.

With the exception of Boscalid (**2**), for which the aggregate scores are not favourable to any of the mechanochemical methods, compared to solution-based approach,[52, 53] for all the other targets **1,3-5** the LA-RAM protocols exhibited better performance with respect to the 12 Principles of Green Chemistry than their ball-milling counterparts (Figures S13 and S14, ESI and excel spreadsheets), attributable both to higher reaction yields (improved resource efficiency in Group 1) and the absence of prolonged reaction times upon scale-up.

Indeed, LA-RAM offers a distinct practical advantage in terms of scalability. Once the reaction conditions have been optimized, the process can be translated to larger scales with minimal adaptation, generally requiring only the use of a larger reaction vessel while maintaining the same operating parameters. This has a significant influence on both reaction time and yield. As the reaction scale increases, and previously demonstrated,[45] complete conversion is achieved more rapidly, while the larger mass of the reaction mixture is likely to facilitate more efficient transmission of mechanical energy,[54] contributing to the improved yields observed at scale.

Having identified LA-RAM as the most effective mechanochemical platform for the synthesis of most of the target compounds, a direct comparison (for both small- and large-scales) with established solution-phase methodologies provides an appropriate benchmark for evaluating its synthetic and environmental performance (Figure S14, ESI). Across the dataset, RAM protocols consistently demonstrate advantages in several critical areas, particularly in terms of energy efficiency and resource utilization.

For Fenfuram (**1**), the RAM-based synthesis achieves notably better DOZN™ scores across all categories, with a significant edge in Group 1, especially at larger scale (Figure 3, Figure S13 and excels spreadsheets). This performance is largely driven by the elimination of solvents and the use of a simple aqueous precipitation for purification, in contrast to the resource- and waste-intensive column chromatography required in the solution-based method[55] (Table S13, ESI). Additionally, the RAM process proceeds faster (2h 15 *vs*. 4h), under ambient conditions, and with higher yield (96% *vs*. 91%), offering a markedly greener and more efficient route.

In the case of Boscalid (**2**), the solution method[52, 53] achieves slightly better aggregate scores, mainly due to a higher yield and despite the concerns related to the use of hazardous reagents such as oxalyl chloride (generating toxic byproduct CO) and solvents (e.g., DCM, DMF, and 1,2-dichloroethane) (Table S14 and Figure S14, ESI). However, RAM offers clear advantages in Group 2, as the reaction is carried out at room temperature in significantly shorter time. Despite the lower yield and the formation of tetramethyl urea (TMU), a known teratogen leading to less favourable Group 3 score, RAM still provides a comparable overall sustainability profile, particularly appealing from in terms of energy efficiency (Group 2). The reactions are conducted at room temperature and with significantly shorter reaction times, reducing both energy input and operational costs. These benefits are captured in the DOZN™ scoring, resulting in aggregate scores that are ultimately very close between the two methods (11.46 *vs* 13.4, Figure 3). These results suggest that with further optimization, especially in workup and coupling reagent selection, RAM could present a fully competitive alternative for further process optimization.

The synthesis of Mepronil (**3**) further highlights the strengths of RAM in terms of efficiency (Figure S14 and Table S15, ESI). The protocol affords a substantially higher yield (91% *vs.* 77%) than solution-based one relying on the use of $POCl_3$,[56] and needing elevated temperatures. However, the disadvantages intrinsically associated to the use of $POCl_3$, requiring greater care during handling due to its high toxicity and corrosiveness, are counterbalanced by the formation of benign phosphate salts as byproducts, which carry no significant toxicological concerns (benefitting Group 3). On the contrarily, by RAM, the DOZN™ score is slightly penalized in Group 3 due to the generation of TMU, the overall performance remains strong, particularly in Groups 1 and 2. Herein, when considering the overall sustainability profile, the TCFH-mediated amidation by RAM shows slightly lower performance in hazard-related metrics (Group

3) but maintains notable advantages in terms of energy and resource efficiency, as reflected in the Group 1 and 2 scores, thanks to the solvent-free conditions, and the lack of heating required, reducing both material intensity and energy input.

For Flutolanil (**4**), the RAM protocol outperforms the solution-based method[57, 58] across all evaluated categories (Figure S14 and Table S16, ESI). The mechanochemical route eliminates the need for hazardous solvents such as DCM and DMF and avoids the use of oxalyl chloride, a chlorinating agent that generates carbon monoxide as a byproduct. These factors negatively impact both Group 1 (Improved Resource Use) and Group 3, due to their waste generation and associated health/environmental risks. In contrast, the methodology by RAM employs an efficient reaction at room temperature with minimal workup, leading to improved safety and environmental metrics in Group 3 (despite the formation of TMU), alongside superior scores in resource use (Group 1) and energy efficiency (Group 2). The high yield achieved (96%) further underscores its potential for further upscaling. Though both protocols achieve excellent yields, the RAM workup is inherently less wasteful, further reinforcing the overall greener profile of the mechanochemical approach.

The comparison for Fluxapyroxad (**5**) presents a more balanced picture, with the solution-based route[59, 60] slightly outperforming RAM in the aggregate score (2.87 *vs* 4.85 respectively, Figure 3), due to a more favourable Group 3 profile (Table S17 and Figure S14, ESI). Nevertheless, RAM excels in energy efficiency (Group 2) and achieves comparable performance in resource use (Group 1), supported by a superior yield (99% *vs*. 83%). The less favourable hazard metrics for RAM-based method are primarily due to higher water consumption during workup, a factor that, as shown elsewhere (see Figure S13, ESI), can be improved at larger scales.

This suggests that, with appropriate process refinement, RAM has the potential to complement conventional approaches, due to its green performance towards the targets investigated in this study.

Overall, this comparative study highlights the clear environmental and operational benefits of RAM-based mechanochemical amidation using TCFH as coupling agent. Across a range of target molecules and scales, RAM consistently offered advantages in terms of energy savings (based on DOZN^{TM} Group 3 scores) and material efficiency (Group 1 scores), while in the case of Fenfuram (**1**) and Flutolanil (**4**), it also achieves much better hazard profiles. While certain limitations remain particularly

related to byproduct toxicity, intrinsically due to TCFH coupling reagent, and workup operations, the last one are addressable through further optimization.

Taken together, at larger scale the metric profile by DOZN^{TM} improves (Figures S13 and S14, ESI), suggesting that RAM can be evaluated as an additional and promising platform well-suited for further development and complementing traditional solution-phase synthesis for the targets under study.

Assessment using CHEM21 tool (Table S18 and excel spreadsheets in ESI). Along the same line, the LA-RAM amidation reaction at large scale for preparing the targets **1-5** (Method C2, ESI) was selected for the comparative assessment against the corresponding solution-based procedures.

In the case of Fenfuram (**1**), the CHEM21 outputs (Table S18, part I, ESI) highlight a clear benefit of the amidation reaction by RAM in terms of overall material efficiency and waste reduction. While the solution-based method shows a higher Optimum Efficiency (OE, 95.4% *vs* 73.6%), the RAM route achieves superior Atom Economy (40.3% *vs* 27.4%), Reaction Mass Efficiency (29.6% *vs* 26.2%), and lower waste-related metrics (PMI: 60.5 *vs* 65.7; E-factor: 59.5 *vs* 64.7). These improvements arise from the complete elimination of acetonitrile and petroleum ether (both flagged as hazardous solvents under CHEM21) during the reaction and the avoidance of column chromatography in favour of simple aqueous filtration, making the LA-RAM amidation reaction safer and with a better ecofootprint.

For the agrochemicals **2-5**, solution-based methods showed a better synthetic efficiency, reflected by higher values of AE, RME and OE metrics (Table S18, ESI). Taken alone, the comparison could suggest a better performance of solution-based procedures. However, the evaluation of waste related metrics such as PMI and *E*-factor reveals a different trend. While in solution, amide bonds were formed by reacting the amine with corresponding acyl chloride, prepared using low molecular weight (toxic and corrosive) chlorinating agents, the synthetic efficiency of the LA-RAM TCFH-mediated amidation generating the activated intermediate is penalized mainly by the mass contribution of the PF_6^- counterion. However, the mechanochemical approach by RAM, provides a safer and more manageable alternative from both a health and environmental perspective, completely eliminating both hazardous reagents (*e.g.*, $POCl_3$, oxalyl chloride, PCl_5, and gaseous dimethylamine) and highly flammable and toxic solvents (*e.g.*, dichloromethane, 1,2-dichloromethane, toluene, xylene, *N,N*-dimethyl formamide,

n-hexane, and Et_2O). The qualitative safety improvements underscore the benefit of the mechanochemical activation (specifically by RAM in this assessment), despite the low synthetic efficiency of the reactions to target agrochemicals **2-5**.

In the case of Mepronil (**3**) and Fluxapyroxad (**5**), the CHEM21 evaluation highlights the importance of balancing efficiency with hazard mitigation in green chemistry design, with the possibility to further improve the waste metrics (for (**3**): PMI: 29.3 *vs* 13.4 and for (**5**): PMI 60.5 *vs* 16.3, for RAM *vs* solution method respectively (Table S18, and excel spreadsheets, ESI) by using a slightly lower volume of water per gram of product needed in the work-up.

The proper design of the entire downstream operations, including those required for work-up and purification (reflected by $PMI_{work\text{-}up}$ values), has a strong impact on the waste-related metrics (Table S18, ESI). For example, in the case of Flutolanil (**4**), solution-based synthesis accounts for approximately 30 times the mass of the actual reagents, leading to an unfavourable PMI value for solution-based synthesis (50.4) compared to RAM method (24.5) (Table S18, and excel spreadsheets, ESI).

Work-up based on precipitation in/filtration of water represents a substantial contribution to the mass-based waste metrics of the LA-RAM protocols. Increasing the reaction scale reduced the water consumption per unit mass of isolated product, highlighting the dependence of these metrics on the work-up procedure and scale. The present procedures were developed using standard laboratory equipment, rather than an optimized manufacturing process, requiring a dedicated optimization of water consumption. Further reductions in the amount of water used in the work-up could improve PMI and E-factor, provided that product recovery and purity are maintained.

Additional environmental advantages come from the easy recovery of the final products by precipitation from water, rather than by more-resource and energy intensive purification procedures. In particular, the solution-based methods required either a column chromatography (for Fenfuram, **1**), a recrystallisation (for Flutolanil, **4**), and/or distillation under reduced pressure (for Boscalid **2**, Mepronil **3**, and Flutolanil **4**).

The DOZN™ and CHEM21 assessments reveal target-dependent trade-offs between the TCFH-mediated LA-RAM protocols and the selected solution-based procedures. The principal benefits of LA-RAM methodology are the limited use of added organic solvent during the reaction, the efficient multigram synthesis, and product isolation by aqueous precipitation. These features improve selected metrics, including a

lower PMI for Flutolanil (**4**) relative to the solution-based procedure examined (24.5 vs 50.4). However, TCFH activation generates stoichiometric tetramethyl urea (TMU), which presents reproductive toxicity concerns, together with PF_6^--containing salt waste. These limitations preclude describing the process as inherently benign or uniformly more sustainable than the reference routes. The present results therefore support LA-RAM as an effective platform for amidation with reduced reliance on bulk reaction solvents, while identifying coupling-reagent selection and waste management as priorities for improving its environmental profile.

However, mass-based metrics alone do not provide a complete picture of process sustainability and the comprehensive assessment of the environmental footprint of each process should be complemented with energy consumption and life-cycle assessment (LCA), ideally using data obtained at comparable scales.[61]

Overall, the laboratory-scale evaluation indicates that the mechanochemical routes provide a more favourable environmental profile than the corresponding solution-based methodologies. This trend was consistently observed using both DOZN™ 3.0 and CHEM21, which highlighted the reduced reliance on solvents and auxiliary materials, and the simplified downstream processing associated with the mechanochemical approach.

Conclusions

Herein, five marketed agrochemicals Fenfuram, Boscalid, Mepronil, Flutolanil, and Fluxapyroxad (**1-5**) have been prepared by TCFH-mediated amidation reaction, conducted across three different mechanochemical platforms: by ball-milling (VBM and PBM) and by LA-RAM (at different scales). Their systematic comparison identified RAM platform as the most efficient, herein delivering comparable or superior performance in terms of yield and operational simplicity.

Although the three mechanochemical approaches enabled the synthesis of the target phytopharmaceuticals, their performance was strongly influenced by the specific characteristics of the mechanical activation and the manner in which energy was delivered to the reaction mixture. Consistent with previous comparisons of mechanochemical technologies,[24] the results indicate that conditions optimized for one platform cannot necessarily be transferred directly to another without further adjustment. Variations in vessel design, mechanical motion, and energy transmission can substantially affect mixing, reactant interactions, and reaction kinetics. Consequently,

adapting a mechanochemical transformation to a different platform requires consideration of the specific operating principles of that technology and, where necessary, re-optimization of the relevant processing parameters. At the same time, the successful application of the TCFH-amidation methodology across different platforms demonstrates its broader versatility while underscoring the importance of technology-specific process development.

To the best of our knowledge, this contribution represents the first example of LA-RAM preparation of marketed agrochemicals. All the targets were obtained in multi-decagram scale by LA-RAM, with excellent reproducibility and consistency of the results across all the targets, with improved yields and conversions at larger scales due to a more efficient energy transfer and better mixing as the total mass increases.

All the phytopharmaceuticals (**1-5**) presented highly pure crystalline phases after work-up, as shown by HR-PXRD and MicroED investigations. In the case of Boscalid (**2**), Flutolanil (**4**) and Fluxapyroxad (**5**), the crystalline structures were identical to previously reported data, while for Fenfuram (**1**) and Mepronil (**2**), their crystalline structure is herein reported for the first time.

Worth of note it is the peculiar reactivity of the selected targets.[24] The identification of the proper mechanochemical amidation method resulted not trivial,[11] considering that commonly used coupling agents such as 1,1'-carbonyldiimidazole (CDI, by ball-milling)[24] or EDCl (by RAM),[20] failed or underperformed. Beyond chemical reactivity, the role of physical factors, particularly thermal behaviour and rheology, were also examined, to understand their influence in mechanochemical processes under LA-RAM conditions.

For each target, the comprehensive assessment of the greenness of the three mechanochemical processes was conducted, also against the most similar solution-based approaches, using both the DOZN™ 3.0 and CHEM21 metrics toolkit. As a result, LA-RAM proved to be the most competitive significantly reducing the overall waste generation compared to solution-based approaches. More generally, the TCFH-mediated amidation by mechanochemical processing (by VBM, PBM and RAM) offered a simplified reaction setups, less demanding workup procedures, and in many cases improved safety and environmental profiles due to the avoidance of hazardous reagents and solvents.

We hope that this contribution will stimulate more investigations in the field towards a more responsible chemistry as recently advocated by IUPAC.[17, 18]

Author contributions

CRediT: A.C. experimental investigations, formal analysis and green metrics; C.M.C. – review and editing (green chemistry metrics); K.-i. O. formal analyses (micro-ED); J.V. – DSC analyses; M.C. and F.D. - writing (section on kinetics), review and editing; E.C. – funding acquisition, conceptualization, supervision, writing original draft, review and editing; A.N. - funding acquisition, review and editing. All authors have approved the final version of the manuscript.

Conflicts of interest

There are no conflicts to declare.

Data availability

The data supporting this article have been included as part of the Supplementary Information. CCDC [NOZKOF02][50] for Boscalid (**2**), [KUYVOQ][51] for Flutolanil (**4**), and [IDECIH][50] for Fluxapyroxad (**5**), contain the supplementary crystallographic data for this paper.

Acknowledgements

A.C. is grateful to Campus France and Tallinn Technological University (TalTech) for the Ph.D. fellowship (co-tutelle de thèse France-Estonie). E.C. and A.N. are grateful to Campus France and French-Estonian cooperation Programme Hubert Curien France-Estonia (PHC PARROT 2021-2023). A.N. is grateful to the French Embassy in Estonia for the mobility grant (2024) and ÕÜF16 for generous funding. E.C. and C.M.C. gratefully acknowledge IMPACTIVE (Innovative Mechanochemical Processes to synthesize green ACTIVE pharmaceutical ingredients),[62, 63] the research project funded from the European Union's Horizon Europe research and innovation programme (European Health and Digital Executive Agency) under grant agreement No. 101057286. Views and opinions expressed are however those of the authors only and do not necessarily reflect those of the European Union or the European Health and Digital Executive Agency. Neither the European Union nor the granting authority can be held responsible for them. The authors acknowledge the European Synchrotron Radiation Facility (ESRF) for provision of synchrotron radiation facilities and Momentum Transfer for facilitating the measurements. Jakub Drnec is thanked for assistance and support in using

beamline ID31. The measurement setup was developed with funding from the European Union's Horizon 2020 research and innovation program under the STREAMLINE project (grant agreement ID 870313). Measurements performed as part of the MatScatNet project were supported by OSCARS through the European Commission's Horizon Europe Research and Innovation programme under grant agreement No. 101129751. The authors acknowledge the iCeMS Analysis Center for analytical support with the MicroED measurements using a Synergy-ED electron diffractometer (Rigaku/JEOL).

Notes and references

Deposited structures in Cambridge Crystallographic Data Centre (CCDC) under deposition number 2584567 for Fenfuram (**1**), and 2584568 for Mepronil (**3**).

References

1. J. Magano, *Org. Proc. Res. Devel.*, 2022, **26**, 1562-1689.
2. R. M. de Figueiredo, J.-S. Suppo and J.-M. Campagne, *Chem. Rev.*, 2016, **116**, 12029-12122.
3. J. Boström, D. G. Brown, R. J. Young and G. M. Keserü, *Nat. Rev. Drug Discov.*, 2018, **17**, 709-727. .
4. J. R. Dunetz, J. Magano and G. A. Weisenburger, *Org. Proc. Res. Devel.*, 2016, **20**, 140-177.
5. B. Luo, Y. Hu, Y. Wu, M. Liu and K. Fang, *J. Agric. Food Chem.*, 2025, **73**, 30582–30600.
6. In 2024, the market was valued at 240–245 billions USD and it is projected to reach 313.89–347.05 billions USD by 2032–2034, reflecting a compound annual growth rate (CAGR) of 3.2%–4.7%.
7. Data Bridge Market Research 'Global Agrochemicals Market – Industry Trends and Forecast to 2031', 2024, p. 350, https://www.databridgemarketresearch.com/reports/global-agrochemicals-market (accessed June 22, 2026).
8. 2025, Precedence Research - report 'Agrochemicals Market Size, Share, and Trends 2025 to 2034', 2025. https://www.precedenceresearch.com/agrochemicals-market#:~:text=Report%2020Code%2020%2023A%201596,Agrochemicals%201520Market%201520Size%201520and%201520Forecast%202025%201520to%202034,201592.201590%201525%201520from%202025%201520to%202034. (accessed June 22, 202026).

9. H. C. J. Godfray, J. R. Beddington, I. R. Crute, L. Haddad, D. Lawrence, J. F. Muir, J. Pretty, S. Robinson, S. M. Thomas and C. Toulmin, *Science*, 2010, **327**, 812-818.
10. M. W. A. Phillips, *Pest. Manag. Sci.*, 2020, **76**, 3348-3356.
11. T. Nikonovich, C. M. Chatzigiannis, C. Bordier, R. Solorzano-Rodriguez, D. M. Baier, F. F. Ort, R. Aav, T. Leyssens, D. Blanco-Ania, F. P. J. T. Rutjes, D. Kananovich and E. Colacino, *Chem. Rev.*, 2026, **126**, 6015-6080.
12. T. s. Čarný, P. t. Kisszékelyi, M. Markovič, T. Gracza, P. Kóóš and R. Šebesta, *Org. Lett.*, 2023, **25**, 8617-8621.
13. N. Fantozzi, J.-N. Volle, A. Porcheddu, D. Virieux, F. García and E. Colacino, *Chem. Soc. Rev.*, 2023, **52**, 6680-6714.
14. E. Colacino, V. Isoni, D. Crawford and F. Garcia, *Trends in Chem.*, 2021, **3**, 335-339.
15. O. Galant, G. Cerfeda, A. S. McCalmont, S. L. James, A. Porcheddu, F. Delogu, D. E. Crawford, E. Colacino and S. Spatari, *ACS Sustainable Chem. Eng.*, 2022, **10**, 1430-1439.
16. M. Patrascu, D. Meuti, O. Galant, S. Nijem, C. E. Diesendruck, A. Casagrande, E. Colacino, M. Felderhoff and S. Spatari, *Sustainable Chem. Pharm.*, 2026, **51**, 102422-102435
17. *IUPAC Guiding Principles of Responsible Chemistry*, https://iupac.org/responsible-chemistry/ (accessed June 22, 2026).
18. E. Lucas, A. J. Martín, S. Mitchell, A. Nabera, L. F. Santos, J. Pérez-Ramírez and G. Guillén-Gosálbez, *Green Chem.*, 2024, **26**, 9300-9309.
19. A. Nanni, P. Bilalis and M. Rueping, *Green Chem.*, 2026, **28**, 255-263.
20. N. Maarouf-Mesli, J. Desjardins-Michaud, Z. Imani, K. Ghosh, F. Polyak and W. D. Lubell, *Green Chem.*, 2026, **28**, 264-276.
21. W. I. Nicholson, F. Barreteau, J. A. Leitch, R. Payne, I. Priestley, E. Godineau, C. Battilocchio and D. L. Browne, *Angew. Chem. Int. Ed.*, 2021, **60**, 21868-21874.
22. A. Nagao, K. Kubota and H. Ito, *Synthesis*, 2026, **58**, 673-678.
23. C. Schumacher, L. Fritz, L. M. Hanek, V. Sidorin, D. Brüx and C. Bolm, *Molecules*, 2023, **28**, 807.
24. A. Casagrande, R. Solorzano-Rodriguez, M. Carta, F. Delogu, J. Vezzani, A. Niidu and E. Colacino, *Chem. Eur. J.*, 2026, **n/a**, e71190.
25. Estimated at 2.65–3.2 billions USD in 2024–2025, the SDHI market is expected to reach USD 5.1–5.43 billion by 2030–2032, with a CAGR of 7.8%–8.2%.
26. L. A. Carpino and A. El-Faham, *J. Am. Chem. Soc.*, 1995, **117**, 5401-5402.

27. T. Dalidovich, K. A. Mishra, T. Shalima, M. Kudrjašova, D. G. Kananovich and R. Aav, *ACS Sustainable Chem. Eng.*, 2020, **8**, 15703-15715.
28. T. Dalidovich, J. V. Nallaparaju, T. Shalima, R. Aav and D. G. Kananovich, *ChemSusChem*, 2022, **15**, e202102286.
29. C. R. McElroy, A. Constantinou, L. C. Jones, L. Summerton and J. H. Clark, *Green Chem.*, 2015, **17**, 3111-3121.
30. A. DeVierno Kreuder, T. House-Knight, J. Whitford, E. Ponnusamy, P. Miller, N. Jesse, R. Rodenborn, S. Sayag, M. Gebel, I. Aped, I. Sharfstein, E. Manaster, I. Ergaz, A. Harris and L. Nelowet Grice, *ACS Sustainable Chem. Eng.*, 2017, **5**, 2927-2935. DOZN™ is a universal tool, suitable for scoring any process, no matter the activation technique used, once the detailed experimental/process conditions are known. The DOZN™ tool is accessible free of charge here: https://bioinfo.merckgroup.com/dozn (accessed July 30, 2026).
31. P. Sharma and E. Ponnusamy, *Sustainable Chem. Climate Action*, 2025, **7**, 100129.
32. P. Sharma, C. Vetter, E. Ponnusamy and E. Colacino, *ACS Sustainable Chem. Eng.*, 2022, **10**, 5110-5116.
33. G. L. Beutner, I. S. Young, M. L. Davies, M. R. Hickey, H. Park, J. M. Stevens and Q. Ye, *Org. Lett.*, 2018, **20**, 4218-4222.
34. N. Shan, F. Toda and W. Jones, *Chem. Commun.*, 2002, **38**, 2372-2373.
35. M. Carta and F. Delogu, *Chem. Eng. Sci.*, 2026, **335**, 124495.
36. A. Polo, M. Carta, F. Delogu, M. Rustici and M. A. Budroni, *Front. Chem.*, 2022, **10**, 915217.
37. M. Broseghini, M. D'Incau, L. Gelisio, N. M. Pugno and P. Scardi, *Mat. Des.*, 2016, **110**, 365-374.
38. L. Vugrin, C. Chatzigiannis, E. Colacino and I. Halasz, *RSC Mechanochem.*, 2025, **2**, 482-487.
39. K. Martina, L. Rotolo, A. Porcheddu, F. Delogu, S. R. Bysouth, G. Cravotto and E. Colacino, *Chem. Commun.*, 2018, **54**, 551-554.
40. A. A. L. Michalchuk and E. V. Boldyreva, in *Encyclopedia of Green Chemistry (First Edition)*, ed. B. Török, Elsevier, Oxford, 2025, DOI: https://doi.org/10.1016/B978-0-443-15742-4.00121-6, pp. 532-541.
41. L. Gonnet, T. H. Borchers, C. B. Lennox, J. Vainauskas, Y. Teoh, H. M. Titi, C. J. Barrett, S. G. Koenig, K. Nagapudi and T. Friščić, *Faraday Discuss.*, 2023, **241**, 128-149.

42. P. Baláž, M. Achimovičová, M. Baláž, P. Billik, Z. Cherkezova-Zheleva, J. M. Criado, F. Delogu, E. Dutková, E. Gaffet, F. J. Gotor, R. Kumar, I. Mitov, T. Rojac, M. Senna, A. Streletskii and K. Wieczorek-Ciurowa, *Chem. Soc. Rev.*, 2013, **42**, 7571-7637.
43. K. Nagapudi, E. Y. Umanzor and C. Masui, *Int. J. Pharm.*, 2017, **521**, 337-345.
44. D. H. Leung, D. J. Lamberto, L. Liu, E. Kwong, T. Nelson, T. Rhodes and A. Bak, *Int. J. Pharm.*, 2014, **473**, 10-19.
45. C. Chatzigiannis, S. Scalzullo, E. Colacino and M. E. Rivas-Velazco, *ChemSusChem*, 2025, **n/a**, e202500110.
46. M. Carta, S. L. James and F. Delogu, *Molecules*, 2019, **24**.
47. A. A. L. Michalchuk, I. A. Tumanov, S. Konar, S. A. J. Kimber, C. R. Pulham and E. V. Boldyreva, *Adv. Sci.*, 2017, **4**, 1700132.
48. D. Braga, L. Casali and F. Grepioni, *Int. J. Mol. Sci.* , 2022, **23**, 9013.
49. D. Braga, *Chem. Commun.*, 2023, **59**, 14052-14062.
50. P. Orecchia, D. S. Petkova, R. Goetz, F. Rominger, A. S. K. Hashmi and T. Schaub, *Green Chem.*, 2021, **23**, 8169-8180.
51. H. Kim, H. Yang, K. J. Sang, S.-H. Moon and T. H. Kim, *Acta Cryst. E*, 2010, **66**, o2471.
52. P. Garrido-García, I. Quirós, P. Milán-Rois, S. Ortega-Gutiérrez, M. Martín-Fontecha, L. A. Campos, Á. Somoza, I. Fernández, T. Rigotti and M. Tortosa, *Nat. Chem.*, 2025, **17**, 734-745.
53. J. Sun and H. Duan, *CN118772051A*, 2024.
54. L. Gonnet, C. B. Lennox, J.-L. Do, I. Malvestiti, S. G. Koenig, K. Nagapudi and T. Friščić, *Angew. Chem. Int. Ed.*, 2022, **61**, e202115030.
55. L. Zhang, N. Ma, M. Wang, W. Gou, J. Tian, Q. Xu, C. Zhao and C. Li, *Org. Chem. Front.*, 2024, **11**, 1796-1803.
56. I. Chiyomaru, S. Kawada and K. Takita, 1976, US3937840A.
57. A. Nandikolla, Y. M. Khetmalis, G. P. V. Sangeetha, A. Chandu, Swati, M. M. K. Kumar, V. Sharma, S. Murugesan and K. V. G. Chandra Sekhar, *New J. Chem.*, 2023, **47**, 15378-15389.
58. K. Yabutani, K. Ikeda, S. Hatta and T. Harada, *US4093743A*, 1977.
59. B. Ke, Y. Wang, H. Pan, X. Cheng, H. Chen, W. He, L. He, X. Yang, Y. Xu, W. Dong and S. Tang, *WO2025074339A1*, 2025.
60. Y. Zhang, Z. Chen, J. Nie, F.-G. Zhang and J.-A. Ma, *J. Org. Chem.*, 2019, **84**, 7148-7158.
61. E. Lucas, A. J. Martín, S. Mitchell, A. Nabera, L. F. Santos, J. Pérez-Ramírez and G. Guillén-Gosálbez, *Green Chem.*, 2024, **26**, 9300-9309.

62. IMPACTIVE: Innovative Mechanochemical Processes to synthesize green ACTIVE pharmaceutical ingredients. https://mechanochemistry.eu/ (accessed 18 June, 2026).
63. J. J. Sáenz de la Torre, L. Flamarique, F. Gomollon-Bel and E. Colacino, *Open Res. Europe*, 2025, **5**, 73. DOI: 10.12688/openreseurope.19848.12681.

Scalable Amidation Reaction by Resonant Acoustic Mixing. Application to the multi-gram scale synthesis of marketed Agrochemicals.

Andrea Casagrande,[a,b] Christos Chatzigiannis,[a] Ken-ichi Otake,[c] Joris Vezzani,[a] Allan Niidu,[b] Evelina Colacino.[a,*]

[a] ICGM, Univ. Montpellier, CNRS, ENSCM, 34293 Montpellier, France

[b] Virumaa College, Tallinn's University of Technology, Ehitajate tee 5, 19086, Tallinn, Estonia

[c] Institute for Integrated Cell-Material Sciences (iCeMS), Kyoto University, Kitagawa Laboratory, iCeMS Research Bldg., 2F, Yoshida-Honmachi, Sakyo-ku, Kyoto, 606-8501, Japan

*E-mail: evelina.colacino@umontpellier.fr

INDEX

EXPERIMENTAL PART S5

Materials and methods S5

Experimental procedures S6

Method A1 – General experimental procedure to prepare compounds **1-5** in a horizontal vibrating ball-mill (VBM, Retsch MM400) – Tables 1 and 2. S6

Method A2 – General experimental procedure to prepare compounds **1** and **2** in a vertical vibrating ball-mill (VBM, Fritsch Pulverisette P23) – Tables 1 and 2. S7

Method B – General experimental procedure to prepare compounds **1-5** in a planetary ball-mill (Fritsch® Pulverisette 7 Premium or Pulverisette 6) – Table 2. S7

Method C1 – General experimental procedure for compounds **1-5** in a resonant acoustic mixer (Resodyn™ LabRAM II) in 2.5 mL polypropylene vials (small scale) – Tables 2, 3 and 4. S8

Method C2 – General experimental procedure to prepare compounds **1-5** by resonant acoustic mixing (Resodyn™ LabRAM II) in a 240 mL PTFE vessel (large scale) – Table 5. S8

Table S1. Scalability studies by LA-RAM for Fenfuram (**1**) using Methods C1 and C2. S9

Figure S1. Scalability studies by LA-RAM for compounds **1-5** using Methods C1 and C2. Isolated yield (%) as a function of reaction scale (mmol) for the targets **1-5** synthesized by TCFH-mediated amidation by LA-RAM. S9

High-pressure DSC screening of the Fenfuram (1) reaction mixture S10

Figure S2. High-pressure DSC thermogram of the premixed Fenfuram reaction mix corresponding in stoichiometry to methods C. Sample mass: 10.0 mg; closed, gold-plated, 100 μL high-pressure crucible; heating rate: 5 K min^{-1} from 20 to 300 °C. S10

SPECTRAL CHARACTERIZATION FOR AGROCHEMICALS 1-5. S11

2-Methyl-*N*-phenyl-3-furamide (Fenfuram) (**1**). CAS [24691-80-3]. S11

Figure S3. Thermal analysis by Differential Scanning Calorimetry (DSC) for Fenfuram (**1**). S11

2-Chloro-*N*-(4′-chloro[1,1′-biphenyl]-2-yl)pyridine-3-carboxamide (Boscalid) (**2**). CAS [188425-85-6]. S11

Figure S4. Thermal analysis by Differential Scanning Calorimetry (DSC) for Boscalid (**2**). S12

2-Methyl-*N*-(3-propan-2-yloxyphenyl)benzamide (Mepronil) (**3**). CAS [55814-41-0]. S12

Figure S5. Thermal analysis by Differential Scanning Calorimetry (DSC) for Mepronil (**3**). S13

N-(3-Isopropoxyphenyl)-2-(trifluoromethyl)benzamide (Flutolanil) (**4**). CAS [66332-96-5]. S13

Figure S6. Thermal analysis by Differential Scanning Calorimetry (DSC) for Flutolanil (**4**). S14

3-(Difluoromethyl)-1-methyl-*N*-(3′,4′,5′-trifluoro[1,1′-biphenyl]-2-yl)-1*H*-pyrazole-4-carboxamide (Fluxapyroxad) (**5**). CAS [907204-31-3]. S14

Figure S7. Thermal analysis by Differential Scanning Calorimetry (DSC) for Fluxapyroxad (**5**). S15

METHODOLOGY VALIDATION FOR AMIDATION REACTION BY RAM (COMPARATIVE EXPERIMENTS) S15

Table S2. Comparative data for the LA-RAM amidation reaction to agrochemicals (**1-5**), prepared via EDC·HCl/Oxyma-mediated synthesis (one-pot/one-step strategy). S15

PXRD PATTERN INDEXING FOR COMPOUNDS 1-5. S16

2-Methyl-*N*-phenyl-3-furamide (Fenfuram) (**1**). CAS [24691-80-3]. S16

Figure S8. Synchrotron PXRD pattern of Fenfuram (**1**), in accordance with CSD deposited structure. S16

Table S3. Most intense peaks for the PXRD diffractogram of Fenfuram (**1**) prepared by LA-RAM and analysed at synchrotron (Table 3, entry 6). S17

2-Chloro-*N*-(4'-chloro[1,1'-biphenyl]-2-yl)pyridine-3-carboxamide (Boscalid) (**2**). CAS [188425-85-6]. S21

Figure S9. Synchrotron PXRD pattern of Boscalid (**2**), in accordance with CSD deposited structure (refcode NOZKOF02). S22

Table S4. Most intense peaks for the PXRD diffractogram of Boscalid (**2**) prepared by LA-RAM (Table 4, entry 3). S22

2-Methyl-*N*-(3-propan-2-yloxyphenyl)benzamide (Mepronil) (**3**). CAS [55814-41-0]. S26

Figure S10. Synchrotron PXRD pattern of Mepronil (**3**), in accordance with CSD deposited structure. S26

Table S5. Most intense peaks for the PXRD diffractogram of Mepronil (**3**) prepared by LA-RAM (Table 2, entry 3). S26

N-(3-Isopropoxyphenyl)-2-(trifluoromethyl)benzamide (Flutolanil) (**4**). CAS [66332-96-5]. S32

Figure S11. Synchrotron PXRD pattern of Flutolanil (**4**), in accordance with CSD deposited structure (refcode KUYVOQ). S33

Table S6. Most intense peaks for the PXRD diffractogram of Flutolanil (**4**) prepared by LA-RAM (Table 2, entry 4). S33

3-(Difluoromethyl)-1-methyl-*N*-(3',4',5'-trifluoro[1,1'-biphenyl]-2-yl)-1*H*-pyrazole-4-carboxamide (Fluxapyroxad) (**5**). CAS [907204-31-3]. S37

Figure S12. Synchrotron PXRD pattern of Fluxapyroxad (**5**), in accordance with CSD deposited structure (refcode IDECIH). S37

Table S7. Most intense peaks for the PXRD diffractogram of Fluxapyroxad (**5**) prepared by LA-RAM (Table 2, entry 5). S37

GREEN CHEMISTRY METRICS: COMPARATIVE ASSESSMENT OF SOLUTION-BASED *vs* MECHANOCHEMICAL METHODS. S43

Back-to-back comparison between solution and LA-RAM (at scale) methods. S44

Table S12. Small-scale, TCFH-mediated mechanochemical amidation reaction to phytopharmaceuticals **1-5**, by ball-milling (VBM and PBM) in LAG conditions, and comparison with the 1,1'-oxalyl diimidazole (ODI)-mediated reaction in a PBM, by LA-RAM, and with solution-based methods. S44

Table S13. Comparison between solution-based method and TCFH-mediated amidation reaction by LA-RAM protocols for the synthesis of Fenfuram (**1**). S45

Table S14. Comparison between solution-based method and TCFH-mediated amidation reaction by LA-RAM protocols for the synthesis of Boscalid (**2**). S46

Table S15. Comparison between solution-based method and TCFH-mediated amidation reaction by LA-RAM protocols for the synthesis of Mepronil (**3**). S47

Table S16. Comparison between solution-based method and TCFH-mediated amidation reaction by LA-RAM protocols for the synthesis of Flutolanil (**4**). S47

Table S17. Comparison between solution-based method and TCFH-mediated amidation reaction by LA-RAM protocols for the synthesis of Fluxapyroxad (**5**). S48

Assessment by DOZN™ 3.0. S49

Figure S13. Comparison of VBM *vs* PBM *vs* RAM (0.58 mmol scale, "small scale") *vs* RAM (93.01 mmol scale, "large scale") protocols for the synthesis of **1-5** by DOZN™ 3.0 Quantitative Scoring tool. S49

Figure S14. Comparison of solution *vs* RAM (0.58 mmol scale, "small scale") *vs* RAM (93.01 mmol scale, "large scale") methods for the synthesis of **1-5** by DOZN™ 3.0 Quantitative Scoring tool. S50

Table S18. Comparison of CHEM21 assessment for solution-based *vs* LA-RAM using TCFH as a coupling agent for the synthesis of compounds (**1**), (**2**) and (**3**). S51

REFERENCES S53

Spectral data (^{1}H, ^{13}C and for compounds 1-5, and ^{19}F NMR for compounds 4 and 5) S54

EXPERIMENTAL PART

MATERIALS AND METHODS

Chemicals. All reagents were commercially available and used without any further purification.

Liquid nuclear magnetic resonance (NMR) spectroscopy. ^{1}H, ^{13}C and ^{19}F NMR spectra were recorded at room temperature on a Bruker 400 MHz spectrometer at room temperature. Chemical shifts (δ) of ^{1}H NMR and ^{13}C NMR spectra are reported in ppm relative to residual solvent signals with the appropriate deuterated solvent (DMSO-d_6 and $CDCl_3$). Chemical shifts (δ) of ^{1}H NMR and ^{13}C NMR spectra are reported in ppm relative to residual solvent signals (DMSO in DMSO-d_6: δ = 2.52 ppm for ^{1}H and δ = 39.52 ppm for ^{13}C NMR; $CHCl_3$ in $CDCl_3$: δ = 7.27 ppm for ^{1}H and $^{13}CDCl_3$: δ = 77.16 ppm for ^{13}C NMR). ^{19}F NMR spectra were recorded at 376 MHz with the same instrument. The chemical shifts are expressed in parts per million (ppm), reported from $CFCl_3$ δ = 0.0 ppm by definition.[1] *J* values are given in *Hz*. ^{1}H and ^{13}C NMR spectra were recorded at 400 MHz and 100.63 MHz respectively. The following abbreviations are used to express the multiplicity: s (singlet), d (doublet), t (triplet), q (quadruplet), dd (doublet of doublet), dt (doublet of triplets), td (triplet of doublets) or m (multiplet). The identity of analytically pure final products was assessed by comparison of the spectral data previously described in the literature and by their fragmentation in GC–MS.

Melting points were measured: i) in an open capillary on a Stuart SMP50 automatic melting point apparatus equipped with a PT1000 Platinum resistance temperature sensor and a heating rate of 2°C/min; and/or ii) by Differential Scanning Calorimetry (DSC).

Differential scanning calorimetry (DSC). Analyses for all compounds were performed with a Netzsch DSC 200F3 calorimeter with intra-cooler, at the heating rate of 2 °C min^{-1}. Samples were placed in hermetic aluminum pans. Constant calibration was performed using adamantane, biphenyl, indium, zinc, tin and bismuth standards. Nitrogen was used as the purge gas.

Temperature of reaction mixture processed by RAM was measured with a 66IR200 InfraRed Thermometer.

Gas Chromatography coupled to Mass Spectrometry (GC-MS). GC-MS analyses were performed using a Shimadzu GCMS-QP2010 SE (Shimadzu, Kyoto, Japan) gas chromatograph, equipped with an AOC-20i autosampler and a Zebron ZB-5ms column equipped and a data processor. The oven program was as follows: temperature increase from 50 °C at a rate of 2°C/min up to 280 °C. Helium was used as carrier gas (0.74 mL min^{-1}). The injector and detector temperatures were set at 250 °C and 280 °C, respectively. 1 μL of the solution was injected with split mode 30; MS range 30-800.

High-Resolution Powder X-Rays Diffraction (PXRD). High-resolution synchrotron X-ray diffraction and total scattering measurements were performed at beamline ID31 at the European Synchrotron Radiation Facility (ESRF). The sample powders were loaded into cylindrical slots (approx. 1 mm thickness) held between Kapton windows in a high-throughput sample holder. Each sample was measured in transmission geometry with an incident X-ray energy of 75.051 keV (λ = 0.16520 Å). Measured intensities were collected using a Pilatus CdTe 2M detector (1679 × 1475 pixels, 172×172 μm2 each) positioned with the incident beam in the corner of the detector. The sample-to-detector distance was approximately 1.5 m for the high-resolution measurements and 0.3 m for the total scattering measurements. Background measurements for the empty windows were measured and subtracted. NIST SRM 660b (LaB_6) was used for geometry calibration performed with the software

pyFAI followed by image integration including a flat-field, geometry, solid-angle, and polarization corrections.

Microcrystal Electron Diffraction (MicroED) measurements were conducted using RIGAKU/JEOL SynergyED electron diffractometer. The samples were continuously rotated along a single axis from –50° to +50° at a rotation rate of 0.2° s^{-1}. The electron dose rate was set to 0.01 el $Å^{-2}$ s^{-1}, thus the total dose was 3 el $Å^{-2}$. No significant beam damage was observed after each 3DED data collection. The data reduction was performed using either CrysAlispro for ED. The intrinsic phase method was applied for structural solution using SHELXT, followed by refinement using SHELXL under Olex2 platform. The crystallographic data have been deposited with the Cambridge Crystallographic Data Centre (CCDC) under deposition number 2584567 for Fenfuram (**1**), and 2584568 for Mepronil (**3**).

Vibrating ball-mill (VBM) experiments were performed in a Retsch® MM400 horizontal vibrating ball mill at 30 *Hz*, in a 10 mL volume ZrO_2 jar using a single 10 mm Ø ZrO_2 ball (m_{ball} = 3.113 g) or in a Fritsch Pulverisette P23 vertical vibrating mill at 30 or 50 *Hz* in a 10 mL volume ZrO_2 jar using a single 10 mm Ø ZrO_2 ball (m_{ball} = 3.026 g).

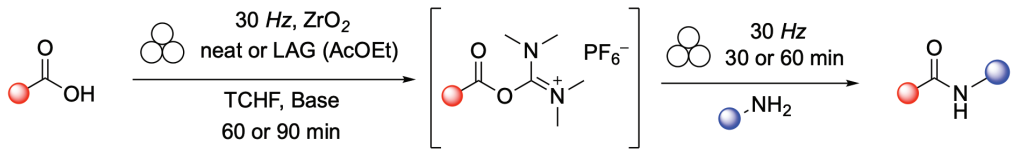
Planetary ball-mill (PBM) experiments were performed in a Fritsch Pulverisette P7 Premium (for compounds **1** and **2**) or Pulverisette P6 (for compounds **3-5**), operating at 500 rpm, in a 45 mL volume ZrO_2 jar, using 50 5 mm Ø ZrO_2 balls (m_{ball} = 0.411 g). Chemical composition for zirconium oxide beads : Zirconium oxide 95% and Yittrium oxide 5% (data source: https://www.fritsch-france.fr/preparation-dechantillons/broyage/broyeurs-planetaires/details/produit/pulverisette-7-premium-line/accessoires/).

Resonant acoustic mixer (RAM) experiments were performed in a Resodyn® LabRAM II mixer at 90 *g* at 60 *Hz* using either a Supelco® polypropylene (PP) limited volume vial (2.5 mL), VWR® PTFE screw top jars (volume either 15 mL, 30 mL, 120 mL or 240 mL) or Supelco® glass vial with polypropylene cap (4 mL). For experiment conducted in parallel, holders for 6 and 14 samples were used.

All the experiments were carried out in duplicate to ensure reproducibility of the experimental data. Yields refer to pure isolated materials.

EXPERIMENTAL PROCEDURES

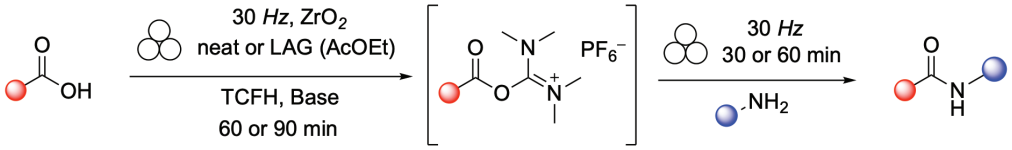
Method A1 – General experimental procedure to prepare compounds 1-5 in a horizontal vibrating ball-mill (VBM, Retsch MM400) – Tables 1 and 2.



Step 1. To a 10 mL ZrO_2 jar equipped with a 10 mm diameter ball of the same material (m_{ball} = 3.113 g), the acid (0.66 mmol, 1.1 equiv.) and *N,N,N',N'*-tetramethylchloroformamidinium hexafluorophosphate (TCFH, 0.66 mmol, 1.1 equiv., 185.2 mg) were added in the presence of a base (1.8 mmol, 3.0 equiv.). For accessing compounds **1-4**, the base was dipotassium phosphate (K_2HPO_4, 313.6 mg) and AcOEt (η = 0.2 μL/mg, LAG solvent) were added. For

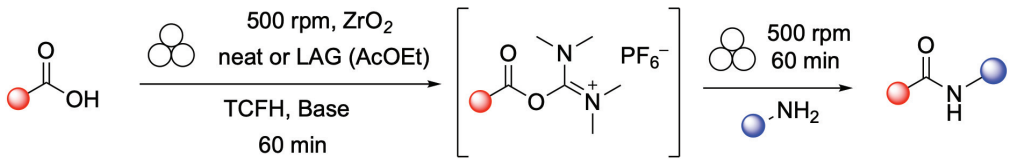
accessing compound **5**, the base was *N*-methylimidazole (NMI, 142.8 μL). Milling occurred at 30 *Hz* during 60 min (for compounds **1**, **3-5**) or 90 min (for compound **2**). *Step 2*. After this time, the amine (0.48 mmol, 0.8 equiv.) was added, and the reaction mixture was further ball-milled at 30 *Hz* for 30 min. (for compound **1**) or 60 min. (for compounds **2-5**). The final product was recovered by precipitation with water i) 10 mL for compounds **1** ii) 20 mL for compounds **3** and **4**, iii) 10 mL and CaO under stirring until pH = 8 (2.0 mg), then filtered under vacuum and washed with 8 mL of 1M HCl and 2 mL of water, for compound **2**; or iv) 18 mL 1M HCl and 2 mL water for compound **5**. The precipitate was dried overnight under vacuum over P_2O_5 to afford the clean products **1-5**.

Method A2 - General experimental procedure to prepare compounds 1 and 2 in a vertical vibrating ball-mill (VBM, Fritsch Pulverisette P23) - Tables 1 and 2.



Step 1. To a 10 mL ZrO_2 jar equipped with one 10 mm diameter ball of the same material (m_{ball} = 3.026 g), the acid (0.66 mmol, 1.1 equiv.), *N,N,N',N'*-tetramethylchloroformamidinium hexafluorophosphate (TCFH, 0.66 mmol, 1.1 equiv., 185.2 mg), dipotassium phosphate (K_2HPO_4, 1.8 mmol, 3.0 equiv., 313.6 mg) and AcOEt (η = 0.2 μL/mg, LAG solvent), were added. Milling occurred at 50 *Hz* during 90 min. *Step 2*. After this time the amine (0.48 mmol, 0.8 equiv.) was added, and the reaction mixture was further ball-milled at 50 *Hz* for 60 min. The final product was recovered by precipitation with water : i) 10 mL for compound **1**, and ii) 10 mL of water with CaO under stirring until pH = 8 (2.0 mg) and washed with 18 mL 1M HCl and 2 mL water for compound **2**. The precipitate was dried overnight under vacuum over P_2O_5 to afford the clean products **1-2**.

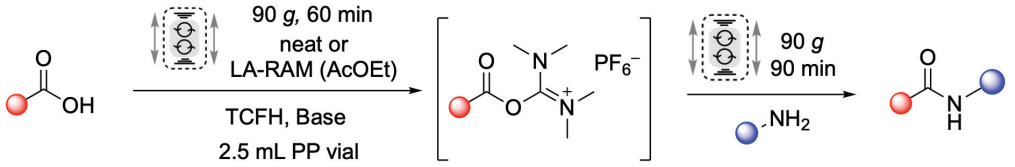
Method B – General experimental procedure to prepare compounds 1-5 in a planetary ball-mill (Fritsch® Pulverisette 7 Premium or Pulverisette 6) - Table 2.



Step 1. To a 45 mL ZrO_2 jar equipped with 50 balls of the same material (5 mm Ø, m_{ball} = 0.411 g), the acid (2.64 mmol, 1.1 equiv.) and *N,N,N',N'*-tetramethylchloroformamidinium hexafluorophosphate (TCFH, 2.64 mmol, 1.1 equiv., 740.7 mg) were added in the presence of a base (7.2 mmol, 3.0 equiv.). For accessing compounds **1-4**, the base was dipotassium phosphate (K_2HPO_4, 1.254 g), and AcOEt (η = 0.2 μL/mg) was added as LAG solvent. For accessing compound **5**, the base was N-methylimidazole (NMI, 142.8 μL) and the reaction was conducted by neat grinding. Milling occurred at 500 rpm for 60 min. *Step 2.* After this time, the amine (1.92

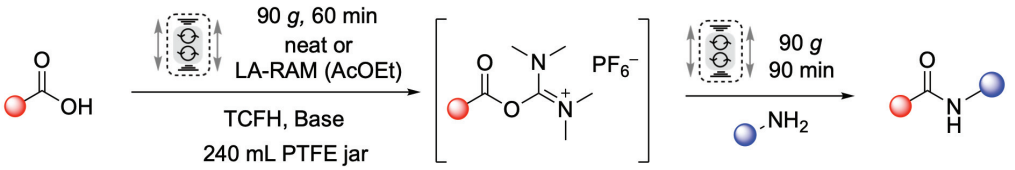
mmol, 0.8 equiv.) was added, and the reaction mixture was further ball-milled at 500 rpm for 60 min. The final product was recovered by precipitation with water i) 45 mL for compounds **1**, **3** and **4**, ii) 45 mL and CaO under stirring until pH = 8 (5.0 mg) then filtered under vacuum and washed with 40 mL of 1M HCl and 5 mL of water, for compound **2**; or iii) 40 mL of 1M HCl and 5 mL of water for compound **5**. The precipitate was dried overnight under vacuum over P_2O_5 to afford the clean products **1-5**.

Method C1 – General experimental procedure for compounds 1-5 in a resonant acoustic mixer (Resodyn™'s LabRAM II) in 2.5 mL polypropylene vials (small-scale) – Table 2, Table 3 and Table 4.



Step 1. To a 2.5 mL PP vial the acid (0.8 mmol, 1.1 equiv.) and *N,N,N',N'*-tetramethylchloroformamidinium hexafluorophosphate (TCFH, 0.8 mmol, 1.1 equiv., 224.5 mg) were added in the presence of a base. For accessing compound **2**, the base was dipotassium phosphate (K_2HPO_4, 2.4 mmol, 3.0 equiv., 380.1 mg) and AcOEt (η = 0.2 µL/mg, 169.8 μL) was used as liquid-assisted RAM (LA-RAM) solvent. For accessing compounds **1**, **3-5** the base was *N*-methylimidazole (NMI, 2.4 mmol, 3.0 equiv., 179.1 μL). The mixture was reacted at 90 *g* for 60 min. *Step 2*. After this time, the amine (0.58 mmol, 0.8 equiv.) was added, and the reaction mixture was further mixed at 90 *g* for 90 min. The final product was recovered by precipitation with i) 10 mL of water for compounds **1**, **3** and **4**, ii) 10 mL of water and CaO under stirring until pH = 8 (2.0 mg) then filtered under vacuum and washed with 8 mL of 1M HCl and 2 mL of water, for compound **2**; or iii) 10 mL 1M HCl for compound **5**. The precipitate was dried overnight under vacuum over P_2O_5 to afford the clean products **1-5**.

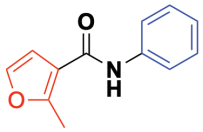
Method C2 – General experimental procedure to prepare compounds 1-5 by resonant acoustic mixing (Resodyn™ LabRAM II) in 240 mL PTFE vessel (large scale) – Table 5.



Step 1. To a 240 mL PTFE screw top vessel, the acid (128 mmol, 1.1 equiv.) and *N,N,N',N'*-tetramethylchloroformamidinium hexafluorophosphate (TCFH, 128 mmol, 1.1 equiv., 35.91 g) were added in the presence of a base. For accessing compound **2**, the base was dipotassium phosphate (K_2HPO_4, 349.1 mmol, 3 equiv., 60.81 g) and AcOEt (η = 0.2 μL/mg, 27.17 mL) was used as liquid-assisted RAM (LA-RAM) solvent. For accessing compounds **1**, **3-5** the base was *N*-

methylimidazole (NMI, 349.1 mmol, 3.0 equiv., 27.69 mL). The mixture was reacted at 90 *g* for 60 min. *Step 2.* After this time, the amine (93.1 mmol, 0.8 equiv.) was added, and the reaction mixture was further mixed at 90 *g* for 90 min. The final product was recovered by precipitation with i) 1 L of water for compound **1**, or ii) 1 L of water and CaO under stirring until pH = 8 (30 mg) then filtered under vacuum and washed with 950 mL of 1M HCl and 50 mL water, for compound **2**; iii) 550 mL of 1M HCl and 50 mL water for compounds **3** and **4**; or iv) 950 mL of 1M HCl and 50 mL water for compound **5**. The precipitate was dried overnight under vacuum in an oven at 80°C to afford the clean products **1-5**.

Table S1. Scalability studies by LA-RAM for Fenfuram (**1**) using Methods C1 and C2.



1

Vial type	Volume (mL)	Scale (mmol)	Amount of 1 (g)	Yield (%)
PP	2.5	0.8	0.10	86
Glass	4	2.0	0.29	94
PTFE	7	3.8	0.51	93
PTFE	15	8.0	1.15	98
PTFE	30	16.0	2.27 (2.34) [a]	97 (100)[a]
PTFE	120	64.0	9.37	100
PTFE	240	128.0	18.00	96

[a] The reaction was performed at 45 *g* (for both steps).

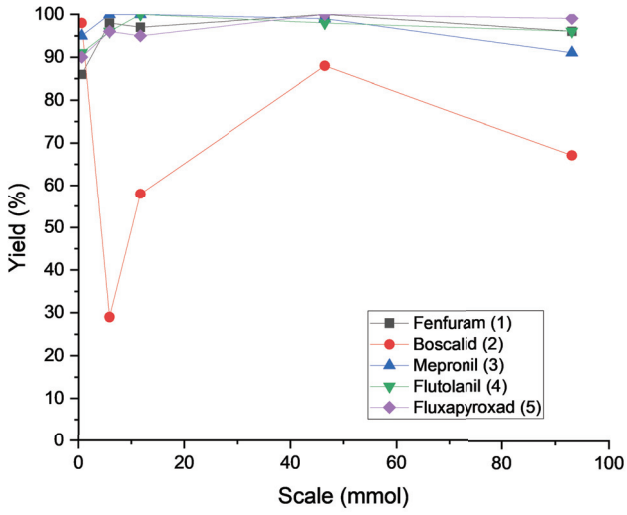


Figure S1. Scalability studies by LA-RAM for compounds **1-5** using Methods C1 and C2. Isolated yield (%) as a function of reaction scale (mmol) for the targets **1-5** synthesized by TCFH-mediated amidation by LA-RAM.

High-pressure DSC screening of the Fenfuram (1) reaction mixture

A formulation containing the carboxylic acid, TCFH, NMI, and aniline in the proportions used for Fenfuram synthesis in Table 3, entry 6, was prepared by combining all components. Approximately 15 min after preparation, a 10.0 mg sample was analyzed using a NETZSCH DSC 200 F3 instrument in a closed, gold-plated, 100 μL high-pressure crucible. The sample was heated from 20 to 300 °C at 5 K min^{-1}. Exothermic heat flow is plotted upwards.

A broad exothermic event was observed with a peak at 98.3 °C and an integrated heat release of 64.4 J g^{-1} under the selected baseline. Additional exothermic events peaked at 167.1 and 207.6 °C, with integrated heat releases of 13.3 and 30.0 J g^{-1}, respectively. The chemical origins of these events were not established. As reaction may occur before measurement, the recorded heat release does not necessarily represent the total enthalpy of the transformation.

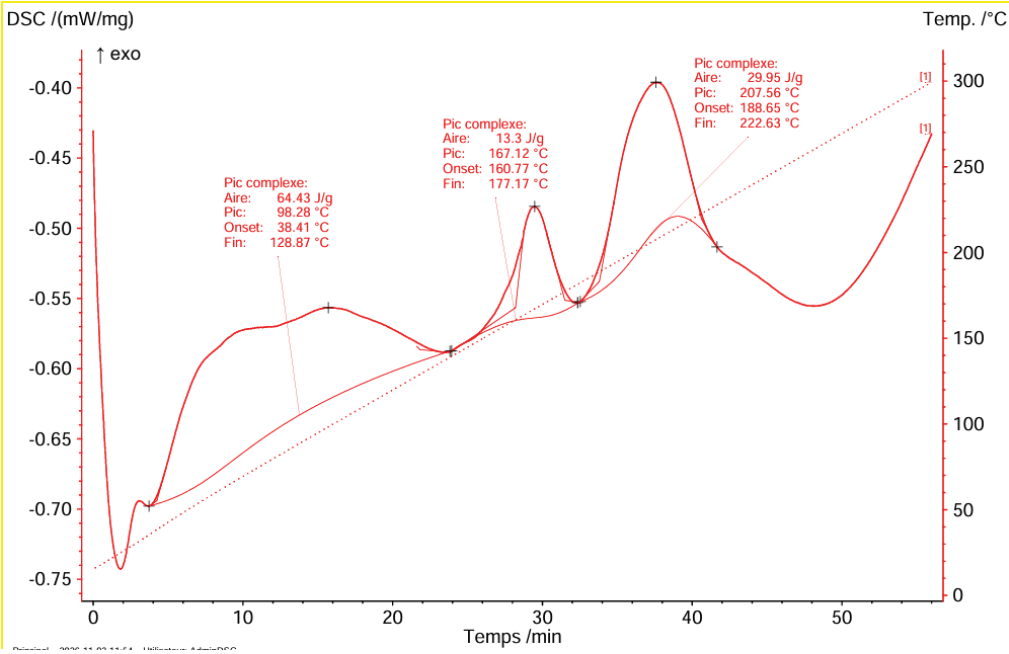
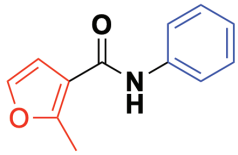


Figure S2. High-pressure DSC thermogram of the premixed Fenfuram reaction mix corresponding in stoichiometry to methods C. Sample mass: 10.0 mg; closed, gold-plated, 100 μL high-pressure crucible; heating rate: 5 K min^{-1} from 20 to 300 °C.

SPECTRAL CHARACTERIZATION FOR AGROCHEMICALS 1-5.

2-methyl-*N*-phenyl-3-furamid (Fenfuram) (1). CAS [24691-80-3].



1

Compound (**1**) was prepared using Method **A1**: 78% (75.4 mg); Method **A2**: 41% (39.5 mg); Method **B**: 84% (324.5 mg); Method **C1**: 86% (100.1 mg); Method **C2**: 96% (18.0 g). Off-white powder, **m.p.** 109.0°C capillary (lit. 109.5°C)[1], **DSC m.p.** 108°C (Figure S3); **^{1}H NMR** (400 M*Hz*, $CDCl_3$)[2] δ (ppm): 7.57 (d, *J* = 7.68 *Hz*, 2H) 7.39 - 7.30 (m, 4H), 7.13 (t, *J* = 7.39 *Hz,* 1H), 2.64 (s, 3H). **^{13}C{^{1}H} NMR** (101 M*Hz*, $CDCl_3$)[2] δ(ppm): 162.2, 158.2, 140.7, 137.9, 129.2, 124.5, 120.3, 115.93, 108.3, 13.8. **^{1}H NMR** (400 M*Hz*, DMSO-d_6) δ (ppm): 9.71 (s, 1H), 7.71 (d, *J* = 7.8 *Hz*, 2H), 7.61 (d, *J* = 2.0 Hz, 1H), 7.34 (t, *J* = 7.9 *Hz*, 2H), 7.09 (dd, *J* = 10.3, 4.5 *Hz*, 2H), 2.56 (s, 3H). **^{13}C{^{1}H} NMR** (101 M*Hz*, DMSO-d_6) δ (ppm): 162.2, 157.4, 141.2, 139.4, 129.0, 123.9, 120.9, 116.5, 109.9, 13.8. **EI-(+)** *m/z*: 201 [M]$^{\bullet}$, 109, 43.

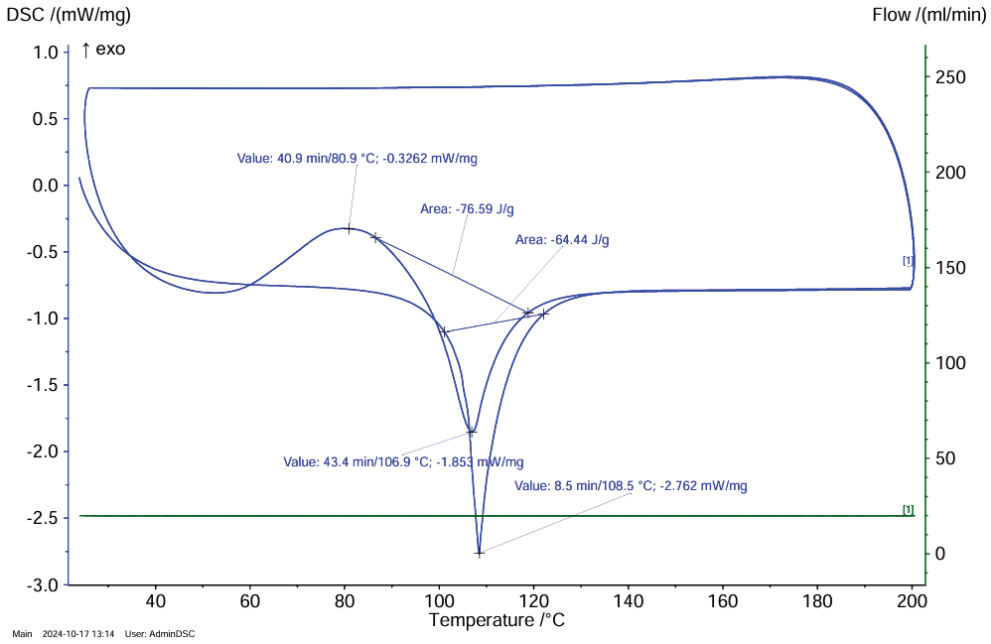
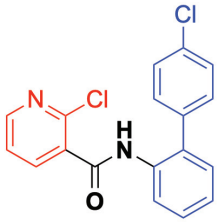


Figure S3. Thermal analysis by Differential Scanning Calorimetry (DSC) for Fenfuram (**1**).

2-chloro-N-(4'-chloro[1,1'-biphenyl]-2-yl)pyridine-3-carboxamide (Boscalid) (2). CAS [188425-85-6].

Compound (**2**) was prepared using Method **A2**: 92% (159.4 mg); Method **B**: 51% (337.0 mg); Method **C1**: 98% (194.7 mg); Method **C2**: 67% (21.46 g). White powder, **m.p.** 144.9°C capillary (lit. 143°C),[3] **DSC m.p.** 142.6 °C (Figure S4); **^{1}H NMR** (400 M*Hz*, $CDCl_3$)[4] δ (ppm): 8.47 - 8.42 (m, 2H), 8.15



2

(dd, *J* = 7.7 *Hz*, *J* = 1.9 *Hz,* 2H), 7.48 - 7.42 (m, 3H), 7.37 - 7.32 (m, 3H), 7.28 - 7.26 (m, 2H). **^{13}C{^{1}H} NMR** (101 M*Hz*, $CDCl_3$)[4] *δ* (ppm): 162.6, 151.5, 140.4, 136.4, 134.6, 134.5, 132.3, 131.2, 131.0, 130.4, 129.5, 129.1, 125.5, 123.1, 122.2. **^{1}H NMR** (400 M*Hz*, DMSO-d_6) *δ* (ppm): 10.17 (s, 1H), 7.88 (dd, *J* = 7.5, 1.9 *Hz*, 1H), 7.60 (d, *J* = 7.8 *Hz*, 1H), 7.56 – 7.35 (m, 9H). **^{13}C{^{1}H} NMR** (101 M*Hz*, DMSO-d_6) δ (ppm): 164.7, 150.8, 146.9, 138.3, 138.2, 136.8, 134.4, 133.4, 132.6, 131.2, 130.8, 128.8, 127.9, 127.5, 123.5. **EI-(+)** *m/z* for ^{37}Cl/^{35}Cl: 346/344/342 [M]•, 142/140, 114/112, 76.

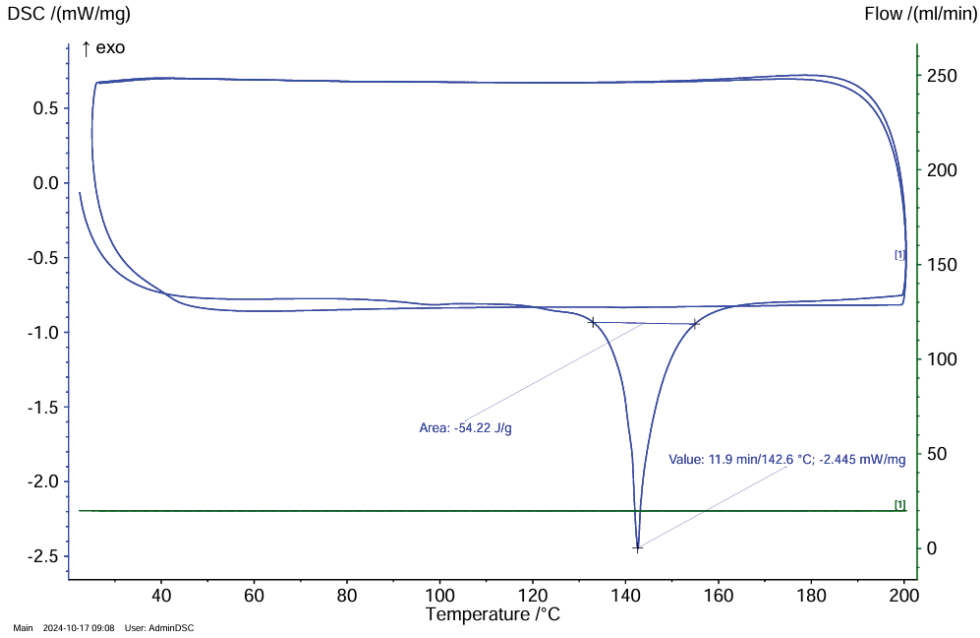
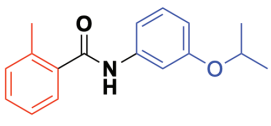


Figure S4. Thermal analysis by Differential Scanning Calorimetry (DSC) for Boscalid (**2**).

2-methyl-*N*-(3-propan-2-yloxyphenyl)benzamide (Mepronil) (3). CAS [55814-41-0].



3

Compound (**3**) was prepared using Method **A1**: 48% (62.6 mg); Method **B**: 71% (367.0 mg); Method **C1:** 95% (148.2 mg); Method **C2**: 91% (22.90 g). White powder, **m.p.** 92.5°-93.3°C capillary (lit. 92°-94°C),[5], by DSC: 92.2°C (Figure S5). **^{1}H NMR** (400 M*Hz*, DMSO-d_6) *δ* (ppm): 10.24 (s, 1H), 7.46-7.38 (m, 3H), 7.33-7.19 (m, 4H), 6.66 (d, *J* = 7.7 *Hz*, 1H), 4.58 (m, 1H), 2.39 (s, 3H), 1.28 (d, *J* = 5.9 *Hz*, 6H); **^{13}C{^{1}H} NMR NOE** (101 M*Hz*, DMSO-d_6) *δ* (ppm): 168.3, 158.2, 141.0, 137.8, 135.6, 130.9, 130.1, 129.9, 127.6, 126.1, 112.2, 111.0, 107.6, 69.6, 22.3, 19.8. **EI-(+)** *m/z*: 269 [M]•, 119 [M-$NH(C_6H_4)OC_3H_7$]•.

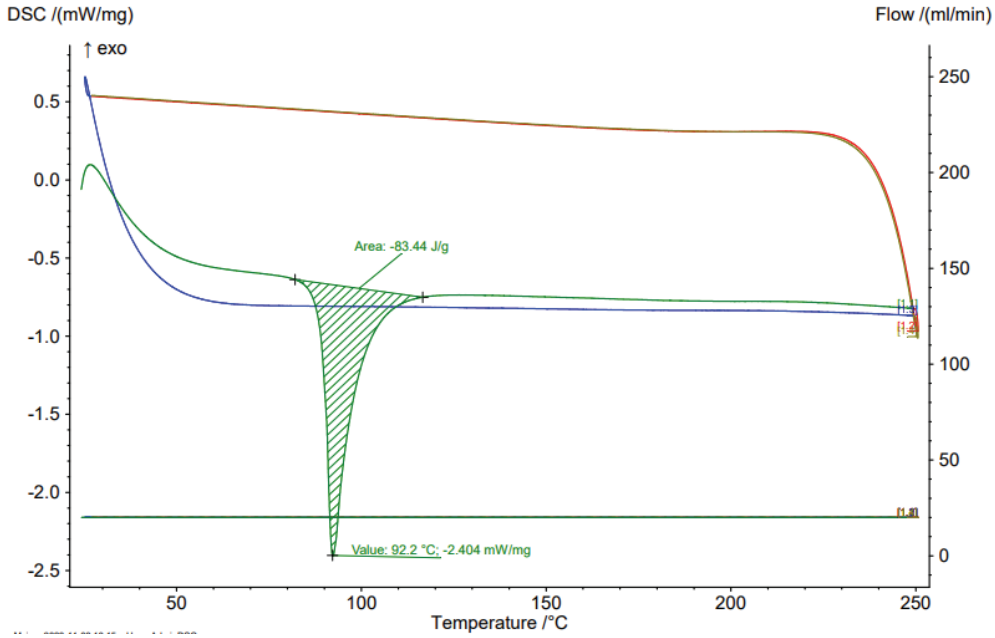
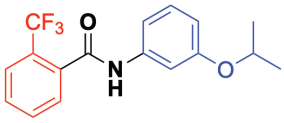


Figure S5. Thermal analysis by Differential Scanning Calorimetry (DSC) for Mepronil (**3**).

***N*-(3-Isopropoxyphenyl)-2-(trifluoromethyl)benzamide (Flutolanil) (4).** CAS [66332-96-5].



4

Compound (**4**) was prepared using Method **A1**: 32% (49.6 mg); Method **B**: 78% (486.6 mg); Method **C1**: 91% (170.4 mg); Method **C2**: 96% (28.94 g). White powder, **m.p.** 100.1°-100.4°C (capillary), by DSC: 99.9°C (Figure S6) (lit. 95°-97°C).[6] **^{1}H NMR** (400 M*Hz*, DMSO-d_6) δ (ppm): 10.49 (s, 1H), 7.86-7.77 (m, 2H), 7.73-7.68 (m, 2H), 7.33 (s, 1H), 7.22-7.20 (m, 2H), 6.67 (d, J = 7.3 *Hz*, 1H), 1.28 (d, J = 6.0 *Hz*, 6H).**^{13}C{^{1}H} NMR** (101 M*Hz*, DMSO-d_6) δ (ppm): 166.0, 158.2, 140.6, 133.1, 130.5, 130.1, 128.9, 126.8, 112.2, 111.3, 107.6, 69.7, 22.3.**^{19}F{^{1}H} NMR** (376 M*Hz*, DMSO-d_6)[6] δ (ppm): -57.93 (s). **EI-(+)** *m/z*: 323 $[M]^{\bullet}$, 173 $[M\text{-}NH(C_6H_4)OC_3H_7]^{\bullet}$.

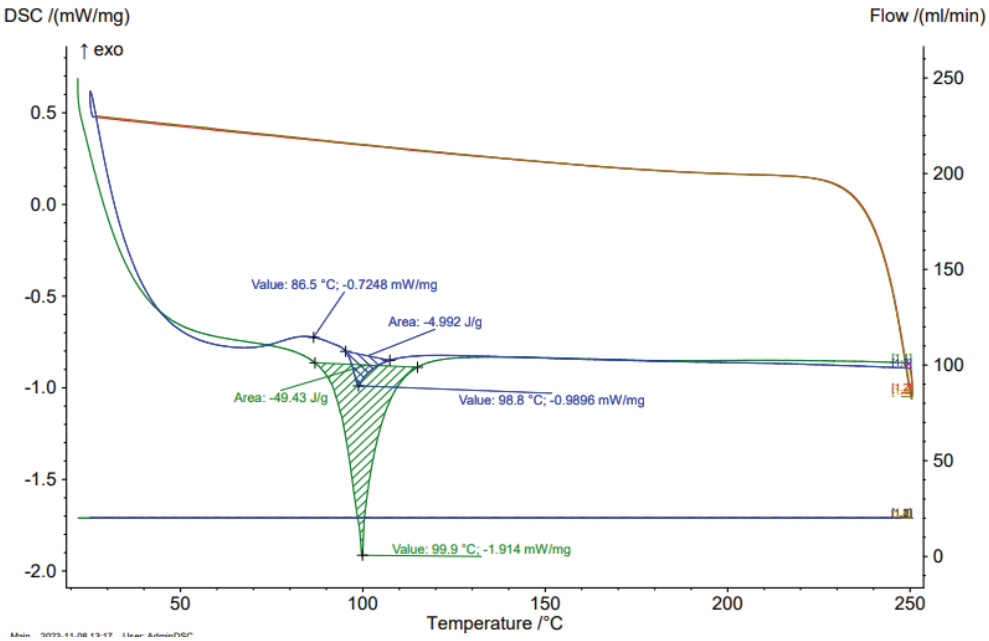
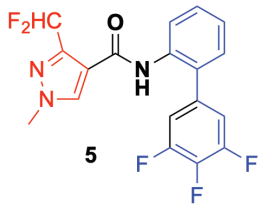


Figure S6. Thermal analysis by Differential Scanning Calorimetry (DSC) for Flutolanil (**4**).

3-(Difluoromethyl)-1-methyl-*N*-(3',4',5'-trifluoro[1,1'-biphenyl]-2-yl)-1H-pyrazole-4-carboxamide (Fluxapyroxad) (5). CAS [907204-31-3].



5

Compound (**5**) was prepared using Method **A1:** 73% (132.9 mg); Method **B:** 79% (578.7 mg); Method **C1:** 90% (199.3 mg); Method **C2:** 99% (34.99 g). White powder, **m.p.** 151.8 °C (by DSC, Figure S7), 157-158°C (capillary) (lit. 155°-158°C).[7] **^{1}H NMR** (400 M*Hz*, $CDCl_3$)[8] *δ* (ppm): 8.13 (d, *J* = 8.2 *Hz*, 1H), 7.89 (s, 1H), 7.73 (s, 1H), 7.38-7.34 (m, 1H), 7.19-7.13 (m, 2H), 6.97- 6.89 (m, 2H), 6.58 (t, *J* = 53 *Hz*, 1H, CHF_2), 3.85 (s, 3H). **^{13}C{^{1}H} NMR** (101 M*Hz*, $CDCl_3$)[8] *δ*(ppm): 159.4, 136.4, 134.6, 131.2, 130.0, 129.3, 125.2, 123.4, 116.7, 113.9 (dd, *J* = 16.6, 4.6 *Hz*), 111.7, 109.4, 39.6. **^{19}F{^{1}H} NMR** (376 M*Hz*, $CDCl_3$)[8] *δ*(ppm): -108.52, -108.72 (m, 2F), -133.61, -133.73 (m, 2F), -161.39, -161.54 (tt, *J* = 20.5 *Hz*, *J* = 6.4 *Hz*, 1F). **EI-(+)** *m/z*: 381 $[M]^{\bullet}$, 159 $[M\text{-}NH(C_{12}H_6F_3)]^{\bullet}$.

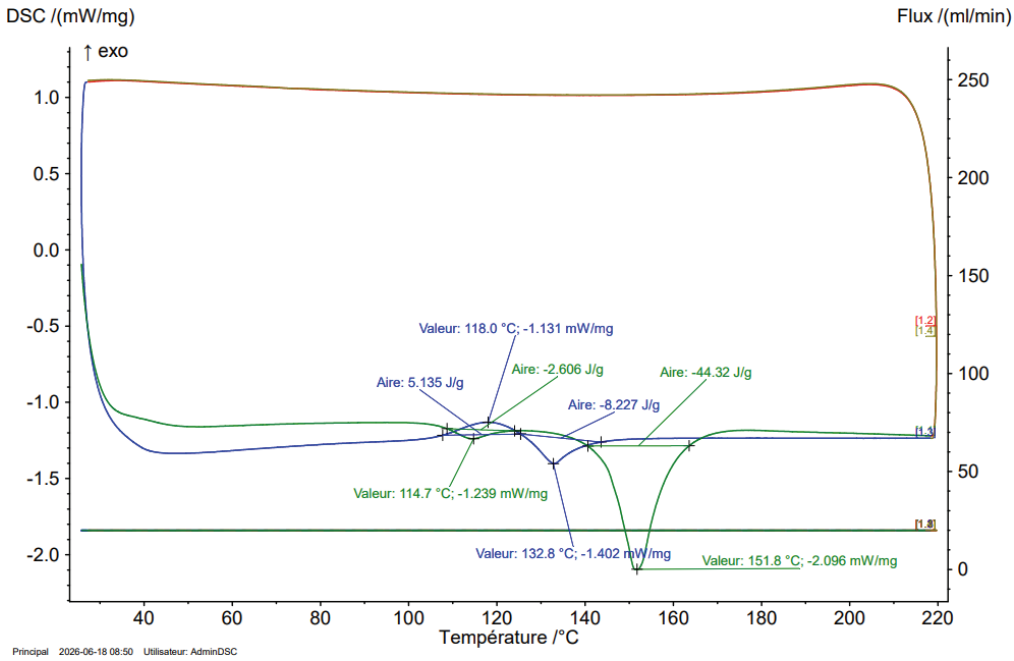
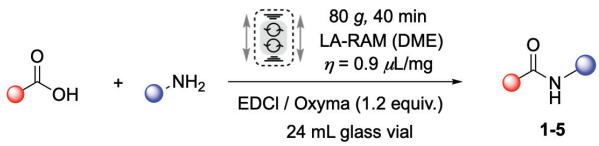


Figure S7. Thermal analysis by Differential Scanning Calorimetry (DSC) for Fluxapyroxad (**5**).

METHODOLOGY VALIDATION FOR AMIDATION REACTION BY RAM (COMPARATIVE EXPERIMENTS)

Table S2. Comparative data for the LA-RAM amidation reaction to agrochemicals (**1-5**), prepared via EDCI/Oxyma-mediated synthesis[9] (one-pot/one-step strategy).

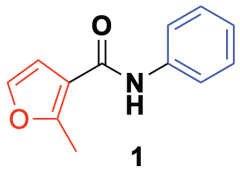


		LA-RAM-mediated amidation	
		EDCI/Oxyma[a,9]	This work (TCFH)
Entry	**Compound**	**qNMR Yield(%)[b]**	**Yield (%)[c]**
1	Fenfuram (**1**)	36	98[d]
2	Boscalid (**2**)	22 / 17[d]	29
3	Mepronil (**3**)	34	100
4	Flutolanil (**4**)	56 / 45[d]	96
5	Fluxapyroxad (**5**)	45	96

[a] Reaction condtions:[9] The acid (3.34 mmol, 1.0 equiv.), the amine (1.5 equiv.), EDCI (1.2 equiv.), Oxyma (1.2 equiv.), and 1,2-dimethoxyethane (DME, η = 0.9 μL/mg) as LAG solvent, were added to a 24 mL glass vial and reacted at 80 *g* during 40 minutes; [b] qNMR yields were measured in $CDCl_3$ (0.6 mL) using cyclododecane (10 mg, 59 μmol for 30 mg of target) as an internal standard for entries 1, 2 and 5 and in DMSO-d_6 (0.6 mL) using 1,3,5-trimethoxybenzene (15 mg, 89 μmol for 30 mg of target) as an internal standard for entries 3 and 4; [c] Isolated yield for compounds **1-5**, prepared as described in Methods C1-C2, at 8 mmol scale (in a 15 mL PTFE jar); [d] from Table S1 (entry 4). [d] LA-RAM solvent used was ethyl acetate (AcOEt, η = 0.9 μL/mg).

PXRD PATTERN INDEXING FOR COMPOUNDS 1-5.

2-methyl-*N*-phenyl-3-furamid (Fenfuram) (1). CAS [24691-80-3].



1

Space Group	$Pna2_1$
Cell Lengths	**a** 9.385(3) **b** 11.017(4) **c** 9.7829(15)
Cell Angles	***α*** 90° ***β*** 90° ***γ*** 90°

Deposited in CCDC Cambridge under number 2584567

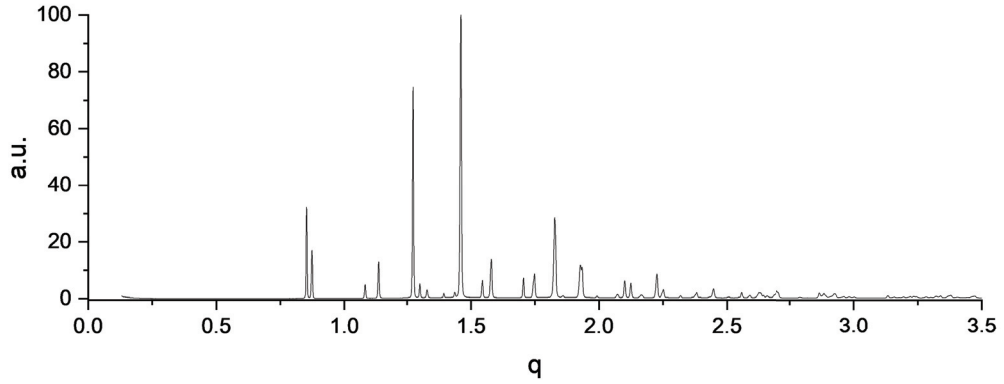


Figure S8. Synchrotron PXRD pattern of Fenfuram (**1**), in accordance with CDS deposited structure (deposited in CCDC Cambridge under number 2584567).

Table S3. Most intense peaks for PXRD diffractogram of Fenfuram **(1)** prepared by LA-RAM and analysed at synchrotron (Table 3, entry 6).

Pos.[°2Th.]	Height [cts]	FWHMLeft[°2Th.]	d-spacing [Å]	Rel. Int. [%]
1,282613(9)	21169(105)	0,00410(3)	68,82171	34,63
1,285800(9)	10584(105)	0,00410(3)	68,82171	17,31
1,31355(1)	9422(65)	0,00597(5)	67,20082	15,41
1,31681(1)	4711(65)	0,00597(5)	67,20082	7,71
1,62647(4)	2855(40)	0,0060(1)	54,27242	4,67
1,63052(4)	1427(40)	0,0060(1)	54,27242	2,33
1,70580(2)	8265(70)	0,00544(6)	51,74866	13,52
1,71004(2)	4132(70)	0,00544(6)	51,74866	6,76
1,916454(6)	47141(155)	0,00503(2)	46,06104	77,11
1,921217(6)	23571(155)	0,00503(2)	46,06104	38,56
1,95721(6)	3053(46)	0,0056(1)	45,10201	4,99
1,96207(6)	1527(46)	0,0056(1)	45,10202	2,50
1,99985(7)	1627(28)	0,0088(2)	44,14047	2,66
2,00482(7)	813(28)	0,0088(2)	44,14047	1,33
2,1287(2)	1526(35)	0,00100(3)	41,46925	2,50
2,1340(2)	763(35)	0,00100(3)	41,46925	1,25
2,1595(2)	668(24)	0,0096(5)	40,87722	1,09
2,1649(2)	334(24)	0,0096(5)	40,87722	0,55
2,197088(9)	61132(153)	0,00730(2)	40,17826	100,00
2,202548(9)	30566(153)	0,00730(2)	40,17826	50,00
2,32381(6)	3555(41)	0,0069(1)	37,98746	5,82
2,32959(6)	1778(41)	0,0069(1)	37,98746	2,91
2,37564(2)	8005(55)	0,00823(7)	37,15894	13,09
2,38154(2)	4003(55)	0,00823(7)	37,15894	6,55
2,56560(4)	3852(44)	0,00609(8)	34,40799	6,30
2,57198(4)	1926(44)	0,00609(8)	34,40799	3,15
2,628(6)	1463(1654)	0,010(3)	33,59368	2,39
2,628(3)	3270(1624)	0,010(2)	33,58879	5,35
2,634(6)	732(1654)	0,010(3)	33,59367	1,20
2,635(3)	1635(1624)	0,010(2)	33,58879	2,67
2,74965(1)	16943(63)	0,01060(5)	32,10529	27,72
2,75648(1)	8472(63)	0,01060(5)	32,10529	13,86
2,8262(3)	449(27)	0,0018(1)	31,23627	0,73
2,8332(3)	225(27)	0,0018(1)	31,23627	0,37
2,90393(3)	7057(36)	0,01553(9)	30,39988	11,54
2,91115(3)	3528(36)	0,01553(9)	30,39988	5,77
2,9995(3)	318(15)	0,0134(9)	29,43155	0,52
3,0070(3)	159(15)	0,0134(9)	29,43155	0,26
3,1180(2)	736(21)	0,0121(5)	28,31296	1,20
3,1258(2)	368(21)	0,0121(5)	28,31295	0,60

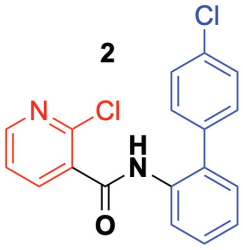
3,16080(5)	3366(34)	0,00751(9)	27,92993	5,51
3,16866(5)	1683(34)	0,00751(9)	27,92993	2,75
3,19688(6)	2706(26)	0,00766(4)	27,61482	4,43
3,20482(6)	1353(26)	0,00766(4)	27,61482	2,21
3,2591(2)	615(13)	0,0169(5)	27,08798	1,01
3,2672(2)	308(13)	0,0169(5)	27,08798	0,50
3,34923(4)	4769(39)	0,00898(9)	26,35899	7,80
3,35756(4)	2385(39)	0,00898(9)	26,35899	3,90
3,38644(8)	1569(25)	0,0116(3)	26,06943	2,57
3,39486(8)	785(25)	0,0116(3)	26,06943	1,28
3,4893(2)	452(17)	0,0101(5)	25,30129	0,74
3,4980(2)	226(17)	0,0101(5)	25,30129	0,37
3,5818(1)	869(17)	0,0165(4)	24,64789	1,42
3,5907(1)	435(17)	0,0165(4)	24,64789	0,71
3,68206(8)	1652(24)	0,0119(2)	23,97704	2,70
3,69121(8)	826(24)	0,0119(2)	23,97704	1,35
3,7723(4)	199(14)	0,013(1)	23,40367	0,33
3,7817(4)	100(14)	0,013(1)	23,40367	0,16
3,8485(1)	864(19)	0,0106(3)	22,94021	1,41
3,8581(1)	432(19)	0,0106(3)	22,94021	0,71
3,8960(2)	509(18)	0,0106(5)	22,66113	0,83
3,9056(2)	254(18)	0,0106(5)	22,66113	0,42
3,9554(8)	1084(77)	0,0203(6)	22,32056	1,77
3,9653(8)	542(77)	0,0203(6)	22,32056	0,89
3,978(4)	247(38)	0,013(5)	22,19357	0,40
3,988(4)	123(38)	0,013(5)	22,19357	0,20
4,0010(6)	445(30)	0,0087(5)	22,06644	0,73
4,0109(6)	222(30)	0,0087(5)	22,06644	0,36
4,056(1)	982(56)	0,0218(8)	21,76558	1,61
4,066(1)	491(56)	0,0218(8)	21,76558	0,80
4,0698(3)	1100(97)	0,0095(3)	21,69342	1,80
4,0799(3)	550(97)	0,0095(3)	21,69342	0,90
4,2008(4)	223(14)	0,014(1)	21,01740	0,37
4,2112(4)	112(14)	0,014(1)	21,01740	0,18
4,244(2)	49(6)	0,017(1)	20,80251	0,08
4,255(2)	24(6)	0,017(1)	20,80251	0,04
4,3164(3)	1036(38)	0,0116(3)	20,45490	1,69
4,3271(3)	518(38)	0,0116(3)	20,45489	0,85
4,3440(3)	943(29)	0,0155(7)	20,32458	1,54
4,3548(3)	471(29)	0,0155(7)	20,32458	0,77
4,398(2)	461(121)	0,032(3)	20,07719	0,75
4,405(1)	574(105)	0,011(2)	20,04371	0,94
4,409(2)	230(121)	0,032(3)	20,07718	0,38
4,416(1)	287(105)	0,011(2)	20,04371	0,47

4,4553(7)	281(20)	0,019(1)	19,81715	0,46
4,4664(7)	140(20)	0,019(1)	19,81715	0,23
4,4904(7)	296(17)	0,014(1)	19,66247	0,48
4,5016(7)	148(17)	0,014(1)	19,66247	0,24
4,5196(7)	244(15)	0,014(1)	19,53552	0,40
4,5308(7)	122(15)	0,014(1)	19,53552	0,20
4,7175(3)	487(14)	0,0119(1)	18,71659	0,80
4,7292(3)	244(14)	0,0119(1)	18,71659	0,40
4,7548(7)	219(20)	0,016(1)	18,56977	0,36
4,7666(7)	110(20)	0,016(1)	18,56977	0,18
4,807(2)	180(29)	0,030(3)	18,36759	0,29
4,819(2)	90(29)	0,030(3)	18,36759	0,15
4,855(3)	248(50)	0,030(4)	18,18801	0,40
4,867(3)	124(50)	0,030(4)	18,18801	0,20
4,882(2)	280(43)	0,020(5)	18,08711	0,46
4,894(2)	140(43)	0,020(5)	18,08711	0,23
4,9426(7)	268(19)	0,016(1)	17,86469	0,44
4,9548(7)	134(19)	0,016(1)	17,86469	0,22
4,972(1)	174(24)	0,010(1)	17,75791	0,28
4,985(1)	87(24)	0,010(1)	17,75791	0,14
5,0020(6)	437(33)	0,014(1)	17,65264	0,71
5,0144(6)	218(33)	0,014(1)	17,65264	0,36
5,0266(5)	429(15)	0,0126(2)	17,56610	0,70
5,0391(5)	214(15)	0,0126(2)	17,56610	0,35
5,078(1)	545(45)	0,0192(9)	17,38791	0,89
5,091(1)	273(45)	0,0192(9)	17,38791	0,45
5,093(1)	285(46)	0,013(1)	17,33625	0,47
5,106(1)	142(46)	0,013(1)	17,33625	0,23
5,1575(7)	176(14)	0,015(1)	17,12046	0,29
5,1704(7)	88(14)	0,015(1)	17,12046	0,14
5(250636109243147)	0(21)	0(298809526288)	16,91598	0,00
5,2257(4)	609(22)	0,0149(5)	16,89737	1,00
5(250636109243147)	0(21)	0(298809526288)	16,91598	0,00
5,2387(4)	304(22)	0,0149(5)	16,89737	0,50
5,3037(8)	146(14)	0,020(2)	16,64889	0,24
5,3169(8)	73(14)	0,020(2)	16,64889	0,12
5,368(2)	46(9)	0,033(9)	16,45010	0,08
5,381(2)	23(9)	0,033(9)	16,45010	0,04
5,4260(8)	173(14)	0,016(2)	16,27389	0,28
5,4395(8)	87(14)	0,016(2)	16,27389	0,14
5,4680(4)	359(16)	0,0135(7)	16,14915	0,59
5,4816(4)	179(16)	0,0135(7)	16,14915	0,29
5,5113(3)	540(16)	0,0156(6)	16,02243	0,88
5,5250(3)	270(16)	0,0156(6)	16,02243	0,44

5,5566(3)	446(15)	0,0185(9)	15,89169	0,73
5,5705(3)	223(15)	0,0185(9)	15,89169	0,36
5,614(2)	53(10)	0,023(7)	15,73059	0,09
5,628(2)	27(10)	0,023(7)	15,73059	0,04
5,704(7)	11(4)	0,03(1)	15,48072	0,02
5,718(7)	6(4)	0,03(1)	15,48072	0,01
5,7933(8)	170(14)	0,015(1)	15,24308	0,28
5,8077(8)	85(14)	0,015(1)	15,24308	0,14
5,8345(8)	161(13)	0,019(2)	15,13534	0,26
5,8491(8)	81(13)	0,019(2)	15,13534	0,13
5,9056(6)	227(12)	0,0156(3)	14,95332	0,37
5,9203(6)	114(12)	0,0156(3)	14,95332	0,19
5,9560(4)	362(14)	0,024(1)	14,82696	0,59
5,9708(4)	181(14)	0,024(1)	14,82696	0,30
6,013(1)	117(12)	0,017(3)	14,68680	0,19
6,028(1)	58(12)	0,017(3)	14,68680	0,10
6,061(2)	90(22)	0,016(3)	14,56933	0,15
6,077(2)	45(22)	0,016(3)	14,56933	0,07
6,092(1)	170(15)	0,016(2)	14,49521	0,28
6,108(1)	85(15)	0,016(2)	14,49521	0,14
6,142(1)	106(11)	0,019(3)	14,37933	0,17
6,157(1)	53(11)	0,019(3)	14,37933	0,09
6,236(3)	28(11)	0,017(9)	14,16257	0,05
6,251(3)	14(11)	0,017(9)	14,16257	0,02
6,303(1)	95(12)	0,013(2)	14,01170	0,16
6,319(1)	48(12)	0,013(2)	14,01170	0,08
6,3670(9)	112(11)	0,019(3)	13,87081	0,18
6,3828(9)	56(11)	0,019(3)	13,87081	0,09
6,481(2)	64(15)	0,012(3)	13,62648	0,10
6,497(2)	32(15)	0,012(3)	13,62648	0,05
7(665966155563867)	0(4)	0(1631675330367)	13,56196	0,00
6,522(6)	21(11)	0,02(2)	13,54097	0,03
7(665966155563867)	0(4)	0(1631675330367)	13,56196	0,00
6,538(6)	10(11)	0,02(2)	13,54097	0,02
6,599(1)	99(11)	0,017(3)	13,38441	0,16
6,615(1)	50(11)	0,017(3)	13,38441	0,08
6,712(1)	98(12)	0,015(2)	13,15762	0,16
6,729(1)	49(12)	0,015(2)	13,15762	0,08
6,981(1)	90(10)	0,021(3)	12,65144	0,15
6,999(1)	45(10)	0,021(3)	12,65144	0,07
7,086(2)	54(7)	0,020(1)	12,46414	0,09
7,104(2)	27(7)	0,020(1)	12,46414	0,04
7,167(1)	77(7)	0,043(6)	12,32483	0,13
7,184(1)	38(7)	0,043(6)	12,32483	0,06

7,259(1)	93(12)	0,020(3)	12,16832	0,15
7,277(1)	46(12)	0,020(3)	12,16832	0,08
7,327(6)	17(6)	0,05(2)	12,05471	0,03
7,346(6)	9(6)	0,05(2)	12,05471	0,01
7,460(2)	61(8)	0,045(8)	11,84124	0,10
7,478(2)	30(8)	0,045(8)	11,84124	0,05
7,533(2)	56(16)	0,015(4)	11,72630	0,09
7,552(2)	28(16)	0,015(4)	11,72631	0,05
7,628(6)	41(6)	0,09(1)	11,57968	0,07
7,647(6)	21(6)	0,09(1)	11,57968	0,03
7,718(3)	50(13)	0,039(8)	11,44589	0,08
7,737(3)	25(13)	0,039(8)	11,44589	0,04
7,787(1)	89(10)	0,027(4)	11,34431	0,15
7,806(1)	45(10)	0,027(4)	11,34431	0,07
7,875(1)	104(9)	0,020(2)	11,21836	0,17
7,894(1)	52(9)	0,020(2)	11,21836	0,08
7,935(1)	112(9)	0,022(2)	11,13362	0,18
7,954(1)	56(9)	0,022(2)	11,13362	0,09
8,111(1)	97(11)	0,037(4)	10,89163	0,16
8,131(1)	49(11)	0,037(4)	10,89163	0,08
8,287(5)	58(3)	0,19(2)	10,66061	0,09
8,308(5)	29(3)	0,19(2)	10,66061	0,05
8,417(2)	45(9)	0,0333(4)	10,49686	0,07
8,438(2)	22(9)	0,0333(4)	10,49686	0,04
8,518(3)	48(6)	0,063(8)	10,37170	0,08
8,540(3)	24(6)	0,063(8)	10,37170	0,04
8,788(9)	39(2)	0,31(2)	10,05382	0,06
8,810(9)	20(2)	0,31(2)	10,05382	0,03
9,644(7)	24(2)	0,22(2)	9,16328	0,04
9,668(7)	12(2)	0,22(2)	9,16328	0,02

2-chloro-N-(4'-chloro[1,1'-biphenyl]-2-yl)pyridine-3-carboxamide (Boscalid) (2). CAS [188425-85-6].



Space Group P $2_1/c$

Cell Lengths **a** 14.811(6) **b** 11.5817(14) **c** 18.721(2)

Cell Angles ***α*** 90° ***β*** 91.126(19)° ***γ*** 90°

Reference code for CCDC Cambridge: NOZKOF02.[10]

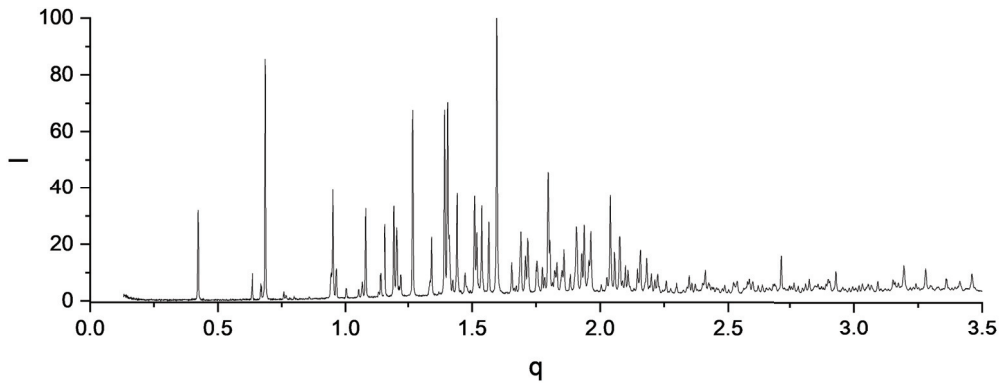


Figure S9. Synchrotron PXRD pattern of Boscalid (**2**), in accordance with CDS deposited structure (refcode NOZKOF02).[10]

Table S4. Most intense peaks for PXRD diffractogram of Boscalid **(2)** prepared by LA-RAM (Table 4, entry 3).

Pos.[°2Th.]	Height [cts]	FWHMLeft[°2Th.]	d-spacing [Å]	Rel. Int. [%]
0,6365(1)	181(9)	0,0045(3)	138,68880	32,15
0,6380(1)	91(9)	0,0045(3)	138,68880	16,07
0,9542(5)	42(7)	0,0031(7)	92,50873	7,49
0,9566(5)	21(7)	0,0031(7)	92,50872	3,74
1,0048(8)	28(6)	0,003(1)	87,84886	5,01
1,0073(8)	14(6)	0,003(1)	87,84885	2,50
1,03230(6)	431(16)	0,0046(2)	85,50928	76,50
1,03486(6)	216(16)	0,0046(2)	85,50928	38,25
1,150(3)	8(5)	0,002(2)	76,74427	1,41
1,153(3)	4(5)	0,002(2)	76,74426	0,71
1,4312(2)	217(13)	0,0048(4)	61,67844	38,41
1,4347(2)	108(13)	0,0048(4)	61,67844	19,20
1,4504(5)	64(8)	0,0047(9)	60,85860	11,39
1,4541(5)	32(8)	0,0047(9)	60,85860	5,69
1,510(1)	21(6)	0,004(1)	58,45974	3,73
1,514(1)	11(6)	0,004(1)	58,45974	1,86
1,589(2)	18(5)	0,004(1)	55,55690	3,13
1,593(2)	9(5)	0,004(1)	55,55690	1,57
1,611(3)	29(9)	0,0042(9)	54,79494	5,08
1,615(3)	14(9)	0,0042(9)	54,79494	2,54
1,6243(2)	173(11)	0,0044(4)	54,34364	30,71
1,6284(2)	87(11)	0,0044(4)	54,34364	15,36
1,7149(5)	50(7)	0,005(1)	51,47543	8,79

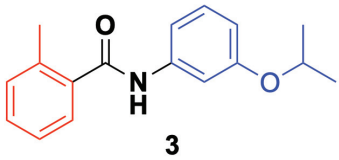
1,7191(5)	25(7)	0,005(1)	51,47543	4,39
1,7447(2)	144(10)	0,0049(4)	50,59562	25,51
1,7490(2)	72(10)	0,0049(4)	50,59562	12,75
1,803(1)	153(19)	0,0045(3)	48,94802	27,19
1,808(1)	77(19)	0,0045(3)	48,94802	13,60
1,8149(4)	188(16)	0,0039(3)	48,63743	33,31
1,8194(4)	94(16)	0,0039(3)	48,63743	16,65
1,829(2)	59(12)	0,0025(4)	48,27084	10,55
1,833(2)	30(12)	0,0025(4)	48,27084	5,27
1,840(1)	43(7)	0,0063(5)	47,96582	7,67
1,845(1)	22(7)	0,0063(5)	47,96582	3,84
1,90911(9)	364(14)	0,0052(2)	46,23815	64,53
1,91386(9)	182(14)	0,0052(2)	46,23814	32,26
2,0219(3)	115(9)	0,0050(5)	43,65928	20,46
2,0269(3)	58(9)	0,0050(5)	43,65928	10,23
2,1006(3)	346(16)	0,0049(2)	42,02268	61,30
2,1059(3)	173(16)	0,0049(2)	42,02269	30,65
2,1200(2)	442(17)	0,0047(2)	41,63808	78,47
2,1253(2)	221(17)	0,0047(2)	41,63808	39,23
2,152(2)	37(9)	0,0051(8)	41,01534	6,61
2,158(2)	19(9)	0,0051(8)	41,01534	3,30
2,1716(3)	178(13)	0,0059(4)	40,64885	31,60
2,1770(3)	89(13)	0,0059(4)	40,64886	15,80
2,2244(6)	52(6)	0,008(1)	39,68581	9,18
2,2299(6)	26(6)	0,008(1)	39,68581	4,59
2,2764(3)	224(13)	0,0065(4)	38,77802	39,65
2,2821(3)	112(13)	0,0065(4)	38,77802	19,83
2,2921(5)	110(9)	0,0041(3)	38,51329	19,44
2,2978(5)	55(9)	0,0041(3)	38,51330	9,72
2,3175(2)	177(10)	0,0051(3)	38,09132	31,40
2,3232(2)	89(10)	0,0051(3)	38,09132	15,70
2,3577(2)	146(8)	0,0057(3)	37,44196	25,88
2,3635(2)	73(8)	0,0057(3)	37,44196	12,94
2,40426(8)	564(15)	0,0059(2)	36,71665	100,00
2,41023(8)	282(15)	0,0059(2)	36,71665	50,00
2,4967(5)	70(7)	0,0066(7)	35,35723	12,50
2,5029(5)	35(7)	0,0066(7)	35,35723	6,25
2,5452(3)	124(9)	0,0080(7)	34,68438	21,93
2,5515(3)	62(9)	0,0080(7)	34,68438	10,96
2,576(1)	99(16)	0,0072(7)	34,27270	17,48
2,582(1)	49(16)	0,0072(7)	34,27270	8,74
2,5881(5)	126(11)	0,0056(5)	34,10866	22,38
2,5946(5)	63(11)	0,0056(5)	34,10866	11,19
2,6413(4)	74(5)	0,012(1)	33,42196	13,07

2,6479(4)	37(5)	0,012(1)	33,42196	6,54
2,6742(8)	67(7)	0,0063(6)	33,01070	11,90
2,6809(8)	34(7)	0,0063(6)	33,01070	5,95
2,696(4)	44(18)	0,0054(6)	32,74958	7,86
2,702(4)	22(18)	0,0054(6)	32,74958	3,93
2,7099(3)	292(13)	0,0070(4)	32,57644	51,74
2,7166(3)	146(13)	0,0070(4)	32,57644	25,87
2,7470(9)	74(8)	0,0083(8)	32,13586	13,13
2,7539(9)	37(8)	0,0083(8)	32,13586	6,56
2,7623(8)	68(7)	0,0053(5)	31,95808	12,00
2,7692(8)	34(7)	0,0053(5)	31,95808	6,00
2,7995(4)	95(7)	0,0075(6)	31,53314	16,85
2,8065(4)	47(7)	0,0075(6)	31,53314	8,42
2,8397(8)	47(5)	0,0069(6)	31,08743	8,26
2,8468(8)	23(5)	0,0069(6)	31,08743	4,13
2,8719(3)	147(8)	0,0107(8)	30,73862	26,01
2,8791(3)	73(8)	0,0107(8)	30,73862	13,00
2,906(1)	105(12)	0,0079(7)	30,37795	18,59
2,913(1)	52(12)	0,0079(7)	30,37795	9,29
2,9205(5)	138(9)	0,0058(4)	30,22732	24,47
2,9278(5)	69(9)	0,0058(4)	30,22732	12,24
2,9568(3)	137(8)	0,0083(6)	29,85687	24,37
2,9641(3)	69(8)	0,0083(6)	29,85687	12,18
3,024(1)	21(2)	0,016(1)	29,19381	3,68
3,031(1)	10(2)	0,016(1)	29,19382	1,84
3,053(2)	45(13)	0,0063(9)	28,91226	7,91
3,061(2)	22(13)	0,0063(9)	28,91226	3,95
3,0709(5)	200(10)	0,0070(4)	28,74762	35,45
3,0785(5)	100(10)	0,0070(4)	28,74762	17,73
3,0970(5)	90(7)	0,0069(5)	28,50529	15,94
3,1047(5)	45(7)	0,0069(5)	28,50528	7,97
3,1278(3)	126(7)	0,0090(7)	28,22499	22,43
3,1355(3)	63(7)	0,0090(7)	28,22499	11,21
3,1611(8)	64(7)	0,0075(7)	27,92769	11,31
3,1689(8)	32(7)	0,0075(7)	27,92769	5,65
3,1812(8)	61(6)	0,0064(6)	27,75052	10,91
3,1891(8)	31(6)	0,0064(6)	27,75052	5,45
3,233(1)	65(11)	0,0076(8)	27,30219	11,56
3,242(1)	33(11)	0,0076(8)	27,30219	5,78
3,2484(8)	89(7)	0,0070(8)	27,17688	15,78
3,2565(8)	44(7)	0,0070(8)	27,17688	7,89
3,2858(6)	76(6)	0,0085(8)	26,86805	13,45
3,2939(6)	38(6)	0,0085(8)	26,86805	6,72
3,312(1)	46(6)	0,008(1)	26,65497	8,23

3,320(1)	23(6)	0,008(1)	26,65497	4,12
3,336(2)	39(9)	0,008(1)	26,46670	6,86
3,344(2)	19(9)	0,008(1)	26,46670	3,43
3,354(1)	51(6)	0,0070(8)	26,32508	9,05
3,362(1)	26(6)	0,0070(8)	26,32508	4,53
3,4045(9)	30(5)	0,010(2)	25,93141	5,28
3,4129(9)	15(5)	0,010(2)	25,93141	2,64
3,463(1)	20(4)	0,015(4)	25,49115	3,50
3,472(1)	10(4)	0,015(4)	25,49115	1,75
3,5424(7)	43(5)	0,011(2)	24,92217	7,66
3,5512(7)	22(5)	0,011(2)	24,92217	3,83
3,6368(6)	53(5)	0,011(1)	24,27521	9,42
3,6459(6)	27(5)	0,011(1)	24,27521	4,71
3,797(5)	27(14)	0,013(3)	23,25257	4,76
3,806(5)	13(14)	0,013(3)	23,25257	2,38
3,817(5)	25(7)	0,013(8)	23,13217	4,46
3,826(5)	13(7)	0,013(8)	23,13217	2,23
3,885(1)	30(3)	0,025(3)	22,72354	5,35
3,895(1)	15(3)	0,025(3)	22,72354	2,67
3,915(2)	29(5)	0,008(1)	22,55154	5,17
3,925(2)	15(5)	0,008(1)	22,55154	2,58
4,0481(9)	30(2)	0,025(1)	21,80951	5,27
4,0582(9)	15(2)	0,025(1)	21,80951	2,64
4,0917(5)	78(5)	0,0083(7)	21,57738	13,85
4,1019(5)	39(5)	0,0083(7)	21,57738	6,93
4,2607(8)	41(4)	0,0094(8)	20,72211	7,31
4,2713(8)	21(4)	0,0094(8)	20,72211	3,65
4,3680(9)	32(2)	0,029(2)	20,21337	5,65
4,3788(9)	16(2)	0,029(2)	20,21337	2,83
4,4129(8)	48(5)	0,010(1)	20,00762	8,50
4,4239(8)	24(5)	0,010(1)	20,00762	4,25
4,6623(9)	31(4)	0,013(2)	18,93808	5,51
4,6738(9)	16(4)	0,013(2)	18,93807	2,75
4,758(1)	26(2)	0,042(4)	18,55627	4,67
4,770(1)	13(2)	0,042(4)	18,55627	2,33
4,8129(6)	60(5)	0,014(1)	18,34561	10,61
4,8249(6)	30(5)	0,014(1)	18,34561	5,31
4,9417(6)	50(4)	0,016(2)	17,86784	8,91
4,9540(6)	25(4)	0,016(2)	17,86784	4,46
5,0648(7)	38(4)	0,015(2)	17,43380	6,82
5,0774(7)	19(4)	0,015(2)	17,43380	3,41
5,1430(9)	29(3)	0,019(3)	17,16893	5,13
5,1558(9)	14(3)	0,019(3)	17,16893	2,57
5,2137(7)	44(4)	0,016(2)	16,93635	7,87

5,2266(7)	22(4)	0,016(2)	16,93635	3,93
5,524(1)	22(2)	0,030(5)	15,98687	3,90
5,537(1)	11(2)	0,030(5)	15,98687	1,95
5,851(1)	20(3)	0,015(3)	15,09167	3,55
5,866(1)	10(3)	0,015(3)	15,09167	1,77
7,83(2)	5,5(3)	1,02(6)	11,28393	0,98
7,85(2)	2,8(3)	1,02(6)	11,28393	0,49

2-methyl-*N*-(3-propan-2-yloxyphenyl)benzamide (Mepronil) (3). CAS [55814-41-0].



3

Space Group P b c n

Cell Lengths **a** 18.825(3) **b** 8.7096(19) **c** 18.064(10)

Cell Angles ***α*** 90° ***β*** 90° ***γ*** 90°

Deposited in CCDC Cambridge under number 2584568

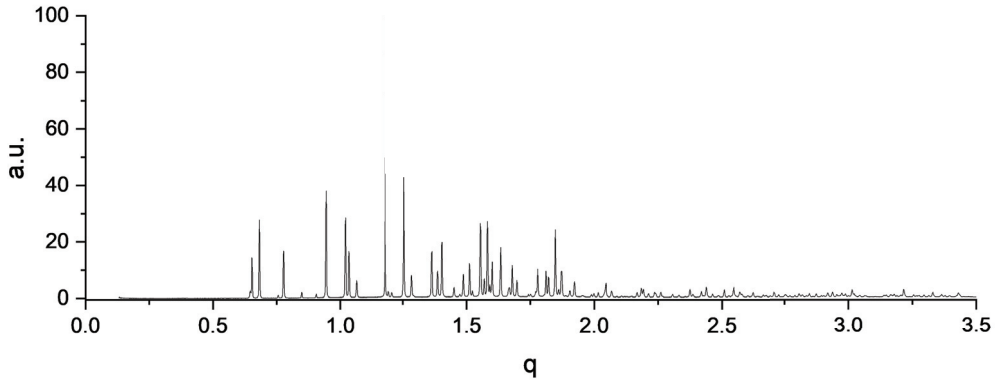


Figure S10. Synchrotron PXRD pattern of Mepronil (**3**), CDS deposited structure (deposited in CCDC Cambridge under number 2584568).

Table S5. Most intense peaks for PXRD diffractogram of Mepronil **(3)** prepared by LA-RAM (Table 2, entry 3).

Pos.[°2Th.]	Height [cts]	FWHMLeft[°2Th.]	d-spacing [Å]	Rel. Int. [%]
0,9792(9)	218(34)	0,0101(4)	90,14587	2,16
0,9816(9)	109(34)	0,0101(4)	90,14587	1,08
0,98263(7)	1960(46)	0,00346(8)	89,83120	19,42

0,98507(7)	980(46)	0,00346(8)	89,83121	9,71
1,02698(2)	3700(43)	0,00416(6)	85,95213	36,67
1,02953(2)	1850(43)	0,00416(6)	85,95213	18,34
1,1357(4)	123(14)	0,0028(4)	77,72468	1,22
1,1385(4)	62(14)	0,0028(4)	77,72467	0,61
1,16975(2)	2482(35)	0,00448(8)	75,46178	24,61
1,17266(2)	1241(35)	0,00448(8)	75,46178	12,30
1,2774(2)	277(15)	0,0042(3)	69,10210	2,75
1,2806(2)	139(15)	0,0042(3)	69,10209	1,37
1,3789(5)	199(8)	0,0010(1)	64,01757	1,97
1,3823(5)	100(8)	0,0010(1)	64,01757	0,99
1,42149(2)	5188(52)	0,00422(5)	62,09835	51,43
1,42502(2)	2594(52)	0,00422(5)	62,09835	25,71
1,53531(3)	3817(43)	0,00447(6)	57,49497	37,83
1,53912(3)	1908(43)	0,00447(6)	57,49497	18,92
1,55619(4)	2491(36)	0,00418(8)	56,72340	24,69
1,56006(4)	1246(36)	0,00418(8)	56,72340	12,35
1,60286(9)	719(22)	0,0056(2)	55,07184	7,13
1,60685(9)	359(22)	0,0056(2)	55,07184	3,56
1,77424(1)	10089(67)	0,00470(4)	49,75278	100,00
1,77865(1)	5044(67)	0,00470(4)	49,75278	50,00
1,8187(2)	588(13)	0,0022(1)	48,53746	5,83
1,8232(2)	294(13)	0,0022(1)	48,53746	2,91
1,8397(3)	487(11)	0,00100(4)	47,98135	4,83
1,8443(3)	244(11)	0,00100(4)	47,98135	2,41
1,88848(2)	4197(43)	0,00434(5)	46,74336	41,60
1,89317(2)	2099(43)	0,00434(5)	46,74336	20,80
1,9426(1)	859(15)	0,00270(8)	45,44048	8,51
1,9475(1)	429(15)	0,00270(8)	45,44048	4,26
2,05178(4)	1978(26)	0,0055(1)	43,02335	19,60
2,05688(4)	989(26)	0,0055(1)	43,02335	9,80
2,08682(7)	1144(21)	0,0056(1)	42,30099	11,34
2,09201(7)	572(21)	0,0056(1)	42,30099	5,67
2,11245(4)	2569(32)	0,00511(8)	41,78793	25,46
2,11770(4)	1285(32)	0,00511(8)	41,78794	12,73
2,1863(2)	380(17)	0,0073(4)	40,37593	3,77
2,1918(2)	190(17)	0,0073(4)	40,37593	1,88
2,2342(8)	322(50)	0,0050(4)	39,51084	3,19
2,2398(8)	161(50)	0,0050(4)	39,51084	1,59
2,2406(2)	844(30)	0,0051(3)	39,39856	8,37
2,2461(2)	422(30)	0,0051(3)	39,39856	4,18
2,27680(7)	1255(26)	0,0062(2)	38,77171	12,44
2,28246(7)	628(26)	0,0062(2)	38,77171	6,22
2,3143(2)	443(10)	0,00142(7)	38,14334	4,39

2,3201(2)	221(10)	0,00142(7)	38,14334	2,19
2,33861(5)	3112(35)	0,00581(8)	37,74717	30,84
2,34442(5)	1556(35)	0,00581(8)	37,74717	15,42
2,3615(2)	677(21)	0,0069(2)	37,38145	6,71
2,3674(2)	338(21)	0,0069(2)	37,38145	3,35
2,38192(6)	3163(40)	0,00584(7)	37,06085	31,35
2,38784(6)	1581(40)	0,00584(7)	37,06085	15,67
2,4060(3)	970(59)	0,0042(1)	36,69057	9,61
2,4112(1)	1165(38)	0,0042(1)	36,61129	11,54
2,4119(3)	485(59)	0,0042(1)	36,69057	4,81
2,4172(1)	582(38)	0,0042(1)	36,61129	5,77
2,45828(5)	1787(25)	0,0058(1)	35,90985	17,71
2,46439(5)	893(25)	0,0058(1)	35,90986	8,85
2,5063(3)	427(16)	0,0101(4)	35,22157	4,24
2,5126(3)	214(16)	0,0101(4)	35,22157	2,12
2,5266(1)	1279(24)	0,0055(1)	34,93890	12,68
2,5329(1)	640(24)	0,0055(1)	34,93890	6,34
2,5546(1)	699(16)	0,0068(2)	34,55640	6,93
2,5609(1)	350(16)	0,0068(2)	34,55641	3,46
2,6357(4)	218(13)	0,0065(3)	33,49327	2,17
2,6422(4)	109(13)	0,0065(3)	33,49327	1,08
2,6617(9)	207(11)	0,0039(4)	33,16626	2,05
2,6683(9)	103(11)	0,0039(4)	33,16626	1,02
2,674(1)	249(46)	0,008(2)	33,01215	2,47
2,6769(3)	831(38)	0,0059(2)	32,97737	8,23
2,681(1)	125(46)	0,008(2)	33,01215	1,24
2,6836(3)	415(38)	0,0059(2)	32,97737	4,12
2,7246(2)	864(28)	0,0058(2)	32,40033	8,56
2,7314(2)	432(28)	0,0058(2)	32,40033	4,28
2,7406(2)	857(22)	0,0059(2)	32,21070	8,50
2,7475(2)	429(22)	0,0059(2)	32,21070	4,25
2,77978(8)	2011(28)	0,00566(8)	31,75739	19,93
2,78668(8)	1005(28)	0,00566(8)	31,75739	9,96
2,7981(6)	302(20)	0,0056(2)	31,54983	2,99
2,8050(6)	151(20)	0,0056(2)	31,54983	1,50
2,8172(1)	1324(23)	0,0068(1)	31,33509	13,12
2,8242(1)	662(23)	0,0068(1)	31,33509	6,56
2,866(2)	188(40)	0,005(1)	30,80095	1,87
2,867(2)	201(17)	0,007(3)	30,79333	2,00
2,873(2)	94(40)	0,005(1)	30,80095	0,93
2,874(2)	101(17)	0,007(3)	30,79333	1,00
2,8932(2)	598(16)	0,0075(2)	30,51213	5,92
2,9004(2)	299(16)	0,0075(2)	30,51213	2,96
2,954(1)	93(16)	0,011(2)	29,88891	0,92

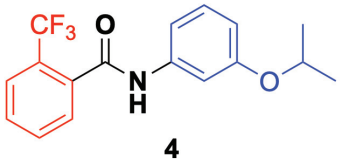
2,961(1)	46(16)	0,011(2)	29,88891	0,46
3,007(1)	137(25)	0,007(1)	29,35744	1,36
3,0097(8)	128(19)	0,0038(6)	29,33195	1,27
3,015(1)	68(25)	0,007(1)	29,35744	0,68
3,0172(8)	64(19)	0,0038(6)	29,33195	0,63
3,0336(4)	201(11)	0,0064(4)	29,10060	2,00
3,0412(4)	101(11)	0,0064(4)	29,10060	1,00
3,0762(1)	472(14)	0,0103(4)	28,69778	4,68
3,0839(1)	236(14)	0,0103(4)	28,69778	2,34
3,1128(2)	305(12)	0,0072(4)	28,36094	3,02
3,1205(2)	152(12)	0,0072(4)	28,36093	1,51
3,1738(4)	154(7)	0,0040(4)	27,81546	1,52
3,1817(4)	77(7)	0,0040(4)	27,81546	0,76
3,2032(4)	204(8)	0,0030(2)	27,56016	2,02
3,2112(4)	102(8)	0,0030(2)	27,56016	1,01
3,2298(9)	50(8)	0,012(3)	27,33356	0,49
3,2378(9)	25(8)	0,012(3)	27,33356	0,25
3,2617(5)	188(12)	0,0077(5)	27,06585	1,87
3,2698(5)	94(12)	0,0077(5)	27,06585	0,93
3,288(1)	304(47)	0,0079(6)	26,85049	3,02
3,296(1)	152(47)	0,0079(6)	26,85049	1,51
3,299(1)	253(22)	0,0092(9)	26,76085	2,51
3,307(1)	127(22)	0,0092(9)	26,76085	1,26
3,3296(5)	144(10)	0,0078(6)	26,51446	1,43
3,3379(5)	72(10)	0,0078(6)	26,51446	0,71
3,3690(2)	294(11)	0,0080(4)	26,20417	2,92
3,3774(2)	147(11)	0,0080(4)	26,20417	1,46
3,4035(3)	228(10)	0,0077(4)	25,93884	2,26
3,4120(3)	114(10)	0,0077(4)	25,93884	1,13
3,4722(5)	119(9)	0,0091(9)	25,42591	1,18
3,4808(5)	60(9)	0,0091(9)	25,42592	0,59
3,5096(6)	89(8)	0,010(1)	25,15459	0,88
3,5184(6)	44(8)	0,010(1)	25,15459	0,44
3,5767(2)	277(11)	0,0096(5)	24,68295	2,75
3,5856(2)	139(11)	0,0096(5)	24,68295	1,37
3,6419(4)	214(10)	0,0092(5)	24,24110	2,12
3,6510(4)	107(10)	0,0092(5)	24,24110	1,06
3,6708(2)	365(12)	0,0086(3)	24,05086	3,61
3,6799(2)	182(12)	0,0086(3)	24,05086	1,81
3,7082(6)	121(9)	0,0086(7)	23,80838	1,20
3,7174(6)	61(9)	0,0086(7)	23,80838	0,60
3,7417(8)	78(8)	0,011(2)	23,59498	0,77
3,7510(8)	39(8)	0,011(2)	23,59498	0,39
3,7766(3)	230(10)	0,0087(4)	23,37729	2,28

3,7859(3)	115(10)	0,0087(4)	23,37729	1,14
3,818(4)	30(12)	0,0029(7)	23,12182	0,30
3,828(4)	15(12)	0,0029(7)	23,12182	0,15
3,8329(3)	356(11)	0,0093(4)	23,03361	3,53
3,8425(3)	178(11)	0,0093(4)	23,03362	1,76
3,8761(3)	228(11)	0,0117(7)	22,77722	2,26
3,8857(3)	114(11)	0,0117(7)	22,77722	1,13
3,9167(9)	75(8)	0,008(1)	22,54144	0,74
3,9264(9)	37(8)	0,008(1)	22,54143	0,37
3,9467(4)	174(10)	0,0105(7)	22,37010	1,73
3,9565(4)	87(10)	0,0105(7)	22,37010	0,86
4,008(2)	97(26)	0,010(2)	22,02726	0,96
4,018(2)	48(26)	0,010(2)	22,02726	0,48
4,024(3)	69(13)	0,010(3)	21,94267	0,68
4,034(3)	34(13)	0,010(3)	21,94267	0,34
4,051(1)	76(12)	0,012(2)	21,79210	0,76
4,061(1)	38(12)	0,012(2)	21,79210	0,38
4,0785(6)	204(11)	0,0098(6)	21,64753	2,02
4,0886(6)	102(11)	0,0098(6)	21,64753	1,01
4,1073(7)	124(10)	0,0083(7)	21,49579	1,23
4,1175(7)	62(10)	0,0083(7)	21,49579	0,61
4,1472(5)	137(10)	0,014(1)	21,28903	1,36
4,1575(5)	68(10)	0,014(1)	21,28903	0,68
4,180(1)	83(12)	0,009(1)	21,12430	0,82
4,190(1)	42(12)	0,009(1)	21,12430	0,41
4,2258(8)	144(15)	0,0119(8)	20,89315	1,43
4,2363(8)	72(15)	0,0119(8)	20,89315	0,71
4,2475(7)	147(13)	0,0077(6)	20,78611	1,46
4,2581(7)	73(13)	0,0077(6)	20,78611	0,73
4,274(2)	81(17)	0,010(1)	20,65873	0,80
4,284(2)	41(17)	0,010(1)	20,65873	0,40
4,289(1)	159(10)	0,0078(6)	20,58484	1,58
4,300(1)	80(10)	0,0078(6)	20,58484	0,79
4,3284(4)	153(8)	0,0104(7)	20,39812	1,52
4,3391(4)	77(8)	0,0104(7)	20,39812	0,76
4,3940(5)	171(9)	0,0134(9)	20,09367	1,69
4,4049(5)	85(9)	0,0134(9)	20,09367	0,85
4,4249(4)	233(11)	0,0093(4)	19,95334	2,31
4,4359(4)	116(11)	0,0093(4)	19,95334	1,15
4,4776(4)	278(18)	0,0096(4)	19,71863	2,75
4,4887(4)	139(18)	0,0096(4)	19,71863	1,38
4,5014(8)	159(17)	0,0094(8)	19,61432	1,58
4,5126(8)	80(17)	0,0094(8)	19,61432	0,79
4,5428(2)	383(12)	0,0102(4)	19,43578	3,80

4,5541(2)	191(12)	0,0102(4)	19,43578	1,90
4,5826(8)	80(8)	0,014(2)	19,26691	0,79
4,5940(8)	40(8)	0,014(2)	19,26691	0,40
4,6194(9)	73(6)	0,020(3)	19,11350	0,72
4,6309(9)	36(6)	0,020(3)	19,11350	0,36
4,729(2)	97(22)	0,015(2)	18,67136	0,96
4,741(2)	49(22)	0,015(2)	18,67136	0,48
4,745(2)	70(18)	0,008(2)	18,60647	0,70
4,757(2)	35(18)	0,008(2)	18,60647	0,35
4,776(1)	152(21)	0,015(2)	18,48836	1,51
4,788(1)	76(21)	0,015(2)	18,48835	0,75
4,806(1)	105(15)	0,009(1)	18,37371	1,04
4,817(1)	53(15)	0,009(1)	18,37371	0,52
4,828(2)	78(20)	0,011(1)	18,28731	0,78
4,840(2)	39(20)	0,011(1)	18,28731	0,39
4,8444(8)	306(14)	0,0095(6)	18,22656	3,04
4,8564(8)	153(14)	0,0095(6)	18,22656	1,52
4,902(1)	116(17)	0,0106(9)	18,01148	1,15
4,914(1)	58(17)	0,0106(9)	18,01148	0,57
4,930(2)	74(7)	0,019(3)	17,90913	0,74
4,943(2)	37(7)	0,019(3)	17,90913	0,37
4,964(1)	105(10)	0,0097(9)	17,78579	1,04
4,977(1)	52(10)	0,0097(9)	17,78579	0,52
4,996(2)	69(20)	0,0095(8)	17,67340	0,69
5,009(2)	35(20)	0,0095(8)	17,67340	0,34
5,0159(9)	215(12)	0,0089(4)	17,60376	2,13
5,0283(9)	108(12)	0,0089(4)	17,60375	1,07
5,0666(9)	119(12)	0,013(1)	17,42756	1,18
5,0792(9)	60(12)	0,013(1)	17,42756	0,59
5,091(2)	74(14)	0,008(1)	17,34500	0,73
5,103(2)	37(14)	0,008(1)	17,34500	0,37
5,117(1)	69(7)	0,013(2)	17,25566	0,68
5,130(1)	34(7)	0,013(2)	17,25566	0,34
5,1664(3)	193(8)	0,0157(9)	17,09103	1,92
5,1793(3)	97(8)	0,0157(9)	17,09103	0,96
5,3384(7)	72(5)	0,019(2)	16,54086	0,71
5,3517(7)	36(5)	0,019(2)	16,54086	0,36
5,4532(8)	71(7)	0,017(2)	16,19282	0,70
5,4668(8)	35(7)	0,017(2)	16,19282	0,35
5,4993(7)	99(8)	0,013(1)	16,05730	0,98
5,5130(7)	49(8)	0,013(1)	16,05730	0,49
5,563(2)	30(6)	0,022(7)	15,87342	0,30
5,577(2)	15(6)	0,022(7)	15,87342	0,15
5,608(1)	77(9)	0,011(1)	15,74700	0,77

5,622(1)	39(9)	0,011(1)	15,74700	0,38
5,646(2)	51(9)	0,012(2)	15,63997	0,51
5,660(2)	25(9)	0,012(2)	15,63997	0,25
5,698(3)	20(4)	0,024(7)	15,49844	0,20
5,712(3)	10(4)	0,024(7)	15,49844	0,10
5,800(1)	55(7)	0,014(2)	15,22588	0,55
5,814(1)	28(7)	0,014(2)	15,22588	0,27
5,840(2)	46(8)	0,012(2)	15,12130	0,46
5,854(2)	23(8)	0,012(2)	15,12129	0,23
5,923(1)	34(3)	0,038(6)	14,90834	0,34
5,938(1)	17(3)	0,038(6)	14,90834	0,17
6,020(2)	23(5)	0,014(3)	14,66859	0,23
6,035(2)	12(5)	0,014(3)	14,66859	0,11
6,219(1)	41(6)	0,017(3)	14,20078	0,41
6,234(1)	21(6)	0,017(3)	14,20078	0,20
6,398(4)	14(6)	0,02(1)	13,80294	0,14
6,414(4)	7(6)	0,02(1)	13,80294	0,07
6,478(8)	10(2)	0,08(2)	13,63256	0,10
6,494(8)	5(2)	0,08(2)	13,63256	0,05
6,869(4)	18(7)	0,013(5)	12,85825	0,17
6,886(4)	9(7)	0,013(5)	12,85825	0,09
6,932(3)	18(4)	0,03(1)	12,74204	0,17
6,949(3)	9(4)	0,03(1)	12,74204	0,09
7,171(8)	8(3)	0,10(3)	12,31725	0,08
7,189(8)	4(3)	0,10(3)	12,31725	0,04
7,57(2)	11(1)	0,5(1)	11,66286	0,11
7,59(2)	5(1)	0,5(1)	11,66286	0,05
8,20(2)	18(2)	0,57(6)	10,77971	0,18
8,22(2)	9(2)	0,57(6)	10,77971	0,09

***N*-(3-Isopropoxyphenyl)-2-(trifluoromethyl)benzamide (Flutolanil) (4).** CAS [66332-96-5].



4

MicroED not performed

Reference code for CCDC Cambridge: KUYVOQ[11]

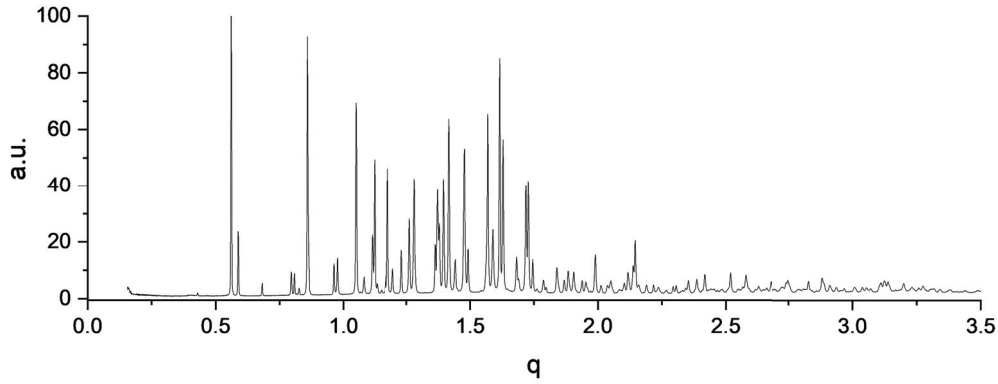


Figure S11. Synchrotron PXRD pattern of Flutolanil (**4**), in accordance with CDS deposited structure (refcode KUYVOQ).[11]

Table S6. Most intense peaks for PXRD diffractogram of Flutolanil **(4)** prepared by LA-RAM (Table 2, entry 4).

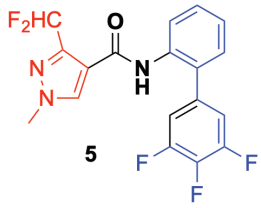
Pos.[°2Th.]	Height [cts]	FWHMLeft[°2Th.]	d-spacing [Å]	Rel. Int. [%]
0,2419	341,11	0,0059	365,17390	2,48
0,6472	95,60	0,0039	136,51010	0,69
0,845117(7)	12052(71)	0,00419(3)	104,44770	87,60
0,847217(7)	6026(71)	0,00419(3)	104,44770	43,80
0,88610(3)	2601(35)	0,00434(7)	99,61749	18,91
0,88830(3)	1301(35)	0,00434(7)	99,61749	9,45
1,0272(1)	506(20)	0,0042(2)	85,92947	3,68
1,0298(1)	253(20)	0,0042(2)	85,92947	1,84
1,1995(1)	995(30)	0,0050(2)	73,59103	7,24
1,2025(1)	498(30)	0,0050(2)	73,59103	3,62
1,2179(1)	896(28)	0,0045(2)	72,48010	6,51
1,2209(1)	448(28)	0,0045(2)	72,48009	3,26
1,2450	342,73	0,0064	70,90080	2,49
1,2481	171,36	0,0064	70,90080	1,25
1,2481	171,36	0,0064	70,90080	1,25
1,25(4)	171(1142)	0,0064(7)	70,90080	1,25
1,2481	171,36	0,0064	70,90080	1,25
1,2941	13757,83	0,0049	68,26737	100,00
1,3028	1755,39	0,0020	67,81158	12,76
1,4499	1640,35	0,0059	60,93230	11,92
1,4706	1919,98	0,0059	60,07592	13,96
1,5807	10120,68	0,0059	55,88977	73,56
1,6270	909,78	0,0079	54,29819	6,61

1,6770	3133,00	0,0059	52,67955	22,77
1,6902	7107,02	0,0049	52,26833	51,66
1,7055	571,96	0,0059	51,80167	4,16
1,7312	243,97	0,0049	51,03301	1,77
1,7565	1102,02	0,0049	50,29724	8,01
1,7719	6453,87	0,0049	49,85847	46,91
1,8021	1343,86	0,0059	49,02406	9,77
1,8541	2349,74	0,0049	47,64961	17,08
1,9011	4017,58	0,0069	46,47189	29,20
1,9303	6140,26	0,0079	45,76797	44,63
2,0543	2671,87	0,0039	43,00602	19,42
2,0676	5574,67	0,0069	42,72862	40,52
2,0783	3727,00	0,0049	42,51019	27,09
2,1032	6002,79	0,0069	42,00665	43,63
2,1344	9214,00	0,0069	41,39184	66,97
2,1721	1823,13	0,0079	40,67468	13,25
2,2259	7698,96	0,0089	39,69181	55,96
2,2480	2404,00	0,0059	39,30091	17,47
2,3638	9517,30	0,0059	37,37597	69,18
2,3942	3381,37	0,0089	36,90180	24,58
2,4342	12641,32	0,0069	36,29456	91,88
2,4538	8009,59	0,0059	36,00552	58,22
2,5340	1996,03	0,0096	34,83729	14,51
2,5453	815,70	0,0072	34,76892	5,93
2,5887	5837,25	0,0084	34,10123	42,43
2,6029	6052,19	0,0072	33,91491	43,99
2,6290	1804,65	0,0084	33,57864	13,12
2,6537	290,68	0,0096	33,26547	2,11
2,6919	751,53	0,0096	32,79437	5,46
2,7075	381,05	0,0060	32,60476	2,77
2,7712	1419,07	0,0096	31,85613	10,31
2,8142	762,73	0,0084	31,36906	5,54
2,8376	1242,01	0,0084	31,10989	9,03
2,8706	1178,81	0,0096	30,75238	8,57
2,9200	731,27	0,0084	30,23304	5,32
2,9419	660,65	0,0072	30,00737	4,80
2,9687	182,97	0,0072	29,73673	1,33
2,9976	2089,95	0,0096	29,44992	15,19
3,0313	480,28	0,0132	29,12331	3,49
3,0693	478,01	0,0096	28,76243	3,47
3,0892	726,10	0,0084	28,57733	5,28
3,1394	258,89	0,0072	28,12027	1,88
3,1681	596,76	0,0096	27,86587	4,34
3,1901	1176,57	0,0096	27,67355	8,55

3,2207	1519,00	0,0084	27,41041	11,04
3,2326	2855,17	0,0072	27,30980	20,75
3,2532	510,18	0,0108	27,13663	3,71
3,2992	497,57	0,0096	26,75826	3,62
3,3407	507,94	0,0072	26,42589	3,69
3,3692	375,56	0,0120	26,20296	2,73
3,4174	222,25	0,0072	25,83347	1,62
3,4562	421,66	0,0072	25,54307	3,06
3,4744	461,45	0,0072	25,40984	3,35
3,5068	177,54	0,0096	25,17497	1,29
3,5298	333,93	0,0084	25,01070	2,43
3,5461	731,75	0,0096	24,89617	5,32
3,5958	792,14	0,0096	24,55192	5,76
3,6430	1042,82	0,0096	24,23431	7,58
3,6802	294,59	0,0096	23,98905	2,14
3,6965	287,06	0,0120	23,88363	2,09
3,7180	217,65	0,0072	23,74556	1,58
3,7449	276,29	0,0120	23,57502	2,01
3,7950	1145,99	0,0084	23,26347	8,33
3,8391	274,11	0,0096	22,99689	1,99
3,8665	402,50	0,0072	22,83355	2,93
3,8853	1019,18	0,0120	22,72306	7,41
3,9432	258,53	0,0096	22,38993	1,88
3,9598	418,70	0,0096	22,29570	3,04
4,0086	334,78	0,0096	22,02477	2,43
4,0342	667,60	0,0108	21,88470	4,85
4,0597	286,52	0,0144	21,74750	2,08
4,1031	420,04	0,0096	21,51737	3,05
4,1302	654,93	0,0072	21,37628	4,76
4,1403	763,69	0,0072	21,32443	5,55
4,1970	281,68	0,0108	21,03657	2,05
4,2612	713,91	0,0096	20,71936	5,19
4,3418	895,51	0,0096	20,33488	6,51
4,3534	608,67	0,0096	20,33146	4,42
4,3874	507,42	0,0108	20,12384	3,69
4,4256	391,88	0,0108	19,95040	2,85
4,4720	338,76	0,0096	19,74346	2,46
4,5321	401,02	0,0108	19,48176	2,91
4,5785	402,30	0,0108	19,28452	2,92
4,6016	378,71	0,0072	19,18738	2,75
4,6283	329,65	0,0120	19,07706	2,40
4,6778	493,62	0,0096	18,87517	3,59
4,6876	641,42	0,0084	18,83577	4,66
4,7080	747,25	0,0132	18,75424	5,43

4,7285	703,69	0,0084	18,71919	5,11
4,7737	264,64	0,0096	18,49610	1,92
4,8210	594,41	0,0120	18,31471	4,32
4,8693	406,25	0,0096	18,13313	2,95
4,9099	367,73	0,0108	17,98355	2,67
4,9349	464,03	0,0132	17,89221	3,37
4,9811	302,83	0,0144	17,72659	2,20
4,9989	328,96	0,0156	17,66356	2,39
5,0339	278,87	0,0168	17,54059	2,03
5,0938	262,09	0,0288	17,33466	1,90
5,1827	227,31	0,0120	17,03743	1,65
5,2571	231,18	0,0144	16,79640	1,68
5,3126	236,03	0,0120	16,62113	1,72
5,3390	250,71	0,0192	16,53909	1,82
5,3833	209,85	0,0120	16,40286	1,53
5,4547	168,04	0,0132	16,18858	1,22
5,5423	228,66	0,0144	15,93273	1,66
5,5629	222,12	0,0192	15,87389	1,61
5,5974	195,83	0,0132	15,77616	1,42
5,7235	236,94	0,0096	15,42866	1,72
5,8276	178,28	0,0120	15,15329	1,30
5,8710	168,26	0,0384	15,04156	1,22
6,0474	171,56	0,0168	14,60300	1,25
6,1497	191,86	0,0144	14,36039	1,39
6,2085	159,85	0,0192	14,22455	1,16
6,3500	150,45	0,0120	13,90784	1,09
6,5387	156,71	0,0144	13,50684	1,14
6,6421	102,03	0,0480	13,29684	0,74
6,8069	93,40	0,0288	12,97535	0,68
7,0122	78,32	0,0960	12,59586	0,57
7,1720	115,57	0,0336	12,31565	0,84
7,4411	159,27	0,0108	11,87081	1,16
7,5470	90,71	0,3072	11,70453	0,66
8,1322	127,74	0,0192	10,86348	0,93
8,2946	112,26	0,0576	10,65117	0,82
8,7094	91,88	0,1152	10,14482	0,67
9,2679	83,03	0,0480	9,53460	0,60

3-(Difluoromethyl)-1-methyl-*N*-(3',4',5'-trifluoro[1,1'-biphenyl]-2-yl)-1H-pyrazole-4-carboxamide (Fluxapyroxad) (5). CAS [907204-31-3].



5

Space Group	P b c a
Cell Lengths	**a** 12.937(2) **b** 9.2697(14) **c** 28.487(17)
Cell Angles	***α*** 90° ***β*** 90° ***γ*** 90°

Reference code for CCDC Cambridge: (refcode IDECIH).[10]

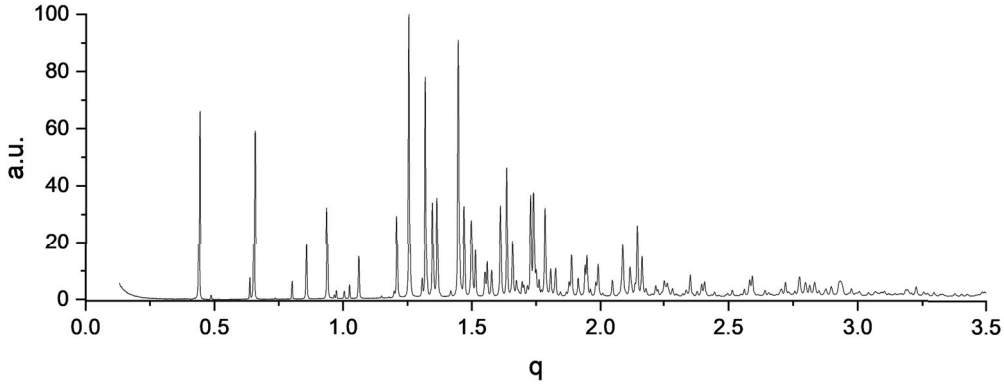


Figure S12. Synchrotron PXRD pattern for Fluxapyroxad (**5**), in accordance with CDS deposited structure (refcode IDECIH).[10]

Table S7. Most intense peaks for PXRD diffractogram of Fluxapyroxad **(5)** prepared by LA-RAM (Table 2, entry 5).

Pos.[°2Th.]	Height [cts]	FWHMLeft[°2Th.]	d-spacing [Å]	Rel. Int. [%]
0,20(2)	566(71)	0,10(4)	435,84130	3,39
0,20(2)	283(71)	0,10(4)	435,84130	1,70
0,6627(1)	10521(819)	0,0054(4)	133,20380	62,96
0,6643(1)	5261(819)	0,0054(4)	133,20380	31,48
0,73(2)	209(429)	0,001(3)	120,71110	1,25
0,73(2)	105(429)	0,001(3)	120,71110	0,63
0,9582(2)	1108(511)	0,003(2)	92,12434	6,63
0,9606(2)	554(511)	0,003(2)	92,12434	3,32
0,9836(1)	9855(966)	0,0051(5)	89,74361	58,98
0,9860(1)	4927(966)	0,0051(5)	89,74360	29,49
1(1513589048595)	0(1025)	0(471200377357)	79,29607	0,00
1(1513589048595)	0(1025)	0(471200377357)	79,29607	0,00
1,206(1)	1105(86)	0,0038(2)	73,18132	6,61

1,209(1)	552(86)	0,0038(2)	73,18132	3,31
1,29120(7)	3315(173)	0,00540(9)	68,36378	19,84
1,29441(7)	1657(173)	0,00540(9)	68,36378	9,92
1,4133(1)	5625(705)	0,00548(7)	62,45762	33,66
1,4168(1)	2812(705)	0,00548(7)	62,45762	16,83
1,46(4)	60(219)	0,0(1)	60,27563	0,36
1,465(6)	352(135)	0,00(2)	60,26517	2,11
1,47(4)	30(219)	0,0(1)	60,27563	0,18
1,468(6)	176(135)	0,00(2)	60,26517	1,05
1,5112(3)	453(38)	0,005(2)	58,41320	2,71
1,5149(3)	226(38)	0,005(2)	58,41320	1,35
1,542(1)	914(135)	0,0038(4)	57,24902	5,47
1,546(1)	457(135)	0,0038(4)	57,24902	2,74
1,59703(5)	2671(77)	0,0054(2)	55,27294	15,99
1,60100(5)	1336(77)	0,0054(2)	55,27295	7,99
1,7460(7)	181(11)	0,0033(8)	50,55774	1,08
1,7503(7)	90(11)	0,0033(8)	50,55774	0,54
1,814(1)	413(111)	0,0066(7)	48,65814	2,47
1,819(1)	206(111)	0,0066(7)	48,65814	1,23
1,8215(2)	4948(228)	0,0054(1)	48,46245	29,61
1,8260(2)	2474(228)	0,0054(1)	48,46245	14,81
1,89295(9)	16710(247)	0,0058(1)	46,63295	100,00
1,89765(9)	8355(247)	0,0058(1)	46,63295	50,00
1,9821(5)	1523(177)	0,0053(3)	44,53585	9,11
1,9870(5)	761(177)	0,0053(3)	44,53585	4,56
1,9899(2)	11664(400)	0,0053(2)	44,36147	69,80
1,9948(2)	5832(400)	0,0053(2)	44,36147	34,90
2,0304(2)	5409(273)	0,0070(7)	43,47663	32,37
2,0354(2)	2705(273)	0,0070(7)	43,47663	16,19
2,05674(4)	5531(93)	0,0068(2)	42,91953	33,10
2,06186(4)	2765(93)	0,0068(2)	42,91953	16,55
2,1376(6)	217(18)	0,010(1)	41,29560	1,30
2,1429(6)	109(18)	0,010(1)	41,29560	0,65
2,1810(1)	14867(514)	0,0068(3)	40,47417	88,97
2,1864(1)	7434(514)	0,0068(3)	40,47417	44,49
2,21367(9)	5286(192)	0,00600(9)	39,87740	31,64
2,21917(9)	2643(192)	0,00600(9)	39,87740	15,82
2,2569(1)	4553(167)	0,0087(5)	39,11430	27,25
2,2625(1)	2277(167)	0,0087(5)	39,11430	13,62
2,2794(2)	2706(179)	0,0063(6)	38,72789	16,20
2,2850(2)	1353(179)	0,0063(6)	38,72789	8,10
2,3437(1)	1906(44)	0,0078(2)	37,66513	11,41
2,3495(1)	953(44)	0,0078(2)	37,66513	5,70
2,3496(2)	1350(61)	0,0042(2)	37,57142	8,08

2,3554(2)	675(61)	0,0042(2)	37,57141	4,04
2,37507(9)	1513(27)	0,0080(2)	37,16772	9,06
2,38098(9)	757(27)	0,0080(2)	37,16772	4,53
2,4261(4)	5335(52)	0,00734(8)	36,38676	31,92
2,4321(4)	2667(52)	0,00734(8)	36,38676	15,96
2,4629(2)	6955(341)	0,0060(7)	35,84235	41,62
2,4690(2)	3478(341)	0,0060(7)	35,84236	20,81
2,4978(3)	2991(49)	0,0084(2)	35,34134	17,90
2,5040(3)	1496(49)	0,0084(2)	35,34134	8,95
2,5342(1)	1208(25)	0,0048(3)	34,83486	7,23
2,5405(1)	604(25)	0,0048(3)	34,83486	3,61
2,5587(8)	939(103)	0,0115(5)	34,50063	5,62
2,5651(8)	470(103)	0,0115(5)	34,50063	2,81
2,5838(5)	847(28)	0,0053(4)	34,16515	5,07
2,5903(5)	423(28)	0,0053(4)	34,16515	2,53
2,600(4)	933(874)	0,0054(5)	33,95404	5,58
2,6039(3)	5510(287)	0,0065(2)	33,90251	32,98
2,606(4)	466(874)	0,0054(5)	33,95404	2,79
2,6103(3)	2755(287)	0,0065(2)	33,90251	16,49
2,6227(5)	6508(509)	0,0074(2)	33,65866	38,95
2,6292(5)	3254(509)	0,0074(2)	33,65866	19,47
2,6502(4)	2035(65)	0,0044(1)	33,31007	12,18
2,6568(4)	1018(65)	0,0044(1)	33,31007	6,09
2,667(2)	724(47)	0,004(1)	33,10276	4,33
2,673(2)	362(47)	0,004(1)	33,10276	2,17
2,684(2)	803(148)	0,0050(7)	32,89441	4,81
2,6876(1)	4946(149)	0,0071(5)	32,84692	29,60
2,690(2)	402(148)	0,0050(7)	32,89441	2,40
2,6942(1)	2473(149)	0,0071(5)	32,84692	14,80
2,7190(6)	1543(54)	0,0086(4)	32,46726	9,23
2,7257(6)	771(54)	0,0086(4)	32,46725	4,62
2,7472(2)	1543(28)	0,0098(2)	32,13337	9,23
2,7541(2)	772(28)	0,0098(2)	32,13337	4,62
2,7969(5)	501(12)	0,0040(2)	31,56332	3,00
2,8038(5)	251(12)	0,0040(2)	31,56332	1,50
2,823(4)	400(119)	0,016(4)	31,27516	2,40
2,830(4)	200(119)	0,016(4)	31,27516	1,20
2,838(2)	739(139)	0,010(2)	31,10327	4,42
2,8421(5)	2088(67)	0,0062(3)	31,06118	12,50
2,845(2)	369(139)	0,010(2)	31,10327	2,21
2,8492(5)	1044(67)	0,0062(3)	31,06118	6,25
2,8822(2)	1122(40)	0,0086(2)	30,62890	6,71
2,8894(2)	561(40)	0,0086(2)	30,62890	3,36
2,922(1)	2045(292)	0,0082(2)	30,21079	12,24

2,929(1)	1023(292)	0,0082(2)	30,21079	6,12
2,9334(5)	2061(207)	0,0066(2)	30,09431	12,34
2,9407(5)	1031(207)	0,0066(2)	30,09431	6,17
2,9601(6)	457(39)	0,0061(2)	29,82329	2,73
2,9674(6)	228(39)	0,0061(2)	29,82329	1,37
2,986(2)	857(86)	0,0096(4)	29,56851	5,13
2,993(2)	428(86)	0,0096(4)	29,56851	2,56
2,9978(2)	1723(50)	0,0079(7)	29,44860	10,31
3,0052(2)	861(50)	0,0079(7)	29,44860	5,15
3,0476(4)	460(15)	0,0053(2)	28,96751	2,76
3,0551(4)	230(15)	0,0053(2)	28,96752	1,38
3,0800(4)	835(18)	0,0107(5)	28,66258	4,99
3,0876(4)	417(18)	0,0107(5)	28,66258	2,50
3,1481(6)	2662(72)	0,0114(2)	28,04281	15,93
3,1559(6)	1331(72)	0,0114(2)	28,04281	7,97
3,1925(2)	1844(63)	0,0095(2)	27,65230	11,03
3,2005(2)	922(63)	0,0095(2)	27,65230	5,52
3,2151(9)	393(76)	0,0081(8)	27,45864	2,35
3,2231(9)	196(76)	0,0081(8)	27,45864	1,18
3,2327(5)	3523(40)	0,0081(7)	27,30902	21,08
3,2407(5)	1761(40)	0,0081(7)	27,30902	10,54
3,2612(2)	2210(41)	0,0089(2)	27,07033	13,22
3,2693(2)	1105(41)	0,0089(2)	27,07033	6,61
3,2894(9)	375(28)	0,011(1)	26,83835	2,24
3,2976(9)	187(28)	0,011(1)	26,83835	1,12
3,3466(4)	351(12)	0,0258(9)	26,37943	2,10
3,3550(4)	176(12)	0,0258(9)	26,37943	1,05
3,3941(5)	850(40)	0,0171(5)	26,01058	5,08
3,4025(5)	425(40)	0,0171(5)	26,01058	2,54
3,4141(6)	682(42)	0,0084(9)	25,85833	4,08
3,4226(6)	341(42)	0,0084(9)	25,85832	2,04
3,4409(4)	489(35)	0,0108(8)	25,65716	2,93
3,4494(4)	245(35)	0,0108(8)	25,65716	1,46
3,4820(7)	286(28)	0,0079(7)	25,35456	1,71
3,4906(7)	143(28)	0,0079(7)	25,35456	0,85
3,506(3)	182(61)	0,011(1)	25,17852	1,09
3,515(3)	91(61)	0,011(1)	25,17852	0,54
3,519(1)	406(27)	0,0085(6)	25,08857	2,43
3,528(1)	203(27)	0,0085(6)	25,08857	1,21
3,5421(2)	1233(39)	0,0094(2)	24,92402	7,38
3,5509(2)	617(39)	0,0094(2)	24,92402	3,69
3,5816(6)	321(18)	0,0109(7)	24,64934	1,92
3,5905(6)	161(18)	0,0109(7)	24,64934	0,96
3,6090(4)	786(48)	0,0095(5)	24,46218	4,70

3,6180(4)	393(48)	0,0095(5)	24,46218	2,35
3,6271(7)	917(27)	0,0084(5)	24,34049	5,49
3,6361(7)	459(27)	0,0084(5)	24,34049	2,74
3,6845(5)	161(8)	0,031(2)	23,96137	0,96
3,6936(5)	80(8)	0,031(2)	23,96137	0,48
3,761(1)	157(9)	0,030(2)	23,47190	0,94
3,771(1)	79(9)	0,030(2)	23,47190	0,47
3,7906(8)	365(19)	0,0099(6)	23,29048	2,19
3,8001(8)	183(19)	0,0099(6)	23,29048	1,09
3,8558(5)	342(16)	0,0158(9)	22,89728	2,05
3,8653(5)	171(16)	0,0158(9)	22,89728	1,02
3,8894(4)	1013(45)	0,0118(5)	22,69917	6,06
3,8991(4)	506(45)	0,0118(5)	22,69917	3,03
3,9051(4)	1010(27)	0,0091(4)	22,60800	6,04
3,9148(4)	505(27)	0,0091(4)	22,60800	3,02
3,9821(8)	364(22)	0,018(1)	22,17123	2,18
3,9920(8)	182(22)	0,018(1)	22,17123	1,09
4,0212(6)	351(27)	0,0081(5)	21,95542	2,10
4,0312(6)	175(27)	0,0081(5)	21,95542	1,05
4,0741(7)	427(16)	0,0221(9)	21,67053	2,55
4,0842(7)	213(16)	0,0221(9)	21,67053	1,28
4,1035(5)	759(33)	0,0101(5)	21,51556	4,54
4,1137(5)	379(33)	0,0101(5)	21,51556	2,27
4,1480(6)	296(22)	0,014(1)	21,28475	1,77
4,1583(6)	148(22)	0,014(1)	21,28475	0,89
4,1775(3)	1176(25)	0,0127(5)	21,13448	7,04
4,1879(3)	588(25)	0,0127(5)	21,13448	3,52
4,2120(3)	863(27)	0,0119(8)	20,96144	5,16
4,2225(3)	431(27)	0,0119(8)	20,96144	2,58
4,2379(5)	696(28)	0,0102(3)	20,83326	4,16
4,2485(5)	348(28)	0,0102(3)	20,83326	2,08
4,2668(4)	844(24)	0,0133(6)	20,69228	5,05
4,2774(4)	422(24)	0,0133(6)	20,69228	2,53
4,2950(9)	282(21)	0,0113(8)	20,55634	1,69
4,3057(9)	141(21)	0,0113(8)	20,55634	0,84
4,3297(6)	442(16)	0,0162(8)	20,39171	2,65
4,3405(6)	221(16)	0,0162(8)	20,39171	1,32
4,3637(3)	582(18)	0,013(1)	20,23289	3,48
4,3746(3)	291(18)	0,013(1)	20,23289	1,74
4,4104(9)	925(89)	0,015(1)	20,01905	5,54
4,4213(9)	463(89)	0,015(1)	20,01905	2,77
4,4262(9)	618(36)	0,013(1)	19,94748	3,70
4,4372(9)	309(36)	0,013(1)	19,94748	1,85
4,4788(8)	330(19)	0,023(1)	19,71330	1,97

4,4900(8)	165(19)	0,023(1)	19,71330	0,99
4,5228(7)	253(12)	0,030(2)	19,52169	1,51
4,5340(7)	126(12)	0,030(2)	19,52169	0,76
4,5789(7)	198(44)	0,017(3)	19,28280	1,18
4,5902(7)	99(44)	0,017(3)	19,28280	0,59
4,626(1)	230(24)	0,041(7)	19,08575	1,38
4,638(1)	115(24)	0,041(7)	19,08575	0,69
4,673(2)	238(36)	0,034(6)	18,89455	1,43
4,685(2)	119(36)	0,034(6)	18,89455	0,71
4,7244(6)	316(24)	0,0092(9)	18,68906	1,89
4,7362(6)	158(24)	0,0092(9)	18,68906	0,95
4,762(2)	229(38)	0,021(3)	18,54193	1,37
4,774(2)	115(38)	0,021(3)	18,54193	0,69
4,8019(8)	533(47)	0,015(1)	18,38750	3,19
4,8139(8)	267(47)	0,015(1)	18,38750	1,60
4,829(1)	285(37)	0,010(1)	18,28571	1,70
4,841(1)	142(37)	0,010(1)	18,28571	0,85
4,8579(3)	558(21)	0,0129(8)	18,17587	3,34
4,8700(3)	279(21)	0,0129(8)	18,17587	1,67
4,9054(6)	323(24)	0,0134(8)	17,99974	1,93
4,9176(6)	161(24)	0,0134(8)	17,99974	0,97
4,9354(8)	234(14)	0,017(2)	17,89049	1,40
4,9477(8)	117(14)	0,017(2)	17,89050	0,70
4,9723(6)	330(15)	0,0130(8)	17,75797	1,98
4,9846(6)	165(15)	0,0130(8)	17,75797	0,99
5,015(1)	282(29)	0,016(2)	17,60706	1,69
5,027(1)	141(29)	0,016(2)	17,60706	0,84
5,049(1)	181(28)	0,0101(8)	17,48751	1,08
5,062(1)	91(28)	0,0101(8)	17,48751	0,54
5,0921(6)	210(11)	0,021(1)	17,34042	1,26
5,1047(6)	105(11)	0,021(1)	17,34042	0,63
5,1366(8)	203(16)	0,016(1)	17,19026	1,22
5,1494(8)	102(16)	0,016(1)	17,19026	0,61
5,1752(9)	184(17)	0,017(2)	17,06222	1,10
5,1880(9)	92(17)	0,017(2)	17,06222	0,55
5,255(1)	319(13)	0,034(2)	16,80406	1,91
5,268(1)	160(13)	0,034(2)	16,80406	0,96
5,285(1)	242(20)	0,011(1)	16,70773	1,45
5,298(1)	121(20)	0,011(1)	16,70773	0,73
5,3292(5)	272(13)	0,021(1)	16,56943	1,63
5,3424(5)	136(13)	0,021(1)	16,56943	0,81
5,3695(6)	455(36)	0,013(1)	16,44499	2,72
5,3829(6)	228(36)	0,013(1)	16,44499	1,36
5,4003(5)	252(16)	0,0066(5)	16,35142	1,51

5,4137(5)	126(16)	0,0066(5)	16,35142	0,75
5,4510(6)	224(19)	0,0154(8)	16,19944	1,34
5,4646(6)	112(19)	0,0154(8)	16,19943	0,67
5,5161(7)	214(5)	0,061(3)	16,00841	1,28
5,5298(7)	107(5)	0,061(3)	16,00841	0,64
5,5792(5)	372(19)	0,0119(8)	15,82755	2,23
5,5930(5)	186(19)	0,0119(8)	15,82755	1,11
5,6106(9)	196(18)	0,013(1)	15,73895	1,17
5,6246(9)	98(18)	0,013(1)	15,73895	0,59
5,6961(6)	285(21)	0,0120(8)	15,50284	1,71
5,7103(6)	143(21)	0,0120(8)	15,50284	0,85
5,7347(7)	216(16)	0,0126(9)	15,39868	1,29
5,7489(7)	108(16)	0,0126(9)	15,39869	0,65
5,790(2)	165(31)	0,016(2)	15,25296	0,99
5,804(2)	83(31)	0,016(2)	15,25295	0,49
5,8211(9)	199(17)	0,016(1)	15,17019	1,19
5,8356(9)	99(17)	0,016(1)	15,17019	0,59
5,873(1)	120(10)	0,033(4)	15,03694	0,72
5,887(1)	60(10)	0,033(4)	15,03694	0,36
5,939(7)	87(64)	0,02(2)	14,87025	0,52
5,953(7)	44(64)	0,02(2)	14,87025	0,26
5,974(4)	143(56)	0,014(2)	14,78173	0,85
5,989(4)	71(56)	0,014(2)	14,78173	0,43
5,994(2)	193(24)	0,011(3)	14,73275	1,16
6,009(2)	97(24)	0,011(3)	14,73275	0,58
6,105(6)	58(3)	0,17(2)	14,46652	0,35
6,120(6)	29(3)	0,17(2)	14,46652	0,17
6,229(1)	154(12)	0,027(3)	14,17838	0,92
6,244(1)	77(12)	0,027(3)	14,17838	0,46
6,272(1)	181(26)	0,010(1)	14,08029	1,08
6,288(1)	91(26)	0,010(1)	14,08029	0,54
6,309(2)	81(10)	0,016(3)	13,99734	0,48
6,325(2)	40(10)	0,016(3)	13,99734	0,24
6,4307(9)	219(31)	0,013(2)	13,73353	1,31
6,4467(9)	110(31)	0,013(2)	13,73353	0,66
6,464(2)	129(25)	0,016(4)	13,66364	0,77
6,480(2)	65(25)	0,016(4)	13,66364	0,39
6,561(2)	65(4)	0,058(6)	13,46122	0,39
6,577(2)	32(4)	0,058(6)	13,46122	0,19
6,798(2)	42(5)	0,059(7)	12,99262	0,25
6,815(2)	21(5)	0,059(7)	12,99262	0,13
6,972(4)	32(4)	0,09(1)	12,66758	0,19
6,990(4)	16(4)	0,09(1)	12,66758	0,10
7,22(2)	3(6)	0,03(1)	12,23446	0,02

7,24(2)	2(6)	0,03(1)	12,23446	0,01
7,337(8)	48(3)	0,22(3)	12,03840	0,29
7,356(8)	24(3)	0,22(3)	12,03840	0,14
7,617(2)	42(8)	0,050(9)	11,59763	0,25
7,636(2)	21(8)	0,050(9)	11,59763	0,13
7,720(2)	63(14)	0,0421(5)	11,44229	0,38
7,739(2)	32(14)	0,0421(5)	11,44229	0,19
7,892(7)	53(7)	0,20(4)	11,19314	0,32
7,912(7)	26(7)	0,20(4)	11,19314	0,16
8,132(9)	54(12)	0,18(4)	10,86362	0,32
8,152(9)	27(12)	0,18(4)	10,86362	0,16
8,383(6)	58(7)	0,19(3)	10,53962	0,35
8,403(6)	29(7)	0,19(3)	10,53962	0,17
8,642(5)	45(7)	0,13(2)	10,22316	0,27
8,664(5)	22(7)	0,13(2)	10,22316	0,13
8,92(1)	45(2)	0,33(2)	9,91005	0,27
8,94(1)	22(2)	0,33(2)	9,91005	0,13

GREEN CHEMISTRY METRICS: COMPARATIVE ASSESSMENT OF SOLUTION-BASED *vs* MECHANOCHEMICAL METHODS.

The calculations of the green metrics using CHEM21[12] and DOZN™ 3.0[13] toolkits for the solution syntheses of compounds **1-5** were performed based on the experimental procedures reported in literature chosen to be the most closely related to the mechanochemical protocol(s) from a synthetic point of view and giving priority to commercially used routes when applicable. A comparison of the results obtained across different mechanochemical methods (TCFH- *vs* 1,1'-oxalyldiimidazole (ODI-mediated), mechanochemical processing methodologies (by VBM, PBM and LA-RAM) with the previously described solution-based syntheses for phytopharmaceuticals **1-5** is given in Table S12 and detailed in Tables S13-S17. Table S18 reports the main assessment by CHEM21.[12] The detailed calculations are also available as separate excel files, as an integrant part of the SI.

BACK-TO-BACK COMPARISON BETWEEN SOLUTION AND LA-RAM (at scale) METHODS.

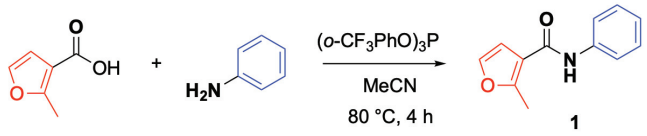
Table S12. Small-scale, TCFH-mediated mechanochemical amidation reaction to phytopharmaceuticals **1-5**, by ball-milling (VBM and PBM) in LAG conditions, and comparison with the 1,1'-oxalyl diimidazole (ODI)-mediated reaction in a PBM,[14] by LA-RAM, and with solution-based methods.

	Yields (%) by Ball-milling *vs* RAM *vs* Solution					
Compound	**VBM**[b]	**PBM**[c]	**TCFH method**[a]	**ODI method**[14] **VBM / PBM**	**TCFH method by RAM**[d]	**Solution method**
(**1**)	78	**84**	A1, A2, B	n.p.[e]	**86**	**91**[15]
(**2**)	**92**	51	A2, B	n.p.[e]	**98**	94[16, 17]

(**3**)	48	**71**	A1, B	90 / 93	**95**	78[5]
(**4**)	32	**78**	A1, B	50 / 64	**91**	90[6, 18]
(**5**)	73	**79**	A1, B	0 / 53	**90**	82[8, 19]

[a] All the reactions were conducted using AcOEt as LAG solvent (η = 0.2 μL/mg) and K_2HPO_4 (3.0 equiv.) as a base, except for Fluxapyroxad (**5**) involving neat grinding with NMI (3.0 equiv.) as a base; [b] The reaction scale was 0.48 mmol; [c] The reaction scale was 1.92 mmol; [d] All the reactions were conducted using AcOEt as LAG solvent (η = 0.2 μL/mg) and NMI (3.0 equiv.) as a base, except for Boscalid (**2**); [e] n.p. = not performed.

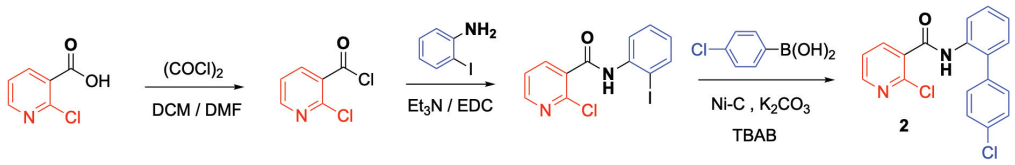
Table S13. Comparison between solution-based method[15] and TCFH-mediated amidation reaction by LA-RAM protocols for the synthesis of Fenfuram (**1**).



	Solution-based route[15]	**RAM route**
Number of steps	1	1
Reagents	$(o\text{-}CF_3PhO)_3P$	TCFH/NMI
Solvent	MeCN	/
Reaction time	4 h	2 h 15
Temperature	80°C	r.t.
Workup	Column chromatography (PE:AcOEt 15:1 v/v)	Precipitation in water
Yield	91% (96 mg)	96% (18 g)

Additional note for Table S13 : the original commercial patented route involves an amidation using thionyl chloride ($SOCl_2$).[1] However, this protocol was excluded from the DOZN™ assessment due to the absence of yield data, which made a quantitative comparison unfeasible. Instead, a more recent solution-phase amidation route reported in the literature[15] was selected as a benchmark, which is carried out in acetonitrile as the solvent using a new generation coupling agent.

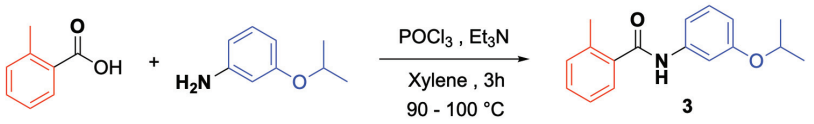
Table S14. Comparison between solution-based method[16, 17] and TCFH-mediated amidation reaction by LA-RAM protocols for the synthesis of Boscalid (**2**).



	Solution-based route[16, 17]	**RAM route**
Number of steps	3	1
Reagents	$(COCl)_2$ / Et_3N, EDC / Ni-C / K_2CO_3 / TBAB	TCFH / K_2HPO_4
Solvent	Dichloromethane / DMF	AcOEt (LAG)
Reaction time	6 h / 12 h	2 h 15
Temperature	0°C / 130°C	r.t.
Workup	Water and HCl washes / extraction with toluene / washing with MeOH	Precipitation in water
Yield	92% (130 g)	67% (21 g)

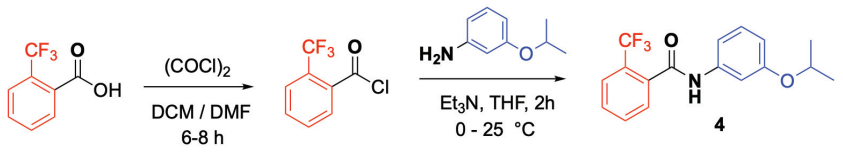
Additional note for Table S14 : The analysis of the comparison for the synthesis of Boscalid (**2**) is based on the commercial route,[17] to which the chlorination step[16] required to convert the acid into the corresponding acyl chloride (similarly to an activation step) was added. This additional step was included to ensure an equivalent starting point with the TCFH-mediated protocol by LA-RAM , where the activated acid is formed after step 1. The chlorination procedure selected for the solution-based route corresponds to the most efficient method reported in the literature, deliberately chosen over more traditional options involving $SOCl_2$,[20-22] which would have resulted in significantly worse environmental and safety scores.

Table S15. Comparison between solution-based method[5] and TCFH-mediated amidation reaction by LA-RAM protocols for the synthesis of Mepronil (**3**).



	Solution-based route[5]	**RAM route**
Number of steps	1	1
Reagents	$POCl_3$ / Et_3N	TCFH / NMI
Solvent	Xylene	/
Reaction time	3 h	2 h 15
Temperature	90°C – 100°C	r.t.
Workup	Precipitation in water	HCl / precipitation in water
Yield	77% (21 g)	91% (23 g)

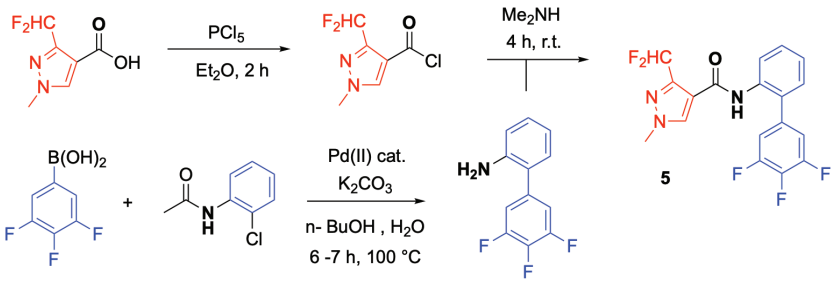
Table S16. Comparison between solution-based method[6, 18] and TCFH-mediated amidation reaction by LA-RAM protocols for the synthesis of Flutolanil (**4**).



	Solution-based route[6, 18]	**RAM route**
Number of steps	2	1
Reagents	$(COCl)_2$ / Et_3N	TCFH / NMI
Solvent	DMF / DCM / THF	/
Reaction time	8h + 2h	2 h 15
Temperature	0°C + 25°C	r.t.
Workup	Vacuum distillation / recrystallization	HCl / Precipitation in water
Yield	91% (2.9 g)	96% (29 g)

Additional note for Table S16 :To compare the protocol used for the synthesis of Flutolanil (**4**), the patented commercial route was taken as reference.[6] However, to ensure a fair comparison based on equivalent starting materials, namely the acid and the amine, which are the inputs in the LA-RAM methods, it was necessary to include the chlorination step[18] in the evaluation of the solution-based process, which starts from the corresponding acyl chloride in the patented route. The chlorination method selected was the most efficient available, with minimal energy and resource-intensive workup requirements, in order to ensure a balanced and conservative comparison.

Table S17. Comparison between solution-based method[8, 19] and TCFH-mediated amidation reaction by LA-RAM protocols for the synthesis of Fluxapyroxad (**5**).



	Solution-based route[8, 19]	**RAM route**
Number of steps	2	1
Reagents	K_2CO_3 / Pd(II) cat. / Me_2NH	TCFH / NMI
Solvent	*n*-BuOH	/
Reaction time	4h + 6h	2 h 15
Temperature	115°C – r.t	r.t.
Workup	Vacuum distillation / Water filtration / Acid and basic washes	HCl / precipitation in water
Yield	83% (85 g)	99% (*ca.* 35 g)

Additional note for Table S17: The comparison between the solution-based route and the mechanochemical RAM protocol for the synthesis of Fluxapyroxad (**5**) follows a similar approach to the one adopted for Boscalid (**2**) and Flutolanil (**4**). The commercial[19] patented route was used as reference, and a chlorination step,[8] starting from the corresponding carboxylic acid, was added to align both synthetic strategies in terms of initial molecular building blocks (Table S17). This adjustment was made to ensure a balanced comparison between the two processes.

ASSESSMENT BY DOZN™ 3.0

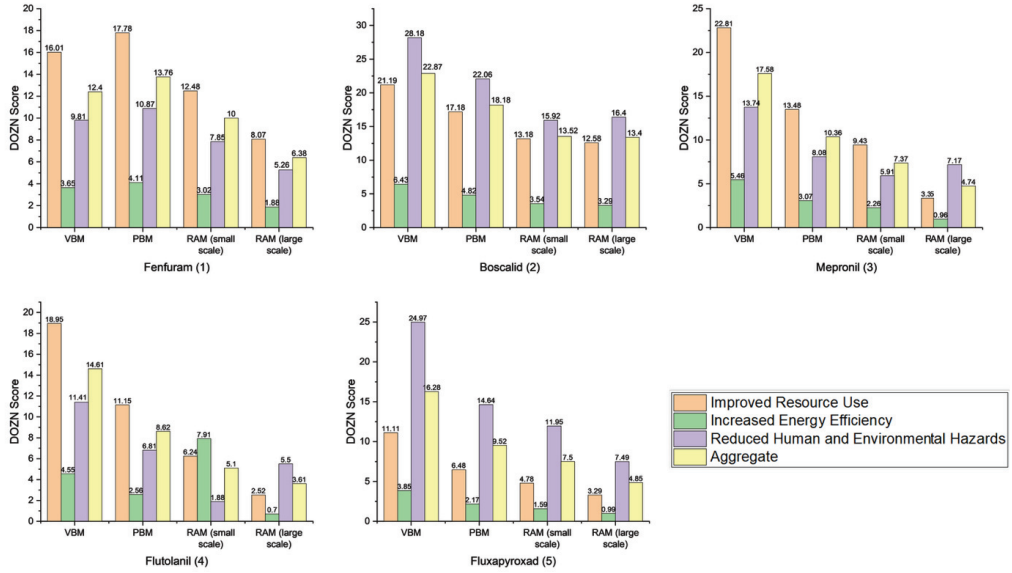


Figure S13. Comparison of VBM *vs* PBM *vs* RAM (0.58 mmol scale, referred as "small scale") *vs* RAM (93.01 mmol scale, referred as "large scale") protocols for the synthesis of Fenfuram (**1**), Boscalid (**2**), Mepronil (**3**), Flutolanil (**4**), Fluxapyroxad (**5**) by DOZN™ 3.0 Quantitative Scoring tool. *Legend*: Aggregate score (**orange**), *Group 1* (Improved Resource Use – **green**), *Group 2* (Increased Energy Efficiency – **violet**), and *Group 3* (Reduced Human and Environmental Hazards – **yellow**).

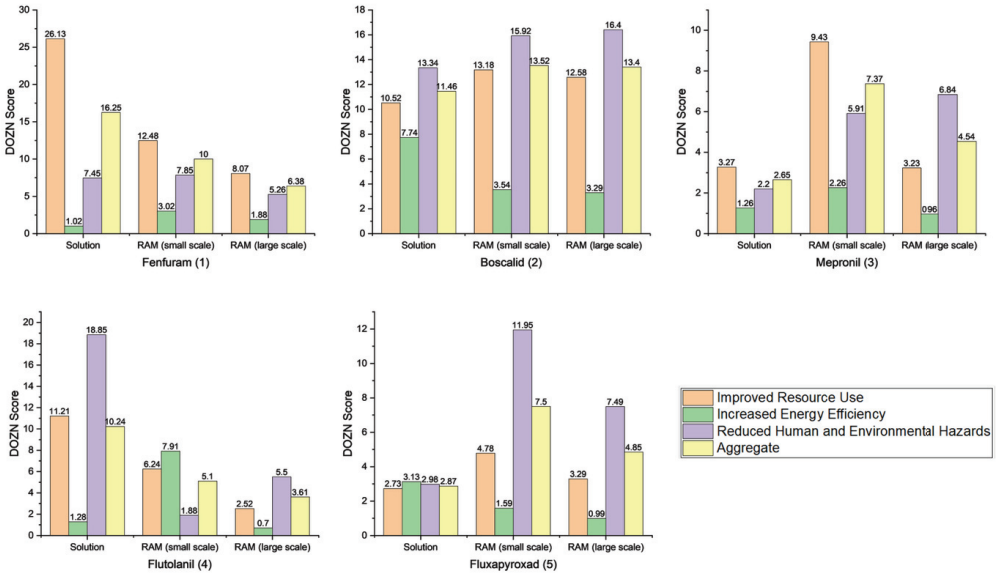


Figure S14. Comparison of solution *vs* RAM (0.58 mmol scale, referred as "small scale") *vs* RAM (93.01 mmol scale, referred as "large scale") methods for the synthesis of Fenfuram (**1**), Boscalid (**2**), Mepronil (**3**), Flutolanil (**4**), Fluxapyroxad (**5**) by DOZN™ 3.0 Quantitative Scoring tool. *Legend*: Aggregate score (**orange**), *Group 1* (Improved Resource Use – **green**), *Group 2* (Increased Energy Efficiency – **violet**), and *Group 3* (Reduced Human and Environmental Hazards – **yellow**).

Table S18 (part I). Comparison of CHEM21[12] assessment for solution-based *vs vs* LA-RAM using TCFH as a coupling agents for the synthesis of compounds (**1**), (**2**) and (**3**) (for the full assessment, *c.f.*, ESI). Legend: Green flag: Preferred; Amber flag: Acceptable with some concerns; Red Flag: Undesirable. [a] Best value for AE, RME and OE is 100%, for PMI is 1 and *E*-Factor = PMI – 1.[23] When comparing two processes, the one with the lowest PMI will be greenest; [b] $OE = {}^{RME}/_{AE} \times 100$;[12] [c] Where precise work-up chemical quantities were unavailable, estimates were derived as detailed in the ESI to ensure fair comparison.

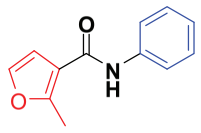
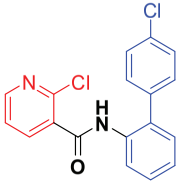
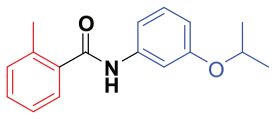
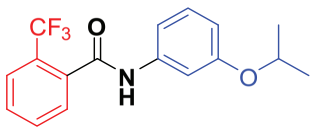
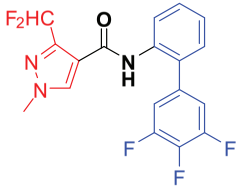
	RAM *vs* Solution method								
METRICS[a]	 (**1**)			 (**2**)			 (**3**)		
AE	40.3	*vs*	27.4	53.5	*vs*	64.4	47.4	*vs*	80.8
RME	29.6	*vs*	26.2	28.6	*vs*	58.7	34.0	*vs*	61.8
OE[b]	73.6	*vs*	95.4	53.5	*vs*	91.2	71.6	*vs*	76.5
PMI[c]	60.5	*vs*	65.7	101.2	*vs*	119.9	29.3	*vs*	13.4
PMI$_{reaction}$	5.0	*vs*	7.9	7.5	*vs*	110.1	4.2	*vs*	6.3
PMI$_{workup}$	55.6	*vs*	57.8	93.7	*vs*	9.8	25.1	*vs*	7.2
***E*-factor**	59.5	*vs*	64.7	100.2	*vs*	118.9	28.3	*vs*	12.4
Solvent	**Water**		**ACN, AcOEt, PE**	**AcOEt, water**		**DCE, DCM, DMF, toluene, MeOH**	**Water**		**Xylene, water**
Work-up, recovery	**Water filtration**		**Column chromatography**	**Water filtration**		**Reduced pressure distillation, extraction, MeOH filtration**	**Water filtration**		**Water washing, reduced pressure evaporation**
Health & safety									
Main hazard statements	H301, H311, H317, H318, H331, H341, H351, H372, H373, H400, H410, H302, H315, H318, H360D H302, H311, H314, H318, H361d		H301, H311, H317, H318, H331, H341, H351, H372, H373, H400, H410, H224, H304, H315, H336, H411	H302, H315, H318, H360D		H225, H302, H304, H315, H319, H331, H335, H350, H226, H312, H319, H332, H360D, H225, H301, H311, H331, H370, H371, H228, H317, H351, H372, H331, H220, H360d, H372, H302, H315, H319, H361fd, H412, H225, H302, H311, H314, H318, H331, H335, H225, H304, H315, H336, H361d, H373, H412, H315, H319, H336, H351, H301, H331	H302, H315, H318, H360D, H302, H311, H314, H318, H361d		H302, H314, H318, H330, H372, H225, H302, H311, H314, H318, H331, H335, H225, H226, H304, H312, H315, H319, H332, H335, H373, H412

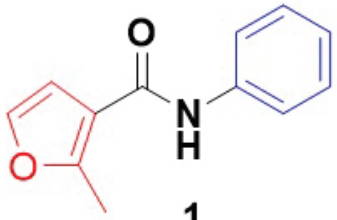
Table S18 (part II). Comparison of CHEM21[12] assessment for solution-based *vs* LA-RAM using TCFH as a coupling agents for the synthesis of compounds (**4**) and (**5**) (for the full assessment, *c.f.*, ESI). Legend: Green flag: Preferred; Amber flag: Acceptable with some concerns; Red Flag: Undesirable. [a] Best value for AE, RME and OE is 100%, for PMI is 1 and *E*-Factor = PMI – 1.[23] When comparing two processes, the one with the lowest PMI will be greenest; [b] $OE = {}^{RME}/_{AE} \times 100$;[12] [c] Where precise work-up chemical quantities were unavailable, estimates were derived as detailed in the ESI to ensure fair comparison.

	RAM *vs* Solution method					
						
METRICS[a]	(**4**)			(**5**)		
AE	52.0	*vs*	69.0	56.1	*vs*	73.1
RME	38.9	*vs*	60.9	44.2	*vs*	58.9
OE[b]	74.9	*vs*	88.1	78.7	*vs*	80.6
PMI[c]	24.5	*vs*	50.4	60.5	*vs*	16.3
PMI$_{reaction}$	3.6	*vs*	49.7	3.1	*vs*	8.9
PMI$_{workup}$	20.9	*vs*	0.7	57.4	*vs*	7.4
***E*-factor**	23.5	*vs*	49.4	59.5	*vs*	15.3
Solvent	**Water**		**DCM, THF, *n*-hexane**	**Water**		**Et_2O, *n*-BuOH, water**
Work-up, recovery	**Water filtration**		**Distillation under reduced pressure, recrystallization**	**Water filtration**		**Water washing, water filtration**
Health & safety						
Main hazard statements	H302, H315, H318, H360D, H302, H311, H314, H318, H361d		H331, H220, H360d, H372, H301, H331, H351	H302, H315, H318, H360D, H410, H302, H311, H314, H318, H361d		H302, H319, H411, H224, H302, H336, H220, H280, H315, H318, H319, H332, H335, H412

REFERENCES

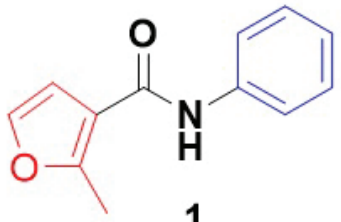
1. H. P. Ten, *DE1914954A1*, 1969.
2. T. Ben Halima, J. Masson-Makdissi and S. G. Newman, *Angew. Chem. Int. Ed.*, 2018, **57**, 12925-12929.
3. N. Oger, E. Le Grognec and F.-X. Felpin, *ChemCatChem*, 2015, **7**, 2085-2094.
4. M. K. Sahoo, S. P. Midya, V. G. Landge and E. Balaraman, *Green Chem.*, 2017, **19**, 2111–2117.
5. I. Chiyomaru, S. Kawada and K. Takita, *US3937840A*, 1976.
6. K. Yabutani, K. Ikeda, S. Hatta and T. Harada, *US4093743A*, 1977.
7. U. Troppmann, W. Mayer, S. Koltzenburg, R. Israels, A. Bauder, U. Schlotterbeck*, US8735321B2,* 2009.
8. Y. Zhang, Z. Chen, J. Nie, F.-G. Zhang and J.-A. Ma, *J. Org. Chem.*, 2019, **84**, 7148-7158.
9. N. Maarouf-Mesli, J. Desjardins-Michaud, Z. Imani, K. Ghosh, F. Polyak and W. D. Lubell, *Green Chem.*, 2026, **28**, 264-276.
10. P. Orecchia, D. S. Petkova, R. Goetz, F. Rominger, A. S. K. Hashmi and T. Schaub, *Green Chem.*, 2021, **23**, 8169-8180.
11. H. Kim, H. Yang, K. J. Sang, S.-H. Moon and T. H. Kim, *Acta Cryst. E*, 2010, **66**, o2471.
12. C. R. McElroy, A. Constantinou, L. C. Jones, L. Summerton and J. H. Clark, *Green Chem.*, 2015, **17**, 3111-3121.
13. K. J. Ardila-Fierro and J. G. Hernández, *ChemSusChem*, 2021, **14**, 2145-2162.
14. A. Casagrande, R. Solorzano-Rodriguez, M. Carta, F. Delogu, J. Vezzani, A. Niidu and E. Colacino, *Chem. Eur. J.*, 2026, **n/a**, e71190.
15. L. Zhang, N. Ma, M. Wang, W. Gou, J. Tian, Q. Xu, C. Zhao and C. Li, *Org. Chem. Front.*, 2024, **11**, 1796-1803.
16. P. Garrido-García, I. Quirós, P. Milán-Rois, S. Ortega-Gutiérrez, M. Martín-Fontecha, L. A. Campos, Á. Somoza, I. Fernández, T. Rigotti and M. Tortosa, *Nat. Chem.*, 2025, **17**, 734-745.
17. J. Sun, X. Feng, H. Chen and L. Sun, *CN 105085389 A*, 2015.
18. A. Nandikolla, Y. M. Khetmalis, G. P. V. Sangeetha, A. Chandu, Swati, M. M. K. Kumar, V. Sharma, S. Murugesan and K. V. G. Chandra Sekhar, *New J. Chem.*, 2023, **47**, 15378-15389.
19. B. Ke, Y. Wang, H. Pan, X. Cheng, H. Chen, W. He, L. He, X. Yang, Y. Xu, W. Dong and S. Tang, *WO2025074339A1*, 2025.
20. S. F. Hunt, S. T. Onions, V. Sherbukhin, E. A. F. Fordyce, J. C. Thomas, P. J. Murray, M. S. Coates, D. W. Brookes, K. Ito and P. Strong, *WO 2017/175000 A1*, 2017.
21. J. Sun and H. Duan, *CN118772051A*, 2024.
22. Y. Tian, J. Wang, B. Yang, H. Yao, S. Liu, S. Deng, et al., *CN119285539A*, 2025.
23. J. Kielhorn, C. Melber, D. Keller and I. Mangelsdorf, *Int. J. Hyg. Environ. Health*, 2002, **205**, 417-432.

^{1}H NMR in DMSO-d_6



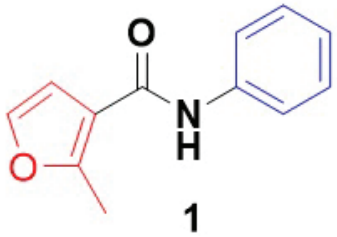
1

$^{13}C\{^{1}H\}$ NMR in DMSO-d_6



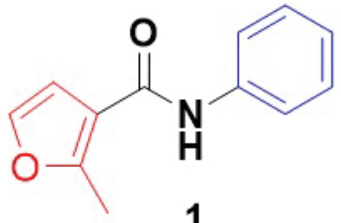
1

^{1}H NMR in $CDCl_3$



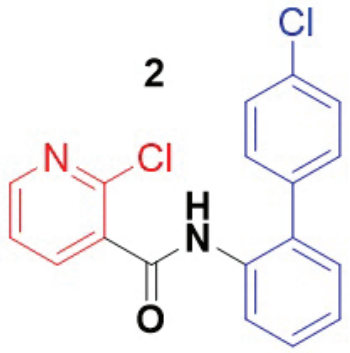
1

$^{13}C\{^{1}H\}$ NMR in $CDCl_3$

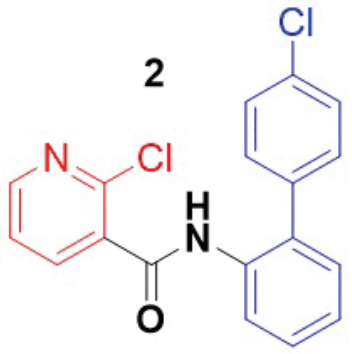


1

^{1}H NMR in DMSO-d_6



$^{13}C\{^{1}H\}$ NMR in DMSO-d_6



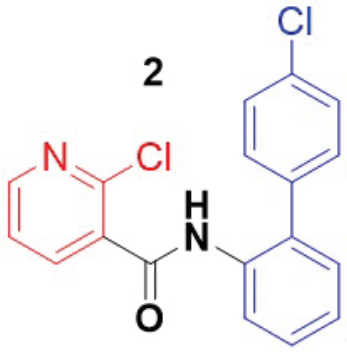
164.19
150.33
146.47
137.82
137.69
136.39
133.96
132.96
132.17
130.72
130.27
128.30
127.46
126.98
123.02
40.15
39.94
39.73
39.52
39.31
39.10
38.89

16524.80
15129.72
14741.58
13870.47
13858.33
13726.87
13482.25
13381.74
13302.16
13156.44
13111.40
12913.29
12828.49
12779.69
12381.73

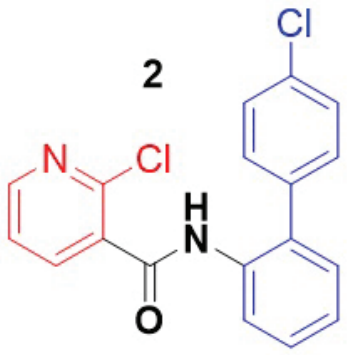
f1 (ppm)

S59

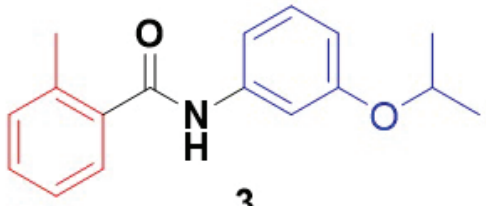
^{1}H NMR in $CDCl_3$



$^{13}C\{^{1}H\}$ NMR in $CDCl_3$

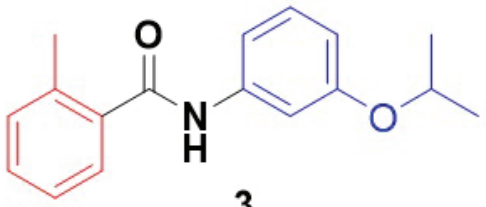


^{1}H NMR in DMSO-d_6



3

$^{13}C\{^{1}H\}$ NMR in DMSO-d_6



3

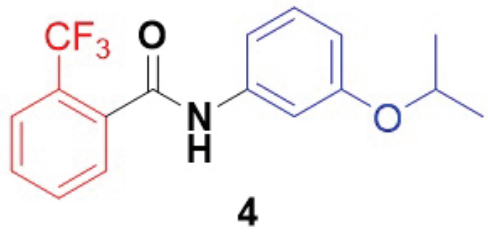
167.87 157.68 140.48 137.30 135.16 130.51 129.61 129.46 127.16 125.64 111.71 110.57 107.10 69.14 40.15 39.94 39.73 39.52 39.31 39.10 38.89 21.86 19.28

14137.62 13817.66 13601.48 13133.63 13042.93 13027.95 12796.94 12644.01 11242.16 11127.34 10778.17

f1 (ppm)

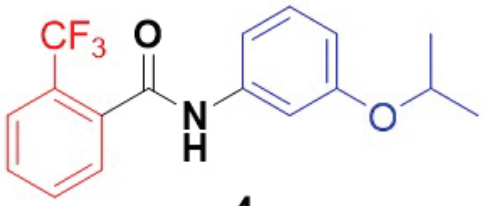
f1 (ppm)

^{1}H NMR in DMSO-d_6



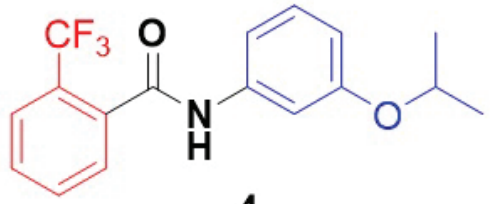
4

$^{13}C\{^{1}H\}$ NMR in DMSO-d_6

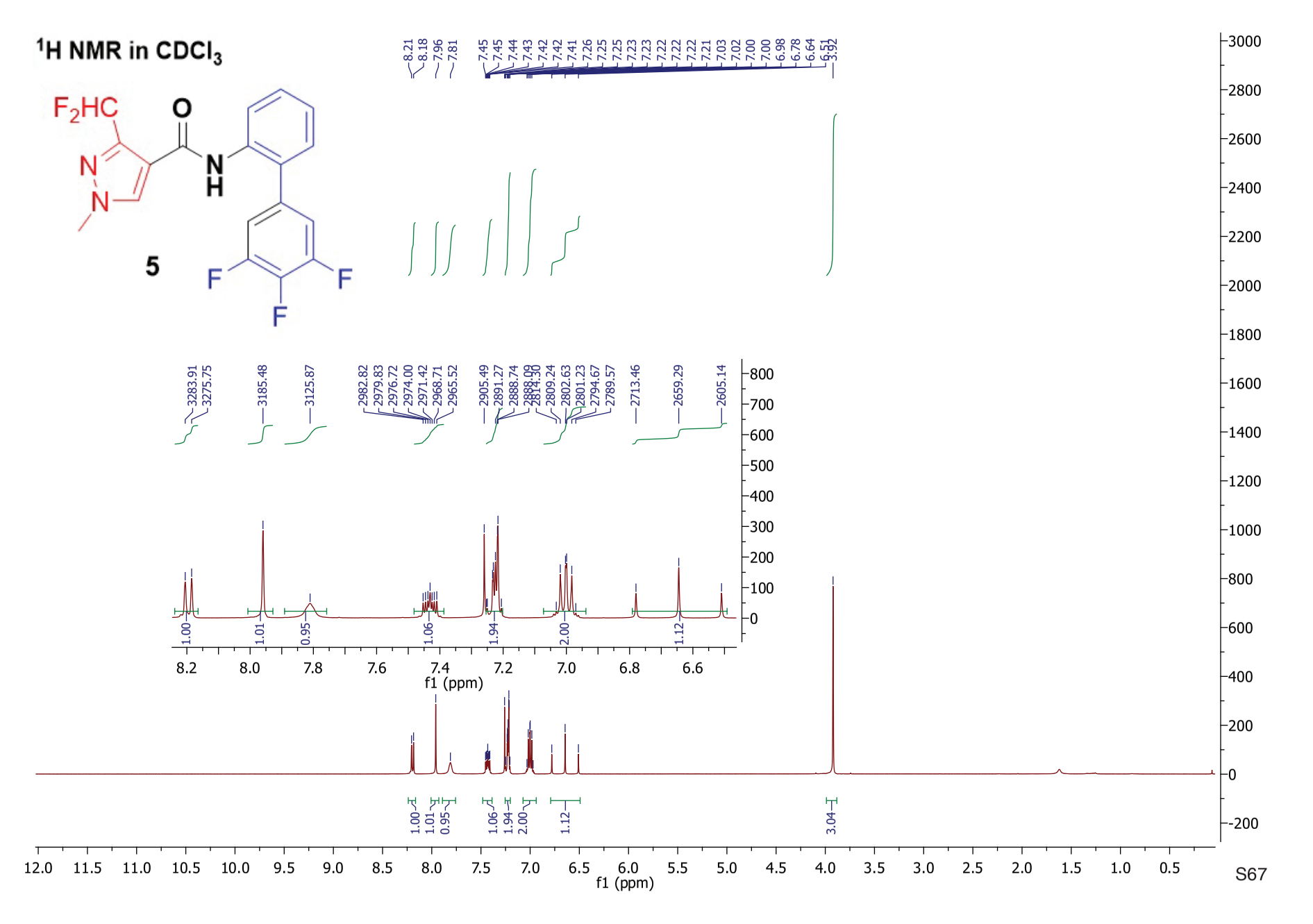


4

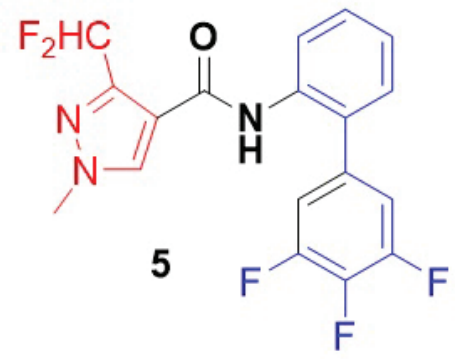
$^{19}F\{^{1}H\}$ NMR in DMSO-d_6



4

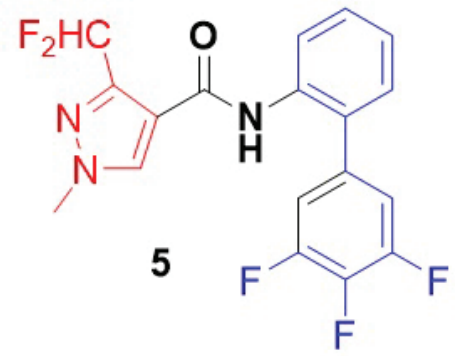

1H NMR in CDCl3
F2HC
O
N
N
N
H
F
F
F
5
8.21
8.18
7.96
7.81
7.45
7.45
7.44
7.43
7.42
7.42
7.41
7.26
7.25
7.25
7.23
7.23
7.22
7.22
7.22
7.21
7.03
7.02
7.00
7.00
6.98
6.78
6.64
6.51
3.92
3283.91
3275.75
3185.48
3125.87
2982.82
2979.83
2976.72
2974.00
2971.42
2968.71
2965.52
2905.49
2891.27
2888.74
2814.30
2809.24
2802.63
2801.23
2794.67
2789.57
2713.46
2659.29
2605.14
1.00
1.01
0.95
1.06
1.94
2.00
1.12
3.04
f1 (ppm)
f1 (ppm)
S67

$^{13}C\{^{1}H\}$ NMR in $CDCl_3$



5

$^{19}F\{^{1}H\}$ NMR in $CDCl_3$



5

Appendix 6

Publication VI
L. Čolakić,[‡] A. Casagrande,[‡] G. Miletić, E. Meštrović, E. Colacino, I. Halasz. Breathing New Life into Old Processes: Continuous Mechanochemistry Enables Green Manufacturing of Essential Pharmaceuticals. **2026**, *submitted to a peer-reviewed journal*.

[‡]Equal contribution.

Breathing new life into old processes: continuous mechanochemistry enables green manufacturing of essential pharmaceuticals silver(I) sulfadiazine and phenytoin.

Lea Čolakić,[1,‡] Andrea Casagrande,[2,3,‡] Goran Miletić,[1] Ernest Meštrović,[4,*] Evelina Colacino,[2,*] Ivan Halasz[1,*]

[1] Ruđer Bošković Institute, Zagreb, Croatia

[2] ICGM, Univ Montpellier, CNRS, ENSCM, 34293 Montpellier, France

[3] Virumaa College, Tallinn's University of Technology, Whitajate tee 5, 19086, Estonia.

[4] Faculty of Chemical Engineering and Technology, University of Zagreb, Zagreb, Croatia

Corresponding authors: ivan.halasz@irb.hr; evelina.colacino@umontpellier.fr; ernest.mestrovic@fkit.unizg.hr.

‡ Equal contribution

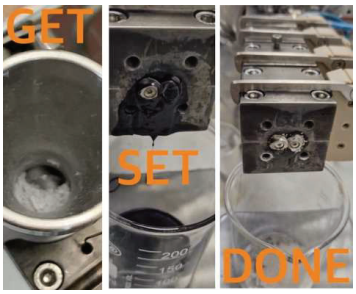
Keywords: Mechanochemistry - Twin Screw Extrusion – Active Pharmaceutical Ingredients - Silver sulfadiazine – Phenytoin – Polymorph.

Abstract

The pharmaceutical industry requires scalable manufacturing strategies that reduce solvent consumption, waste generation, and energy demand while preserving the quality attributes of active pharmaceutical ingredients (APIs). Here, we report the use of continuous mechanochemistry by twin-screw extrusion (TSE) for the preparation of two World Health Organization essential medicines: silver(I) sulfadiazine (SSD), a topical antiseptic, and phenytoin (PHE), an antiepileptic drug. The developed protocols translate mechanochemical synthesis from batch ball-milling to continuous processing and enable scale-up from milligram to decagram quantities using equipment compatible with industrial implementation. Both APIs were obtained as highly phase-pure crystalline materials, with powder X-ray diffraction and infrared spectroscopy confirming the formation of the polymorphic forms corresponding to the approved drug products. Sustainability performance was assessed using Process Mass Intensity (PMI) and *E*-factor metrics and benchmarked against conventional solution-based routes and

previously reported mechanochemical methods. For SSD, the use of Ag_2O in place of $AgNO_3$ affords quantitative conversion with water as the sole by-product, eliminating the need for solvent-intensive precipitation and purification steps. Across both processes, solvent elimination accounts up to 95% of the mass savings relative to the corresponding solution routes. The TSE routes reduce material inputs relative to the corresponding solution-based protocols, although the aqueous purification required for phenytoin contributes substantially to its total process PMI. These results demonstrate that TSE can simplify unit operations, intensify API manufacturing, and extend the sustainability advantages of mechanochemistry beyond laboratory-scale batch processing. Continuous mechanochemical route redesign therefore provides a practical strategy for reducing the environmental footprint of established pharmaceutical processes while maintaining product quality and supporting future industrial implementation.

Graphical Abstract



Twin-screw extrusion is used to continuously manufacture two WHO essential medicines — silver(I) sulfadiazine and phenytoin — at decagram scale, eliminating solvents, simplifying unit operations, and cutting process mass intensity by over 95% relative to conventional solution routes.

Introduction

The pharmaceutical industry faces mounting pressure to cut greenhouse-gas emissions while safeguarding product quality and supply. A large share of the footprint for small-molecule Active Pharmaceutical Ingredients (APIs) stems from solvent manufacture,[1] its extensive use and disposal, driving roughly three-quarters of the overall energy demand, alongside energy-intensive synthesis, drying, and HVAC (heating, ventilation and air conditioning),[2] contributing as much as half of the associated global warming potential.[3] Accordingly, sustainable process design towards green pharmaceuticals[2,4,5] now targets waste elimination, use resources more

efficiently, and improve safety, aligning with the United Nations' 17 Sustainable Development Goals (UN SDGs).[6]

In this context, mechanochemistry is now recognized as a promising and transformative approach that can help advance several of these objectives,[7] providing a solvent-free or solvent-lean alternative, improving green chemistry and sustainability metrics,[8,9] can be characterized by lower energy use,[10,11] and minimized waste,[12] that lowers Process Mass Intensity (PMI) and *E*-factor[13] while preserving critical quality attributes.[14] When these processes are thoughtfully developed and evaluated, they can meet the criteria of Safe and Sustainable by Design (SSbD), and tackle critical societal and environmental challenges,[15] in line with the 'IUPAC Guiding Principles of Responsible Chemistry'.[16]

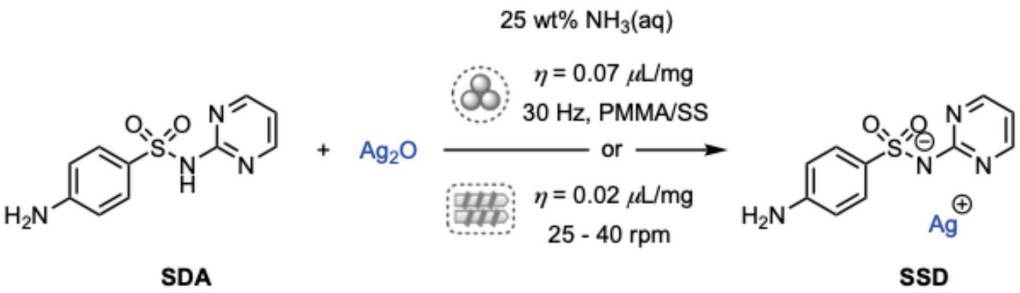
In this context, ball-milling (BM) techniques have been extensively used for the mechanochemical preparation of APIs,[17–21] or their late-stage functionalization,[22] at small, laboratory-scale. In 2019, IUPAC highlighted mechanochemistry, and in particular twin screw extrusion (TSE) as a key technology for sustainable chemical synthesis.[23] Nonetheless, the translation of these batch approaches into continuous methodologies for upscaling have remained limited, with the early contribution published in 2020[24,25] for the mechanochemical preparation of nitrofurantoin,[24,26] a generic antibacterial agent listed as essential medicine by the World Health Organisation (WHO).[26,27] After two-minute residence time, a space-time yield (STY) of 6800 kg m^3 day^{-1} was obtained, with a 8 times lower global warming potential (expressed in kg of CO_2 equivalents) and estimated reduction costs of 12%, than the solution Kg-scale synthesis in batch.[10]

Then, continuous flow mechanochemistry by TSE[28–30] was used to prepare generic APIs such as paracetamol,[31] moclobemide,[32,33] teriflunomide[33] adapting the corresponding batch syntheses by ball-milling (by Beckmann rearrangement for paracetamol,[34,35] amidation reaction for moclobemide,[36] and for teriflunomide).[37] Miltefosine (by salification reaction)[38] and Benodanil[32] were prepared by TSE adapting solvent-based processes, no small-scale methods in batch by mechanochemistry being reported, while a bead-mill (Dyno-mill®) was also used as alternative to TSE for the multi-gram scale of paracetamol,[39] benchmarking the previously reported method by ball-milling.[34,35] Very recently, machine learning approaches based on Bayesian optimisation applied to continuous flow mechanochemistry by TSE,[40] were also implemented for the preparation of moclobemide.[41]

We report herein the implementation of TSE for breathing a new life to old processes to access the metallo-drug silver(I) sulfadiazine (**SSD**), a topical antiseptic, and phenytoin (**PHE**, diphenylhydantoin), an antiepileptic drug, both listed as essential medicines by WHO,[27] simplifying the unit operations and improving the sustainability profile for their manufacturing at scale. Both API were obtained in highly phase-pure crystalline forms. Green metrics such as PMI and *E*-factor were calculated by CHEM21 tool,[42] and the results were assessed, also for their productivity, benchmarking the corresponding methods in solution, by the previously reported mechanochemical processes for these specific targets.

Results and discussion

Mechanochemical synthesis in batch and in continuous of silver (I) sulfadizine (SSD). Conventional **SSD** production uses aqueous precipitation after mixing the solutions of silver nitrate and sulfadiazine (SDA, often partially deprotonated with aqueous ammonia), followed by filtration, drying, milling, and sometimes recrystallization.[43] The process is high-yielding but it is nevertheless solvent-intensive and generates nitrate-bearing effluents. Some of these drawbacks could be previously mitigated by adapting the solvent-based method in a BM, using a catalytic amount of aqueous ammonia.[44,45] The mechanochemical synthesis was validated in different processing conditions,[44] however, *in situ* monitoring studies by Raman spectroscopy showed that the reaction was highly sensitive to the amount of ammonia used.[45] Therefore, aiming to implement by TSE the **SSD** synthesis, and to avoid nitrate effluents, the preparation of **SSD** was initially explored in the BM, specifically substituting silver nitrate by silver (I) oxide, rendering **SSD** formation an acid–base neutralization reaction in which the basic oxide accepts the sulfonamide proton and delivers silver (I) to the deprotonated ligand, producing only water as a stoichiometric by-product that is removable by drying in air or in a vacuum oven (Scheme 1).



Scheme 1. BM and TSE synthesis of silver (I) sulfadiazine (**SSD**) from sulfadiazine (**SDA**) and Ag_2O.

While both $AgNO_3$ and Ag_2O are unreactive under neat conditions by ball-milling,[45] thus requiring the use aqueous ammonia towards the formation of SSD, the use of Ag_2O eliminates nitrate from the bill of materials and salt-laden mother liquors, cutting wastewater treatment burden, lowering PMI and increasing the atom economy (AE) of the reaction. Indeed, material efficiency improved because silver oxide is more silver-dense than silver nitrate and each mole provides two equivalents of silver, as quantified by a better atom economy (AE) for the BM synthesis involving Ag_2O (97.5% *vs* 85%, respectively, *c.f.*, ESI). Moreover, this solid-state route does not stipulate dissolution to enable the reaction allowing for the use of reagents, such as Ag_2O that are not suitable to be used in solution synthesis due to their insolubility.

The BM reaction was conducted in a polymethylmethacrylate (PMMA) 14 mL jar, at 30 Hz during 5 min, using 2 stainless steel (SS) balls of 7 mm diameter. Pure **SSD** was obtained on the 500 mg scale within minutes, as further confirmed by the *in situ* monitoring of the mechanochemical reaction, also displaying complete consumption of Ag_2O and SDA. **SSD** was recovered from the jar by scratching out the product (avoiding any extractive washes or ion-removal steps). Compared to $AgNO_3$-based synthesis, controlling residual nitrate in the product in the current oxide-based process thus becomes obsolete.

Dry mixing of powders of black silver(I) oxide and white SDA provided a grey physical mixture of components, but without **SSD** formation. Prolonged milling of half an hour did not produce **SSD**, but only partial amorphisation of the mixture, as evident from real-time process monitoring using synchrotron X-ray diffraction in situ (Figure 1A). In fact, the physical mixture of Ag_2O and SDA seems to be stable indefinitely. The target **SSD** essentially resulted from a neutralization reaction between SDA and Ag_2O, but proton transfer between SDA and Ag_2O required a catalyst also in this case. One such catalyst is aqueous ammonia, which in trace amounts facilitated rapid conversion of the grey reactant mixture into an off-white powder **SSD** product (Figure 1B). The catalytic action of ammonia may also partially involve stabilisation of silver ions by the formation of $[Ag(NH_3)_2]^+$ complex, as previously observed for the reaction using $AgNO_3$ as the silver source.[45]

Interestingly, the formation of a hitherto unknown intermediate crystalline phase preceded the **SSD** formation, as evidenced by *in situ* PXRD monitoring of the reaction by BM. Formation of the intermediate was independent of the source of silver ions, as it was also

observed in experiments with Ag_2SO_4 and $AgNO_3$ as the silver precursors, indicating that it contains silver ions, but not the counterion or water.

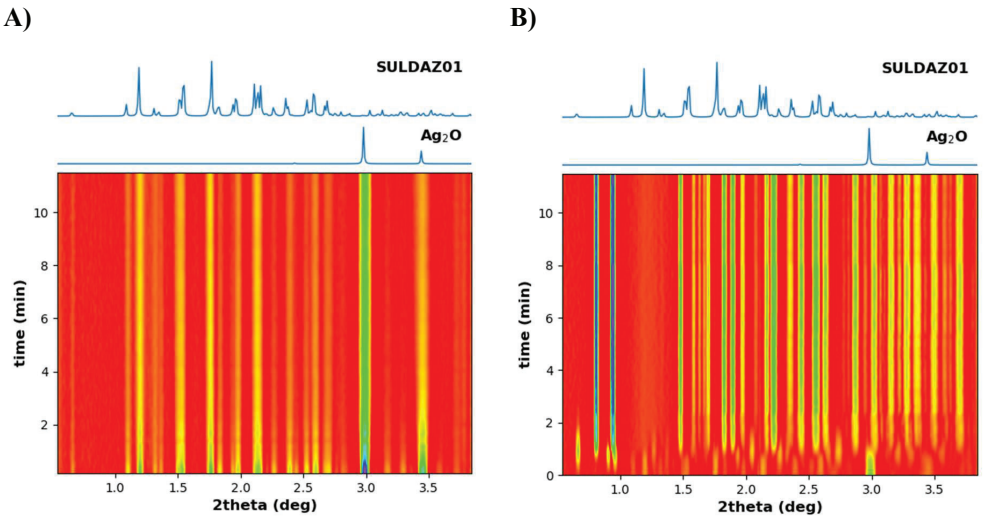


Figure 1. *In situ* PXRD monitoring of **SSD** formation by BM. (a) Neat grinding with no chemical reaction. (b) Grinding using traces of 25 wt% aqueous ammonia (η = 0.07 μL/mg) to provide the target **SSD** via a hitherto unknown intermediate that persisted only in the first two minutes of milling.

The intermediate phase proved too unstable to be isolated or prepared ad hoc for ex situ characterisation, while the poor quality of the in situ diffraction data precluded its structure solution. Therefore, an in situ preparation on a laboratory diffractometer was attempted by mixing Ag_2O and SDA in the 1:2 ratio, placing the resulting mixture on a silicon PXRD holder, moistening it with a small amount of distilled water, and exposing it to gaseous ammonia generated from an aqueous ammonia solution placed at the edge of the holder. The setup was additionally covered with Kapton foil to keep the moist powder in ammonia atmospehere, and PXRD data were collected immediately using a rapid acquisition program. Following several attempts, we have obtained a diffraction pattern dominated by the intermediate phase. The structure was solved by simulated annealing in direct space, using a rigid-body model for sulfadiazine and a free silver ion, and further optimised by solid-state DFT. The optimised model confirmed the symmetry and overall geometry of the experimentally derived structure, providing a structural description of this transient, metastable intermediate (for further information please refer to the SI).

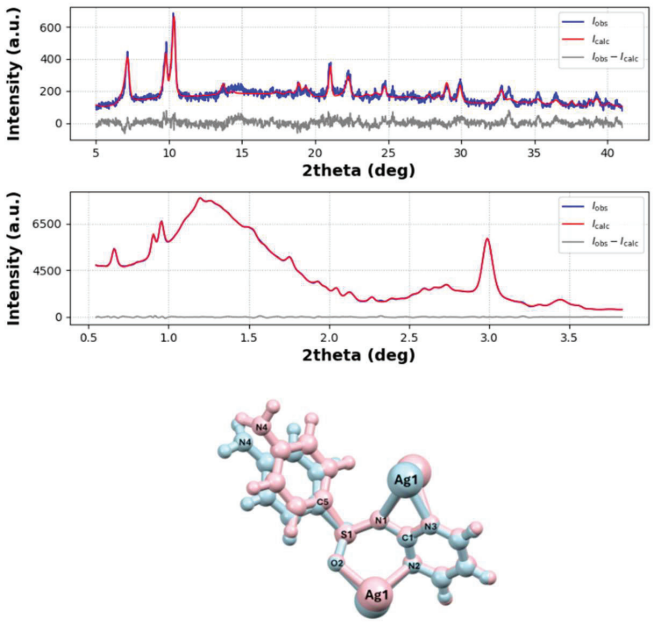


Figure 2. Rietveld refinement of the SSD intermediate structure. (top) Laboratory data, λ = 1.54 Å. (middle) *In-situ* collected synchrotron diffraction pattern during the reaction, λ = 0.14202 Å. The peak at $2\theta \approx 3.0°$ belongs to Ag_2O; (bottom) DFT optimisation of the structure model: (pink) Rietveld-refined and (bluish) after DFT optimization.

In the intermediate, the molecules form one-dimensional chains along the crystallographic *b* axis, bridged by silver ions. Adjacent chains are interconnected along the *c* axis via Ag···Ag contacts, which further link to neighbouring molecules through the sulfadiazine moiety via hydrogen bonds involving the aniline group and the oxygen atom of the sulfonyl group, finally forming a three-dimensional network (Figure 3).

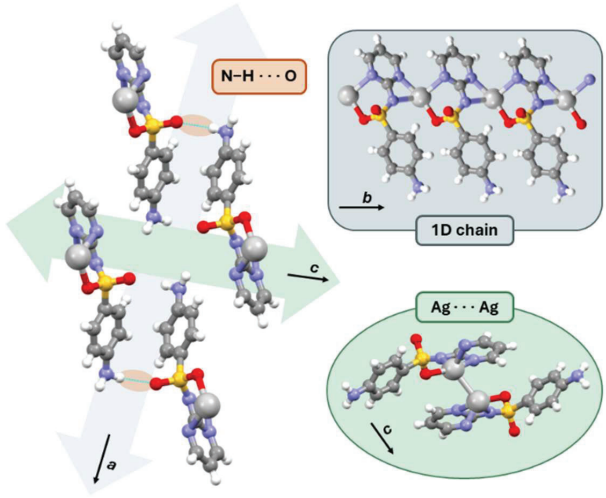


Figure 3. Crystal packing of **SSD** intermediate.

The main structural difference between the product and the intermediate lies in the torsion angle of the aniline ring of the sulfadiazine ligand, as well as in the coordination environment of the silver cation. In the intermediate, one silver ion is coordinated by two sulfadiazine molecules. From the first molecule, it binds to the sulfonamide nitrogen (N1) and one diazine nitrogen (N3), while the coordination sphere is completed by the neighbouring molecule through its diazine nitrogen (N2) and an oxygen atom (O2). In the product, the coordination environment is completed through three different sulfadiazine molecules: the sulfonamide (N1) originates from one molecule, a diazine nitrogen (N3) from a second, and the diazine nitrogen (N2) together with an oxygen atom (O2) from a third neighboring molecule. Also, both structures feature Ag···Ag contacts, measuring 2.76 Å in the intermediate and 2.92 Å in the product. This coordination arrangement promotes a more compact crystal packing, resulting in a product that is denser and more stable than the intermediate.

Having disclosed the reaction pathway to **SSD** by BM, its implementation in continuous by TSE operating at room temperature was straightforward. Being aware of the facile manner in which **SSD** forms upon contacting SDA and Ag_2O in the presence of ammonia, TSE processing with the addition of a few drops of aqueous ammonia under virtually any processing conditions provide **SSD**, avoiding at the same time milling-media abrasion possibly induced by high-energy ball-milling, and being directly compatible with pharmaceutical solids-handling infrastructure.

Therefore, a mixture of black silver(I) oxide (3.83 g, 16.5 mmol) and white sulfadiazine (SDA, 8.27 g, 33.0 mmol) in the 1:2 molar ratio (total initial mass of reactants: 12.1 g) was manually pre-mixed in a glass beaker using a spatula, resulting in a grey powder which was dispensed in portions into the extruder, via the feeder opening, at an initial screw speed of 25 rpm (Scheme 1). A catalytic amount of aqueous ammonia (25% wt%, 300 µL, η = 0.02 µL/mg) was occasionally added in the extruder barrel through the opening port for liquid addition positioned close to the feeder opening.

The basic screw profile consisting of conveying segments and kneading segments, having angles of 90° and 60°, required no further optimization (Figure S1, *c.f.*, SI). The extrudate was, as expected, off-white, slightly moist powder of pure and crystalline **SSD**, as confirmed by PXRD (Figure 4). This process yielded quantitatively and phase-pure **SSD** at the rate of at least 10 g/h and, given the readiness of **SSD** formation by TSE, it could be scaled further. Chemical purity was further established by elemental analysis (c.f., SI). TSE synthesis of SSD is demonstrated in the Supporting Video V1 (c.f., SI). SSD forms virtually immediately upon contact of the reactant solid mixture with ammonia solution while kneading by the extruder ensures proper contact between the reactant particles.

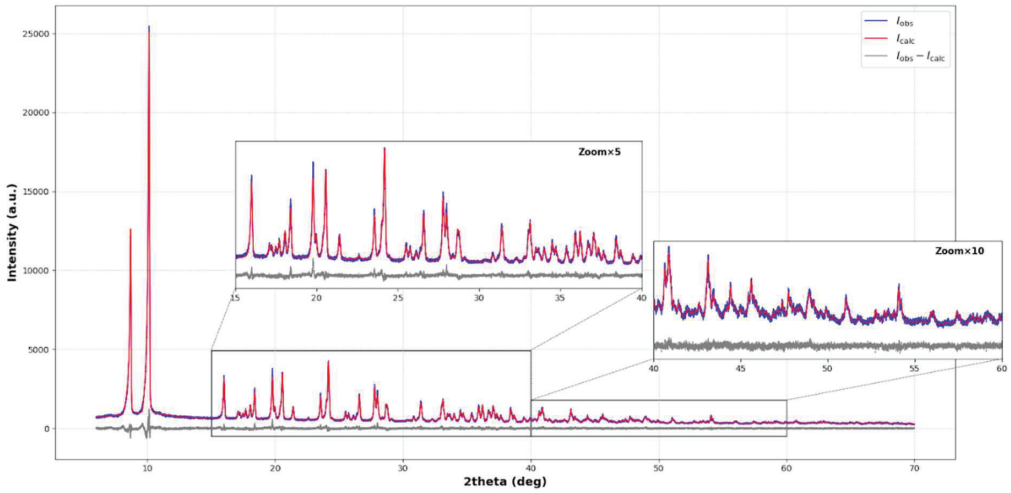


Figure 4. Rietveld analysis of **SSD** obtained by TSE from a 1:2 mixture of Ag_2O, SDA, and a catalytic amount of aqueous ammonia, corresponding to pure **SSD**. Experimental data are shown in blue, calculated data in red, and the difference curve in gray. Calculated data based on the crystal structure from the CSD (refcode: SULPMS).

Mechanochemical synthesis in continuous of Phenytoin (PHE). Because of its significance to the World Health Organization (WHO) as antiepileptic drug,[27] the solution-based

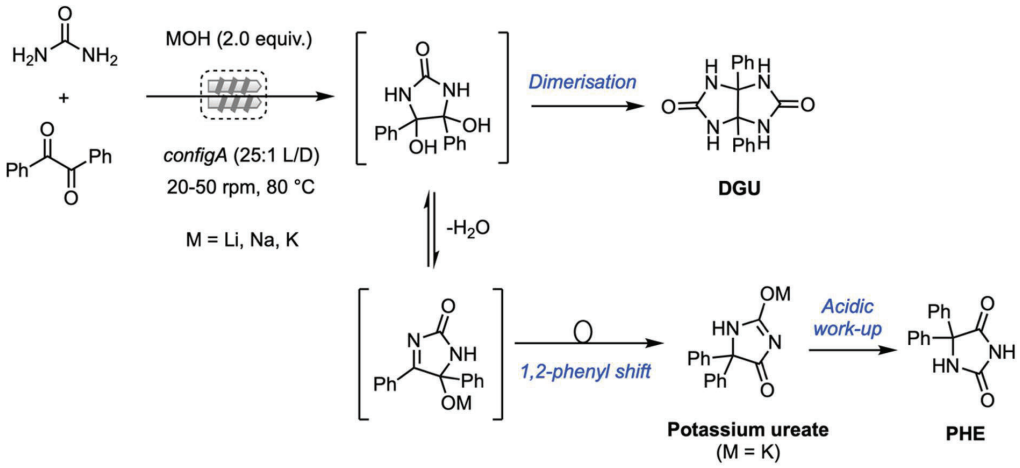
manufacturing route of **PHE** according to Biltz rearrangement[47,48] was implemented by mechanochemical approaches in batch by ball-milling[49,50] and by RAM,[51] up to multigram scale. The commonly accepted mechanism in solution relies on a base-promoted benzil–urea condensation reaction, followed by a [1,2]-intramolecular phenyl shift, competing with a dimerization reaction leading to 3a,6a-diphenylglycoluril (**DGU**) as by-product. The rearrangement by mechanochemistry[35] was also investigated at the solid state by *in situ* monitoring by Raman spectroscopy.[50] Seminal reports showed that mechanochemical rearrangements[35] constitutes a powerful approach for the synthesis of various active pharmaceutical ingredients (APIs),[34,49,52] offering efficient opportunities for derivatization, incorporation of diverse chemotypes into existing molecules, and broader exploration of chemical space.

In this work, we describe the continuous flow mechanochemical synthesis of **PHE** using TSE, with systematic evaluation and optimization of the relevant reaction and processing conditions. This approach is intended to improve process efficiency and enhance the potential for industrial implementation of continuous mechanochemical manufacturing of API.

The initial series of experiments was conducted to determine whether non-hygroscopic bases such as LiOH:H_2O and NaOH, could be employed as alternatives to KOH (Table 1, entries 1-3), commonly used in solution (with EtOH), and being the most suitable also when conducting the reaction in the ball-mill[50] or by liquid-assisted RAM (LA-RAM).[51] Indeed, being the stress phenomena and mechanical inputs technology-dependent, it cannot be excluded that a different reactivity is observed by TSE. The screw configuration used, and referred to as *configA* (Figure S2, ESI), alternates blocks of conveying and kneading screw segments, intercalated by mix reverse, to both increase material retention and mixture homogeneity. The extrusion process occurred at 80°C, and 30 rpm.

The reactivity trend was confirmed also by TSE, with KOH displaying the better yield of **PHE** (entry 3). The results are consistent with earlier studies[53] regarding base behavior in the solid state, rationalized within the Hard and Soft Acids and Bases (HSAB) theory. Specifically, stronger ion pairing is expected when the hydroxide anion, a hard base, is associated with harder cations ($Li^+ > Na^+ > K^+$), which decreases hydroxide availability for reaction. Accordingly, KOH showed the highest reactivity, followed by NaOH and then $LiOH{\cdot}H_2O$. Notably, the formation of the main byproduct, identified as 3a,6a-diphenylglycoluril (**DGU**), was more pronounced (entry 1) when $LiOH{\cdot}H_2O$ was employed, already after short residence time.

Table 1. Selected data to prepare **PHE** by TSE, as function of the base (MOH, M = Li, Na, K), and screw speed (not optimized conditions).[a]



Entry	Base (MOH)	Screw speed (rpm)	Yield (%)[b]	
			PHE	DGU
1	$LiOH.H_2O$	30	3	21
2	NaOH	30	12	3
3	**KOH**	**30**	**55**	3
4[c]	KOH	20[c]	16[c]	1[c]
5	KOH	**40**	**58**	4
6	KOH	50	55[d]	10

[a] Typical experimental procedure: 30.75 g total premix input mass composed of benzil (76.0 mmol, 16.13 g, 1.0 equiv.), urea (76.0 mmol, 4.59 g, 1.0 equiv.) and base (2.0 equiv., M = Li, Na, K) were manually fed into a corotating twin-screw extruder (25:1 length-to-diameter ratio, L/D), kept at the specified screw speed (in rpm). The TSE screw configuration used was *configA* (Figure S2, ESI for the details on the screw profile), the extrusion process occurred at 80°C; [b] Yields were calculated on recovered extrudate after work-up, except when otherwise specified. No purge of the barrel was done; [c] The short extrusion time (and the modest yield) resulted from motor blockage after 16 min due to excessive compaction of the powder mixture inside the barrel; [d] Because the final isolated phenytoin contained unidentified impurities by ^{1}H NMR of the crude, the purity and the corresponding reaction yield were determined by ^{1}H qNMR in DMSO-d_6 (0.5 mL) using 1,3,5-trimethoxybenzene (10 mg) as internal standard, sampling 16.2 mg of the reaction crude after work-up.

This observation suggested that both the nature of the base and the water content could affect the kinetics of the rearrangement, with lower effective basicity prolonging the lifetime of intermediates. As a consequence, the dimerization reaction becomes a more competitive pathway than the rearrangement, with **DGU** being the main reaction product (entry 1, 21% *vs* 3% yield of **DGU** and **PHE** respectively). NaOH was excluded because of the formation of a very compact powder in this processing conditions, with high torque increase stopping the extrusion process. In any case, the low yield observed for $LiOH \cdot H_2O$ and NaOH is also due to

incomplete reaction with a large amount of benzil still present after work-up (also due to motor block hampering the reaction to proceed). For the hydroxide-screening experiments time-resolved recording of torque and barrel-zone temperatures were recorded (Figures S7-S9, SI). The $LiOH \cdot H_2O$ and NaOH runs showed increasing torque towards the instrument limit, whereas the KOH run was completed without reaching this limit. These observations support the selection of KOH on operational grounds, independently of subsequent screw-configuration changes. Because the premix was fed manually, the profiles reflect both material behavior and fluctuations in instantaneous feeding. Therefore, KOH was confirmed as the most suitable base, and the study continued with selected experiments aiming to investigate the influence of the screw speed on the reaction yield. The screw speeds were varied between 20 and 50 rpm (Table 1, entries 4-6) and whether it was not possible to identify a clear trend, 40 rpm was selected as speed for the following investigation, delivering slightly better isolated yield of **PHE** (58%, entry 4), and proportionally lower amount of **DGU** (4%). At higher screw speed, **PHE** yield was not markedly improved; instead, a larger increase in **DGU** formation was observed (10%, entry 6) together with traces of not identified byproducts that co-precipitated with **PHE** during the acidic work-up. In this case, the phenytoin yield was determined by ^{1}H qNMR using an internal standard to account for product impurity.

Although the formation of potassium ureate (Table 1) was a good indication that the reaction is occurring,[50] its physical state (deliquescent liquid) is not optimal from rheological point of view, generating a compact past inside the barrel, making the mixing efficiency and the compression forces of the kneading segments less effective. Therefore, the initial screw profile was slightly modified (*configB*, Figure S3, SI), by inserting in the initial section, alternate mixing and kneading segments, with no further modifications introduced in the second half of the screw profile. A new campaign of optimization was conducted at 40 rpm, aiming to identify: i) the optimal stoichiometry of urea (in the range 1.0-1.6 equiv., Table 2), ii) the effect of thermal energy (explored in the range 70 – 100 °C, Table 2) and iii) the effect of liquid-assisted grinding (LAG) conditions with EtOH (for $0.25 < \eta < 0.75$ mL/g) (Table 3). This part of optimization was conducted using a different screw configuration compared to Table 1 (*configA* to *configB*) was built with a bigger number of mixing elements to ensure a more consistent mixing of the reaction mixture and reflect in generally more robust and reproducible results. A bridging experiment conducted with the same procedure as entry 1 Table 2 but with *configA* screw profile, giving 60% yield, comparable to entry 5 Table 1.

Although an excess of urea is clearly expected to drive the reaction toward an increased formation of **DGU**, the seminal report from Biltz[47] showed that a slight excess of urea can be beneficial to increase the yield to phenytoin. As shown in Table 2 (entries 1-4), the selectivity toward **DGU** was not appreciably affected and remained approximately constant, increasing only slightly, whereas the yield of phenytoin increased more substantially when 1.4 equiv. of urea were used instead of in stoichiometric amount with benzil (61% *vs* 54% for entries 1 and 3 respectively), consistently with the solution-based method, both in terms of **PHE** formation and **DGU** formation.

Table 2. Scouting of the parameters to prepare **PHE** by TSE at 40 rpm: selected data for the optimisation of urea amount and thermal energy effect.[a]

Entry	Urea (equiv.) / Benzil (mmol)	T (°C)	Yield (%)[b]	
			PHE	DGU
1	1.0 / 76.0	90	54	3
2	1.3 / 72.7	90	57	4
3	**1.4** / 71.6	90	**61**	5
4	1.6 / 69.7	90	57	5
5[c]	1.4 / 71.6	70	52	3
6[c]	1.4 / 71.6	80	60	5
7[c]	1.4 / 71.6	100	53	4
8	1.4 / 71.6	25	41	1
9[d]	1.4 / 71.6	90	56	6

[a] Typical experimental procedure: 30.75 g total premix input mass composed of benzil (1.0 equiv.), urea (1.0 - 1.6 equiv.) and KOH (2.0 equiv.) were manually fed into a twin-screw extruder (25:1 length-to-diameter ratio, L/D), the screws co-rotating at a speed of 40 rpm. The TSE screw configuration used was *configB* (Figure S3, SI for the details on the screw profile), the extrusion process occurred at the specified temperature; [b] Yields were calculated on recovered extrudate after work-up, except when otherwise specified. No purge of the barrel was done; [c] 30.75 g total premix input mass composed of benzil (71.6 mmol, 15.21 g, 1.0 equiv.), urea (100.24 mmol, 6.08 g, 1.4 equiv.) and KOH (143.2 mmol, 9.46 g, 2.0 equiv.). [d] 30.75 g total premix input mass composed of benzil (1.0 equiv.), urea (1.0 - 1.6 equiv.) and KOH (2.0 equiv.) were manually fed into a twin-screw extruder (25:1 length-to-diameter ratio, L/D), the screws co-rotating at a speed of 40 rpm. The TSE screw configuration used was *config0* (Figure S5, SI for the details on the screw profile), the extrusion process occurred at the specified temperature.

The effect of thermal energy was also studied in parallel, by extruding at different temperature, while keeping the other process (40 rpm) and chemical parameters (1.4 equiv. of urea) constant (Table 2, entries 3, 5-7). By increasing the temperature, the total process time decreased, the

mixture of reagents becoming ductile (softer), but still remaining a compact, inhomogeneous solid, as it could be deducted by visual inspection of the mixture in a sacrificial experiment. However, no additional advantages were observed when increasing the reaction temperature in the range 70 – 100 °C, but thermal activation resulted somehow beneficial for the reaction, especially when compared to a similar extrusion experiment at 25°C, delivering a lower, but still surprising acceptable yield (41%, entry 8). Indeed, the exothermicity of the reaction, was previously observed for **PHE** synthesis by LA-RAM,[51] and it is in line with solution-phase procedures, where the reaction is typically conducted at reflux in alcoholic media.[47,54] Moreover, the extruder barrel behaves as a sealed system under steady-state operation, the initial mechanical input provided by kneading in the corotating screws was sufficient to initiate the reaction, which then proceeded to a moderate extent as the temperature of the reaction mixture increased and supplied additional thermal energy. This interpretation was supported by the observation that the extrudate was warmer than the barrel, approximately 40 °C as measured by IR thermometer, that beyond the exothermic nature of the reaction, heat can also be due to mechanical energy dissipation. Second, whereas in the other neat experiments conducted at higher temperature the extrudate exited the barrel as a compact powder, in entry 1 the crude material appeared as a homogeneous paste. However, these effects were insufficient to support the reaction to the same extent as in entries 3, 5-7, conducted at higher temperature range, and confirming the need for barrel heating. Additional controls were performed to examine the contributions of heating and mechanical processing. Using the same benzil:urea:KOH ratio (1.0:1.4:2.0), and operating at 90 °C and 40 rpm, extrusion without kneading elements afforded **PHE** in 56% isolated yield (Table 2, entry 9; the details of the screw configuration are indicated in Figure S5, SI). The gross SME was 0.2 MJ kg^{-1}, compared with 1.8 MJ kg^{-1} for *configB* under the corresponding conditions (entry 3), which afforded 61% yield. Substantial product formation was therefore possible at reduced mechanical input, although the conveying screws still provided a slight mechanical action. In a separate non-extrusion control, the same 30.75 g premix was heated in a 250 mL round-bottom flask at a setpoint of 90 °C for 40 min with magnetic stirring, affording **PHE** in 51% isolated yield. This duration was comparable to the 39 min "*pre-purge*" processing time recorded in Table 4, entry 1, although the material-temperature histories and mixing conditions were not matched. The controls support a substantial thermal contribution to **PHE** formation. The higher relative formation of **DGU** under the control conditions is consistent with lower selectivity towards **PHE**, suggesting that the processing conditions affect both product formation and the competing pathway. This set

of experiments help to outline a degree of synergy between thermal and mechanical energy that is needed for the formation of the desired product.

At this stage, implementation of liquid-assisted grinding (LAG) was also evaluated, for comparison with the previously reported mechanochemical protocols based on LA-RAM,[51] where LAG by EtOH (η = 0.75 mL/g) had been reported to be beneficial (97% yield of **PHE** after 20 min.). The investigation of the optimal η value was screened in the range 0.25 < η < 0.75 mL/g (Table 3). EtOH was added using two different manual feeding approach: i) the reagents and the LAG solvent were pre-mixed and the suspension was manually fed (Table 3, entry 4 and Supporting Video V2); and ii) manual feeding of the pre-mixed solid reagents was occurring while the LAG solvent is constantly added at a feeding rate of 0.375 mL/min (volume syringe: 24 mL, diameter of 22 mm), via the dedicated port for liquid addition. With this second approach, although the 'blue state'[50,51] of the extrudate was clearly indicating the formation of **PHE**, the extrudate aspect was not homogeneous and thus not reproducible (Figure S13, SI).

Table 3. Influence of LAG addition to prepare **PHE** by TSE. Screening of the η value.[a]

Entry	η (mL/g)	EtOH (mL)	Torque (N m)[b]	Yield (%)[c]	
				PHE	DGU
1[d]	-	0	7.0	52	3
2	0.25	7.69	3.0	31	3
3	0.50	15.37	1.5	42	4
4	0.75	23.06	1.5	60	6

[a] Typical experimental procedure: 30.75 g total premix input mass composed of benzil (71.6 mmol, 15.21 g, 1.0 equiv.), urea (100.24 mmol, 6.08 g, 1.4 equiv.) and KOH (143.2 mmol, 9.46 g, 2.0 equiv.) was manually fed, together with EtOH (0.25 < η < 0.75 mL/g) into the twin-screw extruder (25:1 length-to-diameter ratio, L/D). The screw (co-rotating) speed was 40 rpm, the barrel was heated to 70°C. The TSE screw configuration used was *configB* (Figure S3, SI for the details on the screw profile); [b] A torque value of about 1 N m corresponds to dry screw rotation (without chemicals); [c] Yields were calculated on recovered extrudate after work-up, except when otherwise specified. No purge of the barrel was done; [d] Data from Table 2, entry 5.

Also, as far as the η value increased, the rheology of the reaction mixture improved, with a decrease in both the residence time and torque value, delivering the better yield for Phenytoin (60%), when extruding at 70°C, with a screw speed kept constant at 40 rpm. Despite the fact that EtOH boiling point (78.4°C) did not allow to conduct the experiments in the optimal temperature range from 80 °C to 90 °C, identified for neat conditions (Table 2, entries 6 and 3 respectively), at the same scale and screw speed, comparable yields were obtained (60% *vs* 61%

for η = 0.75 mL/g and neat conditions respectively), indicating that, under LAG conditions, it was possible to extrude the mixture at a lower temperature.

The inhomogeneous aspect of the pre-mixed reagents with EtOH already at η = 0.75 mL/g, generated a slurry with EtOH as supernatant, hampering to keep constant the relative proportions and concentrations of the reactants during manual feeding: Therefore, higher values of η (up to 1 mL/g) were not investigated further, despite that a better conversion and yield could be reached by extrusion upon controlled addition of the reactants by volumetric/gravimetric feeders.

Aiming to increase the yield upon temperature raise, while exploiting the positive effect of LAG, a control experiment using *i*-PrOH, an alcohol with a higher boiling point (b.p. 82.3°C) than EtOH was conducted by LA-RAM, with η = 0.75 mL/g, on a 35.7 mmol scale, in the same reaction conditions previously described by us (at 90 *g*, during 10 min).[51] However, the yield was 20% lower than the same experiment conducted with EtOH, as LA-RAM solvent. Therefore, no further experiments involving *i*-PrOH were conducted by TSE.

As a final step of the optimization, the effects of screw speed and screw configuration in determining reaction outcome was investigated by modulating both screw speed and screw configuration, for example by varying the number of reverse elements relative to normal conveying elements. In previous experiments, changes in screw configuration had shown only a limited effect on reaction outcome. The configurations used up to that point had mainly been selected to address the mechanical needs of the evolving experimental campaign during reaction processing, for example by increasing mixing elements when the crude appeared insufficiently homogeneous or increasing kneading elements to transfer enough energy to the system, but not so much to avoid motor blockage.

As shown in Table 4, two screw configurations were compared at the optimal reaction temperature of 90°C, from neat processing: *configB*, containing fewer reverse elements in the initial part of the screw profile (Figure S3, SI), and *configC*, in which the number of reverse elements was maximized (Figure S4, SI), thereby increasing the material retention within the barrel. Both configurations were tested at 30 and 40 rpm, at the same extrusion temperature (90 °C). For the same screw profile, no major changes in yield were observed at different screw speed, although, as expected, the extrusion time was shorter at higher rpm for the same configuration. Different screw speeds and profiles delivered comparable results at 30 rpm for

configB (entry 1) and at 40 rpm *config*C (entry 4), however, the retention time was three times longer for the screw profile *configC*. Moreover, for a very similar throughput (entries 1 and 3), at the same screw speed (30 rpm), higher specific mechanical energy (SME)[28] was needed, due to the increased torque value, when *configC* was used, being doubled when conducting the experiment at 40 rpm (entry 4). The lowest SME value was calculated for *configB* operating at 40 rpm (entry 2), providing the highest throughput, but a slightly lower yield after purge (75%) and the highest amount of **DGU** (8% yield) compared to the other processing conditions, delivering respectively 5% (for entries 1 and 4) and 6% (entry 3).

For the experiment delivering the highest yield after purge (78%, entry 1), the real-time collection of the extrudate (Table 4, entry 1) is shown in the Supporting Video V3 (*c.f.*, SI). The aspect of the crude remaining in the barrel before the purges is shown in Figure S6.

To maximise the amount of product recovered, the barrel was purged three times with 9 g portions of urea each. Each portion of extrudate issue of the individual purge was analysed by TLC to identify the presence of **PHE**, which was recovered each time in a separate post-reaction treatment. Clearly, the amount of **PHE** recovered after each purge cycle was linearly decreasing and three purges were sufficient to recover the full amount of the initial crude, with a generally higher yield increase for the screw profile *configC* (entries 3 and 4), may be because the reverse element introduced just after the first kneading section compact the crude mixture more strongly within the barrel, leading to greater mass loss and therefore larger error.

Table 4. Comparisons of screw profiles to prepare Phenytoin in neat, continuous mechanochemistry.[a]

Entry	Screw profile	Screw speed (rpm)	Torque (Nm)[b]	Throughput[c] (g/h)	SME[d] (MJ/kg)	Yield (%) PHE[d]	
						without purge[e]	After purge[f]
1[d]	*configB*	30	7	32.7	2.4	57 (60)[g]	78 (70)[g]
2	*configB*	40	7	60.2	1.8	61[h]	75
3	*configC*	30	10.5	32.3	3.7	48	76
4	*configC*	40	10.5	21.5	7.4	48	78
5[h]	*configB*	30	7	n.c.[j]	n.c.[j]	63	75

[a] Typical experimental procedure: 30.75 g total premix input mass composed of benzil (71.6 mmol, 15.21 g, 1.0 equiv.), urea (100.24 mmol, 6.08 g, 1.4 equiv.) and KOH (143.2 mmol, 9.46 g, 2.0 equiv.) was manually fed into

the twin-screw extruder (25:1 length-to-diameter ratio, L/D). The screw (co-rotating) speed (rpm) was as specified, the barrel was heated at 90°C. The TSE screw configuration used was *configB* or *configC* (Figures S3 and S4 respectively, SI for the details on the screw profile); [b] A torque value of about 1 N m corresponds to dry screw rotation (without chemicals). The torque value decreases to 5.5 – 6.0 N m upon the purging with urea started; [c] Throughput was calculated as the mass of crude extrudate collected before purging divided by the elapsed time from the start of premix feeding to completion of the initial extrusion stage, expressed in g h^{-1}. Both purge duration and purge-fraction mass were excluded. [d] SME = Specific Mechanical Energy[28] calculated from the data set of the experiments before purging; [e] Yields were calculated on recovered extrudate mass before purging; [f] Yields were calculated assuming total recovery of initial premix mass input; [g] Reaction performed with EtOH in LAG conditions (η = 0.75 mL/g). data from Table 3 entry 4 for the experiment without purge; [h] Data from Table 2, entry 3; [i] Experimental procedure: 61.50 g total premix input mass composed of benzil (143.3 mmol, 30.42 g, 1.0 equiv.), urea (200.62 mmol, 12.17 g, 1.4 equiv.) and KOH (286.6 mmol, 18.91 g, 2.0 equiv.), extruded at 90°C; [j] n.c. = not calculated.

To verify this interpretation, an additional experiment was conducted using double the mass employed in the previous experiments (entry 5). The rationale was that, at higher feed mass, the relative errors associated with mass loss should be smaller and the discrepancy between the pre-purge and post-purge yields should therefore decrease. This was indeed observed (63% before purge *vs* 75% with purge). The fact that this experiment confirmed the hypothesis, while also showing no substantial difference between lower and higher feed masses, provides an encouraging starting point for considering the applicability of this reaction under continuous-operation conditions, where errors in yield determination would progressively diminish while reactivity remains robust over extended extrusion times. These observations support a reduced relative end-of-run recovery penalty at higher feed mass. The premix was fed manually in portions because the extruder was not equipped with an automated feeder. These finite-feed experiments demonstrate the feasibility of **PHE** synthesis by TSE, but do not establish sustained steady-state operation or a sustained throughput advantage over RAM. Further evaluation would require controlled feeding over extended runs, together with a steady automated feed of the premix.

The isolation of **PHE**, and its separation from the unavoidable dimerization by-product **DGU** occurred by a sequence of straightforward water precipitation/filtration at different pH, as already reported by us.[51] In particular, the extrudate was stirred in 200 mL of water, to solubilize the potassium salt of phenytoin and to precipitate the water-insoluble **DGU** (for PXRD of DGU, see Table S3 and Figure S12 , SI) together with any possible traces of unreacted benzil. Then, upon acidification using 10% w/w aqueous citric acid until pH = 4, **PHE** was recovered as precipitate and isolated by filtration. Considering the critical role of crystal structure in pharmaceutical applications,[55,56] the extrudate obtained in the better reaction and processing conditions (78% yield, Table 4, entry 1) was also characterized by powder X-ray diffraction (PXRD) to reveal a phase-pure, highly crystalline substance with the crystal structure

corresponding to published structure of phenytoin.[57,58] Diffraction profiles for the samples obtained by LA-RAM[51] and a commercially available phenytoin reference sample are consistent with the diffraction profile of PHE sample obtained by TSE (see Figures 5 and S11 and Table S2 in the Supporting Information).

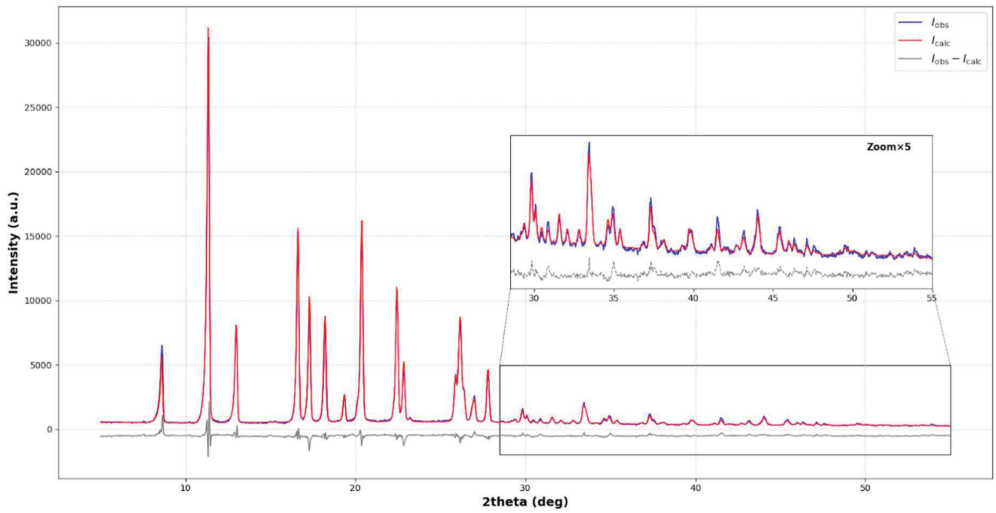


Figure 5. Rietveld analysis of the product obtained by extrusion, corresponding to pure crystalline phenytoin. Experimental data are shown in blue, calculated in red, and the difference curve in gray. Calculated data are based on the crystal structure of phenytoin (CSD refcode: PHYDAN03).

Benchmarking Against the Solution Process. Subsequently, the environmental performance of TSE-assisted syntheses for **SSD** and **PHE** was assessed and compared, not only with the analogous solution-phase synthetic methods, but also against the previously reported mechanochemical processes in batch. Therefore, CHEM21 tool[42] was used to comprehensively evaluate the sustainability of the reactions, considering both quantitative (*e.g,* green chemistry metrics such as atom economy, *E*-factors, reaction mass efficiency and process mass intensity), and qualitative criteria (*e.g.*, energy efficiency, safety, and potential environmental and health risks) (*c.f.*, excel spreadsheets, SI).

From the standpoint of designing a greener synthetic approach, the primary objective is to minimize the quantity of solvent required to obtain the target product. Process Mass Intensity (PMI)[59] evaluates the total amount of material used in relation to the amount of product generated. Total PMI reflects material usage across both synthesis and purification operations.

Although reactive extrusion offers advantages mainly at the reaction stage and can be implemented on a much larger scale, post-reaction processing is not necessarily altered to the same extent, and the recovery of the product in high purity could still require downstream operations, with a negative impact on the green and sustainability metrics.

Table 5 compares the process mass intensity (PMI)[59] values of ball milling (BM), resonance acoustic mixing (RAM), and twin-screw extrusion (TSE), against the corresponding solution-based protocols for the synthesis of **SSD** and **PHE**.

The conventional solution-based synthesis of **SSD**[43] at laboratory scale is characterized by a significantly high Process Mass Intensity (PMI, 43.5 and 62.9 without or with downstream process respectively, Table 5), which served as a benchmark for comparison with greener synthetic routes bases on mechanochemical methods. For comparison, the PMI was also calculated from a patented process[60] on multi kg-scale synthesis of **SSD** in solution, utilizing sulfadiazine, silver nitrate, sodium hydroxide, and purified water as the primary solvent, with the estimated PMI of approximately 42.5.

Table 5. PMI values comparing solution phase, ball mill (BM), resonant acoustic mixing (RAM) and twin-screw extrusion (TSE) methods for the synthesis of **SSD** and **PHE**.

	PMI	**Solution**	**BM**	**RAM**	**TSE**
SSD	*Reaction*[a]	43.5 [c]	1.2[c]/ 1.1[d]	n.p.[e]	1.0[d]
	Total[b]	62.9[c]	1.2[c] / 1.1[d]		1.0[d]
PHE	*Reaction*[a]	32.5[f]	2.0	2.5[f]	2.2
	Total[b]	221.6[f]	383.6	93.9[f]	79.8

[a] PMI of the reaction without considering the downstream process. The data set used for each calculation is indicated in the Chem21 excel spreadsheet (SI). The associated references are also indicated. [b] PMI of the whole process, considering the reaction and isolation process. [c] Source of silver is $AgNO_3$. [d] Source of silver is Ag_2O. [e] Not performed; [f] PMI values already reported in our previous study on LA-RAM synthesis of **PHE**.[51]

This figure indicates that approximately 42.5 kg of total mass - encompassing all reactants, reagents, and the substantial volume of water used for dissolution, reaction, and purification (washing) - is consumed to isolate 1 kg of the final **SSD** product, showing very similar PMI values to the small-scale reaction, due to similar solvent/total mass ratio, the high PMI being due to the solvent and water usage, which accounts for over 96% of the total input mass. When

preparing **SSD** utilizing sodium sulfadiazine as the sulphadiazine starting reagent,[61] the calculated process mass intensity (PMI) is approximately 10 up to the point of isolation of SSD, which may increase significantly if any purification steps are added.

For the synthesis of **SSD**, the mechanochemical protocols by ball-milling achieve near-ideal PMI values, driven primarily by the absence of solvent, which accounts for 97% of the total reaction mass in the solution protocol. Additional contributing factors are the incomplete conversion observed in the solution process, in contrast to the quantitative conversion delivered by all mechanochemical protocols, and the consequent need for a workup step to isolate **SSD** from unreacted starting material. A notable point concerns the impact of the silver source, which can be directly evaluated by comparing the two BM protocols. A small difference in PMI of 0.1 is observed between the use of $AgNO_3$[45] and Ag_2O (1.2 and 1.1, respectively), reflecting the improved atom economy (AE)[62] afforded by Ag_2O (AE = 85.0% for $AgNO_3$ *vs*. 97.5% for Ag_2O). This improvement arises from the halved stoichiometric requirement of Ag_2O, which provides two equivalents of Ag per formula unit compared to $AgNO_3$. Although the gain in PMI is modest, it could represent a meaningful advantage at larger scales, when using the silver source that is accessible exclusively through mechanochemical means: Ag_2O is insoluble in water (the solvent of the solution-based protocol), and ineffective in solution for SSD synthesis, otherwise prepared using water-soluble $AgNO_3$, while sulfadiazine remains in suspension.

The additional marginal improvement observed for the TSE protocol stems from a proportionally lower consumption of aqueous ammonia: 300 μL for 33 mmol scale used in TSE experiment corresponds to an approximately 6-fold increase in volume relative to the 20–50 μL used at 1–2 mmol scale in BM, whereas the scale itself increases 16.5-fold. The TSE protocol thus delivers quantitative yield of **SSD** with a reduced amount of aqueous ammonia, compared to BM approach.

Our current effort demonstrates that novel methods, such as mechanochemical synthesis, achieve a reduction in PMI by one order of magnitude underscoring the high environmental burden of the conventional solvent-based processes. Our solid-state route directly combines silver oxide and sulfadiazine (in the presence of trace aqueous ammonia), targeting quantitative conversion and eliminating nitrate-bearing wastewater. The described process delivers **SSD** in a single step. The mixture of reactants is fed to the extruder to collect pure product that requires only optional drying. With virtually no waste generation, except water which can readily be disregarded, the PMI factor is just above 1 (PMI = *ca.*1.05, *c.f.*,

excel spreadsheet for CHEM21 in supporting information) while the corresponding *E*-factor of the TSE solid-state processing to obtain **SSD** from SDA and Ag_2O approaches 0 (*E*-factor = 0.01).

The purity of the product, however, depends on the purity of the starting substances - any impurity present in the starting reagents will remain in the final product. We note that waste generation may therefore have been moved to earlier steps of purification of starting compounds, which should potentially need to be considered when painting a bigger picture of the greenness of the overall process. If adopted, the solid-state route can also free one reactor train previously dedicated to solution precipitation, improving plant capacity utilization.

For the synthesis of **PHE** in solution, the base-promoted benzil–urea condensation/cyclization occurs in alcoholic or high-boiling media, followed by extractive workups and recrystallizations, steps that inflate PMI, utilities, and isolation cycles (PMI_{total} = 221.6, Table 5). However, a large spread in PMI values is observed across all protocols (solution- or mechanochemistry-based), driven primarily by the workup procedure. With the exception of the BM protocol, which requires column chromatography for purification due to competing reaction pathways that generate several by-products,[50] PMI_{total} for the mechanochemical processes in batch and in continuous decreases as the reaction scale increases (1 mmol in solution, 36 mmol for RAM, 72 mmol for TSE). Indeed, as previously observed for other mechanochemical transformations,[63] upon scale increase, downstream processes could be optimized by reducing the amount of solvent (water in this case) to isolate the product.

Indeed, the weight-to-weight ratio of the chemicals needed for the work-up to isolate 1 g of **PHE** decreases from 186.88 g/g (for solution synthesis) to 91.43 g/g (by RAM) to 66.33 g/g (by TSE). Examining $PMI_{reaction}$, the mechanochemical protocols outperformed the solution-based one, consistent with the trend observed for **SSD**, with solvent constituting 94% of the total reaction mass in the solution protocol. The impact of down-stream operations[64] is evident when comparing the values of $PMI_{reaction}$ with PMI_{total} independently on the methodology used to access PHE (in solution of by mechanochemical activation), with very similar $PMI_{reaction}$ values for the three mechanochemical approaches to **PHE** (BM, RAM and TSE). However, the variations in $PMI_{reaction}$ among the mechanochemical technologies can be rationalized using BM activation as a benchmark ($PMI_{reaction}$ = 2.0), which achieves the lowest value among the three owing to its good yield, strictly stoichiometric reagent quantities, and the absence of liquid-assisted grinding (LAG). The **PHE** synthesis by TSE shows a slightly

higher value (2.2), attributable to the excess of urea (1.4 equiv.) needed to achieved satisfying yield, while the urea used to purge the extruder barrel was excluded from the calculations, as it served as a mechanical push to displace the residual reaction mixture and did not participate in the reaction (see SI for details on the experimental protocol). However, to ensure a fair comparison with the other protocols, the full quantity of workup chemicals required to recover **PHE** from all fractions of the extrudate (including those originating from the urea purge) was accounted for, even though this conservative estimate likely exceeds the quantities that would be needed at an optimized scale. In the case of RAM-mediated synthesis of **PHE**, despite achieving a higher yield than BM (97% *vs*. 76%), presents the highest $PMI_{reaction}$ among the mechanochemical methods (2.5) due to the use of EtOH for LA-RAM (η = 0.75 μL/mg).[51]

In the case of **PHE**, it is worth of note the need of adjusting the processing conditions depending on batch or continuous flow mechanochemistry. In particular, in batch, by BM[50] and RAM,[51] liquid-assisted mechanochemical processing was needed to reach high yields of **PHE**, while LAG results detrimental by TSE. Moreover, RAM-assisted synthesis of **PHE** always delivered a lower amount of **DGU** (2% yield)[51] no matter the processing conditions used, the reaction scale, or the reaction time, compared to TSE (5-8% yield), where changes in scale and processing parameters delivered variable amount of **DGU**.

For each synthetic approach to **SSD** and **PHE**, the productivity (throughput over the time) was also evaluated (Figure 6).

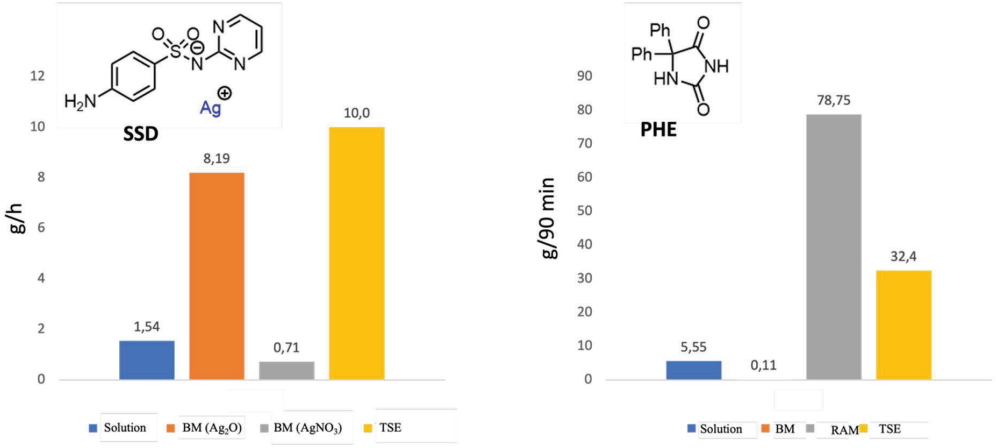


Figure 6. Comparative productivities for **SSD** and **PHE**, by solution-based or by mechanochemically activated processes**.**

For **SSD**, TSE approach displayed the highest productivity (10 g/h), downstream process is not needed, with the reactants continuously fed and less operator intervention (less time to set the experiment), compared to the batch approach, also delivering satisfying values for the BM process involving Ag_2O (8.19 g/h). For the batch processes, the time required to recover the product from the reactor was not considered in the calculation, for sake of comparison with the TSE approach, where the final product is directly extruded. However, although the solution-based synthesis of SSD seemed to outperform compared to BM method employing $AgNO_3$ (1.54 *vs* 0.71 g/h), because the reaction occurs on only 10 min, the real value of productivity should account for the downstream processes to recover the final product, not needed for the BM method, the product being recovered directly from the jar with no additional post-reaction treatment, aspect that counterbalance the apparently lower value of productivity (0.71 g/h) for the BM experiment (Figure 6, left).

In the case of **PHE** (Figure 6, right), the highest productivity (higher throughput) was obtained upon LA-RAM processing conditions (78.75 g / 90 min), while maintaining low waste generation, and enabling the isolation of up to 8.75 g of product in an excellent 97% yield. The low productivity displayed by BM (0.11 g / 90 min) is essentially due to the moderate yield and to the limited reaction scale (below gram level) investigated by this approach.[50] In the selected operating conditions for TSE (Table 4, entry 1), the productivity resulted 32.4 g/90 min (calculated by excluding the downstream operation time), with a 6-fold times increase compared to the corresponding solution process in batch on a similar reaction scale.[65] Although TSE appears less productive than the batch process performed by LA-RAM, it is anticipated that, during longer reaction runs typical of continuous processing, the TSE approach will become superior, with less manual handling for setup, monitoring, transfers, and workup. This reduces labor time and operational bottlenecks. Indeed, in batch processing, production stops between batches for charging reagents, heating/cooling, unloading, cleaning, and restarting. In a continuous process, material flows constantly, so the equipment operates for much longer periods without interruption. Continuous systems can run for hours or days at steady state, meaning the reactor produces material almost all the time. Batch reactors spend a significant fraction of time not reacting. In this specific context, even if TSE shows lower instantaneous productivity than LA-RAM in a short experiment, continuous operation can run for hours or days at steady state, meaning the reactor produces material almost all the time, and may ultimately provide higher overall throughput because setup, shutdown, and crude treatment occupy a much smaller fraction of the total production time.

Conclusion

Overall, the TSE protocols for both **SSD** and **PHE** demonstrate, from a waste-generation perspective, that continuous mechanochemical processing retains and extends the green chemistry advantages established at smaller batch scales: solvent elimination (accounting for over 95% mass saving), and the ability to employ reagents of superior atom economy that are inaccessible in solution, such as Ag_2O in place of $AgNO_3$ for **SSD**. Beyond these intrinsic advantages, the continuous flow nature of TSE further simplifies process streamlining.[66] Looking ahead, additional sustainability gains may be realized by extending extrusion run times and, particularly for **PHE** where downstream operations remain necessary, by also implementing an integrated in-line workup protocol.

Moreover, in the case of **SSD**, its mechanochemical synthesis either in batches using ball mills or in continuous manner using a twin-screw extruder, offers a credible, efficient, and green alternative to the conventional nitrate-based precipitation route, especially since silver nitrate can be replaced by silver oxide to afford quantitative conversion and only water as the byproduct, removal of which requires only drying.

Across both **SSD** and **PHE**, we benchmark against solution routes, apply a common solution and solid-state analytical framework (*c.f.,* SI), and outline scale-up from milligram to decagram scales using equipment already familiar to industry. Framed within a metrics-driven sustainability agenda, these mechanochemical approaches stands as a clear path requiring appropriate regulatory equivalence with existing solution-made products, allowing for : i) retooling and/or retrofitting of existing infrastructure, supported by the further development of existing sustainability laws,[15] and/or ii) route redesign (as for **SSD**) - rather than incremental utilities optimization – that can meaningfully reduce waste, energy demand, and carbon intensity, while meeting pharmaceutical quality standards. Although the **PHE** reaction proceeds without solvent, at the scale explored, its overall material efficiency remains affected by the aqueous work-up required to separate **DGU** and isolate the desired product. Nevertheless, for a continuously running process at larger scale, it is expected a better use of resources, with an increase of overall efficiency, also in terms of reduced downstream waste. Potential reductions in overall energy consumption and carbon emissions remain to be evaluated through process energy measurements and life cycle assessment.

Despite the efficiency of batch processes, intrinsic limitations remain, including increased downtime, longer lead times, and accumulation of work-in-progress between processing steps.

In addition, batch processing is typically associated with higher setup, cleaning, and energy costs, while quality deviations may become apparent only after completion of the entire batch. As expected, continuous-flow mechanochemical approaches, including but not limited to TSE, address these limitations and provide one possible route towards process intensification for mechanochemistry.

Intertwined economic, regulatory, and environmental incentives will contribute to sustainable competitiveness, driving a transformative transition of the fine chemical industry toward more sustainable practices.[15]

Supporting Information

The authors have cited additional references within the Supporting Information.[42–45,47,49–51,67–71] The data supporting this article, including ^{1}H and ^{13}C NMR, and PXRD diffractograms for **SSD**, **PHE** and **DGU**, excel spreadsheets for green chemistry metrics and productivity (Table 5 and Figure 6) calculations by Chem21[42] data input are available as part of the Supplementary Information. TSE syntheses of **SSD** (Scheme 1) and **PHE** (Table 4, entry 1) are shown in the Supplementary videos V1 and V3 respectively. Supporting video V2 refers to a LAG experiment for **PHE**. Crystallographic data for the intermediate SDD crystal structure has been deposited with the CCDC (deposition number 2557865).

Acknowledgments

This article is based upon work from COST Action CA18112 ‘Mechanochemistry for Sustainable Industry’, supported by COST (European Cooperation in Science and Technology).[72–74]



COST (European Cooperation in Science and Technology) is a funding agency for research and innovation networks, helping to connect research initiatives across Europe and enable scientists to grow their ideas by sharing them with their peers. This boosts their research, career and innovation. www.cost.eu.[75] I.H., L.C., G.M. and E.M. acknowledge the Croatian Science Foundation under the project “Coffee ring effect in ‘Lab on Chip’ environments in the

development of new drug formulations" (CoRe4Pharm, gran n° HRZZ IP-2024-05-4339). The authors are grateful to Simon Kimber and Veijo Honkimäki for their help in setting up the *in situ* monitoring at the old ID15B of the ESRF. We thank the ESRF for beamtime. We thank Stipica Tomić, Marin Liović and Petra Pongrac for their help in assessing product purity. A.C. is grateful to Campus France and Tallinn Technological University (TalTech) for the Ph.D. fellowship (co-tutelle de thèse France-Estonie). E.C. is grateful to Campus France and French-Estonian cooperation Programme Hubert Curien France-Estonia (PHC PARROT 2021-2023).

Author Contributions. CRediT: **L. C.** experimental investigations, analysis, writing original draft; **A.C**. experimental investigations, formal analysis and green chemistry metrics; **G. M.** DFT optimisation; **E. M.** funding acquisition, conceptualization; **E.C.** – funding acquisition, conceptualization, supervision, writing original draft, review and editing. **I. H.** funding acquisition, conceptualization, supervision, writing original draft, review and editing. All authors have approved the final version of the manuscript.

Conflicts of Interest

The authors declare no competing financial interest.

Data Availability

All data supporting the findings of this study are available from the corresponding author upon reasonable request.

References

(1) Constable, D. J. C.; Jimenez-Gonzalez, C.; Henderson, R. K. Perspective on Solvent Use in the Pharmaceutical Industry. *Org. Process Res. Dev.* **2007**, *11* (1), 133–137. https://doi.org/10.1021/op060170h.

(2) Gazis, T. A.; Teixeira, R. I.; Volpin, G.; Yewale, A.; Ince, M. C.; Ford, M. J.; Harmsen, J.; Uboldi, M.; Melocchi, A.; Sponchioni, M.; Aramini, A.; Luisi, R.; Benyahia, B.; Vilé, G. Towards Greener-by-Design Fine Chemicals. Part 2: Technological Frontiers. *Chem. Soc. Rev.* **2026**, *55* (2), 675–713. https://doi.org/10.1039/D5CS00930H.

(3) Jiménez-González, C.; Curzons, A. D.; Constable, D. J. C.; Cunningham, V. L. Cradle-to-Gate Life Cycle Inventory and Assessment of Pharmaceutical Compounds. *Int. J. Life Cycle Assess.* **2004**, *9* (2), 114–121. https://doi.org/10.1007/BF02978570.

(4) Kar, S.; Sanderson, H.; Roy, K.; Benfenati, E.; Leszczynski, J. Green Chemistry in the Synthesis of Pharmaceuticals. *Chem. Rev.* **2022**, *122* (3), 3637–3710. https://doi.org/10.1021/acs.chemrev.1c00631.

(5) Gazis, T. A.; Wuyts, J.; Moutsiou, A.; Volpin, G.; Ford, M. J.; Teixeira, R. I.; Wheelhouse, K. M. P.; Natho, P.; Žnidaršič-Plazl, P.; Jost, S.; Luisi, R.; Benyahia, B.; Maes, B. U. W.; Vilé, G. Towards Greener-by-Design Fine Chemicals. Part 1: Synthetic Frontiers. *Chem. Soc. Rev.* **2026**, *55* (2), 619–674. https://doi.org/10.1039/D5CS00929D.

(6) United Nations Sustainable Development Goals (UN's SDG), https://sdgs.un.org/goals (accessed May 4, 2026).
(7)The link between mechanochemistry and the UN SDGs appeared for the first time in the literature in: Virieux, D.; Delogu, F.; Porcheddu, A.; García, F.; Colacino, E. Mechanochemical Rearrangements. J. Org. Chem. 2021, 86 (20), 13885-13894. The concept was further expanded in: Alić, J.; Schlegel, M.; Emmerling, F.; Stolar, T. Meeting the UN Sustainable Development Goals with Mechanochemistry. Angew. Chem. Int. Ed. 2024, 63 (50), e202414745.
(8) Casagrande, A.; Niidu, A.; Aav, R.; Kananovich, D.; Colacino, E. Green Chemistry Tools in Mechanochemistry. In *Encyclopedia of Green Chemistry*; Elsevier, 2025; pp 550–571. https://doi.org/10.1016/B978-0-443-15742-4.00116-2.
(9) Fantozzi, N.; Volle, J.-N.; Porcheddu, A.; Virieux, D.; García, F.; Colacino, E. Green Metrics in Mechanochemistry. *Chem. Soc. Rev.* **2023**, *52* (19), 6680–6714. https://doi.org/10.1039/D2CS00997H.
(10) Galant, O.; Cerfeda, G.; McCalmont, A. S.; James, S. L.; Porcheddu, A.; Delogu, F.; Crawford, D. E.; Colacino, E.; Spatari, S. Mechanochemistry Can Reduce Life Cycle Environmental Impacts of Manufacturing Active Pharmaceutical Ingredients. *ACS Sustainable Chem. Eng.* **2022**, *10* (4), 1430–1439. https://doi.org/10.1021/acssuschemeng.1c06434.
(11) Patrascu, M.; Meuti, D.; Galant, O.; Nijem, S.; Diesendruck, C. E.; Casagrande, A.; Colacino, E.; Felderhoff, M.; Spatari, S. Sustainable Pharmaceutical Manufacturing Based on Mechanochemistry: A Life Cycle Assessment of Rac-Ibuprofen-Nicotinamide Cocrystallization Routes. *Sustainable Chem. Pharm.* **2026**, *51*, 102422. https://doi.org/10.1016/j.scp.2026.102422.
(12) Sharma, P.; Vetter, C.; Ponnusamy, E.; Colacino, E. Assessing the Greenness of Mechanochemical Processes with the DOZN 2.0 Tool. *ACS Sustainable Chem. Eng.* **2022**, *10* (16), 5110–5116. https://doi.org/10.1021/acssuschemeng.1c07981.
(13) Sheldon, R. A. The E Factor: Fifteen Years On. *Green Chem.* **2007**, *9* (12), 1273–1283. https://doi.org/10.1039/B713736M.
(14) Yu, L. X.; Amidon, G.; Khan, M. A.; Hoag, S. W.; Polli, J.; Raju, G. K.; Woodcock, J. Understanding Pharmaceutical Quality by Design. *AAPS J.* **2014**, *16* (4), 771–783. https://doi.org/10.1208/s12248-014-9598-3.
(15) Colacino, E.; Isoni, V.; Crawford, D.; García, F. Upscaling Mechanochemistry: Challenges and Opportunities for Sustainable Industry. *Trends in Chem.* **2021**, *3* (5), 335–339. https://doi.org/10.1016/j.trechm.2021.02.008.
(16) IUPAC Guiding Principles of Responsible Chemistry, https://iupac.org/responsible-chemistry/ (accessed May 4, 2026).
(17) Ying, P.; Yu, J.; Su, W. Liquid-Assisted Grinding Mechanochemistry in the Synthesis of Pharmaceuticals. *Adv. Synth. Catal.* **2021**, *363* (5), 1246–1271. https://doi.org/10.1002/adsc.202001245.
(18) Colacino, E.; Porcheddu, A.; Charnay, C.; Delogu, F. From Enabling Technologies to Medicinal Mechanochemistry: An Eco-Friendly Access to Hydantoin-Based Active Pharmaceutical Ingredients. *React. Chem. Eng.* **2019**, *4* (7), 1179–1188. https://doi.org/10.1039/c9re00069k.
(19) Brandão, P.; Pineiro, M. Mechanochemistry for Sustainable Drug Design and Active Pharmaceutical Ingredient Synthesis. In *Sustainable Approaches in Pharmaceutical Sciences*; 2023; pp 255–272. https://doi.org/10.1002/9781119889878.ch11.
(20) Pérez-Venegas, M.; Juaristi, E. Mechanochemical and Mechanoenzymatic Synthesis of Pharmacologically Active Compounds: A Green Perspective. *ACS Sustainable Chem. Eng.* **2020**, *8* (24), 8881–8893. https://doi.org/10.1021/acssuschemeng.0c01645.
(21) Tan, D.; Loots, L.; Friščić, T. Towards Medicinal Mechanochemistry: Evolution of Milling from Pharmaceutical Solid Form Screening to the Synthesis of Active Pharmaceutical Ingredients (APIs). *Chem. Commun.* **2016**, *52* (50), 7760–7781. https://doi.org/10.1039/C6CC02015A.

(22) Templ, J.; Borchardt, L. Mechanochemical Strategies Applied to the Late-Stage Modifications of Pharmaceutically Active Compounds. *Angew. Chem. Int. Ed.* **2025**, *64* (41), e202503061. https://doi.org/10.1002/anie.202503061.
(23) Gomollón-Bel, F. Ten Chemical Innovations That Will Change Our World: IUPAC Identifies Emerging Technologies in Chemistry with Potential to Make Our Planet More Sustainable. *Chem. Int.* **2019**, *41* (2), 12–17. https://doi.org/10.1515/ci-2019-0203.
(24) Crawford, D. E.; Porcheddu, A.; McCalmont, A. S.; Delogu, F.; James, S. L.; Colacino, E. Solvent-Free, Continuous Synthesis of Hydrazone-Based Active Pharmaceutical Ingredients by Twin-Screw Extrusion. *ACS Sustainable Chem. Eng.* **2020**, *8* (32), 12230–12238. https://doi.org/10.1021/acssuschemeng.0c03816.
(25) Lim, X. Interlocking Screws Crank out Pharmaceuticals. *CE&N* **2020**, *98 (38)*, 11. https://cen.acs.org/pharmaceuticals/process-chemistry/Interlocking-screws-crank-pharmaceuticals/98/i38?utm_source=Synthesis&utm_medium=Synthesis&utm_campaign=CENRSS) (accessed May 4, 2026).
(26) Colacino, E.; Porcheddu, A.; Halasz, I.; Charnay, C.; Delogu, F.; Guerra, R.; Fullenwarth, J. Mechanochemistry for "No Solvent, No Base" Preparation of Hydantoin-Based Active Pharmaceutical Ingredients: Nitrofurantoin and Dantrolene. *Green Chem.* **2018**, *20* (13), 2973–2977. https://doi.org/10.1039/C8GC01345D.
(27) *WHO Model Lists of Essential Medicines*. https://www.who.int/groups/expert-committee-on-selection-and-use-of-essential-medicines/essential-medicines-lists (accessed 2026-07-21).
(28) Bolt, R. R. A.; Leitch, J. A.; Jones, A. C.; Nicholson, W. I.; Browne, D. L. Continuous Flow Mechanochemistry: Reactive Extrusion as an Enabling Technology in Organic Synthesis. *Chem. Soc. Rev.* **2022**, *51* (11), 4243–4260. https://doi.org/10.1039/D1CS00657F.
(29) Reynes, J. F.; Isoni, V.; García, F. Tinkering with Mechanochemical Tools for Scale Up. *Angew Chem Int Ed* **2023**, *62* (44). https://doi.org/10.1002/anie.202300819.
(30) Crawford, D. E.; James, S. L. A Reflection on Synthesis by Extrusion Ten Years on: Achievements, Challenges and Opportunities for Solvent-Free, Sustainable, Continuous Chemical Manufacturing. *Chem. Sci.* **2026**, *17*, 8823–8834. https://doi.org/10.1039/D6SC90085B.
(31) Baier, D. M.; Rensch, T.; Dobreva, D.; Spula, C.; Fanenstich, S.; Rappen, M.; Bergheim, K.; Grätz, S.; Borchardt, L. The Mechanochemical Beckmann Rearrangement over Solid Acids: From the Ball Mill to the Extruder. *Chemistry–Methods* **2023**, *3* (4). https://doi.org/10.1002/cmtd.202200058.
(32) Atapalkar, R. S.; Kulkarni, A. A. Direct Amidation of Acids in a Screw Reactor for the Continuous Flow Synthesis of Amides. *Chem. Commun.* **2023**, *59* (60), 9231–9234. https://doi.org/10.1039/D3CC02402D.
(33) Lavayssiere, M.; Lamaty, F. Amidation by Reactive Extrusion for the Synthesis of Active Pharmaceutical Ingredients Teriflunomide and Moclobemide. *Chem. Commun.* **2023**, *59* (23), 3439–3442. https://doi.org/10.1039/D2CC06934B.
(34) Mocci, R.; Colacino, E.; Luca, L. D.; Fattuoni, C.; Porcheddu, A.; Delogu, F. The Mechanochemical Beckmann Rearrangement: An Eco-Efficient "Cut-and-Paste" Strategy to Design the "Good Old Amide Bond." *ACS Sustainable Chem. Eng.* **2021**, *9* (5), 2100–2114. https://doi.org/10.1021/acssuschemeng.0c07254.
(35) Virieux, D.; Delogu, F.; Porcheddu, A.; García, F.; Colacino, E. Mechanochemical Rearrangements. *J. Org. Chem.* **2021**, *86* (20), 13885–13894. https://doi.org/10.1021/acs.joc.1c01323.
(36) Nicholson, W. I.; Barreteau, F.; Leitch, J. A.; Payne, R.; Priestley, I.; Godineau, E.; Battilocchio, C.; Browne, D. L. Direct Amidation of Esters by Ball Milling**. *Angew Chem Int Ed* **2021**, *60* (40), 21868–21874. https://doi.org/10.1002/anie.202106412.
(37) Métro, T.-X.; Bonnamour, J.; Reidon, T.; Sarpoulet, J.; Martinez, J.; Lamaty, F. Mechanosynthesis of Amides in the Total Absence of Organic Solvent from Reaction to Product Recovery. *Chem. Commun.* **2012**, *48* (96), 11781–11783. https://doi.org/10.1039/c2cc36352f.

(38) Patil, N. B.; Atapalkar, R. S.; Chavan, S. P.; Kulkarni, A. A. Multi-Step Synthesis of Miltefosine: Integration of Flow Chemistry with Continuous Mechanochemistry. *Chem. Eur. J.* **2021**, *27* (70), 17695–17699. https://doi.org/10.1002/chem.202103499.
(39) Geib, R.; Colacino, E.; Gremaud, L. Sustainable Beckmann Rearrangement Using Bead-Milling Technology: The Route to Paracetamol. *ChemSusChem* **2024**. https://doi.org/10.1002/cssc.202301921.
(40) Bordier, C.; Colacino, E. *Method for automatically generating an optimised prediction plan and conducting a mechanochemical reaction* **2026**, *WO2026027590 (A1)*.
(41) Lavayssiere, M.; Bantreil, X.; Lamaty, F. Bayesian Optimization of Solvent-Free Thermal Amidation via Reactive Extrusion. *Chem. Eur. J.* **2026**, e70914. https://doi.org/10.1002/chem.70914.
(42) McElroy, C. R.; Constantinou, A.; Jones, L. C.; Summerton, L.; Clark, J. H. Towards a Holistic Approach to Metrics for the 21st Century Pharmaceutical Industry. *Green Chem.* **2015**, *17* (5), 3111–3121. https://doi.org/10.1039/C5GC00340G.
(43) Borges, Á. D. L.; Ponte, G. D.; Federman Neto, A.; Carvalho, I. Síntese de sulfadiazina e sulfadiazina de prata em escala semi-micro: prática experimental em síntese de fármacos. *Quím. Nova* **2005**, *28*, 727–731. https://doi.org/https://doi.org/10.1590/S0100-40422005000400030.
(44) Ferreira, D. R.; Portet, A.; Alves, P. C.; Rijo, P.; Gomes, C. S. B.; Duarte, M. T.; Halasz, I.; Colacino, E.; Emmerling, F.; André, V. Modulating the Crystalline Forms of Silver–Sulfadiazine Complexes by Mechanochemistry. *CrystEngComm* **2025**, *27* (45), 7287–7294. https://doi.org/10.1039/D5CE00572H.
(45) Sović, I.; Lukin, S.; Meštrović, E.; Halasz, I.; Porcheddu, A.; Delogu, F.; Ricci, P. C.; Caron, F.; Perilli, T.; Dogan, A.; Colacino, E. Mechanochemical Preparation of Active Pharmaceutical Ingredients Monitored by In Situ Raman Spectroscopy. *ACS Omega* **2020**, *5* (44), 28663–28672. https://doi.org/10.1021/acsomega.0c03756.
(46) Lukin, S.; Germann, L. S.; Friščić, T.; Halasz, I. Toward Mechanistic Understanding of Mechanochemical Reactions Using Real-Time *In Situ* Monitoring. *Acc. Chem. Res.* **2022**, *55* (9), 1262–1277. https://doi.org/10.1021/acs.accounts.2c00062.
(47) Biltz, H. Über Die Konstitution Der Einwirkungsprodukte von Substituierten Harnstoffen Auf Benzil Und Über Einige Neue Methoden Zur Darstellung Der 5.5-Diphenyl-Hydantoine. *Ber. Dtsch. Chem. Res.* **1908**, *41* (1), 1379–1393. https://doi.org/10.1002/cber.190804101255.
(48) Konnert, L.; Lamaty, F.; Martinez, J.; Colacino, E. Recent Advances in the Synthesis of Hydantoins: The State of the Art of a Valuable Scaffold. *Chem. Rev.* **2017**, *117*, 13757–13809. https://doi.org/10.1021/acs.chemrev.7b00067.
(49) Konnert, L.; Reneaud, B.; de Figueiredo, R. M.; Campagne, J.-M.; Lamaty, F.; Martinez, J.; Colacino, E. Mechanochemical Preparation of Hydantoins from Amino Esters: Application to the Synthesis of the Antiepileptic Drug Phenytoin. *J. Org. Chem.* **2014**, *79* (21), 10132–10142. https://doi.org/10.1021/jo5017629.
(50) Puccetti, F.; Lukin, S.; Užarević, K.; Colacino, E.; Halasz, I.; Bolm, C.; Hernández, J. G. Mechanistic Insights on the Mechanosynthesis of Phenytoin, a WHO Essential Medicine. *Chem. Eur. J.* **2022**, *28* (13), e202104409. https://doi.org/10.1002/chem.202104409.
(51) Chatzigiannis, C. M.; Scalzullo, S. M.; Colacino, E.; Rivas, M. E. Multigram-Scale Organic Synthesis by Resonant Acoustic Mixing: Application to the Sustainable Preparation of Active Pharmaceutical Ingredients. *ChemSusChem* **2025**, *18* (13), e202500110. https://doi.org/10.1002/cssc.202500110.
(52) Porcheddu, A.; Delogu, F.; De Luca, L.; Colacino, E. From Lossen Transposition to Solventless "Medicinal Mechanochemistry." *ACS Sustainable Chem. Eng.* **2019**, acssuschemeng.9b00709. https://doi.org/10.1021/acssuschemeng.9b00709.
(53) Ortiz-Trankina, L. N.; Crain, J.; Williams, C., III; Mack, J. Developing Benign Syntheses Using Ion Pairs via Solvent-Free Mechanochemistry. *Green Chem.* **2020**, *22* (11), 3638–3642. https://doi.org/10.1039/d0gc01116a.

(54) Lamssane, H.; Haoudi, A.; Thiruvalluvar, A. A.; Hökelek, T.; Varadharajan, V.; Chakroune, S.; Rodi, Y. K.; Mazzah, A.; Mague, J. T.; Alanazi, M. M.; El Monfalouti, H.; Sebbar, N. K. N-Alkylated 5,5-Diphenylhydantoin Derivatives: Synthesis, X-Ray, Spectroscopic Characterization, Hirshfeld Surface Analysis, DFT, Molecular Docking, Molecular Dynamics Simulations, and Cholesterol Oxidase Binding Affinity Estimation. *ACS Omega* **2025**, *10* (27), 29267–29284. https://doi.org/10.1021/acsomega.5c02215.
(55) Braga, D. Crystal Engineering: From Promise to Delivery. *Chem. Commun.* **2023**, *59* (95), 14052–14062. https://doi.org/10.1039/D3CC04313D.
(56) Braga, D.; Casali, L.; Grepioni, F. The Relevance of Crystal Forms in the Pharmaceutical Field: Sword of Damocles or Innovation Tools? *Int. J. Mol. Sci.* **2022**, *23* (16), 9013–9041.
(57) Moriyama, K.; Furuno, N.; Yamakawa, N. Crystal Face Identification by Raman Microscopy for Assessment of Crystal Habit of a Drug. *Int. J. Pharm.* **2015**, *480* (1), 101–106. https://doi.org/10.1016/j.ijpharm.2015.01.031.
(58) Yuminoki, K.; Tachibana, S.; Nishimura, Y.; Mori, H.; Takatsuka, T.; Hashimoto, N. Scaling up Nano-Milling of Poorly Water Soluble Compounds Using a Rotation/Revolution Pulverizer. *Pharmazie* **2016**, *33* (2), 56–64. https://doi.org/10.1691/ph.2016.5093.
(59) Martínez, J.; Cortés, J. F.; Miranda, R. Green Chemistry Metrics, A Review. *Processes* **2022**, *10* (7), 1274. https://doi.org/10.3390/pr10071274.
(60) Shuai, F.; Wang, X.; Zhang, J. 'Method for synthesizing medicinal sulfadiazine silver,' CN101613323B, (2012).
(61) Fox, C. L. Jr. Silver sulfadiazine used in the treatment of burns, US 3.761.590, (1973).
(62) Trost, B. The Atom Economy—A Search for Synthetic Efficiency. *Science* **1991**, *254* (5037), 1471–1477. https://doi.org/10.1126/science.1962206.
(63) Casagrande, A.; Solorzano-Rodriguez, R.; Carta, M.; Delogu, F.; Vezzani, J.; Niidu, A.; Colacino, E. Mechanochemical Amidation Mediated by 1,1'-Oxalyldiimidazole for the Synthesis of Agrochemicals. *Chem. Eur. J.* **2026**, e71190. https://doi.org/10.1002/chem.71190.
(64) Gonnet, L.; Tintillier, T.; Venturini, N.; Konnert, L.; Hernandez, J.-F.; Lamaty, F.; Laconde, G.; Martinez, J.; Colacino, E. *N* -Acyl Benzotriazole Derivatives for the Synthesis of Dipeptides and Tripeptides and Peptide Biotinylation by Mechanochemistry. *ACS Sustainable Chem. Eng.* **2017**, *5* (4), 2936–2941. https://doi.org/10.1021/acssuschemeng.6b02439.
(65) Fan, C.; Lu, H. 'Method for preparing mixed crystal form phenytoin sodium,' CN111303041A (2020).
(66) Moradiya, H. G.; Islam, M. T.; Scoutaris, N.; Halsey, S. A.; Chowdhry, B. Z.; Douroumis, D. Continuous Manufacturing of High Quality Pharmaceutical Cocrystals Integrated with Process Analytical Tools for In-Line Process Control. *Cryst. Growth Des.* **2016**, *16*, 3425–3434. https://doi.org/10.1021/acs.cgd.6b00402.
(67)Baenziger, N. C.; Struss, A. W. Crystal structure of 2-sulfanilamidopyrimidinesilver(I). *Inorg. Chem.* **1976**, *15*, 1807–1809.
(68) *British Pharmacopoeia* Commission. British Pharmacopoeia, 4th ed.; The Stationary Office-TSO publisher, London, 1999; Vol. 1, p. 844.
(69) Arani, N. M.; Safari, J. A Rapid and Efficient Ultrasound-Assisted Synthesis of 5,5-Diphenylhydantoins and 5,5-Diphenyl-2-Thiohydantoins. *Ultrason. Sonochem.* **2011**, *18*, 640–643. https://doi.org/10.1016/j.ultsonch.2010.09.001.
(70) Magd El-Din, A. A.; Roaiah, H. F.; Elsharabasy, S. A.; Hassan, A. Y. A Novel Synthesis of Some New Imidazothiazole and Glycocyamidine Derivatives and Studies on Their Antimicrobial Activities. *Phosphorus Sulfur Silicon Relat. Elem.* **2007**, *182*, 529–536. https://doi.org/10.1080/10426500601013224.
(71) Gbaguidi, F. A.; Kpoviessi, S. S. D.; Kapanda, C. N.; Muccioli, G. G.; Lambert, D. M.; Accrombessi, G. C.; Mansourou, M.; Poupaert, J. H. *African J. Pure Appl. Chem.* **2011**, *5*, 168–175.
(72) For more information on COST Action CA18112 'Mechanochemistry for Sustainable Industry' (MechSustInd): https://www.mechsustind.eu/ (accessed May 4, 2026).

(73) Biela, J.; Stalla, M.; Rabe, L.; Machado, D.; Evers, G.; Ansems, S. *Impact Assessment Study on Innovation in COST Actions (November 2024). https://www.cost.eu/uploads/2025/01/COST-Impact-Assessment-Innovation-112024.pdf (accessed May 4, 2026)*.
(74) Hernández, J. G.; Halasz, I.; Crawford, D. E.; Krupicka, M.; Baláž, M.; André, V.; Vella-Zarb, L.; Niidu, A.; García, F.; Maini, L.; Colacino, E. European Research in Focus: Mechanochemistry for Sustainable Industry (COST Action MechSustInd). *Eur. J. Org. Chem.* **2020**, No. 1, 8–9. https://doi.org/10.1002/ejoc.201901718.
(75) COST | European Cooperation in Science and Technology,https://www.cost.eu/ (accessed May 4, 2026).

Breathing new life into old processes: continuous mechanochemistry enables green manufacturing of essential pharmaceuticals silver(I) sulfadiazine and phenytoin.

Lea Čolakić,[1,‡] Andrea Casagrande,[2,3,‡] Goran Miletić,[4] Ernest Meštrović,[4,*] Evelina Colacino,[2,*] Ivan Halasz[4,*]

[1] Division of Physical Chemistry, Ruđer Bošković Institute, Bijenička cesta 54, 10000 Zagreb, Croatia

[2] ICGM, Univ Montpellier, CNRS, ENSCM, 34293 Montpellier, France

[3] Virumaa College, Tallinn's University of Technology, Järveküla tee 75, Kohtla-Järve, 30322, Estonia.

[4] Faculty of Chemical Engineering and Technology, University of Zagreb, Trg Marka Marulića 19, 10000 Zagreb, Croatia

Corresponding authors: emestrov@fkit.unizg.hr; ivan.halasz@irb.hr; evelina.colacino@umontpellier.fr

This document consists of 22 pages and includes 13 figures and 3 data tables.

[‡] Equal contribution

INDEX

Materials and methods	3
Elemental analysis of SSD and SDA	3
Crystal structure solution of SSD intermediate	4
Screw profiles	5
Figure S1. SSD screw profile	5
Figure S2. PHE screw profile configA	6
Figure S3. PHE screw profile configB	6
Figure S4. PHE screw profile configC	7
Figure S5. PHE screw profile config0	8
Experimental part	8
Preparation of SSD by BM and TSE	9
Table S1. SSD PXRD peaks	10
Preparation of PHE by TSE	10
Figure S6. Residual crude in the barrel	12
Torque and barrel-temperature monitoring	12
Figure S7. LiOH monohydrate monitoring	13
Figure S8. NaOH monitoring	14
Figure S9. KOH monitoring	15
Figure S10. DGU DSC	16
Figure S11. PHE Rietveld comparison	17
Table S2. PHE PXRD peaks	18
Figure S12. DGU PXRD pattern	20
Table S3. DGU PXRD peaks	20
Figure S13. LAG extrudate	21
Technology assessment and green chemistry metrics	22
References	22

MATERIALS AND METHODS

Chemicals. Silver(I) oxide (99+%) was supplied by Alfa Aesar GmbH (Germany) in the form of black powder. Sulfadiazine was supplied by BLD Pharmatech GmbH (Germany) in the form of white powder. Ammonia solution (25%) was supplied by Gram-Mol (Croatia). Benzil (98%) was supplied by Fluorochem (United Kingdom) in the form of yellow powder. Urea (> 99%) was supplied by Fluorochem (United Kingdom) in the form of white powder. Potassium Hydroxide (≥ 85%) was supplied by Sigma Aldrich GmbH (Germany) in the form of white powder. Citric acid (anhydrous, ≤100%) was supplied by BLD Pharmatech GmbH (Germany) in the form of white powder.

Solid-State DFT. Solid-state DFT calculations were performed by using Quantum ESPRESSO package. Plane waves were employed as a basis set with energy cutoff of 60.0 Ry and a cutoff for charge density and potential of 480.0 Ry. Interaction of ion cores with valence electrons was described with standard solid-state pseudopotentials (SSSP). Exchange-correlation energy was calculated within generalized gradient approximation (GGA) according to the Perdew, Burke and Ernzerhof (PBE). Grimme DFT-D3 approximation was employed for description of van der Waals interaction.

Liquid nuclear magnetic resonance (NMR) spectroscopy. *For Silver(I) sulfadiazine (SSD):* ^{1}H and ^{13}C NMR spectra were recorded on a Bruker Avance III HD 600 MHz/54 mm Ascend spectrometer at room temperature in DMSO-d_6. Chemical shifts (δ) of ^{1}H-NMR and ^{13}C-NMR spectra are reported in ppm relative to residual solvent signals (DMSO in DMSO-d_6: δ = 2.50 ppm for ^{1}H NMR and δ = 39.52 ppm for ^{13}C NMR). *For Phenytoin (PHE) and Diglycouril (DGU)*: ^{1}H and ^{13}C NMR spectra were recorded on a Bruker 400 *MHz* spectrometer at room temperature in DMSO-d_6. Chemical shifts (δ) of ^{1}H-NMR and ^{13}C-NMR spectra are reported in ppm relative to residual solvent signals (DMSO in DMSO-d_6: δ = 2.50 ppm for ^{1}H NMR and δ = 39.52 ppm for ^{13}C NMR). The multiplicity was reported with the following abbreviations: s = singlet, m = multiplet.

Elemental analysis. *For silver(I) sulfadiazine (SSD):* The carbon, hydrogen, nitrogen, and sulfur (CHNS) contents were determined by elemental analysis using an Elementar vario MACRO cube CHNS analyzer. Samples weighing up to 5 mg were accurately weighed into tin foil capsules and analyzed by high-temperature combustion, with temperatures reaching up to 1800 °C in the combustion zone. The resulting gaseous combustion products were separated within the analyzer and quantified using a thermal conductivity detector (TCD). Silver sulfadiazine samples were prepared and analyzed according to the standard analytical procedure, using sample masses of up to 5 mg.

For Phenytoin (PHE): The carbon, hydrogen and nitrogen CHN analyses were performed using an Elementar Vario Micro Cube analyzer. Samples were encapsulated in tin and subjected to catalytic combustion at 1150 °C. The combustion gases were passed through a copper reduction furnace at 850 °C under helium, separated by temperature-programmed desorption and quantified using a thermal conductivity detector.

Powder X-ray diffraction (XRD). *For silver(I) sulfadiazine (SSD)*: Powder X-ray diffraction analysis was performed using a Malvern Panalytical Aeris X-ray diffractometer. All samples were placed as a thin layer onto a silicon holder. A copper anode X-ray tube was used as the radiation source, and the beam was passed through a nickel filter. Data was collected using a PIXcel3D-Medipix3 detector. Rietveld analysis was performed using the TOPAS7 software (Figures 4, 5 and S11). *For Phenytoin (PHE) and Diglycouril (DGU):* The PXRD measurements were carried out on a Philips X'Pert PRO MPD diffractometer, fitted with a Reflection-Transmission Spinner for measurements in reflection mode with a X'Celerator Scientific detector with a 0.020 mm nickel Filter. The geometry is Bragg Brentano, radiation is CuK_α (λ = 1.5406 + 1.5444 Å), K_β = 1.3923 Å and scan mode θ/θ coupled.

Differential scanning calorimetry (DSC). *For silver(I) sulfadiazine (SSD)*: Differential scanning calorimetry (DSC) analyses were carried out using PerkinElmer DSC 8500 differential scanning calorimeter. Nitrogen was used as purge gas. The thermal properties were analyzed at 5°C/min between 20 and 500°C. *For Phenytoin (PHE) and Diglycouril (DGU):* Differential scanning calorimetry (DSC) analyses were carried out using a Netzsch DSC200F3 calorimeter with intra-cooler. Constant calibration was performed using adamantane, biphenyl, indium, zinc, tin and bismuth standards. Nitrogen was used as the purge gas. The thermal properties were analyzed at 5°C/min between 20 and 500°C with two dynamic ramps to observe the reaction enthalpy of the cross-linking determined as exothermic peak (1^{st} ramp) and the glass transition temperature determined as the inflexion value in the heat capacity jump (2^{nd} ramp).

IR Thermometer: To record the temperature of experiment listed in Table 2, entry 8, 66IR200 InfraRed Thermometer was used.

Liquid Chromatography coupled to Mass Spectrometry (LC-MS). The samples are dissolved in eluent B before their injection. The analyses were carried out on a microOtof-Q II mass spectrometer (Bruker) coupled to a U 3000 chromatographic chain (Thermoscientific). The analyses are carried out in FIA (Flow Injection Analysis). Eluent A is water acidified with 0.1% formic acid. Eluent B is acetonitrile acidified with 1% formic acid. The flow rate is 0.4 mL/min of a 50-50 mixture of the two eluents. The ionization mode is electrospray. The source parameters are as follows: Capillary voltage 4500 V; nebulizer gas pressure 0.5 Bar; drying gas flow rate: 4 L/min; source temperature 180 °C. The analyses are carried out in both positive and negative modes. The injected volume is 0.1 µL and the analysis time is 1 min.

Ball milling experiments for Silver(I) sulfadiazine (SSD) were performed using a Retsch MM200 laboratory ball mill, modified for *in situ* monitoring, in polymethylmethacrylate (PMMA) reaction vessels of 14 mL internal volume, at the frequency of 30 Hz and using two stainless steel balls of 7 mm in diameter (m_{ball} = 1.4 g each) as the grinding media.

In situ monitoring experiments by ball-milling. The mill was put into operation remotely and in situ data collection at the European Synchrotron Radiation Facility (ESRF) in Grenoble (France) on the old beamline ID15B (this beamline has since been rebuilt for another purpose) was started together with milling, as described in the experimental part. The monochromatic X-ray beam was selected with a bent Laue Si crystal, producing a circular beam footprint of 300 µm² at the sample. A flat-panel Pixium charge-coupled detector collected diffractograms with the time resolution of 10 s. Data analysis of diffraction patterns collected in situ during milling monitoring was performed by Rietveld refinement using the program TOPAS7 as described before. Plotting was done using Matplotlib for Python.

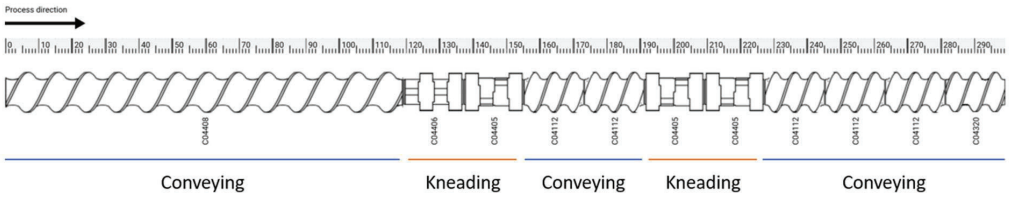
Crystal structure solution of SSD intermediate (new SSD polymorph). This intermediate proved to be too unstable to be isolated or prepared ad hoc for ex situ characterisation. Given the poor quality of the in situ collected diffraction data, attempts of structure solution from in situ data were unfruitful, even towards the identification of the unit cell. Therefore, the preparation of the intermediate phase was attempted ex situ. For this purpose, a mixture of the reactants (Ag2O and SDA in a 1:2 ratio) was mixed in a mortar. The resulting mixture was then placed onto a silicon holder used for PXRD measurements and moistened with a small drop of distilled water. A solution of 25 wt% aqueous ammonia (η = 0.07 µL/mg) was applied at the outer edge of the circular holder so that it did not touch the reactant mixture. This setup was covered with Kapton foil to allow the gaseous ammonia to diffuse towards the sample, and a PXRD experiment on a laboratory diffractometer was immediately initiated using a rapid-acquisition mode, yielding a pattern in which the intermediate phase was the dominant component.

Due to the possible presence of reflections from other phases (unreacted sulfadiazine and silver oxide and SSD, the fractions of which may have changed even during the short data collection time), it was necessary to use in-situ data to correctly assign peaks that belong to the intermediate (Figure 1 in the main manuscript). This tedious procedure by hand ultimately resulted in a set of around 15 reliable peaks that yielded a monoclinic unit cell (a = 18.868 Å, b = 5.327 Å, c = 12.868 Å, β = 106.75°) of the volume V = 1238.49 Å3 and a probable assignment of the C2 space group. The unit cell volume corresponds well to the unit cell volume of the final silver sulfadiazine (V = 1195.91 Å3) indicating that the intermediate phase contains both sulfadiazine and silver(I). Moreover, the slightly larger unit cell volume of the intermediate than the product silver sulfadiazine indicates a lower-density, metastable structure aligning with it presenting as an intermediate.

The crystal structure of the intermediate phase was solved from laboratory powder diffraction data by simulated annealing in direct space, using a rigid-body description for sulfadiazine and a free silver ion, and was confirmed by comparison to the in situ collected data. Since the refined structure model still exhibited some too close intermolecular contacts, the structure was further optimised by solid-state DFT in P1. The optimised model confirmed the C2 symmetry, and the overall geometry did not differ significantly from the experimentally obtained starting model (Figure 2 in the main manuscript). We also noticed that the standard deviations of the experimentally derived atomic coordinates were unusually large, and we have therefore decided to report atom coordinates obtained by the DFT optimisation, except that hydrogen atom positions were additionally normalised to conform to standard crystallographic bond lengths.

SCREW PROFILES

Figure S1. Screw profile for the synthesis of SSD (Scheme 1).

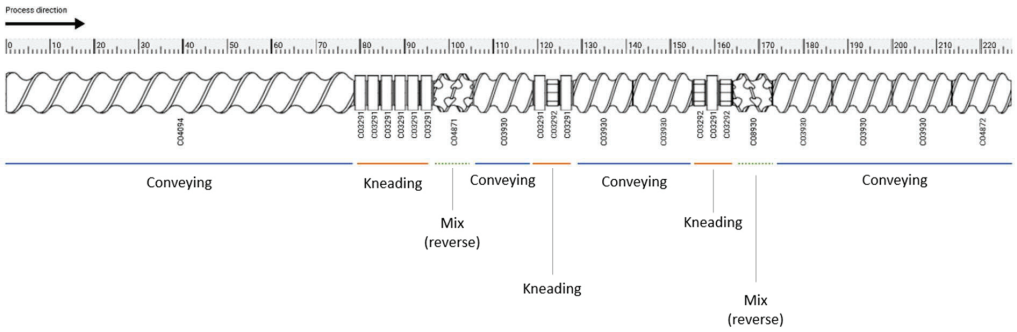


Segment code	Type	Phase	Number of units
C04408	Conveying	n.a.	1
C04406	Kneading	90°	1
C04405	Kneading	60°	1
C04112	Conveying	n.a.	2
C03930	Conveying	n.a.	1
C04405	Kneading	60°	2
C04112	Conveying	n.a.	3
C04320	Conveying (screw end)	n.a.	1

Legend: n.a. = not applicable.

For Phenytoin (PHE): TSE was carried out using a Three-Tec ZE9/12 hybrid extruder, in configuration ZE9 (9 mm, 25:1 length-to-diameter ration, L/D) corotating twin screw extruder with 4 heating zones. Screw profiles were modular. The screw configurations used in the synthesis of **PHE** are indicated in Figures S2-S5. In all configurations the section of six kneading elements C03291 are assembled at a 30° angle the one from the other.

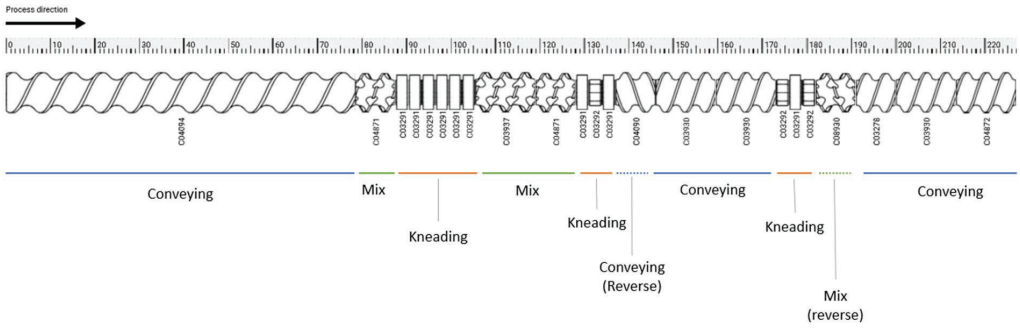
Figure S2. Screw profile for the synthesis of **PHE**, referred to as *configA* (Table 1).



Segment code	Type	Phase	Number of units
C04094	Conveying	n.a.	1
C03291	Kneading	30°	6
C04871	Mix reverse	n.a.	1
C03930	Conveying	n.a.	1
C03291	Kneading	0°	1
C03292	Kneading	90°	1
C03291	Kneading	0°	1
C03930	Conveying	n.a.	2
C03292	Kneading	90°	1
C03291	Kneading	0°	1
C03292	Kneading	90°	1
C08930	Mix reverse	n.a.	1
C03930	Conveying	n.a.	3
C04872	Conveying (screw end)	n.a.	1

Legend: n.a. = not applicable.

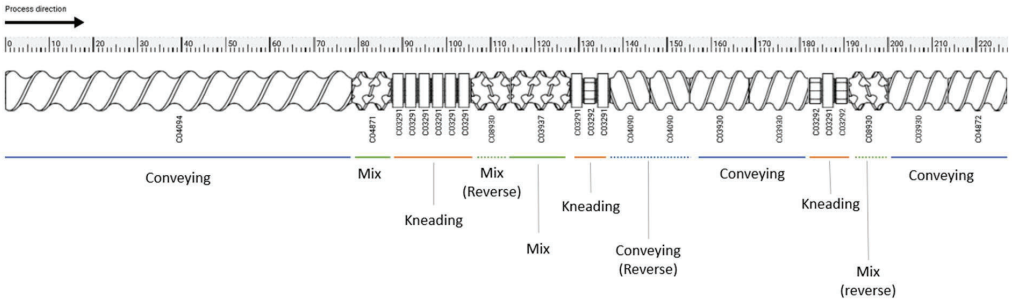
Figure S3. Screw profile for the synthesis of PHE, referred to as *configB* (Table 2, entries 1–8; Table 3; and Table 4, entries 1, 2 and 5).



Segment code	Type	Phase	Number of units
C04094	Conveying	n.a.	1
C04871	Mix	n.a.	1
C03291	Kneading	30°	6
C03937	Mix	n.a.	1
C04871	Mix	n.a.	1
C03291	Kneading	0°	1
C03292	Kneading	90°	1
C03291	Kneading	0°	1
C04090	Conveying Reverse	n.a.	1
C03930	Conveying	n.a.	2
C03292	Kneading	90°	1
C03291	Kneading	0°	1
C03292	Kneading	90°	1
C08930	Mix Reverse	n.a.	1
C03278	Conveying	n.a.	1
C03930	Conveying	n.a.	1
C04872	Conveying (screw end)	n.a.	1

Legend: n.a. = not applicable.

Figure S4. Screw profile for the synthesis of PHE referred to as *configC* (Table 4, entries 3 and 4).

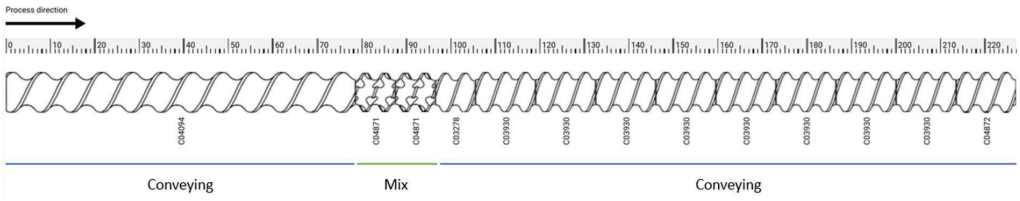


Segment code	Type	Phase	Number of units
C04094	Conveying	n.a.	1
C04871	Mix	n.a.	1
C03291	Kneading	30°	6
C08930	Mix reverse	n.a.	1
C04871	Mix	n.a.	1
C03291	Kneading	0°	1
C03292	Kneading	90°	1
C03291	Kneading	0°	1
C04090	Conveying Reverse	n.a.	2
C03930	Conveying	n.a.	2
C03292	Kneading	90°	1
C03291	Kneading	0°	1
C03292	Kneading	90°	1
C08930	Mix Reverse	n.a.	1
C03930	Conveying	n.a.	1
C04872	Conveying (screw end)	n.a.	1

Legend: n.a. = not applicable.

Reverse elements were incorporated to promote mixing and increase material retention. Residence times and residence-time distributions were not measured.

Figure S5. Screw profile for the synthesis of PHE referred to as *config0* (Table 2, entry 9).

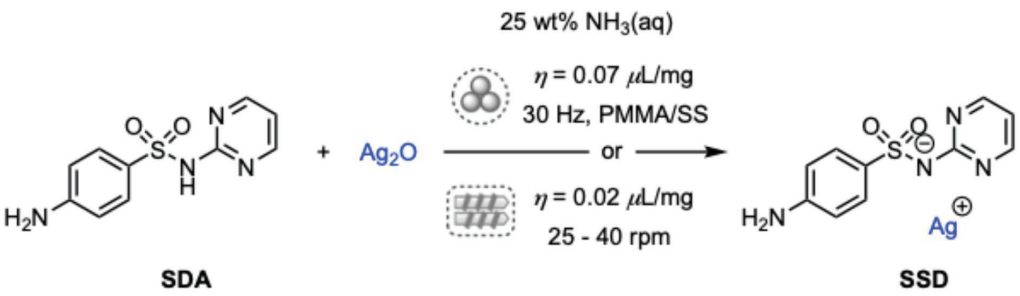


Segment code	Type	Phase	Number of units
C04094	Conveying	n.a.	1
C04871	Mix	n.a.	2
C03278	Conveying	n.a.	1
C03930	Conveying	n.a.	8
C04872	Conveying (screw end)	n.a.	1

Legend: n.a. = not applicable.

EXPERIMENTAL PART.

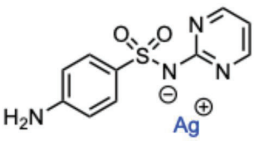
Preparation of Silver(I) sulfadiazine (SSD, Scheme 1) by BM and by TSE.



Ball milling experiments for Silver(I) sulfadiazine (SSD) were performed using a Retsch MM200 laboratory ball mill, modified for *in situ* monitoring, in polymethyl methacrylate (PMMA) reaction vessels of 14 mL internal volume, at the frequency of 30 Hz and using two stainless steel balls of 7 mm in diameter (m_{ball} = 1.4 g each) as the grinding media. The reactants were weighed together in one half of the reaction vessel while 25 wt% aqueous ammonia (50 μL, η = 0.07 μL/mg) was added to the other. Care was taken to ensure that the liquid did not come into contact with the solids during sample preparation and mounting on the mill arm. The mill was put into operation remotely and in situ data collection at the European Synchrotron Radiation Facility (ESRF) in Grenoble on the old beamline ID15B (this beamline has since been rebuilt for another purpose) was started together with milling, as described before. The monochromatic X-ray beam was selected with a bent Laue Si crystal, producing a circular beam footprint of 300 μm² at the sample. A flat-panel Pixium charge-coupled detector collected diffractograms with the time resolution of 10 s. Data analysis of diffraction patterns collected in situ during milling monitoring was performed by Rietveld refinement using the program TOPAS7 as described before. Plotting was done using Matplotlib for Python.

Twin -screw extrusion (TSE) for silver(I) sulfadiazine (SSD). TSE was performed using a Three-Tec ZE12 ECO twin screw extruder (screw diameter 12 mm, L/D ratio = 25:1, with parallel segment orientation) with a screw configuration consisting of both kneading and conveying elements (Figure S1). The screw rotation frequency was initially set to 25 rpm and was increased to 40 rpm after the first portion of product exiting the screws had been collected in the receiving vessel. Aqueous NH_3 (25% wt% , 300 μL, η = 0.02 μL/mg) was occasionally added in the extruder barrel through the opening port for liquid addition positioned close to the feeder opening. The mixture of silver(I) oxide (3.83 g, 16.5 mmol) and sulphadiazine (SDA, 8.27 g, 33.0 mmol) in the 1:2 molar ratio (the total mass was 12.1 g) delivered 10.5 g of **SSD** with additional product material remaining in the extruder barrel. The screw configuration used in the synthesis of **SSD** is indicated in Figure S1.

In situ monitoring studies by PXRD to prepare Silver(I) sulfadiazine (SSD), CAS [22199-08-2], by ball-milling. A seminal example on *in situ* monitoring synthesis of SSD by RAMAN was previously reported.[1] The crystalline form of silver(I) sulfadiazine complexes prepared by mechanochemistry was previously described.[2]



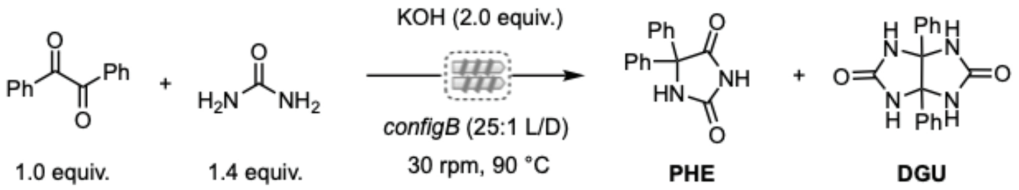
SSD

CAS [22199-08-2].[3] **m.p.** (by DSC) 285.2 °C (litt. 285 °C);[4] **^{1}H NMR** (600 MHz, DMSO-d_6), δ (ppm): 8.42 (d, J = 4.91 *Hz*, 2H), 7.54 (d, J = 8.58 *Hz*, 2H), 6.81 (t, J = 4.03 *Hz*, 1H), 6.52 (d, J = 8.64 *Hz*, 2H), 5.70 (s, 2H). **^{13}C NMR** (151 MHz, DMSO-d_6), δ (ppm): 161.2, 159.2, 151.6, 129.8, 128.2, 111.9, 111.3. **Elemental Analysis** calcd. for [$C_{10}H_9AgN_4O_2S$]: C, 33.63; N, 15.69; H, 2.540. Found: C, 33.31; N, 15.70; H, 2.574, measured purity ≥99.9%; Calcd. for SDA [$C_{10}H_{10}N_4O_2S$]: C, 47.99; N, 22.39; H, 4.03. Found: C, 47.75; N, 22.45; H, 4.083; measured purity ≥99.9%.

Table S1. Most intense peaks for PXRD diffractogram of Silver(I) sulfadiazine (Scheme 1).

Pos. [°2Th.]	Height [cts]	FWHM Left [°2Th.]	d-spacing [Å]	Rel. Int. [%]
8.6756	9997.37	0.0216	10.18419	43.14
8.7013	11506.16	0.0180	10.15417	49.65
8.7190	10672.30	0.0236	10.14204	46.05
10.1567	23173.99	0.0620	8.70935	100.00
16.0137	2698.19	0.0144	5.53011	11.64
18.4068	1938.34	0.0708	4.82016	8.36
19.7870	3121.04	0.0216	4.48325	13.47
20.5528	2848.46	0.0827	4.32147	12.29
23.5497	1602.51	0.0531	3.77788	6.92
24.0054	1180.24	0.0590	3.70717	5.09
24.1644	3566.67	0.0180	3.68010	15.39
26.5772	1565.89	0.0864	3.35122	6.76
27.7875	2300.96	0.0216	3.20794	9.93
27.9998	1844.48	0.0648	3.18410	7.96

Preparation of Phenytoin (PHE, Table 4, entry 1) by TSE.



Benzil (15.21 g, 71.6 mmol, 1.0 equiv.), urea (6.08 g, 100.24 mmol, 1.4 equiv.), and potassium hydroxide (KOH, 9.46 g, 143.2 mmol, 2.0 equiv.) were introduced into a 50 mL glass beaker and premixed using a spatula (total mass of premix 30.75 g). Screw profile *configB* (Figure S3) was used; the screw speed was 30 rpm and the extrusion process was conducted at 90 °C (feeding the reactants in the pre-heated barrel). The premix was introduced into the hopper by approximately continuous sprinkling with a spatula over 37 min. Feeding was manual, and the instantaneous feed rate was not measured. Extrusion continued for a further 2 min after completion of premix feeding. The material collected during this stage was designated F0 (m = 21.26 g), that reflects a 9.49 g of mass holdup in the barrel. After completion of the reaction-premix stage, three successive 9 g portions of urea were introduced to recover material remaining in the extruder. The corresponding extrudates were collected separately and they are referred as F1, F2 and F3, and examined by TLC (eluent: cyclo-octane : AcOEt 1:1 v/v). F0, F1 and F2 were worked up separately. No PHE was detected by TLC in F3, which was discarded without work-up. The extrudate (referred to as F0) and the individual purge fractions (F1 and F2) were treated separately, following identical workup procedure. Therefore, each fraction (F0, F1 and F2) was dissolved in 200 mL of water and stirred for 10 minutes, was then transferred into a vacuum filtration funnel and washed with water (4 x 20 mL) at room temperature. The precipitate was isolated as an off-white solid and dried overnight in oven at 90°C. This solid was identified as 3a,6a-diphenylglycoluril (**DGU**) (0.97 g, 5% yield, calculated from the sum of the mass recovered from individual extrudate fractions: F0: 0.673 g, F1: 0.216 g, F2: 0,081 g). The yellow filtrate (pH = 14) from the individual fractions was collected and acidified with 30 mL of an aqueous solution of 10% w/w citric acid, resulting in a decrease of pH from 14 to 6. The resulting white precipitate (for each fraction) was filtered under vacuum and washed with water (4 x 20 mL) at room temperature (another portion of 20 mL of 10% w/w citric acid was added to each filtrate, to be sure that no more precipitate, **PHE** was formed, this operation was done only as a control and was excluded from the calculations of metrics). The white precipitates from each fraction were dried in oven at 90°C overnight to afford a total amount of 14.04 g (78% yield, calculated from the addition of the mass from individual extrudate fractions: F0: 10.06 g, F1: 2.95 g, F2: 1.02 g) of the phenytoin (**PHE**) compound as a white powder. The ^{1}H and ^{13}C NMR data for both **PHE**[5] and **DGU**[5-6] were consistent with the data published in the literature. The real-time collection of the extrudate (F0) is shown in the Supporting Video V3. As an example, the aspect of the crude remaining in the barrel before the purges is shown in Figure S6.

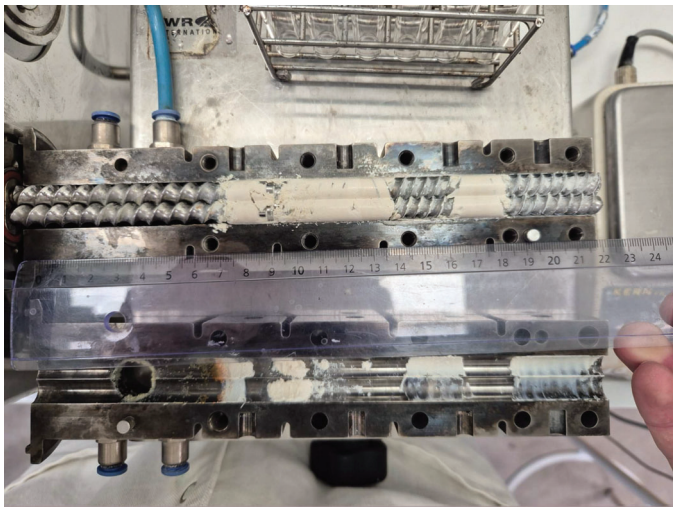


Figure S6. Barrel showing the aspect of the residual fraction of crude before three cycles of purge with urea (*c.f.*, experiment in Table 4, entry 1).

Time-resolved torque and barrel-temperature monitoring during Phenytoin extrusion

Additional extrusion experiments were performed using $LiOH{\cdot}H_2O$, NaOH and KOH with *configA*, a barrel-temperature setpoint of 80 °C and a screw-speed setpoint of 30 rpm. The nominal benzil:urea molar ratio was 1.0:1.0:2.0, and the premix mass was 30.75 g. The premix was introduced by approximately continuous manual sprinkling with a spatula. Torque and temperatures of the individual four-barrel sections (H1 to H4) recorded by the four barrel-zone sensors were monitored over time. Instantaneous feeding rate was not measured. For the experiments that uses $LiOH{\cdot}H_2O$ and NaOH (Figure S7 and S8) as bases it can be seen the torque gradually increasing until reaching the safety instrument limits and triggering the motor block, while for the experiment using KOH (Figure S9) it can be seen the torque gradually decreasing until the extrusion process is terminated after the end of the addition of the premix in the hopper.

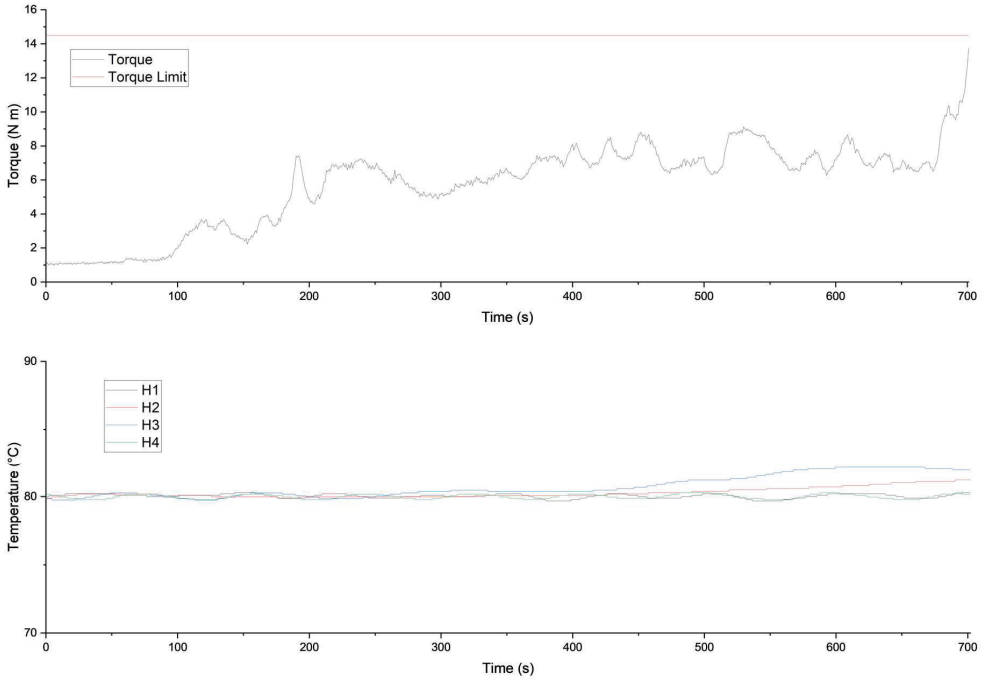


Figure S7. Torque evolution over time (top) and temperature evolution over time (bottom) related to the experiment listed in Table 1 entry 1 (using $LiOH \cdot H_2O$ as base).

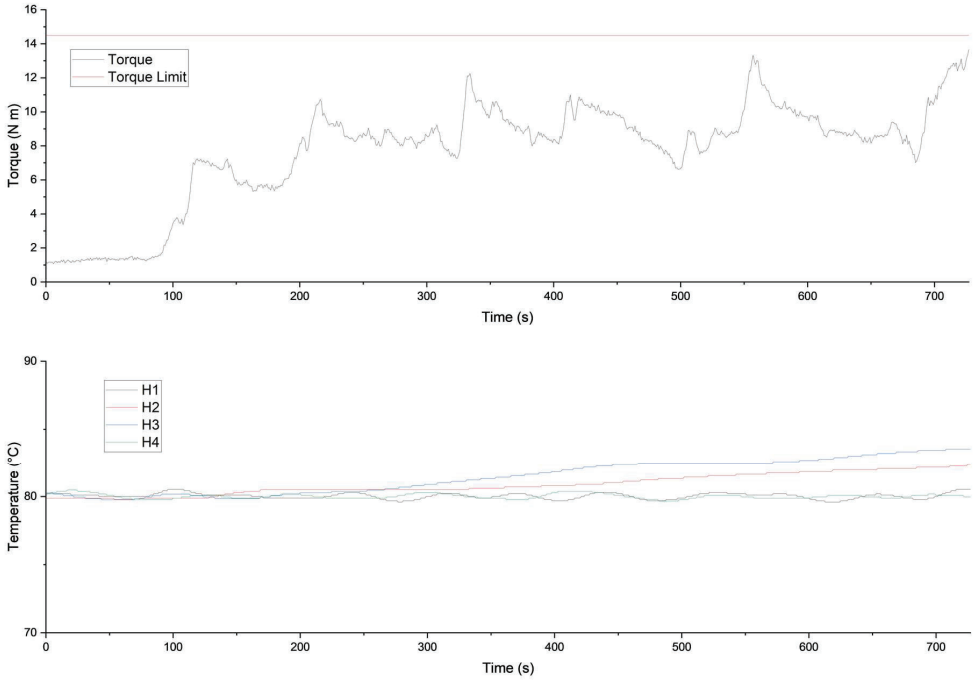


Figure S8. Torque evolution over time (top) and temperature evolution over time (bottom) related to the experiment listed in Table 1 entry 2 (using NaOH as base).

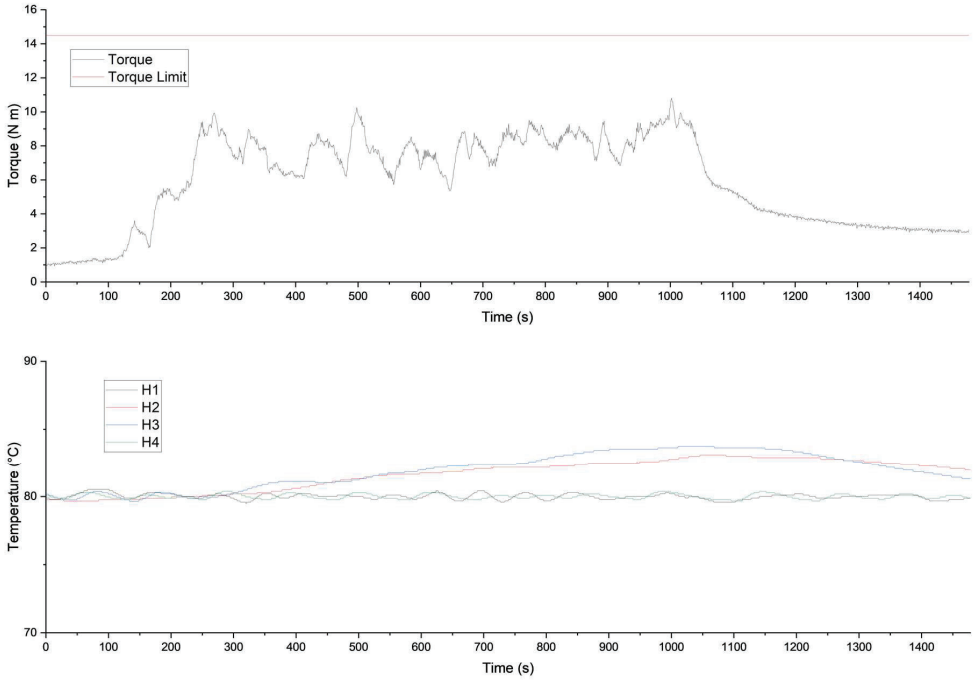
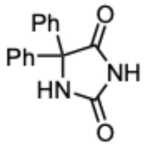


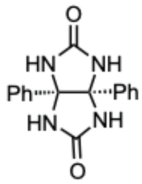
Figure S9. Torque evolution over time (top) and temperature evolution over time (bottom) related to the experiment listed in Table 1 entry 3 (using KOH as base).



PHE

CAS [57-41-0].[7] **m.p.** (by DSC)[5a] 291.1 °C, (litt. 291-294 °C, in a capillary);[8] for commercial phenytoin: 295.6°C determined by DSC.[5a] **^{1}H NMR** (400 MHz, DMSO-d_6),[5] δ (ppm): 11.10 (s, 1H), 9.31 (s, 1H), 7.42 – 7.32 (m, 10H). **^{13}C NMR** (100 MHz, DMSO-d_6),[5] δ (ppm): 174.8, 156.0, 139.9, 128.5, 128.0, 126.6, 70.2. **LC-MS ESI (+)** *m/z*: 253.10 $[M+H]^+$, 182.10 $[M+H-(C_6H_5)]^+$. **HRMS ESI (+)** *m/z* $[M+H]^+$ calcd. for $C_{15}H_{13}N_2O_2$ 253.0972, found 253.0980.**^{1}H qNMR** 400 MHz, DMSO-d_6) purity assay using 1,3,5-trimethoxybenzene as internal standard (20 mg, 0.12 mmol) and 20 mg of analyte (0.08 mmol) in 600 μL of deuterated solvent): 99.9% (w/w). **Elemental Analysis** calcd. for $[C_{15}H_{12}N_2O_2]$: C, 71.42; H, 4.79; N, 11.10. Found (average for two distinct analyses): C, 71.38; H, 4.72; N, 7.60; measured purity ≥99.9%.

***cis*-Tetrahydro-3a,6a-diphenylimidazo[4,5-*d*]imidazole-2,5(1*H*,3*H*)-dione** (or **3a,6a-diphenylglycoluril, DGU). CAS [101241-21-8]**.[9]



DGU

m.p. (by DSC, Figure S10) 331.2 °C (litt. > 320 °C in a capillary).[9] **^{1}H NMR** (400 MHz, DMSO-d_6),[6] δ (ppm): 7.78 (s, 4H), 7.07 (s, 10H, ArH). **^{13}C NMR** (101 MHz, DMSO-d_6),[5a, 6] δ (ppm): 161.2, 138.8, 128.2, 127.8, 127.5, 82.3. **LC-MS ESI (-)** *m/z*: 587.2 $[2M–H]^-$, 293.1 $[M–H]^-$.

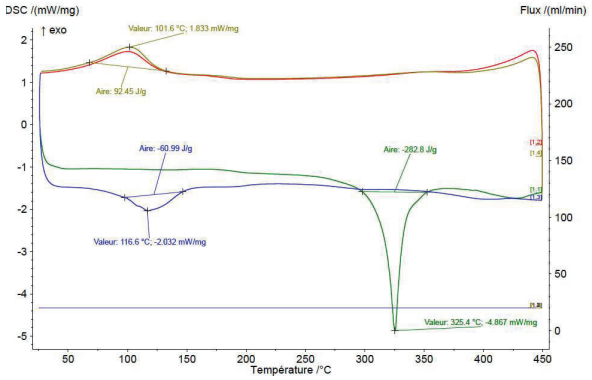


Figure S10. Thermal analysis by Differential Scanning Calorimetry (DSC) for 3a,6a-diphenylglycoluril (**DGU**).

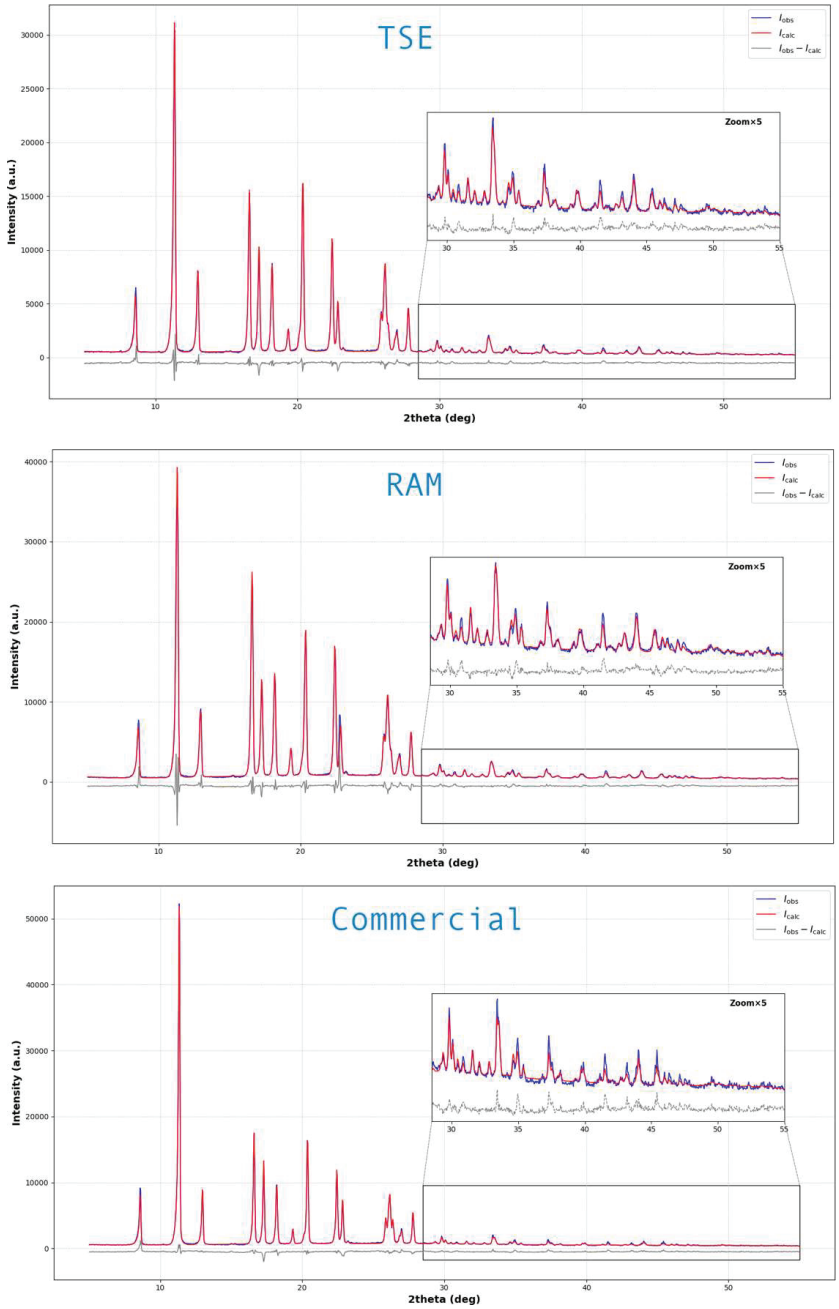


Figure S11. Rietveld analysis of the products obtained by (top) TSE, (middle) liquid-assisted resonant acoustic mixing (LA-RAM)[5a], and the commercial sample of **PHE**, all corresponding to pure phenytoin. Experimental data are shown in blue, calculated data in red, and the difference curve in gray. Calculated data based on the crystal structure from the CSD (refcode: PHYDAN03).

Table S2. Most intense peaks for PXRD diffractogram of **PHE** prepared by TSE (Table 4, entry 1), as per Figure S11.

Pos. [°2Th.]	Height [cts]	FWHM Left [°2Th.]	d-spacing [Å]	Rel. Int. [%]
7.5397	45.43	0.0974	11.72544	0.15
8.6045	5718.61	0.1299	10.27676	19.23
11.3431	29739.36	0.1624	7.80099	100.00
12.9844	7859.74	0.1624	6.81836	26.43
15.1272	337.59	0.5196	5.85700	1.14
16.6120	14617.63	0.1624	5.33668	49.15
17.2899	8824.09	0.1299	5.12895	29.67
18.2062	8461.79	0.1624	4.87282	28.45
19.3448	2290.07	0.1299	4.58851	7.70
20.3734	15422.31	0.1624	4.35911	51.86
22.4397	10471.32	0.1299	3.96218	35.21
22.8391	4249.51	0.1299	3.89378	14.29
23.2148	703.53	0.0974	3.83161	2.37
25.8592	3568.11	0.0974	3.44547	12.00
26.1562	7941.80	0.1624	3.40702	26.70
26.4166	2542.26	0.0974	3.37402	8.55
26.9867	2314.68	0.2273	3.30402	7.78
27.7978	4179.99	0.1624	3.20944	14.06
28.6151	400.53	0.1948	3.11961	1.35
29.3799	541.31	0.0974	3.04011	1.82
29.8289	1358.92	0.1299	2.99537	4.57
30.0868	842.26	0.0974	2.97028	2.83
30.4655	425.11	0.0974	2.93421	1.43
30.8725	593.29	0.1299	2.89645	1.99
31.5732	655.20	0.1299	2.83375	2.20
32.0888	446.02	0.1624	2.78939	1.50
32.8134	446.82	0.1624	2.72943	1.50
33.4395	1792.25	0.1948	2.67974	6.03
34.6406	517.59	0.1299	2.58953	1.74
34.9495	808.94	0.1624	2.56735	2.72
35.3864	460.99	0.1624	2.53664	1.55
36.8426	254.45	0.1948	2.43966	0.86
37.3143	936.59	0.1624	2.40990	3.15
37.5716	478.26	0.0974	2.39398	1.61
38.0968	274.29	0.3247	2.36218	0.92
39.8527	461.27	0.1299	2.26206	1.55
41.5207	664.29	0.2273	2.17496	2.23
43.1651	446.99	0.1948	2.09584	1.50
44.0422	759.81	0.1299	2.05612	2.55
45.4221	504.45	0.2273	1.99681	1.70
46.0079	270.52	0.1299	1.97274	0.91
46.3385	328.23	0.1299	1.95943	1.10
47.1411	301.19	0.1299	1.92793	1.01
47.5822	212.68	0.1299	1.91108	0.72
49.5286	224.93	0.0974	1.84044	0.76

50.8722	111.40	0.1948	1.79495	0.37
51.2624	97.41	0.2598	1.78220	0.33
52.3742	86.50	0.1948	1.74695	0.29
53.3628	104.66	0.2598	1.71690	0.35
53.8932	176.63	0.0974	1.70125	0.59

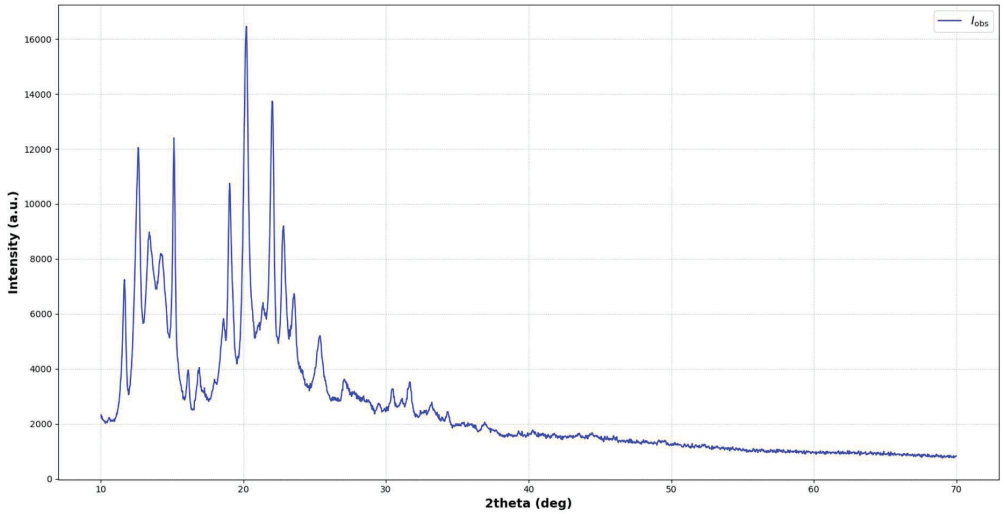


Figure S12. PXRD pattern of **DGU** obtained as a by-product in the synthesis of **PHE** by TSE (Table 4, entry 1 – after purge).

Table S3. Most intense peaks for PXRD diffractogram of **DGU** obtained as by-product in the synthesis of **PHE** by TSE (Table 4, entry 1 – after purge).

Pos. [°2Th.]	Height [cts]	FWHM Left [°2Th.]	d-spacing [Å]	Rel. Int. [%]
11.6618	5081.45	0.1624	7.58851	35.25
12.6371	9994.43	0.2598	7.00496	69.34
13.4105	6844.68	0.2598	6.60267	47.49
14.2568	6104.10	0.3247	6.21254	42.35
15.1373	10333.54	0.1299	5.85310	71.69
16.1273	1938.54	0.1299	5.49598	13.45
16.8818	1934.25	0.2273	5.25200	13.42
17.9885	1639.60	0.1299	4.93130	11.37
18.6097	3834.86	0.2598	4.76807	26.60
19.0448	8708.08	0.1948	4.66012	60.41
20.2025	14414.40	0.2922	4.39560	100.00

Pos. [°2Th.]	Height [cts]	FWHM Left [°2Th.]	d-spacing [Å]	Rel. Int. [%]
21.3760	4446.38	0.1624	4.15687	30.85
22.0321	11832.27	0.2273	4.03455	82.09
22.8037	7258.00	0.2273	3.89975	50.35
23.5512	4839.79	0.1948	3.77764	33.58
25.3611	3374.84	0.2922	3.51200	23.41
27.0761	1823.24	0.1624	3.29332	12.65
28.7019	1081.05	0.3897	3.11036	7.50
29.4967	1000.86	0.1948	3.02834	6.94
30.4521	1548.69	0.1624	2.93547	10.74
31.6740	1822.23	0.2598	2.82497	12.64
33.1924	1051.40	0.1948	2.69912	7.29
34.3286	795.44	0.1948	2.61235	5.52
36.0277	342.29	0.2598	2.49295	2.37
36.9145	420.01	0.3247	2.43508	2.91
40.3154	189.98	0.2598	2.23716	1.32
41.7760	88.70	0.3897	2.16226	0.62
43.4778	115.94	0.3897	2.08149	0.80
44.4567	148.38	0.5196	2.03790	1.03
49.3493	78.32	0.5196	1.84671	0.54



Figure S13. Extrudate obtained upon manual feeding of the pre-mixed solid reagents, while the LAG solvent (EtOH) was constantly added.

Technology assessment and green chemistry metrics. The calculations of the green metrics and productivity carried out by Chem21 toolkit[10] for the synthesis of **SSD** (in solution[11] and by ball-milling using $AgNO_3$[1] or Ag_2O) and **PHE** (in solution,[12] that was previously calculated,[5a] by ball-milling[6] and by Liquid-Assisted Resonant Acoustic Mixing,[5a] LA-RAM) were performed based on the experimental procedures reported in literature, referenced in Table 5, and evaluated by detailed Chem21 calculations, in a separate excel file, being as integrant part of the ESI.

References.

[1] I. Sović, S. Lukin, E. Meštrović, I. Halasz, A. Porcheddu, F. Delogu, P. C. Ricci, F. Caron, T. Perilli, A. Dogan and E. Colacino, *ACS Omega* **2020**, *5*, 28663-28672.

[2] D. R. Ferreira, A. Portet, P. C. Alves, P. Rijo, C. S. B. Gomes, M. T. Duarte, I. Halasz, E. Colacino, F. Emmerling and V. André, *CrystEngComm* **2025**, *27*, 7287-7294.

[3] N. C. Baenziger and A. W. Struss, *Inorg. Chem.* **1976**, *15*, 1807-1809.

[4] *British Pharmacopoeia* 4th ed., The Stationary Office – TSO publisher, London, 1999, vol. 1, p. 844.

[5] a) C. M. Chatzigiannis, S. M. Scalzullo, E. Colacino and M. E. Rivas, *ChemSusChem* **2025**, *18*, e202500110; b) L. Konnert, B. Reneaud, R. M. de Figueiredo, J.-M. Campagne, F. Lamaty, J. Martinez and E. Colacino, *J. Org. Chem.* **2014**, *79*, 10132-10142.

[6] F. Puccetti, S. Lukin, K. Užarević, E. Colacino, I. Halasz, C. Bolm and J. G. Hernández, *Chem. Eur. J.* **2022**, *28*, e202104409.

[7] H. Biltz, *Berichte der deutschen chemischen Gesellschaft* **1908**, *41*, 1379-1393.

[8] A. A. Magd El-Din, H. F. Roaiah, S. A. Elsharabasy and A. Y. Hassan, *Phosphorus Sulfur Silicon Relat. Elem.* **2007**, *182*, 529–536.

[9] F. A. Gbaguidi, S. S. D. Kpoviessi, C. N. Kapanda, G. G. Muccioli, D. M. Lambert, G. C. Accrombessi, M. Mansourou and J. H. Poupaert, *African J. Pure Appl. Chem.* **2011**, *5*, 168-175.

[10] C. R. McElroy, A. Constantinou, L. C. Jones, L. Summerton and J. H. Clark, *Green Chemistry* **2015**, *17*, 3111-3121.
[11] A. D. Lanchote Borges, G. Del Ponte, A. Federman Neto and I. Carvalho, *Quim. Nova* **2005**, *28*, 727-731.
[12] N. M. Arani and J. Safari, *Ultrason. Sonochem.* **2011**, *18*, 640-643.

Appendix 7

Publication VII

A. Casagrande, Y. Li, L. Brandon, V. Flaud, D. Kananovich, R. Aav, A. Niidu, F. Maseras, E. Colacino. Copper-Mediated Mechanochemical Nitrile Reduction in Mild Conditions Using Ammonia Borane and in silico Mechanistic Studies, **2026**, *submitted to a peer-reviewed journal*.

Copper-Mediated Mechanochemical Nitrile Reduction in Mild Conditions Using Ammonia Borane and *in silico* Mechanistic Studies

Andrea Casagrande,[a,b] *Yingzi Li,*[c] *Laurence Brandon,*[c] *Valerie Flaud,*[a] *Dzmitry Kananovich,*[b] *Riina Aav,*[b] *Allan Niidu,*[b] *Feliu Maseras,*[c]* *Evelina Colacino*[a]*

[a]ICGM, University of Montpellier, CNRS, ENSCM, Montpellier, France

[b]Tallinn University of Technology, Tallinn, Estonia

[c]Institute of Chemical Research of Catalonia (ICIQ-CERCA), The Barcelona Institute of Science and Technology, Avgda. Països Catalans 16, 43007, Tarragona, Spain.

KEYWORDS. Ball-milling, mechanochemistry, nitrile reduction, copper catalysis, Density functional theory (DFT).

ABSTRACT. Reduction of nitriles to primary amines is a fundamentally useful yet operationally demanding transformation, traditionally requiring pyrophoric hydride reagents, harsh catalytic hydrogenation, or hazardous ethereal solvents. Here we report the first mechanochemical protocol for the chemoselective reduction of nitriles to primary amines, using bench-stable ammonia borane (AB) as the hydride source and $CuCl_2$ as an activating mediator. The reaction proceeds via sequential, single-jar ball milling: $CuCl_2$ first coordinates and polarizes the nitrile, enhancing its

electrophilicity, before AB delivers hydride directly to the activated substrate, entirely at room temperature and without solvent. The method tolerates aromatic halogens and electron-donating substituents, affording nine primary amines as their hydrochloride salts in 35–92% yield, with selectivity governed primarily by competing dialkylamine over-reduction rather than steric or electronic demand. DFT calculations (B3LYP-D3BJ) support a Cu(II)-mediated activation–hydride delivery mechanism, supported by experimental elucidation of the complex done through FT-IR and XPS. This work fills a longstanding gap in the mechanochemical reduction toolbox and offers a substantially greener entry to primary amine synthesis.

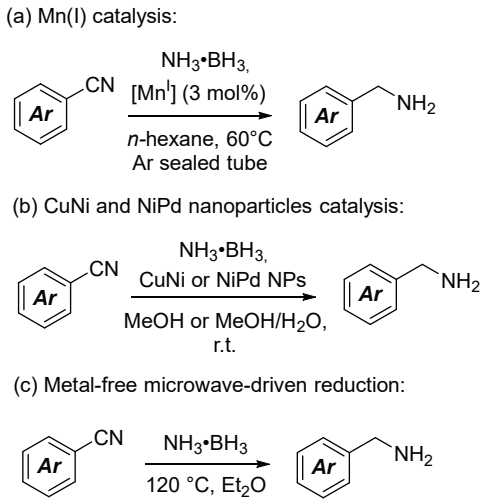
Introduction

Primary amines are essential building blocks for natural products, agrochemicals, dyes, polymers, and a large fraction of marketed pharmaceuticals.[1,2] Among the available transformations, the reduction of a nitrile group is one of the direct methods to install the CH_2–NH_2 functionality in a single step using a readily available precursors. However, the intrinsic thermodynamic stability of the C≡N triple bond (mean bond enthalpy in the range of 887-891 kcal/mol)[3] renders it significantly less reactive toward reduction than other unsaturated functional groups, such as nitro compounds, aldehydes, ketones, and esters. Consequently, conventional synthetic protocols necessitate stoichiometric amounts of powerful hydride reducing agents, including lithium aluminum hydride ($LiAlH_4$),[4] borane (BH_3),[4] or diisobutylaluminum hydride (DIBAlH),[4] or harsh catalytic hydrogenation.[5] These classical approaches present severe operational drawbacks, notably the handling of pyrophoric reagents, poor functional group tolerance, stoichiometric metal-containing waste, and the mandatory use of flammable ethereal solvents such as tetrahydrofuran or diethyl ether. This results in experimental setups that are

hazardous on scale, laborious workup protocols and generate large quantities of waste after workup.[4] Despite decades of effort, the chemoselective reduction of nitrile to primary amine function remains a notoriously demanding transformation: as the forcing conditions inherently mine selectivity. Additionally, imine intermediates and amine products are nucleophilic enough to promote condensation side processes, producing secondary and tertiary amine by-products that contaminate the major primary amine product.[6]

Among the alternative methods reported to date, catalytic hydrogenation with homogeneous or heterogeneous Ru, Rh, Ir, Fe, Co, or Mn-containing catalysts represents more atom-economic, safer and chemoselective alternative, but typically requires elevated temperatures and pressures (up to 60 bar and 160 °C),[5,7–13] custom tailored polydentate or pincer-type phosphine ligands, and external base to suppress over-reduction.[14,15] Additional options involve the use of milder hydride or hydrogen transfer through transition metal catalysts include the use of boranes[16] or silanes[17]. In this context, ammonia borane ($NH_3 \cdot BH_3$, AB) has emerged as an attractive reducing reagent: a non-toxic, bench-stable solid with a remarkable 19.6 wt% hydrogen content, AB has been shown by to act as a reductant for imines, polarized olefins, and carbonyls, using THF as preferred solvent but with option including water and acetonitrile the more readily reactive moieties (Scheme 1).[18,19] When the substrate is a nitrile, however, the solution-phase literature exposes three recurring shortcomings. First, the homogeneous catalytic protocols that achieve selectivity for primary amines rely almost invariably on tailor-made phosphine, nitrogen-nitrogen-phosphorous (NNP), or thiomethoxy-decorated chelating complexes of Fe, Co, or Mn, ligands whose multi-step, often air-sensitive synthesis offsets the cost benefit of using earth-abundant metals.[14,15] Second, the heterogeneous nanoparticle protocols (Pd, Pt, Ni, Cu, and bimetallic systems supported on graphene or oxides) do not use AB as a direct hydride donor. AB is instead dehydrogenated *in situ*

to release molecular H_2, which is then consumed by an entirely separate hydrogenation step, so that AB functions as a hydrogen-storage material rather than as a reductant in its own right.[20,21] Third, the only catalyst-free protocol reported to date, which does exploit AB as a true reductant through its thermally generated aminodiborane (ADB) intermediate, must be run in refluxing diethyl ether at 120 °C inside a sealed autoclave: a combination of a low-boiling, peroxide-forming ethereal solvent with substantial pressure build-up from co-evolved H_2 and NH_3.[22]



Scheme 1. Previous nitrile reduction methods using AB as a reducing agent.

Mechanochemistry, has matured over the past two decades into a solvent-free alternative to solution-phase synthesis, that offers short reaction times, eliminates hazardous organic solvents and has recently begun to build its own dedicated reduction toolbox, most typically explored in a laboratory scale ball mills.[23–26] In this context, hydride transfer reagents such as borohydrides provide bench-stable, mild reducing sources under ball-milling conditions. For example, $NaBH_4$ has been applied to reduce nitrobenzenes to anilines in presence of cyclodextrin-stabilized gold

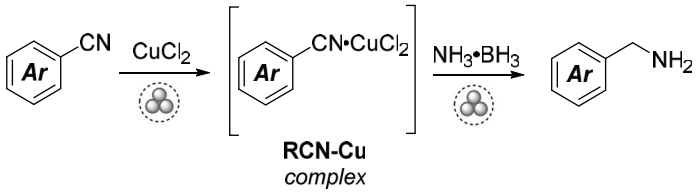
nanoparticles (AuNPs).[27] This borohydride can also reduce aldehydes and ketones, alone or in the presence of LiCl as an additive to generate $LiBH_4$. The latter system is able to reduce esters to alcohols, as reported by Mack and coworkers.[28] Diboron reagents have been reported to reduce alkynes, alkenes or nitro groups through water splitting to generate in situ H_2[29] or to reduce polycyclic aromatic rings or unsaturated carbonyls with a Rh catalyst.[30] Most recently AB itself with NaCl as a solid additive has been reported to reduce nitro groups to amines under ball milling conditions.[31] Other examples of hydride donors are represented by the reduction of nitro group to amine using ammonium formate in a Pd/C-catalyzed process,[32] silanes to reduce carbonyls to alcohols or methylene moiety,[33,34] or to hydrogenate alkenes using piezoelectric catalysts.[35] Bulk low-reactive or zero-valent metals function as highly potent electron donors under ball milling conditions, as continuous grinding activates passivated metal surfaces and generates finely dispersed, highly reactive species without requiring strictly anhydrous conditions, liquid ammonia, or inert atmospheres.[36] Specifically, alkali and alkaline earth metals (Li, Na, Ca, Mg, Ba) have been utilized for Birch-type reductions,[37] mechanochemical generation of polar organometallics and subsequent Barbier-type or Wurtz reductive couplings,[37,38] or Béchamp reduction using Zn.[39] Furthermore, mechanical force can induce single-electron transfer (SET) directly from polarized piezoelectric materials (*e.g.* $BaTiO_3$), driving metal-free mechanoredox reductions and alkene hydrogenations.[35,40]

Direct hydrogenation utilizing molecular hydrogen gas has been successfully adapted to ball-milling reactors, eliminating the waste generation associated with sacrificial hydrogen donors. Using pressurizable stainless-steel jars operated in planetary ball mills, gaseous H_2 and low loadings of palladium on carbon (Pd/C) or direct mechanocatalytic systems (*e.g.* electroplating

catalytically active metals onto the grinding media) enable solvent-free, chemoselective hydrogenation of unsaturated C=C, C=O, N=O, and C-X bonds at ambient temperature and low hydrogen pressures (≤ 1.5 bar).[41,42]

Despite all this works, the mechanochemical reduction protocols for nitriles are still scarce and need to be substantially expanded in chemical diversity. Additionally, chemoselective reduction methods are required. To the best of our knowledge, no mechanochemical protocol has yet been reported for the reduction of nitriles to the corresponding primary amines, leaving a clear gap in the mechanochemical reduction literature. Herein, we report the first mechanochemical protocol for the reduction of nitriles to primary amines using AB as reductant and $CuCl_2$ as mediator.

The strategy is built around a two-step, sequential activation in a single milling jar: (i) $CuCl_2$ should activate the nitrile through coordination, polarizing the C≡N triple bond and substantially enhancing the electrophilicity of the nitrile carbon; (ii) the activated substrate is then reduced by ammonia borane, used directly as a hydride donor rather than as a sacrificial H_2 source (Scheme 2). The combination allows a completely solvent-free, room-temperature reduction of nitriles into the corresponding primary amines using a bench-stable non pyrophoric reductant. The protocol therefore simultaneously fills a long-standing gap in the mechanochemical reduction landscape and offers a markedly greener entry to a transformation of recognized industrial relevance.



Scheme 2. Mechanochemical reduction of nitriles by using AB/$CuCl_2$ system.

Result and Discussion

The preliminary studies have been performed with reductions of liquid benzyl cyanide with several borohydride type reductants in a vibratory ball mill at 30 Hz milling frequency and ZrO_2 milling jars with a single 10 mm ZrO_2 milling ball. Our initial attempts to reduce the nitriles with $LiBH_4$, $NaBH_4$ alone resulted either in no reaction ($NaBH_4$) or trace product ($LiBH_4$). The further reaction design was guided by a single principle: if the nitrile carbon can be turned more electrophilic *before* the reductive step via (κ^1-N) bonded coordination to a metal cation, then the C≡N bond may be reduced more easily. To generate the putative activated nitrile complexes, the nitrile substrate was first milled with a Lewis acid, followed by addition of reducing agent to the same jar and resumed milling. A number of Lewis acid additives ($MgCl_2$, $AlCl_3$, $ZrCl_4$, TiF_4, $FeCl_3$, $ZnCl_2$, $MnCl_2$) resulted in no reduction or only moderate conversion of benzyl cyanide into the corresponding amine (see the Supporting Information, Table S1). The subsequent tests were continued with solid *o*-iodobenzonitrile (**9-RCN**) and liquid *o*-fluorobenzonitrile (**1-RCN**) in order to examine additionally reduction selectivity (to avoid reductive dehalogenation or coupling byproducts, see also SI, Section S1). The iodo-substituted substrate produced high conversion to benzylamine with $NaBH_4/ZrCl_4$ system, indicating on efficient but not selective reduction. When we switch to AB as a milder reductant[43] to our delight, in combination with anhydrous $CuCl_2$ as an activator, we observed promising 60% conversion to *o*-iodobenzylamine with only 20% reductive dehydrohalogenation. This stayed in contrast with $NaBH_4/CuCl_2$ system that resulted in complex mixture of reduction products.

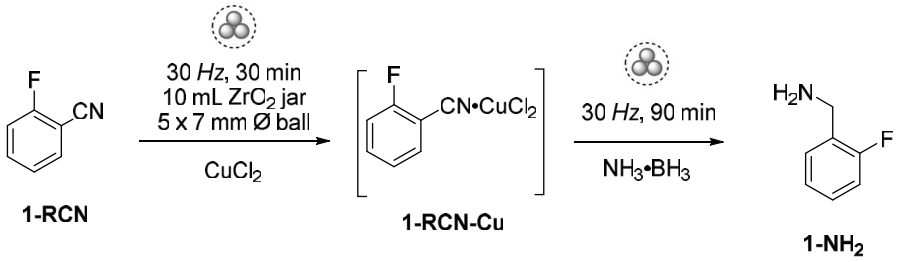
This result manifested $CuCl_2$ as readily available and bench stable inorganic salt that serves as sufficiently strong σ-acceptor to polarize the C≡N triple bond, enhancing its electrophilicity to facilitate an attack from AB as a mild reducing agent. Furthermore, we suggested that typically

strong binding of amine product to copper may assist in sequestering the product by the copper salt and act as a thermodynamic sink that pulls the overall transformation forward.

The subsequent study was focused on finding the optimal loadings of the copper salt and AB with to maximize yields and selectivity in the reduction of **1-RCN** (see Table 1). Main byproducts observed in the case of this substrate are related to coupling of the amines mediated by the copper and the water present in the air trapped in the jar as qualitative GC-MS fragmentation patterns and ^{1}H NMR of the crude analysis showed.

Optimization of the reduction of **1-RCN** to **1-NH₂** was performed by ball milling, using five 7 mm diameter ZrO_2 balls to ensure proper mixing (m_{ball} = 1.03 g, delivering a nominal impact energy[45] E_{imp} = 7.34 mJ), the milling times were chosen to ensure mostly efficient mixing for the complexation to happen, and it was fixed at 30 minutes and for the second step it was fixed at 90 minutes as shorter milling time were not sufficient to ensure total conversion while over-milling (more than 90 minutes) surprisingly resulted in lower conversion. Although the reasons remain unclear, we speculated it could be due to the oxidation of **1-NH₂** to **1-RCN** mediated by the copper species and atmospheric oxygen.[46–48] Both under- and over-loading of either reagent reduced conversion and yields (see more comprehensive optimization results in the SI, Table S2).

Table 1. Stoichiometry optimization for the reduction of **1-RCN** to **1-NH$_2$**.



Entry	$CuCl_2$ equiv.	AB equiv.	Conversion[a] (%)	Yield of 1-NH_2[a] (%)
1	0.5	2	29%	16%
2	0.5	5	100%	93% (92%[b])
3	0.5	7	55%	33%
4	0.2	5	12%	12%
5	0.6	5	94%	92%
6	1	5	88%	2%
7	0.2	2	37%	13%

Typical experimental procedure: To a 10 mL ZrO_2 jar equipped with 5 x 7 mm Ø balls of the same material, the nitrile (1.5 mmol, 1.0 equiv.), $CuCl_2$ were milled for 30 minutes at 30 *Hz* in a mixer mill (*step 1*). After this milling time, AB was added, and the reaction mixture was further milled for 90 minutes at 30 *Hz* (*step 2*). [a] Calculated *via* ^{1}H qNMR, in $CDCl_3$ using cyclododecane as internal standard.[44] [b] Isolated yield.

Thus, the optimal stoichiometry was fixed at 0.5 equiv. of $CuCl_2$ and 5 equiv. of AB (entry 2), giving quantitative conversion and 92% isolated yield. Lowering AB to 2 equiv. (entry 1) gave incomplete conversion, while raising AB loading beyond 5 equiv. (entry 3) also lowered conversion and yield, consistent with over-reduction of Cu(II) to catalytically inactive Cu(0), supported by visible metallic Cu deposits on the jar walls and further supported by DFT studies (see below). A control experiment performed in the absence of $CuCl_2$ showed no reaction, confirming essential role of the copper salt.

Lowering $CuCl_2$ below 0.5 equiv. (entry 4) limited conversion due to insufficient catalyst turnover. Increasing $CuCl_2$ to 1.0 equiv. (entry 6) kept conversion high but collapsed selectivity (2%), attributed to a parasitic C–F activation pathway giving hydrodefluorinated/coupled byproducts (seen in GC–MS and ^{1}H-NMR of crude). Thus 0.5–0.6 equiv. $CuCl_2$ defines the viable window; 0.5 equiv. was adopted as standard in this work. Using $CuCl_2$:AB in the same optimal 1:10 molar ratio but at lower absolute loadings, gave sub-optimal conversion (37%), showing that absolute loadings, not just the ratio, of both reagents are critical for reproducible performance.

With the stoichiometry established, further attention was turned to the technical parameters of the vibratory ball-milling (VBM) setup. We opted to find an optimal duration of both milling steps, the number and size of the milling balls, milling frequency, grinding-media material and also examine transversality between to different shaker mills (both horizontal *vs.* vertical VBM, that use jars of different geometries (see the SI for details). For each configuration, the nominal total energy input per step (E_{tot}) and the energy delivered per ball–reactant impact (E_{imp}) were estimated using the open-source energy calculator developed by the Lungerich group,[45] providing idealized, comparative estimates rather than directly measured values. The key experiments are collected in Table 2.

The influence of ball size and number on reaction efficiency was examined (entries 1–7, Table 2). Variation in the number of milling balls had only a modest effect on yield, with the minor deviations observed most plausibly attributable to changes in mixing efficiency rather than to total energy input. In contrast, E_{imp} emerged as the more decisive parameter: 5 mm balls consistently afforded lower yields even when E_{tot} was held constant (entry 4 *vs.* 6), reflecting insufficient E_{imp} to drive the transformation efficiently. Balls of 10 mm diameter performed comparably to the 7 mm balls, consistent with their higher associated E_{imp}; however, this larger size was more prone to

a "snowballing" effect, with agglomeration of crude material on the ball surface, which in turn compromised reproducibility.[49] Milling frequency was found to exert a further influence: comparison of entries 7 and 8 revealed a 30% decrease in yield upon lowering the frequency, mirroring a corresponding 30% reduction in E_{imp}. Notably, translation of the optimized conditions to a vertical mixer mill (entry 9) gave a different outcome despite nominally equivalent E_{tot} and E_{imp} values, indicating that the mode of mechanical energy transfer and not merely its magnitude, is critical, and that the simplified kinematic model of the milling process is likely insufficient to capture this behavior.[50]

In this regard, jar geometry and internal proportions were found to significantly impact reaction yield. To probe the role of the grinding media, PTFE jars (10 mL) were evaluated in the horizontal mixer mill in combination with various ball materials (see SI, Table S4). PTFE vessels are not recommended for this transformation, as they led to pressure buildup during milling; stainless steel balls were likewise unsuitable, undergoing corrosion and degradation over the course of the reaction. On this basis, ZrO_2 or comparably inert ceramic jars and grinding media are recommended for optimal and reproducible performance.

Following completion of the optimization studies, a general preparative protocol was established: the nitrile substrate was subjected to the optimized conditions reported in Table 2, entry 1, on a 1.5 mmol scale; the final product is afforded by dissolving in green ethereal solvent the crude (methyl *tert*-butyl ether, MTBE) and precipitating selectively the corresponding amine hydrochloride salts by adding HCl in cyclopentyl methyl ether (CPME). The only exception for the workup procedure was for **9-RCN**, which was isolated as free amine (**9-NH$_2$**) through extraction due to more pronounced presence of benzylamine byproduct that rendered impossible isolation *via* precipitation (Figure 3)

Table 2. Technical parameters optimization for the reduction of **1-RCN** to **1-NH$_2$**.

Entry	*f* (Hz)	Balls (n*Ø)	Energy			Yield[a]
			E_{tot} (kJ) (step 1)	E_{tot} (kJ) (step 2)	E_{imp} (mJ)	
1	30 Hz	5*7 mm	19.69	59.06	7.34	93% (92%[b])
2	30 Hz	4*7 mm	15.80	47.40	7.34	60%
3	30 Hz	3*7 mm	11.88	35.62	7.34	90%
4	30 Hz	2*7 mm	7.93	23.78	7.34	84%
5	30 Hz	6*5 mm	9.54	28.62	2.95	54%
6	30 Hz	4*5 mm	7.96	23.88	2.95	50%
7	30 Hz	1*10 mm	11.74	35.23	21.8	91%
8	25 Hz	1*10 mm	6.80	20.39	15.1	61%
9[c]	30 Hz	1*10 mm	11.60	34.81	21.5	34%

Typical experimental procedure: To a 10 mL ZrO_2 jar equipped with specified number and size of balls of the same material, the nitrile (1.5 mmol, 1.0 equiv.), $CuCl_2$ (0.75 mmol, 0.5 equiv.) were milled for the specified amount of time at the specified frequency in a MM400 mixer mill (*step 1*). After this milling time, NH_3BH_3 (7.5 mmol, 5 equiv.) was added, and the reaction mixture was further milled for the specified amount of time at the specified frequency (*step 2*). [a] Calculated *via* ^{1}H qNMR, in $CDCl_3$ using cyclododecane as internal standard.[44] [b] Isolated yield. [c] Mill used was Fritsch's P23 vertical mixer mill.

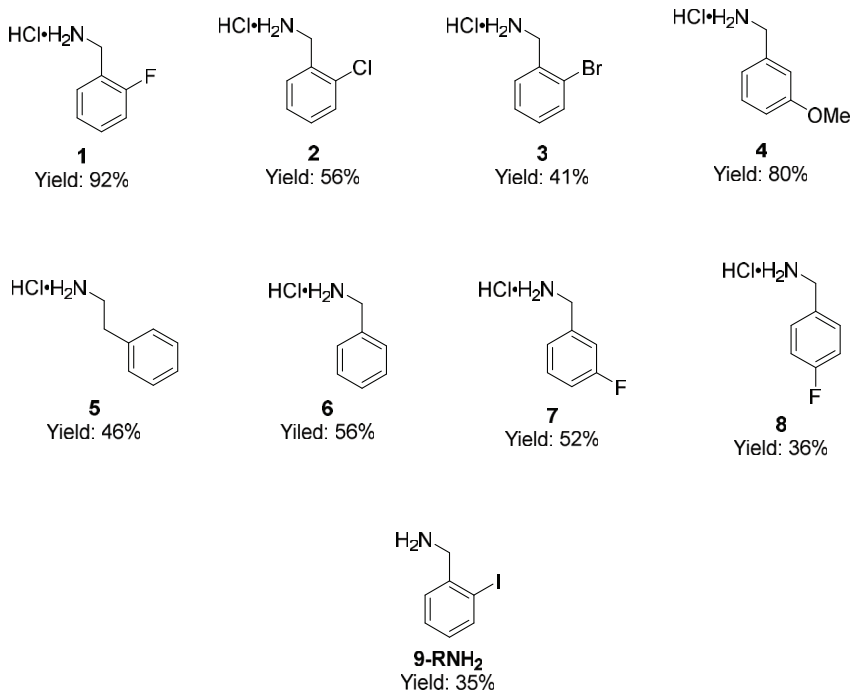
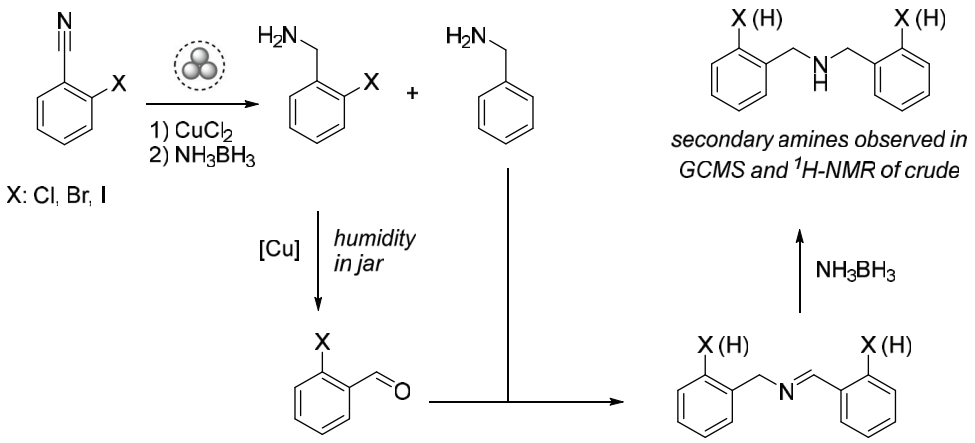


Figure 3. Scope of the reaction.

With an optimized protocol in hand, the generality of the method was assessed on a focused set of aromatic and benzylic nitriles, which were reduced to the corresponding primary amines and isolated as their hydrochloride salts in moderate to excellent yields (35–92%; Scheme 3). Across the full *ortho*/*meta*/*para* series of fluorobenzonitriles (1,7,8), as well as the *ortho*-chloro and *ortho*-bromo analogues (2 and 3), the nitrile was cleanly reduced with minor to no detectable dehalogenated by-products, indicating that the protocol is chemoselective for the nitrile group over the competing carbon–halogen bond, a pathway that frequently complicates nitrile reductions carried out under classical metal/hydride regimes.

Two features of the yield profile merit comment. Within the series of fluorinated substrates, isolated yield decreased in the order *ortho* (1, 92%) > *meta* (7, 52%) > *para* (8, 36%); ^{1}H NMR analysis of the crude reaction mixtures showed that this drop tracks a substantially increased contribution of a dibenzylic secondary amine by-product for the *meta* and *para* isomers that can contain either of the amine also dehalogenated, as well as for the parent benzonitrile (6, 56%), pointing to over-reduction of an imine-type intermediate as the main competing pathway once the *ortho* relationship between the nitrile and the fluorine substituent is lost. A more stable chelation-type engagement of the *ortho*-fluorine by the copper center offers a rationale that is supported by the structural evidence presented in the following sections, although the causal link to the yield ordering remains a working hypothesis.

A related trend was observed across the *ortho*-halogen series, with yield decreasing in the order F (1, 92%) > Cl (2, 56%) > Br (3, 41%) > I (9-NH_2, 35%). For the chloro- and bromo- substrates, the yield decreases again correlated with a greater contribution of the dibenzylic secondary amine byproduct; for the iodo- derivative, a higher degree of competing de-hydroiodination process was observed, consistent with the greater lability of the C–I bond under the reaction conditions. The dehalogenated byproducts are not observed for the fluoro- substrate, and for the chloro- and bromo- substrates is observed only as part of a dybenzylic secondary amine system which side-reaction pathway most probably readily capture the unwanted benzylamine byproduct to transform into a more easily eliminable substrate (Scheme 3).



Scheme 3. Proposed pathway of formation of observed byproducts[11,15] in the synthesis of **2-NH₂**, **3-NH₂**, and **9-NH₂**, see more in the SI, section 1.5.

An electron-donating substituent was nonetheless well tolerated (*meta*-methoxy, 4, 80%), with a comparatively minor contribution of the dibenzylic amine by-product, and the method was not confined to functionalized benzonitriles, since both the parent benzonitrile (6, 56%) and the benzylic nitrile phenylacetonitrile (reduced to phenethylamine, 5, 46%) were reduced efficiently, extending the transformation from aryl to arylaliphatic nitriles; in the latter case, the moderate yield likewise mainly reflects a dominant contribution from the dialkylamine by-product.

Taken together, isolated yields across the substrate scope range from moderate to good, and conditions optimized for substrate 1 may require substrate-specific re-optimization; formation of the dialkylic secondary amine represents the most consistently observed, and currently most significant, competing pathway across the series. The scope therefore appears to be governed less by the intrinsic steric or electronic demand of the nitrile than by whether Cu(II) can engage the nitrogen lone pair in an N-coordinated fashion required for activation, a coordination picture that,

at this stage, remains a solid working hypothesis, to be discussed further in light of the spectroscopic and computational data presented in the following sections.

DFT Calculations

We applied DFT calculations with the ORCA package[51] to better understand the mechanism of the reaction. We have demonstrated in previous publication[52–54] that, at least in some cases, the main role of ball-milling is the efficient mixture of the solids, without an essential role for the explicit introduction of the mechanical energy. Thus, the main difference between ball-milling and solution would be the concentration of the reactants and the polarity of the media, which can be introduced through standard DFT methods. Because of this, we report below calculations carried out with the B3LYP-D3BJ functional in a DCM dielectric media. Full computational details are given in the Supporting Information, and all the computational results are uploaded in the ioChem-BD repository.[55]

We first carried out calculations for the direct reaction between the **1-RCN** reactant and the NH_3BH_3 reducing agent in the absence of copper species. The results, presented in the Supporting Information are conclusive in the sense that the barriers are prohibitively high. The barrier for hydrogenation is 36.1 kcal/mol and for halogen replacement is 45.1 kcal/mol. Analogous calculations for the **9-RCN** reactant, yield values of 36.5 and 41.7 kcal/mol, respectively. Thus, the presence of the copper species is necessary for the reaction to take place, in agreement with experiment.

We next considered the possibilities of modeling the $CuCl_2$ solid through our calculation. This in an ionic solid, with the chloride anions occupying bridging positions between the copper cations. We carried out a series of calculations, reported in the Supporting Information, to evaluate the number of $CuCl_2$ units necessary for a reasonable description. The energy change from a

monomeric $CuCl_2$ description to a dimeric $(CuCl_2)_2$ description is very large, with the dimer being more stable by 27.3 kcal/mol. Further introduction of monomers is not that substantial, to the extent that a tetrameric $(CuCl_2)_4$ unit is less stable than two separate $(CuCl_2)_2$ dimeric fragments. Because of this, we settle on the dimeric $(CuCl_2)_2$ as computational model for the copper system.

The interaction between the copper system and the nitrile molecules was evaluated through geometry optimizations and evaluation of the resulting structures, presented in the Supporting Information. The preferred structure is with the nitrogen atom of the nitrile pointing towards a copper center. Interestingly, the coordination of the nitrile leads to a significant increase on the computed value for the IR frequency associated to the C-N bond, that goes from 2330 cm^{-1} in free **1-RCN** to 2372 cm^{-1} in coordinated **1-RCN**. The corresponding values for **9-RCN** are 2326 and 2334 cm^{-1}, respectively. It is thus clear that coordination to copper activates the nitrile bond, and it makes it more susceptible to reaction.

We confirmed the catalytic role of copper by computing the free energy profile for the hydrogenation reaction, which is presented in Figure 5. The reaction is exergonic by 19.2 kcal/mol (from the initial appearance of **int1a** to its regeneration), and the rate limiting barrier is 24.0 kcal/mol (from **int3a** to **TS2a**). Both results are compatible with the experimental observation of a reaction that takes place at room temperature with a moderate rate.

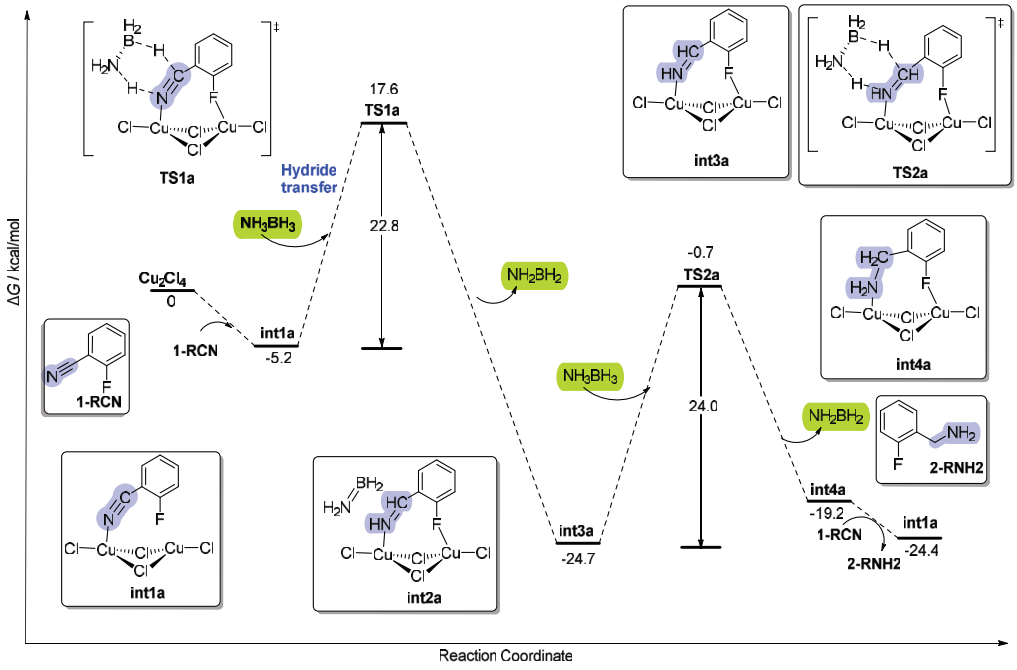


Figure 5. Computed free energy profile (kcal/mol) for the reaction between **1-RCN** and NH_3BH_3 in the presence of Cu_2Cl_4.

The molecule **1-RCN** interacts with the Cu_2Cl_4 unit to form the **Int1a** adduct, where the nitrile is attached to one of the copper centers and the fluorine to the other one. This coordination weakens the triple bond, which can then be hydrogenated by an external NH_3BH_3 molecule with an affordable barrier of 22.8 kcal/mol. The hydrogenated nitrile remains coordinated to the copper center in intermediate **int3a**, and is attacked by a second unit of hydrogenating agent in **TS2a** with a slightly higher barrier of 24.0 kcal/mol.

We also analyzed the behavior of **9-RCN**, where a iodine replaces the chlorine, and where experiment shows a similar rate but a much higher amount of the undesired dehalogenated product. The free energy profile for **9-RCN**, shown in the Supporting Information, was very similar to that

of **1-RCN**, with a slightly higher barrier of 24.2 kcal/mol. No significant difference can be found in the hydrogenation profiles capable of explaining the experimental divergence. We could not find any path leading to the dehalogenated produce when using the Cu_2Cl_4 copper unit, but we succeeded when using a Cu_2Cl_3H unit. The result is shown in Figure 6 for both **9-RNH$_2$** and **1-RNH$_2$**.

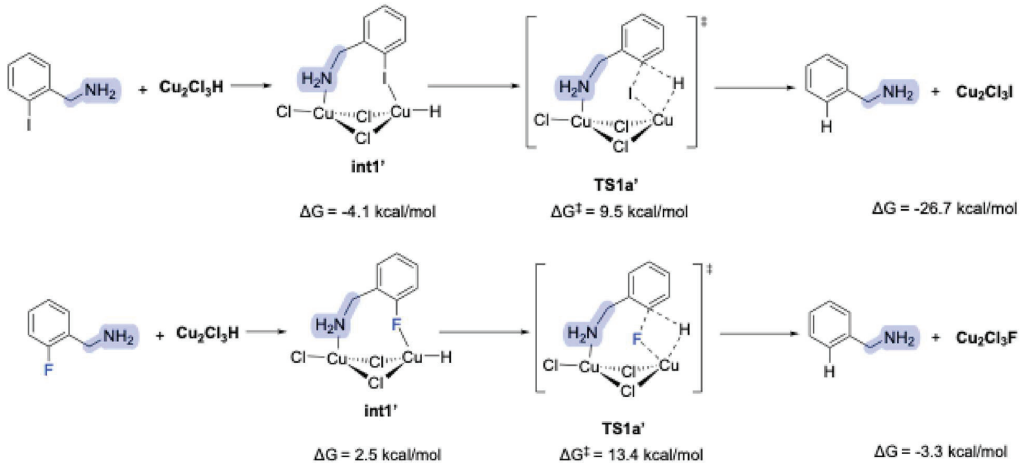


Figure 6. Energetics (kcal/mol) for the reaction between **9-RNH$_2$** and Cu_2Cl_3H (top) and between **1-RNH$_2$** and Cu_2Cl_3H (bottom).

The barriers for the dehalogenation reaction are similar for the compounds with fluorine and iodine are very similar (13.6 kcal/mol for the iodinated species, 13.4 kcal/mol for the fluorinated species), and clearly affordable in the reaction conditions. But the thermodynamics involved are not. The reaction is strongly exergonic (-26.7 kcal/mol) for the iodinated compound **9-RNH$_2$**, but mildly so (-3.3 kcal/mol) for the fluorinated species **1-RNH$_2$**. This means that for the fluorinated species, the dehalogenation step will be in equilibrium, easily inverted, and thus the hydrogenation will predominate. In contrast, the dehalogenation of the iodinated compound will be irreversible,

and explain the significant observation of this product. There is thus a clear difference in reactivity, which follows the experimental trend of a favored dehydrogenation for the iodinated system. The qualitative trend is well reproduced. We cannot expect to have a quantitative reproduction of experimental yields and conversion because we do not know which is the proportion of copper units where a hydride has replaced a chloride, and it is not possible to estimate it with our simple model.

FT-IR Characterization of the Copper – Nitrile complex

Initial characterization of complex **1-RCN-Cu** was performed by ATR FT-IR analysis. The complex was prepared under the same conditions as *step 1* of the reaction: **1-RCN** (1.5 mmol, 1.0 equiv.) and $CuCl_2$ (1.5 mmol, 1.0 equiv.) were milled for 30 min at 30 Hz in a 10 mL ZrO_2 jar with five 7 mm Ø ZrO_2 balls (Figure 5).

The IR spectrum of the resulting crude mixture (Figure 5) shows two bands in the C≡N stretching region (2000–2500 cm^{-1}): we attribute the band at 2237.5 cm^{-1} to the residual uncomplexed **1-RCN**, while the band at 2274.5 cm^{-1}, blueshifted by +37 cm^{-1}, is assigned to the C≡N stretch of the Cu-coordinated nitrile. Blueshifts of this magnitude are characteristic of end-on (κ-N) coordination of a nitrile to a Lewis-acidic metal centre: σ-donation from the nitrile lone pair removes electron density from a weakly C≡N-antibonding orbital, strengthening and shortening the C≡N bond and raising its stretching frequency.[56,57] In Cu(II) (d^9) systems, π-backdonation is negligible, so σ-donation dominates and a positive Δν(C≡N) is expected.

To probe whether complete consumption of free **1-RCN** could be achieved, the milling time was extended in a series of experiments under the same 1:1 stoichiometry (30, 45 and 60 min; Figure 6). With increasing milling time, the free-nitrile band at 2238 cm^{-1} progressively decreases in

intensity while two new bands appear in the coordinated region: an intermediate band at 2254 cm^{-1} and a more strongly blueshifted band at 2275 cm^{-1}.

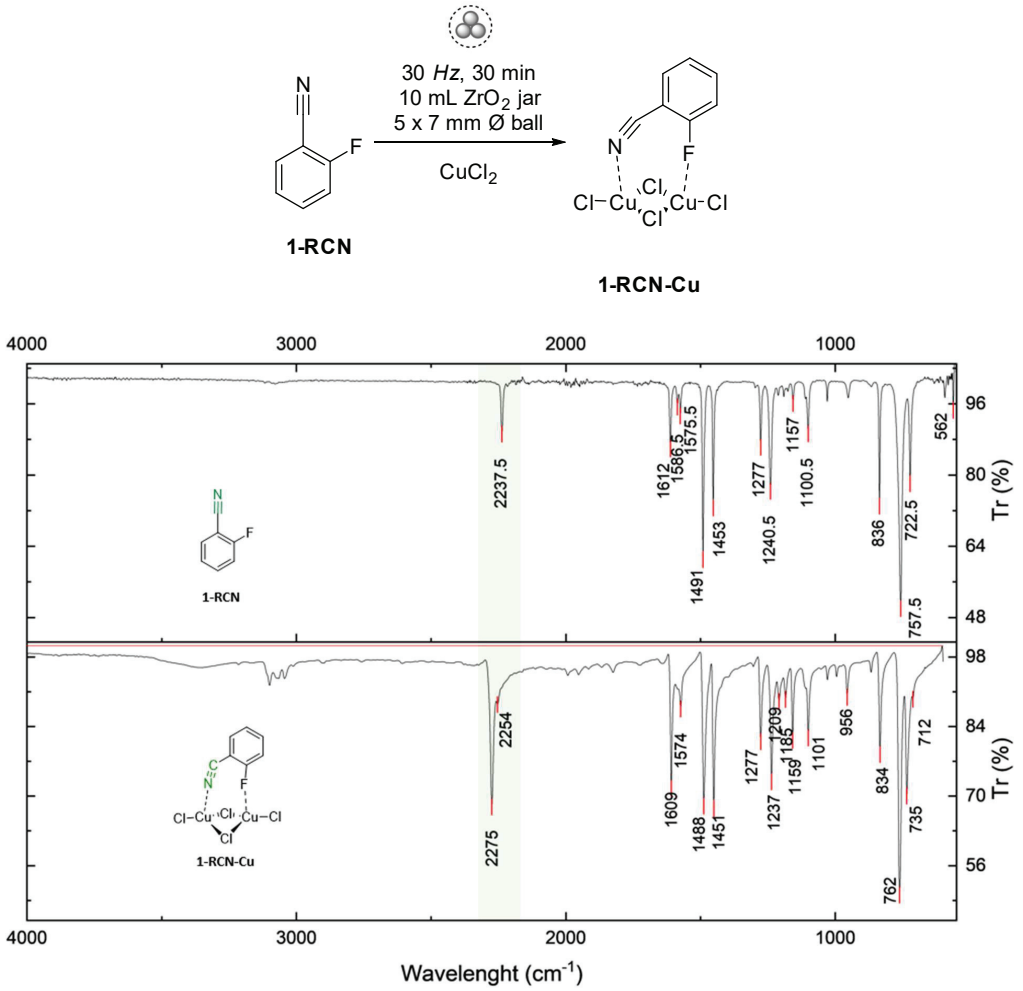


Figure 5. Top: synthesis of **1-RCN-Cu** by mechanochemical milling of **1-RCN** with $CuCl_2$. Bottom: ATR-FT-IR spectra of free **1-RCN** (top trace) and of the crude mixture after milling (bottom trace). The C≡N stretching region is highlighted in green.

We assign the band at 2275 cm^{-1} to a κ^2-N,F chelated form, in which the *ortho*-fluorine engages the second Cu of the dimer, and the band at 2254 cm^{-1} to an open κ^1-N form in which Cu coordinates only through the nitrile nitrogen. The relative C≡N stretching frequencies of the two forms, and the predominance of the chelated species, are supported by DFT calculations (see section above). A full IR characterization of the related complexes **2-RCN-Cu–11-RCN-Cu** is provided in the SI (Section S3).

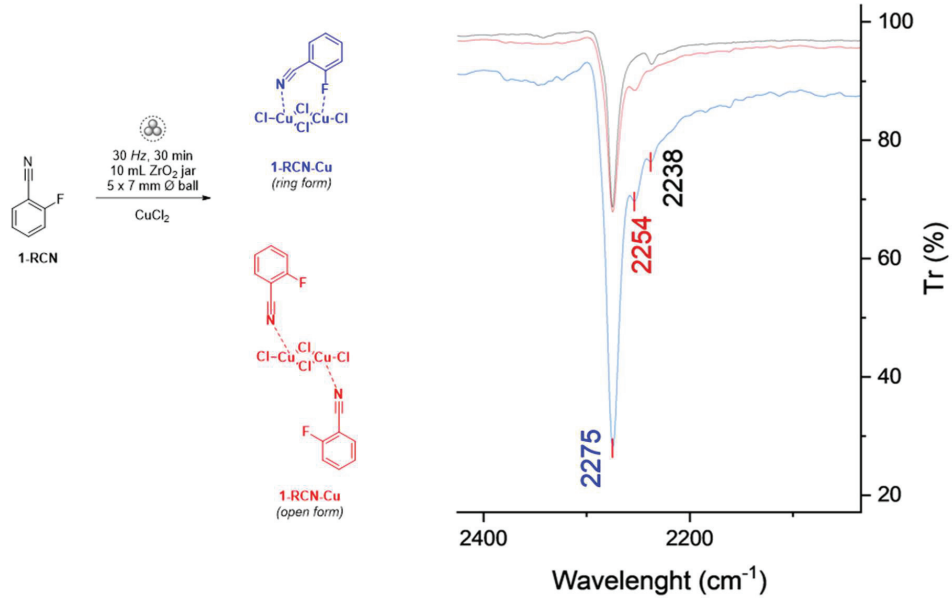


Figure 6. Proposed open and closed (chelated) forms of 1-RCN-Cu, and the C≡N stretching region of the IR spectra after milling at 1:1 Cu:nitrile stoichiometry for extended times. Bands at 2238 cm-1 (free **1-RCN**, black), 2254 cm-1 (open κ^1-N form, red) and 2275 cm-1 (chelated κ^2-N,F form, blue) are highlighted.

XPS Characterization of the Copper – Nitrile complex

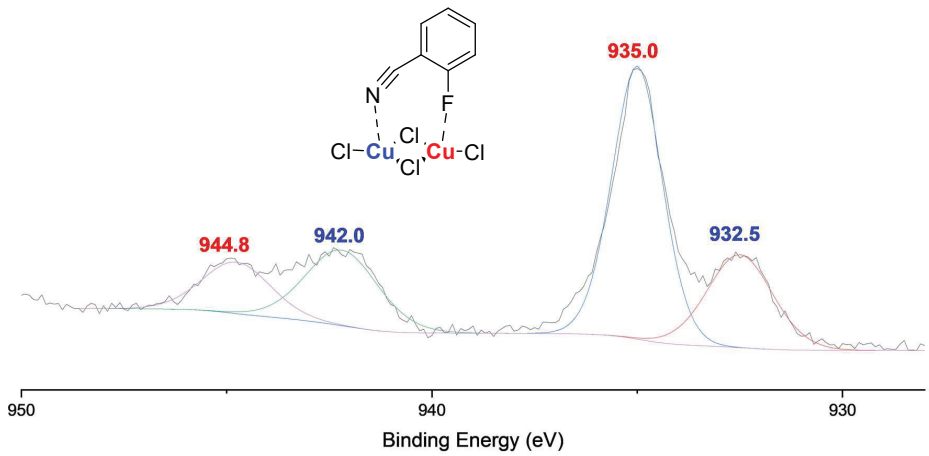
Complex **1-RCN-Cu** was characterized by X-ray photoelectron spectroscopy on the powder recovered directly after *step 1* milling. To obtain information on the structure and chemical environment of both copper and the *ortho*-fluoro nitrile during complexation, the N 1s and Cu 2p photoelectron peaks were monitored and compared between the free components and the complex.

Establishing a reliable free-nitrile N 1s reference is complicated by the fact that **1-RCN** (*o*-fluorobenzonitrile) is a liquid at room temperature and therefore poorly suited to solid-state acquisition under ultrahigh vacuum. To circumvent this, the N 1s spectra of the solid *o*-halo benzonitrile series (*o*-Cl, *o*-Br and *o*-I) were recorded as proxies. The N 1s binding energy proved essentially invariant across the series, 399.1, 399.2 and 399.2 eV for the chloro-, bromo- and iodo-nitriles, respectively (entries 1-3, Table 3 and Section S4 of the SI), demonstrating that the identity of the *ortho*-halogen exerts a negligible influence on the nitrile nitrogen core level. A free-nitrile reference of 399.2 eV is therefore adopted for **1-RCN** by extension.

Table 3. N 1s binding energies of the free *ortho*-halobenzonitriles and of polymethacrylonitrile (PMAN) as a literature reference.

Entry	Compound	N1s Binding Energy (eV)
1	o-Cl-benzonitrile	399.1
2	o-Br-benzonitrile	399.2
3	o-I-benzonitrile	399.2
4	PMAN	399.6[58]

Table 4. Deconvoluted Cu $2p_{3/2}$ XPS spectrum of **1-RCN-Cu**, showing two Cu(II) environments (Cu–N at 932.5 eV; Cu–Cl at 935.0 eV) each with its own shake-up satellite, in agreement with the chelated κ²-N,F structure (inset). On the bottom the XPS core-level binding energies (eV) and surface atomic percentages of the Cu 2p, N 1s and Cl 2p regions of the **1-RCN-Cu** complex.



Entry	Photoelectron	Binding Energy (eV)	Atomic %
1	Cu $2p_{3/2}$ (Cu···NC)	932.5	5.5
2	Cu $2p_{3/2}$ (Cu-Cl)	935.0	12.4
3	Cu $2p_{3/2}$ (sat)	942.2	5.0
4	Cu $2p_{3/2}$ (sat)	944.8	3.2
5	N 1s (N≡C)	399.7	6.9
6	Cl $2p_{3/2}$ (Cl-Cu)	199.0	66.8

This value is independently corroborated by the published N 1s binding energy of the nitrile nitrogen in polymethacrylonitrile (PMAN, 399.6 eV, entry 4 of Table 3),[58] a polymer of entirely

different molecular architecture, notably lacking an aromatic ring adjacent to the C≡N group, whose close agreement, with only a slight shift, confirms that the nitrile N 1s is robust and only weakly perturbed by the second-neighbor environment.

On complexation, the nitrile N 1s shifts from this 399.2 eV baseline to 399.7 eV. A positive N 1s shift (+ 0.5 eV) is precisely what end-on (κ^1-N) σ-donation of the nitrile lone pair to a Lewis-acidic Cu(II) center predicts: donation depletes electron density at the nitrogen and raises its core-level binding energy, mirroring the + 0.3-0.5 eV observed for the nitrogen end of metal-bound cyanides[59] and corroborating, in the electronic domain, the C≡N IR blueshift assigned to the same σ-donation above (entry 5, Table 4).

The Cu $2p_{3/2}$ region resolves into two copper environments, each accompanied by its own shake-up satellite: a component at 935.00 eV (satellite at 944.8 eV, ΔE = 9.8 eV, entry 4) and a second at 932.5 eV (satellite at 942.2 eV, ΔE = 9.7 eV). The presence of a shake-up satellite on both main lines is diagnostic, as such satellites arise only from the open-shell $3d^9$ final state of Cu(II) and are absent for the closed-shell $3d^{10}$ configurations of Cu(I) and Cu(0).[60] Both copper centers are therefore Cu(II), as required, since no reducing agent is present during step 1 and reduction of the metal is chemically precluded until AB is introduced in step 2. The two inequivalent Cu(II) environments constitute direct spectroscopic evidence for the closed-ring (chelated) κ^2-N,F structure indicated by the DFT calculations and inferred from the IR analysis (Section S3 of the SI), in which the two coppers of the Cu_2Cl_4 dimer are distinguished by their coordination spheres. The higher-energy component at 935.0 eV is assigned to the fluorine-bearing copper, whose first coordination sphere consists exclusively of halogens (1 F + 3 Cl); its binding energy coincides with that of uncoordinated $CuCl_2$ (935.5 eV, see SI), as expected since replacing a single chloride by fluoride in an all-halogen sphere does not perturb the Cu $2p_{3/2}$ binding energy appreciably. The

lower-energy component at 932.5 eV is assigned to the nitrogen-bearing copper: σ-donation from the nitrile lone pair increases the electron density at this center and correspondingly lowers its core-level binding energy relative to the all-halogen copper. This metal-centered shift is the exact counterpart of the +0.5 eV N 1s shift, the same Cu-N σ-donation observed from both ends of the bond, raising the binding energy of the donor nitrogen while lowering that of the acceptor copper, and furnishes an internally consistent, two-sided spectroscopic fingerprint of nitrile coordination (figure of Table 4). Consistently, the surface atomic ratio of nitrogen to this lower-energy (nitrogen-bound) copper is 1:1 (N ≈ 7.0 at%; Cu at 932.5 eV ≈ 5.5 at%) within the 10–20% relative uncertainty typical of XPS quantification, as expected for a single κ^1-N-coordinated nitrile per nitrogen-bound copper in the chelate. No separate signal from uncoordinated **1-RCN** is detected in the complex: being a room-temperature liquid, any uncoordinated nitrile is readily volatilized under the ultrahigh vacuum of the spectrometer, and the slight excess of nitrogen beyond the 1:1 ratio is attributed to the minor residual fraction that escaped evaporation and remained adsorbed at the surface of the complex.

The Cl $2p_{3/2}$ peak at 199.0 eV (cf. $CuCl_2$, 199.8 eV, see SI, section S4.3), together with the 4:2 surface atomic ratio, confirms that chloride is retained in the copper coordination sphere, the experimental support for the Cu_2Cl_4-core model used throughout the complexation structure discussion.

CONCLUSIONS

We have developed the first mechanochemical protocol for the chemoselective reduction of nitriles to primary amines, combining ammonia borane (AB) as a bench-stable hydride source with $CuCl_2$ as an activating mediator under solvent-free, room-temperature ball-milling conditions.

Systematic optimization identified 0.5 equiv $CuCl_2$ and 5 equiv AB as the optimal stoichiometry, delivering the target amine in up to 92% isolated yield, and established that both the absolute loadings and the impact energy of the milling event and not solely the total energy input, govern reaction efficiency. The protocol tolerates a range of aromatic halogens and electron-donating substituents, affording nine primary amines as their hydrochloride salts in 35–92% yield, with chemoselectivity for the nitrile group over competing C–X bonds. Complementary FT-IR, XPS, and DFT evidence converge on a Cu_2Cl_4 dimer that activates the nitrile through κ^1-N (and, for *ortho*-halogenated substrates, chelating κ^2-N,F) coordination, polarizing the C≡N bond ahead of hydride delivery from AB, with a computed mechanism consistent with the mild, room-temperature reactivity observed experimentally. By replacing pyrophoric hydrides, high-pressure/temperature hydrogenation, and hazardous ethereal solvents with a solid-state, bench-stable reagent combination, this work closes a longstanding gap in the mechanochemical reduction toolbox and establishes a scalable, green entry point to primary amine synthesis from nitriles.

Supporting information

The following files are available free of charge.

ACKNOWLEDGMENT

A.C. is grateful to Campus France and Tallinn Technological University (TalTech) for the Ph.D. fellowship (co-tutelle de thèse France-Estonie). E.C. and A.N. are grateful to Campus France and French-Estonian cooperation Programme Hubert Curien France-Estonia (PHC PARROT 2021-2023). A.N. is grateful to the French Embassy in Estonia for the mobility grant (2024) and ÕÜF16 for generous funding.

REFERENCES

(1) Hayes, K. S. Industrial Processes for Manufacturing Amines. *Appl. Catal. A Gen.* **2001**, *221* (1–2), 187–195. https://doi.org/10.1016/S0926-860X(01)00813-4

(2) Flick, A. C.; Leverett, C. A.; Ding, H. X.; McInturff, E.; Fink, S. J.; Helal, C. J.; DeForest, J. C.; Morse, P. D.; Mahapatra, S.; O'Donnell, C. J. Synthetic Approaches to New Drugs Approved during 2018. *J. Med. Chem.* **2020**, *63* (19), 10652–10704. https://doi.org/10.1021/acs.jmedchem.0c00345

(3) Luo, Y.-R. *Comprehensive Handbook of Chemical Bond Energies*, 1st ed.; CRC Press, 2007. https://doi.org/10.1201/9781420007282

(4) Seyden-Penne, J.; Seyden-Penne, J. *Reductions by the Alumino- and Borohydrides in Organic Synthesis*, 2. ed.; Wiley-VCH: New York Weinheim, 1997.

(5) de Bellefon, C.; Fouilloux, P. Homogeneous and Heterogeneous Hydrogenation of Nitriles in a Liquid Phase: Chemical, Mechanistic, and Catalytic Aspects. *Catal. Rev.* **1994**, *36* (3), 459–506. https://doi.org/10.1080/01614949408009469

(6) Natte, K.; Jagadeesh, R. V. Amines By Reduction. In *Kirk-Othmer Encyclopedia of Chemical Technology*; Kirk-Othmer, Ed.; Wiley, 2021; pp 1–34. https://doi.org/10.1002/0471238961.0113091419030809.a01.pub3

(7) Reguillo, R.; Grellier, M.; Vautravers, N.; Vendier, L.; Sabo-Etienne, S. Ruthenium-Catalyzed Hydrogenation of Nitriles: Insights into the Mechanism. *J. Am. Chem. Soc.* **2010**, *132* (23), 7854–7855. https://doi.org/10.1021/ja102759z

(8) Feller, M. Hydrogenation of Nitriles and Imines for Hydrogen Storage. *Phys. Sci. Rev.* **2019**, *4* (3). https://doi.org/10.1515/psr-2018-0033

(9) Chen, J.; Jiao, Y.; Qin, X.; Cai, X.; Wang, M.; Diao, J.; Wang, L.; Li, C.; Ren, P.; Wen, X.; Wang, N.; Rong, J.; Xiao, D.; Liu, H.; Ma, D. Atomic-Dispersed Rh Enables Efficient Catalytic Nitrile Hydrogenation: Size Effect and Metal-Dependent Effect. *ACS Catal.* **2023**, *13* (13), 8354–8361. https://doi.org/10.1021/acscatal.3c01562

(10) Chin, C. S.; Lee, B. Hydrogenation of Nitriles with Iridium-Triphenylphosphine Complexes. *Catal. Lett.* **1992**, *14* (1), 135–140. https://doi.org/10.1007/BF00764228

(11) Bornschein, C.; Werkmeister, S.; Wendt, B.; Jiao, H.; Alberico, E.; Baumann, W.; Junge, H.; Junge, K.; Beller, M. Mild and Selective Hydrogenation of Aromatic and Aliphatic (Di)Nitriles with a Well-Defined Iron Pincer Complex. *Nat. Commun.* **2014**, *5* (1), 4111. https://doi.org/10.1038/ncomms5111

(12) Liu, W.; Sahoo, B.; Junge, K.; Beller, M. Cobalt Complexes as an Emerging Class of Catalysts for Homogeneous Hydrogenations. *Acc. Chem. Res.* **2018**, *51* (8), 1858–1869. https://doi.org/10.1021/acs.accounts.8b00262

(13) Elangovan, S.; Topf, C.; Fischer, S.; Jiao, H.; Spannenberg, A.; Baumann, W.; Ludwig, R.; Junge, K.; Beller, M. Selective Catalytic Hydrogenations of Nitriles, Ketones, and Aldehydes by Well-Defined Manganese Pincer Complexes. *J. Am. Chem. Soc.* **2016**, *138* (28), 8809–8814. https://doi.org/10.1021/jacs.6b03709

(14) Lyu, Q.; Qian, X.; Su, Y.; Wang, Y.; Li, L.; Wang, Z.; Ma, Y.; Sun, W.-H. Efficiently Robust Transfer Hydrogenation of Nitriles to Methylamines Achieved by Using Manganese Complexes. *J. Catal.* **2026**, *459*, 116925. https://doi.org/10.1016/j.jcat.2026.116925

(15) Sarkar, K.; Das, K.; Kundu, A.; Adhikari, D.; Maji, B. Phosphine-Free Manganese Catalyst Enables Selective Transfer Hydrogenation of Nitriles to Primary and Secondary Amines

Using Ammonia–Borane. *ACS Catal.* **2021**, *11* (5), 2786–2794. https://doi.org/10.1021/acscatal.0c05406
(16) Hayrapetyan, D.; Khalimon, A. Y. Catalytic Nitrile Hydroboration: A Route to N,N-Diborylamines and Uses Thereof. *Chem. - Asian J.* **2020**, *15* (17), 2575–2587. https://doi.org/10.1002/asia.202000672
(17) Li, B.; Sortais, J.-B.; Darcel, C. Amine Synthesis via Transition Metal Homogeneous Catalysed Hydrosilylation. *RSC Adv.* **2016**, *6* (62), 57603–57625. https://doi.org/10.1039/c6ra10494k
(18) Faverio, C.; Boselli, M. F.; Medici, F.; Benaglia, M. Ammonia Borane as a Reducing Agent in Organic Synthesis. *Org. Biomol. Chem.* **2020**, *18* (39), 7789–7813. https://doi.org/10.1039/D0OB01351J
(19) Yang, X.; Fox, T.; Berke, H. Ammonia Borane as a Metal Free Reductant for Ketones and Aldehydes: A Mechanistic Study. *Tetrahedron* **2011**, *67* (37), 7121–7127. https://doi.org/10.1016/j.tet.2011.06.104
(20) Yu, C.; Fu, J.; Muzzio, M.; Shen, T.; Su, D.; Zhu, J.; Sun, S. CuNi Nanoparticles Assembled on Graphene for Catalytic Methanolysis of Ammonia Borane and Hydrogenation of Nitro/Nitrile Compounds. *Chem. Mater.* **2017**, *29* (3), 1413–1418. https://doi.org/10.1021/acs.chemmater.6b05364
(21) Göksu, H.; Ho, S. F.; Metin, Ö.; Korkmaz, K.; Mendoza Garcia, A.; Gültekin, M. S.; Sun, S. Tandem Dehydrogenation of Ammonia Borane and Hydrogenation of Nitro/Nitrile Compounds Catalyzed by Graphene-Supported NiPd Alloy Nanoparticles. *ACS Catal.* **2014**, *4* (6), 1777–1782. https://doi.org/10.1021/cs500167k
(22) Ding, M.; Chang, J.; Mao, J.-X.; Zhang, J.; Chen, X. Noncatalyzed Reduction of Nitriles to Primary Amines with Ammonia Borane. *J. Org. Chem.* **2022**, *87* (24), 16230–16235. https://doi.org/10.1021/acs.joc.2c01727
(23) Colacino, E.; Isoni, V.; Crawford, D.; García, F. Upscaling Mechanochemistry: Challenges and Opportunities for Sustainable Industry. *Trends in Chem.* **2021**, *3* (5), 335–339. https://doi.org/10.1016/j.trechm.2021.02.008
(24) Friščić, T.; Mottillo, C.; Titi, H. M. Mechanochemistry for Synthesis. *Angewandte Chemie International Edition* **2020**, *59* (3), 1018–1029. https://doi.org/10.1002/anie.201906755
(25) James, S. L.; Adams, C. J.; Bolm, C.; Braga, D.; Collier, P.; Friščić, T.; Grepioni, F.; Harris, K. D. M.; Hyett, G.; Jones, W.; Krebs, A.; Mack, J.; Maini, L.; Orpen, A. G.; Parkin, I. P.; Shearouse, W. C.; Steed, J. W.; Waddell, D. C. Mechanochemistry: Opportunities for New and Cleaner Synthesis. *Chem. Soc. Rev.* **2012**, *41* (1), 413–447. https://doi.org/10.1039/C1CS15171A
(26) Howard, J. L.; Cao, Q.; Browne, D. L. Mechanochemistry as an Emerging Tool for Molecular Synthesis: What Can It Offer? *Chemical Science* **2018**, *9* (12), 3080–3094. https://doi.org/10.1039/C7SC05371A
(27) Menuel, S.; Léger, B.; Addad, A.; Monflier, E.; Hapiot, F. Cyclodextrins as Effective Additives in AuNP-Catalyzed Reduction of Nitrobenzene Derivatives in a Ball-Mill. *Green Chem.* **2016**, *18* (20), 5500–5509. https://doi.org/10.1039/C6GC00770H
(28) Mack, J.; Fulmer, D.; Stofel, S.; Santos, N. The First Solvent-Free Method for the Reduction of Esters. *Green Chem.* **2007**, *9* (10), 1041. https://doi.org/10.1039/b706167f
(29) Cuccu, F.; Basoccu, F.; Fattuoni, C.; Porcheddu, A. Mechanically Accelerated Catalytic Hydrogenation: Correlating Physical State, Reaction Rate, and Interface Area. *Green Chem.* **2024**, *26* (4), 1927–1934. https://doi.org/10.1039/D3GC03783E

(30) Toyama, Y.; Nakamura, T.; Horikawa, Y.; Morinaka, Y.; Ono, Y.; Yagi, A.; Itami, K.; Ito, H. Rh-Catalyzed Mechanochemical Transfer Hydrogenation for the Synthesis of Periphery-Hydrogenated Polycyclic Aromatic Compounds. *Chem. Sci.* **2025**, *16* (21), 9117–9124. https://doi.org/10.1039/d5sc01489a
(31) Mkrtchyan, S.; Purohit, V. B.; Shalimov, O.; Karpun, Y.; Prajapati, R. V.; Prajapati, V. D.; Bielec, B.; Addová, G.; Filo, J.; Jin, P.; Wang, C.; Katayev, D.; Iaroshenko, V. O. Photo and Mechanochemically Induced Reduction of Nitroarenes Using Ammonia Borane. *Org. Chem. Front.* **2026**, *13* (3), 874–883. https://doi.org/10.1039/D5QO01451D
(32) Portada, T.; Margetić, D.; Štrukil, V. Mechanochemical Catalytic Transfer Hydrogenation of Aromatic Nitro Derivatives. *Molecules* **2018**, *23* (12), 3163. https://doi.org/10.3390/molecules23123163
(33) Li, A. Y.; Segalla, A.; Li, C.-J.; Moores, A. Mechanochemical Metal-Free Transfer Hydrogenation of Carbonyls Using Polymethylhydrosiloxane as the Hydrogen Source. *ACS Sustainable Chem. Eng.* **2017**, *5* (12), 11752–11760. https://doi.org/10.1021/acssuschemeng.7b03298
(34) Hanek, L. M.; Bolm, C. Mechanochemical Hydrodeoxygenations. *Eur. J. Org. Chem.* **2026**, *29* (22), e202501222. https://doi.org/10.1002/ejoc.202501222
(35) Ai, Z.; Liu, M.; Wang, X.; He, X.; Zhang, X.; Lian, Z. Mechanochemical Piezoelectric Catalysis: Advancing the Hydrogenation of Alkenes. *Adv. Sci. n/a* (n/a), e76446. https://doi.org/10.1002/advs.76446
(36) Nallaparaju, J. V.; Aav, R.; Kananovich, D. Mechanochemistry: A Transformative Technique for the Synthesis of Polar Organometallics from Zero-Valent Metals. *ChemPlusChem* **2026**, *91* (1), e202500445. https://doi.org/10.1002/cplu.202500445
(37) Nallaparaju, J. V.; Satsi, R.; Merzhyievskyi, D.; Jarg, T.; Aav, R.; Kananovich, D. G. Mechanochemical Birch Reduction with Low Reactive Alkaline Earth Metals. *Angew. Chem. Int. Ed.* **2024**, *63* (20). https://doi.org/10.1002/anie.202319449
(38) Kondo, K.; Lowe, M.; Davison, N.; Waddell, P. G.; Armstrong, R. J.; Lu, E.; Kubota, K.; Ito, H. Mechanochemical Synthesis of Organosodium Compounds through Direct Sodiation of Organic Halides. *Nat. Synth* **2026**, *5* (5), 669–679. https://doi.org/10.1038/s44160-025-00949-7
(39) Kubota, K.; Nagao, A.; Ito, H. Solvent-Free Zinc-Mediated Béchamp Reduction Using Mechanochemistry. *RSC Mechanochem.* **2025**, *2* (3), 389–393. https://doi.org/10.1039/D4MR00138A
(40) Sudrajat, H.; Hsu, H.-Y.; Jérôme, F.; Colmenares, J. C. Mechanoredox-Catalyzed Organic Synthesis with Piezoelectric Materials: Quo Vadis? *ChemCatChem* **2025**, *17* (6), e202401814. https://doi.org/10.1002/cctc.202401814
(41) Bhatnagar, S.; Felderhoff, M.; Schöbel, J.-H. Solvent-Free Mechanocatalytic Reduction of Nitro Compounds with Hydrogen Gas and Its Application in the Synthesis of Drugs and Their Intermediates. *Adv. Synth. Catal.* **2025**, *367* (19), e70071. https://doi.org/10.1002/adsc.70071
(42) Mayer, M.; Wohlgemuth, M.; Salomé Straub, A.; Grätz, S.; Borchardt, L. Hydrogenation of Organic Molecules via Direct Mechanocatalysis. *Angew. Chem. Int. Ed.* **2025**, *64* (16), e202424139. https://doi.org/10.1002/anie.202424139
(43) Heiden, Z. M.; Lathem, A. P. Establishing the Hydride Donor Abilities of Main Group Hydrides. *Organometallics* **2015**, *34* (10), 1818–1827. https://doi.org/10.1021/om5011512
(44) Jarg, T.; Tamm, J.; Suut-Tuule, E.; Lootus, K.-M.; Kananovich, D.; Aav, R. How Reliable Is Internal Standard Method in Monitoring Mechanochemical Synthesis? A Case Study of

Triphenylmethane in HPLC-UV-MS Analysis of Hemicucurbit[*n*]Urils. *RSC Mechanochem.* **2025**, *2* (4), 507–515. https://doi.org/10.1039/D4MR00145A
(45) Jafter, O. F.; Lee, S.; Park, J.; Cabanetos, C.; Lungerich, D. Navigating Ball Mill Specifications for Theory-to-Practice Reproducibility in Mechanochemistry. *Angew. Chem. Int. Ed.* **2024**, *63* (48), e202409731. https://doi.org/10.1002/anie.202409731
(46) Hu, Z.; Kerton, F. M. Simple Copper/TEMPO Catalyzed Aerobic Dehydrogenation of Benzylic Amines and Anilines. *Org. Biomol. Chem.* **2012**, *10* (8), 1618. https://doi.org/10.1039/c2ob06670j
(47) Xu, B.; Hartigan, E. M.; Feula, G.; Huang, Z.; Lumb, J.; Arndtsen, B. A. Simple Copper Catalysts for the Aerobic Oxidation of Amines: Selectivity Control by the Counterion. *Angew. Chem. Int. Ed.* **2016**, *55* (51), 15802–15806. https://doi.org/10.1002/anie.201609255
(48) Patil, R. D.; Gupta, M. K. Methods of Nitriles Synthesis from Amines through Oxidative Dehydrogenation. *Adv. Synth. Catal.* **2020**, *362* (19), 3987–4009. https://doi.org/10.1002/adsc.202000635
(49) Boldyreva, E. Non-Ambient Conditions in the Investigation and Manufacturing of Drug Forms. *Curr. Pharm. Des.* **2016**, *22* (32), 4981–5000. https://doi.org/10.2174/1381612822666160804093120
(50) Carta, M.; Delogu, F. Ball Dynamics and Rate of Mechanically Induced Transformations in Oscillating Ball Mills. *Chemical Engineering Science* **2026**, *335*, 124495. https://doi.org/10.1016/j.ces.2026.124495
(51) Neese, F. Software Update: The ORCA Program System—Version 6.0. *WIREs Comput Mol Sci* **2025**, *15* (2), e70019. https://doi.org/10.1002/wcms.70019
(52) Pladevall, B. S.; De Aguirre, A.; Maseras, F. Understanding Ball Milling Mechanochemical Processes with DFT Calculations and Microkinetic Modeling. *ChemSusChem* **2021**, *14* (13), 2763–2768. https://doi.org/10.1002/cssc.202100497
(53) Galeas, D. M.; Tolbatov, I.; Colacino, E.; Maseras, F. Computational Study on the Mechanism for the Synthesis of Active Pharmaceutical Ingredients Nitrofurantoin and Dantrolene in Both Solution and Mechanochemical Conditions. *Phys. Chem. Chem. Phys.* **2024**, *26* (37), 24288–24293. https://doi.org/10.1039/D4CP01613K
(54) Garcia-Padilla, E.; Maseras, F. Understanding the Divergence in Outcomes between Mechanochemical and Solution Phase Reactivity of Fullerenes. *Cell Reports Physical Science* **2025**, *6* (2), 102434. https://doi.org/10.1016/j.xcrp.2025.102434
(55) Álvarez-Moreno, M.; De Graaf, C.; López, N.; Maseras, F.; Poblet, J. M.; Bo, C. Managing the Computational Chemistry Big Data Problem: The **ioChem-BD** Platform. *J. Chem. Inf. Model.* **2015**, *55* (1), 95–103. https://doi.org/10.1021/ci500593j
(56) N. Storhoff, B.; C. Lewis Jr., H. Organonitrile Complexes of Transition Metals. *Coordination Chemistry Reviews* **1977**, *23* (1), 1–29. https://doi.org/10.1016/S0010-8545(00)80329-X
(57) Reedijk, J.; Zuur, A. P.; Groeneveld, W. L. Complexes with Ligands Containing Nitrile Groups. Part III. Infrared Spectra of Coordinated Methyl Cyanide. *Recl. Trav. Chim. Pays-Bas* **1967**, *86* (10), 1127–1137. https://doi.org/10.1002/recl.19670861012
(58) Beamson, G.; Briggs, D. *High Resolution XPS of Organic Polymers: The Scienta ESCA300 Database*; Wiley: Chichester, 1992.
(59) Cano, A.; Avila, Y.; Avila, M.; Reguera, E. Structural Information Contained in the XPS Spectra of Nd10 Metal Cyanides. *J. Solid State Chem.* **2019**, *276*, 339–344. https://doi.org/10.1016/j.jssc.2019.05.021

(60) Biesinger, M. C. Advanced Analysis of Copper X-ray Photoelectron Spectra. *Surf. Interface Anal.* **2017**, *49* (13), 1325–1334. https://doi.org/10.1002/sia.6239

SUPPORTING INFORMATION

Copper-Mediated Mechanochemical Nitrile Reduction in Mild Conditions Using Ammonia Borane and *in silico* Mechanistic Studies

Andrea Casagrande,[a,b] *Yingzi Li,*[c] *Laurence Brandon,*[c] *Valerie Flaud,*[a] *Dzmitry Kananovich,*[b] *Riina Aav,*[b] *Allan Niidu,*[b] *Feliu Maseras,*[c] *Evelina Colacino*[a]

[a]ICGM, University of Montpellier, CNRS, ENSCM, Montpellier, France

[b]Tallinn University of Technology, Tallinn, Estonia

[c]Institute of Chemical Research of Catalonia (ICIQ-CERCA), The Barcelona Institute of Science and Technology, Avgda. Països Catalans 16, 43007, Tarragona, Spain.

TABLE OF CONTENT

EXPERIMENTAL PART ... 3

S1. General experimental procedure ... 4

S1.1 Initial Lewis' Acids Screening ... 5

S1.2 Comprehensive screening and optimization experiments for *o*-iodobenzonitrile (9-RCN) and *o*-fluorobenzonitrile (1-RCN). ... 6

S1.4 Scope Limitation ... 10

S1.5 Effect of humidity on the reaction outcome ... 11

S2. Characterization data ... 14

S3. FT-IR Spectra of Nitrile-Cu Complexes ... 15

S3.1 Notable IR C≡N stretch peak shifts in RCN-Cu complexes ... 28

S4. XPS spectra ... 29

S4.1 N 1s spectra for the 2-halobenzonitriles series ... 29

S4.2 XPS spectra of 1-RCN-Cu ... 30

S4.3 XPS spectra of $CuCl_2$ ... 31

S5. Additional computational results ... 33

S.5.1 The uncatalyzed reaction ... 33

S5.2 Modeling of the $CuCl_2$ solid ... 34

S5.3 Effect of coordination to copper on the nitrile IR frequencies ... 34

S5.4 DFT calculations of the reduction of 9-RCN ... 35

S5.5 DFT calculations of Cu_2Cl_3H formation ... 36

S5.6 Benchmarking of the DFT functional ... 37

S7. Cartesian coordinates of the computed structures ... 38

References ... 60

EXPERIMENTAL PART

General remarks

All reagents were commercially available and used without any further purification.

NMR spectra were recorded at room temperature on a Bruker 400 MHz spectrometer at room temperature. Chemical shifts (δ) of ^{1}H-NMR spectra are reported in ppm relative to residual solvent signals of the deuterated solvents (H_2O in D_2O: δ = 4.79 ppm, $CHCl_3$ in $CDCl_3$: δ = 7.26 ppm); *J* values are given in *Hz*. $^{13}C\{^{1}H\}$ were recorded at 151 MHz on the same instrument and the chemical shifts (δ) are reported in ppm, referenced against trimethylsilyl propionic acid (TSP) δ = 0.0 ppm; *J* values are given in *Hz*. $^{19}F\{^{1}H\}$ NMR spectra were recorded at 377 M*Hz* with the same instrument. The chemical shifts are expressed in ppm, reported from $CFCl_3$ δ = 0.0 ppm. The following abbreviations are used to express the multiplicity: s (singlet), d (doublet), t (triplet), dd (doublet of doublet), dt (doublet of triplets), td (triplet of doublets) or m (multiplet). The identity of analytically pure final products was assessed by comparison of the spectral data previously described in the literature and by their fragmentation in LC−MS or GC-MS.

Liquid Chromatography coupled to Mass Spectrometry (LC-MS). The samples are dissolved in eluent B before their injection. The analyses were carried out on a microOtof-Q II mass spectrometer (Bruker) coupled to a U 3000 chromatographic chain (Thermoscientific). The analyses are carried out in FIA (Flow Injection Analysis). Eluent A is water acidified with 0.1% formic acid. Eluent B is acetonitrile acidified with 1% formic acid. The flow rate is 0.4 mL/min of a 50-50 mixture of the two eluents. The ionization mode is electrospray. The source parameters are as follows: Capillary voltage 4500 V; nebulizer gas pressure 0.5 Bar; drying gas flow rate: 4 L/min; source temperature 180 °C. The analyses are carried out in both positive and negative modes. The injected volume is 0.1 µL and the analysis time is 1 min.

GC–MS analyses were performed in a GC Agilent 6890 (Agilent Technologies, USA) that was fitted with a mass detector Shimadzu GCMS-QP2010 SE, using a 20 m long capillary column, internal diameter (i.d.) of 0.18 mm and film thickness 0.18 µm (Zebron). GC conditions were: injection split 1:20, injector temperature 250 °C, detector temperature 280 °C. Gas carrier: helium (0.74 mL/min), temperature program: from 50 °C (3 min) to 300 °C at 10 °C/min.

Fourier-transform infrared (FT-IR) spectra were recorded in the ATR mode on a Perkin Elmer Spectrum 100 FT-IR instrument (Attenuated Total Reflectance Infrared ATR-IR device) in reflectance mode. Measurements are performed directly on the powders. The powders were placed on the ATR-IR plate and a constant pressure (*i.e.* force gauge was kept at 19% of the scale) was applied to the powder to bring it into good contact with the ATR crystal. The characteristic IR absorptions mentioned in the text

are reported in cm^{-1}. The application of a force uniformly distributed across the crystal allowed to obtain adequate band intensities and monitor over the time their modifications. Band positions are reported in cm^{-1}.

Density functional theory (DFT) calculations were performed using the ORCA program system.[1] Geometry optimizations for all stationary points, including reactants, intermediates, and transition states, were carried out using the B3LYP-D3BJ functional[2–4] with the def2-TZVP basis set.[5] in a dielectric environment for DCM,[6] which was deemed reasonable for the experimental conditions. Frequency calculations were performed at the same level to confirm the nature of each stationary point (no imaginary frequencies for minima and one imaginary frequency for transition states) and to obtain zero-point energies and thermal corrections to Gibbs energies at 298 K. All computational results have been uploaded to the ioChem-BD repository.[7]

XPS analysis was performed using a Thermo Electron ESCALAB 250 device. The photoelectron emission spectra were recorded using Al–Kα radiation (hν = 1486.6 eV) from a monochromatized source. The spot size was approximately 500 μm^2. The pass energy was fixed at 20 eV for high resolution scan.

The spectrometer energy calibration was made using the Au 4f7/2 (83.9 ± 0.1 eV) and Cu $2p_{3/2}$ (932.8 ± 0.1 eV) photoelectron lines. The binding energy scale was established by referencing the C 1s value of adventitious carbon (284.8 eV). The background signal was removed using the Shirley method.[8] The atomic concentrations were determined with a relative error of 10%-20% from photoelectron peak areas using the atomic sensitivity factors reported by Scofield.[9] The photoelectron peaks were analysed by Gaussian/Lorentzian (G/L = 50) peak fitting.

Vibrating ball-milling experiments were performed in:

a) a horizontal MM400 or MM500 Vario mixer-mill (Retsch GmbH, Haan, Germany) or FTS-1000 (InSolido Technologies jdoo, Zagreb, Croatia) using 10 mL zirconium oxide jar with zirconium oxide ball(s) of 10 mm Ø, 7 mm Ø, 5 mm Ø or 10 mL PTFE jar with either 10 mm Ø PFTE coated SS ball, 10 mm Ø SS ball or 10 mm Ø, 7 mm Ø, 5 mm Ø zirconium oxide ball(s);

b) a vertical mixer-mill Pulverisette 23 (Fritsch GmbH, Idar-Oberstein, Germany) using a 5 mL PTFE jar with 1 zirconium oxide ball of 10 mm Ø.

S1. General experimental procedure

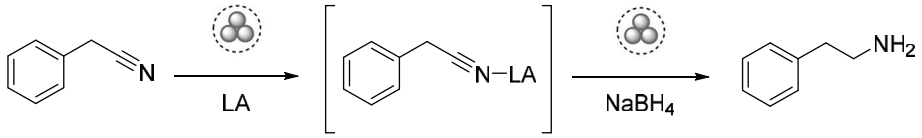
To a 10 mL ZrO_2 jar equipped with 5 7 mm Ø balls of the same material, the nitrile (1.5 mmol, 1.0 equiv.), $CuCl_2$ (0.75 mmol, 0.5 equiv.) were milled for 30 minutes at 30 *Hz* in a MM400 mixer mill (*step 1*). After this milling time, NH_3BH_3 (7.5 mmol, 5 equiv.) was added, and the reaction mixture was furtherly milled for 90 minutes at 30 *Hz* (*step 2*). Then the reaction crude is dissolved in MTBE (30 mL

total to recover the whole crude from the jar) and filtered through celite to remove the black suspended precipitate. After this, N_2 gas is bubbled through the filtrate to remove any dissolved NH_3 and then 1 mL of 3M HCl in CPME is added, causing the white amine hydrochloride **1-8** to precipitate. The solution is filtered under vacuum. At this point, to confirm the absence of NH_4Cl, the precipitate is dissolved in MeOH: while the amine is soluble in the alcoholic media, the NH_4Cl is not and should precipitate. If precipitate is observed is then filtered and discarded, then the amine hydrochloride **1-8** is recovered pure from the solution by evaporating MeOH at reduced pressure at 40 °C. The amine **9-NH_2** was isolated as free amine via extraction: the crude was dissolved in MBTE and filtered through celite to remove the black suspended precipitate, then the filtrate was transferred to a extraction funnel and extracted the amine in water phase with 3x30 mL 1M HCl, then K_2CO_3 was added to the water phase until pH = 10, and the free base amine **9-NH_2** was extracted in MTBE using 4x30 mL of the ether. The organic phase is then dried with $MgSO_4$ and the amine **9-NH_2** is recovered pure by evaporation of the solvent under reduced pressure.

S1.1 Initial Lewis' Acids Screening

Initial screenings were conducted adding to a 10 mL ZrO_2 jar equipped with a single 10 mm Ø ball of the same material, 0.5 mmol of benzyl cyanide (1 equiv., 57.4 μL) and 0.5 mmol of the Lewis' acid (LA, 1 equiv.). They are milled together at 30 Hz for 15 minutes, then the jar is opened and 4.5 mmol of $NaBH_4$ (9 equiv., 170.2 mg) are added and the reaction mixture is further milled for 90 minutes at 30 Hz. The crude is then dissolved in CH_2Cl_2, filtered and analyzed *via* GCMS.

Table S1. Screening of Lewis' acids as nitrile bond activators for reduction through $NaBH_4$.



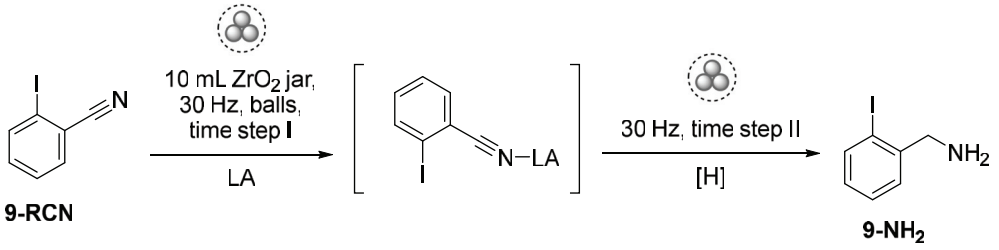
LA	$MgCl_2$	$AlCl_3$	TiF_4	$MnCl_2$	$FeCl_3$	$CuCl_2 \cdot H_2O$	$ZnCl_2$	$ZrCl_4$
Conversion[a] (%)	9%	19%	74%	6%	62%	26%	2%	41%

[a] Conversion calculated via GCMS

Conversion of benzyl cyanide generally follows the hardness of the LA, the fluctuations can be due to several factor such as susceptibility to air/moisture of the LA, specific side reactions that can be promoted by specific metal centers and can alter the conversion reading etc.

S1.2 Comprehensive screening and optimization experiments for *o*-iodobenzonitrile (9-RCN) and *o*-fluorobenzonitrile (1-RCN).

Table S2. Optimization experiments for the reduction of **9-RCN** to **9-NH_2**, LA = Lewis' Acid; [H] = reducing agent.



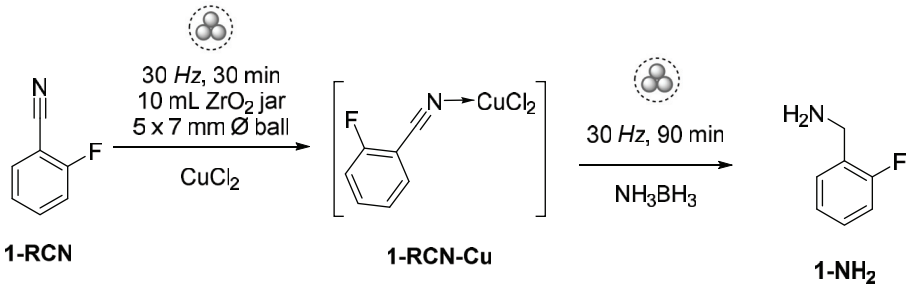
9-RCN **9-NH_2**

Entry	LA	LA equiv.	[H]	[H] equiv.	Balls (n*Ø)	Time (min) (step I + step II)	Conversion[a] (%)	Yield[a] of 9-NH_2 (%)
1	$ZrCl_4$	1	$NaBH_4$	9	1*10	15 + 90	66%	64%
2	$ZrCl_4$	1	$NaBH_4$	9	1*10	15 + 120	38%	5%
3	$ZrCl_4$	0.5	$NaBH_4$	5	1*10	45 + 30	16%	1%
4	$CuCl_2$	0.5	$NaBH_4$	5	1*10	45 + 90	99%	7%
5[b]	$CuCl_2$	0.5	NH_3BH_3	5	1*10	45 + 90	86%	47%
6	$CuCl_2$	0.5	NH_3BH_3	5	1*10	45 + 90	85%	49%
7	$CuCl_2$	0.5	NH_3BH_3	5	1*10	20 + 90	65%	21%
8	$CuCl_2$	0.5	NH_3BH_3	5	1*10	30 + 90	81%	53%
9	$CuCl_2$	0.5	NH_3BH_3	2	1*10	30 + 90	75%	28%
10	$CuCl_2$	0.5	NH_3BH_3	3.5	1*10	30 + 90	80%	40%
11	$CuCl_2$	0.5	NH_3BH_3	6	1*10	30 + 90	67%	28%
12	$CuCl_2$	0.5	NH_3BH_3	7	1*10	30 + 90	87%	33%
13	$CuCl_2$	1	NH_3BH_3	5	1*10	30 + 90	85%	6%
14	$CuCl_2$	0.4	NH_3BH_3	5	1*10	30 + 90	65%	28%
15	$CuCl_2$	0.6	NH_3BH_3	5	1*10	30 + 90	79%	19%
16	$CuCl_2$	0.5	NH_3BH_3	5	3*7	30 + 90	69%	11%
17	$CuCl_2$	0.5	NH_3BH_3	5	1*10	30 + 30	58%	14%
18	$CuCl_2$	0.5	NH_3BH_3	5	1*10	30 + 60	74%	31%
19	$CuCl_2$	0.5	NH_3BH_3	5	1*10	30 + 120	87%	52%
20	$CuCl_2$	0.5	NH_3BH_3	5	5*7	30 + 90	88%	43%
21	$CuCl_2$	0.5	NH_3BH_3	5	1*10	45 + 90	67%	45%

22	$CuCl_2$	0.5	NH_3BH_3	5	1*10	90[c]	83%	28%
23	$CuCl_2$	0.5	NH_3BH_3	5	2*7	30 + 90	65%	16%
24[d]	$CuCl_2$	0.5	NH_3BH_3	5	1*10	30 + 90	92%	57%
25	$CuCl_2$	0.5	NH_3BH_3	5	4*7	30 + 90	91%	36%
26	$AlCl_3$	0.5	NH_3BH_3	5	1*10	30 + 90	60%	25%

Typical experimental procedure: To a 10 mL ZrO_2 jar equipped with the specified amount and size of balls of the same material, the nitrile (1.5 mmol, 1.0 equiv.) and the specified LA were milled for the specified time at 30 *Hz* in a mixer mill (*step 1*). After this milling time, the reducing agent [H] was added, and the reaction mixture was further milled for the specified time at 30 *Hz* (*step 2*). [a] Calculated *via* ^{1}H qNMR, in $CDCl_3$ using cyclododecane as internal standard. [b] Jar assembled in glove box. [c] Experiment performed in a single step adding all the reagents together at the start. [d] The crude was left aging for 24 hours before running the analysis, the jar was never opened before the sampling.

Table S3. Comprehensive AB and $CuCl_2$ loading optimization for the reduction of **1-RCN** to **1-RNH$_2$**.



Entry	$CuCl_2$ equiv.	AB equiv.	Conversion[a] (%)	Yield of 1-RNH_2[a] (%)
1	0.5	2	29%	16%
2	0.5	4	61%	47%
3	**0.5**	**5**	**100%**	**93% (92%)[b]**
4	0.5	6	56%	46%
5	0.5	7	55%	33%
6	0.2	5	12%	12%
7	0.4	5	45%	35%
8	0.6	5	94%	92%
9	1	5	88%	2%
10	0.2	2	37%	13%
11	0.3	3	15%	15%

Typical experimental procedure: To a 10 mL ZrO_2 jar equipped with 5 x 7 mm Ø balls of the same material, the nitrile (1.5 mmol, 1.0 equiv.), $CuCl_2$ were milled for 30 minutes at 30 *Hz* in a mixer mill (*step 1*). After this milling

time, AB was added, and the reaction mixture was further milled for 90 minutes at 30 *Hz* (*step 2*). [a] Calculated *via* ^{1}H qNMR, in $CDCl_3$ using cyclododecane as internal standard.[10] [b] Isolated yield.

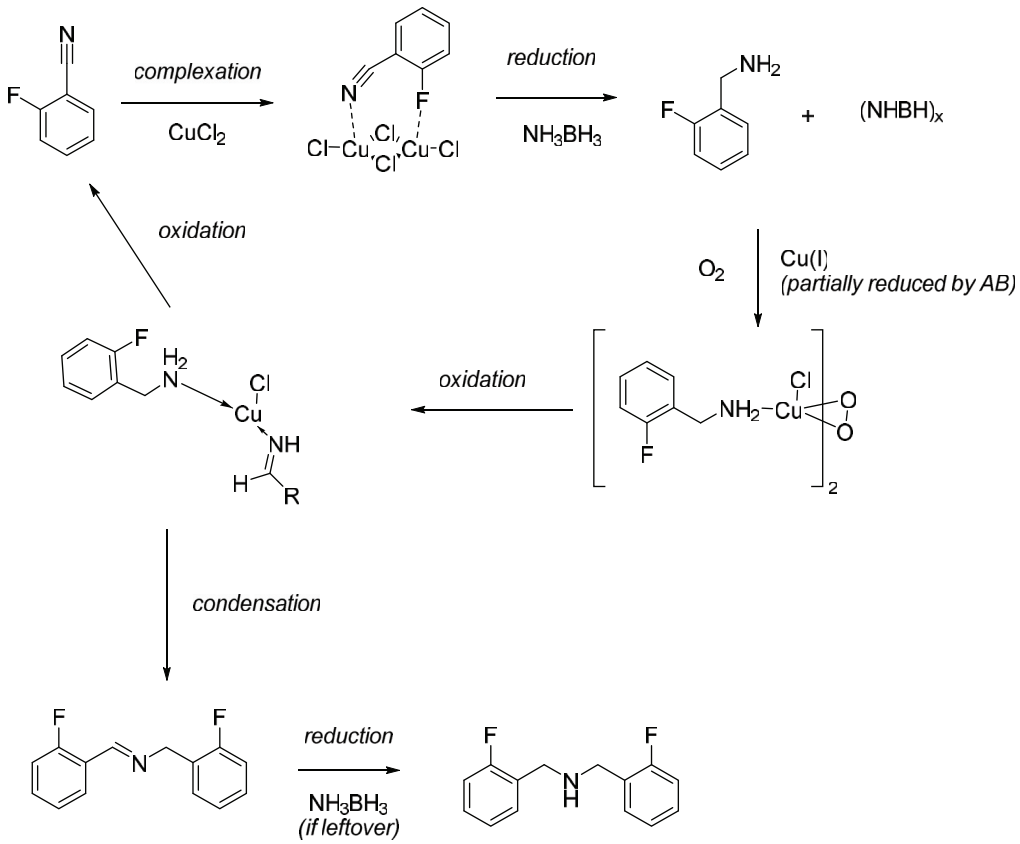
Table S4. Comprehensive technical parameters optimization for the reduction of **1-RCN** to **1-RNH$_2$**.

Entry	Time Step (min.)		Jar material	*f*(Hz)	Balls (n*Ø)	Energy			Conversion[a]	Yield[a]
	1	2				E_{tot} (kJ) (step 1)	E_{tot} (kJ) (step 2)	E_{imp} (mJ)		
1	15	90	ZrO_2	30Hz	5*7	9.8	59.1	7.34	39%	20%
2	30	90	ZrO_2	30Hz	5*7	19.7	59.1	7.34	100%	93% (92%[b])
3	45	90	ZrO_2	30Hz	5*7	29.5	59.1	7.34	65%	38%
4	30	30	ZrO_2	30Hz	5*7	19.7	19.7	7.34	64%	18%
5	30	60	ZrO_2	30Hz	5*7	19.7	39.4	7.34	60%	20%
6	30	120	ZrO_2	30Hz	5*7	19.7	78.8	7.34	16%	14%
7	30	90	ZrO_2	30Hz	4*7	15.8	47.4	7.34	100%	60%
8	30	90	ZrO_2	30Hz	3*7	11.9	35.6	7.34	96%	90%
9	30	90	ZrO_2	30Hz	2*7	7.9	23.8	7.34	99%	84%
10	30	90	ZrO_2	30Hz	6*5	9.5	28.6	2.95	56%	54%
11	30	90	ZrO_2	30Hz	4*5	8.0	23.9	2.95	56%	50%
12	30	90	ZrO_2	30Hz	1*10	11.7	35.2	21.8	100%	91%
13	30	90	ZrO_2	25Hz	1*10	6.8	20.4	15.1	100%	61%
14[c]	30	90	ZrO_2	30Hz	1*10	11.6	34.8	21.5	56%	34%
15[c]	30	90	ZrO_2	50Hz	1*10	53.7	161.2	59.7	75%	37%
16[d]	30	90	PTFE	30Hz	1*10	15.3	46.0	28.5	100%	90%
17[e]	30	n.p.[f]	PTFE	30Hz	1*10	11.7	35.2	21.8	48%[g]	22%[g]
18	30	n.p.[f]	PTFE	30Hz	1*10	6.9	20.6	12.7	91%[g]	13%[g]
19[e]	30	n.p.[f]	PTFE	30Hz	5*7	19.7	59.1	7.34	79%[g]	21%[g]

Typical experimental procedure: To a 10 mL ZrO_2 jar equipped with specified number and size of balls of the same material, the nitrile (1.5 mmol, 1.0 equiv.), $CuCl_2$ (0.75 mmol, 0.5 equiv.) were milled for the specified amount of time at the specified frequency in a MM400 mixer mill (*step 1*). After this milling time, NH_3BH_3 (7.5 mmol, 5 equiv.) was added, and the reaction mixture was further milled for the specified amount of time at the specified frequency (*step 2*). [a] Calculated *via* ^{1}H qNMR, in $CDCl_3$ using cyclododecane as internal standard.[10] [b] Isolated yield. [c] Mill used was Fritsch's P23 vertical mixer mill. [d] Ball material is stainless steel (SS). [e] Ball material is ZrO_2. [f] Not performed due to immediate pressure build up after the start of step *II*. [g] Crude analyzed after deflagration (≈1 s of step 2).

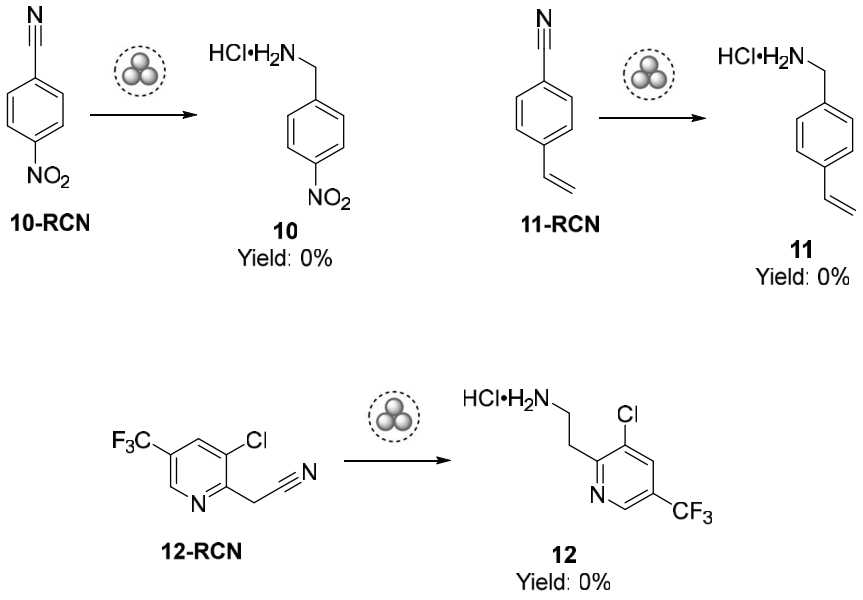
For step 1 (*e.g.* the complexation of $CuCl_2$ with the nitrile), the optimum is 30 min (entry 2). A shorter step 1 of 15 min (entry 1) gives markedly lower conversion (39%), consistent with insufficient time for $CuCl_2$ and **1-RCN** to mix and form the activated complex, whereas a longer

step 1 of 45 min (entry 3) is also detrimental (65% conversion), which we attribute to mechanical degradation of the complex and/or partial passivation of the copper by adventitious air in the jar (*e.g.* $CuCl_2$ to CuO). For step 2 (*e.g.* the reductive step after AB addition), conversion and yield increase progressively with milling time up to 90 min (entries 4, 5, 2: 30 min gives 64%, 60 min gives 60%, 90 min gives 100%). Beyond this optimum, however, over-milling is strongly deleterious: at 120 min (entry 6) the conversion collapses to 16%, far below not only the 90 min optimum but even the shorter 30 and 60 min runs. We rationalize this as a switch in the chemical environment of the jar once AB is exhausted. While AB is present in excess the jar interior is reductive, but once the AB is fully consumed (within ≈90 min) the environment becomes oxidative, only the residual oxygen of the sealed jar headspace and the Cu species remain, and copper is well known to catalyze the aerobic oxidative dehydrogenation of primary (benzylic) amines back to the corresponding nitriles (Scheme S1).[11–13] The product amine is thus partially re-oxidized to the starting nitrile under prolonged milling, eroding the apparent conversion. This interpretation is independently supported by experiments run at controlled humidity levels (see Section S1.5), which modulate the same oxidative pathway.



Scheme S1. Plausible mechanism for dehydrogenation byproducts of the amine.[11]

S1.4 Scope Limitation



Scheme S2. Substrates for which no desired product was observed.

To probe the limitations of this methodology, Scheme S2 reports a number of substrates for which the desired product could not be isolated. During the preparation of **10**, the reaction vessel deflagrated in *step 2*. With our reported scope no deflagration have been reported but is advised extreme precaution when milling in those reported condition when mixing a reducing agent (AB) and an oxidizer bearing group (like -NO_2) do preliminary test like Browne and coworkers advices[14] when applying this method to unreported substrates. Consistent with this, the IR spectrum of **10-RCN** after the *step 1* milling with $CuCl_2$ is essentially superimposable on that of free **10-RCN** (Figure S11), indicating that no Cu–nitrile complex is formed under these conditions, the strongly electron-withdrawing *para*-nitro group lowers the basicity of the nitrile nitrogen and prevents σ-donation to Cu(II). The deflagration is therefore attributed to a direct reaction between AB and the nitro group in *step 2*, not to a Cu-mediated pathway. In the case of **11**, the reaction proved unselective. The IR spectrum of the corresponding complex (Figure S12) shows that the single nitrile stretch of free **11-RCN** (2226 cm^{-1}) is replaced by two bands (2226 and 2246 cm^{-1}), while the vinyl C–H out-of-plane bending bands shift from 988 and 921 cm^{-1} to 996 and 929 cm^{-1}; in addition, the nitrile blueshift (20 cm^{-1}) is notably smaller than that of the analogous *para*-substituted complex **8-RCN-Cu** (45 cm^{-1}). Together these observations are consistent with an additional interaction between Cu and the vinyl moiety of **11-RCN** (Figure S12). The ^{1}H NMR spectrum of the isolated material indicated a mixture of products that could not be individually identified, consistent with the loss of selectivity inferred from the IR data. The synthesis of **12** was likewise unsuccessful, affording dehalogenation and loss of the CF_3 group rather than the desired product. The IR spectrum of

the corresponding complex (Figure S13) reveals a coordination mode distinct from that of the other substrates examined in this study: the C≡N stretch is essentially unchanged on complexation, whereas substantial perturbations of the pyridine ring skeletal modes and of the aromatic and methylene C–H stretches are observed. These changes are consistent with Cu coordination at the pyridine ring nitrogen rather than at the nitrile, a binding mode favored by the stronger donor character of the pyridine nitrogen and reinforced by the reduced basicity of the nitrile nitrogen due to the electron-withdrawing chlorine and trifluoromethyl substituents. The absence of Cu coordination at the nitrile prevents the activation required for reduction by AB, while the observed dehalogenation and loss of CF_3 group, which we were unable to mechanistically rationalize in detail, presumably proceed from this Cu–pyridine adduct as a parallel pathway.

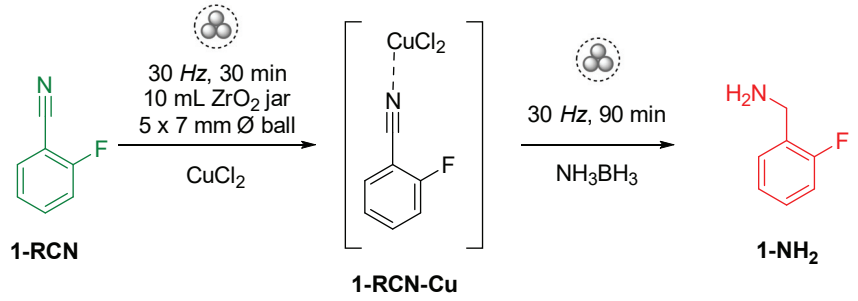
S1.5 Effect of humidity on the reaction outcome

The reaction outcome was found to be slightly but reproducibly affected by the ambient humidity at which the milling jar was assembled. Figure S1 reports the GC-MS chromatograms of three experiments performed at different relative-humidity (RH) levels, together with a control assembled inside an Ar-filled glovebox; the corresponding ^{1}H qNMR conversion and yield data are collected in Table S5.

Table S5. Effect of ambient humidity on the mechanochemical reduction of *o*-fluorobenzonitrile (**1-RCN**) to 2-fluorobenzylamine (**1-NH$_2$**).

Entry	Humidity (%)	Conversion (%)[a]	Yield (%)[a]
1	20%	100%	93%
2	49%	100%	50%
3	65%	94%	41%
4	Ar atm	100%	83%

[a] Calculated *via* ^{1}H qNMR, in $CDCl_3$ using cyclododecane as internal standard.



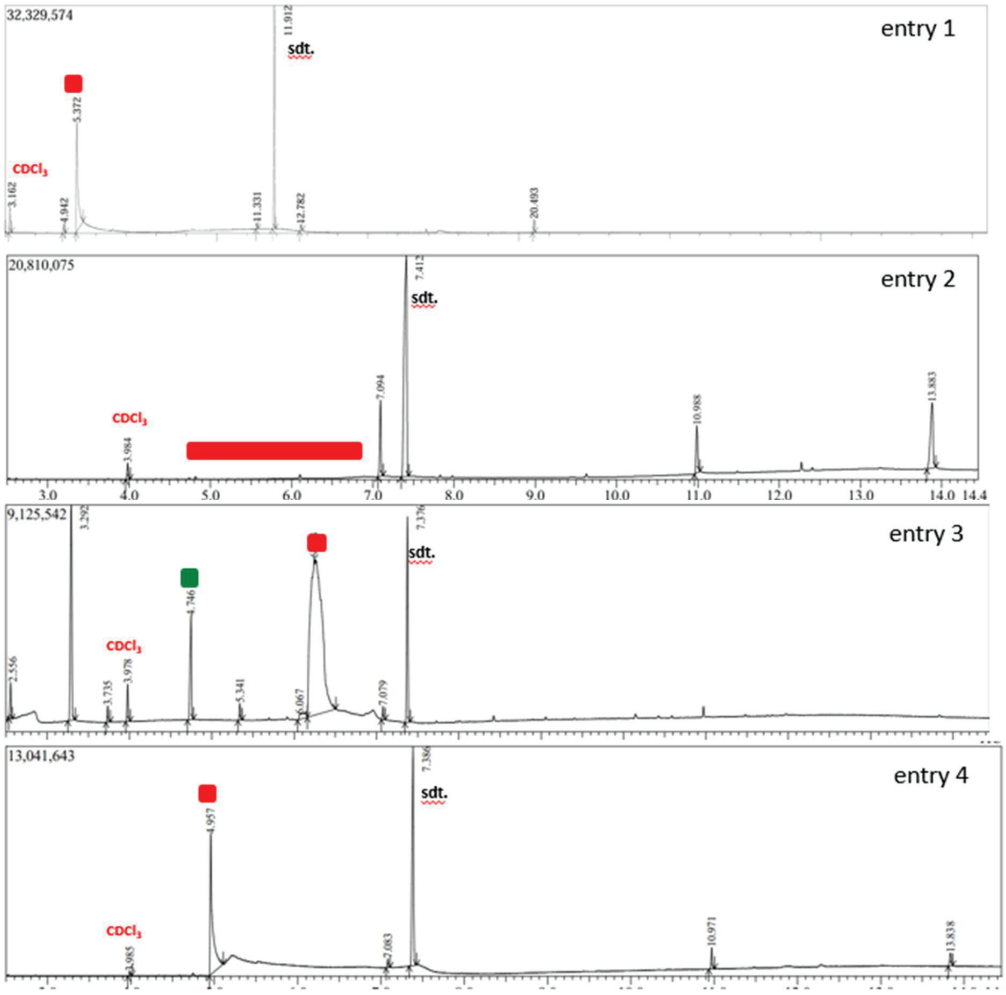


Figure S1. Figure of the 4 GC chromatograms of the 4 entries of Table S5. The GCMS were done on the same sample used previously to run the qNMR analysis of the crude, properly diluted. In the figure are indicated in green the peak of the starting material, in red the amine, then is marked the peak of the NMR solvent (CDCl3), and of the internal standard used (cyclododecane).

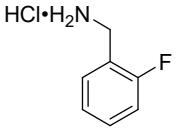
A clear trend emerges from the data: while the conversion of the starting *o*-fluorobenzonitrile remained essentially quantitative across all four experiments, the yield of the desired primary

amine **1-NH_2** dropped from 93% at 20% RH to 50% at 49% RH and 41% at 65% RH, with a parallel growth of GC peaks attributable to secondary-amine and imine by-products. We rationalize this loss of selectivity as the result of water-mediated diversion of the primary aldimine intermediate toward the secondary-amine manifold. Hydrogenation of nitriles with NH_3BH_3/Cu is established to proceed via a primary aldimine (ArCH=NH), which under anhydrous conditions is rapidly reduced to the primary amine.[15,16] In the presence of adventitious water, however, the aldimine can be hydrolyzed to the corresponding aldehyde and ammonia; the aldehyde then condenses with a molecule of the freshly formed primary amine to give a secondary aldimine ($ArCH=NCH_2Ar$), which is in turn reduced by residual NH_3BH_3 to the symmetrical secondary amine ($ArCH_2NHCH_2Ar$), the classical pathway responsible for secondary-amine selectivity losses in catalytic nitrile reductions.[16,17] An additional, slower contribution from Cu(II)/O_2-mediated aerobic dehydrogenation of the primary amine to the same aldimine/imine intermediates[11,12] is also expected to operate under humid conditions, since H_2O is known to accelerate the aerobic Cu(II) amine-oxidation manifold by facilitating proton-transfer steps in the rate-limiting β-H elimination from the Cu–amido intermediate.[11]

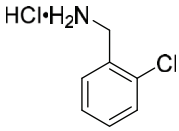
Interestingly, the control experiment assembled under Ar (entry 4) gave the same quantitative conversion as the driest air-assembled run (entry 1) and a very similar by-product profile, but slightly underperformed in terms of isolated amine yield (83% *vs* 93%). We tentatively attribute this small but reproducible difference to the beneficial role of a residual trace of O_2 in the unpurged jar in maintaining the Cu pre-catalyst in its active oxidation state. $CuCl_2$ added at the beginning of step II is rapidly reduced by NH_3BH_3 to Cu(0)/Cu(I) species,[18] in the absence of any O_2 this reduction is irreversible, whereas a sub-stoichiometric amount of O_2 allows re-oxidation of the Cu surface and the establishment of a more productive Cu(0)/Cu(II) redox cycle during milling. This phenomenon, in which atmospheric O_2 activates a Cu pre-catalyst during ball-milling, has been demonstrated and unambiguously assigned by Friščić, Batteas and co-workers for the Cu-catalyzed mechanochemical synthesis of tolbutamide, where Cu(I) precursors are shown to be aerobically oxidized to the catalytically active Cu(II) species directly inside the milling jar,[19] the same group has further shown that the Cu oxide layer formed on metallic copper under milling/RAM conditions can itself act as the catalytically active phase in direct mechanocatalysis of CuAAC reactions.[20] Under our conditions, an analogous trace-O_2 activation of the Cu(0) generated *in situ* from $CuCl_2$/NH_3BH_3 provides a plausible explanation for the small yield advantage of the dry-air run over the strictly inert one.

Together, these observations identify ambient humidity, rather than oxygen *per se*, as the principal external variable affecting the selectivity of the reaction, and justify the routine assembly of the jar under low-RH conditions in the standard protocol.

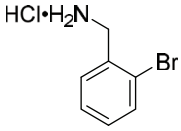
S2. Characterization data



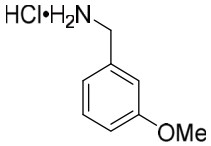
(2-fluorophenyl)methanamine hydrochloride (1). CAS [655-17-4]. White powder (Yield: 92%, 223.8 mg). **^{1}H NMR** (400 M*Hz*, D_2O) *δ* (ppm):[21] 7.54-7.48 (m, 2H), 7.32-7.24 (m, 2H), 4.29 (s, 2H). **^{13}C{^{1}H} NMR** (101 M*Hz*, D_2O) *δ* (ppm):[21] 160.9 (d, *J* = 246.1 *Hz*), 131.7 (d, *J* = 8.5 *Hz*), 131.3 (d, *J* = 2.4 *Hz*), 125.0-124.7 (m), 119.6 (d, *J* = 17.6 *Hz*), 115.7 (d, *J* = 21.0 *Hz*), 37.16. **^{19}F{^{1}H}NMR** (376 M*Hz*, D_2O) *δ*(ppm):[21] -118.19. **LC-MS ESI (+)** *m/z*: 126.02 $[M]^+$.



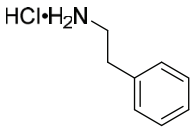
(2-chlorophenyl)methanamine hydrochloride (2). CAS [22680-44-0]. White powder (Yield: 56%, 149.4 mg).[22] **^{1}H NMR** (400 M*Hz*, D_2O) *δ* (ppm):[23] 7.57-7.39 (m, 4H), 4.34 (s, 2H). **^{13}C{^{1}H} NMR** (101 M*Hz*, D_2O) *δ* (ppm):[23] 133.8, 131.3, 131.2, 130.2, 130.0, 127.9, 40.9. **LC-MS ESI (+)** *m/z* for ^{37}Cl/^{35}Cl: 141.9587/143.96 $[M+H]^+$.



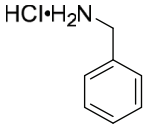
(2-bromophenyl)methanamine hydrochloride (3). CAS [5465-63-4]. White powder (Yield: 41%, 135.7 mg.**^{1}H NMR** (400 M*Hz*, D_2O) *δ* (ppm):[24] 7.74 (dd, *J* = 8.0 *Hz*, *J* = 1.0 *Hz*, 1H), 7.52 (dd, *J* = 7.6 *Hz*, *J* = 1.8 *Hz*, 1H), 7.46 (td, *J* = 7.5 *Hz*, *J* = 1.2 *Hz*, 1H), 7.37 (td, *J* = 7.8 *Hz*, *J* = 1.8 *Hz*, 1H), 4.34 (s, 2H). **^{13}C{^{1}H} NMR** (101 M*Hz*, D_2O) *δ* (ppm):[24]133.6, 131.6, 131.5, 128.8, 124.2, 43.6. **LC-MS ESI (+)** *m/z* for ^{79}Br/^{81}Br: 185.99/187.99 $[M+H]^+$, 168.98/170.96 $[M–NH_2]^+$.



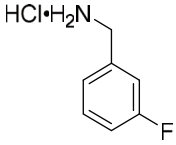
(3-methoxyphenyl)methanamine hydrochloride (4). CAS [3459-14-1]. White powder (Yield: 80%, 207.9 mg). **^{1}H NMR** (400 M*Hz*, D_2O) *δ* (ppm):[21] 7.34 (t, *J* = 7.7 *Hz*, 1H), 6.99-6.97 (m, 3H), 4.08 (s, 2H), 3.77 (s, 3H). **^{13}C{^{1}H} NMR** (101 M*Hz*, D_2O) *δ* (ppm):[21] 159.2, 134.3, 130.6, 121.4, 114.8, 114.5, 55.5, 43.0. **LC-MS ESI (+)** *m/z:* 138.09 $[M+H]^+$, 121.06 $[M–NH_2]^+$.



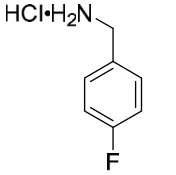
phenethylamine hydrochloride (5). CAS [156-28-5]. White powder (Yield: 46%, 107.8 mg). **^{1}H NMR** (400 M*Hz*, D_2O) *δ* (ppm):[25] 7.44-7.41 (m, 2H), 7.37-7.33 (m, 3H), 3.29 (t, *J* = 7.3 *Hz*, 2H), 3.01 (t, *J* = 7.3 *Hz*, 2H). **^{13}C{^{1}H} NMR** (101 M*Hz*, D_2O) *δ* (ppm):[25] 136.7, 129.1, 128.9, 127.35, 40.6, 32.7. **LC-MS ESI (+)** *m/z:* 122.10 $[M+H]^+$.



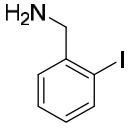
benzylamine hydrochloride (6). CAS [100-46-9]. White powder (Yield: 56%, 121.3 mg). **^{1}H NMR** (400 M*Hz*, D_2O) δ (ppm):[21] 7.50-7.44 (m, 5H), 4.18 (s, 2H). **^{13}C{^{1}H} NMR** (101 M*Hz*, D_2O) δ (ppm):[21] 132.7, 129.2 (d, *J* = 1.7 *Hz*), 128.8, 43.1. **LC-MS ESI (+)** *m/z:* 108.08 $[M+H]^+$, 91.05 $[M-NH_2]^+$.



(3-fluorophenyl)methanamine hydrochloride (7). CAS [658-25-3]. White powder (Yield: 52%, 127.1 mg). **^{1}H NMR** (400 M*Hz*, D_2O) δ (ppm):[26] 7.51-7.46 (m, 1H), 7.28-7.19 (m, 3H), 4.20 (s, 2H). **^{13}C{^{1}H} NMR** (101 M*Hz*, D_2O) δ (ppm)[26]: 162.6 (d, *J* = 244.3 *Hz*), 134.9 (d, *J* = 7.8 *Hz*), 131.1 (d, *J* = 8.5 *Hz*), 124.7 (d, *J* = 3.0 *Hz*), 115.8 (dd, *J* = 39.9 *Hz*, *J* = 21.7 *Hz*), 42.57. **^{19}F{^{1}H}NMR** (376 M*Hz*, D_2O) δ(ppm):[26] -112.84. **LC-MS ESI (+)** *m/z:* 126.07 $[M+H]^+$, 109.04 $[M-NH_2]^+$.



(4-fluorophenyl)methanamine hydrochloride (8). CAS [659-41-6]. White powder (Yield: 36%, 88.2 mg).**^{1}H NMR** (400 M*Hz*, D_2O) δ (ppm):[21] 7.48-7.45 (m, 2H), 7.22-7.18 (m, 2H), 4.17 (s, 2H). **^{13}C{^{1}H} NMR** (101 M*Hz*, D_2O) δ (ppm):[21] 131.04 (d, *J* = 8.7 *Hz*), 115.96 (d, *J* = 22.2 *Hz*), 42.45. **^{19}F{^{1}H}NMR** (376 M*Hz*, D_2O) δ(ppm):[21] -113.29. **LC-MS ESI (+)** *m/z:* 126.07 $[M+H]^+$, 109.04 $[M–NH_2]^+$.



(2-iodophenyl)methanamine (9-NH_2). CAS [39959-51-8]. White powder (Yield: 35%, 142.0 mg); **^{1}H NMR** (400 M*Hz*, $CDCl_3$) δ (ppm):[27] 7.81 (d, *J* = 7.70 *Hz*, 1H), 7.37-7.26 (m, 2H), 6.94 (td, *J* = 7.70 *Hz*, *J* = 2.11 *Hz*, 1H), 3.85 (s, 1H). **^{13}C{^{1}H} NMR** (101 M*Hz*, D_2O) δ (ppm):[28] 145.2, 139.6, 128.8 (d, *J* = 3.5 *Hz*), 128.6, 99.10, 51.46. **GC-MS EI** *m/z*: 233 $[M]^{\bullet}$, 106 $[M-I]^{\bullet}$.

S3. FT-IR Spectra of Nitrile-Cu Complexes

To prepare the sample of 2-F-benzonitrile and $CuCl_2$ (**1-RCN-Cu**), to a 10 mL ZrO_2 jar equipped with 5 7 mm Ø balls of the same material, the nitrile (1.5 mmol, 1.0 equiv.) and $CuCl_2$ (1.5 mmol, 1.0 equiv.) are added and milled for 30 minutes at 30 *Hz* in a MM400 mixer mill. No further purifications were done and the analysis was done promptly after the end of milling.

To prepare the samples of nitrile-Cu complexes (**2-RCN-Cu** – **12-RCN-Cu**), to a 10 mL ZrO_2 jar equipped with 5 7 mm Ø balls of the same material, the nitrile (1.5 mmol, 1.0 equiv.) and $CuCl_2$ (0.75 mmol, 0.5 equiv.) are added and milled for 30 minutes at 30 *Hz* in a MM400 mixer mill.

No further purifications were done and the analysis was done promptly after the end of milling.

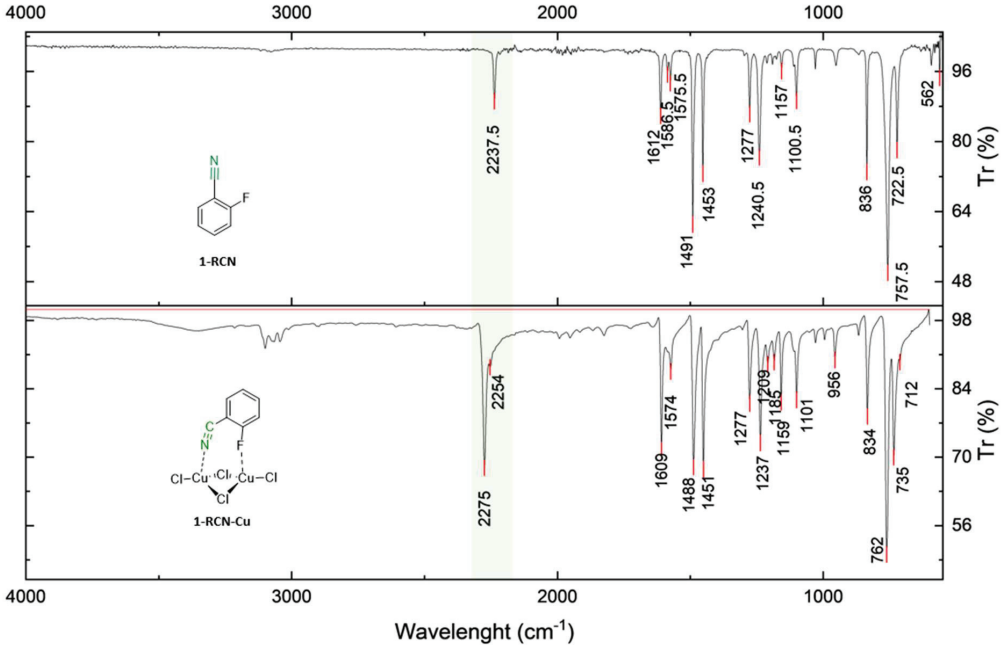


Figure S2. IR-ATR spectra of **1-RCN** (top) and the related $CuCl_2$ complex (**1-RCN-Cu**). In green is highlighted the typical C≡N stretch.

Figure S2 shows the comparison between the free nitrile **1-RCN** and the relative complex with $CuCl_2$, it can be seen an important blueshift for the C≡N stem from the complexation (2237.5 cm^{-1} *vs* 2275 cm^{-1}, a shift of 37.5 cm^{-1}). The proposed structure is supported by DFT calculations and XPS analysis.

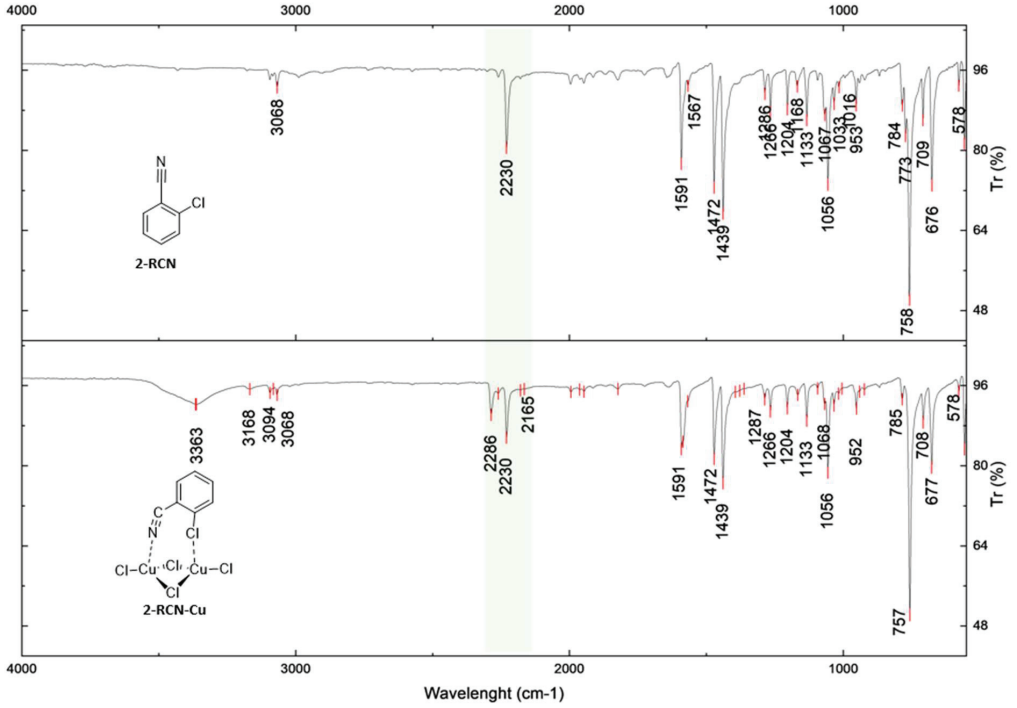


Figure S3. IR-ATR spectra of **2-RCN** (top) and the related $CuCl_2$ complex (**2-RCN-Cu**). In green is highlighted the typical C≡N stretch.

Figure S3 shows the comparison between the free nitrile **2-RCN** and the relative complex with $CuCl_2$, it can be seen an important blueshift for the C≡N stem from the complexation (2286 cm^{-1} *vs* 2230 cm^{-1}, a shift of 56 cm^{-1}). The proposed structure is supported by DFT calculations on **1-RCN-Cu** and **9-RCN-Cu** which both suggest a Cu-X chelation.

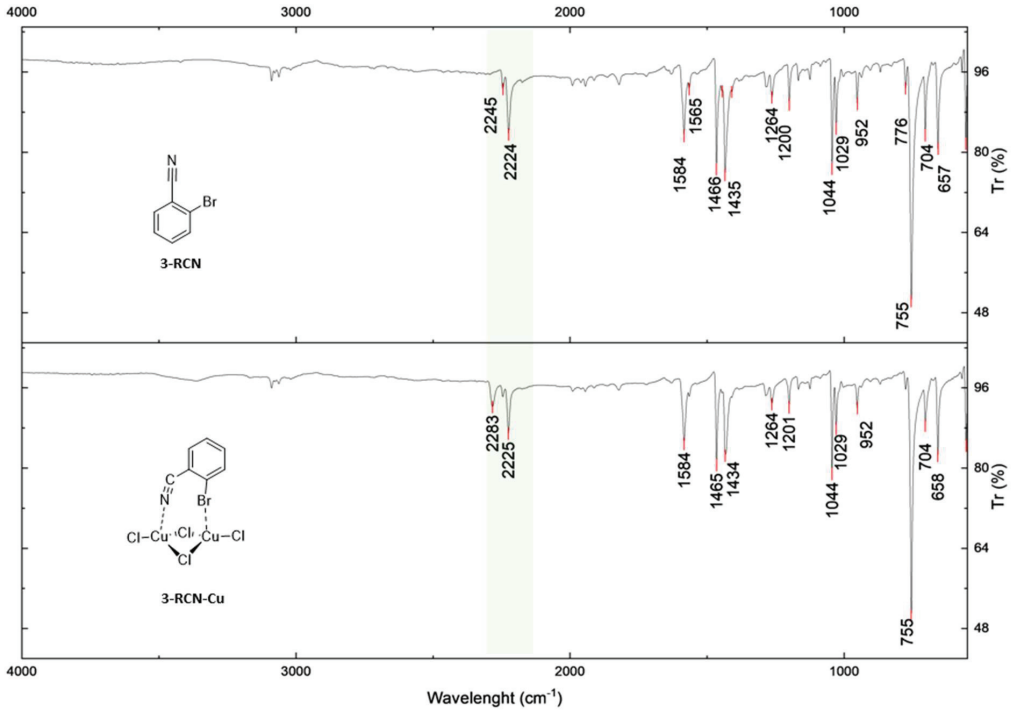


Figure S4. IR-ATR spectra of **3-RCN** (top) and the related $CuCl_2$ complex (**3-RCN-Cu**). In green is highlighted the typical C≡N stretch.

Figure S4 shows the comparison between the free nitrile **3-RCN** and the relative complex with $CuCl_2$, it can be seen an important blueshift for the C≡N stem from the complexation (2283 cm^{-1} *vs* 2225 cm^{-1}, a shift of 58 cm^{-1}). The proposed structure is supported by DFT calculations on **1-RCN-Cu** and **9-RCN-Cu** which both suggest a Cu-X chelation.

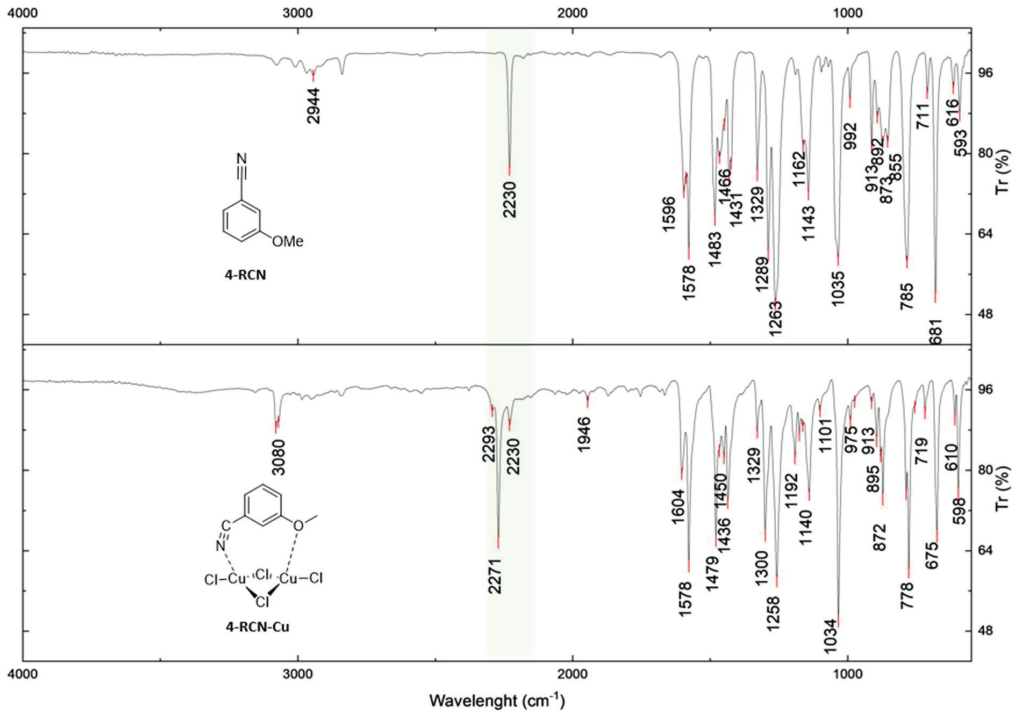
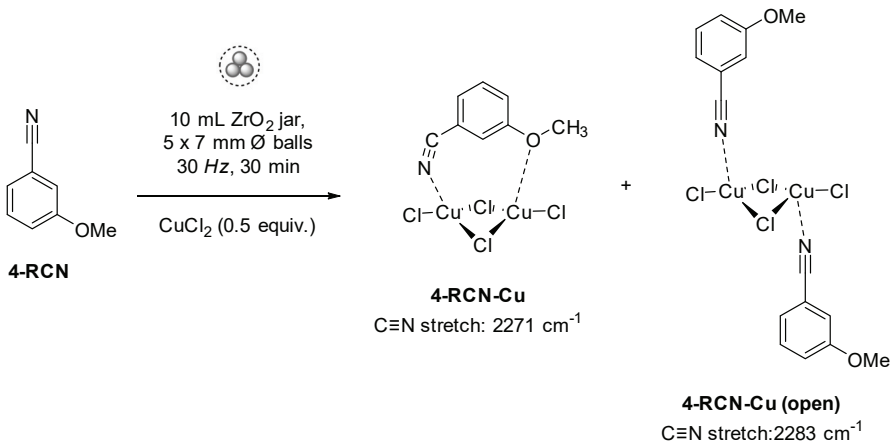


Figure S5. IR-ATR spectra of **4-RCN** (top) and the related $CuCl_2$ complex (**4-RCN-Cu**). In green is highlighted the typical C≡N stretch.

Figure S5 shows the comparison between the free nitrile **4-RCN** and the relative complex with $CuCl_2$, it can be seen a blueshift for the C≡N stem from the complexation (2271 cm^{-1} *vs* 2230 cm^{-1}, a shift of 41 cm^{-1}), also it is noticeable a little peak at 2283 cm^{-1} that may suggest that the methoxy group in meta position of **4-RCN** it may be too distant to close the ring chelating the Cu dimer and the complex can exist in an open form with a 1:1 Cu:nitrile ratio (Scheme S3).



Scheme S3. Scheme of the two plausible forms of **4-RCN-Cu**.

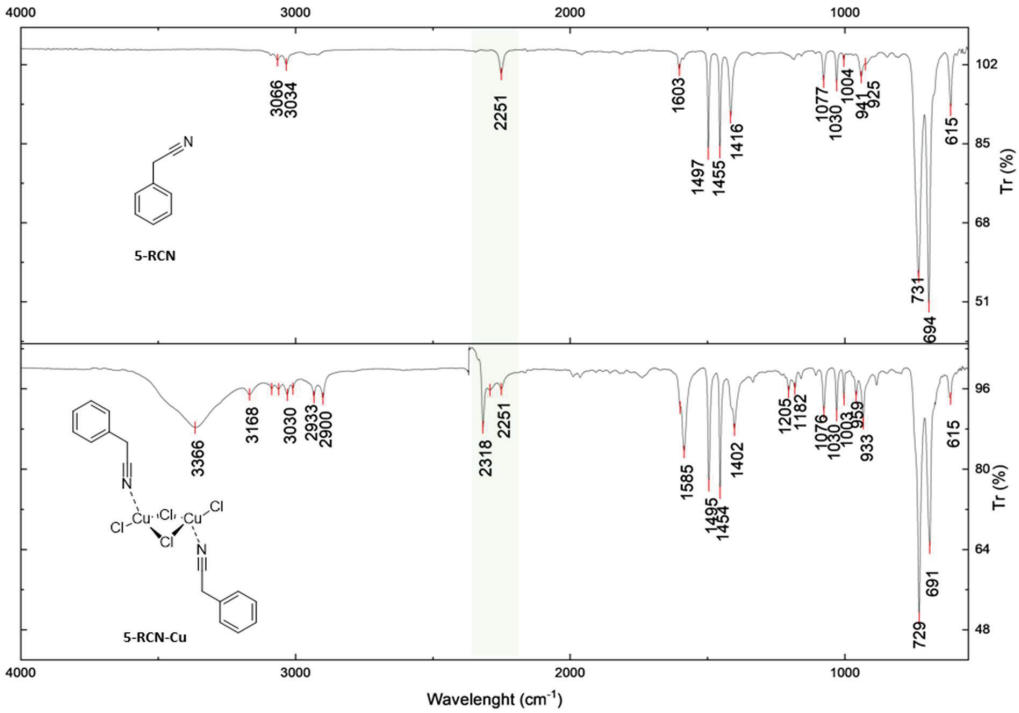
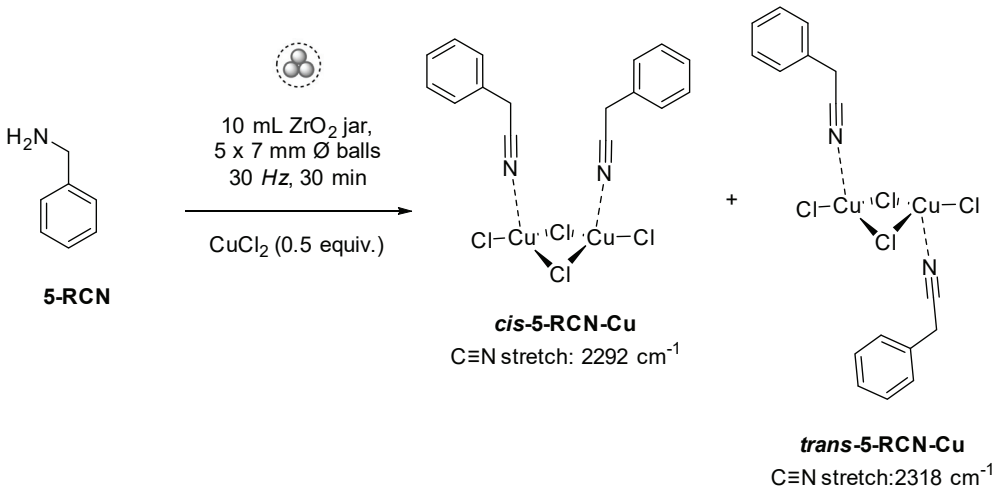


Figure S6. IR-ATR spectra of **5-RCN** (top) and the related $CuCl_2$ complex (**5-RCN-Cu**). In green is highlighted the typical C≡N stretch.

Figure S6 shows the comparison between the free nitrile **5-RCN** and the relative complex with $CuCl_2$, in this case the only possibility for the complex is to be open, as **5-RCN** doesn't have moieties able to chelate the Cu, so a second molecule of **5-RCN** is needed to complete the coordination sphere of both the Cu in the dimer. A shoulder peak at 2292 cm^{-1} near the main C≡N shift of the complex (2318 cm^{-1}) can indicate a cis/trans isomery of the complex (Scheme S4). Also in this case a blueshift (67 cm^{-1} and 41 cm^{-1}) is observed compared to the free **5-RCN** C≡N shift (2251 cm^{-1}). We assign the C≡N band at 2292 cm^{-1} to the cis isomer and the band at 2318 cm^{-1} to the trans isomer, based on two complementary observations. First, the band at 2292 cm^{-1} is the weaker of the two, consistent with the cis isomer being the less abundant species in the mixture, as expected from the greater steric encumbrance of two benzyl groups on the same side of the Cu_2Cl_4 core. Second, the smaller blueshift (41 cm^{-1} *vs* 61 cm^{-1}, *cis* blueshift *vs trans* blueshift) of the cis band relative to free 5-RCN is consistent with a longer (and therefore weaker) Cu–N bond in the cis isomer, where partial elongation of the Cu–N distance would relieve steric strain; weaker σ-donation from the nitrile lone pair gives a less pronounced increase in the C≡N stretching frequency. Unlike the previously reported Cu–benzylcyanide complex, whose doublet was attributed to a Jahn–Teller distortion of an octahedral Cu coordination environment, the present compound cannot be assigned the same solution-derived structure. This conclusion follows from the constraint of our experimental setup that the Cl atoms must remain in the coordination sphere, unlike in the solution-prepared analogue, and is further supported by the different CN stretching frequencies

observed for the two complexes: 2270 and 2305 cm^{-1} for the Jahn–Teller doublet, versus 2292 and 2318 cm^{-1} for our compound.[29]



Scheme S4. The two plausible isomers of 5-RCN-Cu and their assigned C≡N stretching frequencies. The band at 2292 cm^{-1} is assigned to the cis isomer and the band at 2318 cm^{-1} to the trans isomer; the assignment rationale is discussed above.

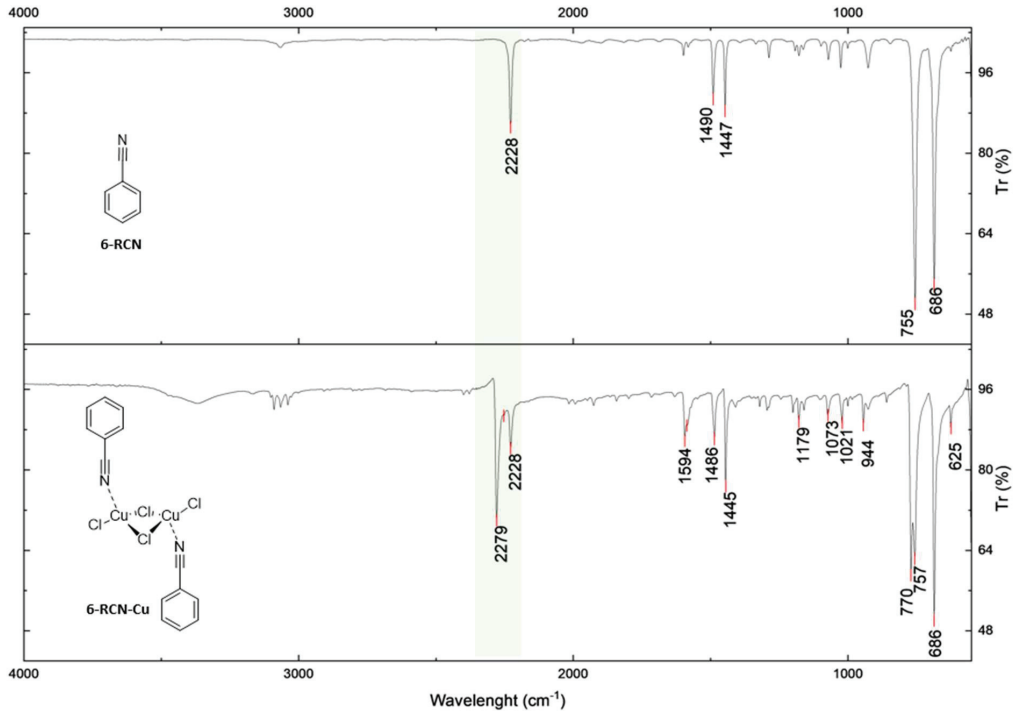


Figure S7. IR-ATR spectra of **6-RCN** (top) and the related $CuCl_2$ complex (**6-RCN-Cu**). In green is highlighted the typical C≡N stretch.

Figure S7 shows the comparison between the IR spectra of the free nitrile 6-RCN and the corresponding $CuCl_2$ complex. As for 5-RCN-Cu, the complex can only exist in an open form, since 6-RCN bears no additional moieties capable of chelating Cu, and a second molecule of 6-RCN is therefore required to complete the coordination sphere of the Cu dimer. A blueshift of the C≡N stretch is again observed upon complexation (2229 cm^{-1} vs 2277 cm^{-1}, a shift of 48 cm^{-1}), and a small shoulder near the main C≡N band of the complex may likewise indicate a cis/trans isomerism. In this case, however, the phenyl group of 6-RCN is directly attached to the nitrile carbon and has fewer degrees of conformational freedom than the benzyl group of 5-RCN, whose additional methylene tether allows the two bulky aromatic rings to be positioned further apart. The cis isomer of 6-RCN-Cu is therefore considerably less stable than its 5-RCN-Cu counterpart, and the cis/trans equilibrium is pushed more strongly towards the trans form, with the cis-related band appearing only as a small shoulder.

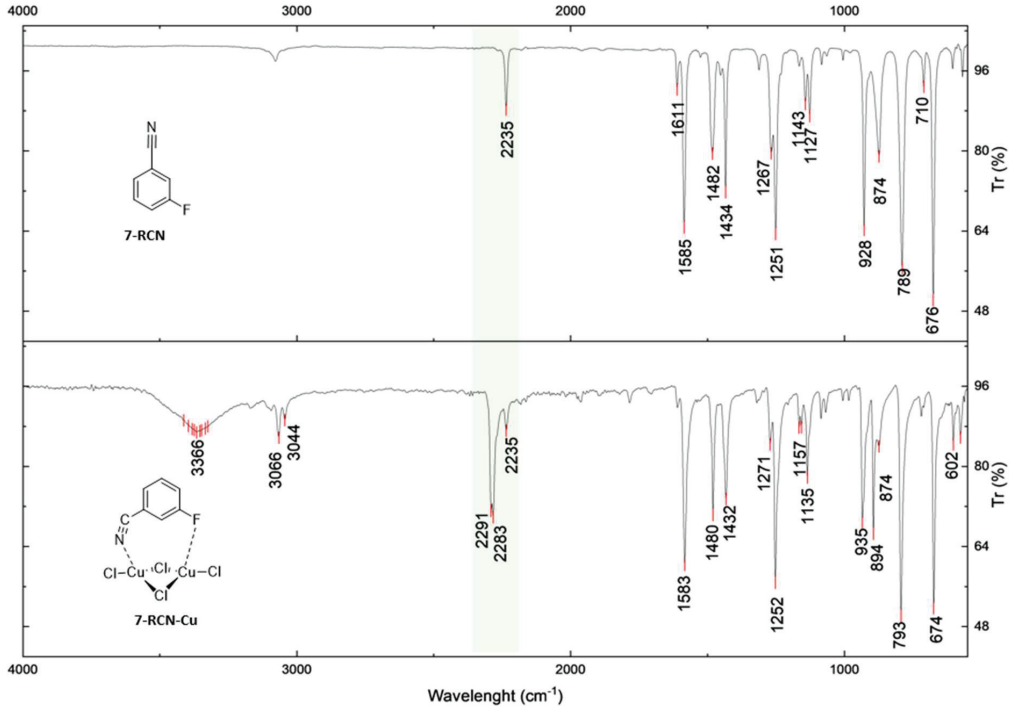
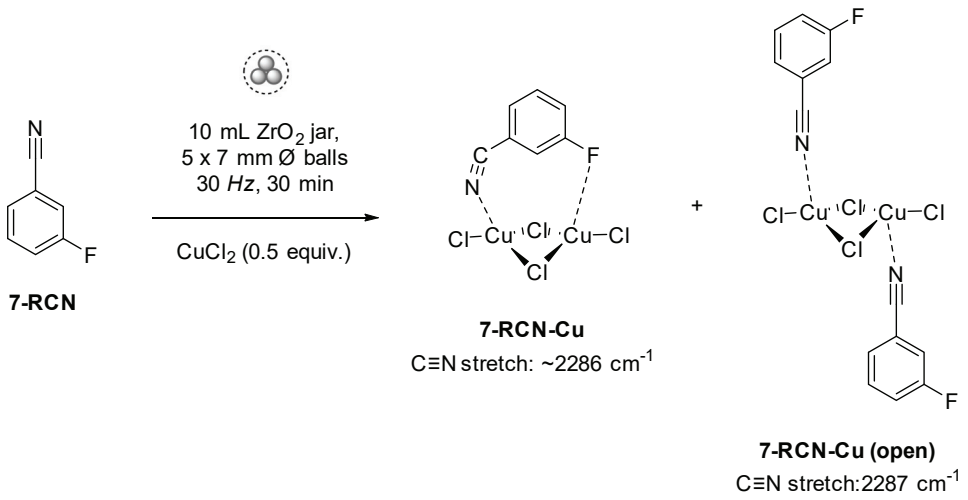


Figure S8. IR-ATR spectra of **7-RCN** (top) and the related $CuCl_2$ complex (**7-RCN-Cu**). In green is highlighted the typical C≡N stretch region.

Figure S8 shows the comparison between the free nitrile 7-RCN and the corresponding $CuCl_2$ complex. A blueshift of the C≡N stretch is observed upon complexation (2287 cm^{-1} vs 2236 cm^{-1}, a shift of 51 cm^{-1}); the band remaining at 2235 cm^{-1} in the complex spectrum is attributed to residual non complexed 7-RCN. As in 4-RCN-Cu, the meta position of the fluorine places the heteroatom far from the second Cu center of the dimer, so that closure of a chelate ring is geometrically disfavored. In contrast to 4-RCN-Cu, however, no significant population of a closed form is observed (a shoulder on the peaks at 2287 cm^{-1} is still visible): the complex appears to exist predominantly in the open form (Scheme S4), in which each Cu of the dimer

is capped by a separate 7-RCN molecule coordinated through the nitrile nitrogen only. We tentatively attribute this difference to the weaker donor character of aryl fluorine toward Cu(II) compared with the methoxy oxygen of 4-RCN: the energetic cost of forming a strained chelate ring from the meta position is insufficiently compensated by Cu–F coordination, whereas in 4-RCN-Cu the stronger Cu–O interaction allows the closed form to be populated.



Scheme S5. Scheme of the two plausible forms of **7-RCN-Cu**.

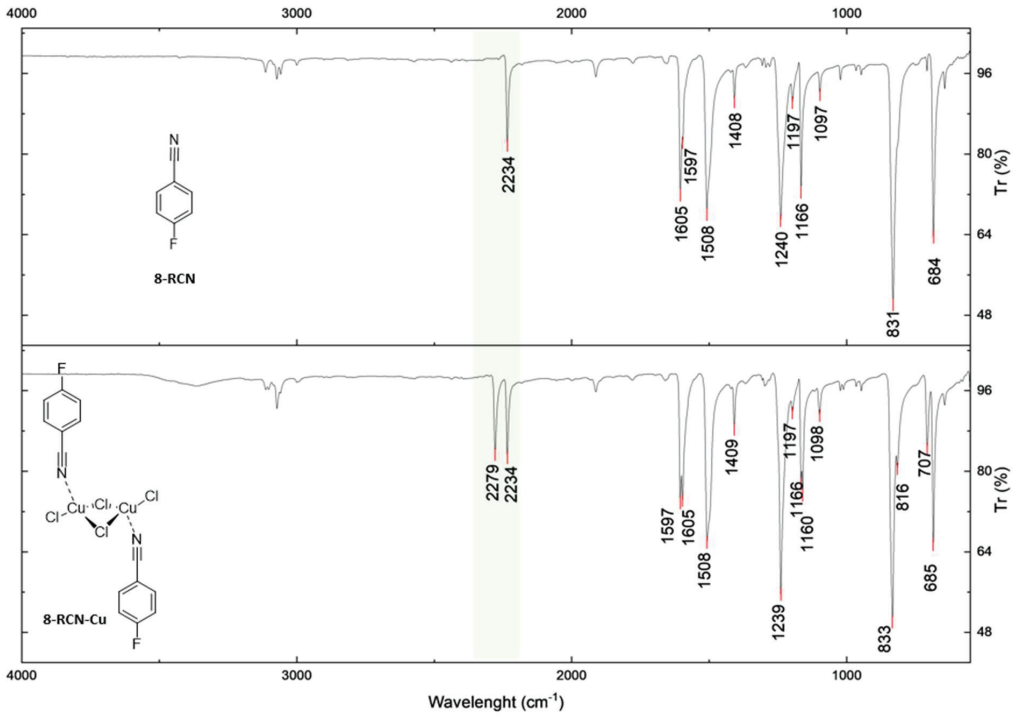


Figure S9. IR-ATR spectra of **8-RCN** (top) and the related $CuCl_2$ complex (**8-RCN-Cu**). In green is highlighted the typical C≡N stretch region.

Figure S9 shows the comparison between the free nitrile 8-RCN and the corresponding $CuCl_2$ complex. A blueshift of the C≡N stretch is observed upon complexation (2279 cm^{-1} *vs* 2234 cm^{-1}, a shift of 45 cm^{-1}); the band remaining at 2234 cm^{-1} in the complex spectrum is attributed to residual non complexed 8-RCN. In this case the para position of the fluorine places the heteroatom on the opposite side of the aromatic ring from the nitrile, so that closure of a chelate ring to the second Cu of the dimer is geometrically impossible. Only the open form is therefore observed, in which each Cu of the dimer is capped by a separate 8-RCN molecule coordinated through the nitrile nitrogen only, as shown in Figure S9.

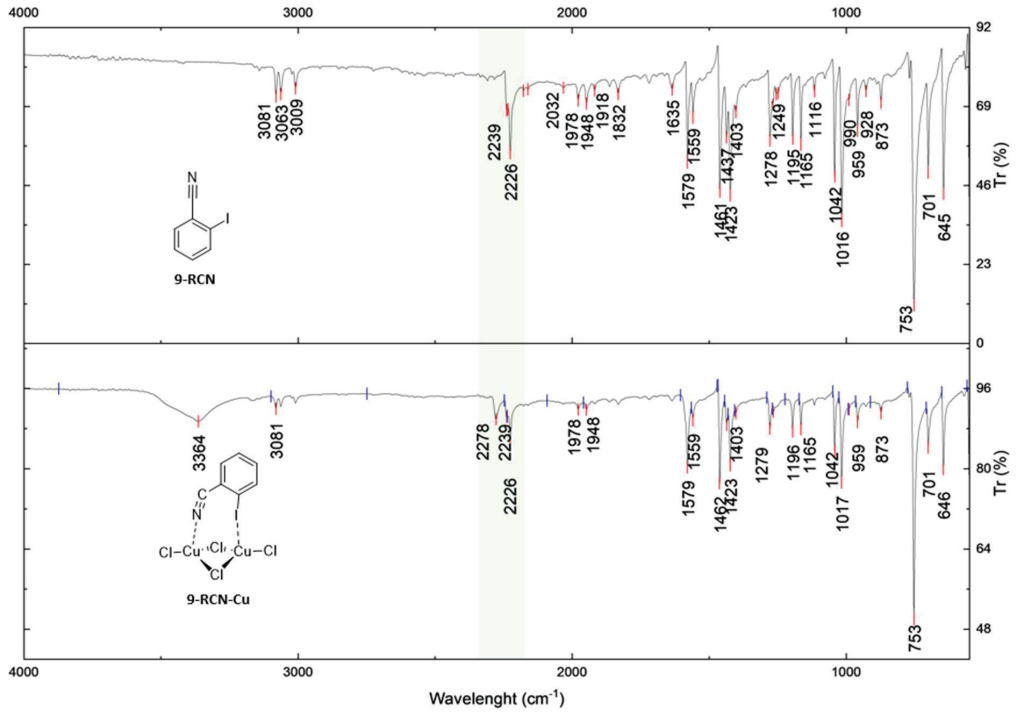


Figure S10. IR-ATR spectra of **9-RCN** (top) and the related $CuCl_2$ complex (**9-RCN-Cu**). In green is highlighted the typical C≡N stretch.

Figure S10 shows the comparison between the free nitrile **9-RCN** and the relative complex with $CuCl_2$, it can be seen an important blueshift for the C≡N stem from the complexation (2278 cm^{-1} *vs* 2226 cm^{-1}, a shift of 52 cm^{-1}). The proposed structure is supported by DFT calculations.

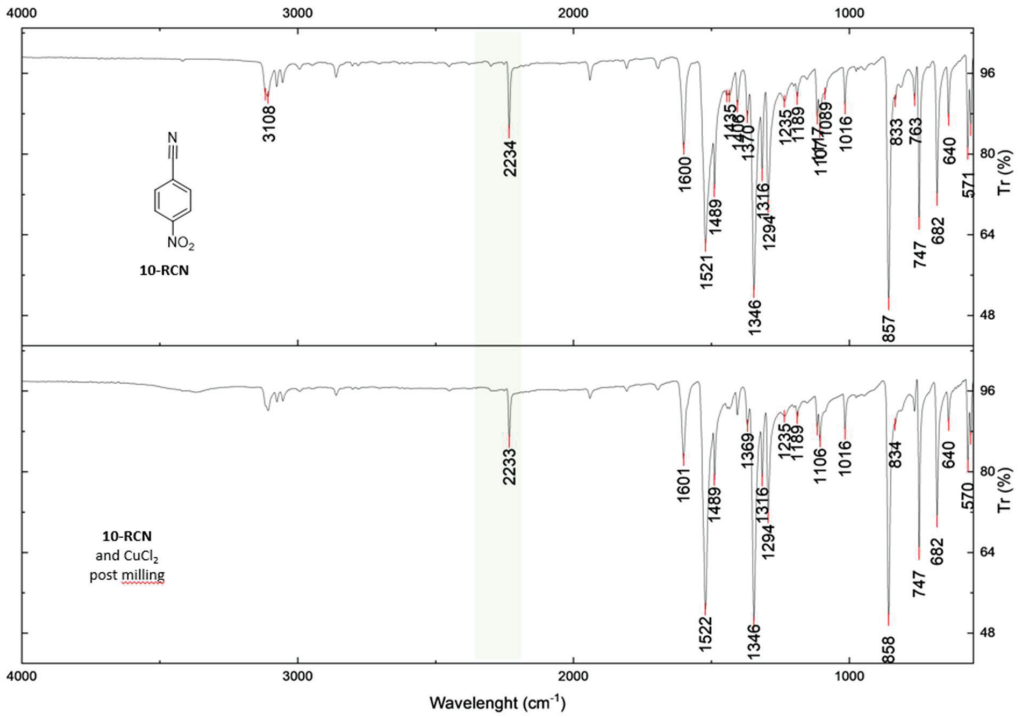


Figure S11. IR-ATR spectra of 10-RCN (top) and of the same sample after milling with $CuCl_2$ under the standard conditions (bottom). The typical C≡N stretch region is highlighted in green.

In contrast to all the previous substrates, no significant change is observed in the IR spectrum of 10-RCN upon milling with $CuCl_2$. The C≡N stretch remains at 2233 cm^{-1} (*vs* 2234 cm^{-1} in free 10-RCN, a shift of only 1 cm^{-1}), and all other ring and substituent bands are also essentially unchanged. We conclude that no complex is formed between 10-RCN and $CuCl_2$ under these conditions. This is consistent with the strong electron-withdrawing character of the para-nitro group, which depletes electron density from the aromatic ring and, through conjugation, from the nitrile nitrogen. The reduced availability of the nitrogen lone pair for σ-donation to Cu(II) prevents formation of a stable Cu–N≡C adduct. The failure of the reduction reaction for 10-RCN (Section S1.1) cannot therefore be attributed to anomalous Cu coordination; we instead ascribe the observed deflagration in step 2 to a direct reaction between AB and the nitro group (*vide supra*).

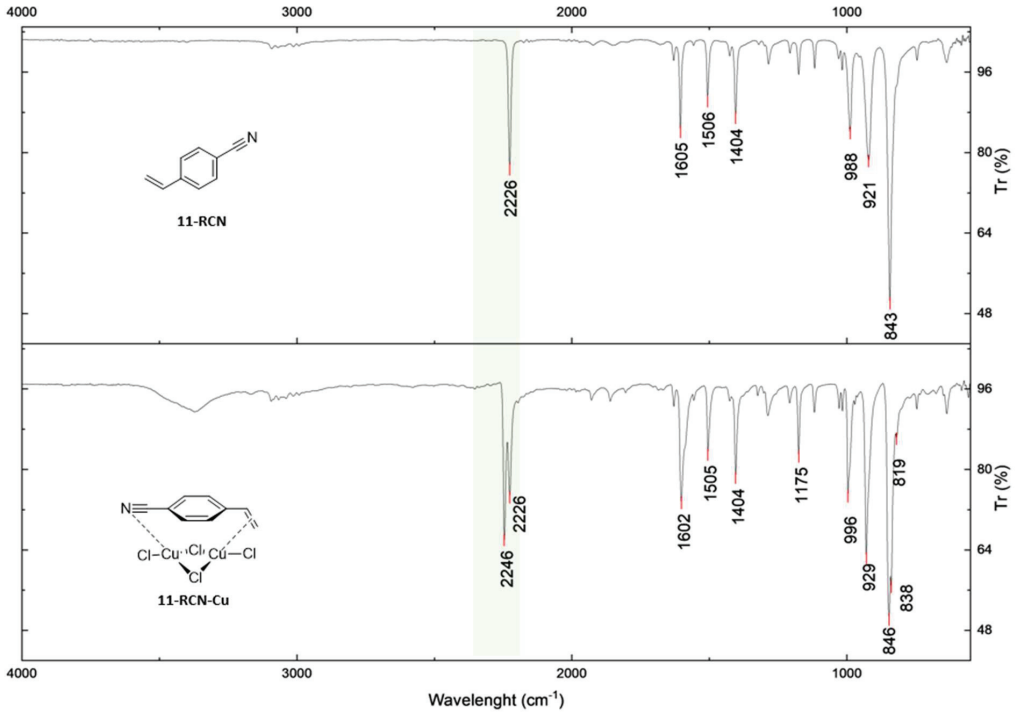


Figure S12. IR-ATR spectra of **11-RCN** (top) and the related $CuCl_2$ complex (**11-RCN-Cu**). In green is highlighted the typical C≡N stretch region.

Figure S12 shows the comparison between the free nitrile 11-RCN and the corresponding $CuCl_2$ complex. A blueshift of the C≡N stretch is observed upon complexation (2246 cm^{-1} vs 2226 cm^{-1}, a shift of 20 cm^{-1}), together with a residual band at 2226 cm^{-1} assigned to non-complexed 11-RCN. The vinyl C–H out-of-plane bending bands also shift on complexation, from 988 and 921 cm^{-1} in free 11-RCN to 996 and 929 cm^{-1} in the complex ($\delta \approx +8$ cm^{-1} for both), while the aromatic C–H out-of-plane bend at 843 cm^{-1} (characteristic of the para-disubstituted ring) is essentially unchanged at 846/838 cm^{-1}. The simultaneous and parallel perturbation of both diagnostic vinyl bands, in the absence of any significant change to the aromatic ring bands, indicates that the local environment of the vinyl group is specifically altered upon Cu binding, suggesting an additional interaction between Cu and the alkene moiety. This interpretation is further supported by the magnitude of the nitrile blueshift: 20 cm^{-1} is significantly smaller than the 45 cm^{-1} observed for the analogous para-substituted complex 8-RCN-Cu, where Cu can bind only at the nitrile nitrogen. If Cu were bound to the nitrile nitrogen only in 11-RCN-Cu as well, a similar blueshift would be expected; the reduced shift is consistent with a weakening of the Cu–N≡C interaction caused by competing

coordination of Cu to the vinyl group, as depicted in the proposed structure (Figure S12). We tentatively attribute the loss of selectivity observed in the attempted reduction of 11-RCN (Section S1.1) to this additional interaction at the vinyl moiety.

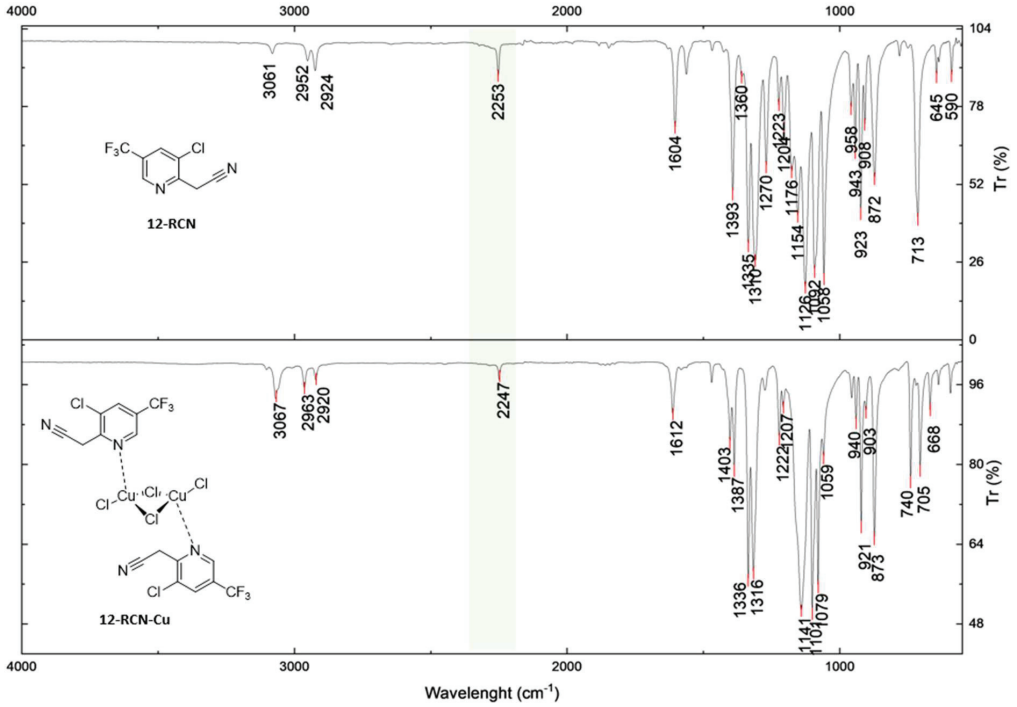


Figure S13. IR-ATR spectra of **12-RCN** (top) and the related $CuCl_2$ complex (**12-RCN-Cu**). In green is highlighted the typical C≡N stretch region.

Figure S13 shows the comparison between the free nitrile 12-RCN and the corresponding $CuCl_2$ complex. The C≡N stretch is essentially unchanged on complexation (2253 → 2249 cm^{-1}, $\delta \approx -4$ cm^{-1}), indicating that the nitrile nitrogen is not the site of Cu coordination. However, substantial changes are observed in the pyridine ring skeletal region: the strong ring band at 1604 cm^{-1} shifts to 1612 cm^{-1} (+8), the band at 1562 cm^{-1} in free 12-RCN loses almost all of its intensity in the complex, and significant reorganization of the bands in the 1400–1100 cm^{-1} region is apparent. The aromatic C–H stretch also shifts (3081 → 3069 cm^{-1}), while the methylene C–H stretch of the CH_2CN arm shifts in the opposite direction (2952 → 2964 cm^{-1}). Together, these changes, particularly the perturbation of the ring skeletal modes and the loss of intensity of the 1562 cm^{-1} band, are characteristic of pyridine coordination to Cu(II) through the ring nitrogen, with concomitant changes in the ring electronics and in the neighboring methylene group. We therefore propose that, 12-RCN coordinates Cu(II) preferentially

through the pyridine nitrogen rather than through the nitrile (Figure S13). The strong electron-withdrawing effects of the chlorine and trifluoromethyl substituents on the ring further reduce the basicity of the nitrile nitrogen, reinforcing this binding-mode preference. This alternative coordination mode is the likely origin of the unsuccessful reduction of 12-RCN to 12: the nitrile is not activated by Cu coordination, and the observed dehalogenation and loss of the CF_3 group are consistent with a parallel pathway initiated from the Cu–pyridine adduct rather than from a Cu–nitrile species.

S3.1 Notable IR C≡N stretch peak shifts in RCN-Cu complexes

Table S6. List of C≡N stretch peaks for compound **1-12-RCN** and related Cu complexes.

Compound	RCN C≡N stretch (cm^{-1})	RCN-Cu C≡N stretch (cm^{-1})	δ (cm^{-1})
1-RCN	2237.5	2275	37.5
2-RCN	2230	2286	56
3-RCN	2224	2283	59
4-RCN	2230	2271	41
5-RCN	2251	2318	67
6-RCN	2229	2277	48
7-RCN	2236	2287	51
8-RCN	2234	2276	42
9-RCN	2226	2278	52
10-RCN	2234	2233	-1
11-RCN	2226	2246	20
12-RCN	2253	2249	-4

S4. XPS spectra

Following are reproduced the spectra for the XPS photoelectron peaks reported in Tables 3 and 4 of the main manuscript.

S4.1 N 1s spectra for the 2-halobenzonitriles series

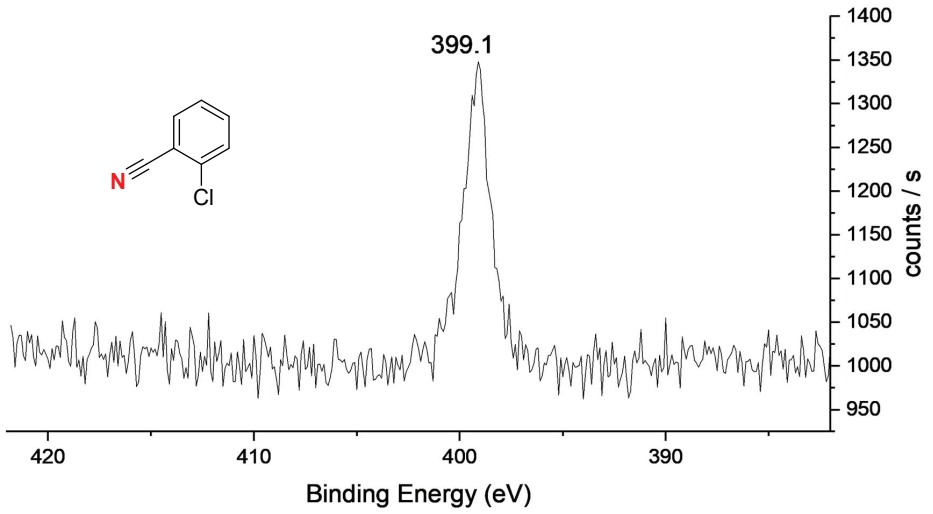


Figure S14. XPS spectra of the N 1s photoelectron for **2-RCN**.

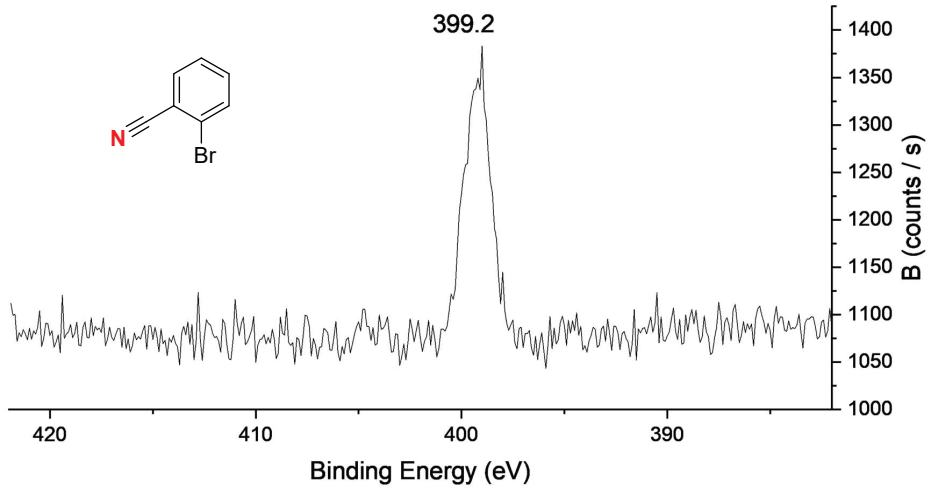


Figure S15. XPS spectra of the N 1s photoelectron for **3-RCN**.

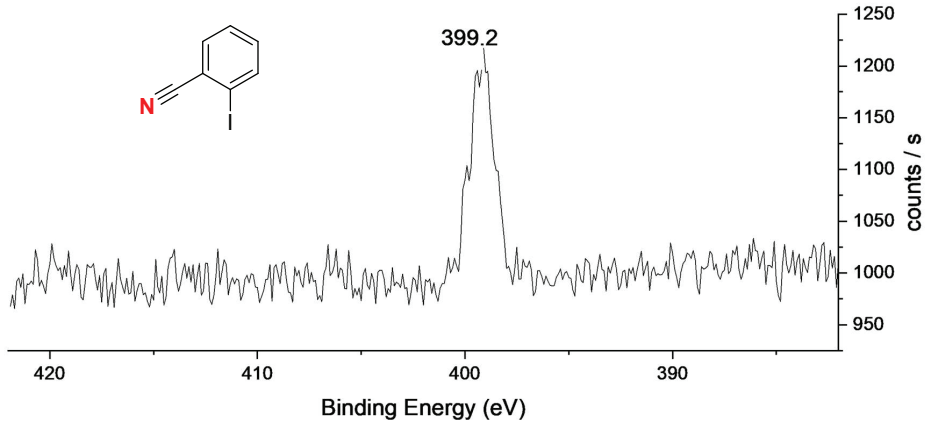


Figure S16. XPS spectra of the N 1s photoelectron for **9-RCN**.

S4.2 XPS spectra of 1-RCN-Cu

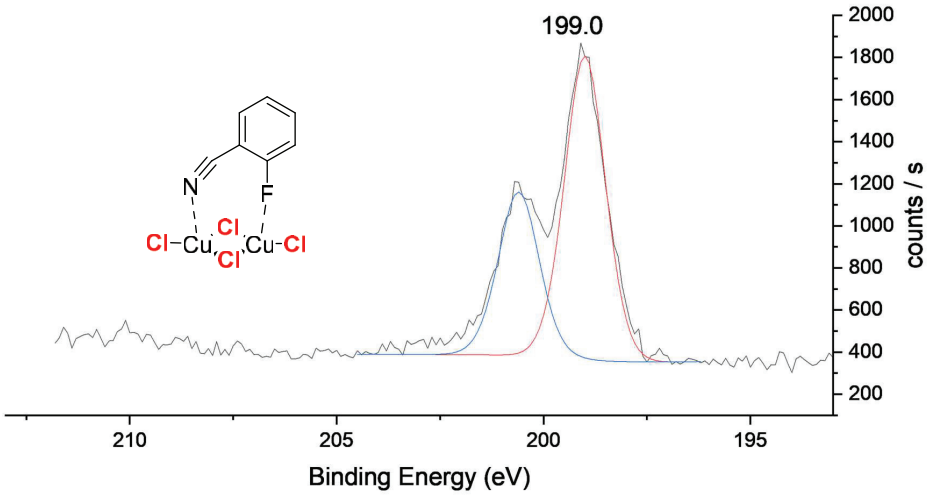


Figure S17. Deconvoluted XPS spectra of the Cl 2p photoelectron of **1-RCN-Cu**. The peaks are fitting respectively Cl $2p_{3/2}$ (in red) and Cl $2p_{1/2}$ (in blue).

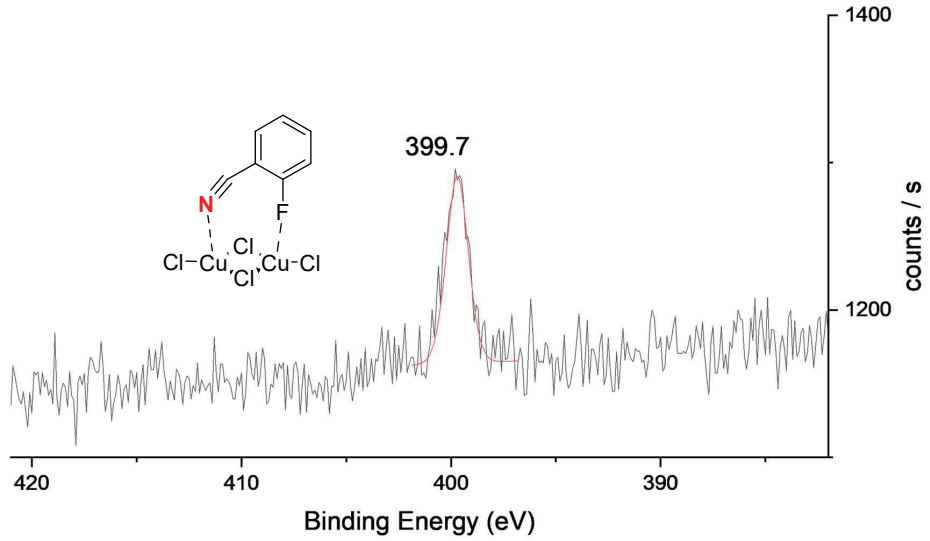


Figure S18. Deconvoluted XPS spectra of the N 1s photoelectron of **1-RCN-Cu.**

S4.3 XPS spectra of $CuCl_2$

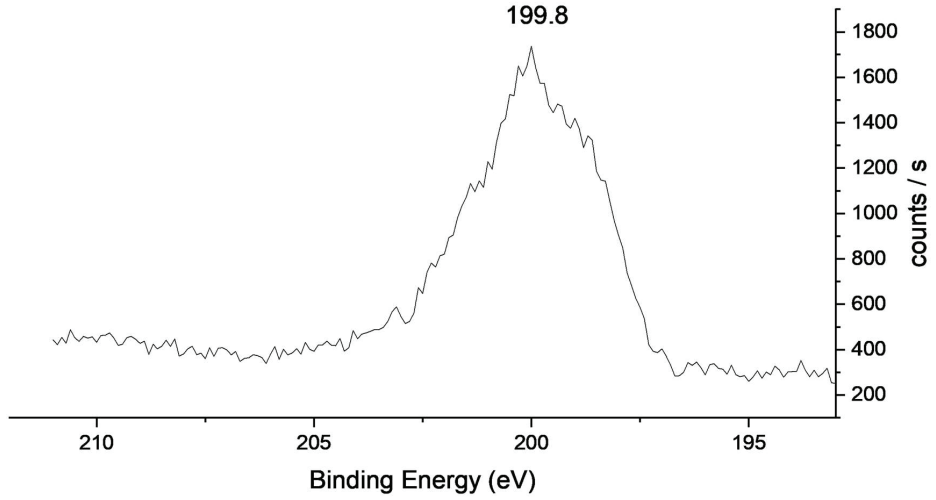


Figure S19. XPS spectra of the Cl $2p_{3/2}$ photoelectron for $CuCl_2$.

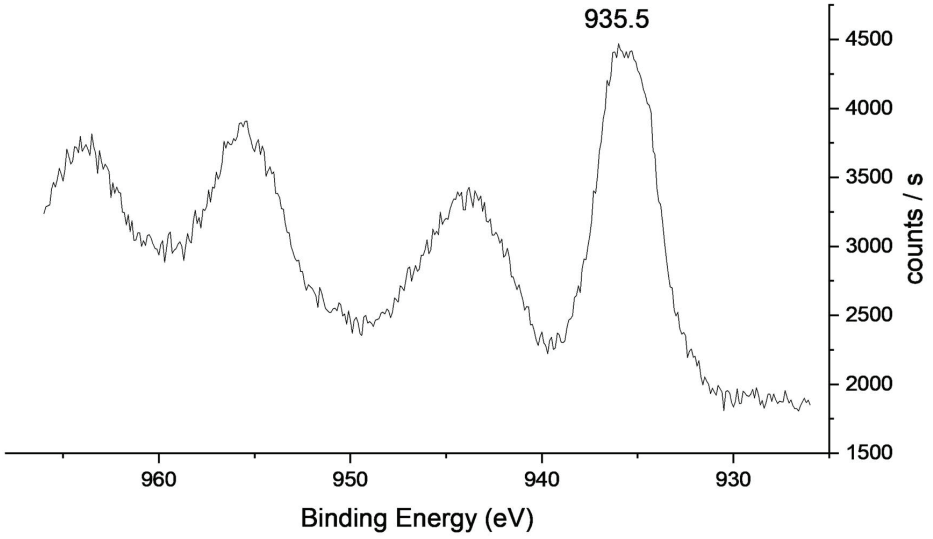


Figure S20. XPS spectra of the Cu $2p_{3/2}$ photoelectron for $CuCl_2$.

S5. Additional computational results

S.5.1 The uncatalyzed reaction

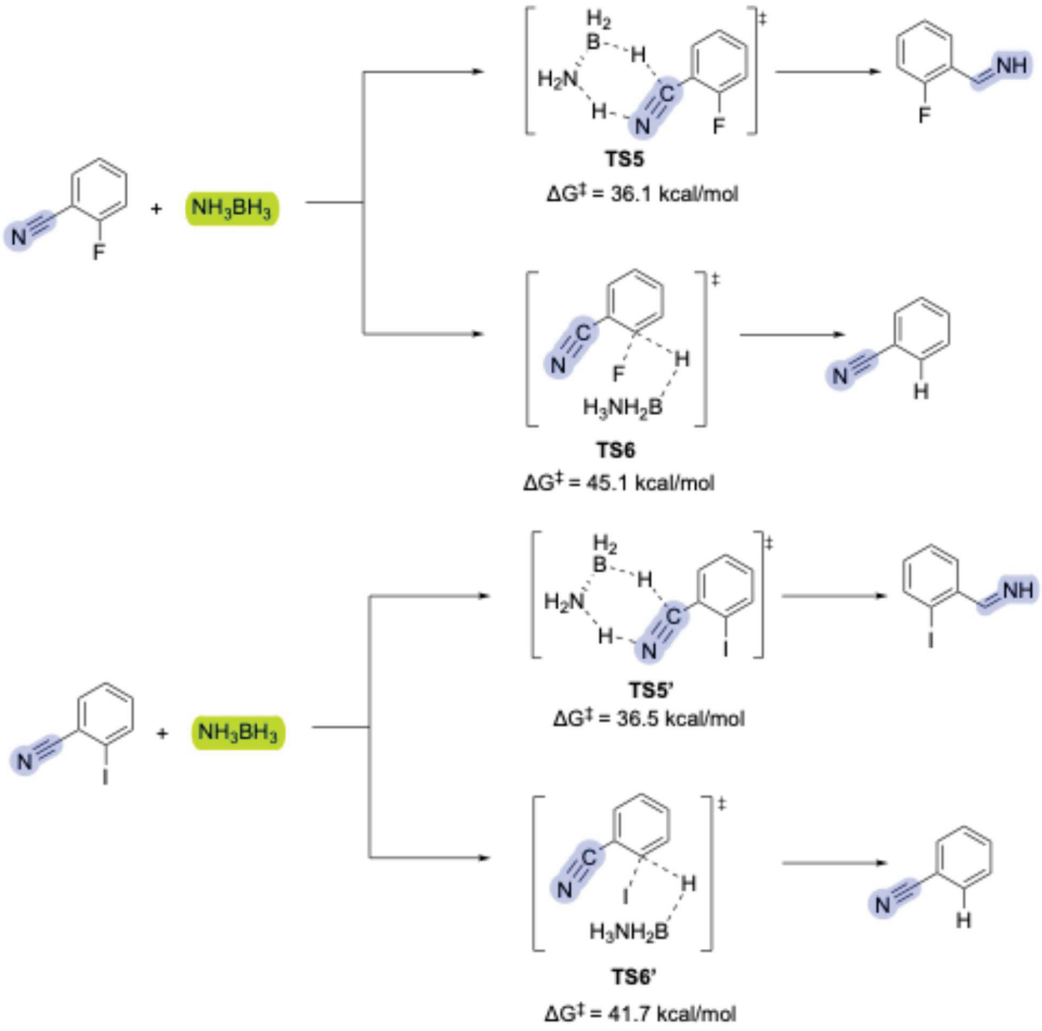


Figure S21. Free energies involved in the uncatalyzed reactions.

We started by computing what would be the barriers for the reactivity in the absence of copper species. The calculated free energy barriers are presented in Figure S21. For the direct reduction of 1-RCN by NH_3BH_3, the calculated activation barrier is 36.1 kcal mol^{-1}. The corresponding direct reduction pathway for 9-RCN has a calculated barrier of 36.5 kcal mol^{-1}. We also examined the uncatalyzed C–X substitution pathways. The calculated activation barriers are 45.1 kcal mol^{-1} for the C–F substitution pathway of 1-RCN-derived substrate and 41.7 kcal mol^{-1} for the C–I substitution pathway of 9-RCN-derived substrate. Both pathways are prohibitively expensive in the absence of copper.

S5.2 Modeling of the $CuCl_2$ solid

Table S7. Free energy associated to the formation of polymeric $(CuCl_2)_n$ units from the $CuCl_2$ monomer.

Monomer	Polymer	ΔG (kcal/mol)
2 $CuCl_2$	$(CuCl_2)_2$	-27.3
3 $CuCl_2$	$(CuCl_2)_3$	-36.1
4 $CuCl_2$	$(CuCl_2)_4$	-51.4
2 $(CuCl_2)_2$	$(CuCl_2)_4$	3.2

Copper chloride is an ionic solid, with bridging chlorides between the copper centers. We evaluated which was the minimum size of the model to have a realistic description of the reactivity. We started from a monomeric unit of $CuCl_2$ and evaluated the free energy associated to the formation of dimeric, trimeric, and tetrameric units. The results are collected in Table S7. It is clear that the monomer is not an acceptable model, as the dimer is −27.3 kcal/mol more stable. In contrast, the series stabilizes fast, with smaller energy costs associated to the addition of additional units. The change from dimer to trimer is below 10 kcal/mol (from -27.3 to -36.1), and the formation of the tetramer is disfavored with respect to two dimers by 3.2 kcal/mol. Based on these results, the dimeric structure was selected as the computational model for subsequent mechanistic investigations.

S5.3 Effect of coordination to copper on the nitrile IR frequencies



Figure S22. Computed IR frequencies for the nitrile group in different compounds.

To gain further insight into the interaction between the nitrile substrate and the copper species, the C≡N stretching frequencies of the free nitrile and the corresponding Cu-coordinated complexes were calculated. As shown in Figure S22, the uncoordinated molecules exhibit a calculated C≡N stretching frequency of 2330 $cm^{-1}$for 1-RCN and 2326 $cm^{-1}$for 9-RCN. Upon coordination to the Cu species, the nitrile stretching frequency shifts to higher wavenumbers, giving calculated values of 2372 and 2334 cm^{-1} for the corresponding Cu–nitrile complexes. The observed blue shift of the C≡N stretching vibration indicates that coordination to the Lewis acidic Cu centers significantly perturbs the electronic structure of the nitrile group.

These results support the experimentally observed interaction between the nitrile functionality and copper species and demonstrate that nitrile coordination can substantially modify the electronic properties of the C≡N bond. The different magnitudes of the calculated

frequency shifts further suggest that the nature of the Cu species and its coordination environment can influence the extent of nitrile activation.

S5.4 DFT calculations of the reduction of 9-RCN

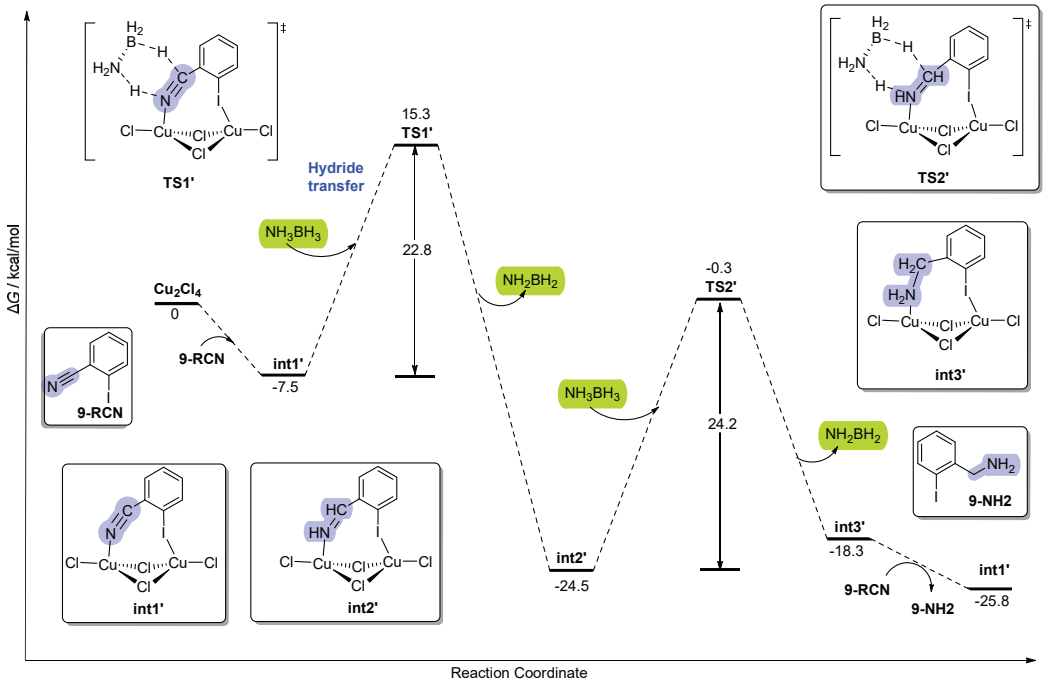


Figure S23. Computed free energy profile (kcal/mol) for the reaction between 9-RCN and NH_3BH_3 in the presence of $CuCl_2$.

To investigate the reduction pathway of 9-RCN, DFT calculations were performed using the Cu_2Cl_4 model under the same computational protocol as that used for 1-RCN. The calculated energy profile is presented in Figure S23. The reaction proceeds through coordination of the nitrile group to the copper complex, followed by two successive hydrogen-transfer steps involving NH_3BH_3-derived species. The calculated activation barriers for the first and second hydrogen-transfer steps are 22.8 and 24.2 kcal mol^{-1}, respectively. These values are comparable to those calculated for the reduction of 1-RCN (22.8 and 24.0 kcal mol^{-1}), indicating that the two substrates have similar calculated energetics for nitrile reduction within the Cu_2Cl_4 model. The results suggest that differences in the intrinsic nitrile-reduction pathways are unlikely to be the sole origin of the contrasting dehalogenation behavior observed experimentally.

S5.5 DFT calculations of Cu_2Cl_3H formation

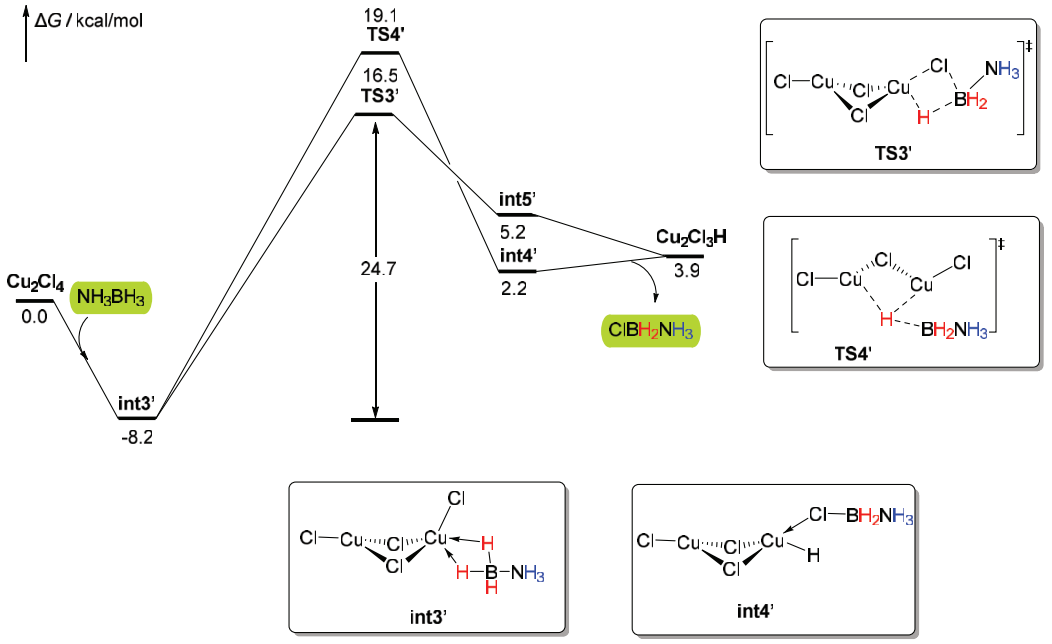


Figure S24. Computed free energy profile (kcal/mol) for the ligand exchange reaction between Cu_2Cl_4 and NH_3BH_3 leading to the formation of Cu_2Cl_3H.

To investigate the possible formation of a hydride-containing copper species under the reaction conditions, we examined the formation of Cu_2Cl_3H in the presence of NH_3BH_3 using DFT calculations. The calculated reaction pathway and corresponding energy profile are shown in Figure S24. The calculations indicate that Cu_2Cl_3H formation is energetically accessible and does not require an exceptionally high energy barrier. This suggests that NH_3BH_3 may serve as a hydride source for the generation of Cu_2Cl_3H under the reaction conditions. The results therefore provide a plausible mechanistic basis for the formation of hydride-containing copper species that could participate in subsequent reaction steps. Although these calculations support the feasibility of Cu_2Cl_3H formation, they do not establish the actual concentration or lifetime of Cu_2Cl_3H under mechanochemical conditions. Accordingly, Cu_2Cl_3H should be considered a plausible intermediate, and its potential role in the subsequent dehalogenation pathway should be interpreted in the context of the calculated reaction energetics.

S5.6 Benchmarking of the DFT functional

Table S8. Comparison of computed activation barriers for Cu_2Cl_3H formation using different computational methods.

Software	Computational method	ΔG (Hartree)	$\Delta G^{\ddagger}$ (kcal mol^{-1})
ORCA	B97-3c (sol)	0.04107646	23.2
ORCA	B3LYP-D3BJ/def2-TZVP (sol)	0.04340686	24.7
ORCA	B3LYP-D3BJ/def2-QZVP (sol)	0.04384315	24.9
ORCA	M06/def2-TZVP (sol)	0.04066066	23.9
ORCA	M06-2X/def2-TZVP (sol)	0.05404148	31.3
ORCA	PBE0/def2-TZVP (sol)	0.04990541	28.7
ORCA	ωB97M-D3BJ/def2-QZVP (sol)	0.04505796	25.7

To assess the sensitivity of the calculated activation barrier for Cu_2Cl_3H formation to the computational method, we compared the results obtained using several density functionals and basis sets (Table S8). Most of the ORCA calculations yielded activation barriers in the range of 25.5–28.3 kcal/mol. M06-2X and PBE0 gave higher values of 33.9 and 31.3 kcal/mol, respectively. Increasing the basis set from def2-TZVP to def2-QZVP at the B3LYP-D3BJ level resulted in a small increase in the calculated barrier, from 27.24 to 27.51 kcal/mol.

With these data, we conclude that the description of the system is not very sensitive to the computational method, and that B3LYP-D3BJ/def2-TZVP (sol) provides a reasonable compromise.

S7. Cartesian coordinates of the computed structures

1-NH2.out

Number of atoms: 17

Coordinates (Angstrom):

N -11.29565600 1.53096500 -12.47291500

C -11.36475500 2.33039600 -11.23796400

C -9.98398800 2.59682600 -10.70237300

C -9.34936000 3.82394200 -10.89400400

C -8.06041500 4.05741100 -10.42594500

C -7.37705200 3.05439100 -9.74797600

C -7.98335900 1.81957800 -9.53803100

C -9.26257700 1.62396400 -10.02086400

H -9.88515700 4.60556400 -11.41953400

H -7.59286300 5.01991200 -10.58886300

H -6.37449700 3.22697700 -9.37815100

H -7.47966600 1.02099900 -9.00936200

H -12.23777700 1.32574300 -12.79232600

H -11.94237800 1.76247400 -10.50679000

H -11.86954100 3.29289800 -11.37838600

H -10.85914100 2.08257700 -13.20586100

F -9.84730600 0.41397400 -9.80536200

1-RCN.out

Number of atoms: 13

Coordinates (Angstrom):

C 1.11970000 -1.60836700 -0.00000300

C 0.54429300 -0.35592200 0.00000900

C 1.30924400 0.81077100 0.00001100

C 2.70569600 0.69901000 0.00000900

C 3.29717100 -0.55283100 -0.00000100

C 2.50708500 -1.69971700 -0.00000800

H 0.48937700 -2.48716200 -0.00000900

H 3.30541500 1.59856600 0.00001300

H 4.37533500 -0.63641800 -0.00000400

H 2.97223000 -2.67667500 -0.00001800

C 0.67419600 2.08383500 0.00001000

N 0.16668700 3.11873800 -0.00003300

F -0.79815300 -0.24540000 0.00001600

9-NH2.out

Number of atoms: 17

Coordinates (Angstrom):

N -11.30448600 1.57061800 -12.49769200

C -11.36775800 2.33777400 -11.24387000

C -9.98502300 2.55719900 -10.68827200

C -9.35805200 3.78834600 -10.89850600

C -8.07212300 4.04395900 -10.44069800

C -7.37957000 3.05746500 -9.75027500

C -7.97760700 1.82310900 -9.52287600

C -9.26384100 1.58421900 -9.99231000

H -9.90250400 4.55701300 -11.43434200

H -7.61566400 5.00905900 -10.62042000

H -6.37761900 3.24111300 -9.38324600

H -7.44423400 1.05435000 -8.98114200

I -10.09619900 -0.32315400 -9.58691800

H -12.24693200 1.37603000 -12.82193300

H -11.96594700 1.76698000 -10.53225700

H -11.84749700 3.31517300 -11.36639200

H -10.86280100 2.13645500 -13.21629300

9-RCN.out

Number of atoms: 13

Coordinates (Angstrom):

C 1.12169500 -1.60877600 -0.00000100

C 0.50678800 -0.36542500 0.00001400

C 1.28799300 0.79901700 0.00001800

C 2.68579800 0.69910500 0.00001300

C 3.29178500 -0.54518300 -0.00000100

C 2.50951000 -1.69502700 -0.00001100

H 0.52306600 -2.50845100 -0.00000900

H 3.27792400 1.60408800 0.00001900

H 4.37097500 -0.61761700 -0.00000800

H 2.97771200 -2.67094700 -0.00002600

C 0.70051700 2.09714400 0.00001400

N 0.25615900 3.16092000 -0.00004900

I -1.59208600 -0.26424300 0.00002300

TS1.out

Number of atoms: 27

Coordinates (Angstrom):

Cu -12.03189200 -2.85518500 -14.62273800

Cl -11.38095000 -1.94686900 -12.65911800

Cl -12.27176100 -0.85671500 -15.57936400

Cu -11.59047900 0.24101600 -13.59148000

Cl -12.06067700 -4.99479000 -14.51943800

N -11.79029300 1.02933000 -11.84133600

C -11.24356000 1.45185200 -10.88476000

C -9.99941700 1.66977700 -10.18474100

C -9.90266200 2.39283900 -8.99380800

C -8.67567400 2.57422000 -8.37859900

C -7.52630500 2.03005000 -8.94386300

C -7.59684700 1.30382200 -10.12707400

C -8.82541100 1.13555000 -10.72865100

H -10.80090800 2.80929600 -8.56082900

H -8.61527200 3.13747600 -7.45749100

H -6.56664200 2.16754000 -8.46320100

H -6.71815600 0.86905900 -10.58393500

Cl -11.00795100 2.14124700 -14.61222600

B -13.41340200 2.24201800 -9.45697400

H -13.59241400 1.39745800 -8.62310100

H -13.47440800 3.38874800 -9.10807500

N -14.25151000 1.96445200 -10.75543200

H -15.08327000 1.40306200 -10.58034700

H -13.67327400 1.43924300 -11.43455700

H -14.55143700 2.81506000 -11.22868800

H -12.20163900 2.07502700 -9.86353300

F -8.89251200 0.43011900 -11.87242200

TS1'.out

Number of atoms: 27

Coordinates (Angstrom):

Cu -8.94515500 -1.38805500 -11.57317800

Cl -8.54330600 0.26485600 -13.29364900

Cl -10.90632200 -2.03749900 -12.42723100

Cu -10.77186200 0.28027400 -13.70167200

Cl -6.90207600 -1.76334900 -10.88479900

N -11.49895900 1.32622000 -12.24104700

C -11.02151200 1.85666000 -11.29132700

C -9.80276600 2.34480800 -10.66496300

C -9.26912100 3.57021500 -11.05862500

C -8.09161300 4.02444900 -10.48208200

C -7.44688100 3.26040500 -9.51629500

C -7.96835200 2.03227900 -9.12269900

C -9.14880200 1.58593000 -9.69269000

H -9.78009500 4.15288900 -11.81302500

H -7.67684700 4.97492900 -10.79004100

H -6.52788800 3.61319600 -9.06676300

H -7.45603100 1.42892800 -8.38707100

I -9.89740600 -0.30964000 -9.15754200

Cl -12.23719900 0.22072600 -15.33229000

B -13.12494000 1.85146800 -9.68040000

H -12.87352200 1.72615900 -8.51750500

H -13.81575500 2.76299900 -10.03824800

N -13.52118900 0.51129900 -10.37887700

H -13.05025100 -0.29626100 -9.96987300

H -13.24778400 0.54024000 -11.37102500

H -14.52569100 0.33705800 -10.34684700

H -11.96044400 2.12578700 -10.23088700

TS2.out

Number of atoms: 29

Coordinates (Angstrom):

Cu -7.44242700 -0.24483500 -12.35112100

Cl -8.81855200 0.94590800 -13.69502300

Cl -9.02883700 -1.71412600 -11.82514500

Cu -10.67270700 -0.14077400 -12.63748900

Cl -5.45086300 0.55185400 -12.42068000

N -11.70789800 1.47493800 -12.37174500

C -11.35370200 2.50154800 -11.56707400

C -10.08423700 2.37997100 -10.79563400

C -9.07838200 3.33165500 -10.95942200

C -7.84356100 3.17764800 -10.34584400

C -7.59556200 2.06484900 -9.54950200

C -8.59054100 1.11500700 -9.34712200

C -9.80824800 1.29979500 -9.96852400

H -9.26861700 4.18543000 -11.59708500

H -7.07049000 3.91863700 -10.49906800

H -6.62963900 1.93166000 -9.08116200

H -8.43284500 0.24427300 -8.72555500

Cl -12.39904100 -1.56904000 -12.77422400

B -13.31936200 2.25762400 -9.82266100

H -12.87467200 2.18257900 -8.71610500

H -14.10940600 3.11574200 -10.08921800

N -13.64570700 0.89354200 -10.47807500

H -13.44406900 0.09162800 -9.88435600

H -13.03723800 0.79262600 -11.33279600

H -14.60951300 0.81154000 -10.79619000

H -12.24689800 2.64244900 -10.53838600

H -11.53255900 3.50592100 -11.94383000

H -12.30287800 1.75114900 -13.14439300

F -10.78098400 0.37083200 -9.76457300

TS2'.out

Number of atoms: 29

Coordinates (Angstrom):

Cu -8.61963400 -1.44222100 -11.52932300

Cl -8.47614000 0.36746700 -13.07320400

Cl -10.38301000 -2.32036100 -12.61075000

Cu -10.79559700 0.03022500 -13.14490600

Cl -6.66354300 -1.59230500 -10.58795400

N -11.60288100 1.58377900 -12.34749700

C -11.31290900 2.43930800 -11.33542500

C -9.93775800 2.52334600 -10.73692000

C -9.24150200 3.70102800 -11.02548400

C -7.95377800 3.91983500 -10.56041000

C -7.33664500 2.96352300 -9.76510600

C -8.01087900 1.79287400 -9.44925700

C -9.29392400 1.57938400 -9.93787100

H -9.72768300 4.45270600 -11.63478500

H -7.44072500 4.83897500 -10.81166600

H -6.33561900 3.12260800 -9.38558900

H -7.53449700 1.04112500 -8.83742700

I -10.14908700 -0.28857600 -9.43354700

Cl -12.42581500 -0.27907300 -14.67153000

B -13.21117900 1.76233700 -9.70592900

H -12.90411600 1.51917300 -8.57927800

H -13.91398300 2.69653800 -9.94902000

N -13.50923100 0.52515700 -10.58353700

H -13.27047800 -0.35893200 -10.13771700

H -12.91247700 0.59890900 -11.44469300

H -14.47601300 0.47250500 -10.90078800

H -12.00782800 2.14822000 -10.23218500

H -11.72802700 3.43539400 -11.46469400

H -12.31389300 1.96120700 -12.96303300

TS3.out

Number of atoms: 23

Coordinates (Angstrom):

Cu 1.40285800 1.13662400 0.19351300

Cl 0.62695100 1.02498300 -1.94794900

Cl 1.55934800 -1.06217200 0.60840900

Cu -0.15380600 -0.95687300 -0.96243700

Cl 1.61015500 3.18317700 0.83074900

H -1.72645100 -1.14569400 -1.17307100

N -1.30515100 -0.81389500 3.02898300

C -2.07461500 -1.33986200 1.90795100

C -2.38687400 -0.29315800 0.87913000

C -2.03418100 1.03887400 0.99161400

C -2.37883500 1.96622400 0.00641500

C -3.13121000 1.58118800 -1.10778600

C -3.49680800 0.26526300 -1.26897400

C -3.00248900 -0.69076300 -0.34984700

H -1.50148800 1.36482700 1.87344800

H -2.08410000 3.00020000 0.12449500

H -3.43998300 2.31910500 -1.83600000

H -4.08477800 -0.07762600 -2.10934600

F -3.58966600 -1.92015500 -0.36750100

H -0.35538200 -0.60870900 2.73332100

H -1.23586900 -1.52532900 3.74811200

H -3.01825300 -1.74041900 2.29095000

H -1.58339500 -2.18040900 1.39523800

TS3’.out

Number of atoms: 14

Coordinates (Angstrom):

Cu 1.37558200 0.33895600 -0.01642200

Cl 0.76259500 1.78664400 -1.56477100

Cl 0.93626100 -1.78524700 -1.08880300

Cu -0.87503100 -1.14802600 0.06069800

Cl 2.73965300 -0.15112300 1.60542400

Cl -2.96430200 -1.08389400 0.64478900

B -1.94861800 1.90061300 1.47159300

N -2.13464000 2.25943700 0.00852800

H -1.29499900 2.06941500 -0.56419800

H -2.29090700 3.27576600 -0.05814400

H -2.90928700 1.60784300 2.08517500

H -0.87063600 2.06599300 1.91854800

H -2.94274600 1.81146600 -0.42878200

H -0.23586100 0.09133300 0.83464700

TS4.out

Number of atoms: 23

Coordinates (Angstrom):

Cu 1.05379900 -2.00742300 0.70912500

Cl 1.88877500 1.79428200 -2.53661400

Cl 0.93690900 -2.34347500 -1.48471400

Cu 1.04383200 -0.07584800 -1.80860900

Cl 1.99239000 -2.04772200 2.63944100

H -0.19550600 0.24107400 -0.82740300

N 1.32113700 2.83983300 1.87821700

C 0.56628000 1.62564800 1.60156400

C -0.65633500 1.85577700 0.76104200

C -1.01776400 3.10984400 0.29856000

C -2.09871500 3.29139400 -0.56475600

C -2.85850700 2.20093800 -0.98261500

C -2.53238900 0.92907600 -0.55276000

C -1.38885600 0.75415000 0.25004800

H -0.43887400 3.96287100 0.62497300

H -2.35326100 4.28871400 -0.89930400

H -3.71091800 2.34200800 -1.63458700

H -3.11023700 0.07042800 -0.86315800

I -1.36826700 -1.10560500 1.32961100

H 1.82273700 3.13809100 1.04710100

H 2.02147200 2.64271000 2.58436300

H 0.27212600 1.17482500 2.55289500

H 1.15937500 0.85784700 1.07662200

TS4'.out

Number of atoms: 14

Coordinates (Angstrom):

Cu 2.07312600 3.01280300 -1.32324900

Cl 2.26504700 1.38632600 0.15075300

Cl -0.18768300 3.19526900 -1.36249500

Cu -0.34353200 1.35860000 0.08338200

Cl 2.89713500 4.45553700 -2.69693100

Cl -1.02434600 0.67997000 2.08542300

B -1.50948400 -1.82004100 0.40388000

N -0.04631600 -2.14629600 0.67787300

H 0.59165200 -1.69927100 0.01460700

H 0.08839400 -3.16112700 0.56856700

H -2.25030200 -1.86948600 1.31633600

H -1.82903000 -1.76555300 -0.72876600

H 0.25532100 -1.90687900 1.62459700

H -0.97998000 0.28015100 -0.81397700

TS5.out

Number of atoms: 21

Coordinates (Angstrom):

C -2.56092400 2.46982400 -0.31352000

C -1.18454100 2.57466600 -0.41303400

C -3.13344700 1.32978000 0.24632300

H -0.72987000 3.45582500 -0.84490400

H -4.20897500 1.24151300 0.32728200

C -0.34230900 1.54946100 0.04165800

C -2.32549100 0.29836300 0.70388900

H -2.74049800 -0.59976700 1.14146400

C -0.95327100 0.42561600 0.59386300

H -3.18917300 3.27495300 -0.67096200

C 1.10939500 1.71748000 -0.09088000

N 1.84766100 2.54257400 -0.57941800

B 2.89504000 0.07333700 0.84167900

H 2.79034900 -0.95795900 0.24659000

N 3.82791600 1.09466600 0.22899400

H 4.40142800 0.74910900 -0.53577000

H 1.66166900 0.69353100 0.49299200

H 3.13576200 1.89522600 -0.22415000

H 2.81424500 0.09057300 2.03425700

H 4.43009900 1.58076200 0.88806300

F -0.19406300 -0.60118100 1.04284800

TS5’.out

Number of atoms: 21

Coordinates (Angstrom):

C -2.40488000 2.57470200 0.14479800

C -1.04404400 2.53902900 -0.11737200

C -3.09811700 1.38967500 0.36445300

H -0.49227000 3.45451800 -0.28565300

H -4.16047000 1.40684000 0.57164200

C -0.35576600 1.32199200 -0.15872000

C -2.43220900 0.17109500 0.31267900

H -2.97451700 -0.75151000 0.46562700

C -1.06695900 0.14109300 0.05665300

H -2.92189400 3.52483400 0.17837800

C 1.09249100 1.36237700 -0.41616500

N 1.82861500 1.85916700 -1.23679100

I -0.12484600 -1.74134700 -0.09312600

B 2.90490400 0.55023200 1.26903500

H 2.89462800 -0.64039600 1.35246900

N 3.80945500 1.13289000 0.21531300

H 4.42852600 0.47047300 -0.24324300

H 1.64497500 0.75189800 0.59499300

H 3.07427700 1.53906100 -0.62028500

H 2.73354000 1.22431900 2.24205100

H 4.35500300 1.93917100 0.50656300

TS6.out

Number of atoms: 21

Coordinates (Angstrom):

N -0.67125500 2.91442700 -1.30240300

C -1.11086200 1.90008200 -0.95156200

C -1.60100400 0.67743200 -0.45668200

C -2.73419400 0.06704400 -1.02346600

C -3.24717900 -1.09970600 -0.50358700

C -2.62475500 -1.66357800 0.62851500

C -1.51158400 -1.10588200 1.20369400

C -0.89899400 0.06129100 0.63924000

H -3.20370200 0.54840500 -1.87248700

H -4.12422000 -1.55970300 -0.93711500

H -3.04072100 -2.56190800 1.07042700

H -1.06079600 -1.54309300 2.08469400

B 0.19715800 1.86281800 2.23907500

H -0.71697500 2.60969700 2.35413800

H 0.56140600 1.13338600 3.10052400

N 1.29804900 2.29976200 1.25238500

H 0.94500600 2.84102200 0.45954400

H 1.98291600 2.88835300 1.73770600

H 1.80405600 1.49436200 0.87672000

H -0.58499700 0.81383400 1.48277900

F 0.58619600 -0.25254700 0.24649000

TS6'.out

Number of atoms: 21

Coordinates (Angstrom):

N -0.38303600 2.45597600 -1.94910600

C -0.87833200 1.58054900 -1.37832200

C -1.47276600 0.51462200 -0.66505200

C -2.80420700 0.15315000 -0.93447700

C -3.42010100 -0.85876600 -0.23074100

C -2.69378000 -1.52390000 0.76888900

C -1.38965500 -1.19166300 1.06093000

C -0.74348600 -0.14959100 0.35878000

H -3.33160800 0.68925800 -1.71315800

H -4.44173300 -1.13731700 -0.44824400

H -3.15894800 -2.32788300 1.32682100

H -0.84932000 -1.72114600 1.83272400

I 1.46829400 -0.70871600 -0.21972600

B 0.02403200 1.67497400 2.19695500

H -1.00615200 2.26823000 2.33610100

H 0.44696000 0.98875700 3.08187500

N 1.14012800 2.54221400 1.51873400

H 0.78277000 3.10535800 0.74695600

H 1.57284700 3.18557000 2.18473600

H 1.88994500 1.95851700 1.14067900

H -0.27462200 0.76823300 1.25215400

int1.out

Number of atoms: 19

Coordinates (Angstrom):

Cu 3.65161300 -2.03196500 0.31657200

Cl 1.47072700 -1.63655900 0.76927000

Cl 3.99770700 0.11278700 -0.19115300

Cu 1.76670200 0.67488200 0.28294100

Cl 4.13245600 -4.09621800 0.60569000

N -0.16771200 0.93843800 0.39786200

C -1.29285500 1.15335600 0.45777200

C -2.67395300 1.44011400 0.53330300

C -3.11897700 2.75215500 0.75446800

C -4.47584000 3.00708600 0.82701500

C -5.39151100 1.96676000 0.68044400

C -4.96638700 0.66101100 0.46013400

C -3.61307100 0.41613500 0.38996500

H -2.39115200 3.54381600 0.86503500

H -4.82349600 4.01659000 0.99734800

H -6.45245200 2.17130900 0.73787800

H -5.66648400 -0.15491300 0.34439400

Cl 2.17479000 2.86749100 0.15117700

F -3.17129700 -0.83455400 0.17810700

int1'.out

Number of atoms: 19

Coordinates (Angstrom):

Cu 0.62266100 -1.37471600 0.26383800

Cl 1.71341200 -0.07034500 1.96985100

Cl 2.25356000 -0.70062600 -1.18347200

Cu 2.18479500 1.27178600 0.17727100

Cl -0.61014300 -2.69131300 1.49443700

N 0.38206100 2.24742500 0.31046700

C -0.74417400 2.02300300 0.38320500

C -2.11049200 1.66560700 0.48622100

C -2.95880100 2.42224500 1.30176100

C -4.28581700 2.05263300 1.44187900

C -4.76731800 0.92812500 0.78200500

C -3.93175000 0.16425400 -0.02800700

C -2.60763400 0.53420000 -0.18296900

H -2.56296900 3.28769300 1.81494500

H -4.94190600 2.63947100 2.06989200

H -5.80270100 0.63449300 0.89487300

H -4.31431700 -0.70953600 -0.53553800

I -1.39806700 -0.59516000 -1.47934300

Cl 3.39724400 2.65123900 -1.01317300

int2.out

Number of atoms: 21

Coordinates (Angstrom):

Cu 1.94119800 -1.38952500 -0.44723000

Cl 3.18644800 0.31514700 0.39075400

Cl 0.68530000 0.01176600 -1.64633600

Cu 1.32060800 1.69868400 -0.03836600

Cl 2.73412200 -3.25906600 0.24385700

H -2.51528300 2.07572500 0.57770500

N -0.52478300 2.33175300 0.18265400

C -1.51664900 1.64584700 0.59794000

C -1.34758800 0.27854600 1.07651900

C -2.27572100 -0.70656800 0.75498600

C -2.08908000 -2.03709000 1.07181700

C -0.93999100 -2.39999900 1.76212200

C -0.00904400 -1.43495400 2.14281100

C -0.21593000 -0.10844100 1.80499400

H -2.82663100 -2.76794500 0.76910400

H -0.77531300 -3.43956600 2.01189600

H 0.86803800 -1.71601600 2.70841300

Cl 2.26189800 3.59879700 0.66671600

H -0.74131600 3.28541100 -0.09518200

H 0.48165600 0.64752600 2.14319900

F -3.37626700 -0.35421700 0.05632900

int2’.out

Number of atoms: 21

Coordinates (Angstrom):

Cu 1.80202400 -1.45084100 -0.49572100

Cl 3.11079400 0.20930500 0.32685200

Cl 0.55915500 -0.01032600 -1.65771300

Cu 1.28445100 1.65081900 -0.05723700

Cl 2.55836800 -3.34532000 0.16919300

H -2.50822200 2.13432500 0.69158200

N -0.52989500 2.34865100 0.20941000

C -1.52134300 1.67945400 0.64796000

C -1.35710800 0.29202600 1.08626100

C -2.21682800 -0.72334600 0.66208400

C -1.96621000 -2.04632200 0.99817300

C -0.86112300 -2.36263500 1.77945200

C -0.01367800 -1.36001800 2.23858600

C -0.26433800 -0.04144900 1.89503200

I -3.84007000 -0.29945100 -0.61230300

H -2.61969300 -2.82967200 0.64093000

H -0.66658400 -3.39689500 2.03087900

H 0.83696600 -1.60293300 2.86028700

Cl 2.30978000 3.51928700 0.61641700

H -0.72579500 3.31686700 -0.03160300

H 0.37191800 0.74656200 2.27839400

int3.out

Number of atoms: 23

Coordinates (Angstrom):

Cu 0.22121100 1.65340000 -0.67966300

Cl 0.31204800 0.17410700 -2.52671500

Cl 1.17953600 0.09216700 0.71231600

Cu 0.23941100 -1.36250600 -0.80744400

Cl 0.32096900 3.62015800 -1.60968800

H -0.39010500 -2.51886800 -1.52241300

N -1.72908600 -1.25185000 3.24241400

C -2.30917900 -1.53861000 1.93539800

C -2.39530100 -0.31720600 1.05658900

C -1.88168200 0.92185000 1.40932700

C -1.91895100 2.00478700 0.52057800

C -2.51824100 1.85687900 -0.73808300

C -3.05300700 0.63165800 -1.10785100

C -2.97168200 -0.41434800 -0.21012800

H -1.43385300 1.04937800 2.38343700

H -1.57503900 2.97751100 0.84840600

H -2.57426700 2.69629000 -1.41574900

H -3.51660500 0.47917800 -2.07253000

F -3.48114500 -1.61069900 -0.57955900

H -0.73594300 -1.05875000 3.15460600

H -1.81033800 -2.07480100 3.82928000

H -3.31504000 -1.93853600 2.08517100

H -1.75682500 -2.30716400 1.37468400

int3’.out

Number of atoms: 14

Coordinates (Angstrom):

Cu 1.81952200 2.44466900 -1.29786100

Cl 1.79121600 0.98552900 0.39726000

Cl -0.36729900 2.95321500 -1.05525400

Cu -0.60250300 1.14185100 0.42988400

Cl 2.66173400 3.55358200 -2.92164900

Cl -2.58686800 1.80122900 1.20812800

B -0.95558800 -1.12350400 0.41782000

N 0.27699400 -2.10964400 0.35479100

H 1.14184600 -1.65241700 0.06571000

H 0.10350600 -2.85816800 -0.31698000

H -1.95319100 -1.68829900 0.76203700

H -1.08351000 -0.57494300 -0.66151400

H 0.46048500 -2.55566400 1.25320600

H -0.70634600 -0.31743500 1.36442100

int4.out

Number of atoms: 23

Coordinates (Angstrom):

Cu 0.41092200 1.22091000 -1.42179400

Cl 0.30413600 -0.03400600 -3.31082900

Cl 0.82197400 -0.48703400 -0.03383000

Cu -0.07853400 -1.85885400 -1.76889500

Cl 0.46193700 3.28993200 -2.02597300

H -0.08356400 -3.06625600 -2.68224200

N -2.05169900 -0.99609000 3.63917000

C -2.24614400 -1.38497000 2.24566800

C -2.38569700 -0.20906900 1.31045800

C -2.27370100 1.10424400 1.76979900

C -2.33500300 2.18757900 0.90338400

C -2.53567300 1.98610100 -0.45705600

C -2.66679700 0.69004900 -0.94421100

C -2.58094900 -0.37558900 -0.05895500

H -2.12549500 1.26819400 2.82795200

H -2.22541600 3.19180200 1.29241500

H -2.59012200 2.82253200 -1.13970700

H -2.81734300 0.51441200 -1.99958300

H -1.11712700 -0.62118900 3.77056900

H -2.11122000 -1.82339700 4.22274700

H -3.15483600 -1.98946400 2.18427300

H -1.43499800 -2.01668700 1.85953200

I -2.59515700 -2.31457300 -0.91671100

int4'.out

Number of atoms: 14

Coordinates (Angstrom):

Cu 2.07416700 0.23401500 -0.17962800

Cl 0.38569900 1.65564700 0.09166000

Cl 0.84805800 -1.61987900 0.22108500

Cu -1.06233900 -0.23425700 0.53923400

Cl 4.10554400 -0.33893600 -0.57712900

Cl -2.99971300 1.05858000 0.07358500

B -4.56176000 -0.09837700 0.28723700

N -4.28370800 -1.37097700 -0.59738000

H -4.15791600 -1.15446300 -1.58659600

H -5.07104900 -2.01934300 -0.53366700

H -4.62511600 -0.40366800 1.43978800

H -5.48024200 0.52644100 -0.15472500

H -3.45278900 -1.87816000 -0.28505800

H -1.86507200 -1.38400000 1.15679700

int5'.out

Number of atoms: 14

Coordinates (Angstrom):

Cu 1.24330200 0.13773800 -0.14782300

Cl 0.49659100 1.84808900 -1.34456700

Cl 0.63101200 -1.85843600 -1.32608700

Cu -1.02747400 -1.29454300 0.05348400

Cl 2.89497000 0.88951100 1.04083700

Cl -3.08612600 -0.91586100 0.86444700

B -3.02963000 0.99270900 1.44650200

N -2.67197800 1.83567200 0.17167000

H -1.72486700 1.67066800 -0.18594100

H -2.71872500 2.82992100 0.40764800

H -4.14885100 1.20696900 1.79889400

H -2.16686900 1.06369500 2.26400400

H -3.32112900 1.69058700 -0.60280600

H -0.16982700 -0.29018000 0.93658600

CuCl2.out

Number of atoms: 3

Coordinates (Angstrom):

Cu 1.36934900 1.76839500 -0.32775700

Cl -0.04385000 0.50960100 -1.23695500

Cl 2.77569500 3.05171900 0.55789200

Cu2Cl4.out

Number of atoms: 6

Coordinates (Angstrom):

Cu 1.57557000 1.21252900 0.26810200

Cl 0.06741200 1.05745400 -1.44083800

Cl 1.11816000 -0.88068200 0.99860100

Cu -0.34357100 -1.06730400 -0.71929800

Cl 2.47460100 3.14113800 0.13988000

Cl -1.77730300 -1.94221400 -2.03106600

Cu4Cl8.out

Number of atoms: 12

Coordinates (Angstrom):

Cu 1.59249900 0.59659900 -2.52986800

Cl -0.17433000 0.59991400 -4.02465400

Cl 1.26393600 -1.60103200 -2.00751600

Cu -0.45750200 -1.65857300 -3.51634300

Cl 2.50412900 2.51435700 -2.71633100

Cl -1.83039800 -2.35804300 -4.99748800

Cu -2.03790300 1.09885100 -1.99991400

Cl -2.31034000 -1.16784000 -1.50822700

Cl -0.34850700 1.28580700 -0.46704300

Cu -0.63771600 -0.91103900 0.07663000

Cl -3.66872600 1.60910700 -3.27878600

Cl -0.51709000 -2.74016900 1.16180500

Cu3Cl6.out

Number of atoms: 9

Coordinates (Angstrom):

Cu 1.79488700 1.27224900 -0.12710600

Cl 0.92479200 0.28792600 -1.96365500

Cl 0.84384100 -0.27500900 1.29494600

Cu -0.71385700 -0.68553700 -0.65759400

Cl 2.96080500 2.95649000 -0.68976200

Cl -1.80671800 -1.73000700 -2.24453500

Cu -1.03247700 0.74175900 2.19555400

Cl -2.41949800 -0.47945400 0.89211300

Cl -2.17075000 2.07294400 3.39670300

References

1. Neese, F. Software Update: The ORCA Program System—Version 6.0. *WIREs Comput Mol Sci* **15**, e70019 (2025).

2. Becke, A. D. Density-functional thermochemistry. III. The role of exact exchange. *The Journal of Chemical Physics* **98**, 5648–5652 (1993).

3. Lee, C., Yang, W. & Parr, R. G. Development of the Colle-Salvetti correlation-energy formula into a functional of the electron density. *Phys. Rev. B* **37**, 785–789 (1988).

4. Grimme, S., Antony, J., Ehrlich, S. & Krieg, H. A consistent and accurate *ab initio* parametrization of density functional dispersion correction (DFT-D) for the 94 elements H-Pu. *The Journal of Chemical Physics* **132**, 154104 (2010).

5. Weigend, F. Accurate Coulomb-fitting basis sets for H to Rn. *Phys. Chem. Chem. Phys.* **8**, 1057 (2006).

6. Marenich, A. V., Cramer, C. J. & Truhlar, D. G. Universal Solvation Model Based on Solute Electron Density and on a Continuum Model of the Solvent Defined by the Bulk Dielectric Constant and Atomic Surface Tensions. *The Journal of Physical Chemistry B* **113**, 6378–6396 (2009).

7. Álvarez-Moreno, M. *et al.* Managing the Computational Chemistry Big Data Problem: The **ioChem-BD** Platform. *J. Chem. Inf. Model.* **55**, 95–103 (2015).

8. Shirley, D. A. High-Resolution X-Ray Photoemission Spectrum of the Valence Bands of Gold. *Phys. Rev. B* **5**, 4709–4714 (1972).

9. Scofield, J. H. Hartree-Slater subshell photoionization cross-sections at 1254 and 1487 eV. *Journal of Electron Spectroscopy and Related Phenomena* **8**, 129–137 (1976).

10. Jarg, T. *et al.* How reliable is internal standard method in monitoring mechanochemical synthesis? A case study of triphenylmethane in HPLC-UV-MS analysis of hemicucurbit[*n*]urils. *RSC Mechanochem.* **2**, 507–515 (2025).

11. Hu, Z. & Kerton, F. M. Simple copper/TEMPO catalyzed aerobic dehydrogenation of benzylic amines and anilines. *Org. Biomol. Chem.* **10**, 1618 (2012).

12. Xu, B. *et al.* Simple Copper Catalysts for the Aerobic Oxidation of Amines: Selectivity Control by the Counterion. *Angew. Chem. Int. Ed.* **55**, 15802–15806 (2016).

13. Patil, R. D. & Gupta, M. K. Methods of Nitriles Synthesis from Amines through Oxidative Dehydrogenation. *Adv. Synth. Catal.* **362**, 3987–4009 (2020).

14. Priestley, I. *et al.* Safety Considerations and Proposed Workflow for Laboratory-Scale Chemical Synthesis by Ball Milling. *Organic Process Research & Development* **27**, 269–275 (2023).

15. Ding, M., Chang, J., Mao, J.-X., Zhang, J. & Chen, X. Noncatalyzed Reduction of Nitriles to Primary Amines with Ammonia Borane. *J. Org. Chem.* **87**, 16230–16235 (2022).

16. Sarkar, K., Das, K., Kundu, A., Adhikari, D. & Maji, B. Phosphine-Free Manganese Catalyst Enables Selective Transfer Hydrogenation of Nitriles to Primary and Secondary Amines Using Ammonia–Borane. *ACS Catal.* **11**, 2786–2794 (2021).

17. Bornschein, C. *et al.* Mild and selective hydrogenation of aromatic and aliphatic (di)nitriles with a well-defined iron pincer complex. *Nat. Commun.* **5**, 4111 (2014).

18. Yu, C. *et al.* CuNi Nanoparticles Assembled on Graphene for Catalytic Methanolysis of Ammonia Borane and Hydrogenation of Nitro/Nitrile Compounds. *Chem. Mater.* **29**, 1413–1418 (2017).

19. Floyd, K., Gonnet, L., Friščić, T. & Batteas, J. The role of the milling environment on the copper-catalysed mechanochemical synthesis of tolbutamide. *RSC Mechanochem.* **1**, 289–295 (2024).

20. Lennox, C. B. *et al.* Direct mechanocatalysis by resonant acoustic mixing (RAM). *Chem. Sci.* **14**, 7475–7481 (2023).

21. Zhang, S., Hu, Y., Li, M. & Xie, Y. Reductive Amination of Aldehyde and Ketone with Ammonia and H_2 by an *In Situ* -Generated Cobalt Catalyst under Mild Conditions. *Org. Lett.* **26**, 7122–7127 (2024).

22. Shapiro, S. L., Parrino, V. A. & Freedman, L. Hypoglycemic Agents. III.[1−3] N^1 -Alkyl- and Aralkylbiguanides. *J. Am. Chem. Soc.* **81**, 3728–3736 (1959).

23. Narobe, R. *et al.* Practical electrochemical hydrogenation of nitriles at the nickel foam cathode. *Green Chem.* **26**, 10567–10574 (2024).

24. Laval, S. *et al.* Straightforward access to cyclic amines by dinitriles reduction. *Tetrahedron* **70**, 975–983 (2014).

25. Dai, H. & Guan, H. Switching the Selectivity of Cobalt-Catalyzed Hydrogenation of Nitriles. *ACS Catal.* **8**, 9125–9130 (2018).

26. Liu, X. *et al.* Recyclable Silver-Catalyzed Selective Hydrogenation of Imides to Primary Amines via Dual C–N Bond Cleavage. *Org. Lett.* **25**, 3066–3071 (2023).

27. Shao, C., Stolte, M. & Würthner, F. Quadruple π Stack of Two Perylene Bisimide Tweezers: A Bimolecular Complex with Kinetic Stability. *Angew Chem Int Ed* **52**, 7482–7486 (2013).

28. Aronica, L. A., Albano, G., Giannotti, L. & Meucci, E. Synthesis of N-Heteroaromatic Compounds through Cyclocarbonylative Sonogashira Reactions. *Eur J Org Chem* **2017**, 955–963 (2017).

29. Complexes with ligands containing nitrile groups. XV. The ligand properties of benzylcyanide. *Inorganica Chimica Acta* **7**, 113–116 (1973).

Curriculum Vitae

Personal data

Name: Andrea Casagrande
Date of birth: 01.04.1998
Place of birth: Rome, Italy
Citizenship: Italian

Contact data

E-mail: andrea.casagrande2@outlook.it

Education

2023–2026	Tallinn University of Technology, Virumaa College, PhD
2023–2026	University of Montpellier, ICGM, PhD
2020–2022	University of Rome – La Sapienza, Chemistry Department, M. Sc.
2017–2020	University of Rome – La Sapienza, Chemistry Department, B. Sc.

Language competence

Italian	Native
English	Fluent
French	Intermediate

Professional employment

2023–2026	Tallinn University of Technology, Virumaa College, early stage researcher

Elulookirjeldus

Isikuandmed

Nimi: Andrea Casagrande
Sünniaeg: 01.04.1998
Sünnikoht: Rooma, Itaalia
Kodakondsus: Itaalia

Kontaktandmed

E-post: andrea.casagrande2@outlook.it

Hariduskäik

2023–2026	Tallinna Tehnikaülikool, Virumaa Kolledž, PhD
2023–2026	Montpellier' Ülikool, ICGM, PhD
2020–2022	Rooma La Sapienza Ülikool, keemia osakond, M. Sc.
2017–2020	Rooma La Sapienza Ülikool, keemia osakond, B. Sc.

Keelteoskus

Itaalia keel	emakeel
Inglise keel	kõrgtase
Prantsuse keel	kesktase

Teenistuskäik

2023–2026	Tallinna Tehnikaülikool, Virumaa Kolledž, nooremteadur

ISSN 2585-6901
ISBN 978-9916-80-610-4